MAR 9 1950

THE PHYSICAL REVIEW

Vol. 77 Second Series NUMBER 5

MARCH 1, 1950

Published for the
AMERICAN PHYSICAL SOCIETY
by the
AMERICAN INSTITUTE OF PHYSICS
Lancaster, Pa. and New York, N. Y.

THE PHYSICAL REVIEW

A journal of exp[erimental and theoretical physics] established by E. L. Nichols in 1[893]

Published by the American Institute of Physics
for the
AMERICAN PHYSICAL SOCIETY

Officers

President

J. J. RABI
Columbia University
New York, New York

Vice-President

C. C. LAURITSEN
California Institute of Technology
Pasadena, California

Secretary

K. K. DARROW
Bell Telephone Laboratories
Office:
Columbia University
New York 27, New York

Treasurer

G. B. PEGRAM
Columbia University
New York 27, New York

Local Secretary
for the Pacific Coast

J. KAPLAN
University of California at Los Angeles
Los Angeles, California

Managing Editor

JOHN T. TATE
University of Minnesota
Minneapolis, Minnesota

The Physical Review

Entered as second-class matter [illegible]
Acceptance for mailing at special rate of [illegible]

BOARD OF EDITORS

[illegible]

Associate Editors

W. E. LAMB, JR. — [illegible]
R. G. HERB — R. F. [illegible]
J. BARDEEN — [illegible]

[illegible] for publication should be submitted to John T. [illegible], University of Minnesota, Minneapolis, Minnesota. The authors' institutions are [illegible] to pay a publication charge of $8 per page which, if [illegible] are not [illegible]. Instructions will be sent with proofs.

[illegible] all correspondence concerning papers in the process of publication [illegible] addressed to the Publication Manager, American Institute of Physics, 57 East 55 Street, New York 22, New York.

Subscription Price

[illegible] and Canada . . . . . [illegible]
[illegible] . . . . . [illegible]

Back Numbers[1]

[illegible] back numbers rates when complete year is available:

Prior to 1940: $20.00
Thereafter: $27.00

[illegible] copies: $2.50 each, prior to July, 1929;
$2.00 each, July, 1929–December, 1941;
$1.50 each, January, 1942–December, 1946;
$1.00 each, January, 1947–December, 1948;
$1.25 each, thereafter.

[illegible] [illegible] (1937–1939) $3.00

[illegible] orders for back numbers should be addressed to [illegible], Lancaster, Pennsylvania, or to the American Institute of Physics, 57 East 55 Street, New York 22, New York.

[illegible] of address in the case of members of the American Physical Society should be sent to the Treasurer; in the case of other subscribers, to the Fulfillment Manager, American Institute of Physics.

[illegible] Cornell University Physics Department, Cornell University, Ithaca, New York.

[illegible] Lancaster, Pennsylvania

[illegible] Lancaster, Pennsylvania, under the Act of [illegible]
[illegible] section 34.40, P. L. & R. of 1948, authorized [illegible]

THE
PHYSICAL REVIEW

A journal of experimental and theoretical physics established by E. L. Nichols in 1893

SECOND SERIES, VOL. 77, NO. 5 MARCH 1, 1950

A New Method for Determining the Relative Phase with Which Slow Neutrons Are Scattered by Nuclei*

P. J. BENDT AND I. W. RUDERMAN
Pupin Physics Laboratories, Columbia University, New York, New York
(Received November 3, 1949)

To determine the relative phase with which neutrons are scattered by an element A, cross-section measurements are obtained for A, for a reference element B, and for a substitutional solid solution of A and B. The experimental value of the effective coherent scattering cross section, σ_{coh}', for the solid solution, when compared with the values calculated from the data for pure A and B, shows whether the two constituent elements scatter neutrons in the same or in opposite phases. Measurements made with the Columbia neutron velocity spectrometer show that copper and nickel scatter with the same phase, and manganese and nickel with opposite phases, in agreement with other methods of phase determination. The following more accurate values of the free scattering cross sections, σ_f, and new values of the effective coherent scattering cross sections, σ_{coh}', were obtained: copper, $\sigma_f=8.2$ barns, $\sigma_{coh}'=6.6$ barns; nickel, $\sigma_f=17.4$ barns, $\sigma_{coh}'=13.9$ barns; manganese, $\sigma_f=1.80$ barns. $\sigma_{coh}'=\sim 1.9$ barns.

INTRODUCTION

IN the course of the systematic investigation of the resonance levels of the elements being carried out with the Columbia neutron velocity spectrometer,[1,2] the free scattering cross sections and the $1/v$ capture slopes of the elements are determined with considerable precision. With relatively little additional work, as will be shown in this paper, it is possible to determine the coherent scattering cross section and the relative phase with which an element scatters neutrons. This new method does not require high resolution, and hence there is no need for the high neutron intensity of a reactor. The data are easily analyzed and the results are obtained directly.

Fermi and Marshall[3] have reported three methods for phase determination: (a) Intensity measurements of different orders of Bragg reflections from the same plane of a crystal and comparison with theoretical values; (b) measurement of the limiting angle for total reflection of neutrons from mirrors; (c) comparison of the observed total cross section of gas molecules at long neutron wave-lengths with values calculated from classical interference theory. The second method is the only one which gives an absolute determination of phase, for only nuclei with positive scattering amplitudes, using the Fermi sign convention, give total reflection. The first two methods require a high neutron flux in order to obtain good resolution in a reasonable period of time. The third method is not a precision experiment and does not require high neutron intensities, but it is limited in its application to gases.

Wollan and Shull[4] made phase determinations by observing the coherent Bragg scattering by different crystal planes, and comparing with theoretical values. Fermi, Sturm, and Sachs[5] and Winsberg, Meneghetti, and Sidhu,[6] have determined phase of scattering by making high resolution transmission measurements of microcrystals, and comparing crystal diffraction peaks of the transmission curve, after identification of the peaks with particular crystal planes, with theoretical values.

THEORY

The theory of the phase of scattering of slow neutrons has been treated in earlier papers.[3,4,7,8] Only the results

* Presented at the Semi-Centennial Meeting of the American Physical Society at Cambridge, Massachusetts, on June 18, 1949.

[1] Havens, Rainwater, Wu, and Dunning, Phys. Rev. **73**, 963 (1948).

[2] Rainwater, Havens, Dunning, and Wu, Phys. Rev. **73**, 733 (1948).

[3] E. Fermi and L. Marshall, Phys. Rev. **71**, 666 (1947).

[4] E. O. Wollan and C. G. Shull, Phys. Rev. **73**, 830 (1948).

[5] Fermi, Sturm, and Sachs, Phys. Rev. **71**, 589 (1947).

[6] Winsberg, Meneghetti, and Sidhu, Phys. Rev. **75**, 975 (1949).

[7] Halpern, Hamermesh, and Johnson, Phys. Rev. **59**, 981 (1941); also O. Halpern and M. H. Johnson, Phys. Rev. **55**, 898 (1939).

[8] Feshbach, Peaslee, and Weisskopf, Phys. Rev. **71**, 145 (1947).

of this theory, and the definitions used in this paper, need be mentioned here. For slow neutron scattering by nuclei, only zero angular momentum or spherically symmetric scattering need be considered. If η is the phase shift relative to the incident neutron wave of the spherically symmetric part of the total wave at large distances, then the free scattering cross section, σ_f, is given by

$$\sigma_f=4\pi(-\lambda\sin\eta)^2, \tag{1}$$

where $\lambda=\lambda/2\pi=1/k$ and λ is the neutron wave-length. For scattering by a nucleus of spin zero, $(-\lambda\sin\eta)$ has a unique value; this quantity is called the free scattering amplitude or scattering length and is denoted by a. For $|\sin\eta|\ll 1$, a is just the value of the radial coordinate r for the (extrapolated) node of the exterior wave function. From general theoretical considerations, the free scattering length is expected to be positive, except in a small energy region on the low side of a resonance, where it is negative. If two nuclei scatter neutrons with the same phase, then the sign of a is the same for both; if they scatter with opposite phases, then a is positive for one nucleus and negative for the other.

If the spin i of the nucleus is not zero, then compound nuclear states of spin $(i+\frac{1}{2})$ and $(i-\frac{1}{2})$ can be formed with relative statistical weights $g_a=(i+1)/(2i+1)$ and $g_b=i/(2i+1)$, respectively. If the corresponding free scattering lengths are a_a and a_b, then the total free scattering cross section for the isotope is

$$\sigma_f=4\pi[g_a a_a^2+g_b a_b^2]. \tag{2}$$

This is the experimentally observed cross section using neutrons of energy >1 ev. At lower energies the binding of the atoms is important and the scattering amplitudes for an infinitely bound atom are increased by the factor $(A+1)/A$, where A is the atomic weight of the nucleus. The bound scattering cross section, σ_b, for a single atom is then

$$\sigma_b=4\pi[g_a f_a^2+g_b f_b^2], \tag{3}$$

where f_a and f_b are the bound scattering amplitudes for the separate spin states.

In a crystalline material containing many atoms, we must take into account that part of the scattering by a single nucleus is coherent relative to scattering by the other atoms, and part is incoherent. The observed scattering at any given energy below about 1 ev is very sensitive to the crystal lattice parameters and to the neutron wave-length on account of interference between the coherent part of the scattering from different atoms. We can define the coherent scattering cross section, σ_{coh}, as that part of σ_b which can be modified by interference effects. Then σ_{coh} is given by

$$\sigma_{coh}=4\pi[g_a f_a+g_b f_b]^2. \tag{4}$$

If measurements are made on an element with several isotopes of relative abundance p_j present, the above averages must also be taken over the isotopes. Then

$$\sigma_f=4\pi\sum_j p_j[g_{aj}a_{aj}^2+g_{bj}a_{bj}^2], \tag{5}$$

$$\sigma_b=4\pi\sum_j p_j[g_{aj}f_{aj}^2+g_{bj}f_{bj}^2], \tag{6}$$

and

$$\sigma_{coh}=4\pi\{\sum_j p_j[g_{aj}f_{aj}+g_{bj}f_{bj}]\}^2. \tag{7}$$

From Eq. (7) we can define the effective bound scattering amplitude, f_{k-eff}, for an element k consisting of more than one isotope by

$$f_{k-eff}=\sum_j p_j[g_{aj}f_{aj}+g_{bj}f_{bj}]. \tag{8}$$

It is the sign of this effective scattering amplitude which is determined by the experiments. The incoherent scattering cross section, σ_{inc}, of an element due to spin and isotope effects is given by

$$\sigma_{inc}=(\sigma_b-\sigma_{coh}). \tag{9}$$

If solid solutions are formed, of two metals for example, there are two cases to consider. If the system is completely disordered with respect to the relative positions of the atoms of the two elements in the lattice, then we may still use Eqs. (5)–(7), but treat p_j as the relative abundance of the jth isotope in the mixture rather than in the element. If the coherent scattering amplitudes are quite different (or of opposite sign) for

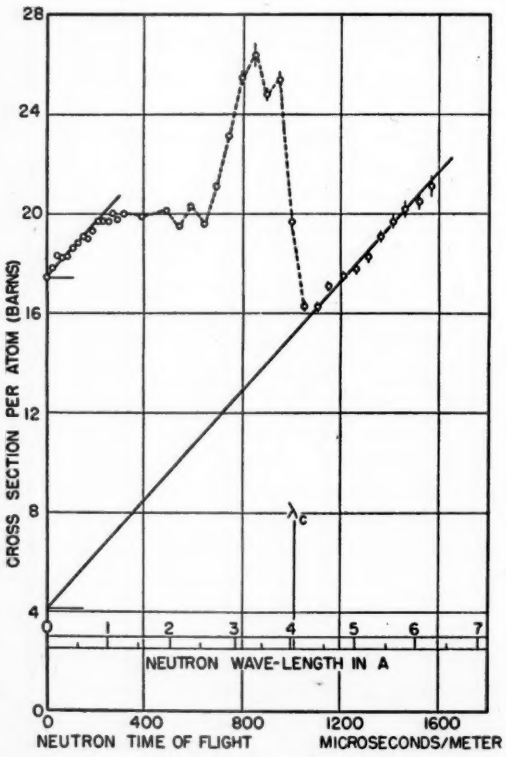

FIG. 1. The slow neutron cross section of nickel as measured with a 9.69-g/cm² sample. The $1/v$ line for the short wave-length region is $\sigma=(17.4+0.79E^{-\frac{1}{2}})$, and the $1/v$ line for data beyond the cut-off for Bragg reflections, λ_c, is $\sigma=(4.1+0.79E^{-\frac{1}{2}})$.

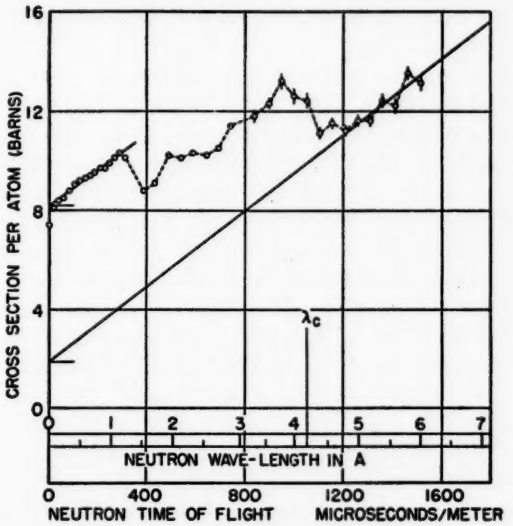

FIG. 2. The slow neutron cross section of copper as measured with a 19.19-g/cm² sample. The $1/v$ line for the short wave-length region is $\sigma=(8.2+0.54E^{-\frac{1}{2}})$, and the $1/v$ line for data beyond the cut-off for Bragg reflections, λ_c, is $\sigma=(1.9+0.54E^{-\frac{1}{2}})$.

the two elements, there will be a large increase in σ_{inc}/σ_b for the mixture relative to either element alone. If there is some degree of order such that the atoms of the two elements tend to take different regular lattice positions, the value of σ_{inc} is reduced, and this offers a method for the study of such order-disorder effects in favorable cases. In the experiments here described, a state of disorder was assured by rapid quenching of the sample from a high temperature.

Let us consider typical transmission data for a microcrystalline sample of an element as obtained with the neutron velocity spectrometer, and plotted as cross section *vs.* neutron wave-length (see, for example, the curve for nickel given in Fig. 1). This curve may be analyzed as follows: The intercept on the zero wave-length axis is σ_f as given by Eq. (5). The curve between the zero wave-length axis and the first crystal diffraction peak is a straight line whose slope is determined by the capture cross section of the sample. The diffraction effects end at the cut-off wave-length, λ_c, for the crystal, since the portion of the curve beyond λ_c is a region in which there is total destructive interference of the various coherent scattering amplitudes. The curve beyond λ_c is again a straight line parallel to the initial part of the curve, and the intercept obtained by extrapolation of this line to zero wave-length gives σ_{inc}. σ_b is obtained by multiplying σ_f by $(A+1)^2/A^2$, and the effective coherent scattering cross section, σ_{coh}', is obtained from $\sigma_{coh}'=(\sigma_b-\sigma_{inc})$. The latter is smaller than σ_{coh} given by Eq. (7) because of thermal motion of the atoms in the crystal.

To determine the sign of the scattering amplitude of an element, a substitutional solid solution is formed of the element and another reference element for which the sign of the scattering amplitude is known or assumed. The coherent scattering cross sections for the elements are known from measurements made on the elements separately. From a modification of Eq. (7),

$$\sigma_{coh}=4\pi[p_1 f_{1-eff}+p_2 f_{2-eff}]^2. \qquad (10)$$

σ_{coh} of the solid solution is calculated assuming f_{1-eff} and f_{2-eff} of the constituent elements to have the same sign, and again assuming opposite signs. A comparison of the measured σ_{coh}' with the two calculated values of σ_{coh} shows whether the phase of scattering of the two elements is the same or opposite.

To be more rigorous, the cross-section data beyond λ_c should be obtained with the sample at a temperature well below the Debye temperature, so as to obtain σ_{coh} rather than σ_{coh}'. However, the difference between these values is small (<0.5 barn) compared with the

TABLE I. Some important observed and calculated cross sections, and the cut-off wave-lengths, λ_c. Cross sections are in barns ($=10^{-24}$ cm²).

	σ_f	σ_b	σ_{coh}'	σ_{coh}, calculated for Same phase	Opposite phase	λ_c in A
Copper	8.2	8.5	6.6			4.16
Manganese	1.80	1.87	~1.9			12.6
Nickel	17.4	18.0	13.9			4.06
Cu–Ni alloy	12.4	12.8	10.1	9.9	0.35	4.11
Mn–Ni alloy	13.6	14.1	5.5	9.5	5.4	6.4

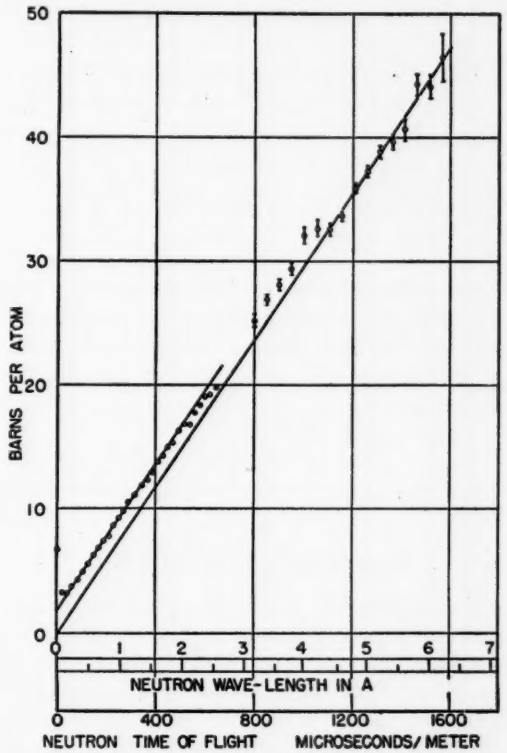

FIG. 3. The slow neutron cross section of manganese as measured with a 16.92-g/cm² sample. The $1/v$ line for the short wave-length is $\sigma=(1.80+2.14E^{-\frac{1}{2}})$.

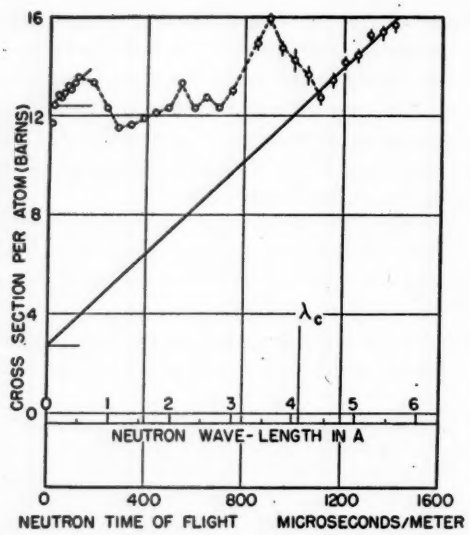

FIG. 4. The slow neutron cross section of disordered copper-nickel alloy composed of 48.10 percent nickel and 51.69 percent copper by weight, and having an area density of 7.48 g/cm². The intercepts of the $1/v$ lines give $\sigma_f=12.4$ barns and $\sigma_{inc}=2.7$ barns.

large difference between the values of σ_{coh} calculated for the same and opposite phases of scattering. By the proper choice of the reference element, and of the relative proportions of the constituents of the solid solution, the difference in σ_{coh} for different phases of scattering can be maximized. The scientific literature[9] provides information on a large number of substitutional solid solutions, from which a suitable reference element may be chosen.

EXPERIMENTAL PROCEDURE

To illustrate this method, transmission measurements were made on samples of pure nickel, copper, manganese, and on copper-nickel and manganese-nickel alloys. The nickel sample was composed of seven micron particles of pure nickel obtained by the decomposition of nickel carbonyl. The copper sample consisted of c.p. copper pellets between 2 and 5 mm diameter. The manganese sample consisted of 99.9 percent electrolytic manganese, which was crushed and screened to give a uniform batch of 0.5- to 1-mm particles, and was outgassed at 400°C for 4 hr. in a high vacuum system to remove hydrogen occluded during the electrolytic process. The samples were packed in flat, cylindrical aluminum containers, 3 in. in internal diameter, and $\frac{3}{8}$ to $1\frac{1}{2}$ in. thick, depending on the desired neutron transmission. After careful outgassing, the containers were filled with helium at atmospheric pressure and sealed.[10]

The copper-nickel alloy was in the form of a plate with an area density of 7.48 g/cm², and analyzed 48.10 percent nickel and 51.69 percent copper by weight. It was heated to 800°C and quenched to room temperature with powdered dry ice in less than 1 min. to insure that it was in a completely disordered state. The manganese-nickel alloy consisted of a plate of area density 3.85 g/cm² and analyzed 27.45 atom percent manganese and 72.55 atom percent nickel. The alloy was heated in an inert atmosphere of argon to 800°C and quenched in dry ice to put it in a disordered state.

The operation of the neutron velocity spectrometer has been described in detail by Rainwater and Havens.[11–13] In order to extend the transmission data in the very low energy region (>5A), the source-to-detector distance was reduced from 6 to 5 meters, and a "cold source" consisting of a liquid-nitrogen-cooled paraffin slab was used. For low energy measurements (>3A), the neutron beam was filtered through 13 g/cm² of Be and 11 g/cm² of BeO so as to reduce the stray neutron background.[10] "Standard filters"[14] were used for the high energy measurements to minimize changes in the counting rate for the "sample in" and "sample out" positions.

RESULTS

The cross-section data for nickel, copper, and manganese are shown in Figs. 1, 2, and 3, respectively. These results are considered more accurate and have been extended to longer neutron wave-lengths than the previously published curves for these elements.[1,13] The

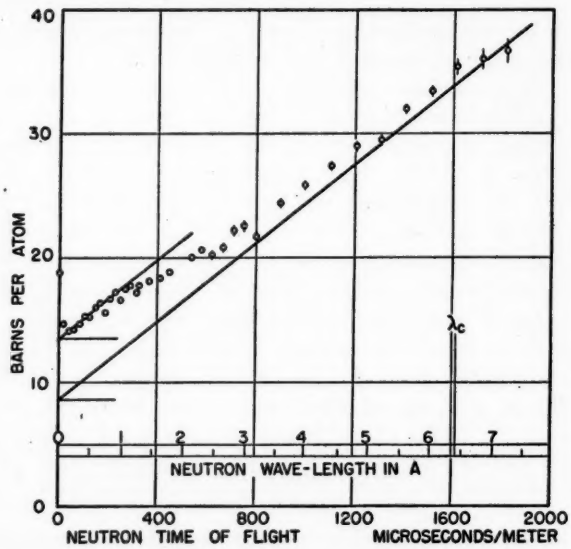

FIG. 5. The slow neutron cross section of disordered manganese-nickel alloy composed of 27.45 atom percent manganese and 72.55 atom percent nickel, and having an area density of 3.85 g/cm². The intercepts of the $1/v$ lines give $\sigma_f=13.6$ barns and $\sigma_{inc}=8.6$ barns.

[9] See, for example, *International Critical Tables* (McGraw-Hill Book Company, Inc., New York, 1927), Vol. II, pp. 400–455.
[10] I. W. Ruderman, Phys. Rev. **76**, 1572 (1949).
[11] J. Rainwater and W. W. Havens, Jr., Phys. Rev. **70**, 136 (1946).
[12] W. W. Havens, Jr., and J. Rainwater, Phys. Rev. **70**, 154 (1946).
[13] Rainwater, Havens, Wu, and Dunning, Phys. Rev. **71**, 65 (1947).
[14] E. Melkonian, Phys. Rev. **76**, 1750 (1949).

best $1/v$ line for nickel in the high energy region (0–0.8A) is given by the equation

$$\sigma=(17.4\pm0.2)+(0.79\pm0.1)E^{-\frac{1}{2}},$$

where σ is the total cross section in barns ($=10^{-24}$ cm^2) and E is the neutron energy in electron volts. Beyond λ_c, the best $1/v$ line is given by

$$\sigma=(4.1\pm1.2)+(0.79\pm0.1)E^{-\frac{1}{2}}.$$

After correcting the free cross section for binding, the best value of σ_{coh}' is 13.9 barns.

Similarly, the best high energy $1/v$ lines for copper and manganese are given by

$$\sigma=(8.2\pm0.2)+(0.54\pm0.05)E^{-\frac{1}{2}}$$

and

$$\sigma=(1.80\pm0.05)+(2.14\pm0.02)E^{-\frac{1}{2}},$$

respectively. Beyond λ_c the cross section for copper is given by

$$\sigma=(1.9\pm0.6)+(0.54\pm0.05)E^{-\frac{1}{2}}.$$

The manganese curve could not be observed out to cut-off, because the neutron intensity at this long wave-length (12.6A) is at present too weak to be useful. However, since the best straight line with the correct capture slope through the points between 4.5 and 6A passes through zero, the incoherent scattering cross section is probably very small, and was indeed taken to be zero for this work. In Table I the important cross sections and values of λ_c for each sample are tabulated.

Using the data from Figs. 1 and 2, f_{eff} was calculated for nickel and for copper. Substituting these f_{eff} values in Eq. (10) together with the appropriate p's shows that σ_{coh} for the copper-nickel alloy should be 9.9 barns if copper and nickel scatter with the same phase, and 0.35 barn if the elements scatter with opposite phases. The measured value of σ_{coh}' for the copper-nickel alloy (Fig. 4) is 10.1 barns. Copper and nickel therefore scatter neutrons with the same phase, in agreement with Fermi and Marshall's results on the basis of the total reflection of neutrons from mirrors[3]. Their measurements also show that the signs of the scattering amplitudes of copper and nickel are positive.

From the manganese-nickel curve (Fig. 5) σ_{coh}' is found to be 5.5 barns. If the two elements scatter with the same phase, then from Eq. (10) σ_{coh} of the alloy should be 9.5 barns, whereas if the elements scatter with opposite phases, then σ_{coh} should be 5.4 barns. It may therefore be concluded that manganese has a negative scattering amplitude, in agreement with Fermi and Marshall's results on the basis of the intensities of Bragg reflections from MnS_2,[3] and Wollan and Shull's measurements of Bragg reflections from MnO.[4] This experiment would have been more sensitive if the alloy contained 72.55 atom percent of manganese instead of 72.55 atom percent of nickel; however, this would have extended λ_c to 10A, in which region measurements are presently impractical to make because of the low neutron intensity.

The greatest uncertainty in the measurements made here is introduced by the long extrapolation from the points beyond λ_c to zero wave-length, using the capture slope. This means that the latter must be determined with high accuracy, and that enough points beyond λ_c must be obtained to enable an accurate extrapolation to be made. Fortunately the capture slope can be measured with good statistical accuracy at short wave-lengths where the neutron intensity is high, and where crystal diffraction effects are not present. Improvements in the spectrometer are now under way which should make it possible to obtain better statistical accuracy at long neutron wave-lengths.

ACKNOWLEDGMENTS

The authors wish to express their appreciation to Professors L. J. Rainwater and W. W. Havens, Jr. for their helpful advice and encouragement. The samples of nickel and nickel-copper alloy were kindly supplied by Mr. W. M. Wise of the International Nickel Company; the electrolytic manganese was furnished by Mr. K. M. Leute of the Electro Manganese Corporation; and the specimen of manganese-nickel alloy was provided by Mr. R. G. Knickerbocker, Rolla Branch, U. S. Bureau of Mines. We should also like to thank the U. S. AEC which aided materially in the performance of this research.

Excited States of Be^7 *

J. C. GROSSKREUTZ AND K. B. MATHER†
Department of Physics, Washington University, St. Louis, Missouri
(Received November 21, 1949)

Evidence for the existence of excited states of Be^7 below 1 Mev has been found from a study of the neutrons produced in the reaction $Li^7(p,n)Be^7$. Using a beam of homogeneous protons of 5 Mev energy from the Washington University cyclotron, the neutrons were detected by a standard photographic plate method. In addition to the ground state group of neutrons, three additional lower energy groups were observed indicating an excited level structure for Be^7. Three separate runs on three separate targets of varying thickness gave the same results. Observations were made at 20° and 90° to the proton beam for each target. In every case the shift in energy of the peaks as one goes from 90° to 20° is consistent with the assignment of definite levels to Be^7. Values obtained for the level excitation energies are: 0.205±0.070 Mev, 0.470±0.070 Mev, and 0.745±0.070 Mev above the ground state. The level at 470 kev is presumably analogous to the well-known level at 478 kev in the mirror nucleus Li^7. Levels in Li^7 corresponding to the other two levels found in Be^7 have as yet not been observed, and may, of course, not exist. The Q for the ground state reaction was found to be −1.65±0.04 Mev in good agreement with previously obtained values.

I. INTRODUCTION

THE assumption of equality between neutron-neutron and proton-proton forces suggests that the level structure of the so-called mirror nuclei is essentially identical. The lightest isotope known to have an excited level is Li^7. Hence it is of interest to inquire as to the level structure of the mirror nucleus, Be^7. In particular, one may expect that there should exist a level in Be^7 corresponding to the well-known 478-kev level in Li^7. A number of workers[1] have looked for such a level in Be^7 but with no success.

One method of attack is to investigate the energy spectrum of the neutrons from the reaction

$$Li^7+H^1\rightarrow Be^7+n^1-1.64 \text{ Mev}. \quad (1)$$

In this reaction, Freier, Lampi, and Williams[2] have shown that for incident protons of energy up to 3.66 Mev, only the ground state group of neutrons is present. Working on the assumption that a greater amount of energy supplied to the compound nucleus, Be^8, might result in the formation of Be^7 in excited states, reaction (1) has been investigated with the 5.11-Mev protons obtained from the Washington University cyclotron.

II. EXPERIMENTAL METHOD

The fringing field of the cyclotron magnet combined with a specially designed slit system is used to isolate a beam of monoenergetic protons for use in the experiment. The beam then passes down a long snout to a point well away from the cyclotron where investigation can be carried out with adequate shielding. The energy of the protons so obtained is determined by allowing them to strike a photographic emulsion at a glancing angle and recording their distribution in range. An energy of 5.11±0.06 Mev with a width at half-maximum of 30 kev is thus found for the proton beam.

A chamber originally designed by one of us (K.B.M.) for use in scattering experiments using photographic emulsions as detectors was modified to give the correct geometry for reaction studies. As seen in Fig. 1, the proton beam enters through a system of collimating slits and strikes a thin target at the center of the chamber. Nuclear track emulsions are arranged radially with respect to the target for detection of the disintegration particles. Since we are interested here in recording only the neutrons produced in the reaction, the emulsions were encased in light-tight steel holders of sufficient thickness to stop any charged particles produced in the target. This thickness is negligible, however, in contributing to a diminution in neutron energy. Neutrons produced in the reaction thus pass freely through the emulsion and an examination of the recoil proton tracks produced in the direction of the neutron flux will give an accurate measure of the neutron energy. Collimation of the neutrons at the various angles of detection results from the fact that the plates are almost tangential to the path of the incident neutrons.

Targets were prepared by evaporation of Li compounds in vacuum onto a 0.1-mil platinum foil supported at the edges by a thin steel frame. Two targets of LiF were prepared, 3.1 mg/cm² and 1.07 mg/cm², and one of LiCl. The thickness of the latter was not determined due to the rapid deliquescence of LiCl when removed from vacuum, but it is believed to have been of the same order of magnitude as the two LiF targets. The uniformity of the LiCl target is in serious doubt as a result of the deliquescence occuring during transfer of the foil from the evaporation chamber to the reaction chamber.

Exposures given the detecting plates were a function of the target thickness used. The thinner of the two LiF targets was given about twice that of the other two targets. The plates were examined by microscope following development and the track lengths recorded

* Assisted by the Joint Program of the ONR and AEC.
† Now at the University of Birmingham, Birmingham, England.
[1] Freier, Lampi, and Williams, Phys. Rev. 75, 901 (1949); W. E. Burcham, and J. M. Freeman, Nature 163, 167 (1949); Mandeville, Swann, and Snowden, Phys. Rev. 76, 980 (1949); A. O. Hanson and R. F. Taschek, National Research Council Preliminary Report No. 4, Nuclear Science Series.
[2] Freier, Lamp, and Williams, Phys. Rev. 75, 901 (1949).

using a procedure that has already been explained in detail.[3]

III. EXPERIMENTAL RESULTS

Figures 2 and 3 give the resulting neutron spectrum at 20° and 90° to the beam, respectively, for the various targets used. The plates exposed at 90° to the LiCl target did not contain sufficient tracks to give a reliable spectrum and it was not felt that an additional run using a longer exposure was justified at the time. A discussion of the data obtained from each target is given below.

160-kev LiF Target

LiF was chosen as a target material because of the ease in evaporation of the compound, plus the fact that neutrons from F(p,n)Ne have quite low energies ($\sim$1.0 Mev at 20° to the beam) in comparison with those from Li^7.

Examination of the spectrum in Fig. 2 obtained at 20° to the incident beam shows what appears to be two unresolved groups at the high end of the energy axis, a well-defined peak at 2.75 Mev, and a point of inflection at $\sim$2.45 Mev. Below this the points do not fall into any definite arrangement. Turning now to the data taken at 90°, shown in Fig. 3, we see again the two unresolved high energy groups while the third group has now lost its definiteness. This "squeezing together" of the groups at 90° to the beam is due to the unfavorable increase of the slope of the range-energy curve for protons in the emulsion at lower energies. Finally a fourth group is now well defined at the 90° position. If one tentatively assigns to Be^7 energy levels correing to the groups observed at 20°, the position on the energy scale of the peaks at 90° is consistent with this assignment. Further, the well-defined fourth group at 90° corresponds in energy to the point of inflection at 2.45 Mev in the 20° data. Since subsequent runs have definitely indicated the existence of this peak at 20°, no explanation is readily forthcoming for its failure to appear in these data.

A run was made on a Pt foil to ascertain what neutrons, if any, were attributable to "background." We were able to show, as a result of this run, that a negligible number of neutrons were present above 2.2 Mev at the 20° position and none above 1.4 Mev at the 90° position. Hence, the four peaks observed are most certainly due to Li^7. ($Li^6(p,n)Be^6$ threshold is quite high. The basis for this statement is a lower limit calculation for the mass of Be^6 from which the Q for the reaction can be estimated. He^6, Li^6, and Be^6 belong to a triplet system and the triplet splitting energy can be found from the known masses of He^6 and Li^6. The Coulomb binding energy for Be^6 and the neutron-proton mass difference are also known; hence a lower limit for the value of the mass of Be^6 can be found.)

[3] J. C. Grosskreutz, Phys. Rev. **76**, 482 (1949).

Thin LiCl Target

As stated previously, the uniformity of this target is in doubt, but the main reason for running it was as a control over the LiF data. Neutrons from Cl^{37} will most certainly be present, as the Q for the reaction $Cl^{37}(p,n)A^{37}$ has been given as -1.596 Mev.[4] The other isotope of Cl will not be effective, the Q for $Cl^{35}(p,n)A^{35}$ being -6.6 Mev.

Figure 2 displays the 20° data from this target, and upon examination one finds again the two unresolved high energy peaks originally found in the LiF data. It must be mentioned that the ground state group of neutrons from $Cl^{37}(p,n)A^{37}$ falls at 3.31 Mev, which further confuses the resolution of the two high energy peaks. However, the intensity of the neutrons from Cl^{37} is probably quite low in comparison to those from Li^7 as a result of barrier penetration. Peaks again occur at 2.75 Mev and 2.45 Mev, corresponding to the ones observed in the case of LiF. Further, two low energy groups are manifest at 1.75 and 2.05 Mev. These two groups agree excellently with the first two excited levels found by Davison[5] in A^{37}. Our data yields values for the levels in A^{37} of 1.40 Mev and 1.65 Mev as compared to 1.38 and 1.63 Mev given by Davison.

50-kev LiF Target

The inability to resolve all groups in the runs just discussed prompted us to do the experiment again some months later using a much thinner LiF target. The uppermost curves in Figs. 2 and 3 display the neutron

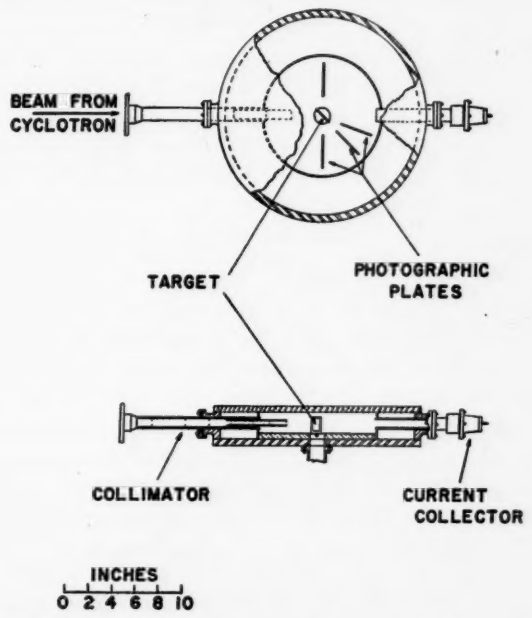

FIG. 1. Experimental arrangement for the study of the neutrons from $Li^7(p,n)Be^7$ by means of photographic plates.

[4] H. T. Richards and R. V. Smith, Phys. Rev. **74**, 1257 (1948).
[5] P. W. Davison, Yale University, Sloane Physics. Lab. Annual Report NR-024-002 (1948).

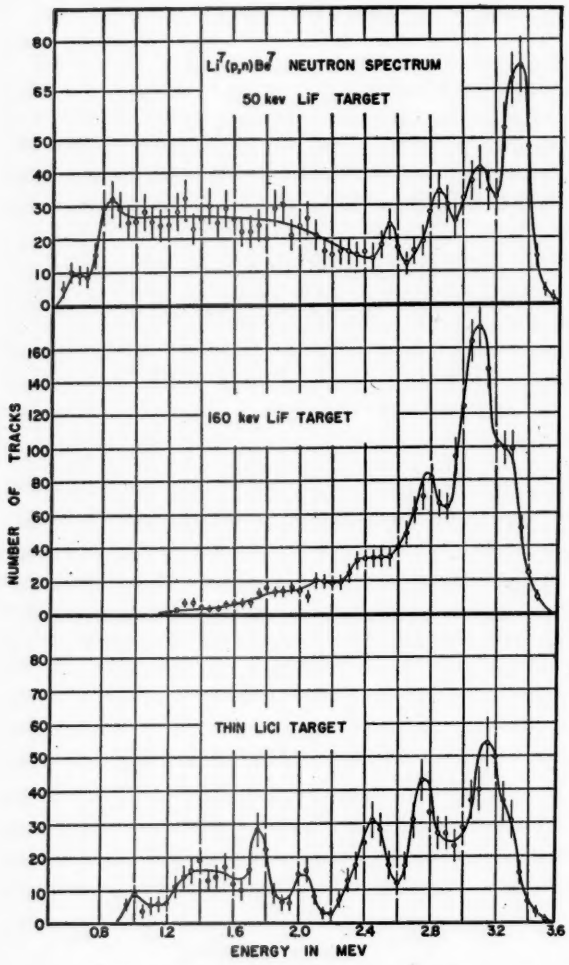

FIG. 2. Energy distribution of neutrons from $Li^7(p,n)Be^7$ observed at 20° to the bombarding beam of protons. The number of tracks in each 100-kev interval has been plotted every 50 kev. Corrections involving geometry and $n-p$ scattering cross section have not been made in this plot. Reading from top to bottom, the spectra represent 772, 962, and 490 acceptable recoil proton tracks.

energy spectra obtained. As is evident from first glance, resolution of the two high energy peaks was indeed achieved. That the relative intensities are consistent with those found in the earlier runs is immediately evident from target thickness considerations; for the general shift of the groups toward lower energies as this thickness increases will cause the second peak to appear to have the greater intensity in the 160-kev LiF case. The position in energy of the ground state group is in excellent agreement with the predicted energy obtained from the known masses and Q-value. The next three groups are in agreement with those found in the earlier runs on thicker targets. The relative intensities of the groups at 20° and 90° are the same within experimental error. The energies of the groups at 20° and 90° correspond to the assignment of definite energy levels to Be^7.

It will be noticed that the background of low energy neutrons is considerably higher in this run than in the first two runs. This can be attributed to two factors. First, the exposure was approximately twice that given the former plates. Second, there is a strong observer bias in favor of the measurement of the long recoil proton tracks over that of the shorter ones. And it was not until scanning of the 50-kev LiF plates began that the microscopist was given strict instructions to measure *every* track that fulfilled the acceptance conditions in an attempt to locate the ground state neutrons from fluorine. These two factors when coupled together will certainly give rise to a higher background than that measured in the original two runs. Whether it accounts for the approximately threefold increase is a matter of conjecture. The significant thing is, however, that no definite grouping emerges from this increased background while the four energy groups found originally are confirmed.

IV. CALCULATIONS AND DISCUSSION

Since in no case are the neutron groups fully resolved into separate peaks, it was necessary to invoke the following procedure for obtaining mean energies for the groups. The ranges of the tracks in terms of the scale divisions of the eyepiece micrometer as recorded by the microscopist were plotted as a histogram. The histogram interval chosen was 1.5 scale divisions (~2 microns)

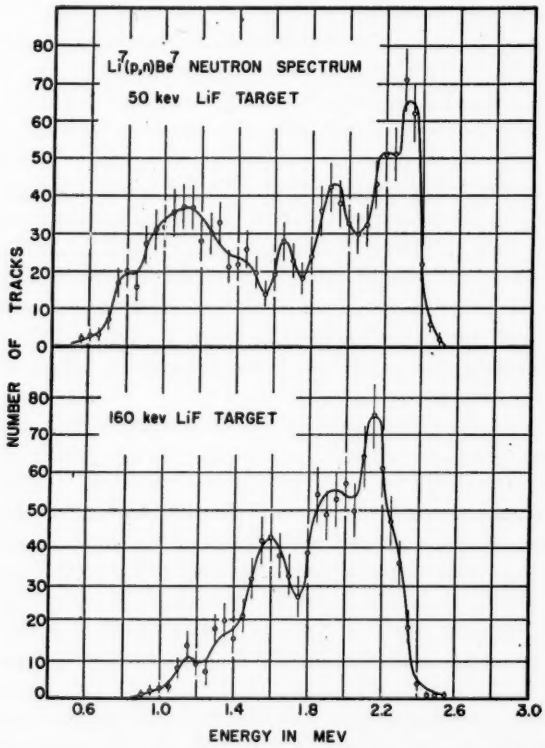

FIG. 3. Energy distribution of neutrons from $Li^7(p,n)Be^7$ observed at 90° to the bombarding proton beam. The number of tracks in each 100-kev interval has been plotted every 50 kev. Corrections involving geometry and $n-p$ scattering cross section have not been made in this plot. Reading from top to bottom, the spectra represent 555 and 565 acceptable recoil proton tracks.

TABLE I. The neutron groups from $Li^7(p,n)Be^7$. Groups are numbered reading from right to left in Figs. 2 and 3. Relative intensities are the mean of the 20° and 90° positions, the differences in the two cases being within the experimental error. An assignment of energy levels is made to Be^7, the values given being the mean of those found at the 20° and 90° positions.

Group	Mean energy of neutrons (Mev) 20° to beam	90° to beam	Q (Mev) 20° to beam	90° to beam	Mean excitation energy of Be^7 (Mev)	Mean relative intensity
I	3.37±0.04	2.37±0.03	−1.64±0.04	−1.67±0.03	0.00	100.0
II	3.14±0.04	2.20±0.03	−1.86±0.04	−1.86±0.03	0.205±0.070	58.5
III	2.88±0.04	1.97±0.03	−2.12±0.04	−2.13±0.03	0.470±0.070	52.5
IV	2.61±0.04	1.72±0.03	−2.38±0.04	−2.42±0.03	0.745±0.070	32.0

which corresponds to approximately 50 kev in energy. The high energy side of the ground state peak was taken to be the true shape of the leading edge of all lower energy groups. This shape was then fitted to the next lowest group and the true shape of the trailing edge of the ground state group ascertained. This gave then a "standard shape" for the highest energy peak which was in turn fitted to all subsequent groups. Because of the fact that no background neutrons contribute to the first three peaks in any appreciable number, the fit was excellent. Only in the case of the fourth group, whose existence is least convincing anyway, did the standard shape fail to fit exactly the experimental points. Even here, however, the fit was satisfactory. Extrapolated ranges were found from the curves so obtained and reduced to mean ranges following the procedure of Bethe.[6] The mean ranges were converted to energy by recourse to the range-energy relation of Lattes, Fowler, and Cuer[7] for Ilford nuclear research emulsions.

The mean energies, Q-values, relative intensities, and a tentative assignment of excitation levels to Be^7 are given in Table I. In order to assign the correct relative intensities, the height of the peaks were corrected in magnitude for the variation with energy of the neutron-proton scattering cross section and for the decreasing probability of recoil protons being fully recorded in the emulsion as their energy increases.

The energy levels as here assigned to Be^7 neither affirm nor deny the expected similarity in structure of the Li^7—Be^7 isobaric pair. Although a level is established at 470 kev which might be analogous to the 478-kev level in Li^7, two additional levels are indicated by the experimental data which have no analog in Li^7. Of course it is possible that such levels do exist in Li^7 but have not yet been observed. To this end, experiments are underway at this laboratory to investigate the inelastic scattering of 5-Mev protons from Li^7, and the energy spectrum of the alpha-particles from the reaction $Be^9(d,\alpha)Li^7$ using 10-Mev deuterons. If additional levels in Li^7 are present, they may well be excited by incident bombarding particles of this energy.

The authors realize of course that the assignment of the proposed level scheme to Be^7 *per se* on the limited amount of evidence available would be somewhat presumptious. However, in order to make our data as convincing as possible, we have endeavored to make an exhaustive search for all possible sources of error. A summary of the conclusions drawn are given herewith.

All that is required of the cyclotron beam is that it be homogeneous in energy. The absolute value of the energy is unimportant since the level values depend only on differences in Q-values. The homogeneity of the proton beam is attested by the small half-width (30 kev) of the range distribution found in a photographic emulsion. That the lower energy groups are not due to inelastically scattered neutrons is borne out by the homogeneity of the groups and further by the fact that their positions in energy at 20° and 90° are entirely consistent with the picture of their having left an excited residual nucleus of Be^7.

One might also expect that (n,p) reactions take place in the AgBr present in the emulsion, thus producing extraneous protons. This is eliminated, however, on the grounds of the relative abundances of hydrogen and AgBr in the emulsion, and on the relative cross sections involved. There are 2.7 times as many atoms of hydrogen as molecules of AgBr present in the photographic plates. Hence, the probability of $n-p$ scattering is 2.7 times as great as an (n,p) reaction on Ag or Br, assuming the cross sections to be the same. A quantitative calculation of the cross sections for (n,p) reactions in Ag and Br at the energies under consideration can be made in the following manner. The actual cross section σ can be thought of as being made up of a geometrical cross section of the nucleus in question times a "penetration factor" P, which accounts for the potential barrier encountered by the emerging proton.

$$\sigma = \pi R^2 P, \tag{2}$$

where $R = 1.45 \times 10^{-13} \times (A)^{\frac{1}{3}}$ is the nuclear radius. The factor P can be taken as simply the transmission coefficient of the potential barrier for a proton in the nucleus. Bethe[8] has worked out formulas for this quantity. Equation (600) of reference 8 has been used to calculate P for Ag and Br and the resulting values inserted in Eq. (2). The cross section σ is then found to be $\sim 10^{-27}$ cm², which is considerably lower than the $n-p$ scattering cross sections at these energies ($\sim 10^{-24}$ cm²). Thus extraneous protons from this source are completely ruled out.

[6] H. Bethe and M. S. Livingston, Rev. Mod. Phys. **9**, 245 (1937).

[7] Lattes, Fowler, and Cuer, Proc. Phys. Soc. **59**, 883 (1947).

[8] H. Bethe, Rev. Mod. Phys. **9**, 69 (1937).

The LiF used for the targets was (C.P.) Baker's analyzed. The known impurities are either incapable of producing neutrons in the energy range considered, or produce them in quantities insufficient to account for the observed peaks.

We may summarize by saying that in the neutron spectra obtained from the reaction $Li^7(p,n)Be^7$, three groups in addition to the ground state groups are observed. The assignment of all these additional groups to the primary reaction seems to be consistent with the group energies at the two angles of observation. The assignment then leads to an energy level scheme for Be^7 in which excited levels are located at 205, 470, and 745 kev above the ground state. The evidence is weakest for the level at 745 kev. In addition, two levels in A^{37} are confirmed in the spectrum obtained from the bombardment of LiCl. These levels fall at 1.40 and 1.65 Mev above ground.

The authors wish to acknowledge the help of Dr. H. Primarkoff who originally suggested the investigation and with whom were held many invaluable discussions. One of us (K.B.M.) acknowledges his Studentship from the Science and Industry Endowment Fund, Commonwealth of Australia. The excellent work of Miss Eileen Dennison in scanning the plates is gratefully acknowledged.

PHYSICAL REVIEW VOLUME 77, NUMBER 5 MARCH 1, 1950

Study of the Multiple Scattering of Fast Charged Particles in a Gas and Its Role in the Interpretation of Cloud-Chamber Tracks*

GERHART GROETZINGER, MARTIN J. BERGER, AND FRED L. RIBE
Institute for Nuclear Studies, University of Chicago, Chicago, Illinois
(Received September 19, 1949)

The curvature of the track of a fast charged particle in a magnetic cloud chamber varies along the track because of the multiple scattering of the particle by the gas in the chamber. By measurement of the mean and the fluctuations of the curvature, it is possible (1) to determine the multiple scattering in a gas of a particle of known mass, and (2) to estimate, on the basis of a verified multiple scattering law, the mass and energy of a particle. The statistical uncertainty inherent in such estimates is discussed. The multiple scattering of 132 beta-particles, ranging in energy from 50 to 1700 kev, with a total path length of 1800 cm in one atmosphere of argon, was measured and compared with the predictions of the theories of Bothe, Williams, Goudsmit and Saunderson, Molière, and Snyder and Scott. The theories of Molière, and Snyder and Scott, as well as that of Williams, if an available parameter is suitably adjusted, agree fairly well with our results.

I. INTRODUCTION

THERE is considerable experimental evidence concerning the multiple scattering of fast charged particles in foils, which in many instances does not conform very well to the various theories of multiple scattering developed by W. Bothe,[1] E. J. Williams,[2] S. Goudsmit and J. L. Saunderson,[3] G. Molière,[4] and H. S. Snyder and W. T. Scott.[5] Multiple scattering in gases, however, has been little investigated so far. During the course of a cloud-chamber investigation of electron-positron pair production, L. Simons and K. Zuber[6] have touched upon the multiple scattering of these particles in the mixture of argon and methyliodide with which their cloud chamber was filled, and found their results in agreement with the theory of Bothe. E. A. Luebke, G. S. Klaiber, and G. G. Baldwin[7] examined the cloud-chamber tracks of protons in air, and L. W. Smith and P. G. Kruger[8] those of electrons in air; their results are consistent with predictions by H. A. Bethe[9] based on the theory of Williams, concerning the errors introduced by multiple scattering in the evaluation of cloud-chamber tracks. On the other hand, Johanna Rüling and Herma Gheri[10] claim that the mean square scattering angle of electrons in air with energies from 4 to 10 Mev, as observed in a cloud chamber, is from five to fifty times greater than predicted by the theory of Williams.

The purpose of this paper is to study the multiple scattering of electrons in argon. Scattering data obtained from the cloud-chamber tracks of beta-particles will be compared with the predictions of various

* Assisted by the Joint Program of the ONR and AEC. Preliminary results of this paper have been presented at the 1948 Chicago meeting of the American Physical Society (Martin J. Berger and Gerhart Groetzinger, Phys. Rev. 75, 342A (1949)). See also Ribe, Berger, and Groetzinger, Phys. Rev. 77, 760 (1950).

[1] W. Bothe, *Handbuch der Physik* (Verlag Julius Springer, Berlin, 1933), Vol. 22, II, p. 1.

[2] E. J. Williams, Proc. Roy. Soc. **169**, 531 (1939); Phys. Rev. **58**, 292 (1940).

[3] S. Goudsmit and J. L. Saunderson, Phys. Rev. **57**, 24 (1940); Phys. Rev. **58**, 36 (1940).

[4] G. Molière, Zeits. f. Naturforsch. **3a**, 78 (1948). (This paper contains a summary of experimental results on scattering by foils.)

[5] H. S. Snyder and W. T. Scott, Phys. Rev. **76**, 220 (1949).

[6] L. Simons and K. Zuber, Proc. Roy. Soc. **159**, 383 (1937).

[7] E. A. Luebke, G. S. Klaiber and G. G. Baldwin, Phys. Rev. **71**, 657 (1947).

[8] L. W. Smith and P. G. Kruger, Phys. Rev. **72**, 357 (1948).

[9] H. A. Bethe, Phys. Rev. **70**, 821 (1946).

[10] Johanna Ruling and Herma Gheri, Acta Phys. Austriaca **2**, 335 (1948).

theories. Furthermore, the role of multiple scattering as a source of error as well as a source of information in the interpretation of cloud-chamber tracks will be discussed.

The amount of information obtainable from the shape of a cloud-chamber track depends on the magnitude of the deflection which the particles undergo under the combined influence of the magnetic field, and of the scattering by the atoms of the gas in the chamber. In the paper by Bethe, mentioned above, the influence of multiple scattering on the mass determination of the meson was investigated. Primarily interested in the tracks of fairly heavy particles, which show little deflection (i.e., tracks short compared to their radius of curvature), Bethe approximated the entire track (as projected on a plane perpendicular to the magnetic field) by a "best circle," whose radius was taken as the mean radius of curvature of the track. In an Appendix dealing with tracks long compared to their radius of curvature, he used essentially the same approximation, the only difference being a small correction due to the increased curvature.

The tracks of electrons will generally have considerable curvature. To extract the maximum amount of information, it is necessary, as already pointed out by Simons and Zuber, to utilize not only the mean curvature, but also the fluctuations of the curvature. This can be done by dividing a strongly curved track into a number of sections whose curvatures are measured separately, a procedure which adapts itself naturally to the case of tracks far from circular (e.g., with sharp bends due to single scattering). This analysis makes it possible to test, by means of a magnetic cloud chamber, the validity of a multiple scattering theory for particles of known mass and charge. Conversely one can, on the basis of a verified multiple scattering law, determine the mass and energy of a particle from the shape of its cloud-chamber track, without having recourse to other information such as that obtained from the ionization of the track.

II. RESUMÉ OF MULTIPLE SCATTERING THEORIES

The angular deflection φ, as projected on a plane containing the direction of incidence, which a particle undergoes as the result of multiple scattering upon traversing a layer of matter, is approximately distributed normally:

$$dF(\varphi)=(2\pi\sigma^2)^{-\frac{1}{2}}\exp(-\varphi^2/2\sigma^2)d\varphi+dF'(\varphi), \quad (1)$$

where the correction term $dF'(\varphi)$ (plural and single scattering tail) is important for large angles only. The variance σ^2 (mean square angular deflection) of the normal part of the distribution can be expressed as the product of two factors, say Q and G, of which Q depends on the interaction between the particle and the nuclei of the scattering atoms, while G takes into account the structure of these atoms (screening, etc.) as well as statistical considerations.

The various theories proposed by Bothe, Williams, Goudsmit and Saunderson, and Molière, all give Q as:

$$Q=\frac{4\pi Nxe^4Z^2}{p^2v^2}, \quad (2)$$

where p and v are the momentum and velocity of the particle; e the charge of the electron; Z the atomic number; N the number of nuclei per cm^3; and x the thickness of the scattering substance (in the direction of incidence).

The various theories differ in their expressions for G, as well as in the small corrections $dF'(\varphi)$.

Bothe and Williams assume that the multiple scattering deflections are the sum of many small individual deflections to which the Gaussian error law is applied. These individual spatial deflections range from a minimum $\theta_{\min}$ (due to screening) up to a maximum $\theta_{\max}$, which must be introduced to keep the mean square deflection finite.

Bothe[1] effectively replaces G, which is approximately independent of the mass and energy of the scattered particle, by the numerical value:

$$G=4.125, \quad (3a)$$

which he derives from a number of experiments on the multiple scattering of alpha- and beta-particles in foils.

According to Williams[2]

$$G=\log(\theta_{\max}/\theta_{\min}) \quad (3b)$$

or

$$G=\log(\varphi_{\max}/\varphi_{\min}), \quad (3c)$$

where $\theta_{\max}$ and $\theta_{\min}$ are spatial, $\varphi_{\max}$ and $\varphi_{\min}$ projected angles. With $\alpha=(mc/p)(Z^{\frac{1}{2}}/137)$ (m is the electronic mass) Williams proposes

$$\theta_{\min}\sim\alpha \quad (4a)$$

and

$$\varphi_{\min}\sim\alpha, \quad (4b)$$

and suggests furthermore that on the basis of a more refined consideration of screening

$$\varphi_{\min}\sim 1.75\alpha. \quad (4c)$$

Williams points out that $\theta_{\max}$ is a somewhat arbitrary quantity without a very clear-cut physical significance. It must be large enough so that angles larger than $\theta_{\max}$ make only a negligible contribution to the scattering. On the other hand, it must be considerably smaller than the mean deflection σ for the path length considered, in order for the application of the Gaussian error law to be justified. Several definitions have been proposed. The definition

$$\varphi_{\max}=(\tfrac{1}{2}Q)^{\frac{1}{2}} \quad (5a)$$

assures (according to Williams) that a particle traversing a layer of matter of thickness x will on the

average make only one collision resulting in a projected deflection greater than φ_{max}. For particles of high momenta one can use the fact that because of the finite size of the nucleus practically no deflections will occur larger than $\lambda\!\!\!^{-}/b$ where b is the nuclear radius and $2\pi\lambda\!\!\!^{-}$ the de Broglie wave-length of the scattered particle, which leads to

$$\theta_{max}\sim\lambda\!\!\!^{-}/b. \tag{5b}$$

Taking $b=0.57e^2Z^{\frac{1}{3}}/mc^2$ and using θ_{min} given by Eq. (4a) gives (see reference 17)

$$G=2\log(181Z^{-\frac{1}{3}}). \tag{3d}$$

Bethe[9] uses Williams theory with

$$\theta_{min}=0.757\alpha(=mcZ^{\frac{1}{3}}/181p) \tag{4d}$$

in connection with

$$\theta_{max}=0.1 \text{ radian}, \tag{5c}$$

which is the approximate magnitude of the smallest single scattering deflection which can be recognized as such in a cloud chamber.

Goudsmit and Saunderson[3] propose

$$G=\log(150/137\alpha) \tag{3e}$$

and

$$G=\log(166/137\alpha) \tag{3f}$$

depending on whether their calculations are based on the Thomas-Fermi model or on the use of a Wentzel potential for the potential distribution in the atom.

Molière[4] adopts a procedure, originally invented by G. Wentzel[11] which consists of first determining separately the contributions to the scattering distribution due to the particles scattered once, twice, $\cdots n$ times in a layer of matter, then summing these contributions to obtain the total angular scattering distribution. The improvement due to Molière is the evaluation of these angular distributions on the basis of an exact quantum-mechanical solution of the single scattering problem.

According to Molière, the angular multiple scattering distribution is again approximately normal, with G defined by

$$\frac{e^G}{(G)^{\frac{1}{2}}}=1.31\frac{Q^{\frac{1}{2}}}{\theta_{min}}, \tag{3g}$$

θ_{min} being a minimum (screening) angle defined as

$$\theta_{min}=1.142\alpha\left[1.13+\left(\frac{3.76Z^2}{137^2\beta^2}\right)\right]^{\frac{1}{2}}. \tag{4c}$$

Molière obtains an explicit expression for the correction $dF'(\varphi)$ to the normal distribution in terms of a power series in $1/G$. Finally it must be mentioned that, in order for the approximations made in Molière's theory of multiple scattering to be justified, it is necessary to have a minimum path length such that $G\gtrsim 2.25$.

[11] G. Wentzel, Ann. d. Physik **69**, 335 (1922).

The most recent theory of multiple scattering is that of H. S. Snyder and W. T. Scott,[5] which is based on an exact solution and numerical integration of an integral diffusion equation. In spite of their different approach their results agree rather closely with those of Molière, so that one could again split off a Gaussian part of the distribution. (For a comparison of the two theories see Section VI.)

It is often advantageous to confine one's attention to the normal part of the distribution (a) for an experimental check of scattering theories because of the rarity of large deflections particularly in a gas, (b) when determining the properties of a particle because of the greater ease of statistical treatment. Fortunately, this is possible in cloud-chamber work, where the entire track of the particle is observable. If one excludes from consideration deflections larger than 2.8σ, the single scattering tail is practically eliminated. It turns out that the variance of this truncated distribution, computed according to Molière's complete expression (including the correction $dF'(\varphi)$) differs from σ^2 by less than 5 percent.

III. ANALYSIS OF A CLOUD-CHAMBER TRACK

Consider a cloud-chamber track, projected on a plane perpendicular to the magnetic field in the chamber, and divided into a number of sections by a set of points equidistant along the track. If these sections are sufficiently small compared to their radii of curvature, the angles between the tangents to the track at successive division points can each be considered as the sum of a constant magnetic deflection and a normally distributed multiple scattering deflection. Thus the set of angles $\varphi_1, \varphi_2, \cdots, \varphi_n$ obtained from one track divided into n sections each of length x, can be considered as a sample of n values of a normal population with the distribution function

$$dF(\varphi)=(2\pi\sigma^2)^{-\frac{1}{2}}\exp[-(\varphi-\mu)^2/2\sigma^2]d\varphi, \tag{6}$$

where

$$\mu=x/\rho_H=xHe/pc \tag{6a}$$

is the magnetic deflection.†

This result is subject to a number of qualifications. For one thing, the multiple scattering theory as set forth in Section II assumes that all angles are projected onto a plane containing the direction of incidence. This condition is not exactly fulfilled if the track is projected onto a plane perpendicular to the magnetic field, which will in general be slightly inclined with respect to the directions of incidence for the various sections of the track. The magnitudes of these angles of inclination depend on the depth of the illuminated region of the cloud chamber (approximately between two parallel planes perpendicular to the magnetic field), and on the length of the track confined to this illuminated region. It may be added here that if the depth of the illu-

† Angular deflection ~path length×"curvature." For the sake of convenience in notation, we keep the discussion mainly in terms of angular deflections rather than "curvatures."

minated region is of the same order of magnitude as the section length x, there will be no limitation on the multiple scattering angle in an individual section of the track, with the possible exception of the last one or two, where the particle may be close to the boundary of the illuminated region. The error due to the projection of the track on the plane perpendicular to the magnetic field is discussed in more detail in Appendix I. It does not exceed ± 2 percent under our experimental conditions. There is an additional error (not greater than 2 percent) due to the inclination of the track with respect to the plane of projection, which makes the effective magnetic field and thus the magnetic deflection somewhat smaller than assumed in Eq. (6a). Of course both these errors can be eliminated, in the interest of accuracy, and at the expense of expediency, if all angles are measured stereoscopically.

Hitherto it has been tacitly assumed, that the energy of the particle remains constant over the entire track. In Appendix II the effect of energy loss is considered. For electrons of initial energies as low as 50 kev in argon at a pressure of one atmosphere it is found to be negligible.

The statistical information contained in the set of observed angles $\varphi_1, \varphi_2, \cdots, \varphi_n$ can be summarized by means of the sample mean

$$m=\frac{1}{n}\sum_{i=1}^{n}\varphi_i, \tag{7}$$

the sample variance about the true mean

$$S^2=\frac{1}{n}\sum_{i=1}^{n}(\varphi_i-\mu)^2, \tag{8}$$

and the sample variance about the sample mean

$$s^2=\frac{1}{n-1}\sum_{i=1}^{n}(\varphi_i-m)^2. \tag{9}$$

As n increases, m approaches μ, while S^2 and s^2 approach σ^2. If, for the sake of convenience, we introduce the auxiliary variables

$$u=(m-\mu)/\sigma n^{\frac{1}{2}}, \tag{10}$$

$$\mathrm{X}^2=nS^2/\sigma^2, \tag{11}$$

$$\chi^2=(n-1)s^2/\sigma^2, \tag{12}$$

$$t=(m-\mu)/sn^{\frac{1}{2}}, \tag{13}$$

their distribution functions are the following standard statistical distributions:[12]

$$dF(u)=\frac{1}{(2\pi)^{\frac{1}{2}}}\exp(-u^2/2)du, \tag{10a}$$

$$dF(\mathrm{X}^2)=\frac{(\mathrm{X}^2/2)^{\frac{1}{2}(n-3)}}{2\Gamma(n/2)}\exp(-\mathrm{X}^2/2)d(\mathrm{X}^2) \tag{11a}$$

χ^2 distribution (with n degrees of freedom).

$$dF(\chi^2)=\frac{(\chi^2/2)^{\frac{1}{2}(n-4)}}{2\Gamma[(n-1)/2]}\exp(-\chi^2/2)d(\chi^2) \tag{12a}$$

χ^2 distribution (with $n-1$ degrees of freedom).

$$dF(t)=\frac{\Gamma(n/2)}{\Gamma[(n-1)/2][(n-1)\pi]^{\frac{1}{2}}}\left(1+\frac{t^2}{n-1}\right)^{-n/2}dt \tag{13a}$$

Student$-t$ distribution (with $n-1$ degrees of freedom).

Integrals of the χ^2 and Student$-t$ distributions are available in tabulated form.[13]

To test the hypothesis that the particle producing the track has a certain mass and energy, we express these quantities in terms of μ and σ^2 and compute by means of expression (10a) or (13a) the probability of obtaining a value of m exceeding the actually found sample mean m_0, and by means of expression (11a) the corresponding probability of obtaining a value S^2 exceeding the actually found sample variance S_0^2. Thus the test of a hypothesis can be based either on a consideration of the mean or the variance of the set of measured angles. For a given energy, the relative accuracy of the two tests depends upon the strength of the magnetic field and vice versa. Let Δm and ΔS be the standard deviations of m and S. Then it follows from (10a), (11a), (12a) and (13a) that

$$\Delta m/m\sim\sigma/n^{\frac{1}{2}}\mu, \tag{14}$$

$$\Delta S/S\sim\Delta s/s\sim 1/(2n)^{\frac{1}{2}}, \tag{15}$$

which indicates that both tests increase in accuracy with increasing n, that the test of the mean increases in accuracy with increasing magnetic field (which is proportional to μ) and that the test of the variance is more accurate than the test of the mean, if $\sigma/\mu>1/\sqrt{2}$. For instance, for electrons with an energy of 1.5 Mev in a cloud chamber filled with argon at a pressure of 1 atmos., the test of the mean is more accurate for magnetic field strengths above, that of the variance for field strengths below 300 gauss.

A remark may be in order concerning the use of the Student$-t$ distribution to test a hypothesis. It is seen that expression (13a) does not contain the theoretical variance σ^2; therefore this test is based merely on the normal form of the angular distribution of multiple scattering deflections, but does not demand a knowledge of the theoretical mean square angle of deflection.

The best estimates of μ and σ^2 are m_0 and s_0^2. The

[12] See H. Cramer, *Mathematical Methods of Statistics* (Princeton University Press, Princeton, 1946).

[13] R. A. Fisher and F. Yates, *Statistical Tables* (Oliver and Boyd, London, 1948).

standard deviations of these estimates have already been given (Eq. (14) and Eq. (15)). The best estimate of a function $F(\mu, \sigma)$ is $F(m, s)$ with a standard deviation

$$\Delta F=\{(\partial F/\partial\mu)_{\mu=m}{}^2(\Delta m)^2+(\partial F/\partial\sigma)_{\sigma=s}{}^2(\Delta S)^2\}^{\frac{1}{2}}. \quad (16)$$

IV. MASS DETERMINATION

The mass of a particle can be estimated in a straightforward fashion from the sample mean and variance of the observed angular deflections of its track with a standard deviation (calculated according to Eq. (16)), proportional to $[1-v^2/c^2]^{-\frac{1}{2}}$ so that for high velocities the statistical error can become considerable.

The mass of a particle can also be estimated by comparing its scattering with that of a particle of approximately the same momentum and known properties, or preferably with the scattering of a group of such particles, an estimate which is nearly independent of the controversial factor G of the scattering law (Eqs. (3a) to (3g)) and of exact knowledge of the experimental conditions, such as the composition of the scattering gas, the magnetic field, etc.

Suppose we have two tracks of n_a and n_b sections, respectively, produced by two particles of the same momentum, but different masses, M_a and M_b. Let $s_a{}^2$ and $s_b{}^2$ be the observed sample variances, and $\sigma_a{}^2$ and $\sigma_b{}^2$ the theoretical variances of the respective normal multiple scattering distributions. If the momenta, i.e., the means of these distributions, are known to be equal, the ratio of the sample variances is distributed according to the Fisher–z distribution $dF(z)$ (see reference 12). Let

$$z=\tfrac{1}{2}\log\{(n_a-1)n_a s_a{}^2/(n_b-1)n_b s_b{}^2\}. \quad (17)$$

Then

$$dF(z)=\frac{\text{const. } e^{(n_a-1)z}}{\{(n_a-1)e^{2z}/\sigma_a{}^2+(n_b-1)/\sigma_b{}^2\}^{\frac{1}{2}(n_a+n_b-2)}}. \quad (17a)$$

Under ordinary circumstances, however, the determination of the momenta will be made from the cloud-chamber tracks and thus be subject to a statistical error, which may amount to 5 percent or more. In this case it is preferable to compare for the two tracks the ratios of their magnetic to their multiple scattering deflections. These ratios, which are proportional to the velocities of the two particles, are rather insensitive to errors in the momentum. Let

$$l_{ab}=(m_a/s_a)/(m_b/s_b) \quad (18a)$$

and

$$\lambda_{ab}=(\mu_a/\sigma_a)/(\mu_b/\sigma_b). \quad (18b)$$

Then it can be shown (see Appendix III), that the variable

$$U=\left(1-\frac{l_{ab}}{\lambda_{ab}}\right)\times\left\{\frac{(1/n_a)(\sigma_a/\mu_a)^2+1}{2(n_a-1)}+\frac{1/n_b+1/\lambda_{ab}{}^2}{2(n_b-1)}l_{ab}{}^2\right\}^{-\frac{1}{2}} \quad (18c)$$

TABLE I. Theoretical (after Molière) root mean square multiple scattering deflections σ_1, σ_3, σ_{10} (in degrees for particles of mass $M=1$, 3, and 10 electron masses, and the corresponding ratios $\lambda_{1,3}$ and $\lambda_{1,10}$

$\lambda_{1,3}=[(\sigma_3{}^2+0.1)/(\sigma_1{}^2+0.1)]^{\frac{1}{2}}$, $\lambda_{1,10}=[(\sigma_{10}{}^2+0.1)/(\sigma_1{}^2+0.1)]^{\frac{1}{2}}$.

$H\rho$ Gauss cm	σ_1 deg.	σ_3 deg.	σ_{10} deg.	$\lambda_{1,3}$	$\lambda_{1,10}$
7500	2.69	3.34	8.35	1.25	3.08
10000	1.99	2.27	4.64	1.14	2.31
12500	1.58	1.73	3.53	1.10	2.20
15000	1.31	1.40	2.22	1.07	1.76
17500	1.12		1.72		1.51
20000	0.98		1.39		1.39
22500	0.87		1.16		1.30
25000	0.78		1.00		1.24

is distributed normally:

$$dF(U)=\frac{1}{(2\pi)^{\frac{1}{2}}}\exp(-U^2/2)dU. \quad (18d)$$

In practice it will often occur that one is comparing one unknown particle with a large group of known particles. In this case one can effectively set $n_b=\infty$. Furthermore, the term $(1/n_a)(\sigma_a/\mu_a)^2$ of Eq. (18c) will often be much less than unity if the magnetic curvature is large enough, and can then be neglected.

Scattering analysis as a means of mass determination is especially suitable for particles of small mass. Recently there have been reports in the literature of particles occuring in the cosmic radiation with masses from three to ten times that of the electron.[14] As an application of the foregoing theory the distribution function $dF(U)$ was used to calculate how well such particles could be distinguished from electrons by their scattering. It was assumed that the tracks are observed

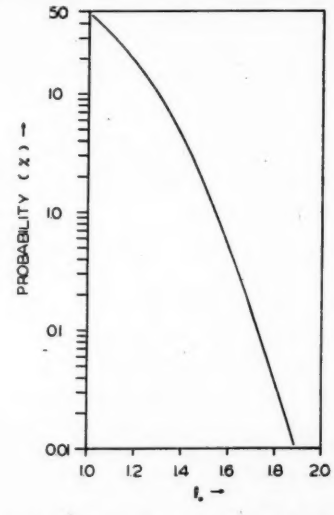

FIG. 1. Statistical fluctuations of the multiple scattering of identical particles: Probability $P_\lambda(l\geq l_0)$ calculated from Eqs. (18c) and (18d) with $\lambda=1$, $n_a=10$, $n_b=\infty$, and $(1/n_a)(\sigma_a/\mu_a)^2\ll 1$.

[14] Cf. L. Janossy and C. B. A. McClusker, Nature **163**, 181 (1949).

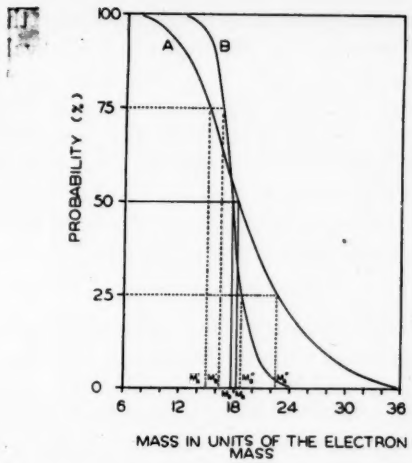

FIG. 2. Mass discrimination on the basis of multiple scattering: Probability $P_\lambda(l \geqslant l_0)$ calculated from Eqs. (18c) and (18d) with $l_0=2$, $\lambda=\lambda(M)$, $n_b=\infty$, $n_a=10$ (curve A), $n_a=100$ (curve B).

in a cloud chamber filled with argon at a pressure of one atmosphere, and that they are divided into sections 2 cm long. One track of an unknown particle, consisting of ten sections, is being compared with many electron tracks of the same momentum. ($n_a=10$, $n_b=\infty$).

Table I gives, for various momenta, the theoretical root mean square multiple scattering deflections σ_1, σ_3, σ_{10} (in degrees) for particles of mass $M=1$, 3, and 10 (in terms of electron mass) calculated according to the theory of Molière as well as the corresponding ratios

$$\lambda_{1,3}=(\mu_1/\sigma_1)/(\mu_3/\sigma_3)=\sigma_3/\sigma_1,$$

and

$$\lambda_{1,10}=(\mu_1/\sigma_1)/(\mu_{10}/\sigma_{10})=\sigma_{10}/\sigma_1.$$

(Here $\mu_1=\mu_3=\mu_{10}$.) These ratios are more likely to be correct than σ_1, σ_3, and σ_{10} because they do not, as pointed out before, depend very much on the factor G of the theoretical variance, which differs for the various theories of multiple scattering. In order to account for the experimental error in measuring the angles of deflection, an "experimental error variance" of $(0.3°)^2$ was added to σ_1^2, σ_3^2, and σ_{10}^2 before the ratios $\lambda_{1,3}$ and $\lambda_{1,10}$ were computed. This value was arrived at by an experimental investigation of the accuracy of measurement to be described later.

Consider the case where the track of the unknown particle is being compared with those of test particles of approximately the same momentum, the ratio l being found experimentally to have the value l_0. Disregarding statistical fluctuations, one would assume that the mass of the unknown particle is such that $\lambda=l_0$. However, in view of the fluctuations, one may test the hypothesis that the unknown particle actually has the same mass as the test particle(s) ($\lambda=1$). In Fig. 1 is plotted, on the hypothesis that $\lambda=1$, the probability $P_\lambda(l \geqslant l_0)$ of obtaining an l greater than or equal to the observed l_0, assuming one "unknown" track of 10 sections and a large number of test particles (electrons). The ordinates corresponding to values of the abscissa $l_0=\lambda_{1,3}$ and $l_0=\lambda_{1,10}$ are then a measure of the likelihood that particles of apparent mass three and ten, respectively, have in reality mass one, $\lambda_{1,3}$ and $\lambda_{1,10}$ become small enough to make this probability appreciable (25 percent) for momenta higher than $H\rho=10{,}000$ and $H\rho=25{,}000$ Gauss-cm, respectively.

Next we consider the use of Eqs. (18c, d) to make a mass estimate. As an example, Fig. 2 describes the hypothetical case of an unknown particle of measured $H\rho=1.7\times10^4$ Gauss-cm which scatters twice as much as electrons of the same momentum with which it is being compared ($l_0=2$). To each assumed mass M (in units of the electron mass) for the unknown particle there corresponds a $\lambda(M)$ and a probability $P_\lambda(l \geqslant l_0)$ of obtaining an $l \geqslant l_0=2$. These probabilities are plotted against different values of M. Curve A refers to the case in which one track, curve B to the case in which a group of 10 tracks of particles (known to be identical) is being compared with a large group of electron tracks.

The best estimates of the mass in these two cases are the values corresponding to the probability level of 50 percent (M_A and M_B, respectively, shown in Fig. 2).‡ The values of the mass corresponding to the 25 percent and 75 percent levels of probability M_A', M_B' and M_A'', M_B'', respectively, are the limits of the "50 percent confidence interval" of the mass estimates.¶

In the interest of accuracy, especially for particles of high energy, it is desirable to have the mean multiple scattering angle as large as possible. This angle is proportional to $Z(A)^{\frac{1}{2}}$ where Z is the atomic number and A the pressure in atmospheres of the scattering gas. Chambers operating at pressures between 100 and 200 atmospheres have recently been described in the literature.[15] It appears possible, by an examination of multiple scattering in such high pressure chambers, to distinguish between mesons of approximately 200 and 300 electron masses, if their energies do not exceed 50 Mev.

TABLE II. Minimum path length in argon (1 atmos., 25°C).

v/c	$x_{\min}$(cm)	v/c	$x_{\min}$(cm)
0.5	0.46	0.9	1.33
0.6	0.63	0.95	1.47
0.7	0.83	0.97	1.54
0.8	1.04	1.00	1.61

‡ M_A differs slightly from M_B due to the fact that the distribution is based on an approximation (see Appendix III).

¶ The limits of the "50 percent confidence interval" are roughly analogous to the limits of the probable error. For an exact definition see, for instance, M. G. Kendall, *The Advanced Theory of Statistics* (Charles Griffin and Company, Ltd., London, 1948), Vol. II, p. 62.

[15] R. Richard-Foy, see L. Le Prince-Ringuet, *Les Rayons Cosmiques* (Michel, Paris, 1945); G. E. Valley and J. A. Vitale, Phys. Rev. **75**, 1328A (1949); Shutt, Hoke, Tuttle, and Neil, Phys. Rev. **75**, 1329A (1949).

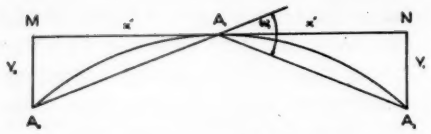

FIG. 3. Geometrical analysis of a cloud-chamber track used in determining multiple scattering.

V. EXPERIMENTAL PROCEDURE

The cloud-chamber tracks of 132 beta-particles from a P^{32} source,‖ ranging in energy from approximately 50 to 1700 kev, were examined. The minimum length of the tracks was 12 cm, the average length 14 cm. They were obtained in a horizontal cloud chamber with a diameter of 24 cm, and an illuminated region 2.5 cm deep, filled with argon at a pressure of one atmosphere at 25°C. The source was mounted about 4 cm from the rim of the chamber in the center of the illuminated region. The magnetic field was produced by a set of Helmholtz coils and ranged from 330 to 355 gauss for different exposures.

Table II gives the minimum path length in one atmosphere of argon which will make the quantity G in Molière's theory larger than 2.25 (condition of applicability of multiple scattering theory). For our experiment we adopted a path-length of approximately 2 cm (i.e., the tracks were divided into 2-cm sections) which satisfied Molière's condition for electrons of all energies. It was this theoretical consideration rather than the difficulty of measurement which put a lower limit on the size of the sections.

Instead of the angles φ_i between the tangents to the projected track at the division points, we preferred to measure the angles ω_i between successive chords connecting these points. (See Fig. 3 in which the curvature is exaggerated.) By an extension of an argument of S. Lattimore[16] to the case of multiple scattering in the presence of a magnetic field it will be shown that the information provided by the angles ω_i is equivalent to that provided by the angles φ_i, except that the number of ω_i's is one less than the number of φ_i's. Figure 3 shows part of a cloud-chamber track, projected on a plane perpendicular to the magnetic field, and passing through the points A_0, A_1, and A_2. The line (NA_1M) is tangent to the track at A_1. It is seen from the figure that the angle between (A_0A_1) and (A_1A_2)

$$\omega_1=y_0/x'+y_1/x'. \tag{19}$$

It can be shown[17] that the lateral deflections y_0 and y_1, each are distributed normally, with mean $x'\mu/2=x'^2/2\rho_H$ $(\rho_H=pc/He)$ caused by magnetic deflection, and variance $\sigma_y^2=\frac{1}{3}x'^2\sigma^2$ due to multiple scattering, where σ^2 is the theoretical mean square angular scattering deflection. Because of the presence of the magnetic field, the distance x' does not correspond exactly to the distance x (thickness of matter traversed) as understood in the theory of multiple scattering. If the total angle subtended by the section of the track considered does not exceed 15°, the chord length (A_iA_{i+1}) will differ at most by 3.5 percent from x', and 0.3 percent from the arclength $[A_iA_{i+1}]$. The length x is larger than x' but smaller than the arc length. The procedure adopted was to make all chords of equal length (2 cm) and consider them equal to x. The mean scattering angle is proportional to the square root of x and will thus be off by at most 1.75 percent. ω_1 is the sum of two normally distributed quantities and is therefore itself normally distributed; this is also true of $\omega_2=(y_1+y_2)/x'$, $\cdots$, $\omega_n=(y_{n-1}+y_n)/x'$. The multivariate distribution function of the angles ω_i is:

$$dF(\omega_1, \omega_2, \cdots, \omega_n) = \text{const.}\exp\left[-\frac{3}{4\sigma^2}\sum_{i=1}^{n}(\omega_i-\mu)^2\right]d\omega_1\cdots d\omega_n. \tag{20}$$

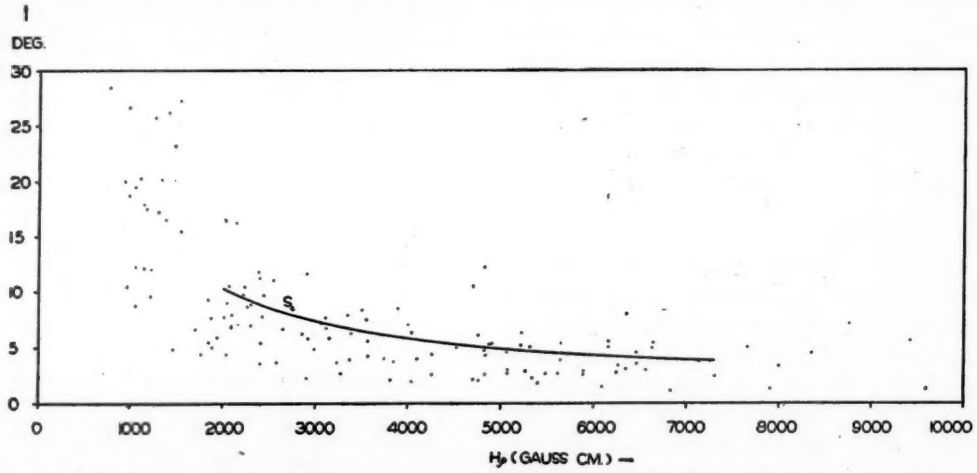

FIG. 4. Multiple scattering of electrons in one atmosphere of argon at 25°C: r.m.s. angular scattering deflection in degrees for 2-cm path length plotted against measured $H\rho$.

‖ The radioactive P^{32} was supplied by the Isotope Branch of the AEC, Oak Ridge, Tennessee.

[16] S. Lattimore, Nature **161**, 518 (1948).

[17] B. Rossi and K. Greisen, Rev. Mod. Phys. **13**, 240 (1941).

Again, as in Section III, we form the sample mean

$$\bar{\omega}=\frac{1}{n}\sum_{i=1}^{n}\omega_i \tag{21}$$

and the sample variances,

$$(\Omega^2)_{Av}=\frac{1}{n}\sum_{i=1}^{n}(\omega_i-\mu)^2 \tag{22}$$

and

$$(\omega^2)_{Av}=\frac{1}{n-1}\sum_{i=1}^{n}(\omega_i-\bar{\omega})^2. \tag{23}$$

As n increases, $\bar{\omega}$ approaches μ, while $(\Omega^2)_{Av}$ and $(\omega^2)_{Av}$ approach $2/3\sigma^2$. The sample mean, in terms of the y's (Fig. 3), can be written

$$\bar{\omega}=(1/nx')(y_0+2y_1+\cdots+2y_{n-1}+y_n). \tag{24}$$

It is distributed normally with mean μ and variance $(4n-2)\sigma^2/3n^2$. The sample variance $(\Omega^2)_{Av}$ is a quadratic form in $n+1$ independent uncorrelated variables y_0, y_1, $\cdots$, y_n, which by a coordinate transformation can be reduced to the sum of the squares of n independent quantities (this number is n rather than $n+1$, because there are only n independent measurements ω_1, ω_2, $\cdots$, ω_n). This transformation will at the same time reduce the exponent of the distribution function (20) to a sum of squares. $3(n-1)(\Omega^2)_{Av}/2\sigma^2$ is then distributed χ^2 with n degrees of freedom (see Eq. (11a), Section III). Similarly it can be shown that $3n(\omega^2)_{Av}/2\sigma^2$ is distributed χ^2 with $n-1$ degrees of freedom, and $(\bar{\omega}-\mu)/[(\omega^2)_{Av}]^{\frac{1}{2}}$ according to the Student$-t$ distribution with $(n-1)$ degrees of freedom.

The angles between successive chords were measured as follows: The image of the track on the 35-mm photographic negative was projected on a sheet of drawing paper with an enlargement giving the original size of the track, and 2-cm sections were then laid off along the image of the track by dividers. The sheet containing the set of division points was mounted on a drafting table, the points were connected by straight lines representing the chords, and the angles between successive chords were measured by means of a drafting machine.

The experimental error due to optical distortions, emulsion distortion, and inaccuracy of angular measurement was estimated as follows: circular arcs of radii 5, 10, 15, and 25 cm were drawn on a sheet of drawing paper and photographed in various orientations in a horizontal plane in the position of the sensitive portion of the cloud chamber, using the same optical arrangement employed originally to photograph the tracks. Each circle was then measured independently by three observers, in the same manner as the cloud-chamber tracks. The resulting error, the apparent root mean square angular scattering deflection, was averaged for all observers for each radius, and found to be almost independent of the radius. The average angle was 1.05°.

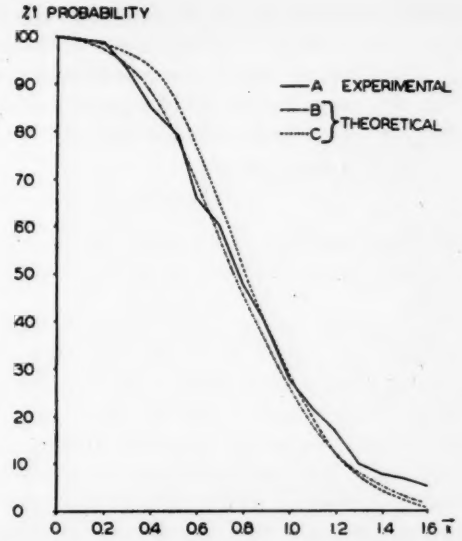

FIG. 5. Statistical fluctuations of multiple scattering: Curve A (experimental): Fraction of tracks from Fig. 4 with $s=ks_{L.SQ.}$ plotted against k. Curves B and C (theoretical): Integrals of χ^2 distributions of $n-1$ degrees of freedom, respectively, between the limits of nk^2 and ∞, plotted against k (with $n=6$, and $n=5$, respectively).

In a separate investigation concerning the accuracy which can be obtained in measuring angular deflections, the same circular arcs were also measured directly on the films by means of a microscope with a mechanical stage, adapted for accurate angular measurements, the magnification used being 51. It was found that this method, while more laborious, will make the experimental error less than 0.3°.

The error due to the turbulence in the chamber is negligible. A few high energy cosmic-ray meson tracks which occured incidentally in the course of the experiment were investigated. They appeared to be slightly curved. By measuring the deviation from a straight line an upper limit of the spurious curvature due to turbulence can be determined. The deviation was measured by means of a micrometer arrangement at points along the track 1 cm apart, and a circle was fitted to the resulting plot of these deviations. The smallest radius of curvature so obtained was larger than 250 cm which corresponds to a negligible error not exceeding 0.3° per 2-cm section.

VI. EXPERIMENTAL RESULTS

The experimental results are shown in Fig. 4, in which the individual root mean square multiple scattering deflections $s=(\frac{3}{2})^{\frac{1}{2}}[(\omega^2)_{Av}]^{\frac{1}{2}}$ are plotted against $H\rho$, each of the 132 points representing one track. 90 percent of these tracks have 6 to 8 sections, the rest 9 to 13. 100 points corresponding to apparent momenta above $H\rho=2000$ Gauss-cm were fitted to a smooth curve by the method of least squares. The lower limit for the momenta was chosen so as to avoid unduly large errors resulting from our only approximately correct manner

of projecting and measuring the tracks. σ^2 can be approximated very well by a second-degree polynomial in $1/(H\rho)^2$. Therefore the least-square curve was obtained by fitting the experimental mean square angles s^2 to such a polynomial, which was found to be:

$$s_{L.SQ.}{}^2=4.307+3.897\times10^8(H\rho)^{-2} -2.294\times10^{14}(H\rho)^{-4}. \quad (25)$$

The probable error in $s_{L.SQ.}{}^2$, calculated from the sum of the residues in least square fitting, was found to be 10 percent.

The least-square fitting had to be carried out as if the momenta for each track were accurately known. The actual statistical uncertainty in $H\rho$ has two effects. Regardless of whether the error in $H\rho$ is negative or positive, it tends to cause an under-estimate of the scattering, since the mean radii (or mean deflections) are calculated in a way which automatically minimizes the mean scattering angles. (See Eq. (22).) This effect has already been accounted for by the use of the sample variance s^2 about the sample mean, which is larger than the sample variance S^2 about the true mean, by a factor $n/(n-1)$. Secondly the uncertainty in $H\rho$ will itself directly affect the shape of the least-square curve. It can be reasonably assumed, however, that with the error in $1/(H\rho)$ equally likely to be positive or negative, the net effect will be insignificant when we are dealing with a large number of particles, in view of the fact that s is very nearly a linear function of $1/(H\rho)$ (see Eq. (25)), where the quadratic term in $(1/H\rho)^2$ is small compared to the linear term.

As mentioned before, the random experimental error due to optics, photography and personal error in measurement, will introduce a spurious root mean square deflection $s_E=1.05°$. On the assumption that the multiple scattering deflections and the "error deflection" s_E are statistically independent one can set the corrected root mean square deflection

$$s_c=(s_{L.SQ.}{}^2-s_E{}^2)^{\frac{1}{2}}. \quad (26)$$

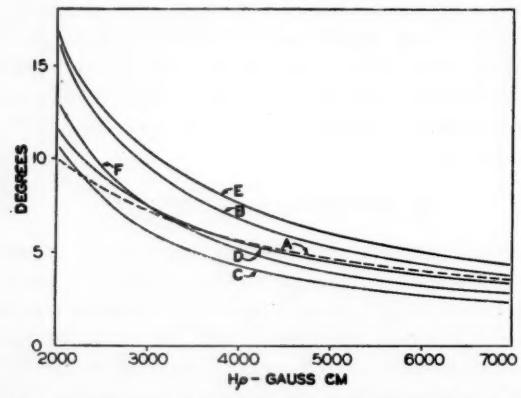

FIG. 6. Comparison of experimental results with various theories of multiple scattering. Curve A: Experimental; Curve B: Bothe; Curve C: Williams ($\varphi_{max}=(\frac{1}{2}Q)^{\frac{1}{2}}$, $\varphi_{min}=(mc/p)\cdot(Z^{\frac{1}{3}}/137)$); Curve D: Williams-Bethe ($\theta_{max}=0.1$ radian, $\theta_{min}=(mc/p)\cdot(Z^{\frac{1}{3}}/181)$; Curve E: Goudsmit and Saunderson (Thomas-Fermi potential); Curve F: Molière.

This correction was applied to the least-square curve. The result is indicated by the solid curve of Fig. 4, which shows s_c as a function of $H\rho$. The curve was broken off at $H\rho=7300$ Gauss-cm, which corresponds to the upper limit of the P^{32} beta-spectrum. Actually there are a few points with an apparently higher $H\rho$ (due to statistical fluctuations) which were included in the fitting of the curve.

Finally, it must be mentioned that sections of track, over which the multiple scattering deflection was more than 2.8 times larger than s for the given momentum, as well as sections with a noticeable single deflection (>0.1 rad.) were excluded from consideration, in order to vouchsafe the Gaussian form of the angular scattering distribution. In fact this exclusion came about almost automatically, since such large deflections were quite rare, and moreover tended to make the track ill-defined and difficult, if not impossible, to measure at the position where they occured.

The dispersion of the experimental points about the "least squares" curve $s_{L.SQ.}$ (Eq. (25)) is indicated in Fig. 5. To each experimental point, with a certain value of apparent $H\rho$ and a root mean square scattering angle, s, there corresponds for the same $H\rho$ a point $s_{L.SQ.}$ on the "least squares" curve. For every number $k\geqslant0$, there is a certain fraction of points such that $s\geqslant ks_{L.SQ.}$. This fraction is plotted for the 100 points above $H\rho=2000$ Gauss-cm, as a function of k (curve A). Theoretically this fraction is given by the integral of the χ^2 distribution of $(n-1)$ degrees of freedom from nk^2 to ∞, where n is the average number of angles ω_i per track. (See Eqs. (9), (12a), and (23).) For the tracks considered here this number was between five and six. Therefore the integrated χ^2-distributions of four and five degrees of freedom are also plotted in Fig. 5 as functions of k (curves B and C). It is seen that for most values of k, the experimental curve falls well between the two theoretical curves, which confirms that

$$[(n-1)s^2/s_{L.LQ.}{}^2]$$

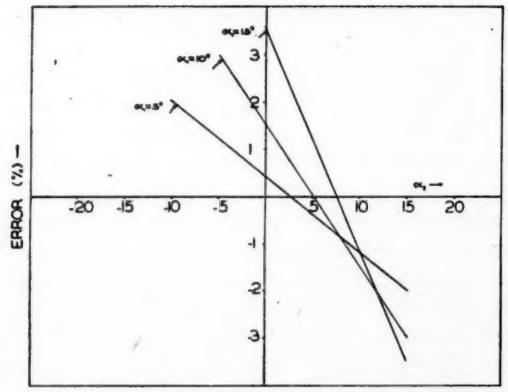

FIG. 7. Error arising from projection of cloud-chamber track section on a plane which does not contain the direction of incidence.

is distributed χ^2, and indirectly that the angular scattering is distributed normally. Only for values of $k \gtrsim 1.3$ is the experimental frequency somewhat too high, which may indicate the presence of a small single-scattering tail.

In Fig. 6 the experimental r.m.s. angle s_c (of the normal part of the multiple scattering distribution) is compared with the corresponding angle σ as given by the various theories. The probable error in s_c is 10 percent and possibly somewhat larger at higher momenta.

The dashed curve A gives our experimental results (s_c). Curve B refers to the theory of Bothe[1] which uses a constant G (Eq. (3a)), curve C to the theory of Williams[2] with a G given by Eq. (3c), and limiting angles given in Eqs. (4b) and (5a), curve D to the same theory with limiting angles due to Bethe[9] (Eqs. (3b), (4d), and (5c)), curve E to the theory of Goudsmit and Saunderson[3] with a G given in Eq. (3e) (based on the Fermi-Thomas potential), and curve F to the theory of Molière.[4] It can be seen that our experimental curve agrees best with the theory of Williams with the limiting angles due to Bethe, and with Molière's theory. The theories of Gousdmit and Saunderson and of Bothe overestimate the multiple scattering throughout the investigated momentum range. In the case of Bothe this may be due to the fact that he obtained the value 4.125 for G from experiments of multiple scattering by foils, which inadvertently may have included a certain amount of single and plural scattering. Numerical results of the theory of Snyder and Scott[5] are not available for our experimental conditions.

According to Snyder and Scott the angular multiple scattering distribution is a function of a parameter z, which is the thickness of the scattering substance in units of the mean free path of the scattered particle. Except for a small difference due to a different expression for the energy dependence of the screening, Molière's theory could also be expressed in terms of this parameter. A comparison of the two theories was made for the smallest $z(=100)$ for which numerical results are given by Snyder and Scott. This corresponds e.g., to the following conditions for electrons in one atmosphere of argon and 20°C.

Kinetic energy	Path length in cm
mc^2	3.42
$2mc^2$	4.05
$3mc^2$	4.28
$4mc^2$	4.37

If the projected angular deflections are expressed in units of $(2GQ)^{\frac{1}{2}}$, it turns out that for angles smaller than 0.5 the complete Molière distribution is larger than the Snyder and Scott distribution by not more than 1 percent. For angles between five and three degrees it is smaller, the maximum discrepancy being 9 percent at an angle of 1.9°. If both distributions are cut off at an angle 1.6° (which is 2.8 times the root mean square of the Gaussian part of the Molière distribution) the root mean square angle of Snyder and Scott is about 2 percent larger than Molière's.

We are indebted to Mr. Watts Humphrey, Jr., and to Mr. Lewis Leder for their valuable help in operating the cloud chamber, measuring the tracks, and performing calculations.

Note added in proof: Our treatment in the text does not do full justice to the theory of Goudsmit and Saunderson. Equations (3e) and (3f) (also quoted by W. T. Scott, Phys. Rev. **76**, 212 (1949)) involve the assumption that $\theta_{max}=\pi$ (all individual scattering angles regardless of magnitude are considered). As Goudsmit and Saunderson point out, it is necessary to introduce a $\theta_{max} \ll \pi$ in order to obtain the normal approximation to the angular multiple scattering distribution. If this had been done, their theory would have been found to be in much better accord with the experimental results.

APPENDIX I: THE PROJECTION OF THE TRACK

Suppose that the magnetic field is directed along the z axis of a cartesian coordinate system. Let u_1 and u_2 be unit vectors, representing the directions of the track at the beginning and the end of the section, inclined at angles α_1, and α_2, respectively, with respect to the $(x-y)$ plane, which is the plane of projection. Let φ be the angle between u_1 and u_2 as projected on the $(x-y)$ plane, and φ' the same angle as projected on a plane containing u_1, which is obtained by rotating the $(x-y)$ plane about an axis perpendicular both to u_1 and the z axis.* It can be easily shown that

$$\tan\varphi/\tan\varphi' = \cos\alpha_1\{1+\tan\alpha_1 \tan\alpha_2/\cos\varphi\}. \quad (27)$$

In Fig. 7 the percentage error in the projected angle is given for values of α_1 and α_2 up to 15° (valid for values of φ ranging from 0° to 20°). All of these angles are larger than these which actually occured in our experiment. The ratio $\tan\varphi/\tan\varphi'$ can either be positive or negative and is almost independent of φ, if φ is small. In this connection it must be pointed out that the error in projection arises only in the part of the angular deflection due to scattering.

APPENDIX II: ENERGY LOSS

Let the track (projected on the plane perpendicular to the magnetic field) be divided into n sections of equal length by means of division points $P_0(a_0)$, $P_1(a_1)$, $\cdots$, $P_n(a_n)$, where a is the arc-length of the track measured from its beginning. The angles $\varphi_1, \varphi_2, \cdots, \varphi_n$, between tangents to the track at successive division points can again be expressed as the sum of a magnetic and multiple scattering deflection. If we consider energy loss, the magnetic deflection and the variance of the multiple scattering deflections, which are functions of the energy, will differ from section to section of the track. The magnetic deflection μ_i in the ith section (bounded by points $P_{i-1}(a_{i-1})$ and $P_i(a_i)$) can be found directly from the theory of energy loss by collision. The scattering variance in the ith section, can be expressed as follows according to Molière, who showed that in order to consider energy loss, his theory must be modified by redefining the variable Q and the screening angle θ_{min}: For the ith section let

$$Q_i = \int_{a_{i-1}}^{a_i} q(a)da \quad (28)$$

and

$$Q_i \log\langle\theta_{i(min)}^2\rangle_{Av} = \int_{a_{i-1}}^{a_i} q(a) \log\theta_{min}^2(a)da, \quad (29)$$

where

$$q(a) = \frac{4\pi NZ^2e^4}{p^2(a)v^2(a)}, \quad (30a)$$

* This happens to be the plane containing u_1, which has the smallest inclination with respect to the $(x-y)$ plane. According to the theory of multiple scattering, this special choice does not affect the distribution of the projected angles.

$$\theta_{\min}(a)=\frac{Z^{\frac{1}{3}}}{120}\frac{mc}{p(a)}\left(1.13+\frac{3.76Z^2}{137^2\beta^2(a)}\right)^{\frac{1}{2}}. \quad (30b)$$

In (28) and (29), $q(a)$ and $\theta_{\min}(a)$ must be expressed as functions of the position along the track according to the theory of energy loss by collision. In terms of these definitions

$$e^{G_i}/(G_i)^{\frac{1}{2}}=1.31(Q_i)^{\frac{1}{2}}\langle\theta_{i(\min)}\rangle_{Av}, \quad (31a)$$

$$\sigma_i^2=Q_iG_i \quad (31b)$$

and

$$dF(\varphi_i)=(2\pi\sigma_i^2)^{-\frac{1}{2}}\exp[-\tfrac{1}{2}(\varphi_i-\mu_i)^2/\sigma_i^2]d\varphi_i. \quad (31c)$$

Define $m_1, m_2, \cdots, m_n$ and $s_1, s_2, \cdots, s_n$ by the equations

$$\frac{1}{n}\sum_{i=1}^{n}\frac{\varphi_i-m_i}{s_i}=0, \quad (32)$$

$$\frac{1}{n-1}\sum_{i=1}^{n}\left(\frac{\varphi_i-m_i}{s_i}\right)^2=1 \quad (33)$$

and by the further condition that the same relations obtain between the m_i and s_i as those which connect the μ_i and σ_i according to the theory of energy loss by collisions and the theory of multiple scattering. These m_i and s_i are the best estimates of μ_i and σ_i, with an accuracy increasing with n. They can be determined, from the conditions defining them in terms of the measured angles φ_i, and in this way the experimental scattering s_i can be expressed as a function of the experimental (apparent) magnetic deflection m_i over the range of energies represented in the track.

If one neglects energy loss and sets all $m_i=m$ (constant), $s_i=s$ (constant), then from (32)

$$\frac{1}{n}\sum_{i=1}^{n}\varphi_i=m$$

and from (33)

$$\frac{1}{n-1}\sum_{i=1}^{n}(\varphi_i-m)^2=s^2.$$

The error thus made is measured by the ratio $R=s/s_i$ between s and the s_i corresponding to the $m_i\approx m$. R is a function of the φ_i, whose distribution function can be determined in terms of those of the φ_i, i.e., the $dF(\varphi_i)$. For electrons with an initial energy of 50 kev and a path length of 14 cm in one atmosphere of argon R_{av} was estimated to differ from unity by less than 1 percent.

APPENDIX III: DERIVATION OF EQ. (18c)

Let m and s be the sample mean and variance, μ and σ the true mean and variance of a normal variable. It was shown by N. L. Johnson and B. L. Welch[18] that the ratio $mn^{\frac{1}{2}}/s$ is distributed approximately normally with mean $(n)^{\frac{1}{2}}\mu/\sigma$ and variance

$$\frac{1+(n\mu^2/\sigma^2)}{2(n-1)}^{\frac{1}{2}}$$

where n is the size of the sample. According to R. C. Geary[19] the ratio v of the two independent normal variables has the distribution function

$$dF(v)=\frac{1}{(2\pi)^{\frac{1}{2}}}\frac{\mu_2\sigma_1^2+\mu_1\sigma_2^2v}{(\sigma_1^2+\sigma_2^2v^2)^{\frac{1}{2}}}\exp\left\{-\frac{1}{2}\frac{(\mu_1-\mu_2v)^2}{\sigma_1^2+\sigma_2^2v^2}\right\}dv \quad (34)$$

so that

$$\frac{\mu_1-\mu_2v}{(\sigma_1^2+\sigma_2^2v^2)^{\frac{1}{2}}}$$

is distributed with mean zero and unit variance, where μ_1 and σ_1 are the mean and variance of the first variable, μ_2 and σ_2 those of the second.

When considering the ratio $(m_a/s_a)(m_b/s_b)$ one can obviously combine the two results quoted above, and obtain Eq. (18c).

[18] N. L. Johnson and B. L. Welch, Biometrika **31**, 362 (1940).
[19] R. C. Geary, JRSS **93**, 447 (1930).

PHYSICAL REVIEW VOLUME 77, NUMBER 5 MARCH 1, 1950

Star Fragments in Oxygen and Helium under Bombardment by 90-Mev Neutrons

JAMES TRACY AND WILSON M. POWELL
Radiation Laboratory, University of California, Berkeley, California
(Received October 17, 1949)

A study has been made of eighty-two stars produced in a mixture of oxygen and helium when a cloud chamber filled with these gases and placed in a magnetic field of 13,000 gauss was bombarded by 90-Mev neutrons. Stars having up to five prongs were observed.

Of the forty-eight 2-prong stars, 14 could be reasonably assigned to oxygen and 14 to helium. The remaining 20 were unidentified. It was found possible to make plausible identifications of all the fragments from only 7 helium stars and one 5-prong oxygen star. The general identification procedure is discussed and the arguments for the one 5-prong oxygen star are presented in some detail. Histograms of the $H\rho$- and scatter-angle distributions of the star fragments are given.

VERY soon after the 184-inch cyclotron[1] began to operate, a cloud chamber was placed in the beam of high energy neutrons[2] that was produced when the 195-Mev deuterons struck a target in the cyclotron tank. These neutrons were observed to produce stars in the gas of the cloud chamber. In individual cases it was always difficult to tell what nucleus was disintegrating. Since oxygen is always present in the cloud-chamber vapor, it was considered profitable to undertake a detailed study of the characteristics of oxygen stars in the hope that they might be distinguished from other stars in future studies.

The cloud chamber[3] contained oxygen, helium, and water vapor with a total pressure of about half an atmosphere. The helium was introduced to minimize multiple scattering and to produce the low stopping power of 0.17 relative to air. Low stopping power was desirable in order to produce long tracks on which accurate curvature measurements could be made. The

[1] W. M. Brobeck, E. O. Lawrence, *et al.*, Phys. Rev. **71**, 449 (1947).
[2] R. Serber, Phys. Rev. **72**, 1007 (1947).
[3] Brueckner, Hartsough, Hayward, and Powell, Phys. Rev. **75**, 555 (1948).

inclusion of the helium had another and unpremeditated advantage; namely, it made possible the study of helium disintegrations which are qualitatively quite different from those in oxygen.

Eighty-two stars were studied. Of 48 two-prong stars, 14 were thought to be helium and 14 to be oxygen stars. The other twenty 2-prong stars could not be identified. In addition there were twenty 3-prong, eight 4-prong and six 5-prong stars all, necessarily, from oxygen. In comparing these oxygen stars with the carbon stars in other cloud-chamber experiments no distinguishing characteristics were found.

The $H\rho$-distribution for the helium, oxygen, and unidentified 2-prong stars is shown in Fig. 1. It was not possible to plot energy rather than $H\rho$ because the mass of the individual particles was usually not known. The angular distribution of all particles from all stars is plotted in Fig. 2. The scatter angle, θ, is measured relative to forward direction of the neutron beam. It has been left in the laboratory system of reference because the momenta of the individual incident neutrons was unknown. There was found to be no marked difference in the angular distribution for the separate categories of stars as listed above. Further, it was impossible to determine whether or not the angular distribution of light and heavy fragments was different.

The analysis of these stars was complicated by the probable presence of secondary neutrons in nearly all cases. This fact, coupled with the energy spread of the incident neutrons, drastically curtailed the effective use of energy, momentum, and mass balances. A charge balance, although ambiguous for two-prong stars where either two or eight charges could have been involved, was more useful. Most important, however, was the identification of as many as possible of the individual prongs. The possible parameters available for this purpose were $H\rho$, range, change of $H\rho$ with range, and specific ionization (as indicated by track density). Generally, good determinations of at least two of these quantities were required. Even then it was possible to identify only the hydrogen and helium isotopes with any certainty because of the overlapping characteristics of heavier particles.

Because of the difficulties, it is not surprising that only one oxygen and seven helium stars could be reasonably well analyzed. The probable fragments of the 5-prong oxygen star (see Fig. 3) were a proton, a triton, three alpha-particles, and a secondary neutron. (The term "secondary neutron" includes any neutron emanating from a disintegration whether it be the scattered neutron or one initially in the target nucleus.) This star was exceptional in that there were at least two parameters applicable to the identification of each prong. Measurement accuracies were enhanced because all tracks lay within 16 degrees of the horizontal. The analysis may be briefly summarized as follows (see Table I): For convenience the prongs are numbered from 1 to 5. Number 1 was very light and had a large $H\rho$ definitely identifying it as H^1 or H^2. The $H\rho$ and density of No. 3 was the same as that of No. 4. Number 3 and No. 4 were, therefore, identical particles. Charge balance considerations required that they have no more than 2 charges apiece and change of $H\rho$ with range data narrowed the choice for No. 3 and No. 4 to He^4 or H^3. Number 5 had a smaller $H\rho$ and slightly less density than No. 3 and No. 4. This comparison with No. 3 and No. 4 together with its change of $H\rho$ suggested No. 5 to be H^2, He^3, or possibly H^3. The $H\rho$, short range, and medium density of No. 2 were such as to strongly suggest a helium or lithium isotope. Finally, after careful comparison of the $H\rho$'s and relative track densities of No. 3, No. 4, and No. 5 while maintaining a charge balance, it was concluded that No. 2 was doubly-charged, No. 3 and No. 4 were He^4's and No. 5 was H^3. Range-$H\rho$-comparison then required that No. 2 be He^4 or He^6. A mass balance eliminated He^6.

At this point the mass and charge of all but prong No. 1 had been assigned. Number 1 was either H^1 or H^2. The total of 17 mass units involved in the reaction required that if No. 1 was a proton that there be a

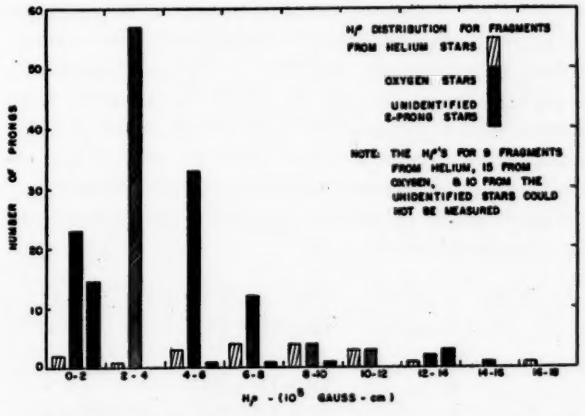

FIG. 1. These $H\rho$'s are the equivalent values which the fragments would have had if traveling normally to the magnetic field. The magnetic field used was 13,000 gauss.

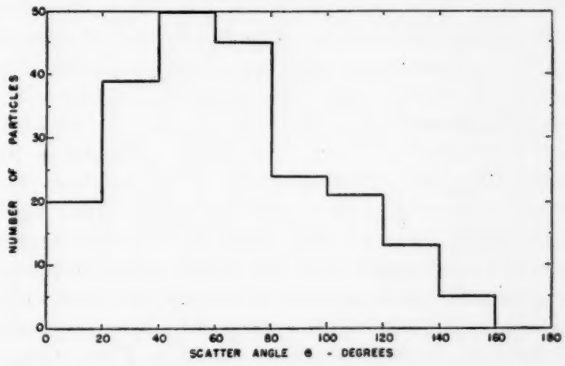

FIG. 2. Angular distribution of all particles from all stars. The distribution is given in the laboratory system. The scatter angle, θ, is measured relative to the forward neutron beam direction.

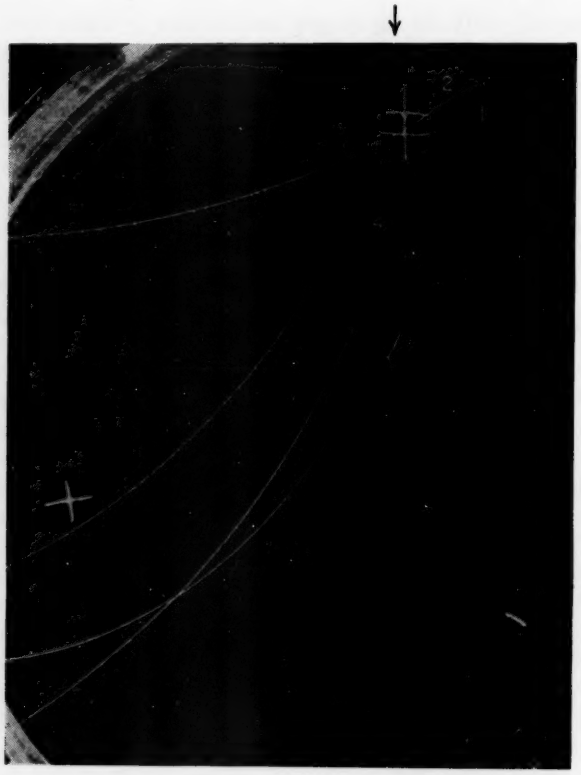

FIG. 3. Five-prong oxygen star. The origin is near the double-cross fiducial mark. The direction of the neutron beam is given by the black arrow.

neutron left over and that if it was a deuteron that there were no secondary neutrons. To decide between these two possibilities and to check further on the reasonableness of the other prong identifications, an energy and transverse momentum balance were attempted. The components of momentum (in units of $H\rho$ times charge) transverse to the incident beam direction did not quite balance out. It should be noted here that momentum in $H\rho$ charge units does not involve mass explicity. The momentum of an unseen neutron could have accounted for this discrepancy. When No. 1 was assumed to be a deuteron, there were no extra neutrons and the kinetic energy of the incident neutron could be calculated in two ways; (1) from the momentum of the incident neutron as given by the sum of the forward components of momentum of the fragments and (2) from the sum of the kinetic energies of the fragments plus the binding energy of the reaction. The former value was 12 Mev greater than the latter value of 74 Mev. On the other hand, a plausible energy balance was achieved when No. 1 was assumed a proton by giving the extra neutron an energy of 4 Mev. This led to an incident neutron energy of 89 Mev very close to the most probable value of 90 Mev. Thus, though the measurement uncertainty extremes were such as not to exclude No. 1 from being a deuteron, it was most probably a proton.

TABLE I. Measured data on the 5-prong oxygen star. (Magnetic field $(H)=1.35\times10^4$ gauss.)

Prong No.	α[a] (deg.)	β[b] (deg.)	ρ_β[c] (cm)	R_G[d] (cm)	ΔR_β[e] (cm)	$\rho_{\beta 2}$[e] (cm)
1	−12±2	114±1	56±1	—	—	—
2	−13±3	130±1	14.0±0.5	4.0±0.1	—	—
3	11.5±2	−60±1	37.5±0.5	—	11	36±1
4	1±1	−10±1	38.5±0.5	—	21	35±1
5	7.5±1	1±1	27.5±0.5	—	20	19±1

[a] α is the dip angle the plane of the track made with the horizontal plane containing the neutron beam.
[b] β is the angle at the origin between the forward direction of the neutron beam and the horizontal projection of the track.
[c] ρ_β is the slant radius of curvature at the origin measured in the plane of the track. The equivalent $H\rho$ is given approximately by $H\rho_\beta \cos\alpha$.
[d] R_G is the range in the cloud chamber. The range in air for the gas mixture used is given by $0.17R_G \pm 10$ percent.
[e] ΔR_β is the distance along the track from its origin at which a second slant radius $\rho_{\beta 2}$ was measured.

The 2-prong stars were not necessarily easier to analyze than other stars. Many consisted of one lightly ionizing track and a very short heavy track for which no $H\rho$ could be measured. Although the light track could usually be identified as an isotope of hydrogen, it was not possible to establish whether the short track was hydrogen or nitrogen since even a proton when of such short range is heavily ionizing. Only when the second track was lightly ionizing or long enough to obtain a good $H\rho$-measurement was it possible to distinguish clearly between helium stars and 2-prong oxygen stars.

In 7 of the 14 identified helium stars, it was possible to obtain an $H\rho$-determination for each of the two prongs and, therefore, to attempt momentum and energy balances. The failure of the transverse momenta to cancel in five of these stars definitely established the presence of one or more secondary neutrons. In the two other cases, the transverse momenta balanced within the experimental errors thus indicating that there may have been no secondary neutrons in the disintegration. The five nucleons and two charges involved in a helium 2-prong star allowed eight possible combinations of fragments. Even where secondary neutrons were assumed present, a minimum energy for the incident neutron could be calculated. Those combinations were rejected which led to energies higher than could reasonably be expected from the known energy distribution of the neutron beam. In most cases it was possible to establish which of the two prongs had the greater mass by comparing $H\rho$'s and track densities.

The probable fragments of these seven helium stars are tabulated below:

Stars No. 1 and 2	$2H^2+n^1$ or H^2+H^3
3 and 4	$H^1+H^3+n^1$
5	$2H^2+n^1$
6	$H^1+H^2+2n^1$
7	$H^1+H^2+2n^1$ or $H^1+H^3+n^1$.

This work was done under the auspices of the AEC.

Elastic Scattering of 84-Mev Neutrons*

A. BRATENAHL, S. FERNBACH, R. H. HILDEBRAND, C. E. LEITH, AND B. J. MOYER
Radiation Laboratory, Department of Physics, University of California, Berkeley, California
(Received November 21, 1949)

Measurements have been made of the angular distribution of 84-Mev neutrons scattered into angles between 2½° and 25° by Al, Cu, and Pb nuclei. Small spheres of these elements were placed in the neutron beam of the 184-in. cyclotron and the scattered neutrons with energies greater than 20 Mev were detected with pieces of carbon activated by the $C^{12}(n,2n)C^{11}$ reaction. Total scattering cross sections were obtained by integration of the differential scattering cross sections and also by attenuation measurements with good and poor geometry.

I. INTRODUCTION

AMALDI *et al.*[1] have observed a portion of the elastic scattering pattern produced by 14-Mev neutrons incident on Pb nuclei. Using a relatively high intensity beam of 90-Mev neutrons from the 184-in. cyclotron the present authors have explored the elastic scattering patterns of Al, Cu, and Pb. The measurements were extended to small enough angles to include a large part of the distribution. By measuring the ratio of the scattered neutron flux to the flux incident on the scattering nuclei it was possible to determine the absolute differential scattering cross sections. Total scattering cross sections were obtained by integration of the differential cross sections. The total scattering cross sections were also measured directly by good and poor geometry attenuation experiments. It is of interest to compare these scattering cross sections to the total collision cross sections determined by Cook *et al.*[2] and by the authors, using the same beam and the same detectors. This comparison provides a test of nuclear models such as the "opaque" model, and the "transparent" model of Fernbach, Serber, and Taylor.[3]

II. GENERAL FEATURES OF THE EXPERIMENT

The neutron source was a ½-in. thick beryllium target bombarded by 190-Mev deuterons in the 184-in. cyclotron. The energy distribution of neutrons from this source has a peak at 90 Mev and a spread at half-maximum of 30 Mev.[4,5]

The scattering experiment was performed in a narrow beam of neutrons defined by a circular hole in the 3-meter thick concrete shielding wall. (See Fig. 1.) The maximum beam intensity was about 10^6 neutrons per square centimeter per second. Some early experiments indicated that the flux density was essentially constant radially out to 4 cm from the axis of the beam and then decreased to less than 0.1 percent at 5 cm.

For the measurements of differential scattering cross sections the disposition of scatterer and detector is shown in Fig. 1A. Spherical scatterers were used to simplify the determination of the effective scattering center and mean angle of scattering. The distance "r" was increased as θ was decreased so that the detector would not be in the beam. It was experimentally established that the activation of the detector at a given angle varied inversely as r^2 indicating freedom from unrecognized sources of detector activation.

The relative intensity of incident to scattered neutrons was measured by placing the detector in the position of the scatterer.

Two types of detection were employed in the course of the study. Most of the work was done with carbon detectors employing the $(n,2n)$ reaction, but a coincidence recoil-proton counter was also used. Both receive discussion in subsequent sections.

The excitation function of the reaction $C^{12}(n,2n)C^{11}$ at high energies has been investigated theoretically by Heckrotte and Wolff,[6] and experimentally by R. L. Mather and H. F. York.[7] Using these results, and the known neutron energy distribution, the mean detection energy is determined to be 84±4 Mev.

The activity of the carbon detectors was compared to the activity of a carbon monitor placed in the beam between the target and the scatterer. The monitor for the recoil proton detectors was a BF_3 slow neutron counter placed in a hole in the concrete shielding wall (position B, Fig. 1). Its response in this location was proportional to the high energy neutron flux incident upon the shielding in the region of collimation.

The measurements of total cross sections and absorption cross sections were obtained simultaneously with the arrangement shown in Fig. 2. The attenuation measured by the "poor geometry" detector gives a cross section for removal of detectable neutron flux from a forward cone extending to the maximum angle, θ_m, subtended by the absorber about the detector. This angle is chosen to be the same as the maximum angle at which differential scattering cross sections were measured, and it includes essentially all of the elastically scattered neutrons. The cross section obtained in this

* This paper is based on work performed under the auspices of the AEC.
[1] Amaldi, Bocciarelli, Cacciapuoti, and Trabacchi, Nuovo Cimento **3**, 15–21, 203 (1946).
[2] Cook, McMillan, Peterson, and Sewell, Phys. Rev. **75**, 7 (1949).
[3] Fernbach, Serber, and Taylor, Phys. Rev. **75**, 1352 (1949).
[4] Hadley, Kelly, Leith, Segrè, Wiegand, and York, Phys. Rev. **75**, 353 (1949).
[5] R. Serber, Phys. Rev. **72**, 1007 (1947).
[6] W. Heckrotte and Peter Wolff, Phys. Rev. **73**, 265 (1948).
[7] R. L. Mather and H. F. York (private communication).

manner is thus approximately equal to the cross section for inelastic collision. A further discussion of this measurement will be found in Section III-B. A good geometry detector shielded from all but the central portion of the absorber was used to measure the total cross section simultaneously.

III. ANALYSIS AND DESCRIPTION OF THE EXPERIMENT

A. Angular Distribution

1. Analysis

Neglecting absorption of the neutrons passing through the scatterer, the activation of a detector of area S placed at angle θ and distance r from the scatterer of volume V and atomic number A is given by

$$D(r,\theta)=(I_0(N_0\rho/A)V)(\sigma(\theta)(S/r^2))\eta, \qquad (1)$$

where I_0 is the incident intensity; $(N_0\rho/A)V$ is the number of scattering nuclei; $\sigma(\theta)$ is the cross section for scattering into unit solid angle at angle θ; S/r^2 is the solid angle subtended by the detector; and η is the efficiency of the detector. If the detector is placed in the neutron beam the activation is given by

$$D_0=I_0S\eta. \qquad (2)$$

Thus from (1) and (2)

$$\sigma(\theta)=\frac{D(r,\theta)}{D_0}\frac{Ar^2}{N_0\rho V}. \qquad (3)$$

Taking absorption and multiple scattering into account a formula is obtained which is the same as (3) multiplied by a factor depending on the radius of the scattering sphere and the total and absorption cross sections.

The method employed in finding the complete expression may be outlined as follows.

A representation of the intensity and angular distribution of the neutrons scattered by a slab of thickness x may be given in the form

$$I(\theta)=I_0\sum_{n=1}^{\infty}\left\{\left[\frac{1}{n!}(x\mu_s)^n\exp(-x\mu_t)\right]\left[\frac{1}{n\sigma_s}\sigma\left(\frac{\theta}{(n)^{\frac{1}{2}}}\right)\right]\right\},$$

where $I(\theta)$ is the flux per unit solid angle in direction θ; μ_t, μ_s are the attenuation constants for collision, and for elastic scattering, respectively; and σ_s is the cross section for elastic scattering.

The first factor of a typical "nth" term gives the probability of just n elastic scattering collisions, and no other collisions, in passing through the slab. Deviations are assumed sufficiently small that the distance traversed in the material is always x.

In the second factor, giving the probability that an n-times-scattered neutron goes in direction θ, the customary assumption has been made that the angular spread after n scatterings is $(n)^{\frac{1}{2}}$ times the spread from single scattering. This implies that the forward scattered intensity shall be correspondingly reduced by the factor $1/n$.

When this type of analysis is applied to the scattering by the spheres used (such as, copper, 2.5 cm diam.), it is found that the coefficient multiplying $\sigma(\theta/\sqrt{2})$ is only 5 percent of the coefficient of $\sigma(\theta/1^{\frac{1}{2}})$. Hence the effect of multiple scattering upon the *form* of the angular distribution from such a sphere is not sufficiently serious to demand attention in treating data of the present accuracy; and it is necessary only to correct for the effects of absorption and multiple scattering in an integral manner rather than to evaluate a correction which depends upon angle.

Having recognized this, it is found to be convenient to evaluate the correction by the following simpler analysis. In traversing a slab of thickness x a neutron will have a probability $[1-\exp(-x\mu_s)]$ of being elastically scattered, and a probability $\exp(-x\mu_a)$ of emerging without an inelastic collision; where μ_a is the attenuation constant for an inelastic or absorbing collision. Since $\mu_t=\mu_a+\mu_s$, the product of these probabilities is $\exp(-x\mu_a)-\exp(-x\mu_t)$.

Applying this to a spherical scatterer of radius a, the expression for the activation of the detector at angle θ

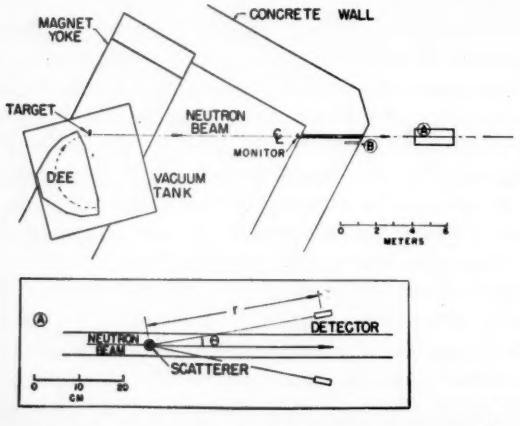

FIG. 1. Plan view of experimental arrangement.

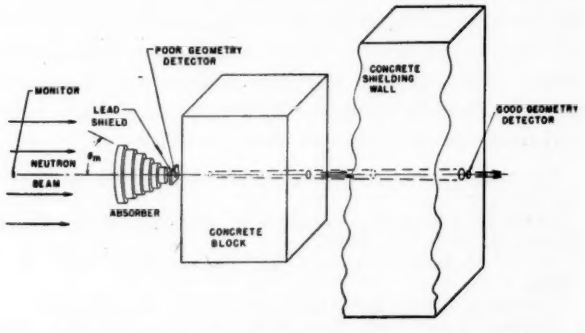

FIG. 2. Schematic drawing of apparatus for attenuation experiments.

and distance r becomes

$$D(r,\theta)=D_0(1/\sigma_s)\sigma(\theta)(1/r^2)\times\int_s[\exp(-x\mu_a)-\exp(-x\mu_t)]ds,$$

where the integration is carried out over the cross-sectional area of the scatterer. The variable x is the length of the chord which is used to approximate the neutron path.

Evaluation of the integral and series expansion results in the equation:

$$D(r,\theta)=D_0(N_0\rho/A)V\sigma(\theta)(1/r^2)K,$$

where

$$K=1-\tfrac{3}{4}a(\mu_t+\mu_a)+\tfrac{2}{5}a^2(\mu_t^2+\mu_t\mu_a+\mu_a^2)-\tfrac{1}{6}a^3(\mu_t^3+\mu_t^2\mu_a+\mu_t\mu_a^2+\mu_a^3)+\cdots.$$

Solving for $\sigma(\theta)$ we have instead of (3):

$$\sigma(\theta)=\frac{D(r,\theta)}{D_0}\frac{Ar^2}{N_0\rho V}\frac{1}{K}. \quad (4)$$

2. *Apparatus and Experimental Procedure*

The scatterers used were 2.54-cm diameter spheres of lead and copper and a 3.81-cm diameter sphere of aluminum. These were suspended in the beam by fine wires. The size of the scatterers was limited to keep the self-attenuation factor K from becoming less than 0.75.

The detectors were stacks of twelve cylindrical sectors of carbon 0.32 cm thick in a copper container (see Fig. 3A). Two such stacks were placed symmetrically about the axis of the beam at distances, depending upon angle, of 18 to 125 cm. The wall of the copper container which faces the scatterer was made 1 cm thick to prevent activation of the carbon pieces by scattered protons. When this thickness was doubled the activity was reduced by the fraction which one would expect if all the activity were due to neutrons. After a 15-minute bombardment at the maximum cyclotron beam intensity the carbon sectors were removed from the copper holders and arranged to surround a set of four thin-glass-walled counting tubes (see Fig. 3B).

The monitors were carbon disks of 4.29-cm diameter and 0.32-cm thickness. These were counted with a mica window bell-jar type counter. All counts were made concurrently; that is, the detector and monitor activities were counted over the same time interval eliminating the necessity of corrections for decay.

In all the experiments described here the basic measurement is the ratio of the activity of the detector to that of the monitor. Calling this ratio A, when the scattering sphere is in place and the detector at (r,θ) (see Fig. 1A); and B, the background ratio when the scatterer is removed but the detector is put in the same position; and C, the ratio when the detector is put in the primary beam in place of the scatterer, we have:

$$D(r,\theta)=(A-B)e, \quad D_0=2Ce,$$

where e is a relative counting tube efficiency factor to allow the results of different runs to be correlated, and $D(r,\theta)$ and D_0 are the quantities to be used in Eq. (4). The value of e is determined before each run by counting standard fixed samples with the detector and monitor counters. The factor 2 in the second equation above is necessary because only one of the copper holders was placed in the beam.

A typical determination of A involved about 2500 net counts from the detector in a period of 15 minutes.

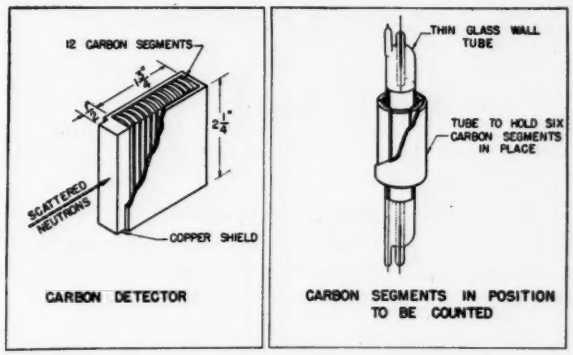

FIG. 3. Detector and detector counting arrangement.

This is about four times the counter background for the set of four tubes used and about four times the net count in determining B. Since the monitor was exposed in the primary beam it gave a much higher count. The ratio $D(r,\theta)/D_0$ was of the order of 0.001.

B. Attenuation Experiments

1. *Analysis*

From the results of the angular distribution measurements one can determine by graphical integration the cross section σ_s' for scattering of detectable neutron flux into a forward cone extending to the widest angle measured θ_m:

$$\sigma_s'=\int_0^{2\pi}d\Phi\int_0^{\theta_m}\sigma(\theta)\sin\theta d\theta. \quad (5)$$

This cross section can also be measured, if inelastically scattered neutrons are not detectable, in an attenuation experiment utilizing the "poor geometry" arrangement of Fig. 4 in which the attenuating material forms the frustum of height x of a cone whose generating angle is θ_m.

For this arrangement the detectable neutron intensity at the detector when the attenuator thickness is x will be

$$I(x)=I_1(x)+2\pi\int_0^{\theta_m}\sin\theta I(\theta,x)d\theta, \quad (6)$$

where $I_1(x)$ is the flux density of unscattered neutrons at a distance x from the base and $I(\theta, x)$ is the intensity at x of previously scattered neutrons moving in direction θ within unit solid angle. This assumes that any increase due to detection of inelastically scattered neutrons is small, as will be justified in Section V.

Consider now the effect of increasing the thickness of the attenuating material by an amount dx. The intensity of detectable neutrons at the vertex of the cone will then be altered by an amount

$$dI(x) = -I_1(x)N\sigma_t dx - 2\pi N\sigma_t dx \int_0^{\theta_m} \tan\theta I(\theta, x)d\theta + 2\pi I_1(x)Ndx \int_0^{\theta_m} \tan\theta\sigma(\theta)d\theta + 2\pi Ndx \int_0^{\theta_m} \tan\theta d\theta \int_0^{\alpha_m} \sigma(\pi-\beta)2\pi \times \sin\alpha I(\alpha, x)d\alpha, \quad (7)$$

where N is the number of nuclei per cm^3 in the attenuator, and σ_t is the total cross section of each nucleus.

The physical meanings of the successive terms on the right-hand side of this equation are as follows:

1. Decrease caused by attenuation in dx of hitherto unscattered neutrons whose flux density is $I_1(x)$.
2. Decrease caused by attenuation in dx of neutrons previously elastically scattered into the direction of the detector.
3. Increase caused by elastic scattering in dx, into the direction of the detector, of hitherto undeviated neutrons.
4. Increase due to elastic scattering in dx of neutrons previously elastically scattered into direction α. The angle β defines the scattering angle necessary to deflect these incident neutrons into the direction of the detector. The angle α_m is to be large enough to include essentially all the elastically scattered flux incident upon dx.

Since $\sigma(\theta)$ and $I(\theta)$ are both strongly peaked at $\theta=0$ the integrals in (7) are not greatly affected by replacing $\tan\theta$ by $\sin\theta$. (In the worst case the difference is only 2.5 percent.) Also for the same reason it may be shown that the angle β may be replaced by θ with an error sufficiently small to be allowable in this experiment. These two approximations are, in fact, partially compensating in their effects.

In view of Eqs. (6) and (5), these approximations permit (7) to be reduced to

$$dI(x) = -I(x)N(\sigma_t - \sigma_s')dx,$$

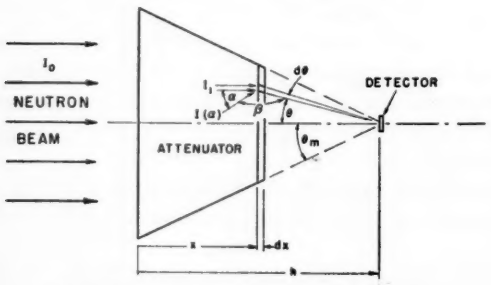

FIG. 4. Geometry of attenuation experiment.

so that an attenuation experiment with this arrangement will measure the difference of cross sections

$$\sigma_t - \sigma_s' = (1/Nx)\ln(I_0/I(x)). \quad (8)$$

The absorption cross section for the nuclei of the attenuating material is related to (8) by

$$\sigma_a = \sigma_t - \sigma_s' - \sigma_1 + \sigma_2, \quad (9)$$

where σ_1 accounts for elastic scattering into angles greater than θ_m, and σ_2 is the cross section for inelastic scattering of neutrons into angles less than θ_m with sufficient energy to be detected.

Subtraction of the measured quantity $(\sigma_t - \sigma_s')$ from the measured value of σ_t yields an evaluation of σ_s'

$$\sigma_s' = \sigma_t - (\sigma_t - \sigma_s'), \quad (10)$$

which may be compared for experimental consistency with that obtained by Eq. (5). If as is shown in Section V the quantities σ_1 and σ_2 are small, then σ_s' is approximately equal to the elastic scattering cross section $\sigma_s = \sigma_t - \sigma_a$.

2. *Apparatus and Experimental Procedure*

The arrangement for the attenuation experiment just discussed is shown in Fig. 2.

The angle θ_m was 27° for dural and copper, and 21° for lead. The maximum attenuator thicknesses were as follows: dural and copper, six 5.08-cm disks; lead, six 2.54-cm disks. In every case a 4-cm lead shield was put just ahead of the poor geometry detector to avoid activation of the carbon by recoil protons from the attenuating material. The uniformity of the incident beam was checked in a preliminary experiment by putting carbon detectors at various points on the base of the absorbing cone. This was also checked by verifying that a single disk at the base of the cone gave the same attenuation as a disk of the same thickness near the vertex. Absorption and total cross sections for aluminum were obtained from the dural measurements making allowance for the other metals in the alloy.

IV. RESULTS

The results are summarized in Tables I and II and Fig. 5.

V. SOURCES OF ERROR

A. Angular Resolution

Because of the finite size of the scatterer and detector a measurement made at a given nominal angle actually corresponds to detection over a fairly wide range of angles as is shown in Fig. 6. A detailed analysis has shown that the errors of the angles and cross sections due to this effect are negligible considering the accuracy of the experiment. This effect alone would not prevent the detection of a minimum of the type theoretically predicted for diffraction by an opaque nucleus.

B. Detection of Inelastically Scattered Neutrons

The 20-Mev threshold of the $C^{12}(n,2n)C^{11}$ reaction made it quite possible that a part of the scattered flux detected in this experiment was due to inelastically scattered neutrons with energies greater than the 20-Mev detection threshold. For this reason the angular distributions were also measured using a recoil proton detector with a BF_3 slow neutron counter as a monitor (see Section II). The detector consisted of a 3.8-cm diameter, 5-cm long paraffin cylinder behind which was placed a set of three cylindrical proportional counters each 5 cm in diameter and 5 cm long which were used in coincidence. A copper absorber was placed between the second and third counter. Its thickness was such that only recoil protons from neutrons with energies greater than 60 Mev could be detected; thus, as a neutron detector this arrangement provided a 60-Mev detection threshold.

Attenuation measurements, made with this detector and monitor combination indicated that under the conditions of operation, it was less reliable than the carbon detectors particularly for the measurement of the very small ratio $D(r,\theta)/D_0$. However, within the accuracy of the measurements the differential cross sections measured by the two methods are in agreement as can be seen in Fig. 5.

TABLE I. Total cross sections and the cross sections σ_s' (see Section III–B1) in units of 10^{-24} cm². The third row of the table gives scattering cross sections obtained from the total and absorption cross sections using Eq. (10). The last row gives the scattering cross section obtained by integration of the differential cross section as in Eq. (5).

Element	Al	Cu	Pb
Total cross sections			
Cook *et al.*[2]	1.12±0.02	2.22±0.04	4.53±0.09
The authors	1.14±0.03	2.15±0.04	4.47±0.11
σ_s'			
By attenuation	0.65±0.04	1.32±0.03	2.64±0.08
By integration	0.71±0.04	1.37±0.07	2.79±0.14
Maximum angle θ_m	27°	27°	21°

TABLE II. Differential cross section in units of 10^{-24} cm² per steradian. The errors shown apply to the relative magnitudes and do not include a 3 percent error in assigning absolute magnitudes.

Angle in degrees	Al	Cu	Pb
2½	5.0 ±0.4	13.8 ±0.9	59.0 ±4.0
3		14.8 ±1.2	54.0 ±6.0
4	4.64±0.18	14.2 ±0.7	53.0 ±5.0
5	4.36±0.23	10.3 ±0.3	34.0 ±7.0
6	4.3 ±0.3	10.6 ±0.3	25.6 ±1.0
7½	3.30±0.15	7.34±0.22	11.3 ±1.1
10	2.24±0.15	4.66±0.07	4.3 ±0.6
12½	1.54±0.13	2.61±0.05	2.1 ±0.3
15	1.08±0.04	1.30±0.02	1.46±0.14
17½	0.66±0.07	0.53±0.03	1.58±0.11
20	0.38±0.02	0.40±0.03	1.04±0.10
22½			0.59±0.13
25	0.17±0.02	0.31±0.05	

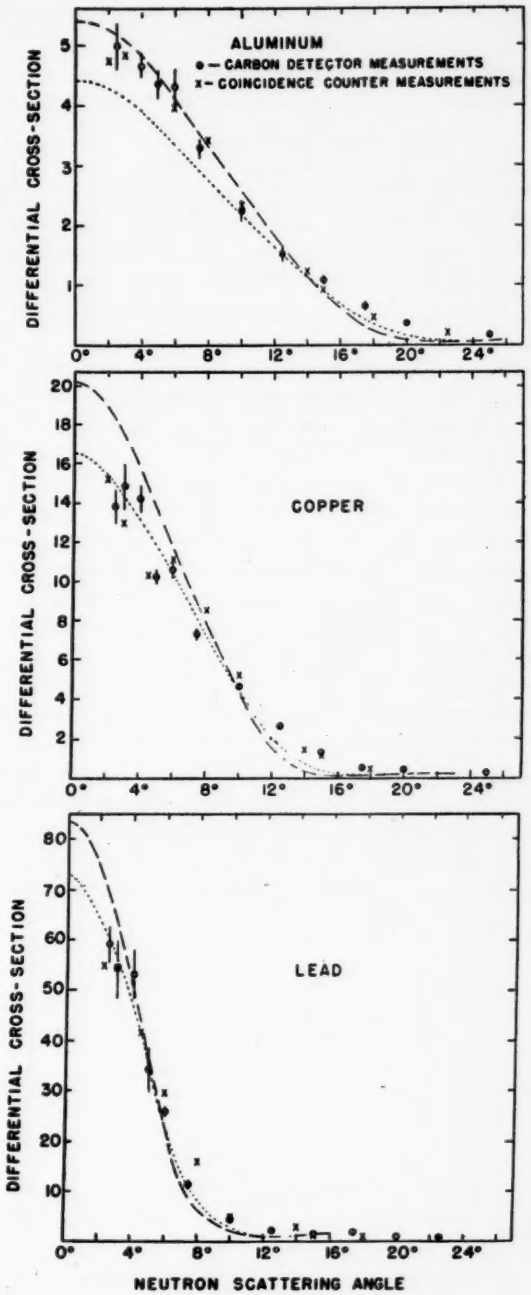

FIG. 5. Differential scattering cross sections in units of 10^{-24} cm² per steradian. The dashed and dotted curves show expected patterns from opaque nuclei with cross sections σ_s' and $(\sigma_s'-\sigma_2)$, respectively. (See Section VI-C.)

The contribution of inelastic scattering is not large enough to be apparent in comparing the results of the two methods.

An estimate of the inelastic contribution can, however, be obtained from measurements of Hadley and York[8] on the differential cross sections of several elements for production of high energy secondary

[8] J. Hadley and H. F. York (to be published).

TABLE III. Observed scattering cross sections σ_s', calculated cross sections σ_2 for producing detectable neutrons by inelastic collisions, and comparisons of ratios of cross sections measured at two energies. (Cross sections in units of 10^{-24} cm^2.)

	Al	Cu	Pb
Observed scattering cross sections σ_s'	0.71	1.37	2.79
Calculated values of σ_2	0.07	0.13	0.17
$(\sigma_s'-\sigma_2)$	0.64	1.24	2.62
σ_s'/σ_t	0.62	0.64	0.62
$(\sigma_s'-\sigma_2)/\sigma_t$	0.56	0.58	0.59
σ_s'/σ_t, measured with Bi fission counters (~95 Mev)	0.58	0.61	0.60

protons by 90-Mev neutrons. At these energies the incident neutron wave-length is sufficiently small to allow the effects of neutron-nucleon collisions to be observed, where the collision event involves primarily only the incident neutron and a neutron or proton of a target nucleus. By this process nucleons may be knocked out of nuclei with energies and angular distributions related to those of $n-p$ or $n-n$ collisions.

Hadley and York have measured differential cross sections for such emission of protons of over 20-Mev energy from C, Cu, and Pb. We shall assume that the neutrons emerging from $n-p$ collisions within the nucleus are described by the same differential cross section as these protons.

There will also be a contribution of high energy neutrons due to $n-n$ collisions. We assume that these events are similar to $p-p$ collisions with respect to cross section and angular distribution. Observations in progress at this laboratory indicate that even at these energies the $p-p$ collisions yield spherical symmetry in the center-of-mass system, and that the collision cross section at these energies is roughly one-half the $n-p$ collision cross section.

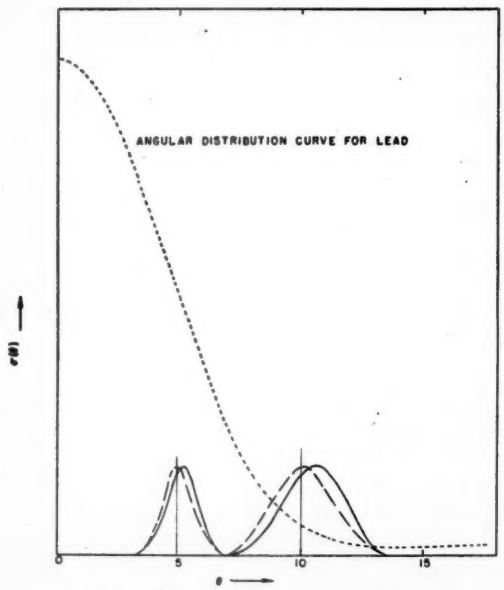

FIG. 6. Angular resolution. The solid bell-shaped curves show the detection efficiency distribution for two typical detector positions in the measurement of the angular distribution from the lead scatterer (5° at 65 cm and 10° at 34 cm). When these are multiplied by the dotted curve which has the form of the angular distribution for lead we obtain the effective detection efficiency distribution shown as dashed curves.

Using these assumptions, and taking account of the relative numbers of neutrons to protons in the nucleus in question, cross sections σ_2 of the target nuclei for delivering detectable neutrons by these "knock-on" processes into the angular range detected have been calculated and are shown in the Table III.

DeJuren and Knable[9] have measured total cross sections and the cross sections for scattering of detectable flux into angles less than θ_m using the same absorbers as those used by the authors. In place of carbon detectors they used bismuth fission chambers for which the neutron counting threshold is about 50 Mev, and the mean detection energy for these neutrons is about 95 Mev. Because of the higher threshold of this detector it is to be expected that the cross sections σ_s' as measured by DeJuren and Knable include smaller contributions from inelastic scattering than the corresponding cross sections measured by the authors. The ratios σ_s'/σ_t and $(\sigma_s'-\sigma_2)/\sigma_t$ from the carbon detector measurements and the ratio σ_s'/σ_t from bismuth fission detector measurements are shown in Table III. Considering this comparison, and the similarity of the angular distributions observed using proportional counters with the 60-Mev threshold with those observed with carbon detectors, it appears likely that these cross sections for inelastic processes yielding detectable neutrons are not underestimated.

In order to estimate the true scattering cross section σ_s one must add the effect of the cross section σ_1 for elastic scattering into wide angles which will be discussed in the next section. Thus:

$$\sigma_s=\sigma_s'-\sigma_2+\sigma_1.$$

Hence the values $\sigma_s'-\sigma_2$ of Table III represent lower limits for σ_s.

C. Elastic Scattering into Wide Angles

The neutron flux per unit solid angle becomes so small at angles greater than θ_m that measurements of the intensity become very inaccurate. However, because of the sine factor which enters into the calculation of the scattering cross sections (see Eq. (5)) the total flux in wide angles may not be negligible. An indication of the order of magnitude of this effect can be obtained from wide angle differential cross-section measurements made with the recoil proton detector.

At 30° the differential cross sections measured were 0.033 ± 0.020, 0.004 ± 0.004, and 0.22 ± 0.13 for Al, Cu, and Pb, respectively. At 45° the value obtained for aluminum was 0.004 ± 0.001 while nothing was detected at this angle from Cu and Pb and nothing was detected in measurements at 60° and 90° from Pb. On the basis

[9] J. DeJuren and N. Knable, Phys. Rev. 77, 606 (1950).

of these observations it has been estimated that the wide angle scattering effect is of the order of 5 percent for Al and less than this for Cu and Pb and is thus somewhat smaller than the inelastic scattering effect. As can be seen from Eq. (9) the two effects tend to cancel each other in the evaluation of the difference between σ_s' and the true elastic scattering cross section σ_s.

It should be noticed that these effects are common to both methods of measuring σ_s, hence the attenuation method serves principally as a check on other systematic errors in the differential cross-section measurements.

VI. ANALYSIS OF RESULTS

A. Description of the Angular Distribution

In the present experiment the de Broglie wave-length of the neutrons is smaller than nuclear dimensions, and it is sensible to speak of a neutron colliding within the area of cross section presented by the nucleus. This implies that neutrons with rather large values of angular momentum will be involved in nuclear collisions.

The quantized values of angular momentum will extend up to $pR=lh$ or $l=kR$; where $k=1/\lambda=p/\hbar$, and l is an angular momentum quantum number. R is the largest value of impact parameter for which observable effects of collision occur, and it may be defined as the nuclear radius.

For 84-Mev neutrons $\lambda=0.48\times10^{-13}$ cm, and for a heavy nucleus R is nearly 10^{-12} cm. Thus values of l will in some cases extend nearly as high as 20.

Since at the degree of excitation which such neutrons could impart to nuclei the nuclear levels will be numerous and overlapping, it is to be expected that such collisions would lead to inelastic events or absorption. Inelastically scattered neutrons or secondary neutrons from such events are almost entirely of energies below the detection threshold as indicated in Section V. Thus it is possible to conceive of the nucleus, for the purpose of this experiment, as an opaque, spherical obstacle absorbing and diffracting the neutron wave.

If a description of the scattering process is represented in partial waves,[10] and the expression for the scattered wave obtained by subtracting the expression for the unperturbed plane wave from that for the wave field with scattering nucleus present, the asymptotic result at a large distance r from the scattering center, and at angle θ from the direction of the incident beam, is:

$$\Psi_{\text{scatt}}\simeq\frac{e^{ikr}}{2ikr}\sum_{l=0}^{\infty}(2l+1)(e^{2i\delta_l}-1)P_l(\cos\theta). \quad (11)$$

When no absorption in the scattering nucleus occurs, δ_l is a real number which measures the phase difference between the lth partial wave in the diverging components of the actual wave field and the corresponding wave in the unperturbed field. But when the scattering nucleus also absorbs neutrons the effect is described by a complex value for δ_l,

$$\delta_l=\xi_l+i\eta_l,$$

where η_l then functions as an absorption exponent affecting the magnitude of the diverging lth wave.

If now the scattering nucleus is considered to be a perfectly absorbing sphere of radius R, the value of η_l for $0\leq l\leq kR$ will be infinite. Also if neutrons passing with $l>kR$ are to be unaffected the value of δ_l will be zero for $l>kR$.

For this approximate model, then, the scattered wave (11) reduces to:[11,12]

$$\Psi_{\text{scatt}}\simeq-\frac{e^{ikr}}{2ikr}\sum_{l=0}^{l=Kr}(2l+1)P_l(\cos\theta). \quad (12)$$

The result (12) can be directly obtained by noting that the effect of the nucleus is to remove from the diverging components of the unperturbed wave those partial waves with values of l up to $l=kR$. This removal is mathematically described by superimposing upon the unperturbed wave a set of partial waves with amplitudes equal to corresponding amplitudes of the unperturbed wave field, with values of l up to $l=kR$, and with each phase shifted by one-half cycle. This superimposed set represents the scattered neutrons and its expression is just (12). This is simply an application of Babinet's principle from physical optics.

From (12) the differential scattering cross section is seen to be

$$\sigma(\theta)=\frac{1}{4k^2}\left[\sum_{l=0}^{l=kR}(2l-1)P_l(\cos\theta)\right]^2. \quad (13)$$

For forward scattering, $\theta=0$, (13) yields

$$\sigma(0^0)=\tfrac{1}{4}k^2(R+1/k)^4. \quad (14)$$

It is to be expected that the opaque nucleus model should give a distribution of elastically scattered neutrons similar to the Fraunhofer diffraction pattern for a plane wave diffracted by an opaque circular disk. It can be shown that expression (13) can be written in the approximate form[11,12]

$$\sigma(\theta)=\tfrac{1}{4}k^2(R')^4\left[\frac{J_1(2kR'\sin(\theta/2))}{kR'\sin(\theta/2)}\right]^2, \quad (15)$$

where J_1 indicates a first-order Bessel function, and $R'=R+1/k$. This is the expression for intensity in the Fraunhofer pattern produced by a disk of radius R' diffracting plane waves with $\lambda=1/k$.

[10] Rayleigh (J. W. Strutt), Proc. Lond. Math. Soc. (1) IV, 253 (1873).

[11] G. Placzek and H. Bethe, Phys. Rev. 57, 1075A (1940).

[12] A. Akhieser and I. Pomeranchuk, J. Phys. U.S.S.R. IX, 471 (1945).

B. Effect of Neutron Energy Spread Upon Angular Distribution

The energy dependence of the differential cross section occurs through the quantity $k=(1/\lambda)=p/\hbar$. In order to compare the theoretical distribution (13) with one observed it is necessary to calculate from (13) or (15) a predicted value of $\sigma(\theta)$ by averaging over the energy spectrum of incident neutrons $G(E)$ modified by the energy dependence of the detection efficiency $\epsilon(E)$.

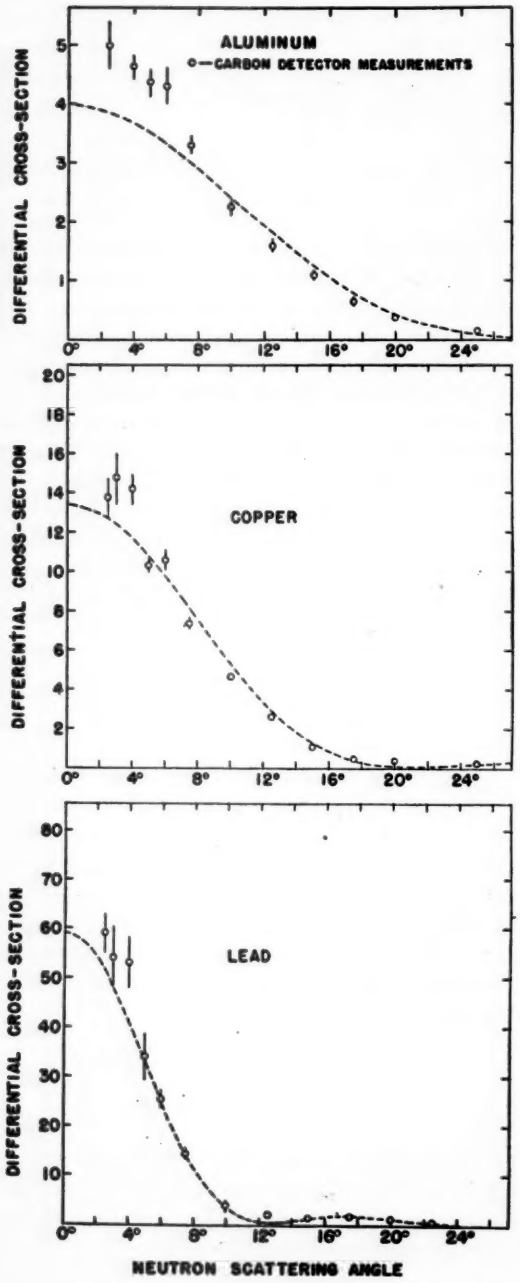

FIG. 7. Comparison of experimental differential cross sections with those calculated from transparent model theory. (Units same as in Fig. 5.)

Thus

$$(\sigma(\theta))_{\text{pred}}=\frac{\int_{E_{\min}}^{E_{\max}}\sigma(\theta, E)G(E)\epsilon(E)dE}{\int_{E_{\min}}^{E_{\max}}G(E)\epsilon(E)dE}.$$

It is not necessary to account for any change in energy of the neutrons upon being scattered, for the lightest nucleus employed is Al, and the scattering is confined to small angles. The averaging is accomplished by graphical integration using information on the neutron energy spectrum previously mentioned, and some approximate experimental data, supplemented by theory,[6,7] on the $C^{12}(n,2n)C^{11}$ cross section and its variation with energy.

The functions (13) and (15) are indistinguishable within the limits of accuracy needed in this comparison, so (15) has been employed. The principal effect of the averaging process just described is to increase the contribution in the vicinity of the first root of the Bessel function above that obtained from a pure spectrum of 84-Mev neutrons.

C. Comparison of Observations with Theory

By integration of the differential scattering cross section as given by (13) the elastic scattering cross section is obtained:

$$\sigma_s=2\pi\int_0^{\pi}\frac{1}{4k^2}\left[\sum_{l=0}^{l=kR}(2l+1)P_l(\cos\theta)\right]^2\sin\theta d\theta \quad (16)$$

$$=\pi(R+1/k)^2=\pi R'^2.$$

An experimental value for σ_s will, by use of (16), allow determination of R', which, in turn, may be used in (15) to construct angular distribution curves appropriate to the opaque model for comparison with the shapes of the experimental distributions.

This comparison is shown in Fig. 5. The dashed curves are the result of determining R' from the values of σ_s' displayed in Table III; and the dotted curves result from using $(\sigma_s'-\sigma_2)$ for determining R'. In each case the distribution given by (15) has been modified as in the preceding Section B to account for the energy spread of the neutrons.

In view of Sections V, B and C, and Eq. (16), we should actually determine R' from $\sigma_s=\sigma_s'-\sigma_2+\sigma_1=\pi(R')^2$. The value of σ_1 is very small in the cases of Cu and Pb, but may be comparable with σ_2 in the case of Al as shown in the experimental results of Section V-C. These facts are consistent with the agreement of the dotted curves with datum points for Pb and Cu, while for Al the points are closer to the dashed curve computed from σ_s'.

To be consistent, one should subtract from the datum point ordinates the values of the differential cross sec-

tions for inelastic collisions delivering detectable neutrons, estimated in the manner described in Section V-B. But this does not significantly alter the positions of the points except at very wide angles where the datum point accuracy does not warrant such correction.

A calculation of the angular distribution has also been made on the basis of the "transparent" model of Fernbach, Serber, and Taylor.[3] This model assumes for nuclear matter an absorption coefficient and an index of refraction. The radius of an individual nucleus according to this scheme can be represented by $r_0A^{\frac{1}{3}}$. In the case previously described, based on the total cross-section measurements of Cook, McMillan, Peterson, and Sewell,[2] the radius of the nucleus is given by $1.37A^{\frac{1}{3}}\times10^{-13}$ cm where K (the absorption coefficient) is chosen as 2.2×10^{12} cm^{-1} and k_1 (the increase of the propagation constant of the neutron wave upon entering the nucleus) as 3.3×10^{12} cm^{-1}.

The angular distributions determined with these constants yield the curves shown in Fig. 7. The theoretical curves are noticeably lower than the experimental values in the forward direction, but fit comparatively well at other angles. The Bessel function obtained from the opaque model on the other hand fits better in the forward direction but not as well at larger angles.

Figure 8 shows the theoretical curve for σ_a/σ_t as a function of nuclear radius. The experimental points are taken from the attenuation data obtained from the poor geometry experiment.

Curve A is calculated with the above mentioned constants, curve B with constants that fit this attenuation data better. Neither the angular distribution nor the total cross sections are very sensitive to changes in the value of the absorption constant, whereas the absorption cross section is a function of KR only. Hence a poor geometry attenuation experiment can be used to make a more critical determination of K. In this case $K=3.0\times10^{12}$ cm^{-1} shows better agreement with the experimental results. It should be mentioned that with this value of K, the value of r_0 necessary to give the best fit for the total cross sections is 1.39×10^{-13} cm.

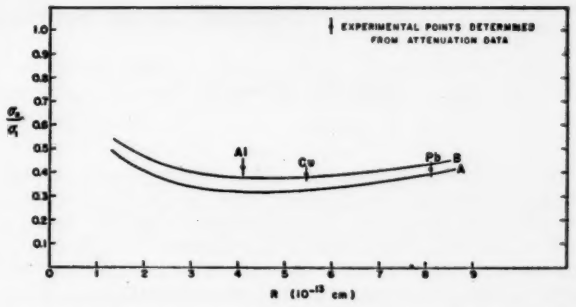

FIG. 8. Theoretical curves for σ_a/σ_t vs. $R(R=1.37A^{\frac{1}{3}}\times10^{-13}$ cm)
A: $K=2.2\times10^{12}$ cm^{-1}, $K_1=3.3\times10^{12}$ cm^{-1},
B: $K=3.0\times10^{12}$ cm^{-1}, $K_1=3.3\times10^{12}$ cm^{-1}.

In Fig. 8 the experimental values have not been corrected for the scattering beyond the maximum angle used. The only appreciable scattering beyond θ_{max} seems to be that for aluminum. Such correction would reduce the ratio σ_a/σ_t and bring the experimental point closer to the theoretical curve.

ACKNOWLEDGMENTS

The authors wish to express their appreciation to Professor E. O. Lawrence for his interest in this work. We are indebted to Professor E. McMillan for originally suggesting the problem and for helpful discussions. We also wish to thank Mr. James Vale and the cyclotron operating crew for their valuable assistance.

Nuclear Cross Sections for 95-Mev Neutrons*

JAMES DEJUREN AND NORMAN KNABLE
Radiation Laboratory, Department of Physics, University of California, Berkeley, California
(Received November 18, 1949)

The total cross sections of twelve different elements were measured using the neutron beam from the 184-inch cyclotron operating with deuterons. Bismuth fission ionization chambers were employed as both monitor and detector in conventional "good geometry" attenuation measurements in the neutron flux emerging from the three-inch diameter collimating port in the 10-foot thick concrete shielding. The mean energy of detection of the neutrons in this experiment is estimated to be 95 Mev.

Measurements were also made with a monitor and detector placed inside the concrete shielding where we could obtain an intense neutron flux over a large area. Attenuators of four different elements were placed in front of the detector in a "poor geometry" arrangement so that attenuation was due essentially to inelastic collisions which degrade the neutron energy below the fission threshold. A second detector was placed outside the concrete shielding in the collimated neutron beam in line with the neutron source, absorber, and first detector. Attenuation in it is caused by both inelastic and elastic scattering. By this arrangement the ratio of inelastic to total cross section can be determined directly in one experiment.

The nuclear radii as calculated from the observed cross sections using the theory of the transparent nucleus vary as 1.38×10^{-13} $A^{\frac{1}{3}}$ cm. In this energy range the ratios of the inelastic to total cross sections are all less than one-half.

INTRODUCTION

SEVERAL experiments have been conducted to measure the cross sections of nuclei with neutrons. They have been spaced at intervals corresponding to the periods when an increase in the energy of the bombarding neutrons was made available. It was thought that as the available energies increased the measured cross sections would tend to become independent of the energy of the bombarding particle. The results of these previous measurements are summarized in a recent paper of Cook, McMillan, Peterson, and Sewell[1] which describes a measurement of cross sections using the neutrons produced by 190-Mev deuterons of the 184-inch cyclotron.

The threshold energy of the reaction used for detecting the neutrons $C^{12}(n,2n)C^{11}$, is 20 Mev and an average cross section is obtained for neutrons having the average energy of the distribution produced in the cyclotron, modified by the $(n,2n)$ cross-section energy dependence. This work showed the expected $A^{\frac{1}{3}}$ variation of the nuclear radius, calculated from an opaque nuclear model, for heavy nuclei but clearly indicated that the light nuclei (carbon and lighter) had smaller apparent radii than would be expected from an $A^{\frac{1}{3}}$ law. This effect was attributed to the transparency of the light nuclei for neutrons of short wave-lengths.

These results indicated the need for a similar experiment to be done at higher energies in order to investigate the energy dependence of the effect. The estimated average energy of detection in the early experiment was 83 Mev. In the experiment to be described, the same source of neutrons was employed, but a bismuth fission ionization chamber[2] with a threshold of about 50 Mev and a mean detection energy of 95 Mev served as the detector. In addition to raising the average detection energy this high threshold served a second purpose; it allowed us to measure the cross sections for inelastic processes.

Such a measurement was necessary for one could no longer assume that the cross sections for inelastic scattering and for elastic scattering were equal to each other and to one-half the total cross sections as would be expected from an opaque model of the nucleus. The nuclear transparency would cause the ratio of inelastic and elastic scattering cross sections to be energy dependent.

Fernbach, Serber, and Taylor[3] have, by assuming a model of the nucleus which has an absorption coefficient and an index of refraction, arrived at a formula for the radius of the nucleus in terms of the total cross section which for the experimental cross sections given shows the radii of the nuclei to be directly proportional to $A^{\frac{1}{3}}$ within the limits of experimental error. The same good fit has been made with the data of the previous experiment using the index of refraction and absorption coefficient corresponding to the neutron momentum of the average energy of detection in that experiment.

The total cross sections of 12 different nuclei are measured employing bismuth fission ionization chambers as both monitor and detector in conventional "good geometry" attenuation measurements in the neutron flux emerging from a three-inch diameter collimating port in the ten-feet thick concrete shielding.

Measurements were also made with a monitor and detector placed inside the concrete shielding where we could obtain an intense neutron flux over a large area. Attenuators of four different elements were placed in front of the detector so that the angle subtended by the attenuator was greater than the angle at which the differential scattering cross section of the attenuator nuclei falls to one percent of its value in the forward direction. This arrangement simulated the situation in which a plane wave of neutrons strikes a slab of material infinite in area so that attenuation is due solely to

* This work was performed under the auspices of the AEC.
[1] Cook, McMillan, Peterson, and Sewell, Phys. Rev. **75**, 7 (1949).
[2] C. Wiegand, Rev. Sci. Inst. **19**, 790 (1948).
[3] S. Fernbach, R. Serber, and T. B. Taylor, Phys. Rev. **75**, 1352 (1949).

inelastic collisions. Measurements with higher threshold detectors gave results which agreed within the probable errors, thus confirming our assumption that an inelastic collision reduces the neutron energy below the threshold for bismuth fission.

A second detector was placed outside the concrete shielding in the collimated beam in line with the neutron source, attenuator, and first detector. Attenuation of the beam for the last detector is caused by both elastic and inelastic scattering. By this arrangement the ratio of inelastic to total cross sections can be measured directly in one experiment.

COUNTERS AND NEUTRON DETECTION

Counters

The ionization chambers[2] employed outside the concrete shielding contained 31 aluminum disks $\frac{1}{32}$-inch thick and two inches in diameter (Fig. 1). Alternate disks were coated with thin layers of bismuth and the separation between adjacent disks was $\frac{3}{8}$ inch. The disks of the chambers used as monitors were plated with bismuth 1.0 to 1.5 mg/cm^2 thick; the detector disks with bismuth 10 mg/cm^2 thick. For exposure to equal neutron flux the detector counting rate is three to four times that of the monitors. The chambers employed in the "poor geometry" measurements inside the shielding were of a shallow design, containing three plates 4.5 inches in diameter, $\frac{3}{4}$ inch apart. Thin bismuth layers were used (as in the monitors described). The fragments produced in fission of bismuth by the high energy neutrons experience their greatest rate of energy loss at the beginning of their ranges since they are initially multiply ionized and recombine with electrons as their velocities decrease. Hence most of the ionization in the argon gas occurs near the negative, bismuth coated plates. The electrons formed are collected on the aluminum plates (field strength 500 v/cm) and the resulting pulses are amplified by means of linear amplifiers.

Pulse Characteristics

The number of ions produced by a bismuth fission fragment is much greater than that by an alpha-particle or proton given off by a spallation reaction in the chamber. Consequently it will take coincidences of several spallation reactions to give a pulse as large as a fission pulse. The gas used in the chambers was argon with 3 percent carbon dioxide, and the pressure was adjusted so that the range of the fission fragments was approximately equal to the separation of the plates, since at a higher pressure the total ionization in the gas from a fission fragment would be unchanged but the ionization from an alpha-particle would increase proportionally with pressure. If at a given neutron intensity the logarithm of the counting rate is plotted against the discriminator voltage (Fig. 2) a curve with a broad plateau is obtained. The variation of the counting rate on the plateau is usually one to two percent, per volt change of discriminator voltage. If the logarithm of the ratio of the number of counts of the chamber to a fixed monitor is plotted against discriminator voltage a similar curve results. If the neutron intensity is increased, the rapidly varying "pile-up" region of the curve, due to pulses from coincident spallation reactions is shifted to the right, but the remainder of the curve is unchanged. This agrees with what we would expect from theoretical considerations, which show the number of "pile-ups" to be a much more rapidly increasing function of the neutron intensity than is the number of fissions. Variation of neutron intensity thus affords a criterion for distinguishing fission pulses from "pile-ups" of spallation products.

The stability of the amplification and discrimination voltages was periodically checked by feeding in fixed voltage pulses and it was determined that the experimental errors so incurred were less than the statistical errors of counting.

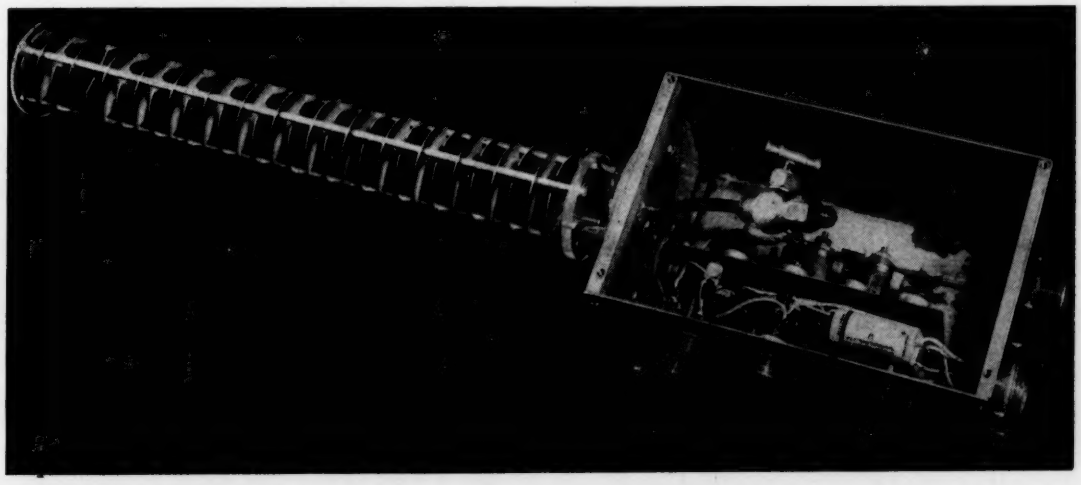

FIG. 1. Internal structure of long fission ionization chamber.

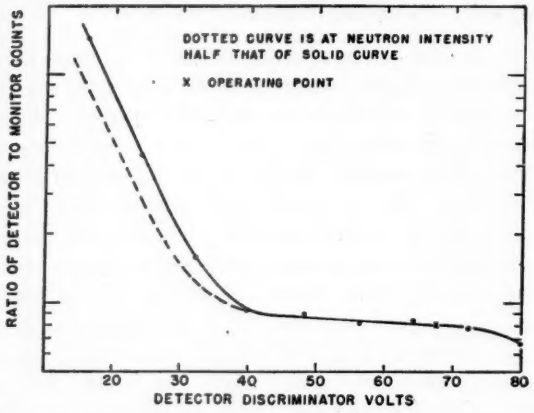

FIG. 2. Discriminator curve: Number of pulses greater than discriminator voltage *vs.* discriminator voltage.

EFFECTIVE NEUTRON DETECTION ENERGY

The neutron beam was produced by bombarding a 0.5-inch Be target with 190-Mev deuterons in the 184-inch cyclotron. The neutrons produced by "stripping" have an energy distribution theoretically predicted by Serber[4,5] and checked experimentally with proton recoil counters[6] and by proton recoils in a cloud chamber.[7] The variation of the fission cross section with neutron energy was investigated by Wiegand and Kelly[8] by varying the radius of the target probe in the 184-inch cyclotron. As there is a spread in neutron energies for each radius and the more energetic neutrons in each energy spectrum have the highest fission efficiency, the curve of bismuth fission cross section as a function of neutron energy may be even steeper than indicated. If the fission cross section and neutron distribution for corresponding energy intervals are multiplied a curve results proportional to the detection efficiency as a function of neutron energy (Fig. 3). The curve is similar to the original neutron distribution; both curves have an energy spread of about 26 Mev at half-maximum, but the average energy of the neutrons detected by fission is about 95 Mev.

EXPERIMENTAL ARRANGEMENTS

Arrangement for Total Cross Sections

The monitors and detectors employed in measuring total cross sections were aligned outside the concrete shielding by means of x-ray film (which was exposed to γ-rays formed when deuterons struck the target). The attenuators were placed behind the monitor at a distance of 100 inches from the detector (Fig. 4), so that the detector subtended a solid angle of 0.0003 steradian at the attenuator. A steel collimator, 18 inches long with a 1-inch×1.5-inch cross-sectional aperture placed in the collimating port through the shielding, was employed in all but the first few experiments. The correction for small angle scattering was negligible when the collimator was used, and the maximum correction without the collimator was only 2.2 percent for the Pb cross section.

Arrangement for Inelastic Cross Sections

The two shallow type chambers mentioned earlier were equipped with cathode followers that would function in the stray magnetic field inside the concrete shielding. These chambers could be placed in the broad neutron beam[5] outside the cyclotron tank. One chamber was placed in the central portion of the beam in line with the probe and collimator (Fig. 4). Absorber slabs could be placed in front of this chamber in "poor geometry" fashion. The second chamber was placed to one side of the absorbers to serve as a monitor (Fig. 5). The absorbers were stacked in a conical array as shown in Fig. 4. The angular distribution of elastically scattered neutrons from nuclei is peaked in the forward direction and even for carbon the fraction singly scattered more than 45° is negligible; so the conical half-angle of 45° employed, permitted essentially all the elastically scattered neutrons to enter the "poor geometry" detector that would have entered even if the slabs were infinite in area. The attenuation, therefore, is a measure of the cross section for inelastic collision.

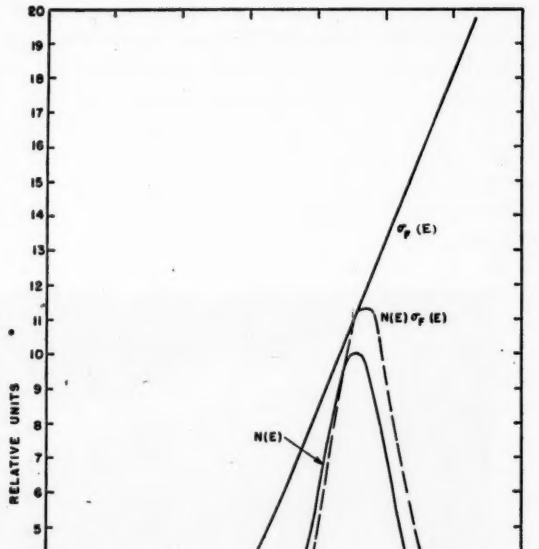

FIG. 3. $\sigma_f(E)$—fission cross section of bismuth, for neutrons $N(E)$—energy distribution of neutrons, and $N(E)\sigma_f(E)$—detection efficiency.

[4] R. Serber, Phys. Rev. **72**, 1008 (1947).
[5] A. C. Helmholz, E. McMillan, and D. Sewell, Phys. Rev. **72**, 1003 (1947).
[6] Hadley, Kelly, Leith, Segrè, Wiegand, and York, Phys. Rev. **75**, 357 (1949).
[7] Brueckner, Hartsough, Hayward, and Powell, Phys. Rev. **75**, 555 (1949).
[8] E. L. Kelly and C. Wiegand, Phys. Rev. **73**, 1135 (1948).

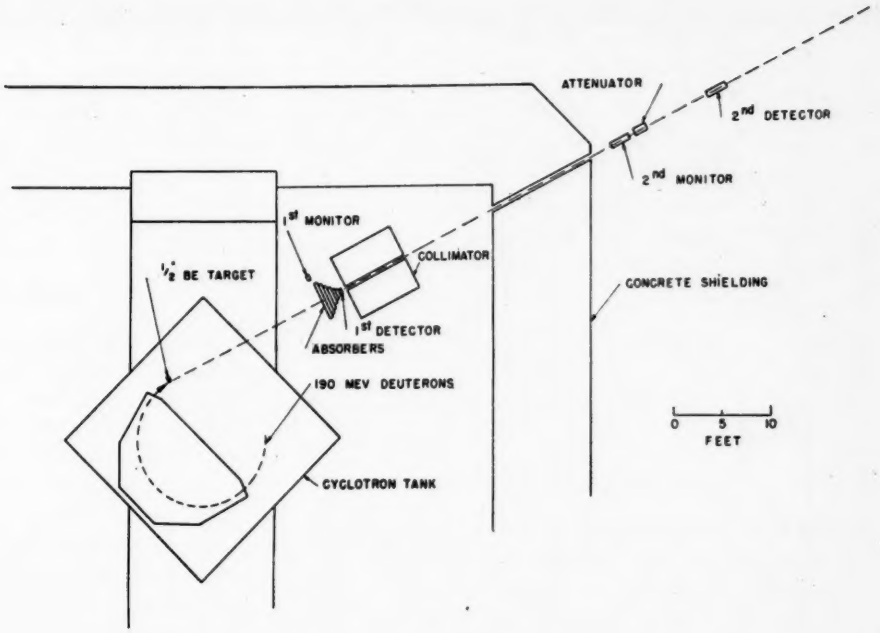

FIG. 4. Arrangement of apparatus.

A detector was also placed outside the shielding, as previously mentioned, in line with the collimated beam, so measurements of total and inelastic cross sections could be measured simultaneously.

The total thickness of attenuators used was restricted by the condition that the flux should be uniform over the first disk (largest in area). A survey of the uniformity was made by moving a shallow fission chamber with 2-inch diameter bismuth-coated plates over the region where the "poor geometry" attenuators were placed. The neutron flux was uniform (within 95 percent of the peak value) over an area 7 inches in radius. Disks greater than 8 inches in radius could not be used because the cyclotron deflector housing reduced the beam intensity at that radius. The attenuation was exponential over more than two inelastic mean free paths of copper, with no transition effects.

Magnitude of Attenuation Employed

As the attenuation was exponential, within the probable errors, for both the "good" and "bad" geometry experiments, it was not necessary to measure the slope of a semi-log plot of the intensity *versus* thickness (Fig. 6). Measurements were made with between one and two mean free paths of material.

For the experiments performed outside the shielding the monitor and detector counting rates were normally about equal with no attenuator present. The statistical error in the value of the cross section measured is equal to the statistical error of counting divided by the number of mean free paths of absorber. The principal counting error results from the detector reading with attenuator present. Slightly over two mean free paths of material was the most efficient length for a cross section determination, but to minimize diffraction scattering into the detector usually less than two mean free paths were employed.

ATTENUATOR MATERIALS

Physical Properties

The metals used in the experiments were usually machined cylinders and were measured by two different observers with micrometer or vernier calipers and carefully weighed. The liquids employed were weighed in a 500-ml volumetric flask, which was first calibrated

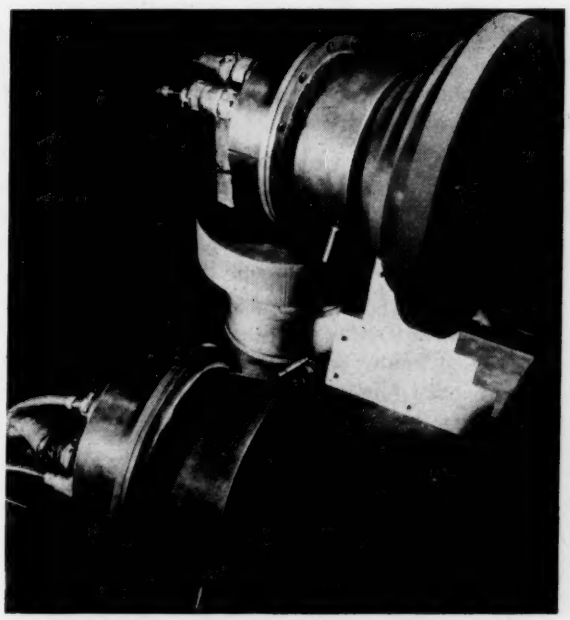

FIG. 5. Fission chambers and absorbers used in "poor geometry" measurements.

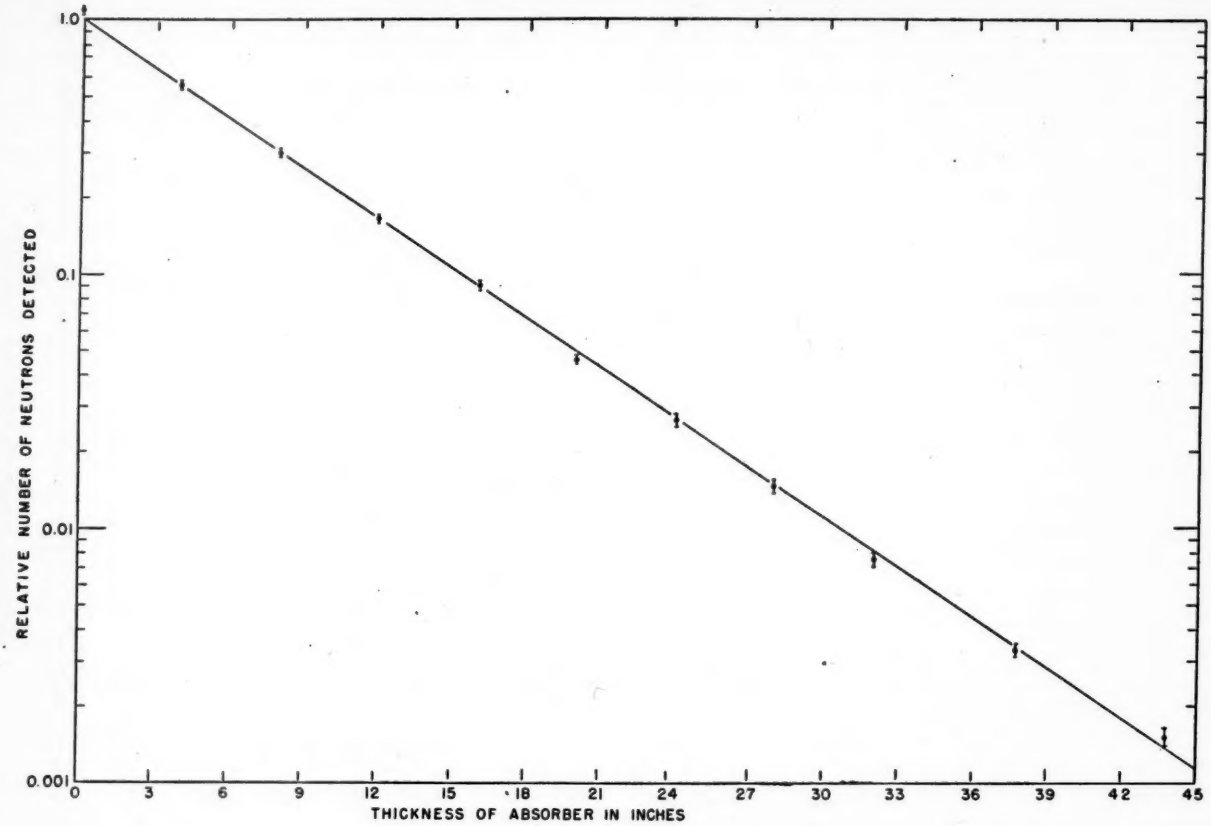

FIG. 6. Absorption of neutrons in Al.

by weighing distilled water at 19.1°. The measured value of the density was 0.9980 g/ml while the accepted value is 0.9984 g/ml.

The liquids were held in a 3-inch inner diameter cylindrical brass holder of variable length with $\frac{1}{16}$-inch thick brass end caps. During an experiment several counting intervals were employed with the holder alternately filled and empty.

The nitrogen cross section was derived from melamine, $C_3H_6N_6$. The melamine was carefully tamped in the brass holder in an effort to make the density as uniform as possible. An alternate empty holder with similar caps was employed during the "blank" counting intervals.

When the holder was used the beam from the 1-inch $\times$1.5-inch collimator was always carefully centered by means of x-ray film to minimize scattering from the brass walls.

Purity of Attenuators

Chemically pure materials were used, and the effect of minute impurities on the values obtained is negligible.

Because of its theoretical importance the total cross section of hydrogen was measured carefully on three separate occasions using pentane-carbon differences. Six graphite cylinders were machined to fit in the brass liquid holder. The length of the holder was adjusted (43 inches) so that the mass per unit area of carbon in the graphite was equal to the carbon in the pentane employed. The graphite cylinders were distributed along the length of the holder to simulate the distribution of carbon in the pentane. A counting interval was first taken with graphite in the holder. When the pentane was substituted the attenuation in the detector over the previous case was due solely to the hydrogen in the pentane. Hence the counting errors are due to these cycles only and the hydrogen cross section is directly obtained without the need of blank cycles, which would introduce added statistical errors. As only 0.5 mean free path of hydrogen was present and the statistical error of the cross section is the counting error divided by the mean free path, it was important to use the counting time efficiently.

The graphite and pentane were analyzed by the Pacific Chemical Laboratories for impurities which were as follows:

Sample	Impurities	Percentage
Graphite	Silicon	0.052
	Sulfur	0.067
	Iron	0.011
	Others	0.020
Pentane	Sulfur	0.045

The error introduced by these impurities is not significant.

The difference between the deuterium and hydrogen cross sections was determined directly in a similar experiment by filling the holder alternately with equal numbers of D_2O and H_2O molecules. The heavy water was 99.87 percent D_2O by weight.

RESULTS

Total Cross Sections

The data for the total cross sections measured outside the shielding are given in Table I. Corrections for diffraction scattering are included in a few cases where this is significant. Statistical errors given are in terms of standard deviations. The effect of background was investigated by placing fourteen mean free paths of various absorbers between detector and monitor. Without absorbers 950 detector counts were obtained for 1000 monitor counts. With absorbers no detector counts were obtained for 3600 monitor counts. Even a few detector counts would have meant negligible error from background. As the chambers have excellent high-voltage and discriminator characteristics, the error introduced by the equipment is probably less than one percent. Repeated measurements have given differences that appear to be purely statistical.

TABLE I. Total cross sections for 95-Mev neutrons measured with bismuth fission chambers.*

Element	Density g/cm³	Atomic number Z	Mass number A	$A^{\frac{1}{3}}$	Cross section $\sigma_t \times 10^{24}$ cm²	Radius, $R \times 10^{13}$ cm from model
Hydrogen		1	1	1.00	0.0745±0.002 0.073 ±0.003 0.071 ±0.002 0.073 ±0.0015 (ave.)	1.69±0.02
Deuterium		1	2	1.26	0.104 ±0.004	1.89±0.03
Beryllium	1.847	4	9	2.08	0.396 ±0.004	2.94±0.015
Carbon	1.580	6	12	2.29	0.502 ±0.004 0.502 ±0.005 0.490 ±0.004 0.494 ±0.004 0.501 ±0.006 0.498 ±0.003 (ave.)	3.20±0.01
Nitrogen		7	14	2.41	0.570 ±0.007	3.35±0.02
Oxygen		8	16	2.52	0.663 ±0.007	3.52±0.02
Aluminum	2.714	13	27	3.00	0.993 ±0.011	4.11±0.02
Chlorine		17	35.46	3.29	1.28 ±0.02	4.55±0.03
Copper	8.90	29	63.57	3.99	2.00 ±0.02 2.00 ±0.03	5.53±0.03
Tin	7.28	50	118.7	4.92	3.18 ±0.03 (3.13)	6.81±0.03
Lead	11.33	82	207.2	5.92	4.48 ±0.03 (4.38)	8.14±0.03
Uranium	18.89	92	238.1	6.20	4.92 ±0.06 (4.89)	8.58±0.05
Deuterium-Hydrogen Compounds		0	1	1.00	0.031 ±0.002	
H_2O	0.998				0.815 ±0.005 0.807 ±0.005	
D_2O	1.104				0.868 ±0.005	
Pentane C_5H_{12}	0.627				3.40 ±0.03 3.37 ±0.03 3.32 ±0.02	
CCl_4	1.592				5.61 ±0.07	
Melamine $C_3H_6N_6$					5.37 ±0.035	

* Values in parentheses are not corrected for diffraction scattering.

TABLE II. Inelastic cross sections for 95-Mev neutrons measured with bismuth fission chambers.

Element	σ_i/σ_t	$\sigma_i \times 10^{24}$ cm²	Total M.F.P. used
Carbon	0.460±0.016 0.457±0.026 0.434±0.023 0.431±0.024 0.454±0.022	0.496±0.012 0.489±0.018 0.497±0.017 0.498±0.017 0.502±0.016	0.60
Aluminum	0.42 ±0.015	0.995±0.02	0.94 (Dural)
Copper	0.39 ±0.005	2.005±0.02	2.5
Lead	0.40 ±0.01 0.38 ±0.01 0.40 ±0.01	4.46 ±0.06 4.46 ±0.06	1.9
Carbon (ave.)	0.45 ±0.015	0.497±0.008	

Inelastic Cross Sections

The inelastic cross-section measurements are subject to greater sources of error. The "poor geometry" detectors count inelastically scattered neutrons or neutrons ejected from nuclei if their energies are above the threshold for bismuth fission. The inelastic cross sections obtained, therefore, represent a lower limit to the true values. However, it is not expected that the contribution of neutrons over threshold energy from inelastic processes is large enough to modify the present interpretations.

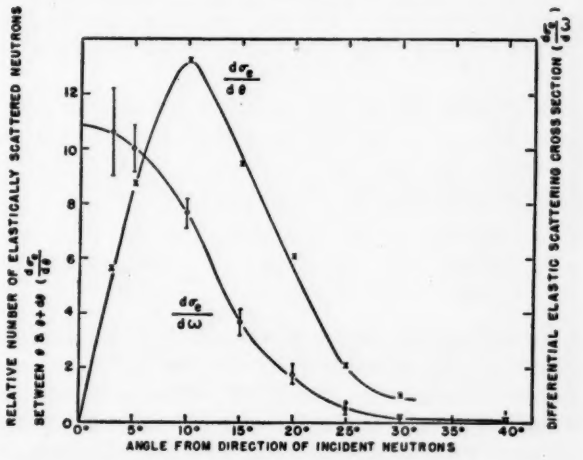

FIG. 7. Angular distribution of elastically scattered neutrons from carbon.

Elastically scattered neutrons will have a greater path length than undeviated neutrons in both the absorber and the bismuth layer of the detector. The relative probability of detection for different neutron paths is discussed in the appendix. Table II contains the experimental results. The ratio of σ_i/σ_t is given, since it is independent of density determinations of the material used and is measured directly. The total cross sections listed in Table II were measured with "better" geometry than those in Table I, and therefore require no corrections for diffraction. Actually dural was used,

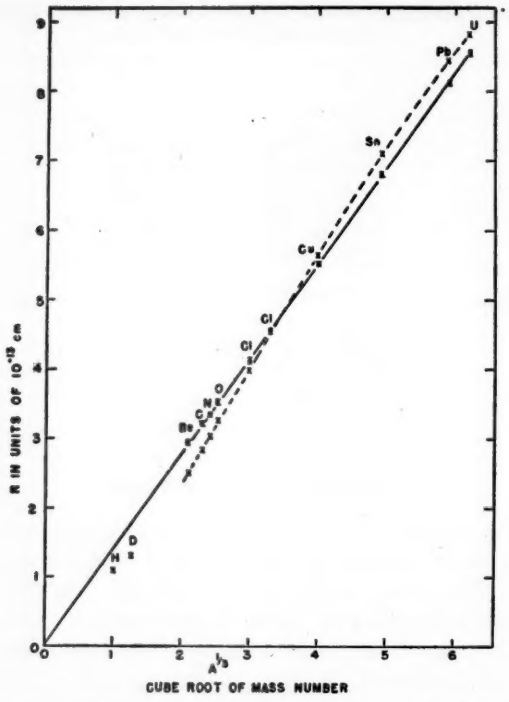

FIG. 8. Radii calculated from model assuming $K=3.00\times10^{12}$ cm^{-1} and $k_1=2.85\times10^{12}$ cm^{-1} define straight line of Eq. $R=1.38\times A^{\frac{1}{3}}\times10^{-13}$ cm. Dotted line is graph of radii calculated from $\sigma_t=2\pi R^2$ (opaque nucleus).

instead of aluminum, but the correction for the impurities (mainly copper) is negligible for the ratio of σ_i/σ_t.

An attempt was made to measure the ratio of σ_i/σ_t for carbon and copper using gold fission for neutron detection, since gold presumably has a higher fission threshold than bismuth. The values obtained were:

Element	σ_i/σ_t	σ_t
Carbon	0.42±0.04	0.48±0.35
Copper	0.38±0.015	1.92±0.06

The counting rate was about a factor of ten less for gold fission than for bismuth. From the total cross sections obtained, the average energy of neutrons detected is estimated to be between 100 and 105 Mev. Evidently the use of a higher threshold did not observably increase the ratio of σ_i/σ_t above the bismuth fission values. Both methods of detection agree, within the statistical errors.

An experiment was made to determine the angular distribution of elastically scattered neutrons from a carbon sphere. A fission chamber mounted on a radial arm pivoted below the sphere was used as the detector. The distribution is plotted in Fig. 7.

DISCUSSION OF RESULTS

The Transparent Nucleus Model

Fernbach, Serber, and Taylor[3] in a recent paper, have assumed a model for nuclei bombarded by high energy neutrons, in which the nucleus is regarded as a sphere of material characterized by an absorption coefficient and index of refraction, both of which are functions of the neutron momentum. Using their notation, k_1 is the increase of the propagation vector of the neutron wave upon entering the nucleus and K is the absorption coefficient. A wave going a distance x in nuclear matter will have its amplitude and relative phase changed by a factor $e^{(-\frac{1}{2}K+ik_1)x}$. The solutions for the inelastic and elastic cross sections are respectively:

$$\sigma_i=\pi R^2\left\{1-\frac{1-(1+2KR)e^{-2KR}}{2K^2R^2}\right\},$$

$$\sigma_e=2\pi\int_0^R|1-e^{(-K+2ik_1)s}|^2sds.$$

The form for σ_e is merely indicated, as the integrated expression is quite complex. R is the radius of the nucleus and $\sigma_t=\sigma_i+\sigma_e$.

Taylor has determined $k_1=2.85\times10^{12}$ cm^{-1} and $K=3.0\times10^{12}$ cm^{-1} to give the best straight line fit for the radii calculated from the total cross sections when R is plotted as a function of $A^{\frac{1}{3}}$. The equation for the line of best fit is $R=1.38A^{\frac{1}{3}}\times10^{-13}$ cm (Fig. 8).

The ratio of σ_i/σ_t for the afore-mentioned values of K and k_1 is given as a function of KR in Fig. 9 and the experimental values are shown.

Comparison with Data at 83 Mev

Cook, McMillan, Peterson, and Sewell[1] have measured total cross sections of the same elements in this laboratory using carbon disks, which have a 20-Mev threshold for the $C^{12}(n,2n)C^{11}$ reaction, for detectors. The average energy of the neutrons detected in their experiments is estimated to be 83 Mev as compared to 95 Mev for bismuth fission. The 95-Mev cross sections are roughly 10 percent smaller than those derived using carbon disks, indicating greater transparency at the higher energy.

ACKNOWLEDGMENTS

The authors wish to express their gratitude to Dr. Burton J. Moyer for his help and suggestions in car-

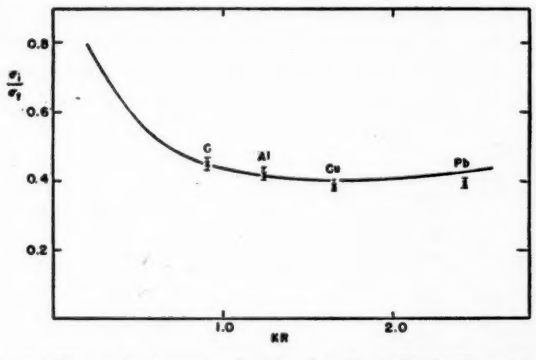

FIG. 9. Theoretical curve of σ_i/σ_t for $K=3.00\times10^{12}$ cm^{-1} and $k_1=2.85\times10^{-12}$ cm^{-1} with experimental points.

rying out the program, to the cyclotron crew for their cooperation in performing the experiments, and to Dr. E. Segrè, E. Kelly, and C. Wiegand for use of their vacuum evaporator for plating the chamber disks with bismuth and gold.

APPENDIX

Effect of Path Length on Inelastic Cross-Section Measurements

If I_0 be the number of neutrons/cm² on a plane absorber of thickness L, the number of neutrons/cm² suffering p elastic scattering events in traversing the material is given by:

$$I_{pL}=I_0\left(\frac{L}{\lambda_e}\right)^p\frac{1}{p!}e^{-L/\lambda_t}, \tag{A}$$

where λ_e and λ_t are the mean free paths for elastic scattering, and for any type of collision, respectively.

If $[d\sigma_e(\theta)]/d\omega$ is the differential cross section per unit solid angle for elastic scattering at angle θ, the number of neutrons/cm² emerging with angles between θ and $\theta+d\theta$ with respect to the incident neutrons is:

$$dI(\theta)=I_0\sum_{p=1}^{\infty}\left(\frac{L}{\lambda_e}\right)^p\frac{1}{p!}e^{-L/\lambda_t}\frac{1}{p}\frac{d\sigma_e(\theta/(p)^{\frac{1}{2}})}{d\omega}\frac{2\pi\sin\theta d\theta}{\sigma_e}$$

$$=\sum_{p=1}^{\infty}I_{pL}\frac{1}{p}\frac{d\sigma_e(\theta/(p)^{\frac{1}{2}})}{d\omega}\frac{2\pi\sin\theta d\theta}{\sigma_e}, \tag{B}$$

where it has been assumed that the effect of p elastic scatterings on the angular distribution is to broaden the distribution by a factor of $(p)^{\frac{1}{2}}$, and to decrease its height by $1/p$. Formulas A and B are only approximate since the path length is equal to L for small angles only.

The probability of a neutron emerging at angle θ, after sustaining an elastic collision into the θ direction within an element dx at depth x, is:

$$e^{-x/\lambda_t}\frac{dx}{\lambda_e}\cdot\exp\left[-\left(\frac{L-x}{\lambda_t\cos\theta}\right)\right].$$

The average attenuation experienced by neutrons following such a path is, from the above expression:

$$\frac{1}{L}\int_0^L\exp\left[-\frac{1}{\lambda_t}\left(x+\frac{L-x}{\cos\theta}\right)\right]dx.$$

The ratio of this attenuation at angle θ to the attenuation when $\theta=0$ is the relative probability of emergence for a neutron at angle θ compared with $\theta=0$.

After integrating, the result is

$$R_A=\frac{\lambda_t}{L}\frac{\cos\theta}{1-\cos\theta}\left\{1-\exp\left[\frac{-L}{\lambda_t}\left(\frac{1}{\cos\theta}-1\right)\right]\right\}.$$

The chance of a neutron inducing fission in the bismuth layer is proportional to its path length in the layer or to $1/\cos\theta$ since the chamber plates are normal to the undeviated neutrons.

In an elastic scattering event in the attenuator the scattered neutron will lose an amount of energy given by

$$\Delta E=\frac{2mE(1-\cos\theta)}{M+m(1-\cos\theta)},$$

where m is the neutron mass, M is the mass of the nucleus and E is the energy of the incident particle. Since the fission cross section is a function of energy the relative chance of producing a fission is

$$\sigma_f(E-\Delta E)/\sigma_f(E).$$

The probability of detecting a neutron scattered through angle θ relative to the probability of detecting an undeflected neutron is the product of the above factors for probability of emergence and probability of producing fission.

$$\frac{\pi_\theta}{\pi_0}=\frac{1-\exp[-n_t(1-\cos\theta)/\cos\theta]}{n_t(1-\cos\theta)}\frac{\sigma_f(E-\Delta E)}{\sigma_f(E)}, \tag{C}$$

where $n_t=L/\lambda_t$, the number of total mean free paths of attenuator.

The change in the bismuth fission cross section is given approximately by

$$d\sigma_f/\sigma_f=9/4(dE/E)$$

in the region of 90 Mev.

In our "poor geometry" experiments either n_t was small or the average angle of deviation was small (due to forward peaking of elastically scattered particles from heavy nuclei); so the exponent in Eq. (C) may be expanded:

$$\frac{\pi_\theta}{\pi_0}=\frac{1-[1-n_t(1-\cos\theta)/\cos\theta+n_t^2/2(1-\cos\theta)^2/\cos^2\theta+\cdots]}{n_t(1-\cos\theta)}\frac{\sigma_f(E-\Delta E)}{\sigma_f(E)}$$

$$\cong\left[\frac{1}{\cos\theta}-\frac{n_t(1-\cos\theta)}{2\cos^2\theta}\right]\frac{\sigma_f(E-\Delta E)}{\sigma_f(E)}. \tag{C'}$$

If we know the angular distribution of elastically scattered neutrons we can correct the inelastic cross section data using C′. For carbon the relative angular distribution of scattered neutrons in the annular region between θ and $\theta+d\theta$ is shown in Fig. 7. If the latter curve is multiplied by C′ which has been evaluated for carbon, the area under the curve increases by about 1.2 percent. Hence the number of singly scattered neutrons detected in the "poor geometry" experiment was increased by 1.2 percent due to the increased probability of detection for $\theta>0°$.

From A with $(L/\lambda_e)=0.33$ the relative number of

neutrons emerging that were elastically scattered p times may be determined:

$p=0$: 71 percent
$p=1$: 25 percent
$p=2$: 4 percent.

Those scattered once and twice will have a greater probability of detection and the increase on the total number of detector counts was roughly 0.25×1.2 percent $+0.04\times1.5$ percent (allowing a greater correction for double scattering) or 0.36 percent. This increase in the detector counts caused the inelastic cross section to be low by the increase divided by the number of inelastic mean free paths, 0.36/0.27 percent, or about 1.3 percent. Since the statistical error is 3.3 percent this correction is hardly significant.

The correction for the heavier nuclei is less, due to the greater forward peaking of the elastically scattered neutrons.

PHYSICAL REVIEW · VOLUME 77, NUMBER 5 MARCH 1, 1950

Neutron-Deficient Cesium Isotopes*

RICHARD W. FINK, FREDERICK L. REYNOLDS, AND D. H. TEMPLETON
Department of Chemistry and Chemical Engineering and Radiation Laboratory, University of California, Berkeley, California
(Received October 31, 1949)

The new isotopes Cs^{127} and Cs^{129} have been produced from iodine by irradiation with high energy helium ions. Their mass assignments were determined with a mass spectrograph. Cs^{127} decays with 5.5±0.5 hr. half-life with emission of positrons (1.2 Mev maximum energy), giving rise to the daughter activity 34-day Xe^{127}. Cs^{129} decays by electron capture with half-life 31±1 hr. A 30-min. activity, presumed to be Cs^{130}, was also produced, but its mass assignment is uncertain.

THE successful completion of a thermally ionizing mass spectrograph in this laboratory and the availability of high energy helium ions from the Berkeley 184-in. cyclotron have led us to investigate neutron-deficient isotopes of alkali metals, which are relatively easy to ionize. Some results for rubidium isotopes have already been reported.[1] This paper is concerned with two new cesium isotopes.

The cesium isotopes of mass 131 and greater have been studied extensively.[2] The only report of lighter isotopes seems to be a 30-min. period produced from iodine with helium ions, presumably of 16 Mev energy from the Purdue University cyclotron.[3]

IODINE BOMBARDMENTS

Stable I^{127} (100 percent abundance) was bombarded in the form of ammonium iodide with 60-Mev helium ions in the Berkeley 184-in. cyclotron for periods of from one to four hours. The ammonium iodide was wrapped in 0.001-in. aluminum foil and irradiated mounted on a water-cooled copper block on the cyclotron probe. Elemental iodine sealed in a platinum capsule was also bombarded. Ammonium iodide was also bombarded with 36-Mev helium ions from the Crocker 60-in. cyclotron.

The cesium radioactivities induced were isolated from the target material by chemical procedures[4] designed to remove Xe, I, Te, Sb, Sn, and most other elements except alkali metals. Carrier cesium was added in some cases, but it was found that very little could be tolerated in samples destined for the mass spectrograph. It was found that sufficient Cs^{133} to serve as a reference line on the mass spectrum was provided

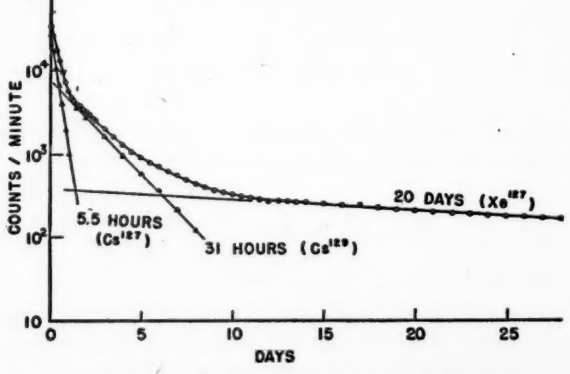

FIG. 1. Decay curve of cesium radioactivities induced by 60-Mev helium ions from ammonium iodide. The points at high counting rates were derived from data obtained at a lower geometry.

* This work was supported by the AEC.

[1] Reynolds, Karraker, and Templeton, Phys. Rev. 75, 313 (1949).

[2] For references, see G. T. Seaborg and I. Perlman, "Table of isotopes," Rev. Mod. Phys. 20, 585 (1948); also, Yaffe, Kirsch, Standil, and Grunlund, Phys. Rev. 75, 699 (1949); N. Sugarman, Phys. Rev. 75, 1473 (1949); J. L. Meem and F. Maienschein, Phys. Rev. 76, 328 (1949); and J. S. Osoba, Phys. Rev. 76, 345 (1949). The assignment of the 10-day cesium to mass 131 has now been confirmed with the mass spectrograph by Karraker, Reynolds, and Templeton, UCRL Report-285 (February 11, 1949) (to be published).

[3] "J. R. Risser and R. N. Smith, private communication from K. Lark-Horowitz," quoted from G. T. Seaborg and I. Perlman, reference 2.

[4] For details, see R. W. Fink, M.S. thesis, University of California, Berkeley, 1949.

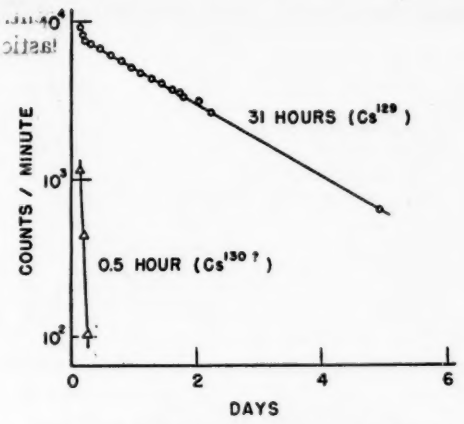

FIG. 2. Decay curve of cesium radioactivities induced from ammonium iodide by 36-Mev helium ions.

by 0.1 μg. Although the first chemical technique yielded sufficient cesium activity for all experimental purposes except mass spectrograph work, it was found that ignition of cesium chloride in an open dish to remove ammoium salts resulted in serious loss of cesium due to the high volatility of CsCl.

To prevent this loss and thereby isolate sufficient cesium activity for mass spectrograph runs, the ammonium iodide was decomposed in moderate vacuum by gentle heating with a drop of nitric acid and a few drops of sulfuric acid. A cold finger cooled with carbon dioxide snow near the sample condensed the iodine and water which escaped. Within three minutes the residue solution could be removed, containing most of the cesium activity and relatively little of the target material. This procedure resulted in substantially better yields of activity.

CESIUM RADIOACTIVITIES

In Fig. 1 is shown the decay curve for the cesium radioactivity from a 60-Mev alpha-bombardment of ammonium iodide. The sample, mounted as cesium chloride and covered with cellulose tape, was counted with an argon-alcohol Geiger tube. The decay curve is resolved into 5.5-hr., 31-hr., and 20-day components. When the chemical procedure was completed rapidly enough, a half-hour period was also observed. With 36-Mev helium ions, only the half-hour and 31-hr. activities were observed in the decay curve, Fig. 2.

After the 5.5-hr. cesium was dead, a portion of the cesium was redissolved, boiled to expel xenon, and evaporated on a counting disk. In Fig. 3 are compared the decay curves of such a sample and a portion which was not disturbed. The 31-hr. activity is not affected by this procedure. The removal of the long 20-day activity by boiling suggested that it is a xenon daughter of the 5.5-hr. cesium. It cannot be the daughter of 31-hr. cesium.

To establish the identity of the long-lived activity, a mixture of freshly isolated 5.5-hr. and 31-hr. cesium activity was placed in a small vacuum line equipped with several glass bulbs. The system was evacuated and the sample was isolated from the pumps and the bulbs. One bulb at a time was opened and cooled with liquid nitrogen, while the sample was heated. Glass wool and loops in the connecting tubing acted as a safeguard against mechanical transfer of non-gaseous material. The bulb was then sealed off and mounted on a holder for counting. The first bulb filled exhibited 109 counts/minute of activity; the walls were too thick for observation of soft radiations. This activity decayed for six weeks with a half-life of 30 to 35 days. Other bulbs filled after the 5.5-hr. activity was dead yielded no observable activity.

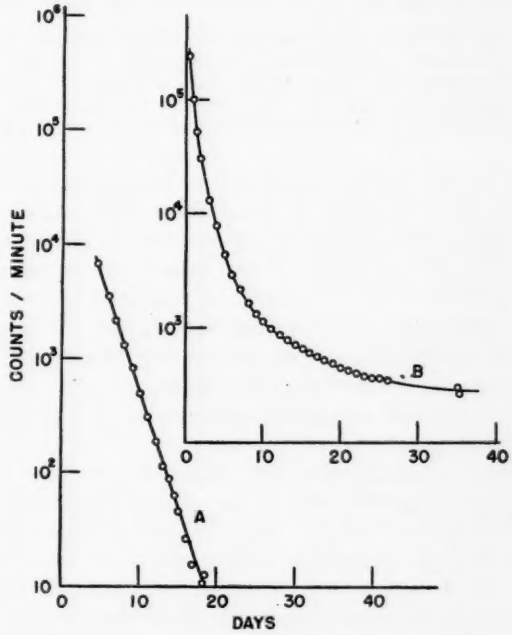

FIG. 3. Effect of repurification. Decay curve A is for a sample from which xenon was expelled by boiling from a solution after the 5.5-hr. cesium was effectively dead. Curve B is for a cesium sample which was not disturbed.

This experiment was repeated twice with similar results. On the basis of these observations, the long-lived activity is identified as the 34-day xenon[5] assigned to Xe^{127}, produced by decay of the 5.5-hr. cesium. Xe^{127} is reported to emit a 0.9-Mev gamma-ray, which is the activity counted in the glass bulb. The shorter half-life observed in cesium samples is caused by diffusion of xenon through the cellulose tape covering the sample.

MASS-SPECTROGRAPHIC EXPERIMENTS

In our mass spectrograph the sample is placed as a solid on a tungsten or platinum filament and is ionized by heat. The efficiency of the ionization for cesium has been found to be strongly dependent on the chemical

[5] Creutz, Delsasso, Sutton, White, and Barkas, Phys. Rev. 58, 481 (1940); M. Camac, Plutonium Project Report CC-2409 (October, 1944); Overstreet, Jacobson, Scott, and Hamilton, Plutonium Project Report CH-379 (December 1942).

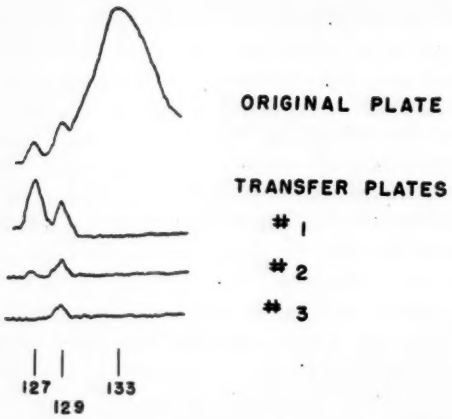

FIG. 4. Microphotometer tracings of mass spectrograph plates. Transfer plate 1 was exposed to the original plate, emulsion to emulsion, immediately after removal from the mass spectrograph, and remained on for 24 hr. Transfer 2 was exposed for the next 48 hr. Then transfer 3 was exposed approximately the next 72 hr.

state of the sample. Similar effects have been noted for some other elements, such as barium and thallium. If the photographic plate is replaced by an electrometer receiver, an integration of the current is a measure of the number of atoms ionized and passed by the slits of the apparatus. The ratio of the amount of sample placed on the filament to the amount found with the electrometer is called the "loss factor."

Experimental values for three cesium salts are listed in Table I.

Since the geometrical loss factor on the mass spectrograph is of the order of 50, with cesium sulfate at least 25 percent of the cesium is ionized. One expects 100 percent ionization under optimum conditions, because of the very low ionization potential (3.87 volts) of cesium. The very low ionization of the chloride and nitrate salts is probably due to greater volatility in vacuum. The presence of ammonium salts or other foreign matter operates to lower the ionization efficiency by increasing mechanical loss of chunks of material from the platinum filament. Only by increasing the yield of activity by use of the vacuum sublimation procedure combined with especial care to prepare practically weightless samples of the sulfate of the radioactive cesium isotopes, instead of the chloride used in early experiments, were successful mass spectrograph results finally attained.

Mass spectrograph plates showing dark lines at mass numbers 127, 129, and 133 (stable carrier) were obtained, and transfer plates showed the radioactivity of lines 127 and 129; after the 5.5-hr. Cs^{127} activity had

TABLE I. Loss factors of various cesium salts on the mass spectrograph.

Salt	Loss factor
Cesium nitrate, $CsNO_3$	1.4×10^6
Cesium chloride, CsCl	8.3×10^4
Cesium sulfate, Cs_2SO_4	180

effectively decayed out, the radioactive line at mass 129 still gave good transfer plates. This is shown in Fig. 4 which consists of microphotometer tracings of an original mass spectrograph plate and three transfer plates made at designated times after bombardment.

RADIATIONS OF 5.5-HR. Cs^{127}

A crude magnetic spectrometer and absorption methods were used to examine the radiations from Cs^{127} and Cs^{129}. Positrons were found with maximum energy about 1.2 Mev. The activity of these positrons decayed with a 5.5-hr. half-life. Lead absorption curves showed 0.5-Mev gamma-rays due to annihilation but no harder gamma-rays. Softer gammas may have been present. Negative electrons of energy of the order of 0.3 Mev and x-rays were also present, but they have not been proved to belong to Cs^{127}.

RADIATIONS OF 31-HR. Cs^{129}

No positrons were observed for Cs^{129}, and it very likely decays entirely by electron capture. It emits 0.3-Mev conversion electrons, K and L x-rays, and gamma-rays of about 0.5 Mev.

RADIATIONS OF THE 30-MIN. CESIUM

We have little data concerning the 30-min. activity. It emits x-rays and gamma-rays of the order 0.5 Mev. We have not tested it for positrons or negative electrons. Its production with 16-Mev helium ions[3] implies that it is Cs^{130}. Our data are consistent with that assignment. Cs^{128} has not been observed, but its half-life must be 30 min., or less. It is conceivable that our 30-min. activity is in part due to Cs^{128}.

ACKNOWLEDGMENTS

We wish to express our sincere appreciation to James T. Vale and B. Rossi and the crews of the 184-in. and 60-in. cyclotrons; to D. G. Karraker, for operation of the mass spectrograph on many night runs; and to Lieselotte K. Templeton, for microphotometer tracings of the mass spectrograph plates.

Nuclear Pairs and Gamma-Radiation from Excited States of O^{16}

V. K. RASMUSSEN, W. F. HORNYAK,* C. C. LAURITSEN, AND T. LAURITSEN
Kellogg Radiation Laboratory, California Institute of Technology, Pasadena, California
(Received November 14, 1949)

The nuclear pairs and gamma-radiation from the reaction $F^{19}(p\alpha)O^{16*}$ have been studied at several of the resonances from 840 to 1380-kev proton bombarding energy. The pair spectrum agrees well with that predicted theoretically for nuclear pairs, showing clearly that the pairs observed are not due to internal conversion of gamma-radiation. The end point observed yields 6.04±0.03 Mev for the location of the first excited state of O^{16}. The gamma-radiation comprises at least two components, with relative intensities differing for the four resonances studied. The energies observed are 6.14±0.04 Mev and 6.99±0.05 Mev at the 873.5 and 1381-kev resonances, and 6.14±0.04 Mev and 7.09±0.06 Mev at the 939-kev resonance.

INTRODUCTION

WHEN fluorine is bombarded with protons in the energy range 0–2 Mev, gamma-radiation, electron-positron pairs not associated with gamma-radiation, and alpha-particles are observed. The several groups of alpha-particles arise from the reaction

$$F^{19}+H^1\rightarrow(Ne^{20})\rightarrow O^{16}+He^4 \quad (Q=8.12 \text{ Mev})$$

in which the residual nucleus, O^{16}, may be left in the ground state or in one of a number of excited levels whose subsequent decay to the ground state accounts for the gamma-radiation and pairs.[1] Which of the O^{16} states is formed depends markedly on the proton energy, and the resonances for production of long range alpha-particles (ground state), pairs, and gamma-rays have been intensively studied.[2]

The pairs arise from the lowest excited state of O^{16}, from which gamma-radiation is presumably forbidden by the selection rule excluding $J=0$ to $J=0$ transitions. The state thus decays by emission of an electron-positron pair which is created by forces acting only within the nucleus.[3] It is this feature of the forces from which the distinction between "nuclear" and "internal conversion" pairs arises since, in the latter case, the pairs are formed in a distance of the order of the Compton wave-length from the emitting nucleus. The maximum energy of the nuclear pairs of O^{16} has been determined by Tomlinson[4] as 4.9±0.2 Mev, giving a level energy of 5.9±0.2 Mev. The spectrum has been investigated by Kojima[2] and shown to be consistent with the hypothesis of their nuclear origin. The angular correlation between electrons and positrons has also been shown by Devons and Lindsay[5] to be consistent with theoretical expectations.* A part of the work of the present paper relates to a more accurate determination of the pair end point and the momentum distribution.

Walker and McDaniel[6] have shown that the gamma-radiation comprises two components, at 6.13±0.06 and 6.98±0.07 Mev, the relative intensities of which depend on bombarding voltage. This result has recently been confirmed by Burcham and Freeman[7] who have observed the corresponding alpha-particle groups but who find indication of a third alpha-group at the 939-kev resonance, suggesting that an additional gamma-ray of energy about 7.2 Mev should exist. These observations have been extended in this laboratory[8] to show that all three groups exist at this and other resonances, with varying relative intensities. Further measurements of

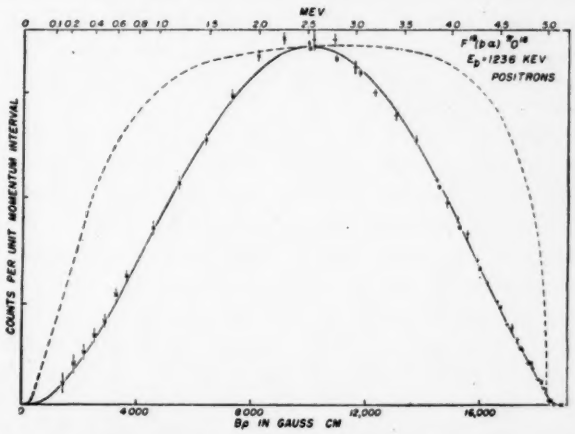

FIG. 1. Momentum distribution of positrons from pair state of O^{16}. Plus signs represent early data, from the CaF_2 on copper target; crosses represent data from the BeF_2 target. The solid curve is the theoretical distribution for nuclear pairs, while the dashed curve gives the distribution expected from pairs due to internal conversion of a gamma-ray.

* Now at the Brookhaven National Laboratory, Upton, Long Island, New York.

[1] Capture gamma-radiation, from transition to the ground state of Ne^{20} has also been observed. S. Devons and H. G. Hereward, Nature **162**, 331 (1948).

[2] See, for example, Streib, Fowler, and Lauritsen, Phys. Rev. **59**, 253 (1941); Bennett, Bonner, Mandeville, and Watt, Phys. Rev. **70**, 882 (1946); S. Kojima, Proc. Imp. Acad. Tokyo **19**, 282 (1943).

[3] J. R. Oppenheimer and J. S. Schwinger, Phys. Rev. **56**, 1066 (1939).

[4] E. P. Tomlinson, Phys. Rev. **60**, 159A (1941); E. P. Tomlinson, thesis, California Institute of Technology (1941).

[5] S. Devons and G. R. Lindsay, Nature **164**, 539 (1949).

* *Note added in proof.*—Devons, Hereward, and Lindsay (Nature **164**, 586 (1949)) have measured the mean lifetime of this state as 7×10^{-11} sec.

[6] R. L. Walker and B. D. McDaniel, Phys. Rev. **74**, 315 (1948).

[7] W. E. Burcham and Joan M. Freeman, Phys. Rev. **75**, 1756 (1949).

[8] Chao, Tollestrup, Fowler, and Lauritsen, Bull. Am. Phys. Soc. **24**, No. 8, 11 (1949).

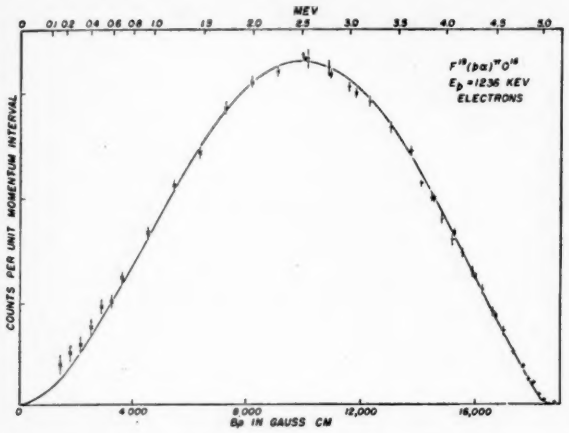
MEV
0 0.1 0.2 0.4 0.6 0.8 1.0 1.5 2.0 2.5 3.0 3.5 4.0 4.5 5.0
$F^{19}(p\alpha)^{17}O^{16}$
E_p = 1236 KEV
ELECTRONS
COUNTS PER UNIT MOMENTUM INTERVAL
0 4,000 8,000 12,000 16,000
Bρ IN GAUSS CM

FIG. 2. Momentum distribution of electrons from the pair state of O^{16}.

the gamma-ray energies and intensities as a function of bombarding voltage are reported in the present paper.

APPARATUS

The instrument used for the study of both gamma-rays and pairs was a magnetic lens spectrometer which has been described previously.[9] Targets placed at the source position of the spectrometer were bombarded by a proton beam entering along the axis. Electrons originating either in the target itself or ejected by the gamma-radiation from suitable converters affixed to the target were focused by the magnetic field onto an annular slit and counted in a bell jar type counter provided with a 2 mg/cm² mica window.[10] The configuration of the magnetic coils and the stops of the spectrometer were such as to yield a resolution (full width at half-maximum) of 2.5 percent; electrons leaving the target at angles of 9° to 16° to the spectrometer axis were accepted. Helical baffles permitted distinction between positive and negative electrons. The target assembly was supported by a fine wire to minimize scattering effects; insulation of the support made possible measurement of the proton beam for monitoring. For targets too thin to stop the protons, the current was measured by means of an insulated collector plate inside the spectrometer. The various resonances were identified by running rough excitation functions, the resonance energies quoted being those of Bennett *et al.*[2] multiplied by 873.5/862 to conform to the presently accepted voltage scale.[11]

Particularly in the work on pairs, considerable attention was given to the problem of distortion of the spectrum by scattering. The first experiments were made with a thin (~50-kev stopping power for 900-kev protons) CaF_2 target evaporated on 0.001-inch copper foil using only the minimum number of baffles required to define the spectrometer acceptance angle and annular focus. The resulting spectra contained a relatively large number of electrons and positrons with energies below 1 Mev. Subsequent work with the spectrometer, using the well-known N^{13} positron spectrum for checking, gave indication of excessive scattering in the arrangement used and led to considerable improvement in the baffling (see Fig. 1 of reference 9). The pair spectrum was then redetermined, with particular emphasis on the low energy region, using, as a further precaution against scattering, a target consisting of a 0.3 mg/cm² Be foil which had been exposed to HF vapor.[12] Data taken with the new arrangement agreed well with the earlier results above 2.0-Mev electron energy, but indicated fewer electrons below this energy, the deviation increasing with decreasing energy to about a factor of 2.5 at 0.5 Mev. All the earlier points below 2.5 Mev have been rejected in plotting the final data.

For gamma-ray measurements, Compton electrons ejected from a 250 mg/cm² beryllium disk roughly 1 cm in diameter were observed. The same CaF_2 on copper foil target used in the early pair measurements served as the target, and a gamma-ray counter, shielded by 1 inch of lead, was used as a monitor.

RESULTS—I. NUCLEAR PAIRS

Figures 1 and 2 present the momentum distribution of positive and negative components respectively, as observed at the 1236-kev pair resonance. Figures 3 and 4 present the portions near the end points. Field insensitive cosmic-ray and local laboratory background of about 3 percent of the peak height has been subtracted from the data presented. Uncertainties in this

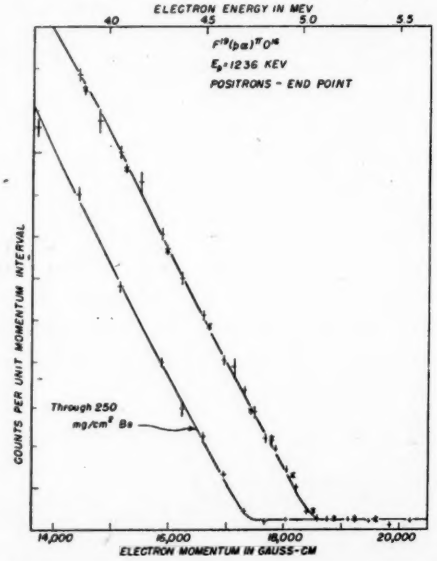

FIG. 3. High energy end of the positron distribution. The lower curve shows the energy loss observed in 250 mg/cm² Be.

[9] Hornyak, Lauritsen, and Rasmussen, Phys. Rev. **76**, 731 (1949).

[10] Radiation Counter Laboratories, Chicago, Illinois.

[11] Herb, Snowdon, and Sala, Phys. Rev. **75**, 246 (1949).

[12] Blank Be foils showed negligible yield at the proton energies used.

background are important only for the first three or four low energy points, where the additional error may amount to as much as the statistical probable error shown.

The solid curves in Figs. 1–4 are calculated from the theoretical expressions given by Oppenheimer,[13] modified slightly by inclusion of the Coulomb factor (as in the case of ordinary pair formation)[14] and including the effect of finite instrument resolution. For comparison, the calculated distribution of internal conversion pairs[15] from electric dipole radiation is shown by the dashed curve in Fig. 1 (higher multipole orders lead to even flatter distributions). It is of interest to observe that the apparent end point of the positron spectrum is some 60 kev higher than that of the electron distribution. The difference results from the effect of the Coulomb factor, which gives a non-zero probability of finding a positron of maximum energy in the primary spectrum but a probability approaching zero of finding an electron of maximum energy. With the resolution used in these experiments, this appears as a difference in the end points for positrons and electrons (compare Figs. 3 and 4).

The choice of the energy parameter in making the best fit of the theoretical distribution to the experimental points permits the determination of the maximum energy of either the positive or negative component to an accuracy that is limited, in our case, only by the accuracy to which the spectrometer calibration is known. This maximum energy was taken as the same for both positive and negative components, 5.017±0.03 Mev, including the most probable energy loss in the copper backing of 18 kev.[16] The energy of the O^{16} level involved is obtained by adding the rest mass of the pair to the obtained maximum energy, yielding 6.04 ±0.03 Mev. No Doppler shift correction has been included in this value, since from the expressions given by Oppenheimer and Schwinger[3] one can estimate that the lifetime of this state is 10^{-12} sec., while the average stopping time for the excited O^{16} nucleus in the CaF_2 target is about 10^{-13} sec.

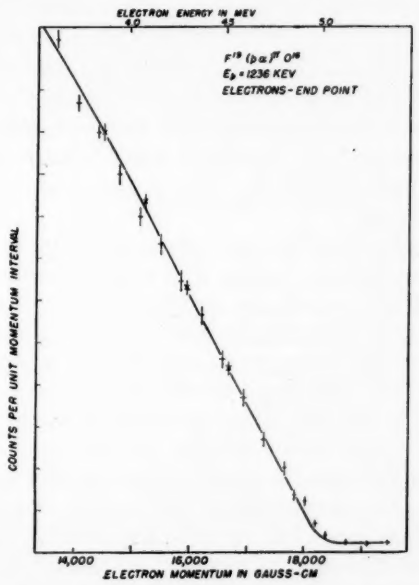

FIG. 4. High energy end of the electron distribution.

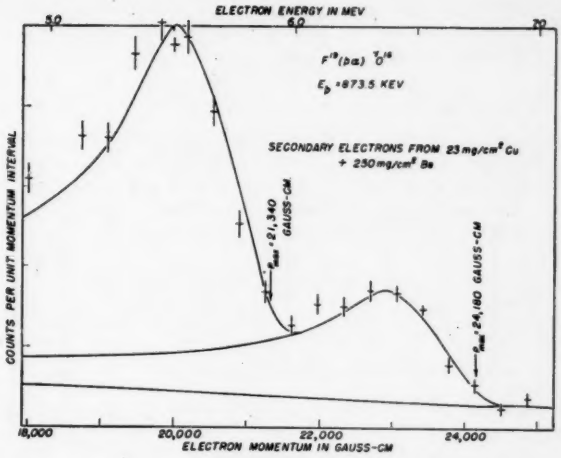

FIG. 5. Compton electrons ejected from 250 mg/cm² Be converter by gamma-radiation produced at the 873.5-kev resonance in $F^{19}(p\alpha)\gamma O^{16}$.

RESULTS—II. GAMMA-RADIATION

Curves showing the distribution of recoil Compton electrons observed for proton bombarding energies corresponding to the gamma-ray resonances at 873.5, 939, and 1381 kev are presented in Figs. 5, 6, and 7. Sufficient data were also obtained at the 1353-kev resonance to make possible an estimate of the relative intensities of the gamma-rays, but not a precise determination of their energies. The energies and relative intensities of the various gamma-rays were determined by comparing the observed distributions with those calculated from the Klein-Nishina formula and the spectrometer geometry, as outlined in the Appendix. This calculation involves assumptions as to the distribution in energy loss for electrons originating uniformly throughout the thickness of the converter. In view of the high energy of the electrons and the low atomic number of the converter, the distribution was taken as rectangular and of constant width, on a momentum scale, over the range of momenta involved. The width of the rectangle was determined experimentally by observing the end point of the nuclear pair distribution

[13] J. R. Oppenheimer, Phys. Rev. **60**, 164A (1941).
[14] W. Heitler, *The Quantum Theory of Radiation* (Oxford University Press, London, 1936), p. 197.
[15] M. E. Rose and G. E. Uhlenbeck, Phys. Rev. **48**, 211 (1935).

[16] The spectrometer calibration is based on $B\rho = 10{,}000$ gauss-cm for the X line from a ThB deposit. The end point quoted was determined from the data taken with the CaF_2 on copper target. Data taken with the BeF_2 target give 5.022±0.04 Mev. The higher energy points taken with this target have been shifted down by approximately 18 kev to facilitate comparison with the earlier data.

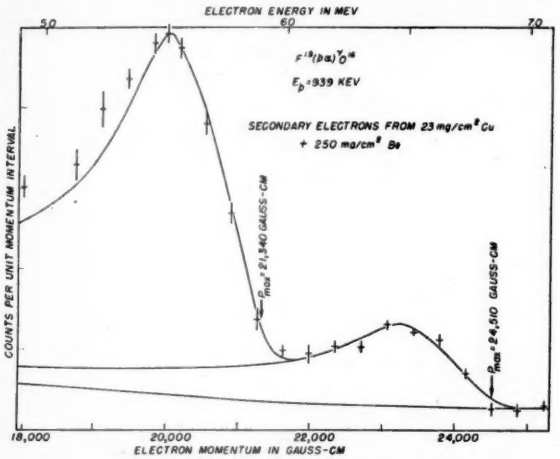

FIG. 6. Compton electrons observed at 939-kev resonance.

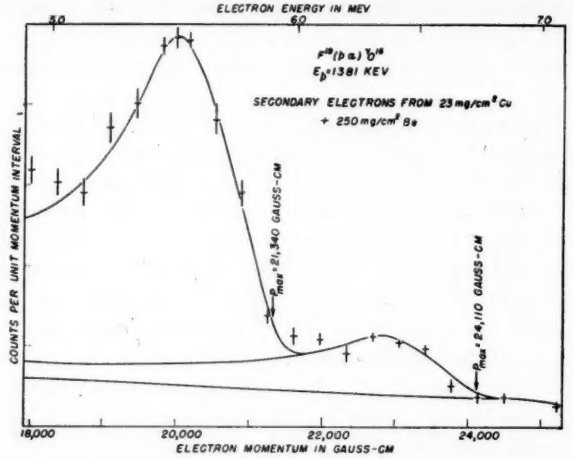

FIG. 7. Compton electrons observed at 1381-kev resonance.

through the same 250 mg/cm² Be that was used as the Compton converter (see Fig. 3). The curve was shifted down by 345±15 kev, which is somewhat larger than the most probable energy loss calculated for this thickness of beryllium. To this number must be added the most probable energy loss of 18 kev for 0.001 inch of copper. The best fits, shown by the curves of Figs. 5–7, were finally obtained by using a rectangle 410 kev wide of which perhaps 10 kev may be attributed to the effect of Doppler broadening. The agreement with the experimental points is considered satisfactory down to and including the peak. The departure below the peak is, possibly, the result of using a rectangular distribution in energy loss; the addition of a tail extending somewhat beyond the average energy loss value would doubtless yield better agreement. The fit on the high energy side is quite insensitive to such modification since both the initial peak of the primary Compton spectrum and the instrument resolution are narrower than the assumed rectangle. For this reason, and because the calculated curve makes more effective use of the data than would a simple extrapolation of the high energy edge, the parameters of the best calculated curves were used to obtain the maximum momentum of the Compton electrons from which the gamma-ray energies are determined by adding the minimum energy of the recoil quanta. A Doppler correction of $\frac{1}{4}$ percent for the center of mass motion is subtracted from the gamma-ray energy to obtain the level energy since the half-life for 6-Mev electric quadrupole radiation, for example, is $\sim 5\times 10^{-15}$ sec., compared to the stopping time for the O^{16} nucleus of $\sim 10^{-13}$ sec. The results are given in Table I, where the relative intensities of the two gamma-rays appearing at each resonance, as obtained from the calculated fits, are also presented.

Although the conditions of the present experiments were not conducive to accurate absolute yield determinations, such yields can be calculated at least to an order of magnitude, and are of interest because they do not involve estimates of the efficiency of gamma-counters, as do previously published values. They are obtained from an estimate of the solid angle of the spectrometer (1.2 percent of a sphere) and the calculated Compton distribution. The first column of yields in Table I are those observed with the 50-kev CaF_2 target. By using the excitation functions of Bennett *et al.*,[2] one may estimate the thin target yields per kev of CaF_2 given in the second column. The thin target yields include the contribution of the continuous background, which is difficult to separate from the resonance yield proper. Because of uncertainties in the solid angle, the current measurement, and the target thickness, the values quoted may be in error by as much as 40 percent.

DISCUSSION

The yields obtained agree reasonably well with the results of others.[2,17] The relative intensities of the 6 and 7-Mev radiation agree with those predicted from the alpha-groups by Burcham and Freeman[7] and are not inconsistent with the thick target work of Walker and McDaniel.[6]

The gamma-ray energies observed at the 873.5 and 1381-kev resonances agree well with those of Walker and McDaniel, while the results at the 939-kev resonance are not inconsistent with the assumption that a higher energy component exists, as suggested by Burcham and Freeman. The resolution and statistical accuracy of individual points obtained in the present experiment are such that one can say only that the difference between the results at the 939-kev resonance and the other resonances is just outside the probable error. However, Chao *et al.*[8] have clearly separated two alpha-groups corresponding to gamma-ray states in O^{16} at around 7 Mev. They find that at the 939-kev resonance only the short range group is of significant intensity but that at the 873.5 and 1381-kev resonances the two groups are of roughly equal intensity. Using

[17] W. A. Fowler and C. C. Lauritsen, Phys. Rev. **76**, 314 (1949).

TABLE I. Summary of results.

E_{res} (kev)	E_{max} (Mev)	E_γ (Mev)	E_{level} (Mev)	I_6/I_7**	$Y\times10^6$† $y\times10^{10}$†† Disintegrations per proton	
γ873.5	5.906	6.151±0.04	6.14±0.04	*2.5		
	6.756	*7.002±0.06	*6.99±0.06			
γ939	5.906	6.151±0.04	6.14±0.04	3.3	15	120
	6.854	7.100±0.06	7.09±0.06			
γ1353		(6.10 ±0.06)	(6.09±0.06)	1		
		(7.05 ±0.1)	(7.03±0.1)			
γ1381	5.906	6.151±0.04	6.14±0.04	*4.7		
	6.735	*6.981±0.06	*6.96±0.06			
π843					0.49	1.1
π1236	5.018±0.03	—	6.04±0.03	—	1.42	3.7

* These values represent two unresolved high energy components.
** Relative intensity of 6- and 7-Mev radiation.
† Yield from CaF_2 target 50 kev thick for 900-kev protons.
†† Estimated thin target yield from CaF_2 one-kev thick at the resonance.

this information, our results may be interpreted as indicating levels in O^{16} that decay by gamma-ray emission at 7.09±0.06, ≈6.9, and 6.14±0.04 Mev.

The nuclear pair level is at 6.04±0.03 Mev, 100±30 kev below the lowest gamma-ray level. The close agreement between the experimental and theoretical pair distributions confirms that these pairs are of nuclear origin, and are not ascribable to internal conversion of gamma-radiation. It may be noted, however, that the pair state may also decay by the emission of two quanta in successive electric dipole transitions.[3] Whether or not such two-quantum decay can compete successfully with pair emission depends principally upon the nuclear matrix elements. Since the two quanta would have a continuous energy distribution, and since it is clear from the work of others[2] that their intensity is at most one or two times that of the nuclear pairs, they would be difficult to detect, and would not have been observed in the present experiments.

ACKNOWLEDGMENTS

We are greatly indebted to Professors R. F. Christy and W. A. Fowler for invaluable assistance on many aspects of this investigation, and to Professor Christy and Dr. E. R. Cohen for calculation of the nuclear pair distribution and of various energy loss values used in the analysis. This work was assisted by the Joint Program of the ONR and AEC.

APPENDIX—COMPTON DISTRIBUTION

The source geometry used in these experiments is shown in Fig. 8a. The converter was a thin disk of beryllium to which the gamma-ray source, much smaller in diameter, was attached directly. The Compton scattering process may then be described in terms of the coordinates of Fig. 8b. Here we have:

θ=angle between the γ-quantum and the spectrometer axis.
θ_0=angle between the recoil electron and the spectrometer axis.
ω=angle between the primary γ-quantum and the recoil electron.
ϵ=angle between the primary γ-quantum and the recoil γ-quantum.
ψ=azimuthal angle of recoil electron about the direction of the primary γ-quantum.
n, t=number of electrons per cm³, and thickness of converter.

If it is assumed that the primary radiation is isotropic and if the differential Compton cross section is represented by $P(\cos\omega)d(\cos\omega)d\psi$, then one primary γ-quantum per unit solid angle in the solid angle $2\pi d(\cos\theta)$ will produce dN recoil electrons per unit solid angle in the solid angle $d(\cos\omega)d\psi$, where dN is given by

$$dN=(nt/\cos\theta)2\pi d(\cos\theta)P(\cos\omega)d(\cos\omega)d\psi. \quad (1)$$

The angles ψ, θ_0, θ, and ω are connected by the trigonometric relation

$$\cos\theta_0=\cos\omega\cos\theta+\sin\omega\sin\theta\cos\psi.$$

Differentiating, putting $d\theta=d\omega=0$, and eliminating $\sin\psi$ one obtains, after some simplification

$$d\psi=\frac{d(\cos\theta_0)}{\{[\cos(\theta_0-\omega)-\cos\theta][\cos\theta-\cos(\theta_0+\omega)]\}^{\frac{1}{2}}}.$$

This expression may be substituted in (1) and the resultant expression for dN integrated from $\theta=\theta_0-\omega$ to $\theta=\theta_0+\omega$, yielding

$$dN'=\frac{4\pi^2ntP(\cos\omega)d(\cos\omega)d(\cos\theta_0)}{[\cos(\theta_0+\omega)\cos(\theta_0-\omega)]^{\frac{1}{2}}}, \quad (2)$$

where a factor of two is necessary to allow for the whole range of ψ.

Using the relations given by the conservation of energy and momentum in Compton scattering one may write the Klein-Nishina formula in terms of a convenient parameter "a" as

$$P(p)dp=\frac{2\pi r_0^2[(\gamma+1)^2+a]^{\frac{1}{2}}}{\gamma\mu(a+1+2\gamma+2\gamma^2)}\times\left\{1+\left(\frac{a-1}{a+1}\right)^2+\frac{4\gamma^2}{(a+1)(a+1+2\gamma)}\right\}dp, \quad (3)$$

where

p=electron momentum times c, in units of m_0c^2,
r_0=classical electron radius,
$\gamma=(h\nu_0)/(m_0c^2)$,
$\mu=m_0c^2$,
$a=(1+\cos\epsilon)/(1-\cos\epsilon)$, $\cos\epsilon=(a-1)/(a+1)$.

The electron momentum is then given by

$$p/p_{max}=\frac{[1+a/(\gamma+1)^2]^{\frac{1}{2}}}{[1+a/(1+2\gamma)]}, \quad \text{where} \quad p_{max}=\frac{2\gamma\mu(\gamma+1)}{2\gamma+1}. \quad (4)$$

Since there is a unique relationship between the momentum of an electron and its recoil angle ω, we may substitute $P(p)dp$ for $2\pi P(\cos\omega)d(\cos\omega)$ in (2). Using the conservation relations again, we rewrite the radical in (2) as

$$[\cos(\theta_0+\omega)\cos(\theta_0-\omega)]^{\frac{1}{2}}=\left[\cos^2\theta_0-\frac{a}{a+(\gamma+1)^2}\right]^{\frac{1}{2}}.$$

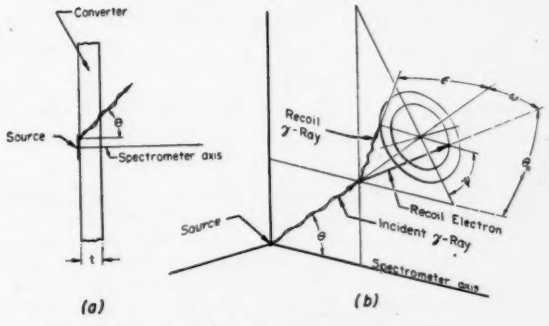

FIG. 8. Geometry of spectrometer source, illustrating typical Compton process.

After making these substitutions, (2) may be integrated from $\theta_0=\theta_1$ to $\theta_0=\theta_2$, the acceptance angle of the spectrometer, to give

$$\frac{dN''}{dp}=\frac{4\pi^2 ntr_0^2[(\gamma+1)^2+a]^{\frac{1}{2}}}{\gamma\mu(a+1+2\gamma+2\gamma^2)}. \quad (5)$$

$$\left[1+\left(\frac{a-1}{a+1}\right)^2+\frac{4\gamma^2}{(a+1)(a+1+2\gamma)}\right]$$

$$\times\cosh^{-1}\left\{\frac{x}{[a/((1+\gamma)^2+a)]^{\frac{1}{2}}}\right\}_{x=\cos\theta_1}^{x=\cos\theta_2}.$$

Equation (5), in conjunction with (4), gives the primary momentum spectrum of the Compton secondaries rigorously, provided that scattering of the electrons and attenuation of the primary gamma-ray intensity are negligible. While it is usually possible to select a converter such that this is so for the converter thickness at the mean spectrometer acceptance angle, scattering for electrons traveling along a radius of the converter, and attenuation of the radiation along a radius may be important. In these cases, however, only the lower energy part of the electron spectrum, which generally is not useful for the determination of quantum energies or intensities, is affected.

Before the primary spectrum of (5) can be compared with the observed distribution, one must allow for the effect of energy loss in the converter, of the finite instrument resolution or "window" and of any inhomogeneities of the primary gamma-ray energy (e.g., Doppler broadening from motion of the excited nucleus). The effect of the converter may be represented by a distribution of energy loss, the details depending on the converter and electron energy involved. After conversion to a momentum scale, this is folded into the primary distribution by numerical integration. The effect of instrument resolution may be similarly treated, using the observed "window" curve of the spectrometer. If any extended range of the spectrum is required, account must be taken of the fact that the instrument window has a constant percentage width by plotting dN''/dp from (5) against $\log p/p_{\max}$ and folding in a window curve of constant width. Such effects as Doppler broadening may also be represented by appropriate distributions and folded into the primary spectrum.

It may be, if the acceptance angle of the spectrometer corresponds to a large range of the angle θ_0, that the window curve of the spectrometer is an implicit function of θ_0, that is, that the window curve for some small part of the accepted range of θ_0 does not coincide with the integrated window curve for the whole range of θ_0. Since dN''/dp is also a function of θ_0, the simple folding operation is then not strictly justified. In the present case, however, the error resulting from the neglect of the finite range of θ_0 is negligibly small.

PHYSICAL REVIEW VOLUME 77, NUMBER 5 MARCH 1, 1950

Theory of the D+D Reactions
Part I. Analysis of the Energy Dependence

F. M. BEIDUK,* J. R. PRUETT, AND E. J. KONOPINSKI
Indiana University, Bloomington, Indiana

(Received October 4, 1949)

The variations with energy of the newly extended observations on the D+D reaction products are analyzed. It is found adequate to assume that all these variations, including details of the angular distributions, are due to differences in centrifugal barriers met by different components of the incident deuteron waves. This is found possible only if considerable spin-orbit interaction is allowed for. The possibility is investigated that numerical measures of the interactions can be obtained from the experimental data. Such conclusions as are permitted by the nature of the data are presented.

1. INTRODUCTION

THE reactions of deuterons with deuterons have been undergoing intensive experimental investigation.[1] There is interest in analyzing the results concerning these simplest of the transmutations. In particular, the extension of the observations to deuteron energies greater than 400 kev was expected[2] to reveal how large a part is played by the spin-orbit coupling during the process of reaction.

Besides the cross section σ as a function of deuteron bombardment-energy, E, the experiments yield the angular distribution with which the products appear, in the form

$$d\sigma=d\omega\sigma'(E)[1+A(E)\mu^2+B(E)\mu^4+C(E)\mu^6+\cdots], \quad (1)$$

$\mu=\cos\vartheta$, with ϑ the angle between the direction taken by the detected product and the incident deuteron beam, as measured in the center-of-mass system.

$$\sigma'=\sigma(E)/[1+(1/3)A+(1/5)B+(1/7)C+\cdots] \quad (2)$$

is the "isotropic cross section" measuring only the products in the isotropic component of (1). A striking feature discovered by the Wisconsin and Minnesota groups[1] is that the "first asymmetry coefficient," $A(E)$, descends from a positive maximum at $E\approx 0.5$ Mev to negative values. This behavior will be seen in Fig. 3. One of the aims of this paper is to show that even such a peculiarity can be attributed entirely to the differences between the centrifugal barriers met by the various components of the incident deuteron wave. A further

* AEC fellow.

[1] The latest and most extensive results are due to G. Hunter and H. Richards, Phys. Rev. **76**, 1445 (1949); we are indebted to Professor Richards for making these data available to us before their publication. Blair, Freier, Lampi, Sleator, and Williams, Phys. Rev. **74**, 1599 (1948) have obtained data on both the He^3 and H^1 production for energies between 1 and 3.5 Mev. The latest low energy measurements were made by Bretscher, French, and Seidl, Phys. Rev. **73**, 815 (1948).

[2] E. J. Konopinski and E. Teller, Phys. Rev. **73**, 822 (1948).

point borne out is, therefore, that the process can be understood as one of "first order," in the perturbation theory sense, not requiring the ad hoc introduction of resonances.

The analysis here is to be based on a minimum of assumptions concerning the basic nuclear forces. Only considerations of barrier penetration (external to the nucleus proper), of symmetry, and of angular momentum conservation will be needed. A second part follows which presents what seems to be the minimal formulation necessary for bringing the basic internucleonic forces into relation with the analyzed experimental observations.

2. THE APPROACH

The two deuterons can meet in 9 distinct spin states, χ_{SM}^0, classifiable into a singlet, a triplet and a quintet. Schiff[3] has listed the state functions for these. Then the incident deuteron wave relative to the center-of-mass is:

$$(9v)^{-\frac{1}{2}}[(\chi_{00}^0+\sum_M \chi_{2M}^0)(e^{ikz}+e^{-ikz}) + \sum_M \chi_{1M}^0(e^{ikz}-e^{-ikz})], \quad (3)$$

aside from well-known modifications required by the irrepressibility of the Coulomb effects. v is the relative velocity and k the corresponding wave number [$k=Mv/\hbar=(ME)^{\frac{1}{2}}/\hbar$, if M is a nucleon mass]. z is the projection on the incidence direction of the separation distance between the deuterons. The wave (3) is normalized to unit current in each of opposite directions, corresponding to bombarding and target deuteron, respectively. Thus, a count of the processes following from (3) gives the cross section directly.

Analyzed into "L-wave components," far from the collision center at $r=0$, (3) is equivalent to:

$$2(4\pi/9v)^{\frac{1}{2}}\sum_{LSM}(2L+1)^{\frac{1}{2}}i^L(kr)^{-1} \times\sin(kr-\tfrac{1}{2}L\pi)Y_{LO}(\vartheta_r)\chi_{SM}^0, \quad (4)$$

where only even integral values of L are to be used with $S=0$ or 2, odd values with $S=1$. The Y_{LO} are the normalized spherical harmonics. ϑ_r is adequately defined through: $z=r\cos\vartheta_r$.

As the first step toward a reaction cross section, we introduce an "approach" cross section, σ_L, which counts the number of collisions in which the deuterons approach within their "sphere" of nuclear interaction or to the "nuclear surface," at radius R. This naturally depends on the boundary conditions adopted for the nuclear surface. Several[4] plausible boundary conditions were investigated with WKB approximation which was deemed adequate considering the uncertainty of the boundary conditions and of the value to be given R. All of them gave approximately:

$$\sigma_L=(4/9)(\pi/k^2)(2L+1)e^{-2C_L} \quad (5)$$

for the number of successful approaches per second from one LSM component of the incident wave (4). Here, (exp: $-2C_L$) is the well-known barrier penetration probability according to the WKB approximation:[5]

$$C_L=k\int_R^{r_L}[(r_c/r)+(L+\tfrac{1}{2})^2/k^2r^2-1]dr \quad (6)$$

with $r_L=\frac{1}{2}r_c+\frac{1}{2}[r_c^2+(2L+1)^2/k^2]^{\frac{1}{2}}$, $r_c=2e^2/E$. The factor "1/9" enters in (5) because it applies to any *one* of the nine spin components of the L-wave. The factor "4" is due to the symmetrization of the deuteron wave.[6] (It has as part of its function, a compensation for the loss of alternate L-values with a given spin.) The importance of σ_L rests on the energy-dependence, $\sim e^{-2C_L}/E$, which will be presumed capable of accounting for all the variations with energy observed by the the experimenters. The energy dependence is demonstrated by the curves drawn in Fig. 1.

3. THE PRODUCT WAVE AMPLITUDES

Since it is the total angular momentum **J**, rather than the individual momenta **L** and **S**, that is conserved we can make general statements only about the results of a collision wave which is an eigenfunction of **J** and its components. We represent the eigenfunction corresponding to an eigenvalue J and its component eigenvalue M by the symbol: ${}^{2S+1}L_J{}^M$. As the symbol implies, the quantity is simultaneously an eigenfunction for the magnitudes of L and S, though not for their components.

For singlet states ${}^1L_L{}^M=\chi_{00}Y_{LM}$, simply, while for triplet states:

$${}^3L_J{}^M=\sum_m(LJM\,|\,m)\chi_{1m}Y_{LM-m}, \quad (7)$$

with $(LJM\,|\,m)$ the elements of the well-known unitary transformation matrix.[7] Following previous treatments,[2] we ignore the quintet contributions and so make no provision for them.[8]

---

[3] L. Schiff, Phys. Rev. **71**, 783 (1937).

[4] One condition tried was the requirement that no reflected wave start at the nuclear surface. This was considered plausible on the supposition that the strong nuclear interactions would make the reflections incoherent with the incoming wave and incapable of interfering with the approach. It led to (5) multiplied by the factor $[1+\frac{1}{4}e^{-2C_L}]^{-2}$, which is nearly unity except near the top of the barrier where $C_L\to 0$. An alternative boundary condition investigated was the requirement of a vanishing amplitude at the nuclear surface. This was suggested by Flügge's (Zeits. f. Physik **108**, 545 (1938)) results showing that the high kinetic energies inside the nuclear surface limited severely the amplitudes that could connect with an external wave function. This procedure led to (5) with a multiplying factor $[(4/5)+(1/5)e^{-4C_L}]^{-1}$, which is unity at the barrier top. The energy dependence included in (5) is the most important part in any case.

[5] We were led to use a centrifugal barrier height of $(L+\frac{1}{2})^2\hbar^2/MR^2$ even for $L=0$ by the findings of Yost, Wheeler, and Breit, Phys. Rev. **49**, 174 (1936).

[6] The factor "4/9" was not included in the definition of σ_L advanced in reference 2. There, a separate weight factor was used in place of the "1/9" and the "4" was ignored, without material effect on the results.

[7] E. Wigner, *Gruppentheorie* (Friedrich Vieweg & Sohn, Braunschweig, 1931), p. 208.

[8] We rely on the usual argument that the Pauli principle hinders a sufficiently close approach in quintet collisions. The

The character of the product wave which may result from an initial state $^{2S+1}L_J{}^M$ is clear from considerations of parity and angular momentum conservation. The product amplitude arising from an initial $^1L_L{}^0$ wave will be written:

$$^1L_L{}^0 \rightarrow \alpha_L\, ^1L_L{}^0 + \beta_L\, ^3L_L{}^0 \quad (\beta_0 = 0;\ L \text{ even}), \quad (8)$$

where α_L, β_L are coefficients (generally complex) which determine the intensity with which various products arise. They are clearly proportional to appropriate matrix elements of whatever "perturbation," $H^{(1)}$, is

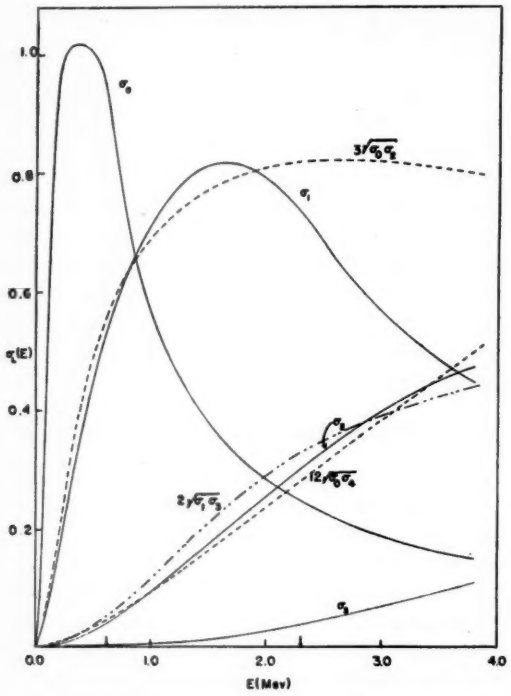

FIG. 1. Approach cross sections as functions of the deuteron energy. The vertical arrows at the bottom give the s and p barrier heights.

responsible for the reaction:

$$\alpha_L \sim \langle ^1L_L{}^0 | H^{(1)} | ^1L_L{}^0 \rangle \quad (9)$$

and

$$\beta_L \sim \langle ^3L_L{}^0 | H^{(1)} | ^1L_L{}^0 \rangle.$$

Here conventional symbols designate the matrix elements and the states they connect. A closer definition of α_L, β_L emerges when the expression for the differential cross section is written below. For triplet collisions (L odd; $M=0, \pm 1$ only):

$$^3L_L{}^M \rightarrow \alpha_{LL}\, ^3L_L{}^M + \beta_{LL}\, ^1L_L{}^M, \quad (10a)$$

$$^3L_{L+1}{}^M \rightarrow \alpha_{LL+1}\, ^3L_{L+1}{}^M + \beta_{LL+1}\, ^3(L+2)_{L+1}{}^M, \quad (10b)$$

$$^3L_{L-1}{}^M \rightarrow \alpha_{LL-1}\, ^3L_{L-1}{}^M + \beta_{LL-1}\, ^3(L-2)_{L-1}{}^M, \quad (10c)$$

where

$$\beta_{LL\pm1} \sim \langle ^3(L\pm2)_{L\pm1}{}^M | H^{(1)} | ^3L_{L\pm1}{}^M \rangle, \text{ etc.} \quad (11)$$

The coefficients α_{LJ}, β_{LJ} are independent of M in consequence of the invariance with respect to absolute orientation of the system.

Since the singlet components of the initial wave are $\sim \chi_{00}{}^0 Y_{LO} = {}^1L_L{}^0$, the differential cross section for the products resulting from singlet collisions can be written (L even, only):

$$d\sigma^{(s)} = d\omega \mathbf{S} \left| \sum_L \sigma_L{}^{\frac{1}{2}} (\alpha_L\, ^1L_L{}^0 + \beta_L\, ^3L_L{}^0) \right|^2, \quad (12)$$

where the symbol $\mathbf{S}$ signifies integration over the spin coordinates. One sees that the definition of α_L, β_L has been so chosen as to allow putting σ_L in evidence. One of course expects the product intensity to be proportional to the number of successful approaches as measured by σ_L. Integrating (12) over all directions gives the total singlet cross section:

$$\sigma^{(s)} = \sum_L \sigma_L (|\alpha_L|^2 + |\beta_L|^2) \quad (13)$$

from which the significance of the coefficients is obvious.

The triplet cross section requires more elaborate treatment because the initial triplet L-wave is proportional to:

$$(\sum_M \chi_{1M}{}^0) Y_{LO} = \sum_{JM} (LJM|M)\, ^3L_J{}^M \quad (14)$$

($J=L$, $L\pm1$) as follows from (7) and the unitary character of the matrix. We then have the triplet differential cross section:

$$d\sigma^{(t)} = d\omega \mathbf{S} \sum_M \left| \sum_{LJ} (LJM|M) \sigma_L{}^{\frac{1}{2}} \times (\alpha_{LJ}\, ^3L_J{}^M + \beta_{LJ}{}^{2s+1} l_J{}^M) \right|^2, \quad (15)$$

where L is odd only; $s=0$, $l=L$ for $J=L$ and $s=1$, $l=J\pm1$ for $J=L\pm1$. No interference between terms of different M is allowed for, since the initial spins are random. The same fact, of course, also allows us to treat the triplet and singlet cross sections as simply additive.

Factoring out explicitly the approach cross section σ_L as done in (12), (15) leaves the "matrix elements" α_L, β_L, α_{LJ}, β_{LJ}, see (9) and (11), independent of the energy on our assumptions. It is plausible that the particular bombardment energy within a fairly wide range make little difference once the specifically nuclear interactions take hold.

4. THE ANGULAR DISTRIBUTION

In order to obtain the angular distribution of the products, the $^{2S+1}L_J{}^M$ waves must be put in terms of

symmetrized wave amplitude for a given spin state may be expressed as

$$\chi_{SM}{}^0(1234)\{F^0[\tfrac{1}{2}(\mathbf{r}_1+\mathbf{r}_2)-\tfrac{1}{2}(\mathbf{r}_3+\mathbf{r}_4)] \pm F^0[\tfrac{1}{2}(\mathbf{r}_3+\mathbf{r}_4)-\tfrac{1}{2}(\mathbf{r}_1+\mathbf{r}_2)]\} - \chi_{SM}{}^0(3214)\{F^0[\tfrac{1}{2}(\mathbf{r}_3+\mathbf{r}_2)-\tfrac{1}{2}(\mathbf{r}_1+\mathbf{r}_4)] \pm F^0[\tfrac{1}{2}(\mathbf{r}_1+\mathbf{r}_4)-\tfrac{1}{2}(\mathbf{r}_3+\mathbf{r}_2)]\},$$

since $\chi_{SM}{}^0(3412) = (-)^S \chi_{SM}{}^0(1234)$. (The lower signs must be used with $S=1$.) $\chi_{2M}{}^0$ is unchanged by any permutation of spins so that there is complete cancellation when $\mathbf{r}_1 \rightarrow \mathbf{r}_3$ (or $\mathbf{r}_2 \rightarrow \mathbf{r}_4$). Inclusion of the small effects remaining because some interaction with $\mathbf{r}_1 \neq \mathbf{r}_3$ can occur would only give us greater freedom in obtaining agreement with the observations.

the spherical harmonics with the aid of (7) and eventually in terms of the cosines, μ, explicitly, as in (1). The first of these steps also permits the completion of the spin coordinate integrations in (12), (15).

The first step is easily carried out for the singlet cross section (12), giving:

$$d\sigma^{(s)}=d\omega\{|\textstyle\sum_L \sigma_L^{\frac{1}{2}}\alpha_L Y_{L0}|^2+|\sum_L \sigma_L^{\frac{1}{2}}\beta_L Y_{L1}|^2\}. \quad (16)$$

Use was made of the facts that $(LL0|0)=0$, $(LL0|\pm1)=\pm 2^{-\frac{1}{2}}$ and $Y_{L1}^*=-Y_{L,-1}$.

The equivalent step for the triplet cross section results in some complexity. First we introduce certain new "matrix elements," $\gamma_{LM-m}{}^m$, such that

$$\textstyle\sum_J (LJM|M)\alpha_{LJ}\,{}^3L_J{}^M=\sum_m \gamma_{LM-m}{}^m Y_{LM-m}\chi_{1m} \quad (17)$$

with the consequence from (7) that:

$$\gamma_{LM-m}{}^m=\textstyle\sum_J \alpha_{LJ}(LJM|M)(LJM|m). \quad (18)$$

From the "matrix element" character of α_{LJ}, one finds:

$$\gamma_{LM-m}{}^m\sim\langle\chi_{1m}Y_{LM-m}|H^{(1)}|\chi_{1M}{}^0Y_{L0}\rangle, \quad (19)$$

that is, a matrix labeled according to the LM_Lsm scheme rather than with $JMLs$ like α_{LJ}. Since they substitute for only three quantities α_{LJ} ($J=L$, $L\pm1$), only three of the $\gamma_{LM-m}{}^m$ can be distinct for a given L. We have first: $\gamma_{L0}{}^0$, $\gamma_{L0}{}^1=\gamma_{L0}{}^{-1}$, $\gamma_{L1}{}^0=\gamma_{L,-1}{}^0$, $\gamma_{L,-1}{}^1=\gamma_{L1}{}^{-1}$ and $\gamma_{L,-2}{}^1=\gamma_{L2}{}^{-1}$ as the only non-vanishing ones. Then, besides,

$$\begin{aligned}\gamma_{L,-1}{}^1-\gamma_{L1}{}^0&=[\tfrac{1}{2}L(L+1)]^{\frac{1}{2}}(\gamma_{L0}{}^0-\gamma_{L0}{}^1)\\&=L(L+1)[2(L-1)(L+2)]^{-\frac{1}{2}}\gamma_{L,-2}{}^1 \quad (20)\end{aligned}$$

serve to reduce the number to three.

To obtain the full amplitude produced by triplet collisions, according to (15), one must add to (17):

$$(LLM|M)\beta_{LL}\,{}^1L_L{}^M=2^{-\frac{1}{2}}\beta_{LL}Y_{LM}\chi_{00} \quad (21)$$

and

$$\begin{aligned}\textstyle\sum_{J=L\pm1}(LJM|M)\beta_{LJ}\,{}^3(L\pm2)_J{}^M&\\=\textstyle\sum_m \chi_{1m}\sum_{l=L\pm2}Y_{l,M-m}\delta_{lM-m}{}^m.& \quad (22)\end{aligned}$$

The "matrix elements":

$$\begin{aligned}\delta^m{}_{L\pm2,M-m}&=(L,L\pm1,M|M)\\&\quad\times(L\pm2,L\pm1,M|m)\beta_{LL\pm1}, \quad (23)\\&\sim\langle\chi_{1m}Y_{L\pm2,M-m}|H^{(1)}|\chi_{1M}{}^0Y_{L0}\rangle \quad (24)\end{aligned}$$

are each numerical multiples of the quantity $\beta_{LL\pm1}$ for all the values of $M(0,\pm1)$ and $m(0,\pm1)$.

Putting the sum of (17), (21), and (22) into (15) and integrating over spins gives:

$$\begin{aligned}d\sigma^{(t)}=d\omega\{&|\textstyle\sum_L \sigma_L^{\frac{1}{2}}\beta_{LL}Y_{L1}|^2\\&+\textstyle\sum_{mM}|\sum_L \sigma_L^{\frac{1}{2}}(\gamma_{LM-m}{}^m Y_{LM-m}\\&\quad+\textstyle\sum_l \delta_{lM-m}{}^m Y_{lM-m})|^2\}. \quad (25)\end{aligned}$$

This expression, as it should be, is independent of the azimuth φ and even in $\mu=\cos\vartheta$ and $(1-\mu^2)^{\frac{1}{2}}$. It is less obvious that, although it contains spherical harmonics to the order $l=L+2$ (for a given L) it nevertheless will give no power of the cosine higher than μ^{2L}. It can be shown with the help of the expansion of the spherical harmonics into their highest powers[9] that the terms in μ^{2L+2} and μ^{2L+4} vanish identically.

To obtain the theoretical equivalent of the experimenters' formula (1), the dependence on the cosine, μ, must be made explicit in $d\sigma=d\sigma^{(s)}+d\sigma^{(t)}$ as given by (16) and (25). This can be done most conveniently for particular values of L, especially since we shall be interested only in the lowest ones. The reason is made obvious by Fig. 1 which shows that the higher centrifugal barriers characteristic of higher L values will make them negligible at less than a given finite energy. Based on this fact, we adopt a systematic procedure which is characterized by a certain definition of "order," n. The cross section $d\sigma$ will have been evaluated to the "nth order" if only terms are included which are proportional to $(\sigma_L\sigma_{L'})^{\frac{1}{2}}$, $L+L'$ having all the possible values $\leqslant 2n$.

To avoid unduly lengthy expressions, we further define new energy-independent coefficients: K_L, A_L, B_L, C_L, $K_{LL'}$, $A_{LL'}$, $B_{LL'}$ and $C_{LL'}$. These will be defined in such a way that the contribution of a single incident L-wave, inferrable from (16) or (25), can be written:

$$d\sigma^{(L)}=d\omega\sigma_L\{K_L+A_L\mu^2+B_L\mu^4+C_L\mu^6+\cdots\}. \quad (26)$$

It is clear from the foregoing discussion that $A_{L<1}=0$, $B_{L<2}=0$, $C_{L<3}=0$. The interference contributions from (16) and (25) are included by introducing $d\sigma^{(LL')}$ such that:

$$d\sigma=\textstyle\sum_L d\sigma^{(L)}+\sum_{L,L'>L}d\sigma^{(LL')}. \quad (27)$$

One has then:

$$\begin{aligned}d\sigma^{(LL')}=d\omega(\sigma_L\sigma_{L'})^{\frac{1}{2}}\{&K_{LL'}+A_{LL'}\mu^2\\&+B_{LL'}\mu^4+C_{LL'}\mu^6+\cdots\}. \quad (28)\end{aligned}$$

Coefficients of any power higher than $\mu^{L+L'}$ will vanish. The convenience of the newest coefficients is made apparent when one now compares (27) with (1) and thus finds:

$$\sigma'=\textstyle\sum_L \sigma_L K_L+\sum_{L,L'>L}(\sigma_L\sigma_{L'})^{\frac{1}{2}}K_{LL'}, \quad (29a)$$

$$\sigma' A=\textstyle\sum_L \sigma_L A_L+\sum_{L,L'>L}(\sigma_L\sigma_{L'})^{\frac{1}{2}}A_{LL'}\ (L\geqslant 1), \quad (29b)$$

$$\sigma' B=\textstyle\sum_L \sigma_L B_L+\sum_{L,L'>L}(\sigma_L\sigma_{L'})^{\frac{1}{2}}B_{LL'}\ (L\geqslant 2), \quad (29c)$$

$$\sigma' C=\textstyle\sum_L \sigma_L C_L+\sum_{L,L'>L}(\sigma_L\sigma_{L'})^{\frac{1}{2}}C_{LL'}\ (L\geqslant 3). \quad (29d)$$

The forms (29), directly comparable with experimental curves for σ', $A\cdots$ make the energy-dependence explicit by putting σ_L and $(\sigma_L\sigma_{L'})^{\frac{1}{2}}$ in evidence. The latter, of course, can be read directly from Fig. 1.

There remains the task of relating the new coefficients with the previously introduced "matrix elements."

[9] Jahnke-Emde, *Tables of Functions* (B. G. Teubner, Leipzig, 1928), p. 110; E. Eisner and R. Sachs, Phys. Rev. **72**, 680 (1947); and C. Yang, Phys. Rev. **74**, 764 (1948) have given proofs of a theorem that this must be so.

Comparison of (26), (27), and (16) gives:

$$K_0=|\alpha_0|^2, \tag{30a}$$

$$K_{02}=-\tfrac{1}{3}A_{02}=-\tfrac{1}{2}5^{\frac{1}{2}}(\alpha_0^*\alpha_2+\alpha_0\alpha_2^*), \tag{30b}$$

$$K_2=(5/4)|\alpha_2|^2, \tag{30c}$$

$$A_2=3K_2-B_2=-(15/2)(|\alpha_2|^2-|\beta_2|^2), \tag{30d}$$

$$K_{04}=-(1/10)A_{04}=(3/35)B_{04}=(9/8)(\alpha_0^*\alpha_4+\alpha_0\alpha_4^*). \tag{30e}$$

To be emphasized is the fact that not all the new coefficients are independent of each other, as the tabulation shows.

For odd L, we compare (26), (27) with (25) and obtain:

$$K_1=\tfrac{3}{2}|\beta_{11}|^2+3|\gamma_{11}{}^{-1}+6^{-\frac{1}{2}}\beta_{12}|^2 +3|\gamma_{11}{}^0-6^{-\frac{1}{2}}\beta_{12}|^2, \tag{31a}$$

$$A_1=3|\gamma_{10}{}^0+(2/3)^{\frac{1}{2}}\beta_{12}|^2+6|\gamma_{10}{}^1-6^{-\frac{1}{2}}\beta_2|^2-K_1. \tag{31b}$$

It would not be of much profit to list further ones of these, particularly because of their inordinate lengthiness.

The quantities occurring in the expressions (30) and (31) are all "matrix elements" which must be considered unknown as long as no calculation of them from assumed internucleonic forces is undertaken. Actually, evaluation of them from experimental data may be regarded as preferable, since it may give more permanently valid results.

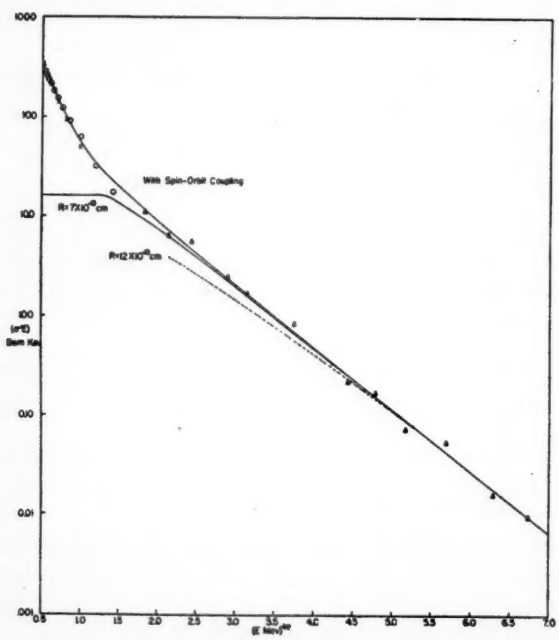

FIG. 2. The isotropic cross section in barns (10^{-24} cm^2) multiplied with the deuteron energy E in kev as a function of $E^{-\frac{1}{2}}$. The two lower curves were calculated without providing for spin-orbit coupling, using two values of the nuclear radius, R. The uppermost curve is also for $R=7(10)^{-13}$ cm. The experimental points designated by circles are due to Hunter and Richards; the crosses are due to the Minnesota group; the triangular points are due to Bretscher, French, and Seidl. (See reference 2.)

5. COMPARISONS WITH EXPERIMENT

The measurements, as extended by Richards and Hunter,[2] are conveniently divided into three deuteron energy ranges: below ~0.5 Mev, where the second and third anisotropy coefficients, B and C, are observed to be negligible; between ~0.5 Mev and ~1.5 Mev, where B rises but C is still negligible; above ~1.5 Mev, where C rises. The three ranges may be appropriately referred to as of first, second, and third "order," in the sense defined in the foregoing section. Thus, for example, the negligibility of B in the lowest range implies that the second-order terms proportional to σ_2, $(\sigma_0\sigma_4)^{\frac{1}{2}}$, $(\sigma_1\sigma_3)^{\frac{1}{2}}$ may be neglected there.

Another point becomes evident immediately. The variations with energy of all the terms of a given order n, proportional to $(\sigma_L\sigma_{2n-L})^{\frac{1}{2}}$ with $L=0, 1, \cdots, n$, are so similar that the experiments should not be expected to differentiate between them, considering that they measure superpositions such as given by (29). Figure 1 exhibits the similarity between[10] $(\sigma_0\sigma_2)^{\frac{1}{2}}$ and $(1/3)\sigma_1$; between $(\sigma_0\sigma_4)^{\frac{1}{2}}$ and $0.08\sigma_2$; and between $(\sigma_1\sigma_3)^{\frac{1}{2}}$ and $\frac{1}{2}\sigma_2$. These facts effectively reduce all the formulas (29) to the form:

$$X\approx\sum_L \sigma_L\bar{X}_L, \tag{32}$$

where X stands for σ', $\sigma'A$, $\sigma'B$ or $\sigma'C$ $(\bar{\sigma}_L'\equiv\bar{K}_L)$

$$\bar{X}_0=X_0;\ \bar{X}_1=X_1+0.33X_{02};\ \bar{X}_2=X_2+0.08X_{04}+0.5X_{13}. \tag{33}$$

From a viewpoint in which the coefficients K_L, $K_{LL'}$, A_L, $A_{LL'}$, $\cdots$ are regarded as unknowns to be obtained from experiment, one sees that the measurements should not be expected to give more than the combinations (33) with any accuracy (except that X_1 and X_{02} are separately obtainable from measurements in the third-order region[10]).

One might also anticipate that the experiments will not *test* the theory very severely. From (32), each measured function of the energy [e.g., $A(E)$], will be represented by a theoretical formula having an unknown constant $[\bar{A}_1, \bar{A}_2, \bar{A}_3]$ for each range of energy. Each will naturally be used as a parameter, adjustable so as to obtain agreement with the data. However, the energy variations given by the σ_L are of a special type, and success in fitting the data with constant coefficients would confirm the assumption that the differences of centrifugal barriers, as represented by the difference of the σ_L, can account for the observations.

The latter conclusion gains support from the following. As a preliminary step, we have considered a simplified version of the theory, for which the separate conservation of spin and orbital angular momenta was assumed. This seems to have some plausibility as a first approximation since it is well known that a rough accounting of the properties of the light nuclei is achievable without introducing spin-orbit coupling.

[10] An exception from the following treatment must be made for $\bar{X}_1$ in the third-order region, as Fig. 1 makes clear.

Reference to the "matrix elements" (9), (11), and (19) shows that, without spin-orbit coupling, all coefficients vanish except α_L and $\gamma_{L0}{}^0=\gamma_{L0}{}^{\pm 1}$. The most striking consequence of this is that the triplet collisions now contribute nothing to the isotropic component ($\sim\sigma'$) of the product distribution [see (29a) and (31)]. One can show that now

$$\sigma'=|\sum_L(-)^{\frac{1}{2}L}[1\cdot 3\cdot 5\cdots(L-1)/2\cdot 4\cdots L] \times[(2L+1)\sigma_L]^{\frac{1}{2}}\alpha_L|^2$$

with *L even only*. Figure 2 demonstrates the result when $R=7(10)^{-13}$ cm and if $R=12(10)^{-13}$ cm. The experimental isotropic cross section increases much more rapidly with energy. To remedy this one might try either to give the higher order coefficients α_2, α_4, $\cdots$ extremely large values or to use a smaller value for the nuclear radius, R. Either procedure would make the coefficients B and C rise far too rapidly. The curves in Fig. 3 are drawn with the inclusion of spin-orbit coupling, as discussed below, but they represent exaggerated lower limits for the rate of increase given when spin-orbit coupling is neglected.

We conclude first from the attempts just described that the D+D reactions cannot be understood without the inclusion of considerable spin-orbit coupling. We also learn that the freedom given by the adjustability of the constants in the forms (32) is limited. The only additional restriction effective with the dropping of spin-orbit coupling had been that odd L-values were excluded from σ', yet this produced strong disagreements with the observations.

All the calculations with spin-orbit coupling to be reported here employed $R=7(10)^{-13}$ cm, arguments for which have been given in reference 2. We found that increasing the radius substantially makes the isotropic cross section difficult to fit, just as without the spin-orbit coupling. (There is a low energy region in which σ_0 predominates, and this is unchanged by introducing the coupling.) On the other hand, the radius adopted represents about the minimum for which the rate of increase of $B(E)$ and $C(E)$ near their beginnings still lies within the experimental uncertainties.

Figures 2 and 3 demonstrate the fitting with the data which were attainable with expressions of the type (32). They are based on the values:

$$\begin{aligned}
&K_0\approx 0.027,\\
&\bar{K}_1=K_1+\tfrac{1}{3}K_{02}\approx 0.030\pm 0.005,\\
&\bar{A}_1=A_1-K_{02}\approx 0.16\pm 0.04,\\
&K_{02}\approx -0.15\pm 0.2,\\
&\bar{K}_2=K_2+0.08K_{04}+0.5K_{13}\approx 0.16\pm 0.04,\\
&\bar{A}_2=A_2-0.83K_{04}+0.5A_{13}\approx -0.8\pm 0.2,\\
&\bar{B}_2=3K_2-A_2+1.05K_{04}+0.5B_{13}\approx 1.07\pm 0.1,\\
&\bar{K}_3\approx 0;\quad \bar{A}_3\approx 0.82;\quad \bar{B}_3\approx -2.3;\quad \bar{C}_3\approx 2.5.
\end{aligned}\tag{34}$$

Coefficients which are *a priori* incapable of independent variation according to the relations (30) and (31) were eliminated from this tabulation as one can see. The uncertainties indicated were estimated for the curve fitting.

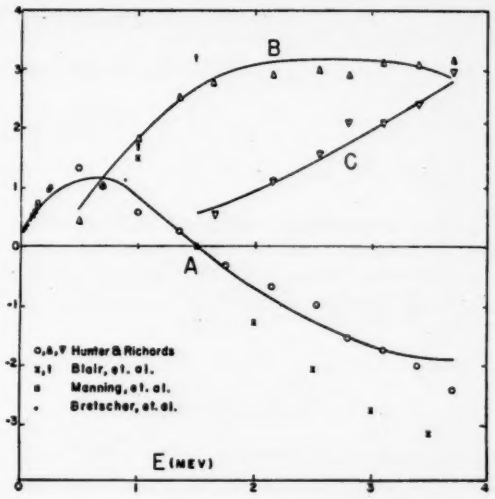

FIG. 3. The anisotropy coefficients as functions of the deuteron energy.

The greatest interest of the numerical results is in the comparison of K_1 and K_0. Whereas K_0 involves no spin-orbit coupling, K_1 can be regarded as a measure of it. This was shown by the discussion above and by formula (31a). If $K_1\approx\bar{K}_1$ could be assumed, then K_1/K_0 has about the value unity signifying that the spin-orbit transitions contribute quite as much as those in which spins are separately conserved. Actually, the entire value of $\bar{K}_1\approx 0.030$ is not due to K_1 but, as shown, $\bar{K}_1\approx K_1+0.3K_{02}$. Now, $K_{02}\sim(\alpha_2{}^*\alpha_0+\alpha_2\alpha_0{}^*)$ also contributed when no spin-orbit coupling was included [see (30)]. It was found then that it could not be given a sufficient magnitude ($\approx 3\bar{K}_1$) without giving α_2 and so A_2, B_2, $\cdots$ too large values. This means that the contribution of K_{02} to $\bar{K}_1$ must be moderate and that K_1/K_0 cannot be much less than unity.

It is also interesting to see that the coefficients listed in (34) associated with larger orbital angular momenta are still of order unity; thus the "intrinsic reaction probabilities" for all values of $L\leqslant 3$ are quite comparable. There are also minor points to be noted: that a negative $\bar{A}_2$ is to be expected since the main term of A_2 is $-(15/2)|\alpha_2|^2$ according to (30); by the same token, a rather larger positive $\bar{B}_2\approx(45/4)|\alpha_2|^2$ should be expected and is found.

Note added in proof.—Since this paper was submitted, work along these lines has been published by Y. Nakano, Phys. Rev. **76**, 981 (1949). This author expanded the results of reference 2 to include the effect of D-waves, without considering, e.g., $S-G$ interference, which becomes effective at the same time. This may be quite defensible. Further, no consideration of the relations between the adjusted constants and matrix elements was attempted. Nakano unfortunately did not possess the information, due to Hunter and Richards (see reference 2), that the $\cos^6\theta$ term is appreciable in the energy range considered, a fact which renders futile a comparison of his numerical results with ours.

Theory of the D+D Reactions
Part II. Relation to the Internucleonic Forces

J. R. PRUETT, F. M. BEIDUK,* AND E. J. KONOPINSKI
Indiana University, Bloomington, Indiana
(Received October 4, 1949)

The adequacy of current ideas about the internucleonic forces in accounting for the observations as analyzed in Part I is investigated. In particular, the adequacy of the spin-orbit coupling provided by the tensor forces is examined. To this end, a "minimal" formulation of the four-body problem is attempted. The interaction responsible for the reaction is derived. Some order-of-magnitude comparisons with the experimental data are presented.

1. INTRODUCTION

IN Part I, the experimental data on the D+D reactions was analyzed for the information it could give when detailed assumptions concerning the internucleonic forces are avoided. It is also of interest to see whether current conceptions of the basic forces are adequate for an understanding of the results of Part I. Such an investigation is necessarily subject to two sources of uncertainty. On the one hand, there is the uncertainty as to the forces. On the other, the complexity of a four-body problem is such that the extensive approximating is necessary and much more than qualitative results cannot be expected. Nevertheless, even with the "minimal" formulation we propose to carry through, some reasonably definite conclusions can be drawn.

2. THE COUPLING OF THE SPIN STATES

The potential[1] V_{ij} which will here be assumed to connect any pair of nucleons i and j is:

$$V_{ij}=[w+bB_{ij}+2wP_{ij}+2bM_{ij}+\tfrac{1}{3}(1+2M_{ij})S_{ij}]U_{ij}(r_{ij}). \quad (1)$$

B_{ij} is the Bartlett spin-exchange operator, M_{ij} is the Majorana space-coordinate exchange operator, and $P_{ij}=B_{ij}M_{ij}$ is the Heisenberg, particle permutation operator. According to the "symmetrical" theory, the constants w and b are to be taken equal to $-\frac{1}{3}$ and $+\frac{2}{3}$, respectively. S_{ij} is the "tensor coupling":

$$S_{ij}=(\boldsymbol{\sigma}_i\cdot\mathbf{e})(\boldsymbol{\sigma}_j\cdot\mathbf{e})-\tfrac{1}{3}(\boldsymbol{\sigma}_i\cdot\boldsymbol{\sigma}_j). \quad (2)$$

$\mathbf{e}$ is a unit vector joining the pair of particles; $\boldsymbol{\sigma}_{i,j}$ are the Pauli spin matrices with unit eigenvalues. We shall find it convenient to adopt the form

$$U_{ij}=-D\exp(-r_{ij}^2/a^2) \quad (3)$$

for the potential well. a is the force range and D is the so-called "singlet depth."

The most immediate results are obtainable by considering first the coupling between our initial and final spin states as provided by an interaction of the form (1). The spin state functions for our four-particle problem have been listed by Schiff[1a]; we rewrite them in terms of two-particle spin functions: the singlet,

$$s_{ij}=2^{-\frac{1}{2}}[\alpha_i\beta_j-\beta_i\alpha_j];$$

and the triplet,

$$t_{ij}^{1}=\alpha_i\alpha_j,\quad t_{ij}^{0}=2^{-\frac{1}{2}}[\alpha_i\beta_j+\beta_i\alpha_j],\quad t_{ij}^{-1}=\beta_i\beta_j.$$

Here α, β are individual particle spin states corresponding to positive and negative spin projections, respectively. We shall associate the indices 1 and 3 with the two neutrons, 2 and 4 with the two protons. The "unpermuted" order will be considered to be the one in which the two deuterons are paired as (1, 2) and (3, 4); and in which the neutron 1 is the ejected particle.

For the initial, two-deuteron states χ_{SM}^{0} we have:

$$\chi_{00}^{0}=(12)^{-\frac{1}{2}}[3s_{13}s_{24}+t_{13}^{0}t_{24}^{0}-t_{13}^{1}t_{24}^{-1}-t_{13}^{-1}t_{24}^{1}]$$
$$\equiv(12)^{-\frac{1}{2}}[3s_{14}s_{23}+t_{14}^{0}t_{23}^{0}-t_{14}^{1}t_{23}^{-1}-t_{14}^{-1}t_{23}^{1}] \quad (4)$$

which is symmetrical in the pairs (12) and (34); and

$$\chi_{1M}^{0}=2^{-\frac{1}{2}}[s_{13}t_{24}^{M}+t_{13}^{M}s_{24}]$$
$$\equiv 2^{-\frac{1}{2}}[s_{14}t_{23}^{M}+t_{14}^{M}s_{23}] \quad (5)$$

which is antisymmetric in the interchange of the pairs (1, 2) and (3, 4). Both the singlet and triplet are symmetric in $1\leftrightarrow2$ and in $3\leftrightarrow4$, as is proper for deuterons.

For the final states χ_{sm} we take functions antisymmetric in $2\leftrightarrow4$, these being the protons within the product triton. We have:

$$\chi_{00}=s_{13}s_{24}\equiv\tfrac{1}{2}[s_{14}s_{23}+t_{14}^{0}t_{23}^{0}-t_{14}^{1}t_{23}^{-1}-t_{14}^{-1}t_{23}^{1}], \quad (6)$$

$$\chi_{1,\pm1}=t_{13}^{\pm1}s_{24}\equiv\tfrac{1}{2}[(s_{14}\pm t_{14}^{0})t_{23}^{\pm1}+t_{14}^{\pm1}(s_{23}\mp t_{23}^{0})], \quad (7a)$$

$$\chi_{10}=t_{13}^{0}s_{24}\equiv\tfrac{1}{2}[s_{14}t_{23}^{0}+t_{14}^{0}s_{23}-t_{14}^{1}t_{23}^{-1}+t_{14}^{-1}t_{23}^{1}]. \quad (7b)$$

The two-particle functions we have chosen to make explicit in (4)–(7) are those most helpful in evaluating the couplings.

In general, the coupling between the spin states χ_{SM}^{0} and χ_{sm} due to the interaction of the particle-pair (i,j)

* AEC fellow.

[1] See, for example, F. Rohrlich and J. Eisenstein, Phys. Rev. **75**, 705 (1949). Our form is equivalent to their: $-(1/3)(\boldsymbol{\tau}_i\cdot\boldsymbol{\tau}_j)\times(\boldsymbol{\sigma}_i\cdot\boldsymbol{\sigma}_j)(1+S_{ij})U_{ij}$, where $\boldsymbol{\tau}_{i,j}$ are the "isotopic spins." We have used the equivalent isotopic spin formulation only in certain checks, having found it unwieldy for our problem.

[1a] L. Schiff, Phys. Rev. **51**, 783 (1937).

is given by

$$(\chi_{sm}\cdot V_{ij}\chi_{SM}{}^0)=[(w+2bM_{ij})(\chi_{sm}\cdot\chi_{SM}{}^0)+(b+2wM_{ij})(\chi_{sm}\cdot B_{ij}\chi_{SM}{}^0)+\tfrac{1}{3}(1+2M_{ij})(\chi_{SM}\cdot S_{ij}\chi_{SM}{}^0)]U_{ij}, \quad (8)$$

where the "dot product" indicates integration over spin coordinates. Actually, only the interacting pairs (1, 3), (1, 4), (2, 3), and (2, 4) need be considered, since, as will be seen below, interaction between the particles within a deuteron does not contribute directly to the formation of the final state.

We first attend to the non-tensor terms of (8), to be designated by the subscript 0. It follows easily from (4)–(7) that the Bartlett and Heisenberg forces vanish for the unlike particle-pairs (1, 4) and (2, 3), leaving:

$$(\chi_{sm}\cdot V_{14}\chi_{SM}{}^0)_0=(\chi_{sm}\cdot\chi_{SM}{}^0)[w+2bM_{14}]U_{14}, \quad (9a)$$

$$(\chi_{sm}\cdot V_{23}\chi_{SM}{}^0)_0=(\chi_{sm}\cdot\chi_{SM}{}^0)[w+2bM_{23}]U_{23}, \quad (9b)$$

$$(\chi_{sm}\cdot V_{13}\chi_{SM}{}^0)_0=(\chi_{sm}\cdot\chi_{SM}{}^0)[(w-(-)^sb)+2(b-(-)^sw)M_{13}]U_{13}, \quad (9c)$$

$$(\chi_{sm}\cdot V_{24}\chi_{SM}{}^0)_0=(\chi_{sm}\cdot\chi_{SM}{}^0)\times[(w-b)+2(b-w)M_{24}]U_{24}, \quad (9d)$$

where

$$(\chi_{sm}\cdot\chi_{SM}{}^0)=\delta_{sS}\delta_{mM}[\tfrac{1}{2}3^{\frac{1}{2}}\delta_{S0}+2^{-\frac{1}{2}}\delta_{S1}]. \quad (10)$$

The direct interaction here gives no spin-orbit coupling.

The tensor couplings will be designated with the subscript T. One finds first that they do not couple the singlet states, either to each other or to the triplets.[2] For the like-particle pair (1, 3), we find:

$$(\chi_{1m}\cdot V_{13}\chi_{1M}{}^0)_T=\kappa_{mM}Y_{2M-m}(\vartheta_{13},\varphi_{13})\cdot\tfrac{1}{3}(1+2M_{13})U_{13}, \quad (11)$$

where Y_{2M-m} is the normalized spherical harmonic and $(5/8\pi)^{\frac{1}{2}}\kappa_{mM}$ is given by Table I. For the unlike particle pairs (1, 4) and (2, 3), the expressions are the same as (11) except that each has also a factor $\frac{1}{2}$ (and, naturally, the coordinates refer to the appropriate separation distance in each case). Whereas the like-particle pair (1, 3) is coupled doubly (no factor $\frac{1}{2}$), the complementary pair (2, 4) leads to a vanishing result with our choice of the states.

The most striking result here is that the spin-orbit coupling due to the tensor forces does not affect the singlet states, and, in particular, provides no triplet ↔ singlet transitions. (Of course, other forms of spin-orbit coupling might arise, as is well known, but the tensor forces can plausibly be expected to be the main source.) This could have had serious implications for the considerations of Part I. It was found there that the experiments required the production of isotropically distributed products from triplet collisions. Such come from triplet to singlet transitions. However, reference to (31a) of Part I shows that the reorientation (change of M) in the triplet to triplet transition also contributes in the manner needed. Thus, the spin-orbit coupling as provided by the tensor forces promises to be adequate for explaining the observations analyzed in Part I.

[2] There is also a quintet to singlet coupling. We follow the procedure of Part I in ignoring it.

TABLE I.

$m \backslash M$	1	0	−1
1	1	$-3^{\frac{1}{2}}$	$6^{\frac{1}{2}}$
0	$3^{\frac{1}{2}}$	−2	$3^{\frac{1}{2}}$
−1	$6^{\frac{1}{2}}$	$-3^{\frac{1}{2}}$	1

3. THE INTERACTION RESPONSIBLE FOR TRANSITIONS

To obtain the transition probabilities, Flügge[3] evaluated matrix elements of potentials connecting *all* pairs of the particles involved. This at least gives correct orders of magnitude, but no straightforward justification of it seems ever to have been given. In the comparison of transitions involving various angular momenta, more attention must be given to the distinctive properties of the interactions responsible. We therefore construct a wave equation for the product wave which will show us how the product amplitude grows from the incident wave as a source.

We construct a description of the process in the form $\Psi=\Psi^{(0)}+\Psi^{(1)}$ where $\Psi^{(0)}$ describes the initial situation, $\Psi^{(1)}$ the final state. At the asymptotes where $\Psi^{(0)}$ describes two separated deuterons, $\Psi^{(1)}$ must vanish. $\Psi^{(0)}$ is to vanish where $\Psi^{(1)}$ describes any one particle as being far removed from the nucleus of the remaining three. We write

$$\Psi^{(0)}=2^{-\frac{1}{2}}(1-P_{13})\psi_D(r_{12})\psi_D(r_{34})\times\textstyle\sum_{SM}F_{SM}{}^0(\mathbf{r})\chi_{SM}{}^0(1234), \quad (12)$$

where $\mathbf{r}=\frac{1}{2}(\mathbf{r}_1+\mathbf{r}_2)-\frac{1}{2}(\mathbf{r}_3+\mathbf{r}_4)$ and the numerals in the argument of $\chi_{SM}{}^0$ stand for spin coordinates. ψ_D is the deuteron ground-state spatial wave function and

$$F_{SM}{}^0(\infty)=2(4\pi/9v)^{\frac{1}{2}}\textstyle\sum_L(2L+1)^{\frac{1}{2}}i^L\times Y_{L0}(\vartheta_r)(kr)^{-1}f_L(r), \quad (13)$$

where f_L has unit amplitude [see Part I, Eq. (4)]. This gives the correct incident current for obtaining the cross section directly by counting the resulting processes. ϑ_r is the angle made by $\mathbf{r}$ with the direction of incidence. P_{13} permutes both space and spin coordinates of the particles (1, 3). It is then obvious that (12) is correctly symmetrized if L is only even when $S=0$, and if L is only odd when $S=1$, considering the symmetry properties of $\chi_{SM}{}^0$.

In describing the final state we neglect the Coulomb effects. On the one hand, the reaction energy available makes the Coulomb barriers fairly negligible. On the other, the experimental observations[4] show that neutron

[3] Flügge, Zeits. f. Physik **108**, 545 (1938).

[4] Blair, Freier, Lampi, Sleator, and Williams, Phys. Rev. **74**, 1599 (1948).

and proton ejections behave in a parallel manner. Thus, the He^3 nuclear state will not be differentiated from the triton state, $\psi_T(\langle 234\rangle)$. Here, the symbol $\langle 234\rangle$ stands for an argument symmetrical in r_{23}, r_{24}, and r_{34}, as befits the expected evenness of the state. Now,

$$\Psi^{(1)}=\tfrac{1}{2}(1-P_{13}+P_{14}P_{23}+P_{12}P_{34})\psi_T(\langle 234\rangle) \times\textstyle\sum_{sm} F_{sm}(\varrho)\chi_{sm}(1234) \quad (14)$$

with $\varrho=\mathbf{r}_1-(1/3)(\mathbf{r}_2+\mathbf{r}_3+\mathbf{r}_4)$. The permutation operators give $\Psi^{(1)}$ the correct symmetry if χ_{sm} is antisymmetric in the spin coordinates, (2, 4). Each permutation term corresponds to the ejection of a different one of the four particles. $F_{sm}(\infty)$ should describe an outgoing wave only.

We introduce the Hamiltonian

$$H=\sum_{i=1}^{4} T_i+\sum_{i,j>i} V_{ij} \quad (15a)$$

$$\equiv H_D(12)+H_D(34)+H_0 \quad (15b)$$

$$\equiv H_T(234)+H_1, \quad (15c)$$

where $H_D\psi_D=E_D\psi_D$, E_D being the deuteron binding energy, and $H_T\psi_T=E_T\psi_T$, E_T being the triton binding energy.

$$H_0=T_0+V_0 =-(\hbar^2/2M)\nabla_r^2+V_{13}+V_{14}+V_{23}+V_{24} \quad (16)$$

is useful to note; H_1 is equally obvious.

Well-known procedures[5] enable one to obtain equations for the F_{sm}, $F_{SM}{}^0$ which make $\Psi=\Psi^{(0)}+\Psi^{(1)}$ as good a solution of $H\Psi=W\Psi$ as is possible with the forms (12) and (14). The wave equation for F_{sm} results from

$$\delta\int\Psi^*(H-W)\Psi d\tau=0 \quad (17)$$

when the variation δ is due to an arbitrary $\delta F_{sm}{}^*$. For this (17) may at once be reduced to

$$\delta\int\psi^{(1)*}(H-W)\Psi^{(1)}d\tau =-\delta\int\Psi^{(1)*}(H-W)\Psi^{(0)}d\tau. \quad (18)$$

Because $(H-W)\Psi^{(1)}$ has only a magnitude determined by the newly growing state $\Psi^{(1)}$, it may be approximated more roughly than $(H-W)\Psi^{(0)}$. Quite in keeping with standard perturbation theory procedures, we shall approximate H on the left-hand side with a Hamiltonian $H^{(0)}$ which differs from (15) in that:

$$V_{ij}{}^{(0)}=[w_0+b_0B_{ij}+2w_0P_{ij}+2b_0M_{ij}]U_{ij} \quad (19)$$

in place of (1). A potential minus the tensor coupling, like (19), is known to give a fair account of the internucleonic forces[6] when $w_0=-0.23$ and $b_0=+0.77$.

The result of (18) has the form:

$$[-\tfrac{2}{3}(\hbar^2/M)\nabla_\rho^2+\bar{V}_{sm}(\varrho)-E_1]F_{sm}(\varrho)=-g_{sm}(\varrho), \quad (20)$$

where $\bar{V}_{sm}$ is an "effective potential," its important characteristic being that it vanishes rapidly outside the "nuclear radius." $E_1=W-E_T$ and the "source function" is:

$$g_{sm}(\varrho)=2^{\frac{1}{2}}\textstyle\sum_{SM}\int\psi_T\chi_{sm}(H-W)\psi_D\psi_D F_{SM}{}^0 \times\chi_{SM}{}^0(d\tau/d\varrho)+\sum_{s'm'}\int K_{sms'm'}(\varrho,\varrho') \times F_{s'm'}(\varrho')d\varrho'. \quad (21)$$

K being obtainable in terms of the potentials and kinetic energies. The first of the "source" terms has the chief interest here, since it is obviously responsible for the D+D reactions.

We follow customary procedures[7] in obtaining a formal solution of (20), of the type:

$$F_{sm}(\varrho)=\textstyle\sum_{lm_l}(k_1\rho)^{-1}f_{lm_lsm}(\rho)Y_{lm_lsm}(\vartheta,\varphi), \quad (22)$$

where $k_1=(3ME_1/2)^{\frac{1}{2}}/\hbar$. At large distances,

$$f_{lm_lsm}(\infty)=-\exp[i(k_1\rho-\tfrac{1}{2}l\pi+\eta_l)] \times\int_0^\infty\varphi_{lm_lsm}(\rho)g_{lm_lsm}(\rho)d\rho, \quad (23)$$

with

$$g_{lm_lsm}=(3M/2\hbar^2)\rho\int d\omega Y_{lm_l}{}^*g_{sm}(\varrho). \quad (24)$$

Here, $\varphi(\rho)$ is the regular solution of the homogeneous part of Eq. (20). η_l is an undetermined phase shift.

We can now put together the complete solution at its asymptote $\rho=\infty$:

$$\Psi=-\tfrac{1}{2}\psi_T(k_1\rho)^{-1}e^{ik_1\rho}\textstyle\sum_{sm lm_l} \times\chi_{sm}Y_{lm_l}(-i)^le^{i\eta_l}\int_0^\infty\varphi g d\rho \quad (25)$$

as follows from (14), (22), and (23). This represents ejected neutrons of index 1. Twice as many are ejected altogether, so that the consequent cross section for neutron production is:

$$\sigma=\int 2(1/4k_1^2)\mathbf{S}\left|\textstyle\sum_{sm lm_l}\chi_{sm}Y_{lm_l}(-i)^le^{i\eta_l}\int_0^\infty\varphi g d\rho\right|^2 \times(3\hbar k_1/4M)d\omega, \quad (26)$$

[5] J. A. Wheeler, Phys. Rev. 52, 1107 (1937).

[6] Rosenfeld, *Nuclear Forces* (Interscience Publishers, Inc., New York), p. 131, gives $V_{ij}=(1-2g)^{-1}[1-\frac{1}{2}g+\frac{1}{2}g(\boldsymbol{\sigma}_i\cdot\boldsymbol{\sigma}_j)]U_{ij}$ for s-states ($M_{ij}=+1$), with $g=0.19$. This leads to

$$w_0=-\tfrac{1}{2}(1-3g)/(1-2g) \text{ and } b_0=\tfrac{2}{3}(1-\tfrac{3}{2}g)/(1-2g).$$

It is equivalent to replacing S_{ij} in (1) with $\frac{1}{2}g(3+\boldsymbol{\sigma}_i\cdot\boldsymbol{\sigma}_j)/(1-2g)$, which also vanishes for singlets.

[7] Mott and Massey, *Theory of Atomic Collisions* (Oxford University Press, New York, 1933).

with the symbol **S** standing for integration over spin coordinates. It is now obvious that the second part of g, as given by (21), should be neglected here since it arises from the newly growing state and must be negligible in comparison with the first term, which comes for the initially established state $\Psi_{LSM}{}^0$ (see below).

As is to be expected, the cross section (26) is given by the square of a matrix element. This is given a standard form in the following. We write the "final state":

$$\Psi_{lm_l sm}=[\rho^{-1}\varphi_{lm_l sm}(\rho)Y_{lm_l}(\vartheta,\varphi)]\psi_T\chi_{sm}, \quad (27)$$

in which $\varphi_{lm_l sm}$ is to be normalized per unit energy.[8] The initial state must be normalized according to (13). We introduce a new "radial function," $\varphi_{LSM}{}^0(r)$, such that $e^{-C_L}\varphi_{LSM}{}^0$ is normalized per unit energy. The exponential represents a diminution of the amplitude at the nuclear surface due to the limited penetrability of the barriers, as evaluated in the WKB approximation.[9] Putting it into evidence as we do here allows us to express the main energy-dependence of the cross section (26) through the factor

$$\sigma_L=(4\pi/9k^2)(2L+1)e^{-2C_L}, \quad (28)$$

which is the cross section for approach to the nuclear surface as defined in Part I. We now write an "initial state wave-function":

$$\Psi_{LSM}{}^0=[r^{-1}\varphi_{LSM}{}^0(r)Y_{L0}]\psi_D(r_{12})\psi_D(r_{34})\chi_{SM}{}^0. \quad (29)$$

Then the differential cross section can be written in the form:

$$d\sigma=d\omega\mathbf{S}\left|\sum\sigma_L{}^{\frac{1}{2}}\chi_{sm}Y_{lm_l}\cdot 4\pi(-i)^l e^{i\eta_l}\times\int\Psi_{lm_l sm}{}^*(H-W)\Psi_{LSM}{}^0 d\tau\right|^2, \quad (30)$$

in which the summation $\sum$ is to be carried out over all the indices: l, m_l, s, m, L, S, M. This is directly comparable with the forms of Part I.

It should be pointed out that the initial wave function (29), and therefore all but the factor $\sigma_L{}^{\frac{1}{2}}$ in (30), can be regarded as practically independent of the deuteron energy. It is well known that a radial function of unit amplitude at infinity, tends to behave $\sim(kr)^{L+1}$ at small distances on account of the centrifugal forces. A function normalized to unit energy will then behave[8] $\sim k^{L+\frac{1}{2}}$. It can easily be shown that when the centrifugal barriers are dominant[8]

$$e^{-C_L}\sim(kR)^{L+\frac{1}{2}},$$

and therefore $\varphi_{LSM}{}^0$ can plausibly be regarded as having its main energy dependence factored out.

Our chief concern is with the matrix element:

$$\langle H-W\rangle=\int\Psi_{lm_l sm}{}^*(H-W)\Psi_{LSM}{}^0 d\tau \quad (31)$$

occurring in the cross section. Recalling (29), (15), (16), (4), and (5), we may write:

$$\langle H-W\rangle=\langle H_0-E_0\rangle, \quad (32)$$

where $E_0=W-2E_D(=\frac{1}{2}E)$ is the relative energy of the deuterons. It is

$$H_0-E_0=T_0-E_0+V_0, \quad (33)$$

which seems to play the part of the interaction responsible for the reaction transitions, in place of

$$V_0+V_{12}+V_{34}$$

as employed by Flügge.[3]

4. THE MATRIX ELEMENTS

The many terms which constitute the matrix elements $\langle H_0-E_0\rangle=\langle T_0-E_0+V_0\rangle$ appearing in (32), after insertion of (16) and (1), can be reduced considerably in number by making use of the symmetries of the wave functions Ψ and Ψ^0. Part of this process has already been carried out when the spin-integrations leading to (9) and (11) are completed. After the Majorana operations still left in (9) and (11) have been performed, it can be shown that:

$$\langle V_0\rangle_0\equiv 3b\langle(-)^S U_{13}+U_{23}\rangle. \quad (34)$$

The precise significance of the bracketing $\langle\ \rangle$ was illustrated in (31). As before, the subscript 0 means that here the tensor coupling has been left out. The tensor terms of V_0 yield the matrix elements:

$$\langle V_0\rangle_T\equiv\langle-\tfrac{1}{2}S_{13}U_{13}+S_{23}U_{23}\rangle=\tfrac{1}{2}\kappa_{mM}\langle U_{23}Y_{2M-m}(\vartheta_{23},\varphi_{23})-U_{13}Y_{2M-m}\langle\vartheta_{13},\varphi_{13}\rangle\rangle. \quad (35)$$

We see that the interactions are expressible entirely as between like-particle pairs (1, 3) and unlike-particle pairs (2, 3).

In the remainder, $\langle T_0-E_0\rangle$, of the matrix element, one can readily show that the proper operator following from (16) is:

$$T_0=\frac{p_r{}^2}{2M}+\frac{L(L+1)\hbar^2}{2Mr^2}, \quad (36)$$

where $p_r=-i\hbar(\partial/\partial r+1/r)$ is the radial momentum operator. Moreover, this operation can, through Green's theorem, be thrown upon functions in the matrix integral other than φ and φ^0 [see (30), (29), and (27)]:

$$\langle T_0-E_0\rangle=(\chi_{sm}\cdot\chi_{SM}{}^0)\int\int d\varrho d\mathfrak{r}(\varphi/\rho)(\varphi^0/r)\times Y_{lm_l}{}^*Y_{L0}(T_0-E_0)\int(d\tau/d\varrho d\mathfrak{r})\psi_T\psi_D\psi_D. \quad (37)$$

The kinetic energy involved here is so large ($\gtrsim$72 Mev, evaluations below will show) that for the deuteron

[8] H. A. Bethe, Rev. Mod. Phys. **9**, 105 (1937). This differs from a function of unit amplitude by the factor $(2/\pi\hbar v_l)^{\frac{1}{2}}$.

[9] Part I, Eq. (6).

energies concerning us ($E_0=\frac{1}{2}E<2$ Mev), E_0 can be neglected and the matrix element regarded as independent of energy.

The greatest difficulty in estimating the matrix elements comes from evaluating the radial functions φ, φ^0 of (27) and (29). Flügge[3] has succeeded in carrying out an approximate valuation for s-states only, with numerical solutions of appropriate wave equations. He thus showed that potentials of the type (19) can lead to a correct order of magnitude for the total cross section. It will therefore suffice for our purposes to estimate ratios between the contributions of more general types of collisions and those due to s-waves. For this, we shall assume that the product $\varphi_{lm_lsm}\varphi_{LSM}{}^0$ is replaceable by an average, $\langle\varphi\varphi^0\rangle_{Av}$, within the nuclear surface; this average value will be assumed independent of angular momenta for the low quantum numbers of interest to us. This has plausibility because the centrifugal forces associated with low quantum numbers should not disturb the effect of the specifically nuclear forces appreciably.

Specific expressions will also be needed for the deuteron and triton ground-state wave functions, ψ_D and ψ_T. The most important characteristics of these for the matrix integrals are their "spreads," which may be well enough represented by the normalized distributions:

$$\psi_D(r_{12})=(2\alpha^2/\pi)^{\frac{3}{4}}\exp(-\alpha^2 r_{12}{}^2), \tag{38}$$

$$\psi_T(\langle 234\rangle)=(3\beta^2/\pi)^{\frac{3}{4}}(4\beta^2/\pi)^{\frac{3}{4}}\times\exp[-\beta^2(r_{23}{}^2+r_{24}{}^2+r_{34}{}^2)]. \tag{39}$$

We have obtained the values of α and β which yield the observed deuteron and triton binding energies when potentials of the type (19) are used, with the singlet depth[5] $D=27.2$ Mev and the range $a=2.1_5(10)^{-13}$ cm. They are $(\alpha a)^2=0.4$ and $(\beta a)^2=0.5$.

Even the integrations over the Gaussian distributions (38), (39), and (3) require undue labor because they are not symmetrical about the collision center. Of course, this non-central character has important effects in that it determines the magnitudes of the angular momentum exchanges between the constituent particles. It manifests itself in the angular integrations. These are threefold, arising from the position vectors of four particles minus the degrees of freedom of the mass center, of the type:

$$\int d\omega_\rho Y_{lm_l}{}^*(\vartheta_\rho,\varphi_\rho)\int d\omega_r Y_{L0}(\vartheta_r)\int d\omega_u Y_{\lambda\mu}(\vartheta_u,\varphi_u)\times\exp[-c_1(\boldsymbol{\rho}\cdot\mathbf{r})-c_2(\boldsymbol{\rho}\cdot\mathbf{u})-c_3(\mathbf{r}\cdot\mathbf{u})], \tag{40}$$

where $\mathbf{u}$ is the third-position vector needed besides the ones originally introduced: $\boldsymbol{\rho}$ and $\mathbf{r}$. $\lambda=2$ for the terms with tensor coupling, *vide* (35), and $\lambda=0$ otherwise. The exponentials arise from the various Gaussian distributions. The approach which could be most consistently carried through was to use a well-known expansion of the exponential, superposed with the addition theorem for spherical harmonics:

$$\exp[-c_1(\boldsymbol{\rho}\cdot\mathbf{r})]=4\pi\sum_{l_1m_1}(-i)^{l_1}j_{l_1}(ic,\rho r)\times Y_{l_1m_1}{}^*(\vartheta_\rho,\varphi_\rho)Y_{l_1m_1}(\vartheta_r,\varphi_r). \tag{41}$$

Here the j_{l_1} are the spherical Bessel functions.[10] This means that the subsequent radial integrations will be over the Bessel function j_{l_1} multiplied with Gaussian distributions. For small arguments[10]

$$j_{l_1}(ic_1\rho r)\approx[ic_1\rho r]^{l_1}/1\cdot3\cdot5\cdots(2l_1+1). \tag{42}$$

This exhibits the most important effect of these functions: they weight outer parts of the particle distributions the more heavily, the larger the number of quanta l_1 of angular momentum that is transferred. We shall approximate this effect by using the evaluation (42), trusting to the Gaussians to "cut off" adequately the regions of large ρ, r when (42) is invalid. The degree of validity of this approximation is unfortunately sensitive to the choice of coordinates, i.e., the choice made for $\mathbf{u}$ in (41). Investigation showed,[11] however, that for *ratios* of matrix elements, adequate accuracy is obtained when $\mathbf{u}=\mathbf{r}_3-\mathbf{r}_4$ (i.e., the separation in that deuteron which captures a nucleon from its fellow deuteron) is used together with the $\boldsymbol{\rho}$ and $\mathbf{r}$ previously introduced.

The procedures described were feasible for $\langle T_0-E_0\rangle$, $\langle U_{13}\rangle$ and $\langle U_{23}\rangle$, but for the tensor terms $\langle S_{13}U_{13}\rangle$ and $\langle S_{23}U_{23}\rangle$ coordinates were dictated which yield poorer accuracy with our approximations. The effect of this was minimized by reevaluating $\langle U_{13}\rangle$ and $\langle U_{23}\rangle$ exactly as $\langle S_{13}U_{13}\rangle$ and $\langle S_{23}U_{23}\rangle$, then employing only the resulting ratios $\langle S_{13}U_{13}\rangle/\langle U_{13}\rangle$ and $\langle S_{23}U_{23}\rangle/\langle U_{23}\rangle$ to obtain the final numerical values.

We now correlate our matrix elements with the coefficients introduced to represent them in Part I. For this, we replace the symbols of the type $\langle H-W\rangle=\langle H_0-E_0\rangle\approx\langle H_0\rangle$ introduced in (31) with the more specific ones:

$$\langle H_0\rangle=\langle lm_lsm|H_0|LSM\rangle. \tag{43}$$

Now, comparison of (30) with (25) of Part I leads to the notational identifications:

$$\alpha_L=4\pi(-i)^L e^{i\eta_L}\langle L000|H_0|L00\rangle, \tag{44a}$$

$$\gamma_{LM-m}{}^m=4\pi(-i)^L e^{i\eta_L}\langle L,M-m,1m|H_0|L1M\rangle, \tag{44b}$$

$$\beta_{LL+1}=4\pi(-i)^{L+2}e^{i\eta_{L+2}}\times[(2L+1)(2L+5)/(L+1)(L+2)]^{\frac{1}{2}}\times\langle L+2,010|H_0|L10\rangle, \tag{44c}$$

$$\beta_{LL-1}=4\pi(-i)^{L-2}e^{i\eta_{L-2}}\times[(2L+1)(2L-3)/L(L-1)]^{\frac{1}{2}}\times\langle L-2,010|H_0|L10\rangle. \tag{44d}$$

As shown in Section 1, $\beta_L=\beta_{LL}=0$, here.

[10] L. Schiff, *Quantum Mechanics* (McGraw-Hill Book Company, Inc., New Yok, 1947) has a convenient summary of these.

[11] Made possible by the fact that in some terms the integration could be carried through exactly.

procedures needed for the numerical evaluation of ratios of the matrix elements (44) to α_0, the s-wave matrix element, have already been described, and the necessary values of numerical quantities introduced. We may therefore list the results:

$$|\alpha_2|^2/|\alpha_0|^2=2.0, \tag{45a}$$

$$|\alpha_4|^2/|\alpha_0|^2=0.50. \tag{45b}$$

These include no tensor coupling since only singlet collisions are involved. For odd L, there are first the matrix elements (with $m=M$) which receive contributions from the non-tensor and the tensor interactions:

$$|\gamma_{10}{}^0|^2/|\alpha_0|^2=2.9; \quad |\gamma_{10}{}^{\pm1}|^2/|\alpha_0|^2=4.0. \tag{46}$$

These would equal each other without the tensor coupling, as would the corresponding matrix-elements for $L=3$:

$$|\gamma_{30}{}^0|^2/|\alpha_0|^2=0.58; \quad |\gamma_{30}{}^{\pm1}|^2/|\alpha_0|^2=1.04. \tag{47}$$

Matrix elements which vanish without spin-orbit coupling are of the type:

$$|\gamma_{11}{}^0|^2/|\alpha_0|^2=|\gamma_{11}{}^{-1}|^2/|\alpha_0|^2=0.0012, \tag{48}$$

and

$$\begin{aligned} &|\beta_{12}|^2/|\alpha_0|^2=0.023_5 \quad (\beta_{10}=0), \\ &|\beta_{34}|^2/|\alpha_0|^2=0.070, \\ &|\beta_{32}|^2/|\alpha_0|^2=0.028. \end{aligned} \tag{49}$$

These numbers are to be regarded only as measures of order-of-magnitude because of the crudity of the representations of the various wave-functions.

The present theory cannot yield the phases of the matrix elements whose magnitudes are given by (45)–(49). This would require much greater accuracy, such as is obtainable only by numerical integration. However, one can get some idea of the consistency of the theory with the experimental data (which does depend on relative phases) by assuming sufficient randomness of the phases to put equal to zero the cross terms between quantities of unequal phase. On this basis, the quantities measured by the experiments according to Part I are:

$$\begin{aligned} &K_1/K_0\approx(6|\gamma_{11}{}^0|^2+|\beta_{12}|^2)/|\alpha_0|^2\approx0.096 \quad (\text{Exp:}\sim1) \\ &A_1/K_0\approx(3|\gamma_{10}{}^0|^2+6|\gamma_{10}{}^1|^2)/|\alpha_0|^2\approx33 \quad (\text{Exp:}\sim6) \\ &\bar{K}_2/K_0\approx(5/4)|\alpha_2|^2/|\alpha_0|^2\approx2.5 \quad (\text{Exp: } 5.9) \\ &\bar{A}_2/K_0\approx-(15/2)|\alpha_2|^2/|\alpha_0|^2\approx-15 \quad (\text{Exp: } -30) \\ &\bar{B}_2/K_0\approx(45/4)|\alpha_2|^2/|\alpha_0|^2\approx22.5 \quad (\text{Exp: } 40) \\ &\bar{A}_3/K_0\approx(63/4)(|\gamma_{30}{}^0|^2+2|\gamma_{30}{}^1|^2)/|\alpha_0|^2\approx42 \\ &\qquad\qquad (\text{Exp: } 300) \\ &\bar{B}_3/K_0\approx-(10/3)\bar{A}_3/K_0\approx-140 \quad (\text{Exp: } -850). \end{aligned} \tag{50}$$

As one sees, there is a general concordance in the way the theoretical and experimental values vary from one case to the other. Considering the crudity of our approximations closer agreements should perhaps not have been expected.

There is just one case in the list (50) which provides a clear measure of the spin orbit coupling: $\bar{K}_1/K_0$. One can see that here the theory gives too small a coupling by a factor 10 or so; this is a somewhat worse comparison than the other values show. There is therefore, this indication that the spin-orbit coupling provided by the tensor forces alone may be insufficient. However, the discrepancy is on the margin of detectability for both the experiments and the present theory.

Part of this work was assisted by the Joint Program of the ONR and AEC.

The Isotopic Constitution of Scandium, Gadolinium, Dysprosium, Holmium, Erbium, and Ytterbium

WALLACE T. LELAND*
University of Minnesota, Minneapolis, Minnesota
(Received November 23, 1949)

The relative abundances of the isotopes of scandium, gadolinium, dysprosium, holmium, erbium, and ytterbium have been redetermined with a mass spectrometer incorporating an electron multiplier to give increased sensitivity. No new isotopes were found although special attention was devoted to this problem and low upper limits were set for nearly all possible isotopes.

ALTHOUGH the isotopic constitution of all the elements has been investigated heretofore, the data on several of the heavier elements are incomplete insofar as no search has been made for very rare isotopes, and in some cases the abundances need revision or confirmation. With these points in mind, several elements were examined with a mass spectrometer which was particularly well suited for the detection of rare isotopes and the measurement of natural isotopic abundances in relatively heavy elements.

APPARATUS AND PROCEDURE

The mass spectrometer employed in this investigation is essentially a modification of one already described in detail by Nier.[1] Figure 1 is a schematic diagram showing the general features of the major parts of the apparatus. Figure 2 gives a more detailed schematic of the source and source end of the spectrometer tube. Ions are obtained by thermionic emission from an appropriate compound with which the under side of the filament is coated. For the elements reported in this paper an oxide of the element in question was used. Adjustment of the current through the filament provided control over the temperature of the oxide coating and the rate of ion emission. In Fig. 2, S refers to a rectangular chamber which surrounds the filament and, along with one side of the filament, is connected to a source of high potential. J_1-J_2 and J_3 are essentially two slotted round plates connected to somewhat lower potentials and serve to draw the ions emitted by the filament down through a slit in S and to form a beam directed in the proper direction. Actually, J_1 and J_2 are a pair of half plates which, if connected to different potentials, provide a cross field capable of deflecting the ion beam to one side or the other. G_1 and G_2 are two grounded plates with fairly small slits, their function being to limit the beam as to size and angular divergence. The nearly monoenergetic beam of ions leaving the source passes through the sector magnet, is bent and dispersed in a spectrum according to the mass to charge ratio of the constituent ions. To measure the intensity of a particular type of ion the ratio of the magnetic field strength to ion energy is adjusted until the trajectory of the ions in question is such that they pass through the adjustable slit in front of the electron multiplier. The slit width is so adjusted that nearly all the ions in question will pass through to the exclusion of those having different mass or charge to mass ratios. The electron multiplier converts the ion current passing through the slit to a considerably larger, but nevertheless proportional, electron current which is then fed to a conventional feedback current amplifier. The design of the electron multiplier corresponds essentially to a scaled down version of one described by Allen.[2] The dynodes are made of a 2 percent beryllium copper alloy and are stacked up and mounted on a flange with a construction similar to that used on the ion source. Potentials and currents for operating the tube were supplied by electronically regulated supplies, a 2500-volt supply for the ion source, a 4500-volt supply for the multiplier and a 0–300 ma supply for the magnet. At 300 ma the magnet produced a field of about 8000 gauss in the air gap of $\frac{5}{8}$ inch. An ionization gauge not shown in the drawings was attached to the vacuum system to indicate the pressure.

The procedure in analyzing an element was quite simple. A clean new filament was prepared and moistened with a drop of pure water. A small amount of powdered oxide was then added to the drop of water so as to form a paste covering one side of the filament. When dry, the filament and source were inserted into the spectrometer tube and the vacuum pump started. After the ionization gauge pressure reading fell below 10^{-6} mm of Hg, the filament was turned on and its temperature raised slowly until adequate ion emission was obtained. Ion currents were metered by feeding the output of the current amplifier to a Brown Strip Chart recording potentiometer. By varying the magnetic field at an appropriate rate a mass spectrum was then traced by the recorder, and by measuring the heights of the various peaks the isotopic abundances could be determined. In order to maintain the desired accuracy over large ranges in intensity the current amplifier was provided with an accurately calibrated divider enabling step-wise changes in sensitivity up to a factor of 500. The usual procedure was to sweep over two or, at most, three adjacent peaks first in one

* A.E.C. Fellow.
[1] A. O. Nier, Rev. Sci. Inst. 18, 398 (1947).
[2] J. S. Allen, Rev. Sci. Inst. 18, 739 (1947).

direction and then the other, the amplifier sensitivity being adjusted for each peak so that the recorder registered almost full scale. Generally twenty or more sweeps were made on a given set of peaks, and in some cases the procedure repeated on different days or at different intensities. The multiplicity of the data permits elimination of errors due to short term fluctuations in the ion current simply by an averaging process while reversing of the sweep direction on successive spectra tends to eliminate errors due to slow drifts in ion current intensity.

ACCURACY OF ABUNDANCE MEASUREMENTS

Obviously the problem of making accurate abundance measurements with a mass spectrometer involves both the production of separated ion beams having intensities of known relation to the isotopic abundances and the subsequent accurate measurement of the individual separated ion currents.

This later problem of measuring small ion currents has been fairly well solved by the development of accurate electrical methods to replace the older and inaccurate photographic plate techniques. The problem of quantitative production of separated ion currents, however, is still subject to many uncertainties which are difficult to detect, since they normally lead to systematic errors and do not affect the consistency or reproducibility of the results. If for the present study it is assumed that the chemicals used as ion sources have not suffered an alteration in isotopic constitution during their preparation, there is still the question of whether there is preferential emission of ions from the source or whether discriminating effects on ions of different mass occurs between the source and ion collector. This latter factor is believed to be negligible in the present experiments. By keeping all potentials fixed and varying only the magnetic field, the trajectories of ions of different mass should be identical in every respect at the time they are metered. Variation of ion source efficiency with voltage is not involved and effects due to initial energies of the emitted ions should be similar for all masses, provided the initial energies are independent of mass. The problem of preferential emission, however, is open to question. Such effects have, for example, been observed by Cook[3] in the case of potassium. A check of potassium with the present apparatus showed similar variations which could not be otherwise understood. Presumably the effect is contingent on the uneven transport of ions or atoms to or from the emitting surface, since if there were no mixing or other means of removing matter from the surface of the emitter, the emission would necessarily reach an equilibrium value giving the proper proportions of each isotope. In this respect, the rare earth oxides should be fairly good sources, since the emission does occur from the solid state at temperature not greatly exceeding 1000°C. Furthermore, the relatively high mass of the ions involved make for small fractional mass differences and less pronounced diffusion effects. To obtain an estimate of the reliability of this type of source, measurements were made on gadolinium on successive days and with different ion intensities. Small variations not exceeding one percent were observed, and it is believed that in the present study this type of error did not exceed one percent.

Errors introduced by the current measuring apparatus should not exceed 0.2 percent. The linearity of the electron multiplier was checked by measuring known isotope ratios such as the K^{40} to K^{39} ratio and found to be adequately linear. The input resistor used in the current amplifier when making abundance

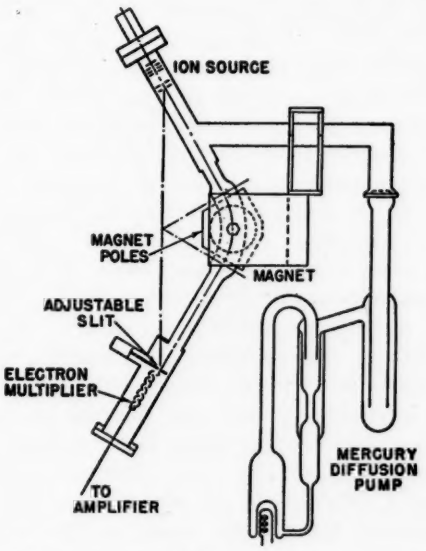

FIG. 1. Schematic drawing showing mass spectrometer tube and auxilliary apparatus.

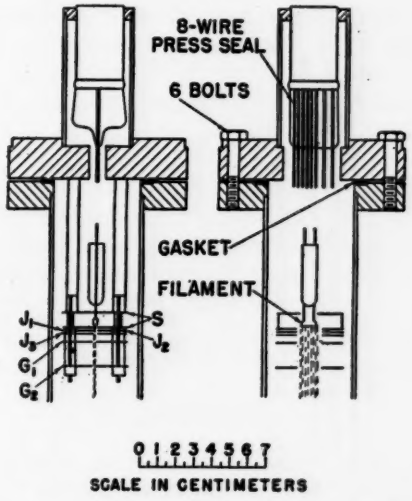

FIG. 2. Schematic drawing of ion sources. The filament is a 0.001-in. tungsten ribbon having a width of 0.030-in. and an overall extended length of about 0.5 inch. Slits in G_1 and G_2 are 0.010 inch by 0.56 inch.

[3] Kenneth L. Cook, Phys. Rev. 64, 278 (1943).

TABLE I. Isotopic constitution of gadolinium.

Isotope	Atomic percentage This study	Hess	Wahl	Dempster	Aston
149	<0.001	<0.005			
150	<0.0005	<0.005			
151	<0.0003	<0.005			
152	0.20±0.005	0.20	0.2	0.2	
153	<0.0005	<0.005			
154	2.16±0.02	2.15	2.86	1.5	
155	14.68±0.15	14.78	15.61		21
156	20.36±0.20	20.59	20.59		23
157	15.64±0.16	15.71	16.42		17
158	24.96±0.25	24.78	23.45		23
159	<0.002	<0.01			
160	22.01±0.22	21.79	20.87		16
161	<0.001	<0.02			
162	<0.002	<0.02			

measurements had a nominal resistance of 2×10^{10} ohms. By placing a charged air condenser in parallel with this resistor and watching the decay in voltage as a function of time, it was ascertained that for the range of voltages used in making abundance measurements, the resistance was independent of voltage to the extent of the 0.1 percent which could have been detected in the test. Response of the amplifier and recorder were checked and the divider used to change amplifier sensitivity carefully calibrated.

The error limits assigned to the measured abundances reported in this paper are estimated maximum errors. They are taken as one percent of the measured value except in special cases where special uncertainties entered.

DETECTION OF RARE ISOTOPES

The detection of rare isotopes poses altogether different problems. Not only is it necessary to measure ion currents having a ratio of say 10^4 to 10^6 in magnitudes, but it is also necessary to produce such well-defined and separated ion beams that the stragglers in the large beams do not mask the presence of the small one. In addition there is the problem of eliminating impurities to a very high degree. If one considers that there is a smallest ion current which can be detected, then there likewise is a minimum total ion current commensurate with measuring a given ratio of ion currents. The higher this ratio is the higher must be the total ion current. Unfortunately, the production of larger ion currents is generally in opposition to the problem of obtaining well-resolved ion beams. Increasing the size of slits to accept a larger and more diverse beam obviously will give more intensity and poorer resolution. Attempts to increase the rate of ion production in the source usually result in an increase in pressure in the spectrometer tube, and an intolerable amount of scattering occurs. In the present apparatus noticeable scattering occurred even at pressures as low as 10^{-6} mm of Hg. It is clear then that there are definite advantages to be gained by using an electron multiplier and working with smaller ion currents. There is, however, no guarantee that the addition of an electron multiplier will enable one to immediately detect rarer isotopes. In the not too unusual cases where there are certain small but relatively fixed impurity peaks already present, one is forced to work at high intensities in an effort to drown out the impurities. Also there are cases wherein resolution is inadequate by virtue of factors fairly independent of the ion intensity or where the samples used contain impurities which remain pretty much in proportion to the element studied. This latter situation proved to be the biggest difficulty in the elements studied in this investigation. All samples used in this work were procured from Johnson, Matthey, and Company, Limited and were of their "specpure" brand. Each

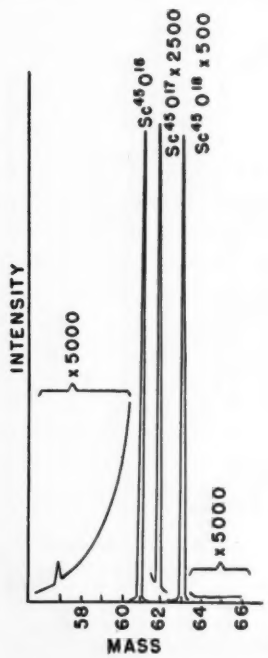

FIG. 3. Mass spectrum of ScO^+ ions. The mass 62 and 63 peaks are due to oxygen isotopes. The mass 57 peak is attributed to an unidentified impurity.

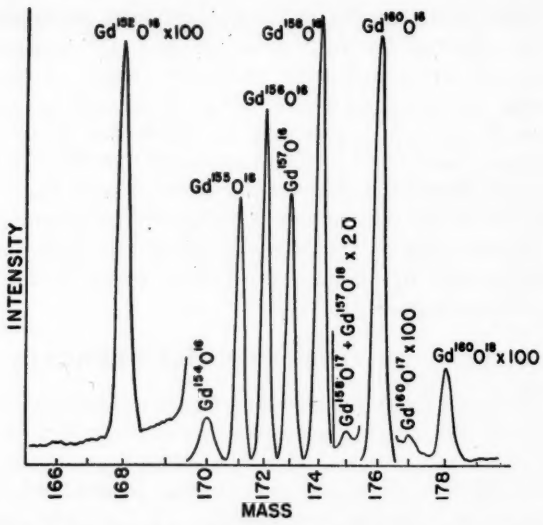

FIG. 4. Mass spectrum of GdO^+ ions showing seven gadolinium isotopes and two oxygen isotopes.

sample had been analyzed spectroscopically by the supplier and detectable traces of impurities reported. Although the spectroscopic analysis generally did not show the presence of troublesome impurities, they invariably turned up in unfortunate amounts. The multiplier used had a gain of about 1000 which is far below its capabilities. In view of the impurity difficulties, however, there was nothing to be gained by taking steps to increase the gain. Also the slits used were larger than would be desirable for best resolution. The lowest upper limits reported in this article occur for scandium and correspond to two parts in 10^6. A better idea of the ultimate capabilities of the apparatus is discerned by the one part in 3×10^6 limit placed on I^{129} as reported in a previous article[4] (erroneously reported one place in the article as three parts in 10^6).

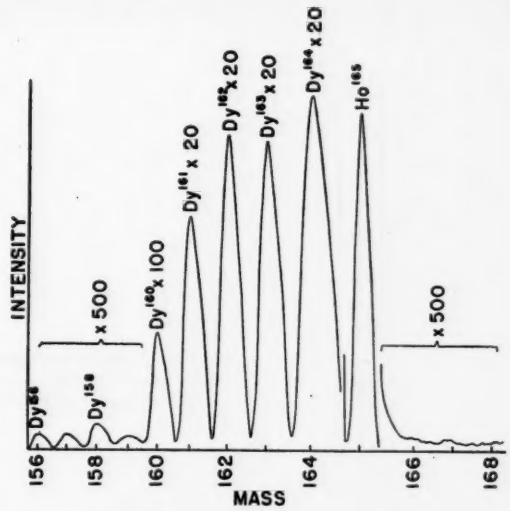

FIG. 6. Mass spectrum of Ho^+ and Dy^+ ions. Peaks at masses 157 and 159 are attributed to impurities.

SCANDIUM

Scandium has been examined by Aston[5] who reported the single isotope Sc^{45}. In this investigation heated Sc_2O_3 was used as a source of thermionic ions. ScO^+ ions were by far the most abundant and, consequently, most suited for the analysis in spite of interference from oxygen isotopes. Figure 3 shows a spectrum of the mass region 57 to 66. Peaks at masses 62 and 63 are accounted for by oxygen isotopes as indicated in the figure. The small peak at mass 57 apparently is due at least in part to an impurity of some sort, since its size relative to the 61 peak did not remain constant with time or with variations in the size of the 61 peak. Upper limits obtained for possible scandium isotopes are as follows: Sc^{41} less than 0.001 percent; Sc^{42}, Sc^{43}, Sc^{48}, and Sc^{49} less than 0.0002 percent; Sc^{44} less than 0.0005 percent; Sc^{46} less than 0.002 percent; Sc^{47} less than 0.01 percent. Limits on Sc^{46} and Sc^{47} are taken to be 5 percent of the abundance of the oxygen isotopes which interfered with these measurements. Actually an analysis of the observed mass 62 and mass 63 peak indicated that they were about 5 percent smaller than would be expected on the basis of the abundances of the oxygen isotopes as given by Thode and Smith.[6] However, comparison of data taken at different times and under different source conditions indicated that, in spite of good internal consistency obtainable for a given analysis for fixed conditions, the result of any one analysis might well be in error to the extent of 5 percent, and no special significance could be attached to lower values obtained for the abundance of the oxygen isotopes. The difficulty probably lies with the type of source used as was discussed earlier in this article.

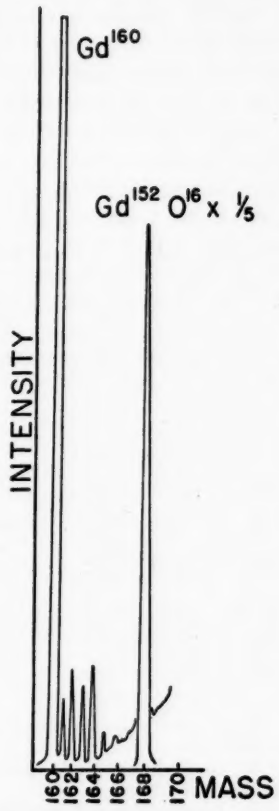

FIG. 5. Expanded view of mass spectrum in region just below lightest known isotope of gadolinium. Unlabeled peaks can be accounted for by rare earth impurities. The flat top in the Gd^{160} peak signifies that it exceeded the maximum travel of the recorder.

With the exception of Sc^{41}, limits on other scandium isotopes are computed on the basis of the estimated size of peak which could have been detected. The size of the mass 57 peak under the most favorable circumstances was used to compute an upper limit for Sc^{41}.

GADOLINIUM

The isotopic constitution of gadolinium has been studied by several investigators, first by Aston,[7] who discovered the five isotopes Gd^{155}, Gd^{156}, Gd^{157}, Gd^{158},

[4] W. T. Leland, Phys. Rev. **76**, 992 (1949).
[5] F. W. Aston, Proc. Roy. Soc. **A134**, 571 (1932).
[6] H. G. Thode and S. R. Smith, National Research Council of Canada, Atomic Energy Project, Report MC-57 (revised) (May, 1949).
[7] F. W. Aston, Proc. Roy. Soc. **A146**, 46 (1934).

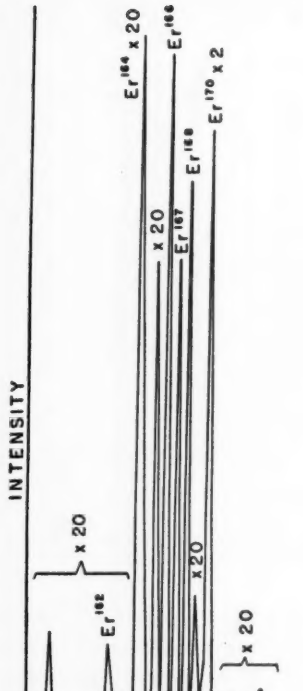

FIG. 7. Mass spectrum of Er^+ ions. Unlabeled peaks are attributed to impurities.

and Gd^{160}, then by Dempster,[8] who also observed the additional less abundant isotopes Gd^{152} and Gd^{154}. Wahl[9] and Hess[10] have since made more precise measurements of the natural isotope abundances but with some disagreement. Further interest in gadolinium centers on the isotope Gd^{150} whose existence in nature has been suggested on the basis of regularities in the isotopic constitution of the heavier elements.[11] Thermionic GdO^+ ions obtained from heated Gd_2O_3 were used in this investigation. The results corrected for the presence of oxygen isotopes are listed in Table I along with those of previous investigations for the sake of comparison. The agreement with Hess' results is quite satisfactory. Actually, if the abundance ratios of adjoining isotopes were compared, the results would be in even better agreement with the exception of the 157/156 ratio. Figure 4 shows a typical mass spectrum of the gadolinium isotopes. The peaks at mass 175, 177, and 178 can be accounted for by oxygen isotopes as indicated in the figure. Computation of the O^{17} and O^{18} abundances on the basis of these peaks gives results agreeing with those of Thode and Smith[6] within 5 percent. The limits placed on Gd^{159}, Gd^{161}, Gd^{162} are consequently computed on the basis of a maximum error in the abundance measurements, namely 10 percent for the peaks of mass 175 and mass 177 and 5 percent for the mass 178 peak.

As is seen in Fig. 5 several peaks occur on the mass range 160 to 169, and in particular a small peak is evident at mass 166 which could be due to $Gd^{150}O^{16}$ in the event Gd^{150} actually existed. However, the 166 peak did not show proper correlation to the other gadolinium peaks, and it is unlikely that more than a small fraction of this peak is due to Gd^{150}. Actually these observed peaks together with their relative abundances are well accounted for by a mixture of NdO^+, Dy^+, and Ho^+ ions which are likely impurities.

The limits placed on the abundances of Gd^{149} and Gd^{150} nevertheless are taken as the size of the corresponding observed impurity peak.

DYSPROSIUM AND HOLMIUM

The holmium oxide secured for the analysis of holmium contained considerable amounts of dysprosia (about 15 percent according to supplier). Because dysprosium has isotopes of mass numbers equal to those of possible holmium isotopes, it was necessary to make an analysis of the dysprosium peaks and compare the results with its previously measured isotopic constitution[12] in order to determine whether or not any holmium peaks were superimposed on those of dysprosium. Although the dysprosium analysis suffered to some extent from the fact that dysprosium occurred in the sample merely as an impurity, the results are nevertheless of interest in that they confirm for the most part the results of Inghram, Hayden, and Hess[12] which do not agree entirely with those of Wahl.[13] In the case of holmium on the other hand, the existence of rare isotopes is still in question. Aston[7] reported a single isotope Ho^{165} but gave no estimate of the sensitivity of his apparatus. Although radioactivities have been reported for most possible holmium isotopes,[14] the isotope assignment in most cases is uncertain. A typical spectrum obtained with Dy^+ and Ho^+ thermionic ions

TABLE II. Isotopic constitution of dysprosium.

Isotope	Atomic percentage				
	This study	Inghram, Hayden, Hess	Wahl	Dempster	Aston
156	0.064+0.001 −0.064	0.0524			
158	0.105+0.001 −0.105	0.0902	0.1	0.1	
160	2.36 +0.02 −0.10	2.294		1.5	
161	18.73 ±0.19	18.88	21.1		22
162	25.36 ±0.25	25.53	26.6		25
163	24.91 ±0.25	24.97	24.8		25
164	28.47 +0.28 −0.56	28.18	27.3		28

[8] A. J. Dempster, Phys. Rev. **53**, 727 (1938).
[9] W. Wahl, Soc. Sci. Fenn., Comment-Physics-Mathematics U, 1 (1941).
[10] D. C. Hess, Jr., Phys. Rev. **74**, 773 (1948).
[11] H. E. Duckworth, Phys. Rev. **75**, 1438 (1949).
[12] M. G. Inghram, R. J. Hayden, and D. C. Hess, Jr., Phys. Rev. **75**, 693 (1949).
[13] W. Wahl, Suomen Kemistiseuran Tiedonatoja **51**, 64 (1942).
[14] G. T. Seaborg and E. Perlman, Rev. Mod. Phys. **20**, 623 (1948).

is shown in Fig. 6. Upper limits obtained for possible holmium isotopes are as follows: Ho^{161}, Ho^{162}, Ho^{163}, and Ho^{164} less than 0.04 percent; Ho^{166}, Ho^{167}, and Ho^{168} less than 0.001 percent; Ho^{169} less than 0.004 percent. The results for dysprosium are given in Table II but must be qualified to some extent due to the presence of impurities as indicated in Fig. 6 by the presence of peaks of mass 157 and mass 159. Assuming the impurities to be rare earths or other common thermionic ion emitters, it is possible to account for all the peaks. Unfortunately, however, it was not possible to make positive identification, and the abundances for the lighter dysprosium isotopes are correspondingly uncertain. Gd^+ ions were pretty much ruled out by noting the inconsequential size of peaks corresponding to GdO^+ ions which are normally the most abundant from a gadolinium oxide source. However, various combinations of CeO^+, NdO^+, PrO^+, Dy^+, and Tb^+ ions giving good account of the peaks in the mass range 156 to 159 could not be ruled out. Actually, it is necessary to assume the presence of only PrO^+, Tb^+, and Dy^+ in which case there would be no interference with the analysis. Taking this last assumption the computed abundances for Dy^{156}, Dy^{158}, and Dy^{160} as given in Table II are higher than those reported by Inghram *et al.*[12] It should be pointed out that since it was not possible to rule out the presence of cerium, this work could not be considered as definite confirmation of the existence of Dy^{156}. The measurement of the Dy^{164} abundance is subject to some error due to imperfect resolution of the mass 164 and mass 165 peaks. This error which is normally negligible is enhanced by the fact the 165 peak is about 20 times as large as the 164 peak. If, for example, in this case the 165 peak has fallen off by a factor of 2000 at the mass 164 position, the 164 peak will still be too high by about one percent. Although it was not possible to ascertain the exact amount of error present on this account, it should not exceed one percent.

The upper limits placed on holmium isotopes lighter than mass 165 are taken as one percent of the corresponding dysprosium peak, while for the heavier isotopes the size of observed impurity peaks is listed.

TABLE III. Isotopic constitution of erbium.

Isotope	Atomic percentage This work	Wahl	Dempster	Aston
160	<0.005		<0.03	
161	<0.01		<0.03	
162	0.154±0.007	0.1	0.25	
163	<0.01		<0.03	
164	1.60±0.02	1.5	2.0	
165			<0.03	
166	33.36±0.33	32.9		36
167	22.82±0.23	24.4		24
168	27.02±0.27	26.9		30
169	<0.15			
170	15.04±0.15	14.2		10
171	<0.01		<0.03	
172	<0.01		<0.03	

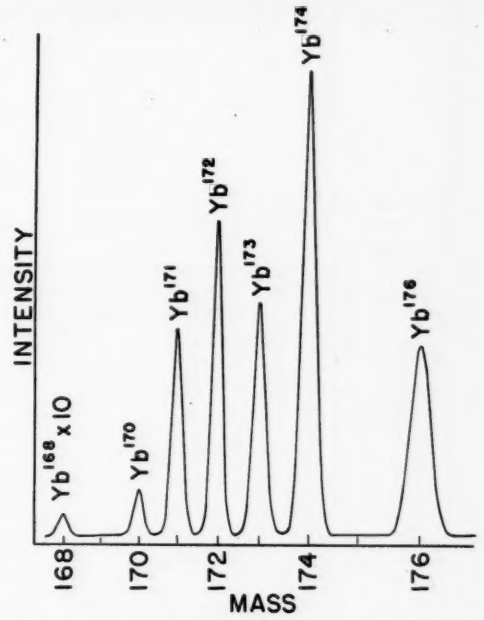

FIG. 8. Mass spectrum of Yb^+ ions showing the seven isotopes of ytterbium.

ERBIUM

Erbium was first studied by Aston[7] who reported the isotopes Er^{166}, Er^{167}, Er^{168}, and Er^{170}. Dempster[8] later found Er^{162} and Er^{164}. More recently Wahl[15] has remeasured the abundances of the natural isotopes. The data obtained by these investigations, however, is based on the photographic plate method of ion detection, and it is of interest to redetermine the abundances using more accurate electrical methods of ion current measurements.

Er^+ ions obtained from heated Er_2O_3 gave the results listed in Table III. A typical spectrum is shown in Fig. 7. As is evident from Fig. 7, there are sizeable peaks at mass 165 and mass 169. However, neither of these peaks maintained a constant ratio to the other erbium peaks with time and with variations in source

TABLE IV. Isotopic constitution of ytterbium.

Isotope	Atomic percentage This study	Hayden, Hess, Inghram	Wahl	Dempster	Aston
166	<0.001	0.002			
167	<0.0005	0.002			
168	0.13±0.005	0.140		0.06	
169	<0.0005	0.01			
170	3.03±0.03	3.034	4.21	2.0	
171	14.27±0.14	14.34	14.26		9
172	21.77±0.22	21.88	21.49		24
173	16.08±0.16	16.18	17.02		17
174	31.91±0.32	31.77	29.58		38
175	<0.005	0.01			
176	12.80±0.13	12.65	13.38		12
177	<0.001	0.01			
178	<0.0005	0.002			

[15] W. Wahl, Suomen Kemist. Tied. **50**, 10 (1941).

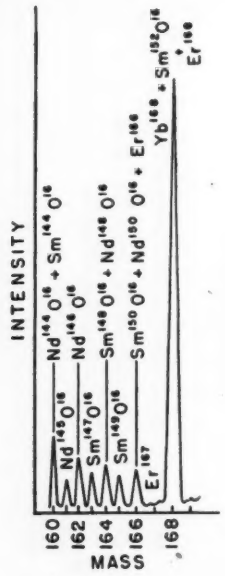

FIG. 9. Mass spectrum showing impurity peaks in mass region below Yb^{168}.

temperature, so they are definitely due, at least in part, to impurities. The corresponding peaks also appeared in the ErO^+ spectrum, but the amounts were significantly different. The most probable impurities are holmium and thulium. SmO^+ ions by virtue of the small mass 163 peak cannot account for the mass 165 peak, while EuO^+ ions are rendered an unlikely source of the 169 peak due to the absence of Eu^+ ions in consequential amounts. Since holmium and thulium have but one isotope, they do not interfere with the analysis other than by making it impossible to detect a small amount of Er^{165} or Er^{169} should they exist. Other peaks in the spectrum indicate the possibility of small amounts of gadolinium, samarium, ytterbium, or dysprosium being present. Allowances for these possibilities have been made by increasing the error limits on abundances in the appropriate direction.

YTTERBIUM

Ytterbium is known to have at least seven naturally occurring isotopes of masses 168, 170, 171, 172, 173, 174, and 176. The five heaviest ones were discovered by Aston,[7] who was the first to investigate the isotopic constitution of ytterbium. Dempster[8] later found the two lighter and rarer isotopes. The relative abundances of the natural isotopes have since been redetermined by Wahl[16] and by Hayden, Hess, and Inghram.[17]

This investigation employed thermionic Yb^+ ions from heated Yb_2O_3. A typical spectrum is shown in Fig. 8, and the results are tabulated in Table IV along with those of other investigators. The measurement of the Yb^{168} abundance was made difficult to some extent by the presence of impurities. Figure 9 shows a typical spectrum of the mass region 160–168. If one makes the very probable assumption that the peaks are due to rare earth ions of the RO^+ or R^+ variety, it is possible to make reasonably positive identification of the impurities by comparing the relative heights of the impurity peaks with the known isotopic abundances of the rare earths. Table V, for example, gives an analysis of the impurity peaks shown in Fig. 9. Examination of the spectrum for lighter masses further substantiates the assignments made. Admitting the presence of samarium of course necessitates a correction in the ytterbium peaks of mass 168 and 170 due to interference from $Sm^{152}O^{16}$ and $Sm^{154}O^{16}$. Under conditions prevalent when the data of Table IV was taken, the correction amounted to 11 percent in the measured abundance of Yb^{168} and 0.4 percent for Yb^{170}. Assignment of upper limits to possible rare ytterbium isotopes has been made on the basis of the heights of observed impurity peaks with the exception of Yb^{175} and Yb^{166} limits. Resolution proved to be a limiting factor in the case of Yb^{175}, while for Yb^{166} allowance has been made for the presence of $Sm^{150}O^{16}$ and $Nd^{150}O^{16}$, the amounts of which are assumed known on the basis of other peaks with an accuracy of 25 percent. Presence of significant amounts of other likely rare earth impurity peaks which might interfere with the analysis has been ruled out. For example, a troublesome amount of gadolinium which would yield GdO^+ ions and give a spectrum coinciding with that of the Yb^+ ions is ruled out by the extreme scarcity of peaks corresponding to Gd^+ ions and to $Gd^{150}O^{18}$.

TABLE V. Analysis of impurity peaks in ytterbium.

Mass	Assumed ions NdO^+	SmO^+	Er^+	Yb^+	Total	Observed peak
160	9.2	0.9			10.1	10.0
161	3.2				3.2	3.4
162	6.6				6.6	6.6
163		4.5			4.5	4.5
164	2.2	3.4			5.6	5.7
165		4.1			4.1	4.1
166	2.2	2.2	0.6		5.0	5.0
167			0.4		0.4	0.5
168		7.9	0.5	52.6	61.0	61.0

I wish to express my sincere thanks to Professor A. O. Nier for his help and encouragement throughout this work. The instrument used in this work was built with a grant from the Graduate School. The research was supported by the Joint Program of the Office of Naval Research and the Atomic Energy Commission. Assistance was also given by the University of Minnesota Technical Research Fund subscribed to by General Mills, Incorporated, Minnesota Mining and Manufacturing Company, Northern States Power Company, Minneapolis Star-Journal and Tribune, and Minneapolis Honeywell Regulator Company.

[16] W. Wahl, Naturwiss. 29, 536 (1941).
[17] Hayden, Hess, and Inghram, Phys. Rev. 75, 322 (1948).

Ionization Chamber Study of the Disintegration of He^3 and N^{14} by Thermal Neutrons*

W. Franzen,† J. Halpern, and W. E. Stephens
University of Pennsylvania, Philadelphia, Pennsylvania

(Received October 31, 1949)

The total ionization produced by the reactions $He^3(n,p)$ and $N^{14}(n,p)$ in a gas mixture consisting mainly of argon was measured by means of a cylindrical ionization chamber operated under conditions of electron collection. High resolution was achieved by suitable choice of chamber geometry and by use of a low noise level amplifier. The total ionization charges collected from polonium alpha-particles, from the disintegration products of $He^3(n,p)$ and from those of $N^{14}(n,p)$ are found to be in the ratio $1:0.145\pm0.002:0.119\pm0.001$, respectively. Comparison with polonium alpha-particles on the assumption of a constant average energy per ion pair in argon then yields reaction energies of 766 ± 10 kev for $He^3(n,p)$ and 630 ± 6 kev for $N^{14}(n,p)$. The difference between these energies agrees well with the difference between the end points of the beta-ray spectra of C^{14} and H^3. This agreement supports the assumption of a proportionality between energy and ionization in argon independent of particle type. A value of 785 ± 6 kev is computed for the neutron-hydrogen mass difference from these data.

INTRODUCTION

A PRECISE measurement of the energy evolved in (n,p) reactions is of interest in view of the fact that the initial and final nuclei involved in such reactions are neighboring isobars. The reaction energy when combined with the neutron-hydrogen mass difference will therefore yield a value for the difference between the masses of the two isobars, a quantity which may also be determined from the radioactivity of the final nucleus. Thus, consider a (n,p) reaction involving an initial nucleus of atomic number Z and mass number A:

$$Z^A+{}_0n^1\rightarrow(Z-1)^A+{}_1H^1+Q_{np}.$$

The reaction will proceed with slow neutrons if $Q_{np}>0$. On the other hand, if $Q_{np}<{}_0n^1-{}_1H^1$, the final nucleus is unstable and decays into the initial nucleus by negative electron emission:

$$(Z-1)^A\rightarrow Z^A+e^-+E_\beta+\nu.$$

If we consider atomic masses, we then have two possible expressions for the mass difference of the two isobars:

$$(Z-1)^A-Z^A=({}_0n^1-{}_1H^1)-Q_{np},$$
$$(Z-1)^A-Z^A=E_\beta+\nu.$$

Here E_β is the *actual* maximum energy of the electrons emitted by the final nucleus and ν is the mass of the neutrino.

In principle, therefore, it is possible to obtain an upper limit on the neutrino mass by use of a reaction cycle which involves the (n,p) reaction energy, the neutron-hydrogen mass difference and the maximum energy E_β of the beta-rays. On the other hand, by assuming that the end point E_{ext} of the beta-ray spectrum of the product nucleus as obtained by extrapolation on the basis of the Fermi theory gives the mass difference of the isobars (independent of the neutrino mass), that is, if $E_{ext}=E_\beta+\nu$, one may calculate the neutron-hydrogen mass difference by adding E_{ext} to

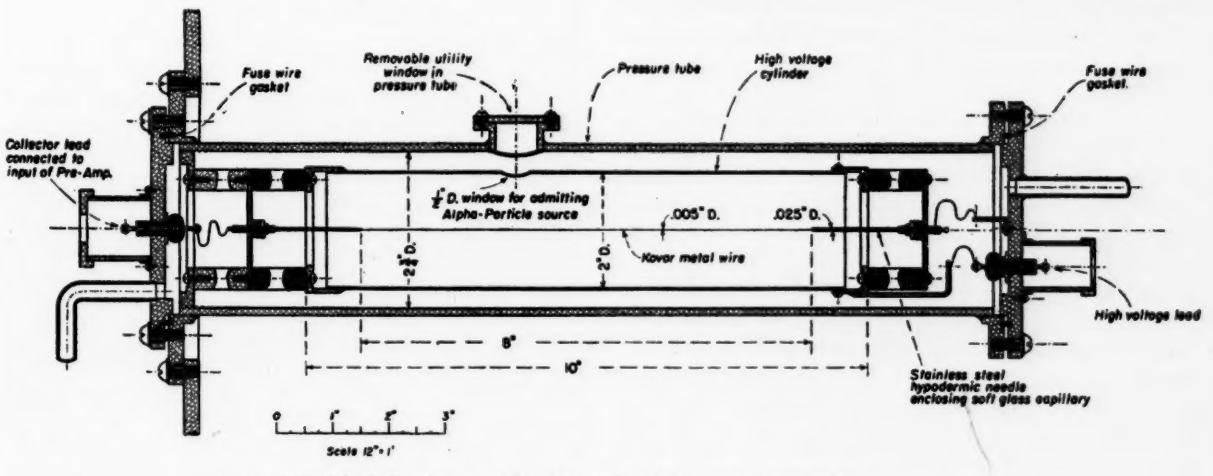

FIG. 1. Cylindrical chamber used for the study of slow neutron reactions.

* Essential portion of a dissertation submitted by W. Franzen to the Graduate School of the University of Pennsylvania.
† Mary Amanda Wood Research Associate at the University of Pennsylvania until August 31, 1949. Now at Palmer Physical Laboratory, Princeton University.

the (n,p) reaction energy: ${}_0n^1-{}_1H^1=E_{ext}+Q_{np}$. The second one of these two alternate procedures was regarded here as the best application of the data obtained.

Previous studies of slow neutron (n,p) reactions have in general fallen into two classes: Cloud-chamber range measurements and total ionization determinations. Despite the precision that can be attained in the measurement of the range of the emitted protons,[1-3] the interpretation of the resulting range values is handicapped by the uncertainty existing in the proton range-energy curve in the low energy region. The total ionization determinations, on the other hand, have been handicapped by the comparatively small energy evolved in slow neutron (n,p) reactions; as a consequence, amplifier noise proved to be a serious limitation on the energy resolution that could be attained, particularly in experiments performed under conditions of total ion collection. The size of the noise level in these cases is caused by the necessity of operating the amplifier with time constants which are long compared to the collection time of the ions; as a consequence, a great deal of low frequency noise (microphonics, line frequency hum, and thermal noise) is present. It is experimentally very difficult to reduce this type of noise below a level which represents an appreciable fraction of the (n,p) reaction energy. A more fundamental limitation on the interpretation of the ionization chamber data has been the absence of any precise knowledge regarding the relationship between energy and total ionization.

We have attempted to overcome the effect of amplifier noise by operating an ionization chamber with electron collection in a gas mixture having high electron drift velocity and by choosing the time constants of the associated amplifier so as to achieve as low a noise level as practicable. A study of the various factors that contribute to the total noise level made it possible to reduce this level to a value of the order of one percent of the energies to be measured. The difficulty introduced by the lack of a reliable energy-ionization relation was minimized to some extent by using argon (in which this relation has been studied more thoroughly than in most other gases) as the principal stopping gas in the chamber. In addition, the two reactions were observed simultaneously so that a cross-check on the validity of the method of calibration could be obtained.

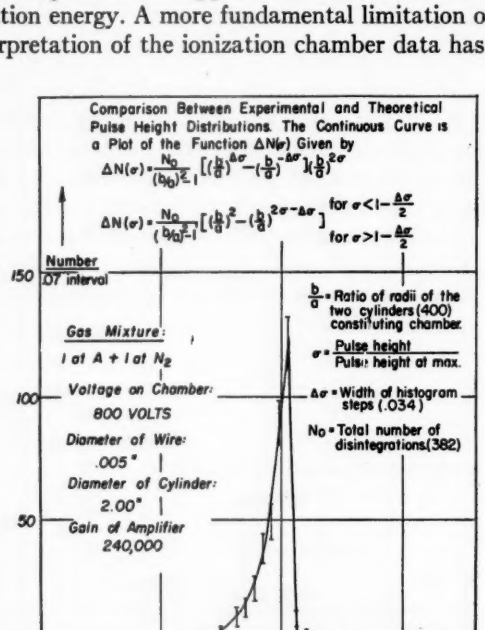
Comparison Between Experimental and Theoretical Pulse Height Distributions. The Continuous Curve is a Plot of the Function ΔN(σ) Given by
ΔN(σ) = N0/(b/a)^2−1 [(b/a)^Δσ − (b/a)^−Δσ](b/a)^2σ
ΔN(σ) = N0/(b/a)^2−1 [(b/a)^2 − (b/a)^2σ−Δσ] for σ<1−Δσ/2
for σ>1−Δσ/2
Number .07 interval
150
100
50
Gas Mixture: I at A + I at N2
Voltage on Chamber: 800 VOLTS
Diameter of Wire: .005"
Diameter of Cylinder: 2.00"
Gain of Amplifier 240,000
b/a = Ratio of radii of the two cylinders (400) constituting chamber
σ = Pulse height / Pulse height at max.
Δσ = Width of histogram steps (.034)
N0 = Total number of disintegrations (382)
1.00
2.00
3.00
Relative Pulse Height

FIG. 2. $N^{14}(n,p)$ reaction. Comparison of experimental pulse-height distribution with the theoretical distribution derived by considering the effect of electron collection on an isotropic distribution of point charges throughout the volume of a cylindrical chamber of the dimensions used.

EXPERIMENTAL METHOD

The cylindrical ionization chamber used in the experiment is shown in Fig. 1. To be noted particularly are the use of guard cylinders to prevent collection of the ionization electrons formed outside the region of cylindrical symmetry, and the large ratio between the diameters of the two cylinders that constitute the chamber.

The reason for using a large ratio of radii is that do to the use of electron collection, the voltage signal induced by the motion of the free electrons from their point of liberation to the collector electrode is in general smaller than the signal which would be induced by the motion of the entire charge, including the positive ions. As a matter of fact, the size of the induced signal is proportional to the fraction of the total potential difference (between the electrodes) which is traversed by the electrons.[4] Thus, corresponding to a known initial geometrical distribution of charges, one obtains a distribution of voltage signals of various sizes. For an isotropic distribution of very short disintegration tracks throughout the volume of a cylindrical chamber, the differential distribution in pulse heights can be computed simply:[5]

$$dN/d\sigma=\frac{2N_0\log(b/a)}{(b/a)^2-1}(b/a)^{2\sigma} \text{ for } 0<\sigma<1,$$

$$dN/d\sigma=0 \text{ for } \sigma>1.$$

Here σ is the ratio of the actual pulse height to the pulse height at the maximum of the distribution curve, N_0 is the total number of disintegrations, and a and b are the radii of the two cylinders constituting the chamber. This distribution is sharply peaked at $\sigma=1$ if $b\gg a$; its width at half-maximum is given by

[1] J. K. Boggild, Kgl. Danske Vid. Sels. Math.-fys. Medd. **23**, 22 (1945).
[2] D. J. Hughes and C. Eggler, Phys. Rev. **73**, 809 (1948).
[3] Cornog, Franzen, and Stephens, Phys. Rev. **74**, 1 (1948).
[4] See, for example, Bridge, Hazen, Rossi, and Williams, Phys. Rev. **74**, 1084 (1948).
[5] P. G. Koontz and T. A. Hall, Rev. Sci. Inst. **18**, 643 (1947).

$[(\frac{1}{2})\log 2]/\log(b/a)$. To make this width as narrow as possible, it is advantageous to use as large a ratio b/a of the radii as possible.

The use of guard cylinders, on the other hand, makes it possible to collect electrons only from those disintegration tracks which are formed in the cylindrically symmetric electric field, and to exclude those which are formed in the distorted field at the ends of the cylinder. As a consequence, the experimentally observed pulse-height distribution closely resembles the theoretical distribution defined above with the modifications that are introduced by the finite size (channel width) of the groups into which the pulses are arranged, and by the presence of wall effect, amplifier noise, straggling in ionization and similar factors. (The close agreement that can nevertheless be achieved between experimental and theoretical distributions is illustrated by Fig. 2.)

Not shown is a retractable thin polonium alpha-particle source on a platinum foil which was attached, by means of a glass rod and a sylphon bellows, to the outside wall of the chamber and which could be positioned in the plane of the high voltage cylinder. When not in use, the source could be withdrawn to a position where none of the alpha-particles emitted by it were able to reach the sensitive volume of the chamber provided the stopping power of the gas filling exceeded one and one-half times that of air at N.T.P. The source itself was made by deposition from 0.1N HCl solution under hydrogen, as described by Erbacher.[6]

The amplifier used with the chamber was a modified version of the Los Alamos Model 100 amplifier designed by Sands.[7] The modifications consisted of operating the first tube of the preamplifier as a triode, of moving the low frequency limiting RC network to a location between the two feed-back loops of the main amplifier (the time constant of this network was 5 μsec.), and of by-passing the plate resistance of the signal inverting stage (last stage of first feed-back loop of main amplifier) with a condenser of such a magnitude as to make the time constant of this network 7.5 μsec., corresponding to a "rise time" of 17 μsec. This combination of time constants was found experimentally to result in the largest attainable signal-to-noise ratio. In the examination of the effect of different combinations of time constants on the signal-to-noise ratio, we were guided to a large extent by the considerations advanced by Elmore.[8] It was found, however, that various low frequency sources of noise (particularly microphonics) made it difficult to approach the optimum combination of time constants predicted by Elmore. Moreover, it was regarded desirable to keep the duration of the pulses observed at the output of the amplifier within a certain limit to prevent excessive "pile-up" of gamma-ray pulses due to gamma-rays emitted by the radium-beryllium neutron source.

Other modifications of the amplifier consisted of careful selection of the input tube of the preamplifier, non-microphonic mounting, selection of other components at critical stages, and use of coupling time constants between stages at least 200 times as large as the time constant of the low frequency limiting network. The last precaution mentioned made it possible to eliminate any evidence of "overshoot." The input tube was operated with floating grid under reduced electrode voltages; the leakage resistance between the input grid and ground was estimated to be 10^{12} ohms by observation of the time constant with which the capacity between the collector wire and the high voltage cylinder charged up when connecting the cylinder to a source of high potential. Under these conditions, the over-all gain of the amplifier was 240,000 for artificial pulses having a "rise time" an order of magnitude shorter than the time constants of the amplifier, and the root-mean-square noise voltage at the input to the amplifier was 2.3 μv, corresponding to 8 kev of ionization for the input capacity used. (This capacity was estimated to be 20 $\mu\mu$f under operating conditions; the measured capacity with input tube turned off was 16 $\mu\mu$f.)

An illustration of the resolution achieved under these conditions is provided by Fig. 2 in which the distribution in size of 382 individual pulses attributed to $N^{14}(n,p)$ is compared with the theoretical distribution derived by considering the effect of electron collection on an isotropic distribution of point charges distributed throughout the volume of a cylindrical chamber of the dimensions used. The theoretical distribution has been normalized to correspond to the same total number of disintegrations as were actually observed, and the effect of the finite width of the individual groups of the histogram has been taken into account. It is evident that the additional spread in pulse height caused by amplifier noise is small; some straggling in ionization undoubtedly also contributes to the observed spread.

Pulses were observed by photographing the face of an oscilloscope tube; for this purpose the shutter of a Sept camera was held open manually until a signal appeared on the face of a coupled monitoring oscilloscope. At this point, the film was advanced by a single frame. Thus signals occurring at a rate as slow as three per minute could be recorded. The linearity of the over-all system was tested by means of a precision pulser and an electronic discriminator.

The gases used in the chamber were carefully purified by use of the purification system illustrated in Fig. 3. Mixtures of argon and nitrogen could be circulated through the calcium oven shown which was maintained at a temperature of 200°C. At this temperature, the calcium does not react with nitrogen, but is nevertheless very effective in removing contaminants that may give rise to electron capture. The calcium itself was outgassed at 400°C for 24 hr. in a vacuum of the order of

[6] O. Erbacher, Zeits. f. physik Chemie **A156**, 142 (1931).
[7] M. Sands, LADC 82.
[8] W. C. Elmore, Nucleonics **2**, No. 3, 16 (1948).

5×10^{-6} mm Hg before use. The progress of the purification could be checked periodically by taking integral bias curves of polonium alpha-particle pulses as a function of applied potential. For the gas mixture used in the helium-nitrogen-argon mixture experiment, the shift that occurred in the position of the maximum of the pulse-height distribution amounted to one percent of the maximum pulse height as the applied potential was increased from 100 volts to 1000 volts after purification had been completed.

The neutrons originated from a 200 mC radium-beryllium source surrounded by a cylinder of paraffin which was placed below the chamber in such a way that the flux of slow neutrons traversed the chamber along its axis. The thickness of paraffin used was not less than 5 cm on all sides; under these conditions, there was an observable background of fast neutron recoil pulses. However, even in the case of the experiment performed with a gas mixture that contained enriched helium in which rather energetic recoils occur, this background was not large enough to interfere with the observation of the monoenergetic disintegration pulses. Approximately 10 cm of lead were placed in the direct path between the source and the chamber in order to keep the background of gamma-ray pulses to a minimum.

RESULTS

The simultaneous observation of the reactions $He^3(n,p)$ and $N^{14}(n,p)$ was accomplished in a gas mixture consisting of two atmospheres argon, one-tenth atmosphere nitrogen, and one-half atmosphere helium which had been enriched by thermal diffusion at the University of Minnesota. The relative isotopic abundance of the two helium isotopes in the sample used was $He^3/He^4=4.9\times10^{-5}\pm25$ percent. The sample was supplied through the kindness of Professor A. O. C. Nier of the University of Minnesota.

Figure 4 shows the resulting pulse-height distributions as recorded photographically. The mixture of the enriched helium with nitrogen thus gives rise to a double peak with two well-resolved components attributed to $He^3(n,p)$ and $N^{14}(n,p)$, respectively. The relative amounts of the isotopes N^{14} and He^3 in the chamber were originally chosen in such a way that, on the basis of the thermal cross sections published by Coon *et al.*,[9] 7500×10^{-24} cm² for $He^3(n,p)$ and 1.75×10^{-24} cm² for $N^{14}(n,p)$, the ratio of the disintegration rate of $N^{14}(n,p)$ to that of $He^3(n,p)$ would be 2:1. This choice of the ratio of disintegration rates was dictated by a desire to avoid interference of the low energy tail of the pulse-height distribution due to $He^3(n,p)$ with the distribution due to $N^{14}(n,p)$. The actual ratio of disintegration rates was nearly 3:1 and is in approximate accord with recently published values of the cross sections for the two reactions,[10–12] averaging about 5000×10^{-24} cm² for $He^3(n,p)$ and 1.76×10^{-24} cm² for $N^{14}(n,p)$. No attempt was made here to measure the relative cross sections for the two reactions because of the uncertainty attached to the isotopic abundance of the He^3 isotope in the gas mixture.

The distribution in pulse heights obtained from a polonium alpha-particle source in the same gas mixture is shown in Fig. 5. For the observation of the alpha-particle pulses, the gain of the amplifier was diminished by a known amount, and the trigger level of the oscilloscope sweep circuit was set so that only alpha-particle signals were recorded. A comparison of the three

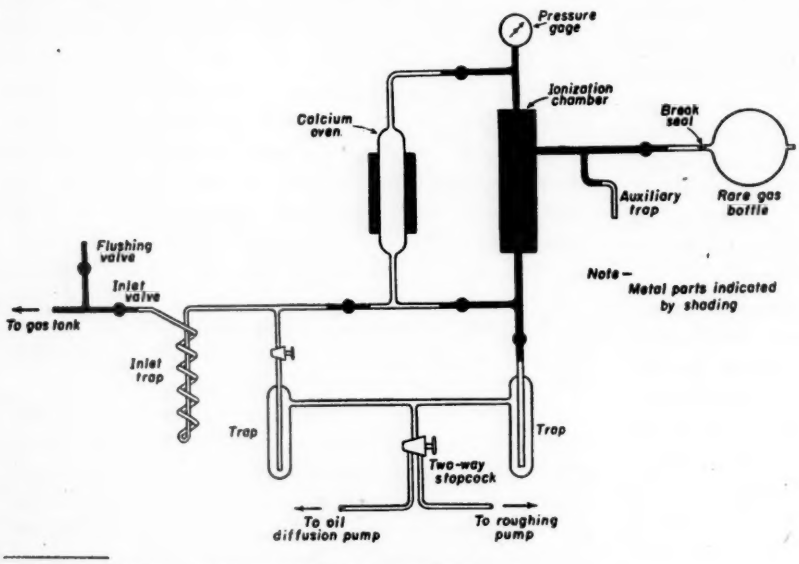

FIG. 3. Schematic diagram of gas-flow and pumping system.

[9] Coon, Goldblatt, Nobles, and Robinson, AECD 2190.
[10] J. H. Coon and R. A. Nobles, Phys. Rev. **75**, 1358 (1949).
[11] L. O. P. King and L. Goldstein, Phys. Rev. **75**, 1366 (1949).
[12] Batchelor, Epstein, Flowers and Whittaker, Nature **163**, 211 (1949).

pulse-height distribution curves reveals the characteristic features previously mentioned that typify the operation of a cylindrical chamber with electron collection. We observe that there is a gradual spread in the low energy direction for the (n,p) reactions, as one would expect for an isotropic distribution of short disintegration tracks throughout the volume of the chamber. The distribution is narrower for the alpha-particles due to the localization of the source on the wall of the ionization chamber. On the high energy side, all distributions fall off sharply in a manner which is determined chiefly by the noise of the amplifier. The sharpness of the location of the high energy edge enables one to deduce the total ionization corresponding to each of the distributions with precision.

A comparison of the three distributions on this basis gives a ratio of $1:0.145\pm0.002:0.119\pm0.001$ for the total ionizations produced in the mixture by polonium alpha-particles, the disintegration products of $He^3(n,p)$ and those of $N^{14}(n,p)$, respectively. The uncertainties indicated for the values of these ratios are estimates of the precision with which the position of the peaks of the pulse-height distributions can be located in view of statistical factors and the finite slope of the distribution curves on the high energy side. Deviations from linearity of the amplifier and recording system are of the order of one-tenth as large as the uncertainties just mentioned.

If we assume that the proportionality between energy and ionization in argon which has been observed by Jesse[13] (although disputed to some extent by the observations of Cranshaw and Harvey[14]) extends to the energy region considered here, and if the effect of the presence of one-tenth atmosphere nitrogen (responsible for approximately 10 percent of the total stopping power of the mixture) on this relation is neglected, we obtain energy values of 766 ± 10 kev for $He^3(n,p)$ and 630 ± 6 kev for $N^{14}(n,p)$ by direct comparison with polonium alpha-particles. (Helium is assumed to be similar to argon in its ionization properties in accordance with the conclusions of Gray.[15]) The polonium alpha-particles were assumed to have an energy of 5298.4 kev.[16] (It should be emphasized that the indicated uncertainties in the Q-values for the (n,p) reactions do not reflect any possible systematic errors arising from the method of calibration.)

Several other gas mixtures containing nitrogen and argon in various proportions were also studied, and a systematic increase with nitrogen concentration of the ratio of the total ionization due to $N^{14}(n,p)$ to that due to polonium alpha-particles was observed. This increase

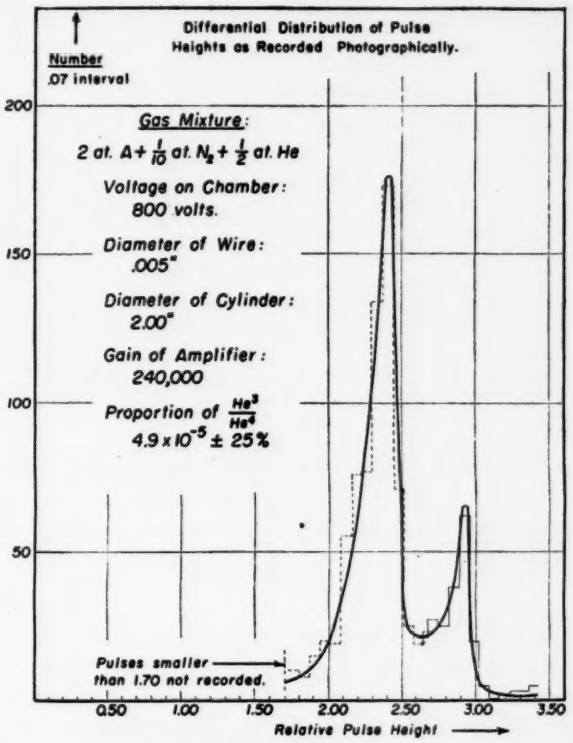

FIG. 4. Pulse-height distribution obtained from the reactions $He^3(n,p)$ and $N^{14}(n,p)$.

amounted to approximately three percent for pure nitrogen as compared to the helium-nitrogen-argon mixture. Thus the correction that would have to be applied to the energy values deduced from the total ionization observed in this mixture to account for the influence of the small concentration of nitrogen present amounts to -0.3 percent. This is negligibly small compared to other uncertainties inherent in the measurement.[17] The cause of the increase in total ionization with nitrogen concentration is not known, but is not necessarily in conflict with two other recent observations[18,19] in which a decrease of total ionization with energy in nitrogen as compared to argon was observed at the energy of the $B^{10}(n,\alpha)$ reaction and the energy of samarium alpha-particles. In the first of these experiments, the total ionization was measured in air, rather than in pure nitrogen. Under such conditions, there is no free electron mobility and saturation conditions are essentially different from those prevailing in purified nitrogen as used here.

DISCUSSION

The difference between the Q-values for $He^3(n,p)$ and $N^{14}(n,p)$ obtained by assuming simple proportionality

[13] (a) W. P. Jesse and H. Forstat, Phys. Rev. **74**, 1259(A) (1948); (b) W. P. Jesse and J. Sadauskis, Phys. Rev. **75**, 1110 (1949).

[14] T. E. Cranshaw and J. A. Harvey, Can. J. Research **26**, 243 (1948).

[15] L. H. Gray, Proc. Camb. Phil. Soc. **40**, 72 (1944).

[16] M. G. Holloway and M. S. Livingston, Phys. Rev. **54**, 18 (1938).

[17] For this reason, the correction of -2 kev that was applied to the energy values for $He^3(n,p)$ and $N^{14}(n,p)$ in a preliminary account of the experiment described here [Franzen, Halpern, and Stephens, Phys. Rev. **76**, 317 (1949)] has not been applied to the values given above.

[18] See reference 13(b).

[19] Stebler, Huber, and Bichsel, Helv. Phys. Acta **22**, 362 (1949).

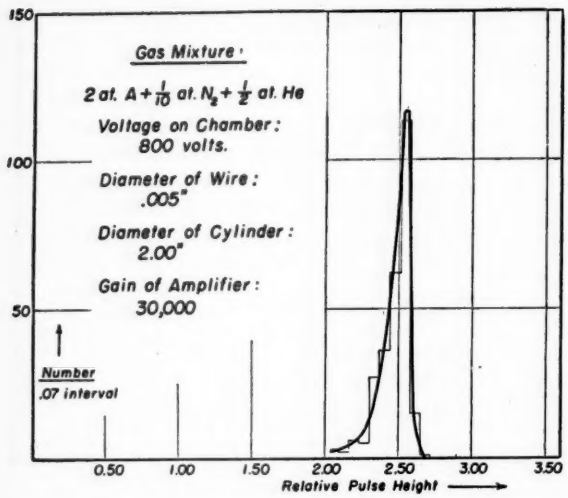

FIG. 5. Pulse-height distribution obtained from a wall source of polonium alpha-particles. The conditions were identical with those used for $He^3(n,p)$ and $N^{14}(n,p)$ experiments.

between energy and total ionization in argon agrees well with the value that one would expect from the end-point energies of the beta-ray spectra of H^3, 18±1 kev,[20,21] and C^{14}, 156±1 kev.[22] This agreement lends support to the method of calibration.

The energies obtained are in good agreement with recent observations of the thresholds for the inverse (p,n) reactions, 620±9 kev for $C^{14}(p,n)$,[23] and 764±1 kev for $H^3(p,n)$.[24] By adding to the measured Q-values the extrapolated end-point energies of the beta-ray spectra of C^{14} and H^3, we obtain an average neutron-hydrogen mass difference of 785±6 kev. This value is definitely smaller than the value obtained by Bell and Elliott (804±5 kev) from study of the gamma-rays emitted in $H(n,\gamma)$[25] and the HH−D mass doublet.[26,*] However, our value agrees well with the value for the neutron-hydrogen mass difference computed by Fowler and collaborators[27] (789±6 kev) from a different transmutation cycle.

The research described in this article was supported in part by the joint program of the Office of Naval Research and the Atomic Energy Commission. We wish to acknowledge with gratitude several grants from the Committee on Advancement of Research of the University of Pennsylvania and the interest and support of Professor G. P. Harnwell. We are indebted to Professor Knut Krieger of the Department of Chemistry for advice on chemical problems of gas purification, to Dr. W. C. Elmore of Swarthmore College for advice on electronic problems connected with the design of a low noise level amplifier, and we wish to thank Professor A. O. C. Nier of the University of Minnesota for supplying the enriched helium that made the He^3 experiment possible.

[20] G. C. Hanna and B. Pontecorvo, Phys. Rev. **75**, 983 (1949).
[21] Curran, Angus, and Cockroft, Phil. Mag. **40**, 53 (1949); Phys. Rev. **76**, 853 (1949).
[22] Cook, Langer, and Price, Phys. Rev. **74**, 548 (1948).
[23] Shoupp, Jennings, and Sun, Phys. Rev. **75**, 1 (1949).
[24] Taschek, Jarvis, Argo, and Hemmendinger, Phys. Rev. **76**, 325 (1949).
[25] R. E. Bell and L. G. Elliott, Phys. Rev. **74**, 1552 (1948).
[26] W. R. Cohen and W. F. Hornyak, Phys. Rev. **72**, 1127 (1947).
* *Note added in proof:* A revised value for the energy of the gamma-rays emitted in $H(n,\gamma)$, as obtained from the latest work performed by Bell and Elliott, leads to a neutron-hydrogen mass difference of 799 kev when the value cited in reference 26 for the HH−D mass doublet is used. (This result was communicated to the authors by Dr. W. B. Lewis of Chalk River.) On the other hand, if this revised gamma-ray energy is combined with the new value for the HH−D mass doublet recently obtained by Nier [T. R. Roberts and A. O. C. Nier, Phys. Rev. **77**, 746 (1950)] one obtains a value of 789 kev for $n-H$, in substantial agreement with the results of the disintegration experiments.
[27] Tollestrup, Jenkins, Fowler, and Lauritsen, Phys. Rev. **75**, 1947 (1949).

The Effective Range of Nuclear Forces
II. Photo-Disintegration of the Deuteron

H. A. BETHE
Cornell University, Ithaca, New York*

AND

CONRAD LONGMIRE**
Columbia University, New York, New York

(Received November 25, 1949)

The theory of the effective range is applied to the photo-disintegration of the deuteron. For the photo-electric effect, the only important influence of the range is through the normalization of the ground state wave function. We find that this is given by an energy-independent factor $(1-\gamma r_{0t})^{-1}$, where r_{0t} is the effective range of the forces in the triplet state, and γ is related to the binding energy of the deuteron. With the most likely experimental constants, this factor is 1.58, irrespective of the shape of the nuclear potential.

In the photomagnetic case, the effect of the range on the matrix element nearly compensates that on the normalization. The cross section is thus nearly the same as for zero range of the forces. However, the cross section is sensitive to the *difference* of the effective ranges for triplet and singlet state, and can thus be used to determine the latter (r_{0s}). The capture of slow neutrons by protons gives $r_{0s}\approx 2.6\pm 0.6\times 10^{-13}$ cm, in good agreement with the proton-proton scattering results.

In the last section, we show that the effect of tensor forces is unimportant.

1. INTRODUCTION

IN the first part of this paper[1] (quoted as I), we have given the definition of the effective range and the reasons why it depends so little on the energy of the system. We then discussed the cross sections of neutron-proton and proton-proton scattering in terms of it. We made extensive use of the quantitative calculations by Blatt and Jackson[2] which we shall again use in this paper (quoted as BJ).

In this paper, we shall discuss the two photo-effects of the deuteron, the electric and the magnetic one, in terms of the effective range. No thorough comparison with the experimental material is attempted, but we shall find it possible to determine the effective range of the forces in the singlet state from the observed cross section for capture of neutrons by protons.

Throughout this paper, as in I, we assume central forces independent of velocity. A further paper (III) will be concerned with the theory of the effective range in the presence of tensor forces.

2. THE PHOTOELECTRIC EFFECT

The matrix element for the electric dipole transition of the deuteron from its ground state (normalized radial eigenfunction $N_g u_g$) to a P-state of energy E (wave number k, radial eigenfunction v) is proportional to

$$M_e = N_g \int_0^\infty r u_g v dr. \tag{1}$$

It is well known that for moderate energies E the P-state function may be replaced by that for a free particle,[3] that the latter behaves as r^2 for small r, and that therefore the contribution of small r (within the range of the nuclear forces) to the integral is small. Explicitly, the fraction of the integral contributed by the region between $r=0$ and b, is

$$F(b) = (\gamma^2+k^2)^2 b^4/24, \tag{2}$$

where

$$\gamma = 2.31\times 10^{12}\ \text{cm}^{-1} \tag{2a}$$

is the "reciprocal radius" of the deuteron ground state (see (I, 2)). If we set for b the width of a square well which will give the correct effective range ($b=1.8_5\times 10^{-13}$ according to I), and take $k=\gamma$ (corresponding to a γ-ray energy of 4.4 Mev), we find

$$F(b) = 0.005. \tag{2b}$$

Only for $r<b$ does u_g deviate from the asymptotic expression

$$\psi_g = e^{-\gamma r}. \tag{3}$$

It is therefore a very good approximation to replace u_g by ψ_g; in fact, doing so changes the matrix element only by $0.08F(b)$ if we use a square well and assume $\gamma b \ll 1$. It is likely that for other potentials the error will be about the same for the same effective range because this quantity determines the deviation of u_g from ψ_g. This would mean that the matrix element M_e

* A part of this investigation was made while the first author was at Columbia University as a Visiting Professor.

** Now at Los Alamos Scientific Laboratory, Los Alamos, New Mexico.

[1] This paper is a continuation of the paper "Theory of the effective range in nuclear scattering," Phys. Rev. 76, 38 (1949). This paper will be quoted as I, and equations from it as, e.g., (I, 24).

[2] J. M. Blatt and J. D. Jackson, Phys. Rev. 76, 18 (1949).

[3] H. A. Bethe and R. Peierls, Proc. Roy. Soc. A148, 146 (1935).

TABLE I. Photoelectric cross sections.

γ-ray	ThC″	Na	*	$F+H$
Energy (Mev)	2.618	2.76	4.47	6.13
σ_e (10^{-28} cm^2)	7.93	10.8	22.5	20.1

* Maxinum of cross section.

is obtained correctly within 0.4 parts in 1000 by using ψ_g instead of u_g. This approximation will, of course, break down at high energies (above 10 Mev, say) where explicit calculation is necessary.

The only point where the range of the forces comes in is therefore in the normalizing factor N_g which is defined by the condition

$$N_g^2\int_0^\infty u_g^2 dr=1. \tag{4}$$

Using (3), and the definition (I, 14) of the effective range,

$$\int u_g^2 dr=\int \psi_g^2 dr-\int(\psi_g^2-u_g^2)dr$$

$$=1/(2\gamma)-r_0/2=(2\gamma)^{-1}(1-\gamma r_0). \tag{5}$$

Therefore

$$N_g^2=N_0^2/(1-\gamma r_0), \tag{5a}$$

where $N_0^2=2\gamma$ is the normalizing factor for zero range. Therefore we find for the photoelectric cross section

$$\sigma_e=\sigma_{e0}/(1-\gamma r_0), \tag{6}$$

where σ_{e0} is the often-quoted cross section for zero range[3]

$$\sigma_{e0}=(8\pi/3)(e^2/\hbar c)(\hbar^2/M)(W_1^{\frac{1}{2}}E^{\frac{1}{2}}/(E+W_1)^3), \tag{7}$$

where W_1 is the binding energy of the ground state of the deuteron and E the energy of the system after disintegration. The range correction is therefore directly given by the effective range, independently of the shape of the potential.

The result (6) was obtained independently by Blatt and Jackson (unpublished). It explains the fact, already noticed by Bethe and Bacher,[4] that the photoelectric cross section depends on the range in the same way as the elastic scattering (I, 18). The correction in (6) is independent of energy; with the value $r_0=1.56\times10^{-13}$ cm, given in (I, 27), the factor by which the cross section (7) must be multiplied, is 1.562.

For all quantitative calculations in this paper, we prefer to use the value[5] $W_1=2.235$ Mev for the binding energy of the deuteron, rather than 2.21 as used in I. The main reason is that 2.235 is based on the direct comparison by Bell and Elliot[5] of the energy of the capture γ-ray from $H+n=D$ with the ThC″ γ-ray, so that this choice is likely to give the best possible value for the difference $E=h\nu-W_1$, i.e., for the kinetic energy of the neutron and proton, to which the cross section (7) is very sensitive. We therefore set

$$W_1=2.235(1+\epsilon_1). \tag{8}$$

Leaving the values of the other constants the same as in I, we get

$$r_{0t}=1.59\times10^{13}\text{ cm} \tag{8a}$$

and the factor $(1-\gamma r_{0t})^{-1}=1.586$. Combining all information, and indicating the influence of the possible experimental errors ϵ_1, ϵ_2, ϵ_3 in (8), (I, 20b) and (I, 20c), we find for the photoelectric cross section

$$\sigma_e=17.98\times10^{-27}w^{\frac{1}{2}}(w+1)^{-3}$$
$$\times[1+0.32\epsilon_1+1.87\epsilon_2-0.56\epsilon_3]\text{ cm}^2, \tag{9}$$

where

$$w=E/W_1.$$

Assuming for the relative probable errors $\epsilon_1=\pm0.010$, $\epsilon_2=\pm0.005$, $\epsilon_3=\pm0.08$ (as in I), the contributions to the uncertainty of the photoelectric cross section are

±0.3 percent from the binding energy,
±0.9 percent from the free scattering cross section,
±4.5 percent from the parahydrogen cross section.

Only the last of these is appreciable.

For some commonly used γ-rays the photoelectric cross sections are given in Table I. These values agree, of course, quite well with those previously calculated from special models. They are also in reasonable agreement with recent experimental values on the absolute cross section.

3. INFLUENCE OF THE *P*-PHASE SHIFT ON THE PHOTOELECTRIC EFFECT

In the last section we have calculated the photoelectric cross section, assuming the P state (final state) to be completely free. This would be exactly true if we assumed the potential between the nucleons to be that suggested by Serber,[6,7] i.e., half-ordinary and half-exchange: This potential gives no interaction in states of odd orbital momentum. However, it seems premature to restrict the choice of potential so much at the present time, and it is therefore interesting to investigate the effect of a P phase shift on the cross section.

The radial P wave function is

$$v=\frac{\sin(kr+\delta)}{kr}-\cos(kr+\delta)=\text{R.P.}\frac{e^{i(kr+\delta)}}{ikr}(1-ikr), \tag{10}$$

where δ is the phase shift. If we take for the ground state wave function simply $u_g=\psi_g\equiv e^{-\gamma r}$, the matrix

[4] H. A. Bethe and R. F. Bacher, Rev. Mod. Phys. 8, 82 (1936) (see p. 125).

[5] We are taking the result of R. E. Bell and L. G. Elliot, Phys. Rev. 74, 1552 (1948), for the ratio of the energy of the capture γ-ray to that of the ThC″ γ-ray, and the value of T. Lauritsen, 2.618 Mev, for the energy of the latter.

[6] See, e.g., R. S. Christian and E. W. Hart, Phys. Rev. 77, 441 (1950).

[7] See G. F. Chew, Phys. Rev. 74, 809 (1948).

element (1) can easily be evaluated and we get

$$M_e = \text{R.P.} N_0 \frac{e^{i\delta}(\gamma - 2ik)}{ik(\gamma - ik)^2}. \tag{11}$$

Now δ is small; therefore δ^2 and higher powers may be neglected and elementary algebraic evaluation gives

$$M_e = \frac{2N_0 k^2}{(\gamma^2+k^2)^2}\left[1+\delta\frac{\gamma}{2k^3}(\gamma^2+3k^2)\right]. \tag{12}$$

The phase shift causes the matrix element to be multiplied by the square bracket in (12), and therefore the cross section by

$$F(\delta) = 1+\delta k^{-3}\gamma(\gamma^2+3k^2). \tag{13}$$

We shall calculate δ below, and find it to be proportional to k^3.

For the correction to M_e due to δ, it is no longer true that almost the entire contribution comes from large r. This is easily seen by expanding v, Eq. (10), up to the linear term in δ:

$$\begin{aligned} v &= v_0 + \delta v_1 \\ v_0 &= \sin kr/kr - \cos kr \\ v_1 &= \cos kr/kr + \sin kr, \end{aligned} \tag{14}$$

v_0 is the regular and v_1 the irregular P-wave function for a free particle; for small r, v_1 behaves as $1/kr$. Therefore, the contribution of the region from $r=0$ to $r=b$ to the correction term in M_e is

$$N_0\int_0^b re^{-\gamma r}(\delta/kr)dr \approx N_0\delta b/k. \tag{14a}$$

Now this contribution is certainly *not* given correctly by our procedure of setting $u_0 = e^{-\gamma r}$ and v equal to expression (10): Both of these functions are actually smaller than these approximations, and therefore we must subtract, from the result (12), a quantity of the order of magnitude of (14a) (in general somewhat less). Therefore the correction factor (13) should be modified to:

$$F(\delta) = 1+\delta k^{-3}[\gamma(\gamma^2+3k^2) - \lambda b(\gamma^2+k^2)^2], \tag{15}$$

where λ is a numerical factor between 0 and 1 depending on the shape of the potential. For k^2 between 0 and $2\gamma^2$, the second term in the bracket is very nearly $\lambda\gamma b$ times the first, and γb is about 0.6 for the Yukawa potential. Thus the finite range of the forces reduces the effect of the P phase shift considerably.

We shall now calculate δ, using the Born approximation and assuming $kb \ll 1$ where b is the intrinsic range. Generally, the Born approximation gives

$$\delta = k^{-1}\int W v_0^2 dr, \tag{16}$$

where

$$W = -M\hbar^{-2}V(r) \tag{16a}$$

is the potential defined by BJ, Eq. (2.8). For the unperturbed P-function v_0, Eq. (14), we may set its expression for small kr,

$$v_0 = \tfrac{1}{3}k^2r^2 \tag{16b}$$

since $r \leqq b$ and kb is assumed small. Then (16) becomes

$$\delta = \tfrac{1}{9}k^3\int W r^4 dr. \tag{17}$$

Blatt and Jackson, in their Eq. (4.5), have given W for the 4 customary potentials in terms of r and b. Integration gives[8]

$$\delta = cs(kb)^3, \tag{18}$$

where s is the depth parameter of the potential, as defined by BJ, and the constant c depends on the shape of the potential; its value is

$$c = \pi^2/180 = 0.0549 \quad \text{for the square well} \tag{18S}$$

$$c = 0.0670 \quad \text{for the Gaussian} \tag{18G}$$

$$c = 0.0868 \quad \text{(Exponential)} \tag{18E}$$

$$c = 0.1176 \quad \text{(Yukawa).} \tag{18Y}$$

We can draw the following conclusions:

(1) δ is proportional to k^3, therefore the correction in $F(\delta)$, Eq. (15), is in first approximation independent of k.

(2) The numerical coefficient of $s(kb)^3$ increases as the "tail" of the potential becomes more pronounced, as is to be expected. This effect, however, is not very large (about a factor 2) once the potentials have been made comparable by introducing the intrinsic range; this is another evidence for the usefulness of the concept of the intrinsic range. However, if the intrinsic range is determined from the "observed" effective range in the ^3S state (BJ and I), it comes out smaller for the square well (1.85×10^{-13}) than for the exponential or Yukawa potential (2.5×10^{-13}): This difference makes the P-phase shift considerably (about 4 times) larger for the latter potentials than for the square well, for given s.

(3) For $F(\delta)$ we obtain approximately

$$F(\delta) \approx 1+0.1s(\gamma b)^3 \approx 1+0.02s \tag{19}$$

if we (a) use a long-tailed (exponential or Yukawa) potential, (b) assume $k \ll \gamma$, (c) neglect the second term in the bracket in (15) and (d) put for b its value in the ^3S state ($\sim 2.5\times10^{-13}$ cm). The second term in (15) may reduce the correction to $0.01s$ or $0.015s$. Now, if the potential in the ^3P state is the same as in ^3S (ordinary forces), s is about 1.4 (BJ, Fig. 4) and we get an increase of the cross section by about 2 percent; for pure exchange forces, the cross section would be reduced by the same amount; but if the P potential is only

[8] These results, as well as those for $l=2$ and 3, have been obtained by J. D. Jackson (private communication).

about 1/10 of the potential in the S state, as is suggested by the neutron-proton scattering at 90 Mev,[9] the correction is only about 0.2 percent. In any case, it is unlikely that experiments on the absolute photoelectric cross section at energies of a few Mev would reveal much about the forces in the P state.

(4) At higher energies (γ-rays of 10 Mev or more, say), the correction in $F(\delta)$ increases linearly with the energy (Eq. (15)), so that it becomes more hopeful to obtain information about the forces in the P state. However, it is then necessary to evaluate the second term in the bracket in (15) more carefully; our theory of the effective range then ceases to be useful, and calculations have to be made with special models; the result will be sensitive to the shape of the potential, not only to its strength.

It is interesting to compare the effect of the P phase shift to the effects of retardation and higher multipole transitions. We may calculate the quadrupole transition probability, which is representative of these effects though not the only one. The ratio of the matrix elements of quadrupole to dipole is:

$$\frac{M_q}{M_d}=\frac{\frac{1}{2}iq\int xz\psi_0\psi_d d\tau}{\int x\psi_0\psi_p d\tau}, \tag{19a}$$

where q is the wave number of the light, ψ_0 the wave function of the ground state, ψ_d and ψ_p those of the final d- or p-state, respectively, x the coordinate of proton relative to neutron in the direction of polarization, and z in the direction of propagation of the light. Elementary evaluation of the integrals, assuming no phase shifts for ψ_p and ψ_d, and use of the relation

$$q=(\hbar/Mc)(\gamma^2+k^2) \tag{20}$$

gives for the ratio of the cross sections

$$\frac{\sigma_q}{\sigma_d}=\left|\frac{M_q}{M_d}\right|^2=\frac{4}{5}\frac{E}{Mc^2}, \tag{21}$$

where $E=(\hbar^2/M)k^2$ is the kinetic energy of proton plus neutron after disintegration. This is of the same order of magnitude as the effect of the P phase shift if the interaction in the P state is 1/10 of that in the S state, as is likely. If the P-interaction were of the same order as in the S state, its effect on the photo-disintegration could be observed without much disturbance from higher multipoles, retardation and relativity.

4. PHOTOMAGNETIC EFFECT: THEORY

We shall now calculate the photomagnetic effect. The matrix element for the magnetic dipole transition to a ^1S state of energy E (eigenfunction $N_s u_s$) is proportional to

$$M_m=N_0N_s\int_0^\infty u_0u_s dr, \tag{22}$$

where N_0 and N_s are the normalizing factors for ground and singlet state, respectively. Ordinarily, one calculates the integral by replacing the wave functions by their asymptotic expressions, ψ_0 (see Eq. (3)) and

$$\psi_s=\sin(kr+\delta_s)/\sin\delta_s, \tag{23}$$

where δ_s is the phase shift for the singlet state of energy E. The normalizing factor is

$$N_s=\sin\delta_s/k. \tag{23a}$$

Elementary integration gives

$$\int_0^\infty \psi_0\psi_s dr=\frac{\gamma+k\cot\delta_s}{\gamma^2+k^2}. \tag{24}$$

The effect of the finite range on this result is less easy to obtain than for the electric dipole moment, but its numerical value will turn out to be much smaller.

We consider the difference between the integrals in (22) and (24) and get

$$\begin{aligned}2D\equiv 2\int_0^\infty(\psi_0\psi_s-u_0u_s)dr&\\ =\int_0^\infty(\psi_0^2-u_0^2)dr+\int_0^\infty(\psi_s^2-u_s^2)dr&\\ -\int_0^\infty[(\psi_0-\psi_s)^2-(u_0-u_s)^2]dr.&\end{aligned} \tag{25}$$

The first integral is by definition one-half of the effective range r_{0t} for the triplet state of the deuteron, the second is one-half of the singlet effective range r_{0s} which may be different from r_{0t}. The last term is likely to be very small: In the first place, the integrand differs from zero only within the range of the nuclear forces; but within this range ψ_0 and ψ_s are nearly equal because they are both normalized to one at $r=0$; likewise, u_0 and u_s are both zero at $r=0$. Thus each of the two parts of the integrand is small, and moreover they tend to compensate. For an estimate, consider a square well of width b, and approximate ψ_0 by the triplet wave function for zero energy,

$$\psi_{t0}=1-r/a_t \tag{26}$$

and ψ_s by the singlet function for zero energy, $\psi_{s0}=1-r/a_s$, where a_t and a_s are the scattering lengths (I, 26); these approximations are good because of the arguments given at the beginning of Section 4 of I. Then

$$\int_0^b(\psi_0-\psi_s)^2dr=\tfrac{1}{3}(1/a_t-1/a_s)^2b^3. \tag{27}$$

[9] Hadley, Kelly, Leith, Segrè, Wiegand, and York, Phys. Rev. 75, 351 (1949). Also private communication from R. Serber.

Using the experimental values of a_t and a_s (I, 26) and $b=1.9\times10^{-13}$ cm (which corresponds to the experimental value of the triplet effective range, (8a)) this is 7 percent of the sum of the first two terms in (25). However, a large fraction of this will be compensated by $\int_0^b(u_0-u_s)^2dr$ because for r near b, where $\psi_0-\psi_s$ becomes largest, u_0-u_s is equally large. Probably the last term of (25) is actually about 2 percent of the first two in typical cases, and these two terms in turn are only about 20 percent of the total matrix element (22).

If the last term in (25) is neglected, we get

$$D\equiv\int_0^\infty(\psi_0\psi_s-u_0u_s)dr=\tfrac{1}{4}(r_{0t}+r_{0s}). \tag{28}$$

This result, which is independent of the energy of the state s, should be subtracted from (24). For very high energy, when (24) becomes less than (28), the approximation breaks down, of course; but then the photomagnetic effect is negligible compared with the photoelectric.

Collecting terms, our approximate result for the photomagnetic matrix element becomes

$$\int u_0u_s dr=\frac{\gamma+k\cot\delta_s}{\gamma^2+k^2}-\tfrac{1}{4}(r_{0t}+r_{0s}). \tag{29}$$

We have tested this result against four direct numerical calculations for zero energy of the singlet state. If $E=0$, we have

$$k\cot\delta_s=-1/a_s\equiv-\alpha, \tag{30}$$

where a_s is the singlet scattering length. For this quantity, and for γ, we have taken the experimental values (see I). The models tested were:

1. Square well, width $b=1.85\times10^{-13}$ cm, for both singlet and triplet.

Results: $r_{0t}=1.582\times10^{-13}$ cm, $r_{0s}=1.905\times10^{-13}$ cm,
Elementary result (24):

$$(1/\gamma)(1-1/\gamma a_s)=5.121\times10^{-13}\text{ cm},$$

Correction (28): $D=0.872\times10^{-13}$ cm,
Corrected value (29) (difference of above):

$$=4.249\times10^{-13}\text{ cm}, \tag{31}$$

Numerically calculated value: 4.250×10^{-13} cm.
The agreement is better than could be expected.

2. Square well, triplet range 1.85 (as in example 1), singlet range zero. Result:

From formula (29)	4.72×10^{-13},
From numerical calculation	4.45×10^{-13}.

(32)

The agreement here is not good but the conditions are very unfavorable: the term $(u_0-u_s)^2$ in the last integral of (25), which normally is rather less than $(\psi_0-\psi_s)^2$, is here very much greater because u_s remains equal to ψ_s all the time. The case in which the intrinsic range for the singlet is *longer* than for the triplet, is less unfavorable.

3. Yukawa potential. To simplify the calculation, we have used the Hulthen potential (Eq. (33)) as a stand-in for the Yukawa potential. The Hulthen potential has the advantage that analytical wave functions are obtained, but the disadvantage that the shape of the potential must be taken slightly different for the ground state and the singlet state. Explicitly, we take for the ground state potential

$$V_t=-(\beta^2-\gamma^2)/(e^{(\beta-\gamma)r}-1), \tag{33}$$

where γ has the usual meaning and β can be arbitrarily chosen to fit the observed effective range r_{0t}. The relation is

$$r_{0t}=4/(\gamma+\beta)-(1/\beta). \tag{33a}$$

Choosing $r_{0t}=1.60\times10^{-13}$ cm, we get

$$\beta=15.5\times10^{12}\text{ cm}^{-1}. \tag{33b}$$

The potential (33) yields the (exact) wave function

$$u_0=e^{-\gamma r}-e^{-\beta r}. \tag{33c}$$

For the singlet state of energy zero, we take as the potential

$$V_s=-\frac{\eta^2}{(1-\alpha r)e^{\eta r}-1}, \tag{34}$$

where $\alpha=1/a_s$ (a negative quantity). The effective range is then

$$r_{0s}=(3/\eta)(1-4\alpha/3\eta) \tag{34a}$$

and can be adjusted by choice of η. The wave function is

$$u_s=1-\alpha r-e^{-\eta r}. \tag{34b}$$

It is possible to choose η so that the two potentials (33) and (34) have almost the same dependence on r: This can be done by choosing $\eta-\alpha=\beta-\gamma$ which gives $\eta=12.8\times10^{12}$ cm^{-1} and $r_{0s}=2.43\times10^{-13}$, a value very close to the experimental result, Section V. With this choice, the ratio V_t/V_s becomes

$$\frac{V_t}{V_s}=\text{const.}\cdot\frac{1-\alpha r-e^{-\eta r}}{e^{-\alpha r}-e^{-\eta r}} \tag{35}$$

and changes by only 0.5 percent from $r=0$ to $r=r_{0s}$. An even smaller variation of this ratio could presumably be obtained if η were chosen so as to make the intrinsic ranges of (33) and (34) equal. The potentials (33) and (34) may therefore be considered as having essentially the same "shape."

With these potentials and wave functions, D can be calculated explicitly and is

$$D=\frac{1}{\beta}\left(1-\frac{\alpha}{\beta}\right)+\frac{1}{\eta+\gamma}-\frac{1}{\eta+\beta}. \tag{36}$$

Computation shows that with very good accuracy, for

r_{0t} in the neighborhood of 1.60×10^{-13},

$$D=0.52r_{0t}+0.15_5r_{0s}-0.24\times10^{-13}. \quad (36a)$$

The difference from (29) is appreciable. However, the numerical values for D from (36) and (29) agree for $r_{0s}=2\times10^{-13}$ (if we assume $r_{0t}=1.6\times10^{-13}$). It is reasonable that (29) is a good approximation when the effective ranges are nearly equal because then the neglected term in (25) is likely to be small. The sensitivity of the cross section to the singlet range is less according to the exact formula (36a) than accordng to the approximate one, (29), but is still appreciable.

4. Exponential potential, of the same intrinsic range for triplet and singlet state. The range was chosen so that the wave function of the ground state would be given by the tabulated function $J_{1/3}$ (see reference 4, Eq. (42c, d)). The potential is then

$$-V_0e^{-2r/a} \quad (37)$$

with

$$a=1.44\times10^{-13}\text{ cm} \quad (37a)$$

$$V_0=168\text{ Mev (triplet state)} \quad (37b)$$

$$V_0=104\text{ Mev (singlet state).} \quad (37c)$$

The intrinsic range defined by BJ is 2.55×10^{-13} cm. The effective ranges are $r_{0t}=1.82$ and $r_{0s}=2.70\times10^{-13}$; they were obtained by direct integration. The quantity D defined in (25) is 1.09×10^{-13} cm whereas the approximate value (28) is $\frac{1}{4}(r_{0t}+r_{0s})=1.13\times10^{-13}$ cm. The agreement is very good; the deviation is in the same direction but not as large as for the Hulthen potential, Eq. (36).

On the basis of these test examples we believe that, for most potential shapes, (29) will give a good approximation to $\int u_gu_s dr$. The effective range then enters the matrix element (22) in two places, *viz.* (a) in the normalizing factor and (b) in the integral. The former is increased by the finite range, the latter decreased; the former involves the triplet range only, the latter the mean of triplet and singlet ranges.

The theory so far outlined is useful for numerical work (see Section 5). However, the effect of the range of the forces can be brought out more clearly with the help of some algebra. First we use in (24) the fundamental relation of the effective-range theory (I, 16)

$$k\cot\delta_s=-1/a_s+\tfrac{1}{2}k^2r_{0s}. \quad (38)$$

Next, we *define* a quantity β for the virtual singlet state in analogy with γ for the ground state by setting[10] (see I, 19)

$$-1/a_s=\beta+\tfrac{1}{2}\beta^2r_{0s}. \quad (39)$$

Then the matrix element becomes

$$\int_0^\infty u_gu_s dr=[\gamma^2+k^2]^{-1}[\beta+\gamma+\tfrac{1}{2}\beta^2r_{0s} -\tfrac{1}{4}\gamma^2(r_{0s}+r_{0t})+\tfrac{1}{4}k^2(r_{0s}-r_{0t})] \quad (40)$$

and the normalizing factor

$$N_s=\sin\delta_s/k=(k^2+\beta^2)^{-\frac{1}{2}}[1+\beta r_{0s}+\tfrac{1}{4}(k^2+\beta^2)r_{0s}^2]^{-\frac{1}{2}} \quad (40a)$$

while N_g is given by (5a). Then the dipole moment may be written

$$M_m=M_{m0}F(r_{0s},r_{0t}), \quad (41)$$

where M_{m0} is the value for zero range,

$$M_{m0}=(\beta+\gamma)(2\gamma)^{\frac{1}{2}}/(\gamma^2+k^2)^{-1}(\beta^2+k^2)^{\frac{1}{2}} \quad (41a)$$

and F the correction factor. After some algebra, one finds

$$F=1+\tfrac{1}{4}(r_{0t}-r_{0s})[\gamma(\gamma+2\beta)-k^2]/(\beta+\gamma) +\tfrac{1}{8}[\gamma(\gamma+4\beta)-k^2]r_{0t}^2+0(\gamma^2r_{0t}[r_{0t}-r_{0s}]) +0(\gamma^3r_{0t}^3). \quad (42)$$

The first correction term in this expression is proportional to the *difference of the effective ranges* for triplet and singlet, $r_{0t}-r_{0s}$. The photo-magnetic effect is therefore a sensitive way to determine this difference.[11] The absolute value of the range is immaterial in this approximation, it comes in only in the correction of relative order $(\gamma r_0)^2$. For the observed value of r_{0t}, this correction is about 3 percent (increase of the cross section). Terms of second-order *and* proportional to the range difference are likely to be considerably smaller. Terms of order r_0^3 have been neglected already in (28).

5. COMPARISON WITH EXPERIMENT

The only accurate experiments on the photomagnetic effect, so far, are those on the capture of slow neutrons by protons. The most exact determination, to our knowledge, is that of Whitehouse and Graham[12] who found for the ratio of the capture cross sections of boron and hydrogen

$$\sigma_B/\sigma_H=2270\pm30. \quad (43)$$

The error given is statistical only; there may be an additional systematic error, therefore we adopt a probable error of ±45, i.e., 2 percent. The boron absorption cross section is given by Fermi and Marshall[13] as

$$\sigma_B=703\pm7\text{ barns} \quad (44)$$

at a neutron velocity of 2200 meters per second. Velocity selector measurements by Sutton *et al.*[14] favor

[10] This choice gives the formula for the singlet scattering cross section

$$\sigma_s=\frac{4\pi}{k^2+\beta^2}[1+\beta r_{0s}+\tfrac{1}{4}(\beta^2+k^2)r_{0s}^2]^{-1}$$

similar to (I, 18). This is a more convenient definition of the virtual state than that of S. Flügge and E. Hückel, Phys. Rev. **73**, 520 (1948).

[11] This was first pointed out by W. M. Woodward on the basis of qualitative considerations.

[12] W. J. Whitehouse and G. A. R. Graham, Can. J. Research **A25**, 261 (1947).

[13] E. Fermi and L. Marshall, Phys. Rev. **72**, 193 (1947).

[14] Sutton, McDaniel, Anderson, and Lavatelli, Phys. Rev. **71**, 272 (1947).

a somewhat higher value (717); we shall adopt 703±14. Then

$$\sigma_H = 0.310 \text{ barn} \pm 4 \text{ percent (at 2200 m/sec.)}. \quad (45)$$

It is convenient to write

$$\sigma_H v = 6.81 \times 10^{-20} \text{ cm}^3/\text{sec.}(1+\epsilon_4), \quad (46)$$

where $\epsilon_4 = \pm 0.04$.

The theoretical prediction, according to (12) and (16), is

$$\sigma_H v = 2\pi \frac{e^2}{Mc} \frac{\hbar}{Mc} \left(\frac{W_1}{Mc^2}\right)^{\frac{1}{2}} \frac{(\mu_p - \mu_n)^2}{(1-\gamma r_{0t})\beta'^2} \times [\gamma + \beta' - \gamma^2 D]^2, \quad (47)$$

where μ_p and μ_n are the proton and neutron moment in units of the proton magneton and $\beta' = -1/a_s$. D is given in first approximation by (28), corrections are discussed in (36) and elsewhere in Section 4. We use $\mu_p - \mu_n = 4.707$, γ corresponding to the binding energy Eq. (8), the other experimental constants as given by (I, 20). Then, including probable errors, the theoretical result for *zero range* of the forces is

$$\sigma_H v = 6.64 \times 10^{-20}(1 + 2.35\epsilon_1 + 0.80\epsilon_2 + 0.05\epsilon_3) \text{ cm}^3/\text{sec}. \quad (48)$$

To include the dependence on the difference of singlet and triplet range in a convenient way, we set

$$D = \tfrac{1}{2} r_{0t} + \tfrac{1}{4} D' \quad (49)$$

so that in the approximate theory of Eq. (28) we have

$$D' = r_{0s} - r_{0t}. \quad (49a)$$

If we then express D' in units of 10^{-13} cm, the theoretical result is

$$\sigma_H v = 6.64 \times 10^{-20}(1 + 0.126 - 0.124 D' + 2.8\epsilon_1 + 1.5\epsilon_2 - 0.15\epsilon_3) \text{ cm}^3/\text{sec}. \quad (50)$$

Equating this to the experimental value (46) gives

$$D' = (0.81 + 23\epsilon_1 + 12\epsilon_2 - 1.2\epsilon_3 - 8.2\epsilon_4) \times 10^{-13} \text{ cm}. \quad (51)$$

If we use (49a) and $r_{0t} = 1.59 \times 10^{-13}$ (Eq. (8a)) we get

$$r_{0s} = 2.40 \times 10^{-13} \text{ cm}. \quad (52)$$

Because of the large coefficients of the ϵ's, the probable error of this result is considerable. Using the values of ϵ_1, ϵ_2, ϵ_3 given below Eq. (9a), and ϵ_4 from (46), we get for the contribution to the probable error in D' (and therefore in r_{0s}):

from the binding energy of the deuteron	±0.23,
from the free proton scattering	±0.06,
from the parahydrogen scattering	±0.10,
from the capture cross section	±0.33.

Assuming these errors to be independent,

$$r_{0s} = (2.4 \pm 0.4) \times 10^{-13} \text{ cm}. \quad (52a)$$

The binding energy of the deuteron will probably soon be known with much better accuracy; an accuracy of ±5 kev would reduce the error due to this datum to ±0.05. It would therefore seem important to improve the measurement of the capture cross section.

To appraise the reliability of the approximate formula (29), we use the examples of the last section. For the square well, the approximation is likely to be very good. For the Hulthén (near-Yukawa) potential, our value of D, $1.00 \pm 0.10 \times 10^{-13}$ cm, leads to $r_{0s} = 2.6_5 \pm 0.65 \times 10^{-13}$. For the exponential potential, we may estimate $\frac{1}{4}(r_{0s} + r_{0t}) = 1.04D = 1.04 \times 10^{-13}$ cm, which leads to $r_{0s} = 2.5_5 \pm 0.5 \times 10^{-13}$. All of these values are reasonably close together; the shape of the potential has less influence on the result than the present experimental error.

The effective singlet range here obtained is within experimental error equal to the proton-proton effective range of 2.7×10^{-13}. This lends support to the charge-independence of nuclear forces. Moreover, the difference between singlet and triplet effective range is just of the magnitude required for a long-tailed (Yukawa or exponential) potential if the intrinsic ranges for singlet and triplet are assumed equal.

A further uncertainty in our theory arises from our neglect of *exchange currents*.[15] These are known to give no contribution to the magnetic moment of the deuteron in any stationary state but they contribute about 6 percent to the magnetic moments of H^3 and He^3. They must also be expected to contribute to the photomagnetic transition probability.[16] The magnitude of this contribution is not known, but it might be possible to correlate it theoretically with the measured extra magnetic moments of H^3 and He^3, and with the effective ranges.

If the contribution of the exchange currents to the matrix element M_m is coherent with the main part of M_m, which is likely, a 1 percent exchange contribution to M_m will cause a change of D' by 0.16×10^{-13} cm which is quite appreciable, and a change of r_{0s} by the same amount.

Apart from the uncertainty due to exchange currents, the photomagnetic effect appears to be a good way to determine the effective range in the singlet state, which may compete in accuracy with the determination of r_{0s} from the neutron-proton scattering at a few Mev. According to BJ Fig. 8, 1 percent error in the scattering cross section at 5-Mev leads to an error of about 0.5×10^{-13} in r_{0s}, if r_{0t} is known with infinite precision; any error ϵ in r_{0t} causes an additional error of about 4ϵ in r_{0s}. In the case of the photomagnetic effect, r_{0s} is rather insensitive to the measurements which determine r_{0t}; moreover, 1 percent error in the capture cross section means an error of only 0.08×10^{-13} in r_{0s}. One must of course remember that it is more difficult

[15] F. Villars, Phys. Rev. **72**, 256 (1947).

[16] A. Pais, Kgl. Danske Vid. Sels. Math.-Fys. Medd. **20**, No. 17 (1943).

to measure the capture cross section precisely than the scattering of 5-Mev neutrons. Still, it seems worth while to improve the accuracy of the measurement of the capture cross section, including that of boron which serves as standard: Such a measurement will either give a better value of r_{0s}, if the contribution of the exchange moment can be shown to be small, or it will, in conjunction with an independent determination of r_{0s} from scattering, give a direct result for the contribution of the exchange magnetic moment.

In concluding this section, we want to discuss briefly the photomagnetic effect at higher energy. This effect is more difficult to measure accurately, but it is almost uniquely determined by the capture cross section at low energy. From (24), (25), (38) we have

$$\int_0^\infty u_g u_s dr=(\gamma^2+k^2)^{-1}[\gamma+\beta'-\gamma^2 D+k^2(\tfrac{1}{2}r_{0s}-D)]. \quad (53)$$

Taking the approximation (28) for D, the factor of k^2 is

$$\tfrac{1}{4}(r_{0s}-r_{0t})=\tfrac{1}{4}D'=0.20\times10^{-13}. \quad (53a)$$

Inserting this, and introducing the ratio

R=actual photomagnetic effect/
photomagnetic effect for zero range (54)

we find

$$R(E)=R(0)(1+0.045E), \quad (55)$$

where E is measured in Mev and $R(0)$ refers to zero *energy*. From (46) and (50),

$$R(0)=1.026. \quad (55a)$$

For ThC'' γ-rays, $E=0.383$ so that $R=1.043$. The cross section for zero range is

$$\sigma_{m0}=\frac{2\pi}{3}\frac{e^2}{\hbar c}\left(\frac{\hbar}{Mc}\right)^2(\mu_p-\mu_n)^2\frac{k\gamma(\gamma+\beta')^2}{(k^2+\gamma^2)(k^2+\beta'^2)}$$
$$=7.02\times10^{-28}\frac{(E)^{\frac{1}{2}}}{(E+2.235)(E+0.0735)}\ \text{cm}^2, \quad (56)$$

where E is the energy in Mev. For ThC'' γ-rays, $E=0.383$ yields $\sigma_{m0}=3.63\times10^{-28}$ and, after correction by the factor R above, $\sigma_m=3.79\times10^{-28}$. The total photo-cross section is then (see Table I)

$$\sigma_t=11.72\times10^{-28}\ \text{cm}^2 \quad (57)$$

and the ratio of differential cross sections in the forward and sideward directions

$$\tau=\frac{\sigma(0)}{\sigma(\pi/2)}=\frac{3.79}{\frac{3}{2}(7.93)+3.79}=0.242. \quad (58)$$

6. MODIFICATIONS DUE TO TENSOR FORCES

The effective range in the presence of tensor forces will be discussed in paper III. The main result from that paper is that the anisotropy of the forces has a negligible effect on the photo-disintegration. Transitions from the ^3D part of the ground state to either ^3P or ^3F states in the continuum by the electric dipole moment are negligible, as are transitions to ^1D by the magnetic moment, and also electric quadrupole transitions. All these results confirm, under more general assumptions, the conclusions of Rarita and Schwinger.[17]

For the electric dipole moment there is virtually no change at all. It can be shown that the normalization factor of the ground state function, N_g, still depends on the effective range r_{0t} by (5a). The only change is in the shape of u at small distances, but this, as we have shown in Section 2 of this paper, has practically no effect on the photoelectric cross section.

For the photomagnetic effect, there is a slight modification because, as will be shown in III,

$$2\int_0^\infty(\psi_g^2-u_g^2)dr=r_{0t}-P_D(1/\gamma-r_{0t}) \quad (59)$$

instead of simply r_{0t}. Here P_D is the fraction of D-state in the ground state wave function which is experimentally about 0.04. The correction (second term) in (59) is -0.11×10^{-13}. According to (25), the quantity $4D$ is equal to the expression (59), plus the singlet effective range r_{0s}, minus the last term of (25) which we have neglected. Since D is essentially determined by experiment, the decrease of (59) must be compensated by a corresponding increase in r_{0s}. Therefore, with tensor forces,

$$r_{0s}=2.5\times10^{-13} \quad (60)$$

if Eq. (29) is used, or about 2.8 for the Hulthén potential, Eq. (36a). This makes the agreement with the proton-proton scattering even better.

We are very grateful to Dr. John Blatt for many valuable suggestions regarding this paper.

[17] W. Rarita and J. Schwinger, Phys. Rev. **59**, 436, 556 (1941)

The Beta-Spectra of Cs^{137}, Y^{91}, Pm^{147}, Ru^{106}, Sm^{151}, P^{32}, and Tm^{170}

HAROLD M. AGNEW*
Institute of Nuclear Studies, University of Chicago, Chicago, Illinois
(Received October 11, 1949)

The beta-spectra of Cs^{137}, Y^{91}, Pm^{147}, P^{32}, Ru^{106}, Tm^{170}, and Sm^{151} have been investigated using a large double-magnetic lens spectrometer. The investigation of these materials was carried out with sources whose thicknesses were less than 0.1 mg/cm². The sources were mounted on thin foils in such a manner that they did not accumulate charge. Cs^{137} and Y^{91} were found to have distinctly non-linear Fermi plots. Ru^{106}, Pm^{147}, and Sm^{151} have linear Fermi plots, and the Fermi plot of Tm^{170} is slightly curved. P^{32} had an unusual Fermi plot at the low energy end. Auger electrons have been found associated with the Ba^{137} decay product of Cs^{137}, and the internal conversion electrons have been found accompanying the continuous beta-radiation from Tm^{170}. The energy of the gamma-ray giving rise to the Yb^{170} conversion electrons is 85.4±0.6 kev. The end points of the continuous beta-spectra of these materials have been determined as follows: Low energy group of Cs^{137}, 0.523±0.004 Mev; Y^{91}, 1.56±0.010 Mev; Tm^{170}, 0.990±0.007 Mev; Sm^{151}, 0.0755±0.0010 Mev; P^{32}, 1.718±0.01 Mev; Pm^{147}, 0.229±0.001 Mev; Ru^{106}, 0.0392±0.0003 Mev.

INTRODUCTION

THE work reported here was begun in the hope of finding forbidden spectra which could be analyzed by using the existing theory of forbidden spectra.[1,2] At the time that this work was begun, there had been no reported instances of a beta-emitter exhibiting a Fermi plot which is concave toward the energy axis at the high energy portion of its spectrum. Actually, most of the experimental data indicated a straight line Fermi plot for the high energy portion of the spectrum, and then some deviation at the low energy end. Generally, the deviation at the low energy end was attributed to thickness of source and backing, lack of detection efficiency, and scattering in the spectrometer. In view of the advantages of the spectrometer[3] used in the work reported here—small scattering and high transmission—it was decided to investigate spectra using thin sources and a known detection efficiency.

Experimentally, allowed and forbidden transitions of nuclei undergoing beta-decay are distinguishable through the comparison of their half-lives after taking into account differences brought about by their nuclear charge and the maximum energy of the beta-particles emitted. This classification is given in terms of the so-called ft value. (The notation used here is that adopted by Konopinski.[2]) It should be understood that the ft value is only a rough guide to be used in distinguishing between various types of transitions. However, it is generally agreed that if the ft value lies between 10^3 and 10^4, the transition involved is an allowed one. Another indication of an allowed transition is obtained from the so-called Fermi or Kurie plot. This is a plot of $\{N/[p^2f(Z,W)]\}^{\frac{1}{2}}$ plotted against the total energy of the particles emitted. N is the number of beta-rays per unit momentum interval Δp. The energy-dependent function $f(Z,W)$ shows the effect of the Coulomb field on the emission of the beta-ray. A straight-line Fermi plot is an indication of an allowed transition. The Fermi plot of a forbidden transition should deviate from a straight line if one uses the $f(Z,W)$ corresponding to an allowed spectrum. Konopinski[2] gives in his review article a list of correction factors C_{ij}. According to the present theory, these should be used to correct $f(Z,W)$ in order to get a straight-line Fermi plot in the case of a forbidden transition.

During the progress of this work, several papers[4–6] have appeared reporting the observation of forbidden-type spectra. The work reported here is in agreement with the results reported on Cs^{137} and Y^{91}. In the case of

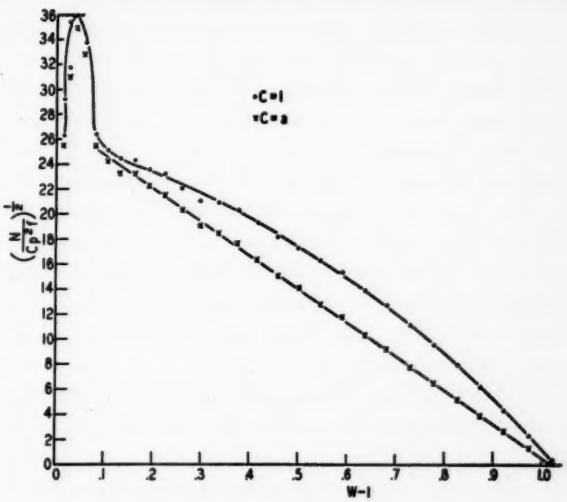

FIG. 1. Fermi plots of the low energy group of beta-rays of Cs^{137} with and without the correction factor a. The hump at the low energy end is due to Auger electrons.

* Now at Los Alamos Scientific Laboratory, Los Alamos, New Mexico.

[1] E. Fermi, Zeits. f. Physik **88**, 161 (1934).

[2] E. Konopinski, Rev. Mod. Phys. **15**, 209 (1943).

[3] H. M. Agnew and H. L. Anderson, Rev. Sci. Inst. **20**, 869 (1949).

[4] C. L. Peacock and A. C. G. Mitchell, Phys. Rev. **75**, 1272 (1949).

[5] L. M. Langer and H. Clay Price, Jr., Phys. Rev. **75**, 1109 (1949).

[6] E. N. Jensen and L. Jackson Laslett, Phys. Rev. **75**, 1949 (1949).

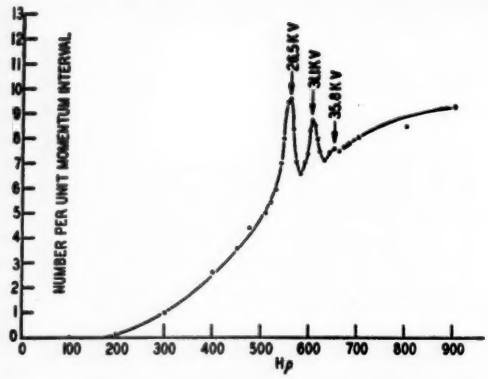

FIG. 2. Auger electrons identified as resulting from Ba^{137}.

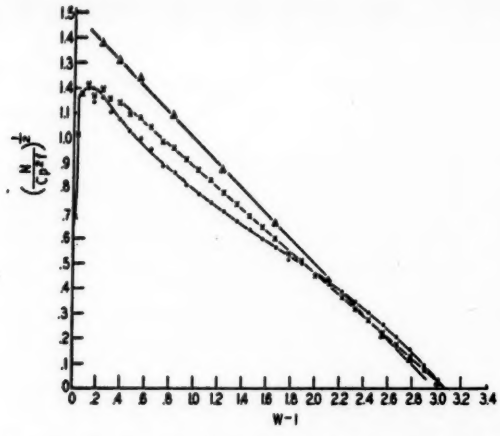

FIG. 3. Fermi plots of the beta-rays of Y^{91} corrected as follows: •$C=1$; ×$C=a$; Δ$C=c$.

Cs^{137}, very distinct Auger lines were detected. From their spacing, it can be shown that they result from the K internal conversion line of the Ba^{137} decay product. Ru^{106}, Pm^{147}, and Sm^{151} were found to have straight-line Fermi plots. Internal conversion electrons were detected accompanying the continuous beta-radiation of Tm^{170}. They result from an excited state of Yb^{170}, the emitted gamma-ray having an energy of 85.4±0.6 kev. Seaborg's[7] table reports, instead, a gamma-ray of energy 0.84 Mev associated with the Tm^{170} activity. If such a gamma-ray exists, its intensity is weaker by a factor of one thousand than the one with energy 85.4 kev. It is suggested that there is an error in the literature and in reality reference is made to a gamma-ray having an energy of 0.084 Mev. The Fermi plot of Tm^{170} was slightly concave toward the axis and an attempt has been made to apply one of the forbidden-type correction factors to it. P^{32} gave a Fermi plot of unexpected shape. The end point of P^{32} has long been used as an energy standard by many investigators to calibrate their spectrometers. It was believed that P^{32} had been thoroughly investigated.[8,9] It was found, however, that the data at energies below 150 kev were not complete. The work here shows a sharp increase in slope of the Fermi plot at about 150 kev and a slight curvature from there to the end point. The source was followed over five half-lives with no change in the position of the break.

It is believed that all materials used were essentially free from radioactive impurities. However, it should be realized that the presence of an impurity in one of the materials could cause a change in the shape of its spectrum. Because of the long lives of the materials reported here, it was not feasible to take separate data from the same materials over a period of several half-lives.

APPARATUS

Spectrometer

The spectrometer[3] used in this work consisted of two large identical coils spaced 95.5 cm apart. The intervening space was evacuated and contained the baffle system. The source was placed in the center of one coil and the detector was placed in the center of the other. In addition to the ordinary type of annular baffles, a helical baffle was used to select the desired trajectories. In the work reported here, the spectrometer was used with a resolution corresponding to a half-width at half-maximum of 1.1 percent and a transmission of 1.4 percent using sources 0.12 cm^2 in area.

All measurements are based on a value of 629 kev for the K internal conversion line of Ba^{137}. This line has been measured by several workers.[4,10,11] The value of 629 kev agrees with their reported results to within one-half percent and, considering the resolution employed in these measurements, it was decided to use it as a standard because of its convenience. On the basis of this value, the energies of the Auger electrons from Ba^{137} agreed very well with their calculated values. The end point of P^{32} agreed with the accepted value of 1.71 Mev.

Detector

A Geiger counter of special design was used to detect the beta-rays. The counter had a thin Nylon window which would transmit electrons having an energy greater than 8.8 kev. The thin Nylon window was supported on a grid and the counter was one electrode of an accelerating system which made it possible to detect a known fraction of the low energy electrons. Electrons of the proper momentum passed through a defining annulus and by means of a potential difference maintained between the counter and the annulus could

[7] G. T. Seaborg and I. Perlman, Rev. Mod. Phys. **20**, 585 (1948).
[8] E. M. Lyman, Phys. Rev. **51**, 1 (1937).
[9] K. Siegbahn, Phys. Rev. **70**, 127 (1946).
[10] Townsend, Owen, Cleland, and Hughes, Phys. Rev. **74**, 99 (1948).
[11] M. Friedman (private communication).

be accelerated before entering the counter. By taking spectra with and without the applied accelerating voltage, it was found that the detecting system was 100 percent efficient for 30-kev electrons with no accelerating voltage.

Using the accelerating section, it was 100 percent efficient for electrons with an energy equal to 30 kev minus the applied accelerating voltage. An $8\frac{1}{2}$ percent correction had to be applied for electrons having an energy of 16 kev when an accelerating voltage of 7 kev was used. The extent of these corrections is illustrated in Figs. 4 and 5. Because of the finite thickness of the sources, it is probable that the spectrum is distorted below 20 kev due to scattering in the source itself. The counting rate, when the counter was operated on its plateau, was constant for counter filling pressures ranging from 3 to 9 cm. This was checked using cobalt gamma-rays and beta-particles from uranium.

Sources

The sources were mounted on either zapon or LC600 films* weighing less than 0.01 mg/cm². The actual weight of the source was estimated by using a measured fraction of a solution in which the total non-volatile mass was known. The sources were made to spread out uniformly over an area of about 0.12 cm² by first placing a dilute drop of insulin on the foils. Experience proved that a very satisfactory method of preventing a source of high specific activity from charging up on the type of mounting employed was to cover it with a thin conducting foil after the source had been vacuum dried. Since scattering for low energy electrons is proportional to Z^2, it is important not only to use a thin foil but to use a thin foil of low atomic number. For this reason, an organic material was used for the foil to give it strength, and the foil was made conducting by coating it with Be metal using standard evaporating techniques. Care was taken not to inhale any of the Be fumes or dust. Foils whose total weight including Be was less than 0.006 mg/cm² were prepared in this manner. Such a foil 2 in. in diameter has a resistance from edge to edge of between 50 and 800 megohms as measured with an ohmmeter. These foils were placed Be side down on top of the dried radioactive source and were grounded to the spectrometer. No effect on the spectrum other than the removal of accumulated charge could be detected when such a foil was placed over the source. At least two different sources were run on each material and one percent statistics were obtained at all points of the spectrum except where the counting rate was less than four times the counter's natural background. In these instances, the data checked to within two percent.

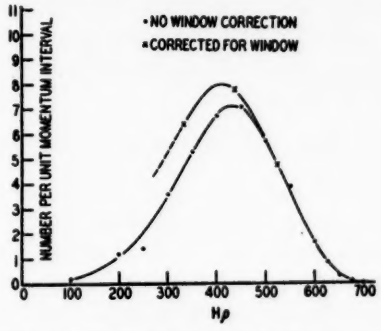

FIG. 4. Momentum distribution of the beta-rays of Ru^{106}.

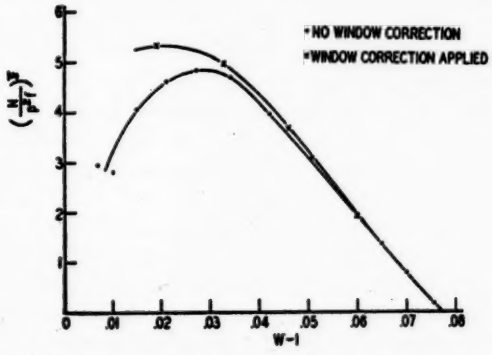

FIG. 5. Fermi plot of the beta-rays of Ru^{106}.

RESULTS

Cs^{137} (Half-Life† 37 Years: $ft = 4.41 \times 10^9$)

Three separate sources of Cs^{137} were prepared from material obtained from Oak Ridge. In each case, the source thickness was less than 0.05 mg/cm². The results are in agreement with those reported by Peacock and Mitchell.[4] The high energy group was not investigated. Figure 1 is a Fermi plot showing how the uncor-

FIG. 6. Fermi plot of the beta-rays of 61^{147}.

* A plastic resin manufactured by the Lithgow Corporation, Chicago, Illinois.

† Half-lives are those given by Seaborg (see reference 7).

rected plot curves toward the energy axis and how using the correction factor $[(W_0-W)^2+W^2-1]$ transforms the curve into a straight line. The hump at the low energy end is due to the presence of Auger electrons. From the end point of 0.523±0.004 Mev, one calculates ft to be equal to 4.41×10^9. Consequently, one would ordinarily classify this material as being second forbidden. Konopinski gives in his reference article various correction factors C_{ij} which one must apply to the function $f(Z, W)$, corresponding to an allowed spectrum, in order to get a straight line when $[N/C_{ij}p^2f(Z, W)]^{\frac{1}{2}}$ is plotted against the energy for an ith-forbidden spectrum. In the case of Cs^{137}, the correction factor a corrected the data extremely well. The only correction factors whose energy dependence is upon the factor a alone are C_{1A} and C_{1T} which are first-forbidden correction factors occurring with G-T selection rules corresponding to $\Delta J=\pm2$(yes). As pointed out by Konopinski, except for the case $\Delta J=\pm2$(yes), if $Z\gg Z_c$ with $Z_c\sim1.6\ W_0^{\frac{1}{2}}$ (W_0 is the total maximum energy of the beta-particle emitted) then all the C_{1j}'s are essentially independent of energy. For Cs^{137}, $Z=55$, whereas $Z_c=4.57$, hence, $Z\gg Z_c$. The correction factors C_{2j} all decrease as $(W_0-W)^2$ for $Z\gg Z_c$ except for $\Delta J=\pm3$(no). For this exception, the correction is determined by the factor

$$c=[3(W^2-1)+3(W_0-W)^4+10(W^2-1)(W_0-W)^2]/90.$$

When the factor c was applied as a correction factor, the Fermi plot was convex with respect to the energy axis. The use of $(W_0-W)^2$ as a correction factor did not give a straight-line Fermi plot. In view of this, one can exclude the possibility $\Delta J=\pm3$(no) and any of the other C_{2j}'s. Consequently, it may be assumed that the low energy group of Cs^{137} is first-forbidden and the large ft value is due to other reasons not included in the theory.

Figure 2 illustrates the Auger electrons occurring at 26.5±0.2 kev, 31.1±0.2 kev, and 35.8±0.2 kev. Using an average of the values of the critical absorption edges of the L and M shells of Ba given by Compton and Allison,[12] one may calculate that Auger electrons associated with Ba should have energies corresponding to 26.1 kev, 31 kev, and 35.8 kev. The experimental results agree very well with these values. With the resolution used, it is very difficult to determine from the separation of the K and L internal conversion lines whether they occur in the Ba or Cs, since it is a problem of measuring 3 kev in 629 kev. However, in the case of the Auger electrons, it is easy to identify them as belonging to the Ba since one needs only to measure 2 kev in 25 kev.

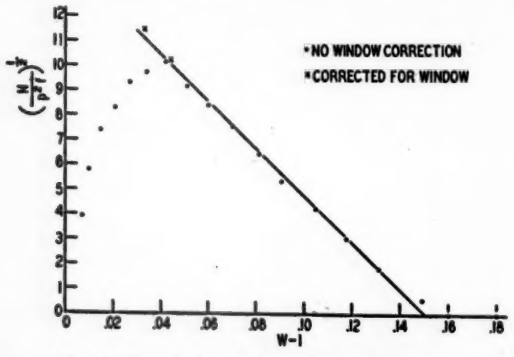

FIG. 7. Fermi plot of the beta-rays of Sm^{151}.

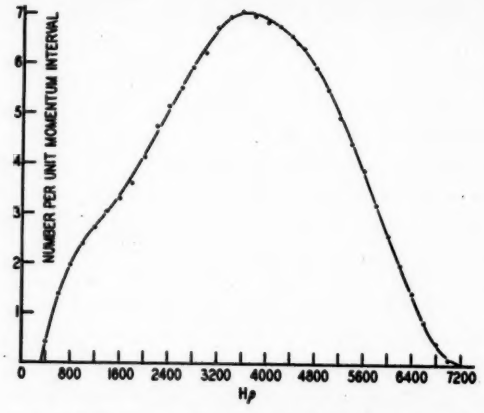

FIG. 8. Momentum distribution of the beta-rays of P^{32}.

It should be pointed out that this material, because of its long half-life, high specific activity, and the presence of the Auger and internal conversion electrons accompanying the continuous beta-spectrum, should be an extremely useful substance for workers in this field. A complete spectrum is shown in Fig. 5 in the report on the spectrometer.

Y^{91} (Half-Life 61 Days: $ft=5.7\times10^8$)

Sources less than 0.05 mg/cm² thick of Y^{91} were prepared from material obtained from Oak Ridge. Figure 3 is a Fermi plot of the spectra of Y^{91} showing the effect of using the correction factors a and c on the allowed $f(Z, W)$. From the end point of 1.56±0.01 Mev, one may calculate Y^{91} to have an ft value equal to 5.7×10^8 and consequently it may be classified as being second forbidden. As in the case of Cs^{137}, the correction factor a, when applied to $f(Z, W)$, gives a straight-line Fermi plot.

The nuclear shell model examined by Feenberg and Hammack[13] predicts that Y^{91} be first forbidden with maximum spin change of ±2. This is consistent with the interpretation of the use of the correction factor a. However, by using the correction factor c, one obtains a Fermi plot which deviates only slightly from a straight line at the high energy end. This would indicate that Y^{91} belongs to the second-forbidden group with $\Delta J=\pm3$(no). This is in contradiction with the conclusions one would arrive at from the use of the factor a. In view of this contradiction, it seems unlikely that one

[12] A. H. Compton and S. K. Allison, *X-Rays in Theory and Experiment* (D. Van Nostrand Company, Inc., New York, 1935), p. 792.

[13] E. Feenberg and K. C. Hammack, Phys. Rev. **75**, 1887 (1949).

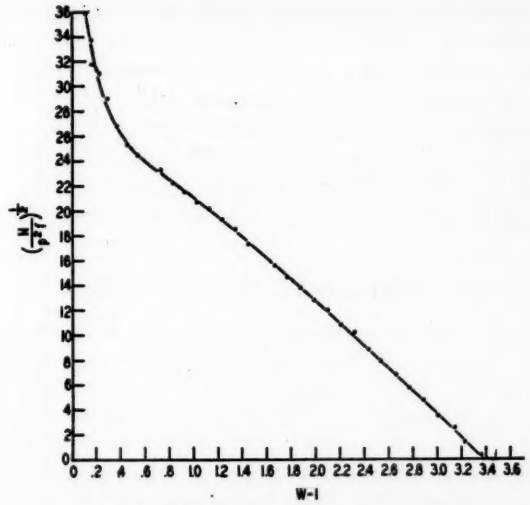

FIG. 9. Fermi plot of the beta-rays of P^{32}.

can determine the type of transition Y^{91} undergoes from an analysis of this type. Langer and Price[5] report using the correction factor a, but do not state whether they have tried any other factors on their data.

Ru^{106} (Half-Life 1 Year: $ft=2.14\times10^4$)

Ru^{106} was prepared by distillation of fission product solution. The author wishes to thank Dr. Ellis Steinberg of the Argonne National Laboratory for his assistance in preparing the material. It was hoped that the source would be free from solid matter except for the Ru^{106}. However, on evaporation, some deposit was visible. The sources used were less than 0.1 mg/cm², but their weights could only be estimated.

Figure 4 gives the momentum distribution of the electrons and shows the effect of the accelerator. Figure 5 is a Fermi plot of the data. From this, one obtains an end point of 0.0392 ± 0.0003 Mev, corresponding to an ft value of 2.14×10^4 which places it in the allowed group. This is an unusually low ft value for a substance with such a high atomic number. Because of the low upper energy limit of this spectrum, only a short stretch of the plot is experimentally significant. With this reservation, the data are compatible with a straight-line Fermi plot. No gamma-ray was observed.

Pm^{147} (Half-Life 3.7 Years: $ft=4.01\times10^7$)

Sources of Pm weighing less than 0.05 mg/cm² were prepared from material obtained from Oak Ridge. Figure 6 is a Fermi plot of the data. From the end point of 0.229 ± 0.001 Mev, an ft value of 4.01×10^7 was computed. This would place Pm^{147} in the first-forbidden group. However, Fig. 6 indicates that it has an allowed shape. As pointed out by Konopinski, if $Z\gg Z_c$, with $Z_c\sim1.6W_0^{\frac{1}{2}}$, then the first-forbidden spectra are nearly identical with allowed spectra for $\Delta J=0\pm1$. In this case, $Z_c=2.18$, whereas $Z=61$; therefore, $Z\gg Z_c$. Consequently, the data are not incompatible with the assumption that the β^--emission of Pm^{147} is first forbidden with $\Delta J=0\pm1$.

Sm^{151} (Half-Life 20 Years: $ft=7.5\times10^6$)

Two sources of Sm^{151} were prepared from material obtained from Dr. M. G. Inghram of the Argonne National Laboratory. Because of the extremely high activity of the material, it was possible to prepare sources weighing less than 0.03 mg/cm². Figure 7 is a Fermi plot of the data. An end point of 0.0755 ± 0.001 Mev was obtained. Using a half-life of 20 years, the corresponding ft value is 7.5×10^6 which classifies it as

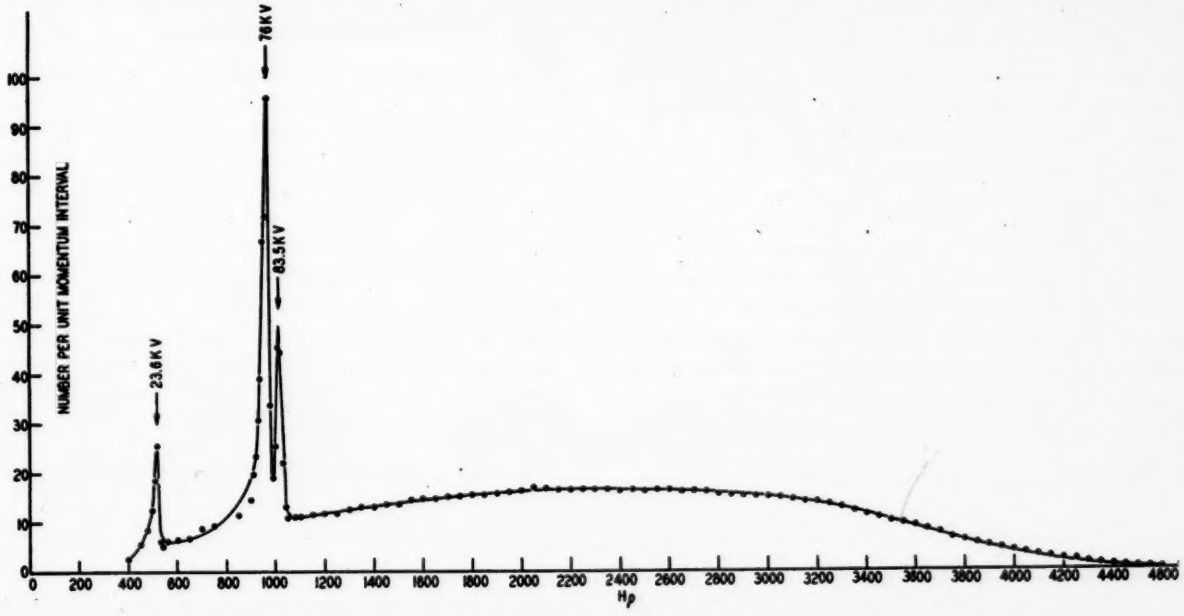

FIG. 10. Momentum distribution of the beta-rays of Tm^{170} showing the internal conversion lines of Yb^{170}.

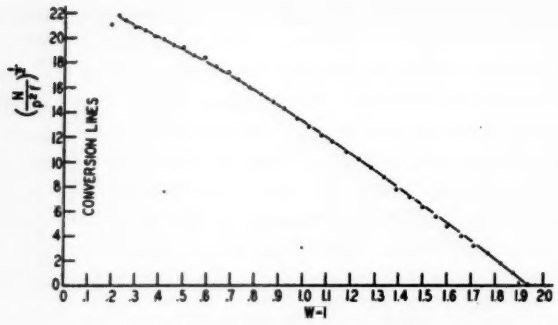

FIG. 11. Fermi plot of the beta-rays of Tm^{170}.

being first forbidden. However, Fig. 7 indicates an allowed-type Fermi plot. Z_c for Sm is 1.79. Hence, $Z \gg Z_c$ so it may be expected that the first-forbidden shape resembles the allowed shape. This would indicate that Sm^{151} is first forbidden with $\Delta J = 0, \pm 1$. Again it should be remarked that, because of the low upper energy limit of this spectrum, only a short stretch of the plot is experimentally significant. The situation is much better than in the case of Ru^{106}, but the errors involved should be realized.

P^{32} (Half-Life 14.3 Days: $ft = 8.60 \times 10^7$)

P^{32} was obtained in carrier-free form from Oak Ridge, and sources weighing less than 0.04 mg/cm² were prepared from it. Figure 8 shows the momentum distribution obtained. The large number of electrons at low energies was not expected, and its effect is shown clearly in Fig. 9 which is a Fermi plot of the data. From this plot, an end point of 1.718±0.01 Mev was obtained. The work of Siegbahn[9] presents a Fermi plot which is only given down to 150 kev; however, there seems to be an indication of the rise which is so noticeable in Fig. 9. This rise is also evident in the momentum plot given by Lawson.[14] From the end point of 1.718±0.01 Mev, P^{32} has an ft value of 8.60×10^7, which places it in the second-forbidden group. The P^{32} was followed for five half-lives with no change in the Fermi plot. Consequently, Fig. 9 must represent the spectrum of P^{32}. If it is complex with a low energy group, then S^{32} must have an isomeric state in which a gamma-transition is strictly forbidden since none is observed. On the basis of the assumption that it is not complex, an attempt has been made to apply a correction factor of the type C_{2j} to the data. The use of the factor c alone did not give a straight line; hence, this rules out the possibility of $\Delta J = \pm 3$(no). Since for these selection rules C_{2A} and C_{2T} depend upon the factor c alone. The use of the factor D_- was of no value, ruling out C_{2S} and C_{2P} corresponding to pure scalar and pseudoscalar interactions. This also rules out C_{2A} for $2 \leftrightarrow 0$ transitions. The use of the factor a alone is also unsatisfactory, ruling out the possibility of P^{32} being first forbidden with $\Delta J = \pm 2$(yes). The factor A_- alone was unsatisfactory, ruling out C_{1S} and C_{1P}. An attempt was made to use C_{2A} assuming various values for $(S_{ijk}/T_{ij})^2$, but no satisfactory fit was obtained.

Tm^{170} (Half-Life 127 Days: $ft = 7.05 \times 10^8$)

Tm^{170} was also obtained from Dr. M. G. Inghram of the Argonne National Laboratory, and sources were prepared which weighed less than 0.03 mg/cm². Figure 10 shows the momentum distribution obtained. Figure 11 is a Fermi plot of the data. The internal conversion lines correspond to a gamma-ray having an energy of 85.4±0.6 kev being emitted by the Yb^{170} decay product. From the Fermi plot, an end point of 0.990±0.007 Mev has been obtained which corresponds to an ft value of 7.05×10^8. This places Tm^{170} in the second-forbidden group. The Fermi plot is slightly concave toward the energy axis and an attempt has been made to apply one of the C_{ij} correction factors. The factors a and c distort the curve considerably thus ruling out the possibility of Tm^{170} being first forbidden with $\Delta J = \pm 2$(yes) or second forbidden with $\Delta J = \pm 3$(no). The factor D_- does not give satisfactory results nor does the factor A_-, thus ruling out C_{2S}, C_{1S}, and C_{1P}. For Tm^{170}, $Z_c = 4.48$, hence $Z \gg Z_c$. Consequently, there are really only two choices of C_{2j}; either $C \sim c$ or $C \sim (W_0 - W)^2$, neither of which is satisfactory in this case. It may be that Tm^{170} is actually first forbidden, and with $Z \gg Z_c$, the Fermi plot could resemble an allowed one. These results are in agreement with those recently reported by Saxon.[15]

ACKNOWLEDGMENTS

It is a pleasure for me to express my appreciation to Professor Enrico Fermi for his continued advice and encouragement. I am indebted to Professor Herbert L. Anderson for his interest in this work, and for initiating the construction of the spectrometer. I also wish to thank Mr. C. Y. Fan for his assistance in the latter stages of the work.

I wish to acknowledge the use of the tables of screening factors and the tables of $f(Z, W)$ made available to me by Dr. John Reitz and Mr. Steven Moszkowski.

A major portion of this work was made possible through the use of materials made available by the Isotope Division of the Oak Ridge Laboratory.

[14] J. L. Lawson, Phys. Rev. **56**, 131 (1939).

[15] D. Saxon and J. Richards, Phys. Rev. **76**, 186 (1949).

Drift Velocities of Electrons in Argon, Nitrogen, and Argon-Nitrogen Mixtures

E. D. KLEMA* AND J. S. ALLEN
Department of Physics, University of Illinois, Urbana, Illinois
(Received October 25, 1949)

The drift velocities of electrons produced by polonium α-particles in a parallel-plate ionization chamber have been measured for pure argon, pure nitrogen, and argon-nitrogen mixtures. The argon data agree with the results of other investigators using the same method, but disagree with those obtained from the pulsed x-ray method. The nitrogen data agree with the results published by early investigators.

INTRODUCTION

BECAUSE of the increasing use of electron collection in ionization chambers, it is of interest to measure the drift velocities of electrons in the gases commonly employed in such chambers. Such measurements enable one to calculate the time of collection of electrons in a given ionization chamber. It is of practical importance to make this time of collection as short as possible, and it has been shown[1] that in certain gas mixtures one can obtain electron drift velocities which are higher than the drift velocity in either component of the mixture alone. It seemed of interest to repeat the measurement of the drift velocity in pure argon because of the discrepancies among the results obtained by various investigators.[1–3]

EXPERIMENTAL METHOD

The ionization chamber used in the present work consisted of two circular brass plates 5 in. in diameter and separated by 2.65 cm in a brass cylinder 6 in. in inside diameter. The chamber was sealed with a koroseal gasket, and a calcium-filled convection-current purifier whose volume was about 1/20 of that of the ionization chamber was used in obtaining the data for purified gases. The purifier was kept in operation, usually at 300°C, while the measurements were being made. Although calcium reacts with nitrogen rapidly at 400°C, the rate of reaction at 300° is low enough to enable one to remove the oxygen and water vapor from nitrogen by circulating it over calcium at this temperature.[4] In the present work, no appreciable pressure change occurred at 3 atmospheres of nitrogen in 24 hours with the purifier at 300°. A polonium α-particle source emitting about 3000 particles/min. was evaporated directly on the negative electrode.

The amplifier used was a "model 500," designed by W. C. Elmore,[5] and modified slightly so that one cathode follower output tube fed the voltage pulses from the chamber to trigger the sweep circuit of the oscilloscope and the other cathode follower fed the pulses from the first triplet feedback loop of the main

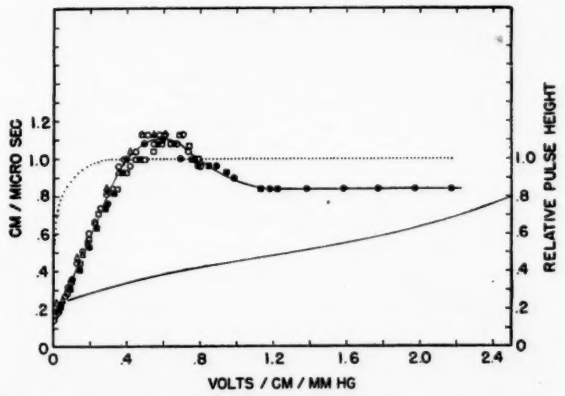

FIG. 1. Electron drift velocity curves obtained with pure argon. The open circles represent data obtained at a pressure of 3 atmos. and a purifier temperature of 160°C. The open triangles represent data at 3 atmos. and 300°C. The open squares, the solid squares, and the solid circles represent the data obtained at pressures of 2, 1, and ½ atmos., respectively. The dotted curve represents the relative pulse height and is referred to the scale at the right of the figure. The lower solid curve represents the data obtained by Nielsen (see reference 7) using the electrical shutter method.

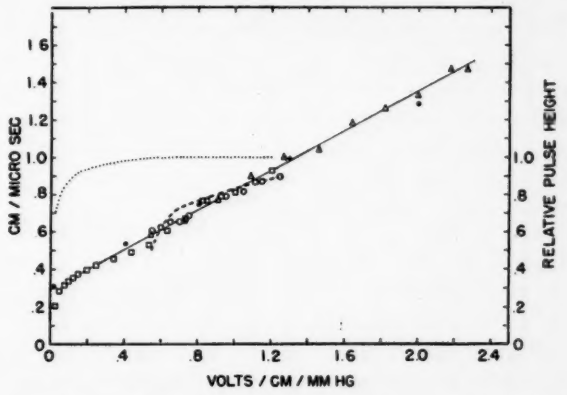

FIG. 2. Electron drift velocity curves for nitrogen. The open circles represent the data obtained with commercial water-pumped nitrogen at a pressure of 2 atmos. The open squares represent the data obtained at 2 atmos. after purification. The open triangles represent the data obtained at 1 atmos. with the purifier turned off after the gas had been purified. The dashed curve is the pulse height curve for the unpurified gas. The dotted curve is the pulse height curve for the purified gas. Several values of the drift velocity obtained from the published curves of Nielsen (see reference 7) are indicated by the solid circles.

* Now at Department of Physics, The Rice Institute, Houston, Texas.

[1] J. S. Allen and Bruno Rossi, MDDC 448, p. 1.
[2] Pierre Herreng, Comptes Rendus **217**, 75 (1943).
[3] Donald E. Hudson, MDDC 524.
[4] P. de Cori, IX Congr. intern. quim. pura aplicada (Madrid) **6**, 225 (1934) (published in 1936).
[5] W. C. Elmore, LADC 89 and LADC 91.

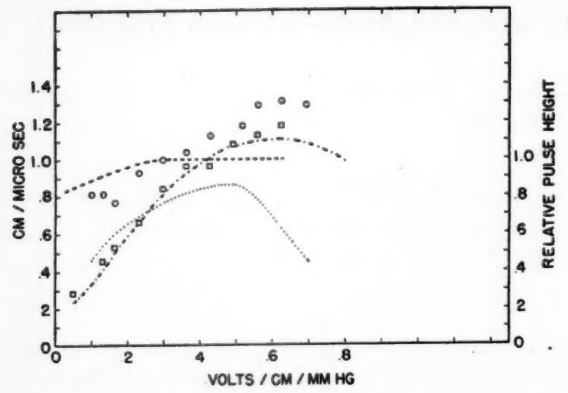

FIG. 3. Electron drift velocity curve for 1 percent of oxygen in argon at 3 atmos. The open circles represent the data obtained with the unpurified mixture. The open squares represent the data obtained after the mixture was passed over hot calcium and the oxygen removed. The alternate dot and dash curve represents the data previously obtained with pure argon. The dotted curve is the pulse height curve of the mixture before purification; the dashed curve is the pulse height curve after purification.

amplifier through a 0.15 μsec. delay line to the amplifier of the oscilloscope. The rise time of the entire amplifying system, including the delay line, was 0.08 μsec., and the time constant determining the low frequency response (the "clipping time") was 50 μsec. From the decay of the pulses as observed on the oscilloscope screen, the effective "clipping time" was about 25 μsec. The signal-to-noise ratio at 3 atmospheres pressure was about 8 to 1 for the pulses of maximum height, corresponding to those α-particles coming off at small angles with respect to the surface of the negative electrode.[6]

The oscilloscope used was a Tektronix Model 511. The sweep speeds were calibrated by means of an oscillator and an accurate wave meter. It was found that the sweeps were slightly non-linear at their starts, and so the positions of the peaks of a known sine wave were determined accurately and a curve of time against distance along the sweep was obtained for each of the sweep speeds used in the experiments.

The output pulses of the amplifier were observed visually on the oscilloscope screen, and the time from the beginning of the sweep to the maximum height of the pulse was measured in each case. The entire pulse was not visible because the time necessary for the pulse to rise to the voltage required to trigger the sweep of the oscilloscope was longer than the delay introduced by the delay line. The pulses were extrapolated back to zero pulse height by means of a transparent straight edge, and the time corresponding to the extrapolation to zero pulse height was added to the time from the beginning of the sweep to the maximum pulse height, as discussed to obtain the total time of the voltage pulse from the chamber. Since the leading edges of the pulses were quite linear, this correction should not introduce a serious source of error. That this is the case was shown by observing the pulses obtained with a given set of experimental conditions in turn on each of two sweeps, the speeds of which varied by about a factor of three. The measurements made on the two sweeps agreed to within the uncertainty of observing the positions of the maxima of the pulses. This check was made each time the sweep speed was changed to accommodate for the change in the drift velocity as the field across the chamber was varied.

Error may be introduced by the observed effective "clipping time" owing to its distortion of the linear leading edge of a pulse from the ionization chamber. This possibility was considered by plotting to the same scale as that of the oscilloscope screen the effect of the observed time constant on a pulse rising linearly to the saturation value in 5 μsec. It was found that the position of the maximum pulse height was still well defined for this case and that no appreciable error in the measurement of the rise time resulted. Since the rise time of the entire amplifying system was about 7 percent of the minimum electron collection time, the effect of this on the observed shapes of the pulses was considered to be negligible in comparison with the errors resulting from the time measurements on the scope screen. The largest pulses were always used for the measurements since for this case the slope of the expected voltage pulse should be accurately constant until the maximum, and then the amplitude should decay with the effective "clipping time" of the amplifier. The drift velocity of the electrons is then given by the distance between the plates of the ionization chamber

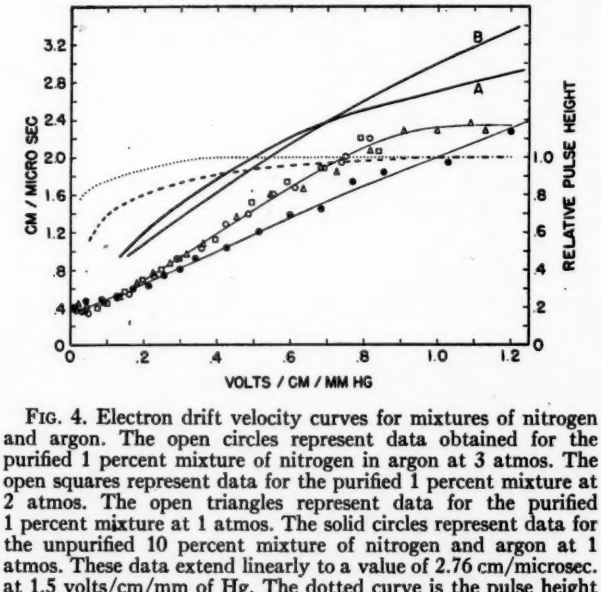

FIG. 4. Electron drift velocity curves for mixtures of nitrogen and argon. The open circles represent data obtained for the purified 1 percent mixture of nitrogen in argon at 3 atmos. The open squares represent data for the purified 1 percent mixture at 2 atmos. The open triangles represent data for the purified 1 percent mixture at 1 atmos. The solid circles represent data for the unpurified 10 percent mixture of nitrogen and argon at 1 atmos. These data extend linearly to a value of 2.76 cm/microsec. at 1.5 volts/cm/mm of Hg. The dotted curve is the pulse height curve for the purified 1 percent mixture. The dashed curve is the pulse height curve for the unpurified 10 percent mixture. The solid curve *A* is a computed electron drift velocity curve for 1 percent of nitrogen in argon based on the data for argon and nitrogen given by Townsend (see reference 11). The solid curve *B* is a similarly computed curve for 10 percent of nitrogen in argon.

[6] Rubby Sherr and Rolf Peterson, Rev. Sci. Inst. **18**, 568 (1947).

divided by the observed total time to the maximum of the voltage pulse from the chamber. The relative accuracy of the drift velocity measurements was estimated to be ±5 percent.

RESULTS

The argon used in this experiment was 99.6 percent pure according to the manufacturer. The drift velocities of electrons in purified argon were measured at pressures of ½, 1, 2, and 3 atmospheres, and the results are given in Fig. 1. The drift velocity in cm/μsec. is plotted against the field strength per unit pressure in volts/cm/mm of mercury. For the case of a pressure of 3 atmospheres, it was found necessary to outgas the calcium in the purifier at a temperature higher than that used for purifying the gas in order to get a reproducible drift velocity curve. When this was done, the data obtained at a purifier temperature of 160°C agreed with those obtained at a purifier temperature of 300°. The dotted curve is the plot of the relative pulse height as a function of the field strength per unit pressure. One sees that at values of E/p greater than 0.3 all the electrons produced by the α-particles are collected.

The data obtained with nitrogen are shown in Fig. 2. The nitrogen used was the water-pumped grade sold commercially in metal cylinders. It is seen that one obtains the same drift velocity curve with tank as with pure nitrogen. However, the saturation properties of the gas improve markedly with purification. The data at 1 atmosphere were obtained with the purifier having been turned off for 2 hours after having been on for about 24 hours. The drift velocity curve obtained for nitrogen agrees with the data of Nielsen.[7]

The effect of introducing 1 percent of commercial tank oxygen into argon at 3 atmospheres pressure is shown in Fig. 3. The drift velocity of the electrons is increased because their average energy is decreased, and the pulse height is decreased because of capture of electrons by oxygen molecules to form negative ions. It is seen that above $E/p=0.5$, as the field strength is increased, the pulse height decreases because the electrons increasingly excite the electronic excitation level of the oxygen molecule at 1.62 electron volts.[8] The fact that the oxygen was removed by the purifier is shown by the agreement of the observed points with the curve obtained for pure argon.

The results obtained with mixtures of argon and nitrogen are shown in Fig. 4. The data for the mixture of 1 percent of nitrogen in argon were limited by the fact that a discharge in the gas occurred at a field strength of 1280 volts/cm at a pressure of 2 atmospheres and at a field strength of 940 volts/cm at a pressure of 1 atmosphere. When the chamber was filled with the 10 percent mixture of nitrogen in argon at 1 atmosphere, a field strength of 1360 volts/cm was reached before breakdown occurred.

One sees that at low values of E/p the electron drift velocity is higher for the 1 percent mixture than for the 10 percent mixture. However, the fact that one can reach higher values of E/p before breakdown with the 10 percent mixture enables one to reach higher values of drift velocity with it than with the 1 percent mixture. The data for the 10 percent mixture shown in Fig. 4 were extended, and the drift velocity continues to increase linearly with E/p to a value of 2.76 cm/μsec. at $E/p=1.5$ volts/cm/mm of mercury.

The Drift Velocity of Electrons in Mixtures of Gases

As mentioned earlier, Allen and Rossi[1] have developed a procedure for the calculation of the drift velocity of electrons in mixtures of two or more gases when the appropriate data for the individual gases are available. A short description of this method has been given by Healey and Reed,[9] and a more detailed discussion has been given by Staub and Rossi.[10] Since this method has proved to be extremely valuable when used to predict the behavior of an ionization chamber, the predicted values of the drift velocity were compared with the observed values for the argon-nitrogen mixtures in order to indicate the accuracy of this method.

For convenience a summary of the method developed by Allen and Rossi[1] will be presented here using the same notation. Consider a gas such as argon in which the probability of negative ion formation is extremely small. When an electric field E volts/cm is applied, a drift velocity W is superimposed upon the irregular thermal motion of any free electrons present in the gas and their average energy is increased above the thermal value. Let $K(3/2kT)$ be the new value of this average energy.

The values of K and W are determined by an equilibrium condition between the energy and momentum imparted by the electric field to the electrons and the energy and momentum transferred by the electrons to the gas molecules through collisions. These two equilibrium conditions may be expressed by the following equations:

$$eEW=p\epsilon(K) \tag{1}$$

$$eE=pW\pi(K) \tag{2}$$

where e is the electronic charge, p is the pressure of the gas in mm of Hg, $\epsilon(K)$ is the average energy transfer per second for $p=1$ mm of Hg and $\pi(K)$ is the average momentum loss per second for $W=1$ and $p=1$ mm of Hg. In general, ϵ and π are functions of K.

For a mixture of n gases with partial pressures p_1, p_2

[7] R. A. Nielsen, Phys. Rev. **50**, 950 (1936).

[8] Leonard B. Loeb, *Fundamental Processes of Electrical Discharge in Gases* (John Wiley & Sons, Inc., New York, 1939), p. 190.

[9] Healey and Reed, *The Behavior of Slow Electrons in Gases* (Iliffe and Sons, Ltd., London, 1941).

[10] H. H. Staub and B. Rossi, National Nuclear Energy Series, Los Alamos Project (McGraw-Hill Book Company, Inc., New York, 1949), Vol. 2.

$\cdots p_n$ and total pressure p, the quantities $p\epsilon(K)$ and $p\pi(K)$ of Eqs. (1) and (2) may be written as

$$p\epsilon(K)=p_1\epsilon_1(K)+p_2\epsilon_2(K)+\cdots p_n\epsilon_n(K), \quad (3)$$

and

$$p\pi(K)=p_1\pi_1(K)+p_2\pi_2(K)+\cdots+p_n\pi_n(K), \quad (4)$$

where ϵ and π now refer to the mixture. In the present experiment the drift velocities were computed for mixtures of 1 percent and 10 percent of nitrogen in argon. The procedure was as follows:

A. $\epsilon_1/e=W_1E_1/p_1$ and $\pi_1/e=E_1/p_1W_1$ were plotted as functions of K for argon, and corresponding curves were plotted for nitrogen. The values of W as functions of E/p and K for the two gases were obtained from tables published by Townsend.[11]

B. Curves showing ϵ and π as functions of K were obtained after substitution of the appropriate values of ϵ_1, ϵ_2, π_1 and π_2 in Eqs. (3) and (4).

C. The curve for ϵ obtained in step B was replotted as a function of E/p, using the relation $\pi/e\times\epsilon/e=(E/p)^2$ for a given value of K.

D. The drift velocity W as a function of E/p was computed for each mixture using the curve obtained in step C and the relation

$$W=\epsilon/e\times p/E \quad \text{(Eq. (1))}.$$

The computed values of the drift velocity in mixtures of $0.01N_2+0.99A$ and $0.10N_2+0.90A$ are shown by curves A and B of Fig. 4. Although the computed values of W are considerably higher than the experimental data, the two sets of curves show the same general shape and indicate that the drift velocities in either of the mixtures are approximately twice the values in either A or N_2 at the same E/p. The physical reason for this increase in the drift velocities can be understood from an analysis of the behavior of electrons in A and in N_2. The curves of ϵ against K show that the energy loss in A is very small until K reaches a value of about 270 (which corresponds to 10 ev) and then starts rising abruptly, while in N_2 the energy loss increases rapidly above $K=30$. This is due to the fact that in A no inelastic collisions occur unless the electrons have an energy larger than the first excitation potential of 11.6 ev. In N_2 however, inelastic collisions occur at much smaller energies because of the vibrational excitation levels of the molecule beginning at about 1 ev. The effect of the addition of N_2 to A is to reduce the average energy of the electrons from about 10 ev for A at $E/p=1$ to about 1 ev for the mixture at the same value of E/p.

The curves of π as a function of K for either of the two mixtures show that the average momentum loss of the electrons is only slightly greater than that in pure argon because of the small proportion of nitrogen. Hence, we can say that the main effect of the addition of a small amount of N_2 to A is to bring the average energy of the electrons from a high value, for which π is large, to a low value, for which π is small. Since the electron drift velocity is inversely proportional to π, this will result in an increased value of the drift velocity.

Since it was necessary to use the values of W and K given by Townsend,[11] a close agreement between the computed and experimental curves was not expected. However, the agreement is sufficiently close to indicate that this method can be used to estimate the behavior of ion chambers containing a mixture of two gases such as argon-nitrogen or argon-carbon dioxide.

[11] J. Townsend, *Electrons in Gases* (Hutchinson's Scientific Publications, London, 1947), pp. 72, 73.

CONCLUSIONS

As mentioned in the introduction, large discrepancies exist between the data published by various investigators for the drift velocity of electrons in argon. Since the drift velocity in this gas is extremely sensitive to small amounts of impurities, the values of W and also of K obtained by Townsend[11] probably are not representative of a pure gas. In recent years, discrepancies have appeared among the results obtained with modern vacuum techniques, but with different methods of drift measurement. The values of W obtained in the present experiment and shown in Fig. 1 are considerably above the curve representing the work of Nielsen[7] for values of E/p less than 2.6. The two sets of data apparently agree at $E/p=2.6$. Nielsen used the electrical shutter method with a thermionic source of electrons. The purity of the argon was stated to be 99.8 percent and the gas was introduced in to the apparatus through a liquid air trap.

The data of Nielsen are in close agreement with those obtained by Herreng.[2] In this latter experiment the electrons were produced by a narrow beam of x-rays parallel to the surface of the upper plate of the ionization chamber. No information regarding the purity of the gas has been published. Hudson[3] has measured the drift velocity of electrons in argon using the pulsed x-ray method. In his experiment, the entire sensitive volume of the ionization chamber was irradiated by the x-ray beam. The gas was purified by the same type of purifier used in the present experiment. He obtained a curve for W as a function of E/p which agrees with our data for low values of E/p, but rises to a maximum of $W=2.1$ cm/μsec. at $E/p=1.0$. This is about twice the maximum value of W observed in our experiment and occurs at about twice the value of E/p.

An obvious explanation for the discrepancies which still exist between the values of the drift velocity of electrons in argon as reported by various investigators is that the methods of purification used at present do not result in the degree of purity required for consistent results. In the present experiment, reproducible drift velocity curves were obtained when the calcium purifier had been evacuated and outgassed prior to the circulation of the gas through the system. The curves of Fig. 3 indicate that the purifier will remove relatively large amounts of oxygen from argon. Since the argon was

allowed to circulate continuously through the purifier during the experiment, all impurities other than inert gases should have been removed. It is possible that impurities were present in the gas used by Nielsen[7] or by Herreng[2] since continuous purification was not used in these experiments.

In contrast to the results for argon the curves shown in Fig. 2 indicate that, in the case of nitrogen, there is a close agreement between the drift velocity data of the present method and those of Nielsen.[7] Apparently, the drift velocity in this gas is less sensitive to the purity of the gas than in the case of argon.

PHYSICAL REVIEW VOLUME 77, NUMBER 5 MARCH 1, 1950

On a New Theory of Nuclear Forces*

H. J. BHABHA
Tata Institute of Fundamental Research, Bombay, India
(Received October 17, 1949)

A new theory of nuclear forces is based on the result established in an earlier paper that if the matrix α^0 in the field equations $(\alpha^k p_k+\chi)\psi=0$ satisfies the minimal equation $\{(\alpha^0)^2-1\}^2(\alpha^0)^s=0$, any integer, then every component of the field ψ satisfies the iterated generalized wave equation $(\Box+\chi^2)^2\psi=0$ of the fourth order. The static potential between two nucleons is then a sum of the interaction (29) between two point charges and the dipole-dipole interaction (30) multiplied by numerical coefficients and isotopic spin factors. This interaction, unlike the usual one based on the Yukawa theory, allows an exact solution of the deuteron problem. The potentials based on more complicated fields satisfying the n times iterated generalized wave equation are also given.

1. INTRODUCTION

THE present theories of nuclear forces are all essentially based on Yukawa's original idea that the force between two nucleons results from the interaction of the nucleons with a field which satisfies the generalized second-order wave equation. For brevity we call this the meson field. All such theories lead in essence to a static potential between two point charges at a distance r of the form**

$$e^{-\chi r}/r, \tag{1}$$

and a static potential between two dipoles of the form

$$e^{-\chi r}\left[\left(\frac{\chi}{r^2}+\frac{1}{r^3}\right)(\boldsymbol{\sigma}^{(1)}\cdot\boldsymbol{\sigma}^{(2)}) - \left(\frac{\chi^2}{r}+\frac{3\chi}{r^2}+\frac{3}{r^3}\right)\left(\boldsymbol{\sigma}^{(1)}\cdot\frac{\mathbf{r}}{r}\right)\left(\boldsymbol{\sigma}^{(2)}\cdot\frac{\mathbf{r}}{r}\right)\right]. \tag{2}$$

χ is the constant associated with the field and equal to the meson mass in suitable units. Here $\boldsymbol{\sigma}^{(1)}$ and $\boldsymbol{\sigma}^{(2)}$ stand for two three component vectors representing the directions of the moments of the two dipoles. The potentials (1) and (2) may be multiplied by isotopic spin factors depending on whether the meson field is neutral or charged or both. The potential between two nucleons is essentially a sum of these two potentials multiplied by numerical factors, the sign and magnitude of the factors depending on the spin of the meson field and the type of coupling assumed between the nucleons and the meson field. All such theories have proved unsatisfactory, not only because of the inability of any of them to describe the properties of the deuteron and the scattering of nucleons correctly, but because of the fundamental difficulty that the potential (2) between two nucleons becomes so singular as their mutual distance r diminishes, that no rigorous quantum mechanical solution of the deuteron problem exists.

Both the classical and quantum theories agree in giving the same potentials (1) and (2) between two nucleons, with the typical r^{-3} singularity in the interaction of two dipoles. This singularity is the same as that for the potential between two dipoles interacting through the electromagnetic field, and is unaffected by letting $\chi\to 0$ in (2). Since this very singular potential means that the kinetic energy of the two nucleons must become very large at close distances, one might for a moment suppose that a relativistic calculation of the potential taking into account the reaction of the emitted mesons might diminish the order of the singularity. This is however extremely unlikely, in my opinion, since every component of the meson field satisfies the

* The main ideas and results of this paper were contained in my lectures to the Canadian Mathematical Seminar, August 15–September 3, 1949, but they have not been published before.

** x^k, $k=0, 1, 2, 3$, are the four coordinates, and the metric tensor is taken in the form $g^{00}=-g^{11}=-g^{22}=-g^{33}=1$, $g^{kl}=0$ for $k\neq l$. A summation from 0 to 3 is understood over every index occurring both above and below. A letter in heavy type, for example $\mathbf{r}$, denotes a space-vector with three components r_1, r_2, and r_3, and absolute length $r=+\{\sum_{k=1}^{3}(r_k)^2\}^{\frac{1}{2}}$. We use the vector product notation $(\mathbf{a}\cdot\mathbf{b})=\sum_{k=1}^{3}a_k b_k$. The four coordinates of a nucleon are denoted by z^k and the suffices (1) and (2) in brackets are used to identify variables belonging to the two nucleons. $r_k=z_k^{(1)}-z_k^{(2)}$, for $k=1, 2, 3$.

generalized second-order wave equation

$$(\Box+\chi^2)U=j, \tag{3}$$

where j is the corresponding source function, and $\Box$ stands for the d'Alembertian $\partial^2/\partial x^k\partial x_k$. Now the exact solution of (3) for arbitrary relativistic movements of the sources is known[1] and we know from this that although the field of a point charge then no longer has its non-relativistic form (1), nevertheless, the order of the singularity is in no way changed. The non-relativistic dipole-dipole interaction (2) is simply obtained from (1) by operating on it with the operator

$$\left(\boldsymbol{\sigma}^{(1)}.\frac{\partial}{\partial \mathbf{z}^{(1)}}\right)\left(\boldsymbol{\sigma}^{(2)}.\frac{\partial}{\partial \mathbf{z}^{(2)}}\right), \tag{4}$$

and is the non-relativistic limit of the exact interaction derivable from the corresponding exact solution of Eq. (3) for arbitrary relativistic movements of the dipole point sources.[2] As long as one works within the framework of the present theory of elementary particles,[3] and the field responsible for the force obeys the generalized second-order wave Eq. (3), there is no possibility of avoiding the r^{-3} singularity in the dipole-dipole interaction which robs even the two nucleon problem of all meaning. The reaction of radiation is no more likely to change the order of the r^{-3} singularity than it changes the order of the r^{-1} singularity between two point changes.

2. GENERAL THEORY AND THE FUNDAMENTAL EQUATIONS OF THE FIELD

In a recent paper[3] the following results have been established. On the basis of six quite general postulates it can be shown that all quadratic terms in the Lagrange function must be of the form $\psi\dagger(\gamma^k p_k+\gamma\chi)\psi$, where the γ^k and γ are five hermitian matrices and $p_k=-i\partial/\partial x^k$. From this it can be deduced that every elementary particle field whose rest mass is not zero must satisfy a linear equation of the type

$$(\alpha^k p_k+\chi)\psi=0 \tag{5}$$

in the absence of interaction, the α^k being four square matrices. It was proved next that as a consequence of (5) every component of the wave function ψ must satisfy a generalized wave equation of the type

$$(\Box+\chi_1^2)(\Box+\chi_2^2)\cdots(\Box+{}_n\chi^2)\psi=0, \tag{6}$$

where $\chi_1^2=\chi^2/a_1^2$, $\chi_2^2=\chi^2/a_2^2$, $\cdots\chi_n^2=\chi^2/a_n^2$, if the minimal equation of α^0 is

$$\{(\alpha^0)^2-a_1^2\}\{(\alpha^0)^2-a_2^2\}\cdots\{(\alpha^0)^2-a_n^2\}(\alpha^0)^s=0, \tag{7}$$

where s is any non-negative integer, and $a_1, a_2, \cdots a_n$ are the non-zero real eigenvalues of α^0, each of which may occur more than once without changing the minimal Eq. (7). The special case of iterated roots in the minimal equation of α^0 is covered by permitting two or more of the numbers $a_1, a_2, \cdots a_n$ to be equal to each other.

Lemma 10 of the paper quoted above states that if the particle described by Eq. (5) is to have only one real mass value then α^0 must have one and only one pair of real eigenvalues $\pm a$ (which may occur several times). Without loss of generality the minimal equation of α^0 is then

$$\{(\alpha^0)^2-1\}^n(\alpha^0)^s=0, \tag{8}$$

where $n\geqslant 1$, $s\geqslant 0$ are non-negative integers. Every component of the wave function then satisfies the generalized wave equation of order $2n$

$$(\Box+\chi^2)^n\psi=0. \tag{9}$$

The effect of the cubic and higher degree interaction terms is to add a non-zero source function to the right-hand side of (5), and therefore to replace (6) and (9) by

$$(\Box+\chi_1^2)(\Box+\chi_2^2)\cdots(\Box+\chi_n^2)\psi=j(x^k) \tag{10}$$

and

$$(\Box+\chi^2)^n\psi=j(x^k) \tag{11}$$

respectively, where the source function j has the same transformation properties as ψ.

The general solution of equations of the type (10) of order $2n$ in m space dimensions has been given recently by Surya Prakash.[4] It consists in finding the elementary solution of Eq. (10), which plays the same part in the theory of hyperbolic equations as the Greens function in the theory of elliptic equations. The elementary solution is defined as the solution of (10) when

$$j(x^k)=\delta(x^0-x'^0)\delta(x^1-x'^1)\delta(x^2-x'^2)\delta(x^3-x'^3), \tag{12}$$

δ being Dirac's delta-function. I give here Prakash's result for the special case of four-dimensional space time in which we are interested. The elementary solution which vanishes on any space-like surface in the past of the point x'^k is

$$G_i(u)=\frac{(-1)^n}{4\pi}\frac{\partial}{u_r\partial u_r}\left\{\sum_{s=1}^{n}\frac{F(\chi_s u)}{\prod_{t\neq s}(\chi_s^2-\chi_t^2)}\right\}, \tag{13a}$$

where

$$F(\chi_s u)=\begin{cases} J_0(\chi_s u) & \text{for } u^0\geqslant u_r \\ 0 & u^0<u_r, \end{cases} \tag{13b}$$

J_0 being the zero order Bessel function, and

$$\begin{aligned} u^k&=x^k-x'^k \\ u&=+(u^k u_k)^{\frac{1}{2}} \\ u_r&=+\left\{\sum_{k=1}^{3}(x^k-x'^k)^2\right\}^{\frac{1}{2}}. \end{aligned} \tag{14}$$

[1] H. J. Bhabha, Proc. Roy. Soc. A, **172**, 384 (1939). See formulas (4) and (9).

[2] H. J. Bhabha and H. C. Corben, Proc. Roy. Soc. A **178**, 273 (1941). See formulas (23) and (114). H. J. Bhabha, Proc. Roy. Soc. A **178**, 314 (1941). See formulas (29) to (35).

[3] H. J. Bhabha, Rev. Mod. Phys. **21**, 451 (1949).

[4] S. Prakash, Proc. Ind. Acad. Sci. A (in course of publication).

The general solution of (10) when $j(x^k)$ is an arbitrary function of x^k is then

$$\psi=\int\int\int\int_{-\infty}^{\infty}G(u)j(x'^k)dx'^0\cdots dx'^3. \quad (15)$$

This is the solution corresponding to the usual retarded potentials. Another solution corresponding to the usual advanced potentials is obtained by replacing u_r by $-u_r$ and reversing the inequality signs in (13b). All the above results can be given a rigorous mathematical formation through the theory of distributions developed by Laurent Schwartz. The Dirac delta-function and the elementary solution (13) are not strictly functions but distributions.

The elementary solution of Eq. (11) is obtained by confluence from that of (10). Since the denominator of every term in (13a) vanishes when all the χ's are put equal, some care has to be exercised in approaching the limit. Denote the coefficient of the sth term in curly brackets in (13a) by

$$a_s=\{\prod_{t\neq s}(\chi_s^2-\chi_t^2)\}^{-1}. \quad (16)$$

Consider the matrix

$$M=\begin{bmatrix}1 & 1 & \cdots & 1\\ \chi_1^2 & \chi_2^2 & \cdots & \chi_n^2\\ \cdot & \cdot & \cdots & \cdot\\ \chi_1^{2n-2} & \chi_2^{2n-2} & \cdots & \chi_n^{2n-2}\end{bmatrix}. \quad (17)$$

Its determinant has the well-known value

$$|M|=\prod_{s,t<s}(\chi_s^2-\chi_t^2) \quad (18)$$

while the determinant of the matrix obtained from (17) by omitting the last row and sth column is just the right-hand side of (18) with all the factors containing χ_s omitted. a_s is therefore just the minor of χ_s^{n-2} in M. Hence, denoting the elements of M by M_{rs},

$$\sum_{s=1}^{n}M_{rs}a_s=\begin{cases}0 & \text{if } r\neq n\\ 1 & \text{if } r=n.\end{cases} \quad (19)$$

This is equivalent to

$$\sum_{s=1}^{n}(\chi_s^2)^r a_s=\begin{cases}0 & \text{if } r<n-1\\ 1 & \text{if } r=n-1.\end{cases} \quad (20)$$

We now expand $F(\chi_s u)$ which is a continuous and differentiable function of χ_s^2 in terms of its Taylor series about the point $\chi_s=\chi$, thus

$$F(\chi_s u)=\sum_{p=0}^{\infty}\frac{(\chi_s^2-\chi^2)^p}{p!}\frac{\partial^p}{\partial(\chi^2)^p}F(\chi u). \quad (21)$$

On inserting (21) into the expression in curly brackets in (13a) the coefficients of $F(\chi u)$ and its first $p-2$ derivatives vanish on account of (20). We can now proceed to the limit of letting every $\chi_s\to\chi$, and obtain

$$G(u)=((-1)^n/4\pi)(\partial/u_r\partial u_r)[1/(n-1)!]\times\{[\partial^{n-1}/\partial(\chi^2)^{n-1}]\}F(\chi u) \quad (22)$$

on account of (20) and the fact that the coefficients of the nth and higher order derivative in (13a) vanish in the limit all $\chi_s\to\chi$. On account of the property $u^{-n}J_n(u)=[-(\partial/u\partial u)]^n J_0(u)$, where $J_n(u)$ is the Bessel function of order n, (22) can also be written

$$G(u)=-\frac{1}{4\pi}\cdot\frac{\partial}{u_r\partial u_r}F_n(\chi u), \quad (23)$$

where

$$F_n(\chi u)=\begin{cases}[1/(n-1)!](u/2\chi)^{n-1}J_{n-1}(\chi u) & \text{for } u^0\geqslant u_r\\ 0 & \text{for } u^0<u_r\end{cases} \quad (24)$$

(22) with $F(\chi u)$ again defined by (13b) or (23) and (24) give the exact elementary solution of Eq. (11). The general solution of (11) is obtained by inserting (23) in (15). Putting $n=1$ we just get the well-known elementary solution corresponding to the retarded potentials of the generalized second-order wave equation.

3. THE TWO-NUCLEON POTENTIAL

To obtain the field of an arbitrarily moving point charge one has simply to put in (15)

$$j(x^k)=\int_{-\infty}^{\infty}j(\tau)\delta(x^0-x'^0)\delta(x^1-x'^1)\times\delta(x^2-x'^2)\delta(x^3-x'^3)d\tau, \quad (25)$$

where τ is the proper time and z^k the coordinates of the arbitrarily moving nucleon. The resulting expression can be calculated without much difficulty, and one obtains a generalization of the well-known expression for the field of a relativistically moving point charge. For the moment we are only interested in the expression when the nucleon is moving with non-relativistic velocities. One then obtains, for the field of a point charge, if the field satisfies Eq. (10), the expression

$$(-1)^{n+1}\left\{\sum_{s=1}^{n}\frac{1}{\prod_{t\neq s}(\chi_s^2-\chi_t^2)}\frac{e^{-\chi_s r}}{r}\right\}. \quad (26)$$

The expression (26) then also gives the simplest type of interaction between two point sources through this field. As a particular case, one gets for $n=2$

$$\frac{1}{(\chi_2^2-\chi_1^2)}(e^{-\chi_1 r}-e^{-\chi_2 r})/r. \quad (27)$$

One could have obtained a potential of the type (27) by taking two separate fields each satisfying the general-

ized second-order wave Eq. (3) and suitably adjusting the interaction constants, as has been done by Møller and Rosenfeld.[5] The main difference in the present case is that when the field satisfies a fourth-order equation of the type (10), the two exponentials appear with predetermined factors such that as $r\to 0$ the field (27) does not tend to infinity as r^{-1}, but tends to a constant value.

One gets something essentially new, however, if the field ψ satisfies the iterated generalized wave Eq. (11) of order $2n$ instead of Eq. (10). The field of a slowly moving point charge is then

$$[(-1)^n/(n-1)!][\partial^{n-2}/\partial(\chi^2)^{n-2}](e^{-\chi r}/2\chi). \quad (28)$$

In particular, for $n=2$ we get the potential

$$(1/2\chi)e^{-\chi r}. \quad (29)$$

(28) and (29) would then be the corresponding potentials between two point sources in the two cases. The corresponding dipole-dipole interaction is obtained by operating on (28) and (29) with the operator (4). One gets in the case (29)

$$\frac{e^{-\chi r}}{2}\left[\frac{(\boldsymbol{\sigma}^{(1)}\cdot\boldsymbol{\sigma}^{(2)})}{r}-\left(\chi+\frac{1}{r}\right)\left(\boldsymbol{\sigma}^{(1)}\cdot\frac{\mathbf{r}}{r}\right)\left(\boldsymbol{\sigma}^{(2)}\cdot\frac{\mathbf{r}}{r}\right)\right]. \quad (30)$$

(30) lacks the singular r^{-3} term which made any sensible calculation on the Yukawa theory impossible. We thus arrive at the central result of this paper, namely:

If the field responsible for nuclear forces satisfies a wave Eq. (5) in which the α-matrices have a minimal equation of type (8) with $n=2$, then the interaction between two nucleons is a sum of (29) and (30) multiplied by numerical factors depending on the magnitude of the interaction constants and the spin of the field, and isotopic spin factors depending on whether the field is neutral or charged or both.

Just as there are several elementary fields with different spins satisfying the second-order generalized wave equation, and the particular mixture of the interactions (1) and (2) depends on whether the pseudoscalar or vector meson theory is taken, or a mixture of both, so here, the relative sign and magnitude of the numerical factors multiplying (29) and (30) depend on the spin properties of the field chosen, that is on the form of the α-matrices in (5). An equation of the type (5) having the required property (8) will be published elsewhere.

It is interesting to note that in the limit $\chi\to 0$ the potentials (28) and (29) become infinite and of infinite extension, as indeed follows generally from (24). Thus, if the field is of zero rest mass, it could have an interaction with point charges only if it satisfied a wave equation of *the second order*, but *not* of higher order. In my opinion, it is a satisfactory feature of this theory that the field responsible for nuclear forces does not differ from the Maxwell field in a rather simple way, but that the differences are much deeper. For one would ultimately expect every particle field in nature to be not just a slight modification of something else, but *sui generis*.

[5] C. Møller and L. Rosenfeld, Nature **143**, 241 (1939).

An Approximate Theory of Order in Alloys*,**

J. M. COWLEY***
Department of Physics, Massachusetts Institute of Technology, Cambridge, Massachusetts
(Received October 26, 1949)

Short-range order parameters α_i are defined to express the interaction of a given atom in an alloy with the atoms of the ith shell of atoms surrounding it. From simple thermodynamic reasoning, involving a certain degree of approximation, equations relating the α_i with energy terms and the temperature are derived. Equations for the long-range order parameter, S, are obtained by considering the limiting case of i very large. The values of the long- and short-range order parameters obtained by solving these equations are in good agreement with experimental values recently found by x-ray diffraction methods. The theory is extended to the calculation of configurational energy and specific heat, and to the determination of order parameters for alloys of arbitrary composition in such binary systems as that of the copper-gold alloys. In these cases qualitative agreement with experimental observations is obtained.

INTRODUCTION

OF the many theoretical approaches to the phenomena of ordering in alloys, those which are mathematically rigorous have been applied only to simple cases, such as the two-dimensional square net,[1] and have not to date given results directly comparable with experiment. Various approximate theories have given predictions of long-range order and nearest-neighbor order for some special cases. Bragg and Williams[2] introduced the long-range order parameter, S, and devised a simple theory giving S as a function of temperature. Bethe[3] considered nearest-neighbor order, measured by the parameter σ, and determined long-range order and nearest-neighbor order for the case of AB alloys. Peierls[4] extended this theory to the case of the face-centered cubic A_3B alloys such as Cu_3Au. Similarly other approximate theories, such as that of Kirkwood[5] have given results for nearest-neighbor order and long-range order for a few special cases.

Recent advances in x-ray diffraction techniques have made possible the quantitative determination of the long-range order parameter, S, and short-range order parameters for several shells of neighbors. Thus, for the alloy Cu_3Au, Wilchinsky[6] measured S and the short-range order parameters for the first three shells, using powder diffraction methods. The present author has measured the short-range order parameters for the first ten shells of neighbors, using single-crystal techniques.[7] The x-ray diffraction methods involved may be applied equally well to a wide range of compositions in a number of alloy systems. For most of the results so obtainable, no theoretical results are available for comparison.

With this situation in mind, it seems worth while to present the following theory which, although admittedly of a very approximate nature, has shown good agreement with the available experimental data, and may be extended to the consideration of a wide range of structures and compositions without undue mathematical difficulty.

DEFINITION OF SHORT-RANGE ORDER PARAMETERS

For an alloy consisting of A and B atoms, present in the proportions m_A and m_B, we define the short-range order parameter for the atomic site with coordinates l, m, n with respect to a given B atom as $\alpha_{lmn}=1-p_{lmn}/m_A$ where p_{lmn} is the probability that the atomic site is occupied by an A atom. Then

$$p_{lmn}=m_A(1-\alpha_{lmn}).$$

If an A atom is taken as origin, $p_{lmn}=m_A+m_B\cdot\alpha_{lmn}$.

Alternatively, if the atom with coordinates l, m, n is considered to belong to the ith shell of neighbors surrounding a B atom, we may write $\alpha_i=1-n_i/m_Ac_i$, where n_i is the number of A atoms among the c_i atoms of the ith shell.

The short-range order parameters were initially defined in this way for convenience in considerations of the x-ray diffraction effects for alloys above the critical temperature of ordering, since the α_{lmn} are the coefficients of the three-dimensional Fourier series expressing the "scattering power" caused by short-range order as a function of the reciprocal-lattice coordinates. However, they were found to be very convenient for thermodynamic considerations also, and have been used in preference to parameters defined in analogy to Bethe's σ. They have the conventional properties of order parameters in that they are zero for the completely random state, and have a maximum (absolute) value for perfect order. The value for perfect order, α_i^0, is unity, however, only for even-numbered shells; for odd-numbered shells it is negative and fractional

* Work supported in part by the U.S. ONR under Contract N5ori-07832.
** Extract from a thesis submitted in partial fulfillment of the requirements for the degree of Doctor of Philosophy in Physics at the Massachusetts Institute of Technology.
*** Now with the Division of Industrial Chemistry, Commonwealth Scientific and Industrial Research Organization, Australia.
[1] G. H. Wannier, Rev. Mod. Phys. **17**, 50 (1945).
[2] Bragg and Williams, Proc. Roy. Soc. **A145**, 699 (1934).
[3] H. A. Bethe, Proc. Roy. Soc. **A150**, 552 (1935).
[4] R. Peierls, Proc. Roy. Soc. **A154**, 207 (1936).
[5] J. G. Kirkwood, J. Chem. Phys. **6**, 70 (1938).
[6] Z. W. Wilchinsky, J. App. Phys. **15**, 806 (1944).
[7] J. M. Cowley, J. App. Phys. (to be published).

except in the case of some AB alloys. Thus, for Cu_3Au, $\alpha_i^0=1$ for i even, and $-1/3$ for i odd. For the case of AB alloys, the α_{lmn} are equivalent to the parameters r_{hkl} defined by Zernike[8] and used by him in theoretical considerations of ordering at this composition. For β-brass, CuZn, at the 50:50 composition, $-\alpha_1=-\alpha_{111}=r_{111}=\sigma(=1$ for perfect order).

Long-range order may be said to exist in an alloy if the value of the parameter α_i does not tend to zero, but approaches a finite limiting value as i becomes very large. The relation between the limiting value of the short-range order parameter and the long-range order parameter depends on the nature of the ordered structure and the composition of the alloy. As an example, the derivation of the relation will be indicated for an alloy of arbitrary composition forming a face-centered cubic lattice such as that of Cu_3Au.

The long-range order parameter S for the face-centered cubic lattice may be defined as the average of the values of S for the four simple-cubic lattices of which the face-centered lattice is composed. If three of the simple-cubic lattices are considered to be α-sites, properly occupied by A atoms, and the other one is considered to consist of β-sites, properly occupied by B atoms,

$$S=\frac{3}{4}\left(\frac{r_\alpha-m_A}{1-m_A}\right)+\frac{1}{4}\left(\frac{r_\beta-m_B}{1-m_B}\right),$$

where r_α and r_β are the fractions of α and β-sites rightly occupied. By summing the total number of A or B atoms, one derives the relation, $r_\beta=3r_\alpha+4m_B-3$, from which it follows that $r_\alpha=(4/3)m_Am_BS+m_A$ and $r_\beta=4m_Am_BS+m_B$.

In order to establish the relationship between the imiting value of the α-coefficients and S, we consider a lattice with long-range order S. If we pick an atom at random as origin, there is a relative probability $r_\beta/4$ that it is a B atom on a β-site, in which case $\alpha_{i\ \text{even}}\rightarrow 4m_BS$. The probability that the origin is a B atom on an α-site is $\frac{3}{4}(1-r_\alpha)$, and for this case $\alpha_{\text{even}}\rightarrow -4m_BS/3$. Similarly, if the origin chosen is an A atom. Taking the weighted average of the limiting values of α_{even} for the various cases, we get, for the whole lattice,*

$$\alpha_{\text{even}}\rightarrow\frac{16}{3}m_Am_BS^2.$$

The limiting value for $\alpha_{i\ \text{odd}}$ is equal to $-\alpha_{\text{even}}/3$.

In the same way it can be shown that, if the numbers of α and β-sites are equal, $\alpha_{\text{even}}\rightarrow 4m_Am_BS^2$.

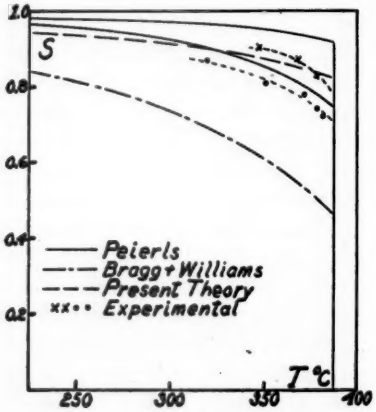

FIG. 1. Variation of long-range order with temperature for Cu_3Au, theoretical and experimental.

THEORY FOR SHORT-RANGE ORDER

In a crystal having zero long-range order, the atomic sites are occupied at random in that each site is occupied by an A atom with probability m_A, and by a B atom with probability m_B. To investigate the influence of one atom on its neighbors, we choose a particular atom as origin—that is, increase the probability of a particular site being occupied by an A, or a B, to unity, and consider the associated change in free-energy. The free-energy change is given by $F-F_0=(U-U_0)-T(S-S_0)$, where U is the configurational energy of the lattice, and S is the entropy of configuration.

The configurational energy is made up of the energies of interaction between pairs of atoms. We denote by $V_{AB,\,lmn,\,l'm'n'}$ the energy of interaction between an A atom with coordinates l, m, n and a B atom with coordinates l', m', n'. For convenience, we substitute the symbol I for the coordinates l, m, n in the subscript, so that the symbol I represents the atom with coordinates l, m, n, which is considered to be a particular atom of the ith shell of atoms about the origin. Similarly we replaced l', m', n' by the symbol J, and the atom with these coordinates is considered to be a particular atom of the jth shell. Similarly we define $V_{AA,IJ}$ and $V_{BB,IJ}$ as the energies of interaction of pairs of A and B atoms at these particular sites. For considerations of ordering, it is necessary to deal with only the linear combination,

$$V_{IJ}=\tfrac{1}{2}(V_{AA,IJ}+V_{BB,IJ})-V_{AB,IJ},$$

which represents the average change of energy when a pair of like atoms is replaced by two unlike atoms at the same positions.

* B atom on a β-site, relative probability $r_\beta/4$.

With respect to this position shells with i=even represent β-sites.

$$\alpha_{i\ \text{even}}\rightarrow 1-\frac{P_{lmn}}{m_A}=1-\frac{(1-r_\beta)}{m_A}=4m_BS.$$

B atom on an α-site, relative probability $3/4(1-r_\alpha)$.

With respect to this position shells with i=even represent α sites.

$$\alpha_{i\ \text{even}}\rightarrow 1-\frac{P_{lmn}}{m_A}=1-\frac{r_\alpha}{m_A}=-\frac{4m_BS}{3}.$$

Weighted average of $\alpha_{i\ \text{even}}$ for all B atoms as origin

$$\alpha_{i\ \text{even}}\frac{(r_\beta/4)4m_BS-\frac{3}{4}(1-r_\alpha)(4m_BS/3)}{r_\beta/4+\frac{3}{4}(1-r_\alpha)}=\frac{16}{3}m_Am_BS^2.$$

[8] F. Zernike, Physica 7, 565 (1940).

If the atom in the position denoted by J is in the kth shell of atoms with respect to the atom I, we write $V_{IJ}=V_k$.

The change in configurational energy involved in the fixing of an A or B atom as origin may be found by summing the average values of the energy changes for all possible pairs of atoms. With respect to the origin, the probabilities of the atoms I and J being A or B atoms are given in terms of α_I and α_J, and the average change in the energy of interaction between these atoms may be found in terms of α_I, α_J, and V_{IJ}. The total configurational energy change for the whole lattice when one atom is fixed as origin is then found to be, on the average,

$$U-U_0=m_Am_B\sum_I\sum_J\alpha_I\cdot\alpha_J\cdot V_{IJ},$$

where a summation with respect to I or J is a summation over every atom in the lattice, that is, over all possible values of the coordinates l, m, n or l', m', n'.

The change of entropy involved in fixing an A or B atom as origin may be expressed as $S-S_0=k\ln W-k\ln W_0$, where k is Boltzman's constant, W is the number of ways of arranging the atoms so that the short-range order parameters will have the values α_i, and W_0 is a constant. In the ith shell about a B atom at the origin, on the average $c_im_A(1-\alpha_i)$ of the c_i atoms will be A atoms.

This arrangement may be obtained in

$$W_{B,i}=\frac{c_i!}{[c_im_A(1-\alpha_i)]![c_i(m_B+m_A\alpha_i)]!}\text{ ways.}$$

This term is multiplied by similar terms for all values of i to give W_B, the total number of arrangements when the origin is a B. Analagous expressions are obtained considering an A at the origin. The entropy-change may thus be found. The simple method of its calculation involves the approximation that only the average distributions have been considered, and fluctuations in the distribution of atoms have been ignored.

For equilibrium, the values of the variables α_I will be such as to make the free-energy a minimum, so that $\delta F=\delta U-T\delta S=0$.

Substituting the expressions obtained for the energy and entropy in this equation gives

$$m_Am_B\sum_I\delta\alpha_I\left[2\sum_J V_{IJ}\alpha_J+kT\ln\left\{\frac{(m_A+m_B\alpha_i)(m_B+m_A\alpha_i)}{m_Am_B(1-\alpha_i)^2}\right\}\right]=0,$$

where the atom I is taken as a particular atom of the ith shell, so that $\alpha_I=\alpha_i$, and Stirling's approximation has been used to simplify the entropy terms.

If it is assumed that all the α_I are independent variables, it follows that all the terms in the square brackets must be zero, so that

$$2\sum_J V_{IJ}\alpha_J+kT\ln\left\{\frac{[m_A/m_B)+\alpha_i][(m_B/m_A)+\alpha_i]}{(1-\alpha_i)^2}\right\}=0. \quad (1)$$

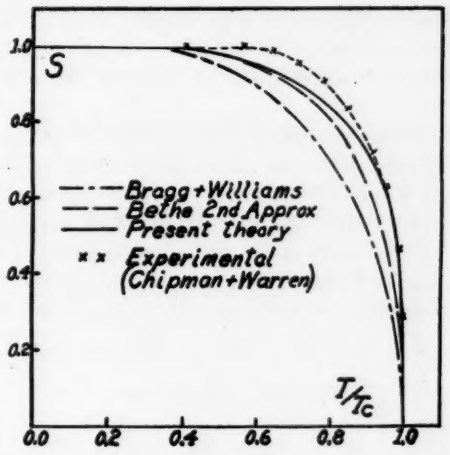

FIG. 2. Variation of long-range order with temperature for CuZn, theoretical and experimental.

The assumption that the α_I are independent is not strictly valid, and must be regarded as a rough approximation only. It is justified in the present case only in that it leads directly to the Eqs. (1) which appear to represent the relations between the order coefficients and energy terms with fair accuracy.

There is an equation of the type (1) for every value of i, and the summation over J is the summation over all atoms of the lattice of the product of the α-coefficient of each atom and its interaction energy with a particular atom of the ith shell.

For Cu_3Au the equations are:

$$-kT\ln\left\{\frac{(\tfrac{1}{3}+\alpha_1)(3+\alpha_1)}{(1-\alpha_1)^2}\right\}=2V_1(1+4\alpha_1+2\alpha_2+4\alpha_3+\alpha_4)+2V_2(2\alpha_1+2\alpha_3+2\alpha_5)+\cdots,$$

$$-kT\ln\left\{\frac{(\tfrac{1}{3}+\alpha_2)(3+\alpha_2)}{(1-\alpha_2)^2}\right\}=2V_1(4\alpha_1+4\alpha_3+4\alpha_5)+2V_2(1+4\alpha_4+\alpha_8)+\cdots,$$

$$-kT\ln\left\{\frac{(\tfrac{1}{3}+\alpha_3)(3+\alpha_3)}{(1-\alpha_3)^2}\right\}=2V_1(2\alpha_1+\alpha_2+2\alpha_3+2\alpha_4+2\alpha_5+\alpha_6+2\alpha_7)+2V_2(\alpha_1+2\alpha_3+2\alpha_7+\alpha_9)+\cdots.$$

On the right-hand side of the first equation, V_1 is multiplied by the α-coefficients of all the atoms which

are nearest neighbors of a particular atom of the first shell, V_2 is multiplied by the α's of all atoms which are second-nearest neighbors of an atom in the first shell, and so on.

For any temperature T, this infinite set of equations could be solved to give short-range order parameters for given values of the energy terms. Conversely, the energy terms may be calculated from experimental values of the short-range order coefficients. This has been done for Cu_3Au using the values for the first ten order coefficients found from x-ray diffraction measure-

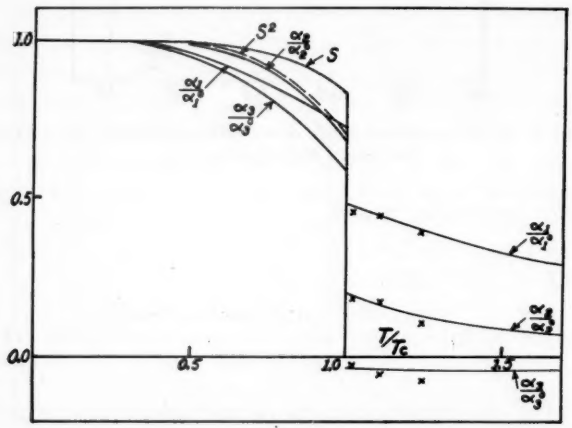

FIG. 3. Short-range order parameters for the first three shells of neighbors, for Cu_3Au, as functions of temperature.

ments,[7] assuming that only V_1, V_2, and V_3 were appreciable. The values obtained, $V_1=358k$, $V_2=-34k$, $V_3=-19k$, are of the right order of magnitude.

LONG-RANGE ORDER FOR PARTICULAR COMPOSITIONS

If, in the lattice of a binary alloy, two kinds of sites are available in exactly the same ratio as the two kinds of atoms, an equation for the long-range order parameter, S, is obtained by considering the limiting case of Eq. (1) for i very large. For example, for Cu_3Au the limiting values of α_i for i large are S^2 if i is even and $-S^2/3$ for i odd. The long-range order parameter is defined by considering the correlation of atoms in a given simple-cubic sub-lattice and the atoms on the same simple-cubic sub-lattice as the origin are those contained in shells with i even. Hence S is given by the limiting form of the equations for α_i with i even. This limiting form is

$$\ln\left\{\frac{(\frac{1}{3}+S^2)(3+S^2)}{(1-S^2)^2}\right\}=+\frac{8S^2}{kT}(V_1-3/2V_2+\cdots).$$

This equation predicts a "critical temperature," T_c at which the long-range order drops to zero. By considering $S\to 0$ one finds

$$T_c=\frac{3}{2k}(V_1-3/2V_2+\cdots).$$

Substituting for the energy terms in the first equation, we have an equation giving S in terms of the ratio T/T_c only, thus,

$$\ln\left\{\frac{(\frac{1}{3}+S^2)(3+S^2)}{(1-S^2)^2}\right\}=\frac{16}{3}\cdot\frac{T_c}{T}\cdot S^2.$$

In Fig. 1 the values of S from this equation are plotted against temperature, assuming $T_c=390°C$, and compared with the values predicted by the theories of Bragg and Williams[2] and Peierls,[4] and experimental values obtained by the present author.[7] The present theory appears to agree with experiment within the limits of experimental error.

For a body-centered cubic structure such as that of β-brass, the analogous equation is

$$\ln\left\{\frac{1+S^2}{1-S^2}\right\}=2\cdot\frac{T_c}{T}\cdot S^2.$$

The values of S found from this equation are plotted against the ratio T/T_c in Fig. 2. It is seen that the present theory is in better agreement with the experimental values of Warren and Chipman[9] than the Bragg and Williams theory or Bethe's second approximation for this case.

CALCULATION OF SHORT-RANGE ORDER COEFFICIENTS

The short-range order parameters α_i may be found for any temperature by solving the Eqs. (1), if the energy terms are known. The values of the first three order parameters for Cu_3Au have been calculated for a number of temperatures with the use of certain simplifying assumptions. It was assumed that for temperatures greater than the critical temperature all $\alpha_i=0$ for i greater than 5, and for temperatures less than the critical temperature all α_i had the limiting value of S^2 or $-S^2$ for i greater than 3. All V_i were assumed zero for i greater than 2, and V_2 was taken as $-V_1/10$, as found by calculation from experimental order coefficients. Both V_1 and V_2 could then be expressed in terms of the critical temperature by use of the relation given in the previous section. For T greater than T_c, the equations to be solved were then

$$\begin{aligned}
-f(\alpha_1)&=1.160T_c/T\cdot(1+3.8\alpha_1+2\alpha_2\\
&\qquad+3.8\alpha_3+\alpha_4-0.2\alpha_5),\\
-f(\alpha_2)&=1.160T_c/T\cdot(-0.1+4\alpha_1+4\alpha_3-0.4\alpha_4+4\alpha_5),\\
-f(\alpha_3)&=1.160T_c/T\cdot(1.9\alpha_1+\alpha_2+1.8\alpha_3+2\alpha_4+2\alpha_5),\\
-f(\alpha_4)&=1.160T_c/T\cdot(\alpha_1-0.2\alpha_2+4\alpha_3+2\alpha_5),\\
-f(\alpha_5)&=1.160T_c/T\cdot(0.1\alpha_1+\alpha_2+2\alpha_3+\alpha_4+1.9\alpha_5),
\end{aligned}$$

where

$$f(\alpha_i)=\ln\left\{\frac{(\frac{1}{3}+\alpha_i)(3+\alpha_i)}{(1-\alpha_i)^2}\right\}.$$

This set of equations was solved by trial-and-error methods through a series of successive approximations

[9] Warren and Chipman, Phys. Rev. 75, 1629 (1949).

leading to a consistent set of parameters. Three equations of the same sort, but involving the values of S^2, were solved for T less than T_c.

The curves so obtained, giving the order parameters as functions of temperature, are shown in Fig. 3. For convenience the values of α_i/α_i^0 rather than α_i have been plotted, α_i^0 being the value of α_i for the case of perfect order. Thus all variables plotted vary from zero for zero order to unity for perfect order. The experimental values obtained by x-ray diffraction methods for temperatures of 405, 460, and 550°C,[7] are added for comparison. The agreement is within the limits of experimental error. In particular, the theory agrees with experiment in giving a negative value for α_3/α_3^0, that is, a positive value for α_3, for T greater than T_c. From the experimental observations of this, and other, reversals of sign it was deduced[7] that there was a "liquid-like" distribution of atoms about a given atom, with the tendency for defect or excess of one kind of atom being more dependent on the radial distance from the origin than on the lattice coordinates. It appears that such a distribution is predicted directly by the theory, and may be regarded as a natural consequence of the structure and energy relations within the crystal lattice. This prediction, and the general magnitudes found for the order parameters are not affected by any reasonable change in the value assumed for the ratio of V_2 to V_1.

In the same way, values of the order parameters have been calculated for AB alloys with structures that are simple-cubic, body-centered cubic, and face-centered cubic. No experimental results are available for comparison. For the hypothetical case of an AB alloy with simple-cubic structure, values of α_i were calculated on the assumption that all α_i with i greater than 3 had the limiting values of zero for T greater than T_c, or $\pm S^2$ for T less than T_c, and $V_i=0$ for i greater than 1. The values found for $-\alpha_1$ are compared with the values of $\sigma(=-\alpha_1)$ given by Bethe's second approximation for this structure, in Fig. 4. The present theory gives a much sharper drop in the value of $-\alpha_1$ for temperatures just below the critical temperature.

CONFIGURATIONAL ENERGY AND SPECIFIC HEAT

The average energy of ordering associated with a particular pair of atoms, one of which is one of the ith—nearest neighbors of the other, is given by $2m_Am_BV_i\alpha_i$. There are $Nc_i/2$ such pairs of atoms in the system. Hence the total configurational energy for the whole system, referred to the state zero order, is given by

$$E'=Nm_Am_B\sum_i c_i\alpha_iV_i.$$

If, as is usual, the energy is referred to the perfectly ordered state, we may write

$$E=E'+E_0=Nm_Am_B\sum_i c_iV_i(\alpha_i-\alpha_i^0).$$

Since the energy terms V_i decrease rapidly with i, the summation contains very few terms of appreciable magnitude, and both the configurational energy and the configurational specific heat, given by dE/dT, may be calculated readily from the values found for the order parameters.

In Table I the values, obtained from such calculations, for various energies and relevant ratios are compared with the values obtained from other theories and experimentally, as reported by Nix and Shockley.[10]

A failing common to most theories of order is that the value of the specific heat predicted by them for alloys such as CuZn is much too low for temperatures just below the critical temperature. Thus the table shows that the values given by Bethe and Kirkwood are less than half the experimental value for CuZn. The present theory gives a much sharper decrease in the order coefficients in this temperature range, and so gives a higher value for the specific heat. It can be shown, in fact, that the order coefficients given by the Eqs. (1) decrease infinitely fast just at T_c, so that the specific heat increases without limit, although there is no discontinuity in energy, and so no latent heat. Such an infinity in the specific heat could not be observed in practice. In any measurement the value of the specific heat obtained is an average taken over the range of fluctuation in temperature and composition in the specimen. Hence the maximum observable specific heat will be finite. For example, for an effective temperature fluctuation of $0.01T_c$, the maximum specific heat observable for CuZn would be $7R$.

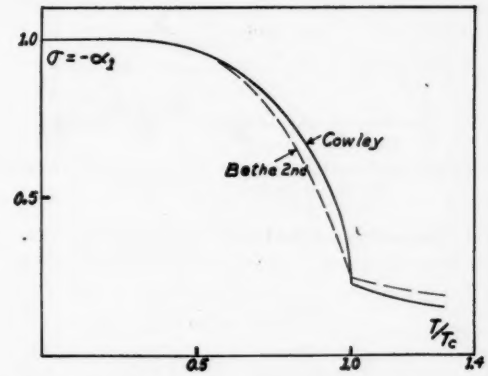

FIG. 4. Nearest neighbor order parameter for simple-cubic lattice.

VARIATION OF ORDER WITH COMPOSITION

For temperatures above the critical temperature, the general Eqs. (1) are valid for all compositions, and may be solved for various values of the ratio m_A/m_B to give the order parameters as functions of composition for given values of the energy terms and temperature. This has been done for the Cu—Au system assuming the value of V_1 found for Cu_3Au, and disregarding other energy terms.

If the same value of V_1 is assumed for all compositions, the values of α_i are symmatrical about the 50:50

[10] Nix and Shockley, Rev. Mod. Phys. **10**, 1 (1938).

composition. However, it seems probable that V_1 varies rapidly with the average distance between neighboring atoms, and in the Cu−Au system the unit-cell dimension varies approximately linearly from 3.61kX for pure copper to 4.07 kX for pure gold. For the calculation of order parameters it was assumed that V_1 was proportional to the inverse sixth power of the unit cell dimension, and so of the average distance between atoms. The results for α_1 and α_2 for $T=770$°C are shown in Fig. 5. The maximum values occur at about 45 percent gold. The experimental values plotted are values of α_1 calculated by Professor B. Averbach from the emf data given by Weibke and Quadt[11] for the same temperature.

The case of long-range order in an alloy of arbitrary composition has been treated by Easthope[12] and by Shockley.[13] Both treatments lead to the prediction of only one maximum in the value of the critical temperature for Cu−Au alloys; that at the 50:50 composition. No indication of the experimentally observed maximum at the 3:1 composition was obtained.

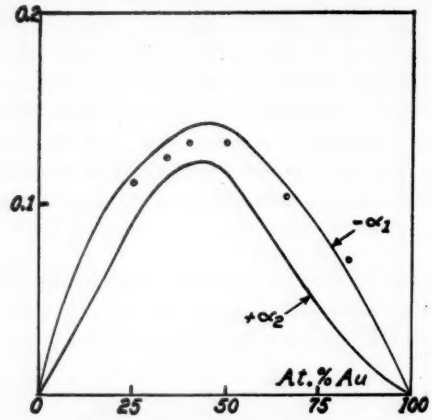

FIG. 5. Variation of short-range order parameters with composition in Cu-Au system for $T=770$°C.

If a direct substitution of the limiting values of α_i, as worked out above, is made in the general Eq. (1), the resulting equations for S give a critical temperature varying parabolically with m_A or m_B, with a maximum at the CuAu composition, as found by Shockley. However, this direct substitution involves the assumption that for any composition a super-lattice exists for which two kinds of atomic sites are present in exactly the same ratio as the two kinds of atoms. For the face-centered cubic structure of the Cu−Au alloys, the available sites can be divided only in the ratios 1:1 or 3:1 unless a super-structure "unit-cell" consisting of two or more face-centered cubic cell is considered. The formation of such a multiple "unit-cell," however, would involve, in effect, an ordering of atoms separated by distances greater than the nearest-neighbor distance in the lattice. Hence the ordering energies involved would be small, and the formation of a multiple unit-cell super-lattice would not take place except at temperatures too low for the rate of formation to be observable. Hence it may be assumed that the available atomic sites may be divided only in the ratios 1:1 or 3:1. For an arbitrary composition, then, limitations are imposed on the values of the order parameters by the conditions that r_α and r_β, the fractions of α- and β-sites rightly occupied, cannot exceed unity. The relation between the limiting value of α_i and S then varies with the amount of long-range order present.

For example, for an alloy near the 3:1 composition, but with an excess of A atoms, the restriction that r_α is less than unity leads to the conditions, $S<3/4m_A$, and the limiting value of α_i for i even, $\alpha_{\text{even}}<3m_B/m_A$. When the amount of long-range order present is very small the restriction is ineffective, and we may write as before, $\alpha_{\text{even}}=(16/3)m_Am_BS^2$. For the maximum value of long-range order, $S=3/4m_A$, the second term of Eq. (1)

TABLE I. Comparison of the values for various energies and relevant ratios as obtained from various theories and by experiment.*

Structure	Source	E_0	$\frac{RT_c}{E_0}$	$\frac{E(T_c-)}{E_0}$	Q/R	$\frac{E(T_c+)}{E_c}$	$E_c(\sigma)$	$\frac{RT_c}{E(T_c+)}$	$\frac{C(T_c-)}{R}$	$\frac{C(T_c+)}{R}$
	$B+W$	$NV_0/8$	2.0	1.0	0	1.0	0	2.0	1.50	0
AB alloy	Bethe no. 1	$3NV/2$	1.65	0.80	0	0.800	0.200	2.06	1.90	0.119
Simple cubic	Bethe no. 2	$3NV/2$	1.581	0.754	0	0.754	0.246	2.10	2.14	0.203
	Kirkwood	$3NV/2$	1.577	0.789	0	0.789	0.211	2.00	4.23	0.134
	Present	$3NV/2$	2.0	0.780	0	0.780	0.220	2.56	∞	0.17
	Bethe no. 1	$2NV$	1.738	0.857	0	0.857	0.143	2.03	1.78	0.081
AB alloy	Kirkwood	$2NV$	1.707	0.854	0	0.854	0.146	2.00	2.21	0.086
Body-centered cubic	Present	$2NV$	2.00	0.823	0	0.823	0.172	2.42	∞	0.12
	Experiment								5.1	
	$B+W$	$3NV_0/32$	2.19	0.792	66	1.00	0	2.19	2.36	0
A_3B alloy	Peierls	$3NV/4$	1.33	0.18	78	0.54	0.46	2.38	—	0.16
Face-centered cubic	Present	$3NV/4$	2.00	0.308	84	0.748	0.44	2.68	0.43	0.17
	Experiment				63			2.60		

* $E(T_c-)$ = configurational energy just below T_c. $E(T_c+)$ = configurational energy just above T_c. Q = latent heat of ordering at the critical temperature. $E_c(\sigma)$ = energy retained by short-range order just above T_c. $C(T_c-)$ = configurational specific heat just below T_c. $C(T_c+)$ = configurational specific heat just above T_c. E_0 = energy difference between perfect order and complete randomness for N atoms.

[11] Weibke and Quadt, Zeits. f. Elektrochemie **45**, 715 (1935).
[12] C. E. Easthope, Proc. Camb. Phil. Soc. **33**, 502 (1937).
[13] W. Shockley, J. Chem. Phys. **6**, 130 (1938).

must be written

$$kT \ln\left\{\frac{(3+\alpha_i)[(3m_B^2/m_A^2)+\alpha_i]}{(3m_B/m_A-\alpha_i)^2}\right\}$$

in order to give the correct values of α_i for $T\to 0$. The change is equivalent to the substitution in this term of $(m_A/3m_B)\alpha_i$ for α_i, so that we put

$$\alpha_{\text{even}}=\frac{16}{3}m_Am_BS^2\cdot\frac{m_A}{3m_B}.$$

For intermediate states of long-range order, it is reasonable to assume that the restriction on r_α introduces a correction to the value of α_{even} which varies with S, or, more probably, S^2. Hence we substitute in the second term of Eq. (1), the relation

$$\alpha_{\text{even}}=\frac{16}{3}m_Am_BS^2\cdot\left\{1-\left(\frac{4m_A}{3}\right)^2\left(1-\frac{m_A}{3m_B}\right)S^2\right\}.$$

For considerations of the critical temperature, the correction to be applied will involve S_c, the value of the long-range order immediately below the critical temperature. This will be zero for the 1:1 composition, but finite for all other compositions. For the case under consideration, we find

$$T_c=\frac{8}{k}\cdot m_Am_B\left(V_1-\frac{3}{2}V_2+\cdots\right)\cdot\left[1-\left(\frac{4m_A}{3}\right)^2\left(1-\frac{m_A}{3m_B}\right)S_c^2\right]^{-1}.$$

Similar expressions may be obtained for other composition ranges.

From such expressions the values of T_c were obtained by a series of approximations. The values of S_c first used were those calculated from the simple theory giving a parabolic variation of T_c. The values of T_c so obtained were then used to recalculate S_c, and second approximations for T_c were found. These second approximations were used to give the plot of T_c against composition shown in Fig. 6. For comparison, the experimental phase-diagram determined by Haughton and Payne[14] from electrical resistance measurements is added.

It is seen that the main features of the phase-diagram have been correctly predicted. The theory gives a broad maximum at the 1:1 composition, and a sharper maximum at the 3:1 composition. In the theoretical calculation, the value of T_c for Cu_3Au was assumed, and the assumption that V_1 varies with the inverse sixth power of the average distance between atoms was again employed. This latter assumption rendered the curve

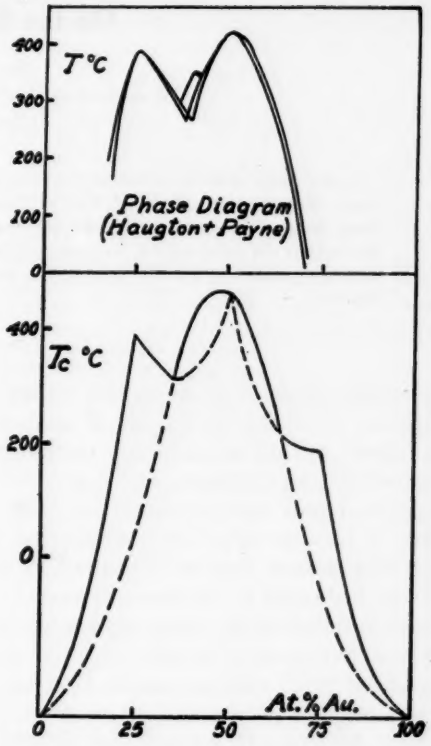

FIG. 6. Theoretical variation of T_c with composition in Cu-Au system, compared with experimental phase-diagram.

unsymmetrical, and depressed the maximum at the 1:3 composition to about 190°C. At temperatures as low as this, the rate of ordering is very low, so that the failure of experimental measurements to reveal a maximum in T_c at the $CuAu_3$ composition is accounted for. The assumption of a more rapid variation of V_1 with interatomic distance would depress this maximum still further.

No account has been taken of the change in structure from face-centered cubic to tetragonal near the CuAu composition. However, the critical temperature predicted for CuAu is 460°C, in reasonable agreement with the experimental value of 425°C.

It thus appears that the present theory is capable of predicting short-range order parameters with fair accuracy, and long-range order and critical temperature rather more approximately for alloys of arbitrary composition in such a system that of Cu—Au. Similarly it could be applied to a wide range of other alloy systems, showing ordering, and could be extended to the consideration of various related problems without undue difficulty. Where experimental data have been available for comparison, the agreement has in most cases been within the limits of experimental error.

In conclusion I wish to thank Professor B. E. Warren for the interest he has shown in this work, and the Commonwealth Scientific and Industrial Research Organization for a research studentship.

[14] Haughton and Payne, J. Inst. Metals 46, 457 (1931).

On the Emission Bands of CF_2

PUTCHA VENKATESWARLU*
Department of Physics, University of Chicago, Chicago, Illinois
(Received November 7, 1949)

A new band system attributed to a non-linear CF_2 molecule has been obtained by exciting the flowing vapor of carbon tetrafluoride. The symmetric stretching frequencies and the bending frequencies in the lower and upper states have been determined. From a study of the sub-band heads (K-structure), it is shown that the band system is of the parallel type, that is, the electric moment associated with the transition vibrates parallel to the line joining the fluorine atoms. The band system is identified with the transition $^1B_2 \rightarrow {}^1A_1$.

IN an earlier communication by the writer,[1] it was mentioned that the excitation of carbon tetrachloride vapor by an uncondensed transformer discharge gave CCl and Cl_2 bands, and that in the case of CBr_4 only Br_2 bands were obtained. The same kind of excitation, in the case of carbon tetrafluoride, gave an extensive band system attributed to the CF_2 molecule. This will be dealt with in the present paper.

The carbon tetrafluoride vapor was kept flowing at a low pressure, estimated to be about 0.1 mm, through a discharge tube fitted with aluminum electrodes and a quartz window. The gas was excited by an uncondensed transformer discharge ($\frac{1}{2}$ kw and 5000–10,000 volts). The color of the discharge was yellowish white. The spectrum obtained was photographed on Hilger medium quartz and E_1-quartz spectrographs. The dispersion of the E_1-quartz spectrograph is about 2.6A/mm at 2500A.

Part of the spectrum obtained is shown in Fig. 1. An extensive band system from 3250–2400A was obtained. The bands are degraded to longer wave-lengths. The wave-lengths and wave numbers along with the visually estimated relative intensities are given in Table I. The structure of the bands, each of which is made up of a series of sub-bands attributable to rotational structure, is similar to that of the NO_2 absorption bands† near 2500A. The presence of the sub-band heads rules out the diatomic molecule CF as the emitter of the band system. The similarity of this band system to the λ2500 system of NO_2 strongly suggests that the emitter is an obtuse-angled non-linear triatomic molecule CF_2. This idea is supported by the vibrational analysis discussed.

All the bands given in Table I can be fairly well represented by the formula

$$\nu = 39195 + 750v_1' ‡ + (495.5v_2' - 0.5v_2'^2) - (1162v_1'' - 0.2v_1''^2 - 0.08v_1''^3) - (666.5v_2'' - 1.0v_2''^2 - 0.5v_2''v_1''), \quad (1)$$

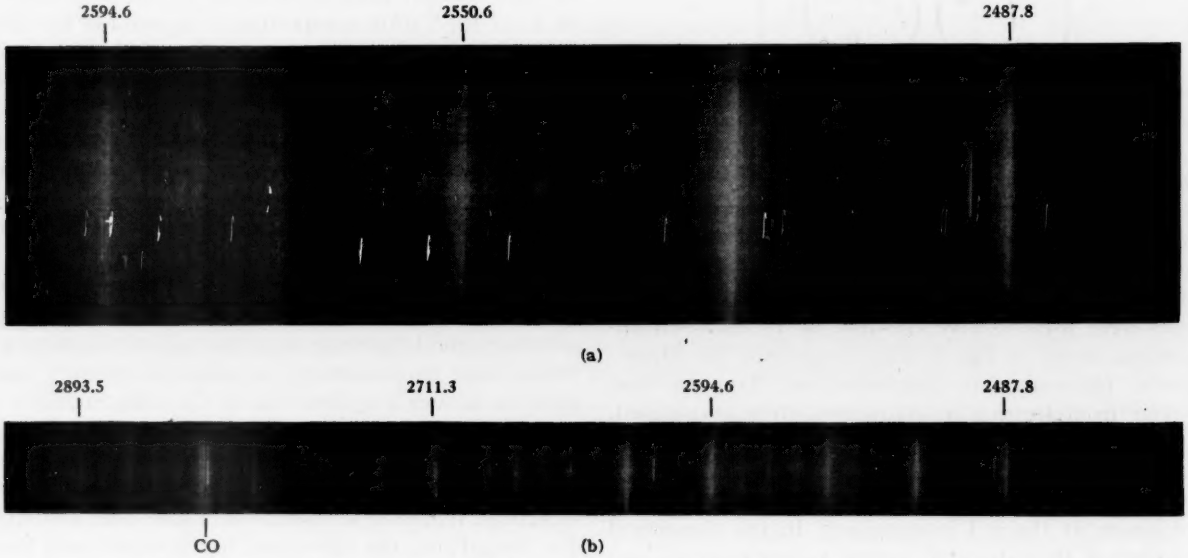

FIG. 1. The spectra of CF_2 taken on the E_1 quartz spectrograph. (b) is from the original and (a) is three times enlarged. Wave-lengths of some of the bands are marked.

* Post-Doctoral Research Fellow, Molecular Spectra Research Project. Now with the Division of Physics, National Research Council, Ottawa, Canada.

[1] P. Venkateswarlu, Phys. Rev. 77, 79 (1950).

† A good photograph of these bands is given in Mulliken's paper (see reference 4) referred to later.

‡ This frequency 750 cm^{-1} for v_1' is doubtful, as there are only two weak bands which are represented by this.

where v_1'' and v_2'' are vibrational quantum numbers here interpreted as those of the symmetric stretching and deformation frequencies in the lower state, while v_1' and v_2' are corresponding quantum numbers for the upper state.

The (v_1'', v_2'', v_1', v_2') values and the corresponding wave numbers for the band heads are also given in Table I. To some of the observed bands alternative assignments of (v_1'', v_2'', v_1', v_2') could be given with the same frequencies; probably experiments with higher resolution might show two bands instead of one in some of these cases. As all the bands can be well explained by formula (1), the analysis indicates that the emitter is a CF_2 molecule with a stretching frequency of 1162 cm^{-1} and a deformation frequency of 666.5 cm^{-1} in the lower state, and a deformation frequency of 495.5 cm^{-1} (and also a probable stretching frequency of 750 cm^{-1}) in the upper state.¶

The idea that the CF_2 molecule is non-linear like NO_2 is supported by the following considerations. The allowed changes in the vibrational quantum numbers according to the selection rules and the most probable changes according to the Franck-Condon principle assuming moderate changes in the nuclear configurations are summarized in Table II.

From the analysis (Table I) it is evident that bands with Δv_2 values from zero to five as well as those with Δv_1 values from zero to seven are all present. Hence, from Table II it follows that the molecule is non-linear. Further, as discussed below, the rotational structure shows the existence of two rotational quantum numbers K and J, which is possible only for a non-linear molecule.

For comparison the vibrational frequencies of some triatomic molecules[2] are given in Table III, and the frequencies obtained for the lower electronic state in the present band system of CF_2 are seen to be of about the right magnitudes for that molecule.

Mulliken[3] has discussed quite extensively the spectra of triatomic molecules. Non-linear triatomic molecules of the type AB_2 fall into the asymmetric top class; that is, they have three unequal moments of inertia. However, the analysis of the band structure of such molecules can be carried out, to a considerable extent, as if they were the bands of symmetrical top molecules. The electronic as well as vibration-rotation bands of symmetric top molecules fall into parallel and perpendicular types. We call the bands parallel or perpendicular according as the electric moment associated with the transition in question vibrates parallel or perpendicular to the symmetry or quasi-symmetry axis.** The selection rule for parallel bands is $\Delta K=0$ and for perpendicular bands $\Delta K=\pm 1$, where K is the quantum number of rotation around the symmetry or quasi-symmetry axis. The structure for parallel-type bands

TABLE I. Experimental data and the vibrational analysis.

Intensity	λ_{air}	ν_{vac}	v_1'', v_2'', v_1', v_2'	ν_{calc}
0	2399.24	41667	0,0,0,5	41660
0	2409.44	41491	0,1,0,6	41485
3	2428.32	41168	0,0,0,4	41169
2	2438.51	40996	0,1,0,5	40995
7	2457.64	40677	0,0,0,3	40677
2	2467.82	40509	0,1,0,4	40504
2	2472.31	40436	0,0,1,1	40440
9	2487.80	40184	0,0,0,2	40184
2	2502.60	39946	0,0,1,0	39945
9	2518.65	39692	0,0,0,1	39690
2	2530.0	39514	1,0,0,3; 0,1,0,2	39515; 39519
3	2541.34	39339	1,1,0,4	39342
8	2550.56	39195	0,0,0,0	39195
4	2561.81	39023	1,0,0,2; 0,1,0,1	39022; 39025
4	2573.17	38851	1,1,0,3; 0,2,0,2	38850; 38855
3	2583.56	38695	0,3,0,3	38687
9	2594.60	38530	0,1,0,0	38530
?·	2594.96	38525	1,0,0,1	38528
2	2606.68	38352	2,0,0,3; 1,1,0,2	38354; 38357
3	2617.90	38187	1,2,0,3	38187
9	2628.51	38033	1,0,0,0	38033
6	2652.38	37691	1,2,0,2; 2,1,0,3	37694; 37690
4	2663.39	37535	1,3,0,3	37526
6	2675.47	36366	1,1,0,0; 2,0,0,1	37368; 37367
5	2688.14	37189	1,2,0,1; 2,1,0,2	37200; 37197
3	2699.06	37039	1,3,0,2	37033
9	2711.30	36872	2,0,0,0	36872
8	2736.40	36534	2,2,0,2	36534
4	2749.09	36365	2,3,0,3	36367
5	2761.24	36205	2,1,0,0; 3,0,0,1	36208; 36208
5	2774.16	36036	2,2,0,1; 3,1,0,2	36040; 36038
3	2787.07	35869	2,3,0,2; 3,2,0,3	35874; 35869
8	2799.81	35706	3,0,0,0	35713
2	2812.92	35540	3,1,0,1; 4,0,0,2	35544; 35544
2	2839.41	35208	3,3,0,3	35209
6	2852.47	35047	3,1,0,0; 4,0,0,1	35049; 35050
6	2866.14	34880	3,2,0,1; 4,1,0,2	34882; 34881
4	2879.73	34715	3,3,0,2	34716
7	2893.54	34550	4,0,0,0	34555
3	2907.51	34384	4,1,0,1	34387
6	2921.28	34222	4,2,0,2	34219
3	2935.17	34060	4,3,0,3	34053
2	2949.82	33891	4,1,0,0	33892
2	2978.92	33559	4,3,0,2	33560
2	2993.69	33394	5,0,0,0	33400
3	3007.53	33240	5,1,0,1	33232
5	3022.76	33073	5,2,0,2	33065
5	3038.09	32906	5,3,0,3	32899
5	3053.66	32738	5,1,0,0	32737
3	3069.61	32568	5,2,0,1	32571
2	3084.57	32410	5,3,0,2	32406
1	3164.6	31590	6,1,0,0	31585
2	3181.0	31428	6,2,0,1	31420
4	3197.5	31265	6,3,0,2	31265
6	3214.1	31104	7,0,0,0	31098
2	3231.1	30940	7,1,0,1	30931
1	3249.5	30765	7,2,0,2	30765

¶ It may be mentioned that the bands can also be explained with a deformation frequency in the lower state of 340 cm^{-1} instead of 667 cm^{-1}. But the calculated values for the band heads in general agree better with the observed values if we use 667 cm^{-1}. Further, a comparison with the frequencies of the triatomic molecules NO_2 and O_3 (Table III) suggests that 667 cm^{-1} is of about the right magnitude.

[2] G. Herzberg, *Infrared and Raman Spectra of Polyatomic Molecules* (D. Van Nostrand Company, Inc., New York, 1945).

[3] R. S. Mulliken, Rev. Mod. Phys. 14, 204 (1942); see also reference 7.

** In asymmetric top molecules like AB_2 the quasi-symmetry axis is the axis of smallest moment of inertia. The other two moments of inertia, which are roughly equal, are much larger in the case that the asymmetric simulates a symmetric top molecule. The quasi-symmetry axis in CF_2 is the line joining the two fluorine atoms.

TABLE II.[a] The allowed changes in the vibrational quantum numbers according to the selection rules, and the most probable changes according to the Franck-Condon principle.

Selection rules		Franck-Condon principle	
Linear molecule	Non-linear molecule	Linear molecule	Non-linear molecule
Δv_{ss}=any	Δv_{ss}=any	Δv_{ss}=any	Δv_{ss}=any
$\Delta v_{\pi d}$=even	Δv_{sd}=any	Δv_{d}=0	Δv_{sd}=any
Δv_{as}=even	Δv_{as}=even	Δv_{as}=0	Δv_{as}=0

[a] In this table, Δv_{ss} and Δv_{as} are the changes in the quantum numbers of the symmetric and antisymmetric stretching frequencies. $\Delta v_{\pi d}$ and Δv_{sd} are the changes in the deformation frequency quantum numbers for linear and non-linear molecules, respectively.

TABLE III. Comparison of the vibrational frequencies.

	ν_1	ν_2	ν_3
CF_2 (bent)	1162	667	—
NO_2 (bent)[4]	1306	755	1621
O_3 (bent)[4]	1110	705	1043
SO_2 (bent)	1151	524	1361
CO_2 (linear)	1337	667	2349

consists of a series of sub-bands (K-structure) each characterized by a definite value of K. These follow the parabolic formula

$$\nu=\nu_0+(C'-C'')K^2, \tag{2}$$

where C' and C'' are related†† to the moments of inertia in the upper and lower states, respectively. Further, each sub-band has fine structure, called J-structure, consisting of Q, R, and P branches corresponding to changes $\Delta J=0, \pm1$ in the over-all rotational quantum number J.

A complete study of the rotational structure of CF_2 could be made only by using high dispersion. But the dispersion of the instrument used at present is enough to analyze the K-structure for some of the higher frequency bands and this, as we shall see, gives the proof that the present band system of CF_2 corresponds to a parallel-type transition. Each band, as stated, consists of a series of sub-bands each of which has a definite K value. The K-structure is shaded toward shorter wave-lengths, but the J-structure of each sub-band, and so the band as a whole, is shaded toward longer wave-lengths.‡‡ That is, $C'>C''$ and $B'<B''$, B' and B'' being the constants¶¶ of the J-structure in the upper and lower states. From considerations of Metropolis,[5] which need not be repeated here, this shows that the apex angle α' in the upper state is larger than α'' in the lower state, but leaves open the question as to whether $r'-r''$ is positive or negative, where r' and r'' correspond to the CF distances in the upper and lower states, respectively. The existence of a long v_1'' series, but with maximum intensity for Δv_1 perhaps about one or two, indicates that $|r'-r''|$ is appreciably different from zero, but not large.

As an example, the wave numbers of the sub-band heads of the band at 2487A are given in Table IV with the assigned values for K.

The sub-heads or in other words the K-structure can be well represented for this band by the parabolic formula

$$\nu=40185+2.35K^2, \tag{3}$$

which shows that the transition involved for the band system is of a parallel type.

The value of $C'-C''$ from Eq. (3) is 2.35 cm^{-1}, not far different in magnitude from the value[6] -3.78 cm^{-1} in the case of NO_2. An accurate determination of $B'-B''$ would require higher dispersion. However, by measuring the second differences in the J-structure for a few higher frequency bands, a rough value of -0.13 ±0.03 cm^{-1} is obtained, as compared with the value -0.06 cm^{-1} in the case of NO_2 (λ2500) and -0.03 cm^{-1} for ClO_2.[7]

Besides the main band system discussed, there are additional weak bands on the longer wave-length side (3300–3700A) which appear to be of a different structure. These may probably form a second CF_2 system. However, it is not yet certain whether these bands belong to CF_2, and further work is needed to determine definitely the nature of these bands.

Following are some comments by Professor R. S. Mulliken on the probable electronic states responsible for the band system and relative to certain states of CH_2. These are included with his kind permission.

[The foregoing results on CF_2 have a bearing on the

TABLE IV. K-structure of the band at 2487A.

K	ν_{obs}	$\nu\Delta$	ν_{calc}
0	40184.0		40185.0
		3.1	
1	40187.1		40187.4
		7.1	
2	40194.2		40194.4
		13.6	
3	40207.8		40206.2
		17.3	
4	40225.1		40222.6
		21.2	
5	40246.3		40243.8
		25.8	
6	40272.1		40269.6
		30.9	
7	40303.0		40300.2
		32.5	
8	40335.5		40335.4
		39.8	
9	40375.3		40375.4

[4] M. Kent Wilson and R. M. Badger, Phys. Rev. **76**, 472 (1949) and J. Chem. Phys. **16**, 741 (1948).

†† $C'=h/(8\pi^2c)[1/I_a'-\frac{1}{2}(1/I_b'+1/I_c')]$, where I_a', I_b', and I_c' are the three moments of inertia of the molecule in the upper state, with $I_a'<I_b'<I_c'$; C'' stands for a similar expression in the lower state.

‡‡ Here the CF_2 bands differ from the bands of NO_2 at 2500A, where the K-structure and the J-structure are both shaded toward longer wave-lengths.

¶¶ $B'=(h/8\pi^2c)\frac{1}{2}(1/I_b'+1/I_c')$, with a similar relation for B''.

[5] N. C. Metropolis, Phys. Rev. **60**, 283 (1941).

[6] L. Harris and G. W. King, J. Chem. Phys. **8**, 775 (1940).

[7] J. B. Coon, J. Chem. Phys. **14**, 665 (1946).

question of the structure of the CH_2 radical.[8,9] From general considerations of valence theory it is fairly certain that CH_2 is a non-linear symmetrical molecule with a singlet ground electronic state. For an s^2p^2 carbon atom, CH_2 would have the same type of electronic and geometrical structure as H_2O, except for the absence of two non-bonding p electrons from the central atom. For an sp^3 carbon atom, CH_2 would be a linear molecule with a triplet ground state. The actual condition of the carbon atom must certainly be intermediate between s^2p^2 and sp^3, but probably nearer the former. This leads to the prediction of an apex angle in the range 110°–130° (or possibly somewhat more) with in all probability a singlet ground state. A triplet ground state would occur if the angle sufficiently approached 180°, but it is improbable that this happens.

For an obtuse-angled model in the range 110°–130° or somewhat more, the electronic structure of the ground state and probable lowest excited states of CH_2 may be described as follows:

$$\begin{array}{l}(1a_1)^2(2a_1)^2(1b_2)^2(3a_1)^2,\ {}^1A_1\\ (1a_1)^2(2a_1)^2(1b_2)^2(3a_1)(1b_1),\ {}^3B_1 \text{ and } {}^1B_1\\ (1a_1)^2(2a_1)^2(1b_2)^2(3a_1)(2b_2),\ {}^3B_2 \text{ and } {}^1B_2.\end{array} \qquad (4)$$

The electron configurations are stated here in terms of MO's (molecular orbitals) classified according to the appropriate symmetry group (C_{2v}), with z axis bisecting the HCH angle and x axis taken as perpendicular to the plane of the nuclei. The y axis, parallel to the H—H line, is the quasi-symmetry axis for the rotation of CH_2 as a quasi-symmetric top—a valid approximation for apex angles in the indicated range. The forms of the various MO's may be described approximately, in LCAO approximation, as follows:

$$\begin{array}{l}1a_1 = 1s_C;\quad 2a_1 \approx s_H h_C s_H;\quad 3a_1 \approx h_C'(?);\\ 1b_2 \approx s_H y_C \bar{s}_H;\quad 2b_2 \approx \bar{s}_H y_C s_H;\\ 1b_1 = x_C.\end{array} \qquad (5)$$

Here $1s_C$, x_C (meaning $2p_x$ of carbon), y_C (meaning $2p_y$), h_C (meaning a hybrid of $2s_C$ and $2p_z$ of C), and h_C' (another hybrid of $2s_C$ and $2p_z$ of C) are carbon atom AO's; s_H is a $1s$ hydrogen atom AO. A symbol such as $s_H h_C s_H$ indicates a linear combination of the three AO's named, all with positive signs; a bar over s_H means that this AO is to be taken with negative sign in the linear combination. The MO's $2a_1$ and $1b_2$ are C—H bonding MO's. The MO $3a_1$ as described in (5) is nearly non-bonding; however, for pure s^2p^2 carbon, $2a_1$ would be non-bonding of the form $2s_C$, and $3a_1$ would be bonding of the form $s_H z_C s_H$; the actual forms of $2a_1$, $3a_1$, and $4a_1$ are subject to considerable uncertainty. The excited MO's $2b_2$ and $1b_1$ are C—H antibonding and non-bonding, respectively; for this reason, $2b_2$ should be considerably higher than $1b_1$ in energy, making the ${}^3B_2$ and ${}^1B_2$ excited states in (4) higher than the ${}^3B_1$ and ${}^1B_1$, respectively.

On the basis of (4) and what has just been said, the known visible emission bands* which are attributed to CH_2 most probably represent the transition ${}^1B_1 \rightarrow {}^1A_1$.[10] Although it has not been proved that their lower state is the ground state of CH_2, the conditions of excitation of this spectrum in comets, as well as the fact that the best known spectra of molecules possessing fairly low excited electronic levels are usually transitions from these to the ground state, make this probable. The observed structures of the bands seems to be consistent[10] with the indicated transition in an obtuse-angled CH_2 molecule.

Although the CF_2 molecule contains additional electrons, an examination of its expected MO's indicates that its normal and low excited states are probably similar to those of CH_2. In the bonding MO's, a linear combination of $2p_y$ and $2p_z$ of fluorine plays the role that $1s_H$ has in CH_2. There are also various interactions involving the fluorine non-bonding electrons, of which perhaps the most significant is one between the carbon $2p_z$ and the fluorine $2p_z$ AO's. This should give some added stability to the ground state (partial C—F double-bond formation), and at the same time makes the excited b_1 MO now somewhat C—F antibonding. This should raise the energy of the ${}^3B_1$ and ${}^1B_1$ excited states of (5) but still probably leave them somewhat below the ${}^3B_2$ and ${}^1B_2$ excited states, respectively.

The parallel-type CF_2 emission band system described earlier in this paper can now probably be identified with the transition ${}^1B_2 \rightarrow {}^1A_1$ involving states analogous to those in (4). The only other *allowed types* of transitions to the assumed ${}^1A_1$ ground state (${}^1B_1 \rightarrow {}^1A_1$ and ${}^1A_1 \rightarrow {}^1A_1$) would give perpendicular-type bands. (A transition of the type ${}^1A_2 \rightarrow {}^1B_1$, ${}^1B_1 \rightarrow {}^1A_2$, ${}^3A_2 \rightarrow {}^3B_1$, or ${}^3B_1 \rightarrow {}^3A_2$ would give parallel-type bands, but would involve two excited states.) It might be hoped that the appreciable though not large decrease in apex angle and change in interatomic distance during the emission process in the observed parallel-type transition would throw light on the electron configurations involved. However, in view of the qualitative nature of the information available and the uncertainty as to the exact form of the (CF_2 analog of the) $3a_1$ MO, all that can be said at present is that there seems to be no obvious inconsistency with the $\cdots(3a_1)(2b_2), {}^1B_2 \rightarrow (3a_1)^2, {}^1A_1$ interpretation.

The possible second system of CF_2 bands at longer wave-lengths than the main system, if confirmed by further work, should according to the preceding dis-

[8] For a review and discussion, see, e.g., R. G. W. Norrish and G. Porter, Discussions Faraday Soc. No. 2, 97 (1947); C. A. McDowell, *ibid.*, p. 143. Discussions Faraday Soc. No. 2, 143 (1947).

[9] Molecular orbital theory of CH_2, see R. S. Mulliken, Phys. Rev. **41**, 751 (1932); J. E. Lennard-Jones, Trans. Faraday Soc. **30**, 70 (1934).

* The emitter of these bands has now, however, become doubtful because of the recently reported results of Monfils and Rosen (Nature **164**, 713 (1949)).

[10] G. Herzberg, Rev. Mod. Phys. **14**, 195 (1942); Astrophys. J. **96**, 314 (1942).

cussion be identified with the transition $^1B_1 \rightarrow {}^1A_1$ and should consist of perpendicular-type bands.

The preceding probable identification of the CF_2 bands lends support to the obtuse-angled model with $^1A_1$ ground state for CH_2. The presence of partial double-bond formation in CF_2 does not alter this conclusion, since the strength of π (i.e., $2p_z$) bonding in an AB_2 molecule is readily seen to be insensitive to the apex angle.]

The writer wishes to express his thanks to Professor Robert S. Mulliken for his kind interest and suggestions during the course of the work.

PHYSICAL REVIEW VOLUME 77, NUMBER 5 MARCH 1, 1950

Internal Conversion in Ni^{60}

MARTIN DEUTSCH* AND KAI SIEGBAHN
Nobel Institute for Physics, Stockholm, Sweden
(Received November 1, 1949)

The coefficients of internal conversion for the two gamma-rays accompanying the decay of Co^{60} have been measured. For the 1.17-Mev gamma-ray we find $\alpha = 2.3 \times 10^{-4}$, for the 1.33-Mev ray $\alpha = 1.8 \times 10^{-4}$. Comparison with theoretical values indicates that the parity change must be the same in both transitions and that the two gamma-rays are probably electric quadrupoles.

ALTHOUGH the decay of Co^{60} has been studied in considerable detail, no measurement of the coefficients of internal conversion of the two well-known gamma-rays has been published. We have used a large, double-focusing spectrometer of 50-cm radius of curvature to measure these coefficients. This instrument admits a solid angle of about 0.12 steradian and, with the extended sources used in these experiments, permits a resolution of about one percent. The magnetic field is measured by balancing the induced e.m.f. of a rotating coil against that of another coil rotating on the same shaft in the field of a set of Helmholz coils. The current through the latter is measured with a precision ammeter. The precision of the field measurements is estimated to be about ± 0.1 percent. An absolute momentum calibration was obtained by the measurement of several well-known electron lines from ThB and of secondary electrons produced by annihilation radiation.

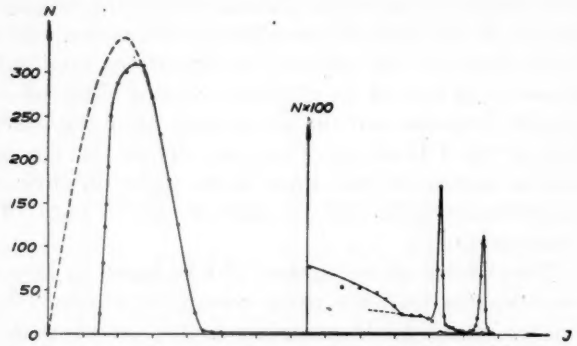

FIG. 1. The electron spectrum of Co^{60}.

Figure 1 shows a momentum spectrum of the electrons from Co^{60}. A counter window of about 3 mg/cm² thickness was used. The two internal conversion lines are shown again in the insert, with the ordinate multiplied by 100. Although the number of conversion electrons is only of the order of 10^{-4} of the number in the primary spectrum, the peaks are well resolved since they appear beyond the end point of the continuum. The low intensity continuous high energy "tail" on the distribution is due to Compton electrons ejected from the source and parts of the spectrometer. The conversion coefficients were determined by comparing the area under each of the peaks with that under the continuous spectrum. The integration of the latter is made difficult by the effect of the counter window, which seriously distorts the spectrum below about 0.15 Mev. Above this energy the observed spectrum is well represented by an allowed Fermi plot and we assumed that the low energy part also follows the allowed shape. The effect of source thickness is probably to cause us to underestimate the number of beta-rays since retardation in the source will reduce the relative number of high energy particles on which our extrapolation is based. The two sources used in our experiments were 8 mg/cm² and 2 mg/cm² thick, respectively, which may cause some error in this direction. Another factor which may cause us to overestimate the conversion coefficients is the production of photo-electrons in the cobalt of the source material. These could not be resolved from the conversion electrons from the nickel product nucleus. From the known source thickness we estimate that this error should be only a few percent. This was confirmed by the fact that the area under the two peaks remained practically unchanged when the source was covered with 18 mg/cm² of copper. If the peaks were largely due

* On leave from Massachusetts Institute of Technology, Cambridge, Massachusetts.

TABLE I. Experimental and theoretical values of internal conversion in the K shell, $\alpha K \times 10^4$.

Gamma-energy Mev	Experiment	Electric 2^l-pole $l=1$	$l=2$	$l=3$	Magnetic 2^l-pole $l=1$	$l=2$
1.17	2.12	0.74	1.58	3.17	1.24	2.93
1.33	1.68	0.60	1.17	2.11	0.97	2.13
Ratio	1.26	1.23	1.35	1.50	1.28	1.37

to external photo-electrons, the additional conversion in the copper would have increased their intensity. Instead, their height was decreased and their width increased as one would expect from straggling of electrons traversing the copper. At the same time the peaks were shifted to lower energies by 16 kev as shown in Fig. 2. The magnitude of this shift is in good agreement with theoretical expectation[1] and agrees within about ten percent with a value for the stopping power of copper obtained by interpolation between the experimental values for other elements.[2]

Using the areas under the distribution as described above, we find for the internal conversion coefficients of the two gamma-rays the values $\alpha_{1.17}=2.32\times10^{-4}$ and $\alpha_{1.33}=1.83\times10^{-4}$. If we subtract from these values eight percent for the unresolved L conversion electrons, as indicated by the calculations of Hebb and Nelson,[3] we obtain the values for the K conversion coefficients shown in Table I. This table also gives the theoretical coefficients according to recent calculations of M. E. Rose and co-workers.† Three significant figures are given for the experimental values because their *ratio*, also indicated in Table I, is known with much greater accuracy than the absolute values. The latter seem to be in error by about 30 percent, the discrepancy from the nearest theoretical values which are believed to be quite accurate. From our discussion of experimental errors it seems more probable that we overestimated the coefficients so that it is likely that the two gamma-rays are both electric quadrupole transitions. This would be in good agreement with their angular correlation.[4] If one prefers to be more conservative in evaluating the experimental uncertainties, it can still be stated that both radiations are either quadrupole or possibly electric octupole. Thus the first excited state in Ni^{60} has probably spin 2 or possibly 3. From the ratio of the two conversion coefficients it is also quite certain that the

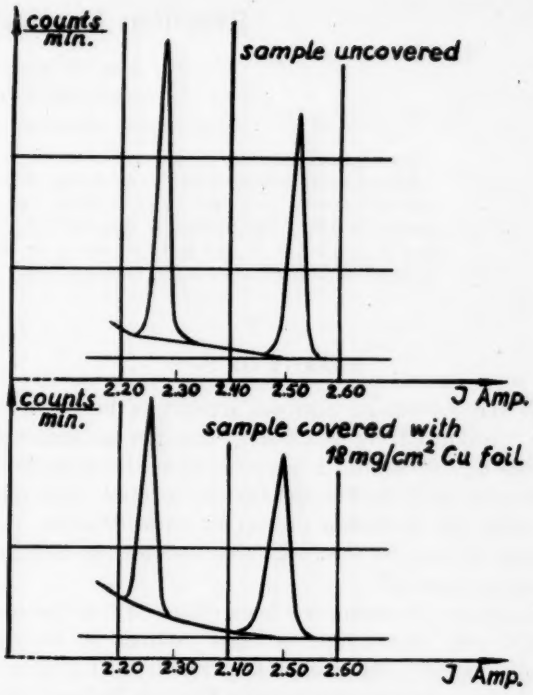

FIG. 2. Photo-electron lines of Co^{60}.

two gamma-rays have the same parity. For example, if one of them is a magnetic quadrupole having odd parity, the other cannot be an electric quadrupole (even parity) but could be either magnetic quadrupole or electric octupole. Thus the total change in parity for the cascade must be even and the 2.50-Mev state in Ni^{60} has the same parity as the ground state.

In the course of these experiments we also measured the energies of the two gamma-rays both by the energies of the conversion lines and by those of photo-electrons ejected from a 4-mg/cm² lead converter. Internal conversion electrons from the thinner sample gave the energies 1.177 Mev and 1.342 Mev, those from the thicker sample 1.171 Mev and 1.332 Mev, respectively. A weighted mean of the K and L photo-electrons from the lead converter yielded the values 1.172 Mev and 1.335 Mev. We adopted the values $E_1=1.174\pm0.005$ Mev and $E_2=1.338\pm0.005$ Mev until we became aware of the results of Lind, Brown, and DuMond.[5] The excellent agreement of these two very different determinations is gratifying.

It is a pleasure to express our gratitude for the cooperation of our colleagues at the Nobel Institute and for the hospitality extended by the Institute to one of us (M.D.) during his stay in Sweden.

[1] See W. Heitler, *Quantum Theory of Radiation* (Oxford University Press, London, 1944), p. 219, Eq. (5) and p. 221, Eq. (9).
[2] Rutherford, Chadwick, and Ellis, *Radiations from Radioactive Substances* (Cambridge University Press, London, 1930), pp. 98–100.
[3] M. H. Hebb and E. Nelson, Phys. Rev. 58, 486 (1940).
† Private communication.
[4] E. L. Brady and M. Deutsch, Phys. Rev. 74, 1541 (1948).
[5] Lind, Brown, and DuMond, Phys. Rev. 76, 591 (1949).

Reactions Leading to Fe^{53}, Mn^{57}, and Cr^{55}

M. E. NELSON* AND M. L. POOL
Ohio State University, Columbus, Ohio
(Received November 21, 1949)

An end point corresponding to an energy of 2.8±0.1 Mev has been determined for the Fe^{53} 8.9-minute positron activity. (α,p) and (n,p) reactions on enriched Cr^{54} and Fe^{57} respectively failed to produce any activity in Mn^{57}. The previously reported 1.3- to 2.3-hour activity of Cr^{55} was shown not to be produced by a (d,p) reaction on enriched Cr^{54} nor by an (n,α) reaction on enriched Fe^{58}. The 3.9-minute V^{52} activity is readily produced by a $Cr(d,\alpha)$ reaction, using Cr enriched in isotope 54.

ENERGY OF Fe^{53}

THE 8.9-minute positron activity of Fe^{53} was first produced by a $Cr(\alpha,n)$ reaction on naturally occurring chromium.[1] It was subsequently shown to be produced by $Fe(n,2n)$ and $Fe(\gamma,n)$ reactions and more recently by spallation of copper with 190-Mev deuterons.[2] In none of these experiments were the radiation energies reported.

Recently chromium has been obtained** in the form Cr_2O_3 with the isotope of mass number 50 enriched electromagnetically from 4.31 percent to 41.2 percent. By bombarding the enriched Cr_2O_3 with 20-Mev alpha-particles it has been possible to produce the 8.9-minute Fe^{53} activity in sufficient intensity to allow absorption measurements of its radiations to be made. The presence of positrons and the value of the half-life were confirmed.

Figure 1 shows a plot of aluminum absorption measurements with an end point of 1.40 g/cm², corresponding to a positron energy of 2.8±0.1 Mev. Lead absorption measurements made on several samples indicate that gamma radiation, if present, is of low intensity compared to annihilation radiation.

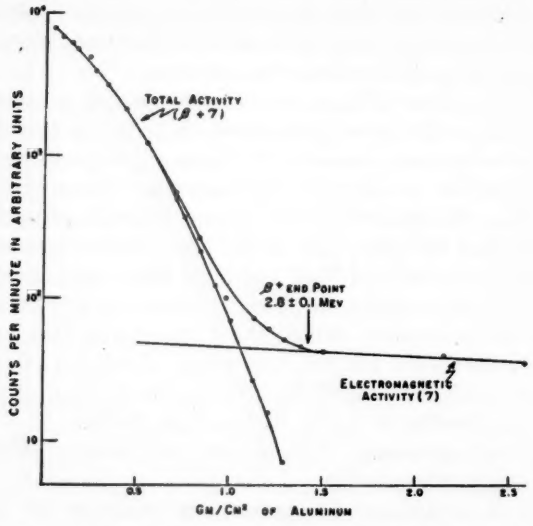

FIG. 1. Aluminum absorption measurement showing the 2.8±0.1 Mev positron endpoint of the 8.9-minute Fe^{53} activity.

Mn^{57}

Radioactive isotopes of Ga^{73}, Cu^{67}, and Co^{61} have recently been reported.[3] Each of these radioactive isotopes is characterized by being two mass units heavier than its nearest stable isotope. If this pattern were to continue, Mn^{57} would be expected to be radioactive. Consequently an attempt was made to produce Mn^{57} by a $Cr^{54}(\alpha,p)$ reaction. A sample of Cr_2O_3 in which the isotope of mass number 54 was electromagnetically enriched** from 2.38 percent to 83.1 percent was bombarded with alpha particles. The 2.6-hour Mn^{56} activity was produced by the $Cr^{53}(\alpha,p)$ reaction since Cr^{53} was present to 4.3 percent abundance in the enriched Cr^{54} sample. No activity, however, attributable to Mn^{57} was observed. The cross section of the $Cr^{54}(\alpha,p)$ reaction for the production of Mn^{57} with a possible half-life of a month or less must be less than 1/500 of that of the $Cr^{53}(\alpha,p)$ reaction for the production of Mn^{56}.

To determine whether a Mn^{57} activity might be produced by a $Fe(n,p)$ reaction a sample of Fe_2O_3 with the Fe^{57} isotope enriched** from 2.20 percent to 77.6 percent abundance was bombarded with fast neutrons from the Li+d reaction. The Fe^{56} isotope was present in 21.7 percent abundance in this sample. The (n,p) reaction cross sections for these two iron isotopes would be expected to be of the same order of magnitude. However, only the 2.6-hour Mn^{56} activity was observed. Consequently no activity was detected which could be assigned to Mn^{57}. These experiments do not preclude the possibility of a very short or a very long half-life activity belonging to Mn^{57}.

ABSENCE OF Cr^{55} ACTIVITY

Activities of half-lives 2.27, 1.6, and 1.3 hours[4] have been attributed to Cr^{55} which has been given an isotopic

* Department of Physics, College of Pugent Sound, Tacoma, Washington.

[1] L. N. Ridenour and W. J. Henderson, Phys. Rev. **52**, 889 (1937).

[2] G. T. Seaborg and I. Perlman, Rev. Mod. Phys. **20**, 585 (1948). Josef Mattauch and Arnold Flammersfeld, "Isotopenbericht," Zeits. f. Naturforschung (Tübingen, 1949).

** Supplied by the Y-12 Plant, Carbide and Carbon Chemicals Corporation, through the Isotopes Division, U. S. AEC, Oak Ridge, Tennessee.

[3] J. M. Siegel, L. E. Glendenin and J. A. Marinsky, reported in Plutonium Project Report CN-2596, p. 10 (Mar. 1945). H. H. Hopkins, Jr. and B. B. Cunningham, Phys. Rev. **73**, 1406 (1948). T. J. Parmley, B. J. Moyer, and R. C. Lilly, Phys. Rev. **75**, 619 (1949).

[4] G. Dickson, P. W. McDaniel, and E. J. Konopinski, Phys. Rev. **57**, 351 (1940). Toshio Amaki, Takeo Iimori, and Asao

assignment classification of B.[2] An attempt was made to produce the reported activity by a deuteron bombardment of Cr_2O_3 in which the isotope of mass number 54 was enriched from 2.38 percent to 83.1 percent abundance. With this enrichment factor of 36 times, the conditions for producing any Cr^{55} activity were most favorable.

No activities with half-lives in the neighborhood of the periods mentioned above were found that could be attributed to Cr^{55}. From the activities measured any (d,p) reaction cross section for the production of a two-hour Cr^{55} activity must be at least 2000 times smaller than the $Cr^{54}(d,\alpha)V^{52}$ reaction cross section. This ratio suggests that neither this activity nor any activity with a half-life of this order of magnitude is due to Cr^{55}. The 3.9-minute V^{52} activity is produced in great intensity by the (d,α) reaction.

Sugimoto, Phys. Rev. **57**, 751 (1940). L. Seren, H. N. Friedlander, and S. H. Turkel, reported in Plutonium Project Reports CP-1592 (May 1944) and CP-2376 (Dec. 1944).

As an additional check on the possible existence of an activity in Cr^{55} fast neutron bombardments of equal intensity and duration were made on two enriched** Fe_2O_3 samples in which the percent abundances of isotopes of mass number 56, 57, and 58 were:

Sample A: 50.4, 6.9 and 42.0,
Sample B: 21.7, 77.6 and 0.2.

The 2.6-hour Mn^{56} activity was produced in each sample by the $Fe^{56}(n,p)$ reaction. The ratio of the observed intensities was the same as that of the abundances of the Fe^{56} isotopes in the two samples; namely 50.4/21.7. This indicates that the activity in each sample was due only to Mn^{56}. Even though the enrichment ratio for the Fe^{58} isotope in sample A was 210 times greater than that in sample B, no additional activity was observed which could be attributed to Cr^{55} produced by an $Fe^{58}(n,\alpha)$ reaction.

The assistance received from the Ohio State University Development Fund is gratefully acknowledged.

PHYSICAL REVIEW VOLUME 77, NUMBER 5 MARCH 1, 1950

On Wave Equation Vector-Matrices and Their Spurs

R. J. DUFFIN
Department of Mathematics, Carnegie Institute of Technology, Pittsburgh, Pennsylvania
(Received September 1, 1949)

If a system of tensor (or spinor) equations may also be written in the matrix form $P\psi=\psi'$ where the column matrices ψ and ψ' undergo the same transformation under a change of coordinates, then the square matrix P is termed a *vectrix*. General considerations indicate that P should obey invariant matrix identities. Of course, the matrix P merely images an operation implicitly defined in the original system of equations in terms of a set of tensor parameters p. A natural method to seek identities is to iterate this operation in the original system with different values ascribed to the parameters. Of especial interest are the vectrices defined by wave equation systems such as those of Dirac and Proca. Here p is to be interpreted as the four-vector of momentum and energy. By carrying out the iteration process, various identities are found. In particular, formulas are obtained for the spur of the product of an arbitrary number of Proca vectrices.

ACCORDING to several familiar theories of particles, the wave function ψ of a free particle satisfies a matrix wave equation of the form

$$\sum_{\mu=1}^{4} p_\mu\beta_\mu\psi=k\psi. \tag{1}$$

Here p_1, p_2, p_3 are the momentum components of the particle and $-icp_4$ is the energy of the particle. The constant $k=im_0c$ where m_0 is the rest mass of the particle. (This assumes, of course, a momentum-energy representation of the wave function. If the wave function were represented in space-time coordinates p_μ is given the interpretation $\hbar\partial/i\partial x_\mu$; however, this representation shall not be employed here.) The β_μ are matrices of constants which satisfy certain commutation identities. For instance, in the Dirac theory

$$\beta_\mu\beta_\nu+\beta_\nu\beta_\mu=2\delta_{\mu\nu}. \tag{2}$$

A still more compact notation is obtained by writing $P=\sum p_\mu\beta_\mu$. Then (1) becomes

$$P\psi=k\psi. \tag{3}$$

Since p_μ is a relativistic four-vector, it is appropriate to term P a vector-matrix or *vectrix* for short. If q_μ is another four-vector, let $Q=\sum q_\mu\beta_\mu$. It is easy to see from (2) that for two Dirac vectrices P and Q,

$$PQ+QP=2(p\cdot q). \tag{4}$$

Here $p\cdot q=\sum p_\mu q_\mu$, the scalar product.

Three methods of performing the algebraic manipulations of a calculation in these particle theories may be distinguished: First, Eq. (1) could be expressed in terms of its components. Second, Eq. (1) could be manipulated directly by matrix methods. This requires a knowledge of the algebraic properties of the β_μ. In particular it happens that the spurs of the multiple

products of the β_μ play an important role. Third, the calculations could be carried out in terms of vectrices. This method bears the same relation to the second method that vector analysis bears to coordinate analysis. This method is the least familiar, so it may be well to give an example. Consider a particle with charge e in a field with vector potential v_1, v_2, v_3 and scalar potential $-iv_4$ considered as functions of space and time. Let a_μ be the fourfold Fourier transform of the vector ev_μ/c. Then if A signifies the vectrix $\sum a_\mu\beta_\mu$, the wave equation is

$$P\psi-k\psi=A*\psi. \tag{5}$$

Here the $*$ indicates the Fourier faltung, for instance in the case of functions of one variable

$$f(x)*g(x)=\int_{-\infty}^{\infty} f(x-t)g(t)dt.$$

Thus $\psi=(P-k)^{-1}A*\psi$. To solve this integral equation one might try successive approximations, i.e., substitution of a first approximation on the right side gives a second approximation on the left side, etc. Note that in the case of a Dirac vectrix, $(P-k)^{-1}=(p^2-k^2)^{-1}\times(P+k)$. It is clear that the formula resulting would contain the products of several vectrices. In a forthcoming article on the space-time approach to quantum electrodynamics, R. P. Feynman arrives at expressions of the same general nature. Actually his calculations are carried out for a Dirac particle; however, he points out that his formalism could be carried over to other particles which satisfy an equation of the form (1), in particular to the Proca particle. He notes that for a Proca vectrix

$$(P-k)^{-1}=(kp^2-k^3)^{-1}(P^2+kP+k^2-p^2).$$

The Proca wave equation, when written in terms of components, is the system

$$p_\mu\phi_\nu-p_\nu\phi_\mu=k\zeta_{\mu\nu},\quad p_\mu\zeta_{\mu\nu}=k\phi_\nu. \tag{6}$$

Here ϕ_μ is a four-vector and $\zeta_{\mu\nu}$ is an antisymmetric tensor. Then ψ is a column matrix consisting of the four components of ϕ_μ and the six independent components of $\zeta_{\mu\nu}$. The following commutation relations were found to hold[1]

$$\beta_\mu\beta_\nu\beta_\rho+\beta_\rho\beta_\nu\beta_\mu=\delta_{\mu\nu}\beta_\rho+\delta_{\rho\nu}\beta_\mu. \tag{7}$$

These were found by "cut and try," i.e., by actually carrying out various multiplications of the ten-row matrices when (6) is put in the form of (1). In this note it is shown how to obtain (7) and other properties of these matrices directly from (6). The method is to regard the left sides of (6) as a linear operation on the set $\{\phi_\mu, \zeta_{\mu\nu}\}$ and to ignore the right sides. By iterating this operation with different values of the parameters p_μ, it turns out to be relatively easy to find identities. The matrix P is, of course, the matrix representation of this operation and must satisfy the same identities. The power of this method depends on the fact that it does not lose track of the manifest relativistic invariance of (6) as would be the case if Eq. (6) were immediately written in matrix form. But this invariance must somehow govern the character of the identities obtained.

Consider first the so-called scalar wave equation

$$p_\mu\phi_\mu=k\sigma,\quad p_\mu\sigma=k\phi_\mu. \tag{8}$$

Here ϕ_μ is a vector and σ is a scalar. Define the operation P as taking the set $\{\sigma, \phi\}$ into the set $\{p\cdot\phi, p\sigma\}$. (The omission of indices here should cause no confusion.) Thus QP gives $\{q\cdot p\sigma, qp\cdot\phi\}$ and RQP gives $\{(r\cdot q)(p\cdot\phi), r(q\cdot p)\sigma\}$. On the other hand, PQR gives $\{(p\cdot q)(r\cdot\phi), p(q\cdot r)\sigma\}$; hence,

$$PQR+RQP=(p\cdot q)R+(r\cdot q)P. \tag{9}$$

Take the vector p to have a unit μ component and no other components; then P becomes β_μ. Likewise let Q and R become β_ν and β_ρ, respectively. In this case (9) becomes (7). In general

$$PQR\cdots XYZ+ZYX\cdots RQP = (p\cdot q)\cdots(x\cdot y)Z+(z\cdot y)\cdots(r\cdot q)P$$

for odd products and

$$PQR\cdots XYZ+ZPQR\cdots XY = (q\cdot r)\cdots(x\cdot y)PZ+(p\cdot q)\cdots(v\cdot x)ZY$$

for even products. These identities are derived by the same method as that used in obtaining (9). However, these identities are not consequences of (9).

Let A signify the space of σ and B the space of ϕ. Then P may be aptly termed a *cross* transformation between these spaces. More precisely, let P_A be the operation taking $\{\sigma, \phi\}$ into $\{p\cdot\phi, 0\}$, and let P_B be the operation giving $\{0, p\sigma\}$. Then $P=P_A+P_B$ and $P_BQ=PQ_A$. Hence, for an even product

$$PQ\cdots YZ=P_AQ\cdots YZ+PQ\cdots YZ_A.$$

Let Sp stand for the operation of taking the sum of the diagonal elements of a matrix, the spur. By the definition of matrix multiplication, it follows that $\mathrm{Sp}XY=\mathrm{Sp}YX$. Hence,

$$\mathrm{Sp}PQ\cdots YZ_A=\mathrm{Sp}Z_APQ\cdots Y=\mathrm{Sp}_AZPQ\cdots Y.$$

Here Sp_A signifies the part of the spur in A. This proves the following lemma for the product of an even number of cross transformations

$$\mathrm{Sp}PQ\cdots YZ=\mathrm{Sp}_APQ\cdots YZ+\mathrm{Sp}_AZPQ\cdots Y. \tag{10}$$

An odd product of cross transformations is a cross transformation; hence there are no diagonal matrix elements, and the spur vanishes. It follows immediately from (10) that

$$\mathrm{Sp}PQ\cdots YZ=(p\cdot q)\cdots(y\cdot z)+(z\cdot p)\cdots(x\cdot y). \tag{11}$$

[1] R. J. Duffin, Phys. Rev. 54, 1114 (1938); N. Kemmer, Proc. Roy. Soc. A173, 91 (1939).

This formula was derived by Feynman and Slotnick by making use of expression for the spurs of the β_μ-matrices given by Kemmer,[1] together with symmetry arguments. They were unable to obtain a spur formula for the more complicated vectrices of the Proca equation by their method. Dr. Feynman asked the writer to investigate this question, and this note resulted.

Turning now to the Proca Eq. (6), let $p\cdot\zeta$ signify $p_\mu\zeta_{\mu\nu}$, and let $p\phi-\phi p$ signify $p_\mu\phi_\nu-p_\nu\phi_\mu$. Define the operation P as taking the set $\{\phi, \zeta\}$ into the set $\{p\cdot\zeta, p\phi-\phi p\}$. Thus the operation QP gives

$$\{(q\cdot p)\phi-(q\cdot\phi)p, qp\cdot\zeta-p\cdot\zeta q\}$$

and RQP gives

$$\{(r\cdot q)p\cdot\zeta-(p\cdot\zeta\cdot r)q, (q\cdot p)r\phi-(q\cdot\phi)rp -(q\cdot p)\phi r+(q\cdot\phi)pr\}.$$

Here $p\cdot\zeta\cdot r=p_\mu\zeta_{\mu\nu}r_\nu$, so because of the antisymmetry, $p\cdot\zeta\cdot r=-r\cdot\zeta\cdot p$. It is clear, therefore, that $PQR+RQP$ gives

$$\{(p\cdot q)r\cdot\zeta+(r\cdot q)p\cdot\zeta, (q\cdot r)p\phi-(q\cdot r)\phi p +(q\cdot p)r\phi-(q\cdot p)\phi r\}.$$

Hence (9) is again satisfied. Let A now denote the space of ϕ. Let $P_1Q_1P_2Q_2\cdots P_mQ_m$ be an even product of $2m$ operations; then in the space A this operation may be expressed in a convenient notation as

$$\phi^{(2m)}=(q_1\cdot p_1-q_1p_1\cdot)(q_2\cdot p_2-q_2p_2\cdot)\cdots \times(q_m\cdot p_m-q_mp_m\cdot)\phi. \quad (12)$$

This formula was seen to hold above for two factors QP, so it must hold in general. It is easy to see from (12) that for four operations, say $SRQP$, in the space A the following reduction formula holds

$$SRQP=(s\cdot r)QP+(q\cdot p)SR-(s\cdot p)QR +(s\cdot p)(q\cdot r)-(s\cdot r)(q\cdot p). \quad (13)$$

It is clear that P is again a cross transformation, so (13) may be used to reduce a product containing six or more factors in the space B, such as $XSRQPY$.

To evaluate $\mathrm{Sp}_A P_1Q_1P_2Q_2\cdots P_mQ_m$, formula (12) is expanded in ascending powers of the operator terms $q_ip_i\cdot$ appearing. Let $[i, j, \cdots, t]$ stand for

$$(p_i\cdot q_1)(p_j\cdot q_2)\cdots(p_t\cdot q_m).$$

The zero power term is $(q_1\cdot p_1)(q_2\cdot p_2)\cdots(q_m\cdot p_m)\phi$, so the spur of this term is $n[1, 2, \cdots, m]$ where n is the dimensionality of coordinate space; of course, $n=4$ for space-time. The first power terms are of the form $-(q_2\cdot p_2)\cdots(q_m\cdot p_m)q_1(p_1\cdot\phi)$. The spur of this term is $-[1, 2, \cdots, m]$. Hence the spur of zero and first power terms add to $(n-m)[1, 2, \cdots, m]$. The spurs of the remaining terms are distinct and are of the form $\pm[i, j, \cdots, t]$ where disregarding the symbols which are in natural order the others shift to the right one place (the last one coming around to the front). If an even number shift, the positive sign is taken. Adding the same expression for $Q_mP_1Q_2\cdots P_m$ gives, by virtue of the lemma (10), a formula for $\mathrm{Sp}P_1Q_1P_2Q_2\cdots P_mQ_m$.

From the spinor form of Dirac's equation it is manifest that the Dirac vectrix is also a cross transformation; hence, the spur of an odd product vanishes. For an even product

$$\mathrm{Sp}P_1P_2\cdots P_{2m}=4\sum\pm(ij)(kl)\cdots(st).$$

Here $(ij)=(p_i\cdot p_j)$, and the term $(12)(34)\cdots(2m-1,2m)$ occurs with a positive sign. The other terms are obtained by successive transpositions of consecutive integers between parentheses until no new terms arise. Each transposition is accompanied by a change of sign. By induction this formula may be shown to follow from the commutation identity (4).

What sort of identities and formulas are to be expected in such theories *a priori*? The following general considerations are of some help concerning this difficult question. A square matrix P whose matrix elements are functions of a set p of tensors and spinors shall be termed a *vectrix* if each transformation of coordinates defines at least one matrix S such that P transforms to SPS^{-1}. Obvious consequences of this definition may be noted: If P has an inverse, the inverse is a vectrix. The secular equation, $\det(P-\lambda I)=0$, is invariant. In particular the spur and determinant are coefficients of the secular equation, so they are scalars. If q is a set of the same type as p, let Q be the corresponding vectrix. Then PQ and $P\pm Q$ are vectrices, so vectrices of the same type generate a vectrix ring. A matrix satisfies its own secular equation, so a vectrix satisfies an invariant identity. Then because of the ring property, commutation identities between $P, Q, \cdots$ are not surprising.

The concept of a vectrix is not limited to cartesian coordinates or euclidean spaces. In general the set p might contain the metric tensor $g_{\mu\nu}$. However, by a well-known principle of tensor analysis, it is sufficient to consider a locally cartesian coordinate system in order to find identities.

Considering a vectrix to be a linear operation on a column matrix ψ, say $P\psi=\psi'$, then this relation is of invariant form if ψ and ψ' are taken to transform as $S\psi$ and $S\psi'$ under a transformation of coordinates. Conversely, if a set of tensor or spinor equations may be written in the form $P\psi=\psi'$ where ψ and ψ' undergo the same transformation under a transformation of coordinates, then P is a vectrix.

A Study of Penetrating Showers at 3260 Meters

WILLIAM D. WALKER*
Cornell University, Ithaca, New York
(Received November 7, 1949)

A series of experiments on local penetrating showers is described. Neon bulbs electronically connected to Geiger counters were lighted and photographed when those counters were struck in a simple coincidence. One row of counters recorded delayed coincidences. Most of the experiments described were performed at Echo Lake, Colorado, elevation 3250 meters.

The experiments indicate that there are approximately equal numbers of charged and neutral primary particles. The measured mean free path is found to decrease with increasing energy. The charged primary particles are shown to have a very strong zenith angle dependence.

Properties of the secondary particles of the showers were also studied. A large fraction of the penetrating particles locally produced are shown to be mesons. Of all the mesons that stop and decay in the apparatus, apparently about 16 percent are locally produced in penetrating showers. There are many short range particles produced that are not mesons. The angular distribution of the penetrating secondaries about the shower axis shows a strong concentration of the particles in the forward direction, such that they could not be emitted symmetrically in the center of gravity system.

I. INTRODUCTION

A LOCAL penetrating shower is usually defined experimentally as the local production of several charged particles, heavier than electrons and each capable of traversing several inches of lead.

The rate of occurrence of these showers increases very rapidly with altitude.[1] This indicates that few, if any, of the showers are produced by μ-mesons. The absorption of the shower primaries has been shown to be greater in carbon than in lead,[2] and therefore the primaries are not photons or electrons. The primaries of the penetrating showers have been called by the collective name "N component,"[3] which is thought to include nucleons and π-mesons (or possibly only nucleons). The present work is intended to be a study of showers produced by the N component and not those produced by μ-mesons or the cascade particles. In some phases of the work it was possible to detect showers whose secondaries were not at all penetrating. In spite of this apparent contradiction, the term "penetrating shower" used in this paper is intended to mean a shower produced by the N component.

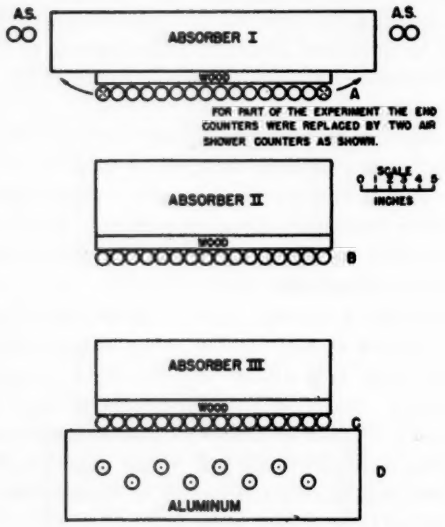

FIG. 1. Counter arrangement.

In investigating penetrating showers there are two general ways of selecting the events to be studied:

(a) Selecting so as to guarantee with high probability that only penetrating showers will be recorded, although certain classes of penetrating showers may be missed entirely.

(b) Selecting so that, as nearly as possible, every penetrating shower will be recorded, although other types of showers may also be recorded.

In this experiment a method of selection intermediate between (a) and (b) was used, in that the simplest coincidence which triggered the apparatus did not require that the secondaries of the shower be penetrating. As a result, a part of this paper is devoted to estimating the rate of showers produced by μ-mesons. Most of the arguments used in evaluating the correction depend upon the fact that the rate of penetrating showers increases much more rapidly with altitude than does the rate of showers produced by μ-mesons.

II. DESCRIPTION OF APPARATUS

The apparatus consisted of an array of 16-inch by one-inch Geiger-Mueller counters pictured in Fig. 1. Each counter was attached to a circuit which would light a neon bulb when the counter pulse was in coincidence with a master pulse. For the major part of the experiment the master pulse was triggered by the simple coincidence $A^{>0}B^{>0}C^{>2}$ (at least one counter struck in row A, at least one in B, and at least three in row C). The use of blocking oscillators in the mixing produced a resolving time of 1.2 μsec. for the production of a master pulse. The length of the master pulse was about 25 μsec.

The counters in tray D were employed in the detection of counts delayed in time between one and four μsec. from the coincidence $A^{>0}B^{>0}C^{>2}$. Pulses were

* Now at Rice Institute, Houston, Texas.
[1] J. Tinlot, Phys. Rev. 74, 1197 (1948).
[2] G. Cocconi, Phys. Rev. 75, 1974 (1949).
[3] B. Rossi, Rev. Mod. Phys. 20, 537 (1948).

TABLE I. Corresponding coincidence rates at Echo Lake and Ithaca.

	Absorber $I=0$, $II=0$, $III=8$-in. Pb				
Coincidence	$A^1B^1C^3$	$A^1B^1C^{4,5}$	$A^1B^1C^{>5}$	$A^1B^1C^{>7}$	$A^1B^{>0}C^{>2}$
Echo Lake rate (min.$^{-1}$)	1.63 ±0.025*	0.614±0.018	0.233 ±0.006	0.0735±0.003	0.41 ±0.015
Ithaca rate (min.$^{-1}$)	0.415±0.01	0.140±0.004	0.0339±0.002	0.006 ±0.0008	0.055±0.004
Ratio	3.95	4.4	6.9	12.5	7.5

* Errors indicated are the standard or r.m.s. errors.

channelled as to delay times 1–2 μsec., 2–3 μsec.,† etc., and as a check the lifetime of the meson was continuously measured.

Because of the very short resolving time, the probability of a chance coincidence triggering the apparatus was completely negligible (less than 0.05 percent of the observed rate). The most probable chance coincidence was the lighting of one extra neon bulb. The calculated probability for this is ½ percent per photograph.

III. CORRECTIONS

A. Soft Component

It is necessary to investigate the possibility that electrons and photons, as well as μ-mesons, can produce background showers.

In order for a single electron or photon to trip the apparatus the cascade would have to traverse, in all cases, at least 180 g/cm² of lead. This requires that it be of energy greater than about 10^{11} ev. An electron or photon of this energy will only be found within a few centimeters of the core of an air shower. In the core of an air shower having electrons of this energy the density is so high that it is extremely improbable to have only one particle incident, and therefore only the case of many particles incident need be considered.

The following precautions were taken to avoid recording particles accompanied by air showers:

(1) There were always at least four unshielded counters in anti-coincidence (415 cm² total area) within one foot of row A.

(2) The absorber was always placed so that, in order to have counters struck in all three rows, several inches of lead had to be traversed, unless the particles were incident horizontally.

Because of the small total area of the air shower counters it was feared that some air showers might escape detection. With no lead above A such events would produce coincidences of the type $A^{>1}B^{>0}C^{>2}$ −A.S.,‡ and the rate of these would decrease markedly with increasing thickness of absorber. The following data show no strong decrease, and it is concluded that the rate of such events is not more than 0.04 min.$^{-1}$.

$A^{>1}B^{>0}C^{>2}$−A.S. with $I=0$, $III=8$-in. Pb			
Absorber II	0	4-in. Pb	8-in. Pb
Rate (min.$^{-1}$)	0.10±0.005	0.072±0.005	0.060±0.004.

The rate of coincidences $A^1B^{>0}C^{>2}$, which is used frequently in analysis in most of the experiments, is always between 1.7 and 2.91 min.$^{-1}$. We see that the estimated upper limit of the background rate, 0.04 min.$^{-1}$, is forty to seventy times smaller. It is therefore concluded that the soft component need not be considered as contributing to the background.

B. Meson Background

μ-mesons can produce showers of electrons and photons either by knock-on or radiation processes. An attempt will now be made to estimate the rate of such showers recorded at Echo Lake. This will be done by comparing the rates of identical coincidences at Echo Lake and at Ithaca (see Table I), using the fact, shown below, that the increase in vertical intensity of mesons of energy greater than 1 Bev between Ithaca and Echo Lake is a factor of 1.5, while the N component increase is between 8 and 15.[3]

Let

$E.L.$ = counting rate of a given coincidence at Echo Lake (elevation 3250 m).
I = counting rate of the same coincidence at Ithaca (elevation 260 m).
x = the number of such coincidences produced by mesons at Echo Lake.
y = the number produced by the N component at Echo Lake.
N = ratio of the rate of nucleon-produced showers at Echo Lake to that at Ithaca.
Δ = ratio of rates of meson produced showers.

Then

$$E.L.=x+y$$
$$I=x/\Delta+y/N.$$

TABLE II. Rates with two different absorber thicknesses (Ithaca)

Coincidences $A^1B^1C^{>2}$	
Absorber (Pb)	Rate
$I=0$, $II=0$, $III=8$ in.	0.61 ±0.02 min.$^{-1}$
$I=4$ in., $II=8$ in., $III=8$ in.	0.565±0.03 min.$^{-1}$

TABLE III. Ratio of vertical intensity of μ-mesons, Echo Lake to Ithaca.

Minimum range	Δ = ratio of vertical intensity	P(ev/c) (momentum)
196 g/cm²/Pb +200 g/cm² Fe	1.55	$\geqslant 6\times10^9$
196 g/cm² Pb +342 g/cm² Fe	1.50	$\geqslant 9\times10^9$
196 g/cm Pb +485 g/cm² Fe	1.50	$\geqslant 11\times10^9$

† The delay time was not indicated on each separate photograph.
‡ "−A.S." means no air shower counters were struck.

Solving these equations for y, the corrected rate, or the rate produced by the N component, of any given coincidence is found.

$$y=\frac{E.L.-\Delta I}{1-(\Delta/N)}. \tag{1}$$

Notice that the calculated value of y is not strongly dependent on the assumed value of N, which is taken as 12.

$$\frac{1}{y}\frac{\partial y}{\partial N}=\frac{1}{N}\frac{\Delta}{N-\Delta}\approx\frac{1}{85}\quad\begin{cases}N=12\\ \Delta=1.5.\end{cases}$$

Δ is estimated from the following evidence. According to the cloud-chamber data of J. G. Wilson,[4] nearly all of the μ-mesons which produce knock-on electrons have an energy of greater than 3×10^9 ev, and therefore we should expect that only high energy mesons produce coincidences. This is substantiated by data taken in Ithaca, shown in Table II, since the counting rate is changed very little by increasing the absorber on the apparatus.

If we suppose that only mesons of residual range greater than R are capable of producing a recorded shower, then after we add δR absorber, only mesons of initial range greater than $R+\delta R$ can be recorded. By examining the integral range spectrum at sea level given by Rossi,[3] we see that a decrease of 10 percent (roughly the change shown in Table II) by an increase of 350 g/cm² Pb (the change in absorber in this case) corresponds to a minimum energy of greater than 10^9 ev.

A direct measurement of the difference in intensity of mesons of energy $>10^9$ ev between these two altitudes has never been made. However, Rossi, *et al.*,[5] have measured the integral range spectrum at Echo Lake. Also the curve for the integral range spectrum at sea level has been given by Rossi,[3] as well as the decrease in mesons of range greater than 167 g/cm² Pb between altitudes corresponding to Echo Lake and Ithaca. Using this information an estimate of the decrease of mesons of $E>10^9$ ev has been made, and the results are given in Table III.

The ratio Δ is observed to change very slowly with the minimum energy selected. Since the probability of creating a knock-on shower goes rapidly to zero for energies less than 10^9 ev, and the number of mesons decreases rapidly with energy above 10^{10} ev, we consider that most of the knock-on showers are generated by mesons in the energy interval 10^9–10^{10} ev, and we have used $\Delta=1.50$ in making the corrections for μ-meson-produced showers. The uncertainty in the factor is considered to be less than 0.1, which makes very little difference in the calculated correction.

In the following sections, whenever a correction for μ-mesons seems necessary for interpretation of the data, it will be made in the way indicated above, by using Eq. (1) and the measured rates at the two different elevations.

IV. PROPERTIES OF THE PRIMARY PARTICLES

A. Mean Free Path *Versus* Energy

This experiment was performed in an attempt to learn whether the mean free path for absorption or

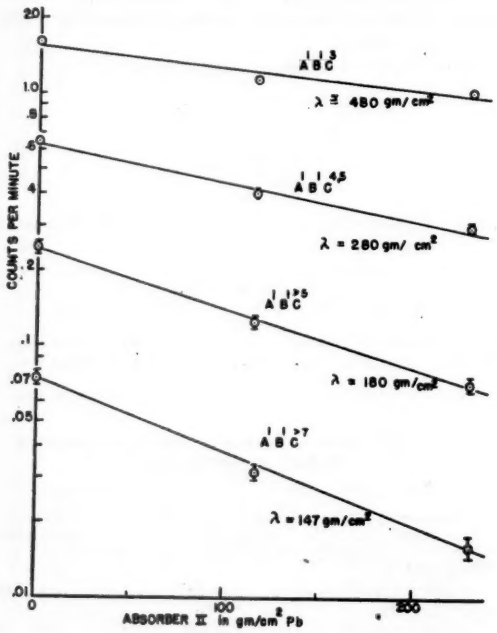

FIG. 2. Uncorrected rate $A^1B^1C^N$ *vs.* thickness of absorber *II*.

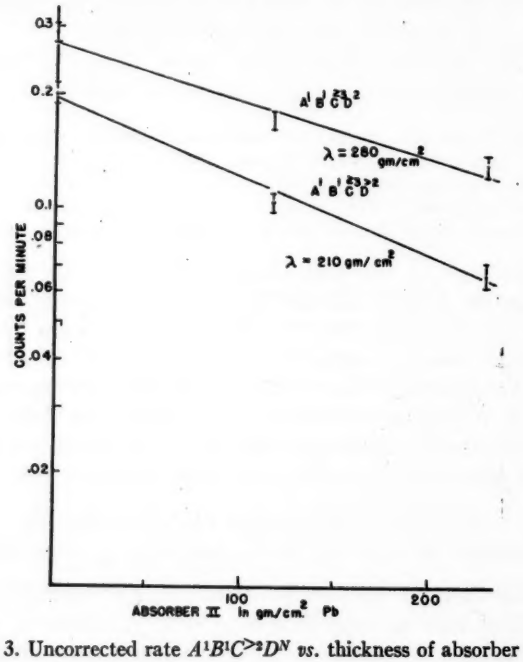

FIG. 3. Uncorrected rate $A^1B^1C^{>2}D^N$ *vs.* thickness of absorber *II*.

[4] J. G. Wilson, Nature 142, 72 (1938).

[5] Rossi, Greisen, Stearns, Froman, and Koontz, Phys. Rev. 61, 675 (1942).

shower production¶ varied with the energy of the primary particle.

Eight inches of lead was kept fixed in position *III*. The lead in position *II* was varied between zero and eight inches. The coincidences of interest were $A^1B^1C^{>2}$. These were thought to be caused by primary charged particles interacting in absorber *III* after traversing *II* with no interaction. We study the rate of these coincidences as a function of the thickness of absorber *II*. A decrease in this rate with increased absorber could be from the following causes:

1. Production of penetrating showers in absorber *II*. (Note that because of the 8-in. lead in *III* these showers may not be recorded at all.)
2. Loss of primary energy by collision processes in *II*.

The energies of the primaries were not measured directly, but it was assumed that the showers of many penetrating particles were made by primaries of very high energy, while the showers of fewer particles were made by primaries of lower energy. The data were therefore subdivided according to the number of counters struck into the following classifications:

(1) $A^1B^1C^3$	(4) $A^1B^1C^{>7}$
(2) $A^1B^1C^{4,5}$	(5) $A^1B^1C^{>2}D^2$
(3) $A^1B^1C^{>5}$	(6) $A^1B^1C^{>2}D^{>2}$

The uncorrected rates *vs.* absorber thickness *II* are shown in Fig. 2 for types 1, 2, 3, 4 and in Fig. 3 for types 5 and 6.

As discussed in Section I, because of the simplicity of the triggering coincidence, a sizeable percentage of background showers due to μ-mesons is expected. The curves in Fig. 4 have been corrected for this background by the method described in Section IIIB. Note that the coincidence rate $A^1B^1C^{>7}$ requires no correction, and that the mean free path from this curve is very close to that calculated from the geometric cross section.

It is found in Section VA that a large percentage of the showers observed have mostly short range secondaries. The following experiment was performed in order to find a separate mean free path for the primaries of these showers. Absorbers *II* and *III* were made 6 in. and $1\frac{1}{2}$ cm of lead respectively, while absorber *I* was varied from 0 to 8-in. lead. The coincidences $A^1B^1C^{>2}$ should be largely due to showers with secondaries of range less than $1\frac{1}{2}$-cm Pb, and $A^1B^{>1}C^{>2}$ should be caused by showers with 3 or more secondaries of range greater than $1\frac{1}{2}$-cm Pb. The results of this experiment, after correction for showers caused by μ-mesons, may be seen in Fig. 5.

It seems that the primary particles of the showers with mostly short range secondaries show a very long mean free path, 360 g/cm² of lead. This is in approximate agreement with measurements of absorption of star-producing radiation in lead ($\lambda = 300$ g/cm², see Bernardini *et al.*[6]) which supports our belief that the penetrating showers with short range secondaries are essentially the same as high energy stars.

In conclusion, there seems to be little doubt that the measured mean free path of the primary particles increases with decreasing energy of the primary. However the presence of many showers with mostly short range secondaries means that there is the possibility of having the primary interact in the absorbing layer without the interaction being detected. Therefore, particularly for the smaller showers, we may no longer be measuring the mean free path for shower production, but rather the mean free path for absorption of the primary. The same is probably true of the experiments of Tinlot and Gregory,[7] and Cocconi,[2] particularly for thick absorbers.

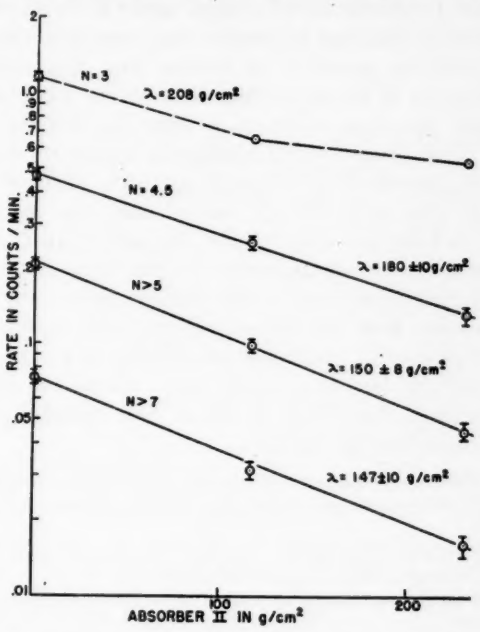

FIG. 4. Rate $A^1B^1C^N$ *vs.* thickness of absorber *II*. Corrected using $\Delta = 1.50$.

B. Ratio of Charged to Neutral Primaries

The purpose to this experiment was to establish the relative number of charged and neutral particles producing penetrating showers. The experimental procedure was as follows.

Keeping eight inches of lead in position *III* fixed, two inches of lead were moved from position *II*, just below the counter tray *A*, to position *I*. We shall denote this lead by *M*. The counting rate of the coincidence $A^{>0}B^{>1}C^{>2}$—A.S. was taken for the two positions of *M*, and the rates were corrected for showers produced by μ-mesons.

¶ We are primarily interested in that for shower production, but the two effects are not separable with this experiment.

[6] Bernardini, Cortini, and Manfredini, Phys. Rev. **74**, 845 (1948).

[7] J. Tinlot and B. Gregory, Phys. Rev. **75**, 519 (1949).

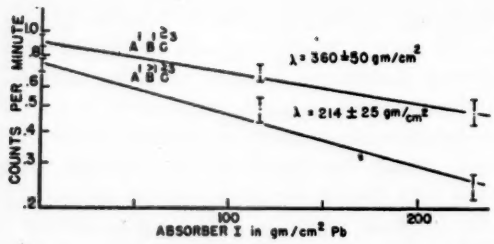

FIG. 5. Corrected absorption curves (I variable, II=6 in. III=1.5-cm Pb). Corrected using Δ=1.50.

When M is in position II, showers originated in it by neutral particles will not be recorded unless the neutral particle is accompanied by one or more charged particles which strike row A, or unless a back projected charged particle produced in M strikes row A. With M in position I, charged primaries may produce showers that will be recorded as before, but also showers produced in M by neutral particles will be recorded.

There are three sources of error in this method. First, there was a slight change in geometry for the showers produced by charged particles when M was moved. The layer, M, was moved only four inches in order to keep this effect small. Second, because of the fact that the two measurements were, of course, taken at different times, barometric changes might influence the results. For this reason, several runs were made with the lead in each position. Third, it was noticed that with no lead in I and II some showers appeared to originate above row B. These were thought to be from the following causes:

(1) Particles producing, in addition to a shower starting in absorber III, one or more knock-on electrons striking counters in row B.

(2) Single primary particles striking two or more counters in row B because of large angle of incidence.

(3) Particles starting a shower in the counter walls or wood above B.

(4) Showers starting in III with back projected particles striking row B.

Since we are interested only in showers actually beginning in II a correction must be made for these four types of events.

As the absorber II is increased, the number of showers starting in III is decreased, and likewise it was estimated that the number of background events is decreased in the same proportion. Then

$$F=\frac{\text{rate } A^1B^{>1}C^{>2}}{\text{rate } A^1B^1C^{>2}} \quad (I=0,\ II=0,\ III=\text{8-in. Pb})$$

gives the fraction which the rate $A^1B^{>1}C^{>2}$ caused by background events (1), (2), (3), and (4) is of the rate $A^1B^1C^{>2}$ for any amount of lead in II. To show that this fraction is essentially constant for any amount of lead in II, we consider how the various events listed above are affected by increasing absorber II.||

|| As noted above, the correction for knock-ons due to μ-mesons has already been made.

The fraction, rate (1)/rate ($A^1B^1C^{>2}$) may increase because of the additional material in which knock-ons can be generated, but the increase must be slight because saturation for the production of knock-ons is known to occur at very small thicknesses, and the material above row B was never less than the counter walls of row A (1 g/cm²) plus two wooden shelves (2 g/cm²), almost enough for saturation.

The zenith angle dependence of the primaries has been measured (see Zenith Angle Dependence) and found to be very steep, so that background due to events of type (2), and particularly the variation of this type of background, is negligible.

The background effects of types (3) and (4) would be expected to decrease in the same proportion as $A^1B^1C^{>2}$. (We assume that the addition of a small amount of lead** in II will not produce much change in the shape of the energy spectrum of the primaries.) We expect (4) to be a large effect because Cocconi and Tongiorgi[8] have found that there is an increase of 30 percent in their counting rate of penetrating showers when a ½-inch lead absorber is placed beneath their detecting apparatus.

To summarize, because Cocconi and Tongiorgi have shown that a large effect due to back projected particles does exist, and because (2) is negligible and the change

TABLE IV. Absorption of primary particles.

Absorber: I=0, II variable, III=8-in. Pb

Uncorrected Echo Lake data

Absorber II	Coincidence rate (min.$^{-1}$)		
	$A^1B^1C^3$	$A^1B^1C^{4,5}$	$A^1B^1C^{>5}$
0	1.63±0.025	0.614±0.018	0.233±0.008
4-in. Pb	1.13±0.02	0.404±0.012	0.123±0.004
8-in. Pb	1.01±0.02	0.287±0.008	0.070±0.003

Corrected Echo Lake data

Absorber II	$A^1B^1C^3$	$A^1B^1C^{4,5}$	$A^1B^1C^{>5}$
0	1.15±0.025	0.462±0.018	0.208±0.008
4-in. Pb	0.65±0.02	0.252±0.012	0.098±0.008
8-in. Pb	0.53±0.02	0.135±0.008	0.045±0.003

Absorber: I variable, II=6-in. Pb, III=1½-cm Pb

I=0	$A^1B^1C^{>2}$ (min.$^{-1}$)	$A^1B^{>1}C^{>2}$ (min.$^{-1}$)
Echo Lake	1.76±0.05	1.17 ±0.04
Ithaca	0.64±0.02	0.347±0.02
Ratio, EL/I	2.76	3.35

Uncorrected Echo Lake data

Absorber I	$A^1B^1C^{>2}$	$A^1B^{>1}C^{>2}$
0	1.76±0.05	1.17 ±0.04
4-in. Pb	1.53±0.05	0.925±0.05
8-in. Pb	1.32±0.06	0.67 ±0.03

Corrected Echo Lake data

Absorber I	$A^1B^1C^{>2}$	$A^1B^{>1}C^{>2}$
0	0.91±0.05	0.73 ±0.04
4-in. Pb	0.68±0.05	0.49 ±0.05
8-in. Pb	0.47±0.06	0.24 ±0.03

** Absorber II was never more than 2-in. Pb when this correction was used.

[8] G. Cocconi and V. C. Tongiorgi (private communication).

in (1) is probably small, we shall use the correction, as outlined above, treating it as a constant fraction, F, of the showers starting below row B. We now calculate F from the data given in Table I.

$$F=\left[\frac{\text{rate } A^1B^1C^{>2}}{\text{rate } A^1B^1C^{>2}}\right]^{\dagger\dagger}=\frac{0.38}{1.82}=0.21.$$

$$I=0$$

$$II=0$$

$$III=\text{8-in. Pb.}$$

The results of the experiment, after correction, are given in Table V.

In interpreting these data we must first consider the possibility that showers produced by neutral particles may occasionally be recorded when M is in position I by (a) being accompanied from the air by a charged particle that strikes row A; (b) producing a back-projected particle that strikes row A.

The column +A.S. in Table V indicates that probably less than 10 percent of the penetrating showers were accompanied by air showers. Previous investigators (Cocconi and Greisen,[9] Treat and Greisen,[10] Tinlot,[1] and Tinlot and Gregory[7]) have also found that only a few percent (less than 5 percent) of the penetrating showers are associated with air showers.

We estimate the effect of (b) by noting that such events would also produce a decrease in the rate $A^1B^1C^{>2}$, when absorber M is moved from position I to position II. The only other effect which might change the rate, the production in M of a single charged primary by a neutral primary, would also make the rate decrease when M was moved from I to II. Therefore the difference between the two rates, which from Table V is 0.02 ± 0.04 min.$^{-1}$, is an upper limit on the rate of these coincidences produced by events of type (b).

Since these two effects are small, it is assumed that

$$R=\left[\frac{\text{rate } (A^{>0}B^{>1}C^{>2}),\ M \text{ in } I,\ II=0,\ III=\text{8-in. Pb}}{\text{rate } (A^{>0}B^{>1}C^{>2}),\ I=0,\ M \text{ in } II,\ III=\text{8-in. Pb}}\right]_{\text{corrected}}=\frac{N+C}{C},$$

where N = number of showers produced in M by neutral particles, and C = number of showers produced in M by charged particles. From Table V,

$$(N+C)/C=R=1.87\pm0.2;\quad \text{and}\quad N/C=0.87\pm0.2.$$

If the neutral and charged particles have the same cross section for interaction, then the ratio N/C represents the ratio of the number of neutral and charged primaries of the penetrating showers. The results indicate that the numbers of charged and neutral primaries are about equal.

It was mentioned above that two effects, back projected charged particles from neutral primaries, and production in M of single charged primaries, would cause a decrease in the rate of $A^1B^1C^{>2}$ when M was moved from I to II. The small change in this rate is also interesting because it sets an upper limit on the second effect. Actually the small difference might be explained in terms of showers too small or too narrow to be detected by the top rows of counters, so it is concluded that the transition $N\rightarrow P$ without penetrating shower production probably does not occur for neutrons of sufficient energy to produce a penetrating shower.

The fact that there are such large numbers of neutral particles capable of producing penetrating showers seems to indicate some sort of heavy particle cascade phenomenon occurring in air. This experiment shows that it may be difficult to interpret absorption experiments (particularly in air) directly in terms of interaction cross sections.

TABLE V. Charged *vs.* neutral primaries.

Uncorrected Echo Lake data

Absorber (Pb)			Coincidence rate (min.$^{-1}$)		
I	II	III	$A^1B^1C^{>2}$	$A^{>0}B^{>1}C^{>2}$−A.S.	+A.S.
0	2 in.	8 in.	1.95±0.03	0.55±0.02	0.16±0.02
2 in.	0	8 in.	1.97±0.05	0.76±0.04	0.18±0.02
0	8 in.	8 in.	1.32±0.04	0.38±0.02	0.08±0.01
2 in.	6 in.	8 in.	1.38±0.03	0.54±0.02	0.11±0.01

Echo Lake data corrected for μ-meson background

I	II	III	$A^1B^1C^{>2}$	$A^{>0}B^{>1}C^{>2}$−A.S.	Difference
0	2 in.	8 in.	1.30±0.03	0.52±0.02	
2 in.	0	8 in.	1.32±0.03	0.73±0.04	0.21±0.05
0	8 in.	8 in.	0.67±0.04	0.35±0.02	
2 in.	6 in.	8 in.	0.73±0.03	0.51±0.02	0.16±0.04

(1) $F\times1.31=0.21\times1.31=0.275$ min.$^{-1}$*

(2) $\frac{N+C}{C}=\frac{0.73-0.275}{0.52-0.275}=1.87\pm0.2$

* Background number of showers that appear to originate between tray A and tray B even when the material M is absent.

C. Zenith Angle Dependence

Using the apparatus as an array of counter telescopes, the primary particle zenith angle, projected on a vertical plane, was measured. Greisen[11] has shown that if the zenith angle distribution is of the form $\cos^n\theta$, then the projected zenith angle distribution is of the form $\cos^n\theta_{\text{proj}}$. We expect this type of distribution if the charged particles producing showers have come undeviated through the atmosphere from outer space, or if, in case they are the progeny of a cascade phenomenon

†† Corrected for showers produced by μ-mesons.

[9] G. Cocconi and K. I. Greisen, Phys. Rev. **74**, 62 (1948).

[10] J. E. Treat and K. I. Greisen, Phys. Rev. **74**, 414 (1948).

[11] K. I. Greisen, Phys. Rev. **61**, 212 (1942).

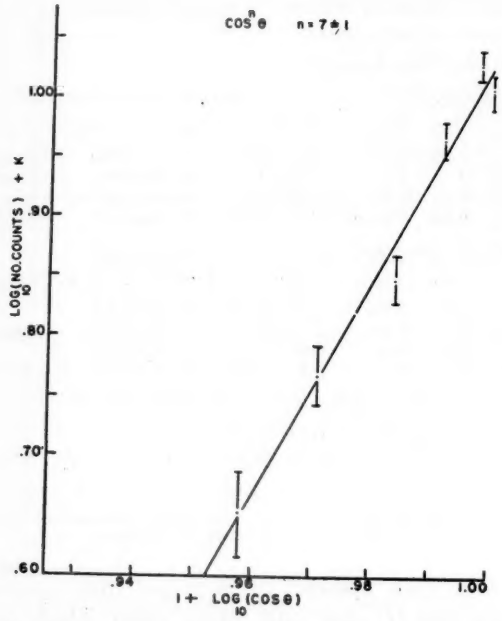

FIG. 6. Zenith angle dependence of primaries producing coincidences $A^1B^1C^{>3}D^{>1}$ (at Echo Lake).

(see Ratio of Charged to Neutral Primaries), they maintain the initial direction. The zenith angle distribution would then be of the form $\exp[-l/\lambda\cos\theta]$, l being the depth of the atmosphere, and λ the mean free path for disappearance. It will be noticed that $\exp[-n/\cos\theta]\approx e^{-n}\cos^n\theta$ for $n\leq 8$, $\theta\leq 30°$.

$A^1B^1C^{>3}D^{>1}$‡‡ was selected as the coincidence to be studied for two reasons. First, A^1B^1 was necessary in order that the direction be determined. Second, a complex event was chosen to insure smaller background due to showers produced by μ-mesons. The corresponding rate was not measured in Ithaca, and no correction for meson-produced showers was made.

The number of primaries from each direction was multiplied by a weighting factor determined by the following geometrical considerations:

(1) The number of telescopes available decreases with angle. (Telescopes whose inclination and position were such that the secondaries might miss the bottom row were not counted.)

(2) Counters forming large angle telescopes are farther apart.

(3) Inclined particles may go through two counters in a given row, and will sometimes not be counted in this measurement. This decreases the area of the telescope by a factor of $(2\cos\theta-1)\approx\cos^2\theta$. This correction was reduced slightly because the sensitive areas of the counters were not immediately adjacent.

The weighted results of this tabulation are shown in Fig. 6. The zenith angle dependence is seen to be $\cos^7\theta$, and since $l=700$ g/cm² at Echo Lake, this gives $l/\lambda=7$; $\lambda=100$ g/cm² as the mean free path for absorption of the primaries in air.

In Figs. 7, 8, and 9 are plotted the zenith angle distributions of the primaries for the simplest type of coincidence (uncorrected), i.e., $A^1B^1C^3$, for $I=II=0$, $III=8$-in. Pb at Echo Lake (Fig. 8), for $I=0$, $II=8$-in. Pb, $III=8$-in. Pb at Echo Lake (Fig. 7), and for $I=II=0$, $III=8$-in. Pb at Ithaca (Fig. 9). From Greisen's measurement[11] we expect the zenith angle distribution for μ-mesons to be approximately $\cos^2\theta$, or likely even less steep because only mesons of energy above 10^9 ev produce such showers with much probability. We see that the zenith angle distributions for this simple event are not as sharp as for the more complex one shown in Fig. 6, and also that the curve becomes less steep with more absorber, either air or lead, above the apparatus. This is what we expect if

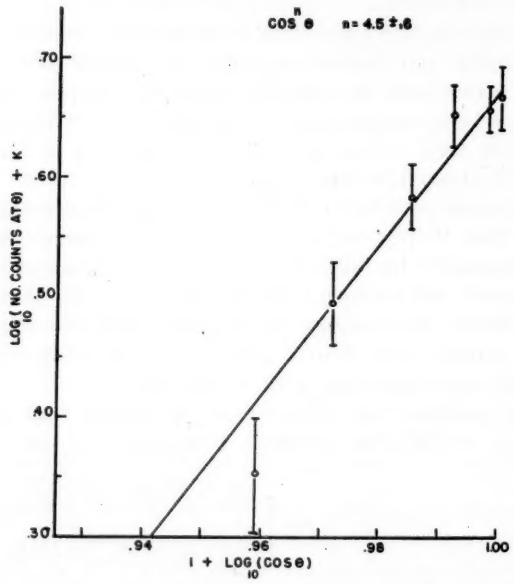

FIG. 7. Zenith angle dependence for primaries producing coincidences $A^1B^1C^3$ ($I=0$, $II=8$ in., $III=8$-in. Pb, at Echo Lake).

part of these coincidences are the result of meson-produced showers, although a real variation of the mean free path of the N component with energy may be a contributing factor. However, these results do show that even the simplest coincidence at Ithaca, or with the maximum amount of lead on the apparatus at Echo Lake, was not entirely background caused by knock-ons of μ-mesons. The fraction, α, of the coincidences $A^1B^1C^3$, $I=II=0$, $III=8$-in. Pb, caused by μ-mesons is known approximately, so one may attempt to correct the zenith angle curves for this background by subtracting $\alpha\cos^2\theta$ from the curve. The results of this subtraction give a curve (see Fig. 10) which is of the form $\cos^{7.3}\theta$. This is in agreement with the zenith angle dependence for the more complex showers that were not corrected for showers produced by μ-mesons. As mentioned above, a zenith angle dependence of $\cos^{7\pm1.2}\theta$ implies a mean free path in air of 100 ± 17 g/cm². This value of λ is somewhat smaller than that obtained by Tinlot[1] (118 ± 2 g/cm²) but the difference

‡‡ Also coincidences were accepted in which 3 counters were struck in row C, but with at least one counter separated from the other two by one counter space.

is within the statistical errors of the present measurements.

V. PROPERTIES OF THE SECONDARY PARTICLES

A. Range and Identity

In order to study the absorption of the secondary particles, one would like to observe the variation in the number of secondaries penetrating a lead absorber of variable thickness, these particles having been produced in a thin generator above the absorber. Actually we measured the rate of coincidence $A^1B^{>1}C^{>2}$, corrected for showers produced by μ-mesons, with $I=0$, $II=6$ in., and III variable. We assume that in this arrangement II is the generator and III is the variable absorber.

It is necessary to point out that there is an uncertainty of 6-in. Pb in the absorber thickness because of the thickness of the generator. However the *increase* in absorber thickness upon addition of absorber in position III is known accurately. If the absorption were exponential the effect of a given increase in the

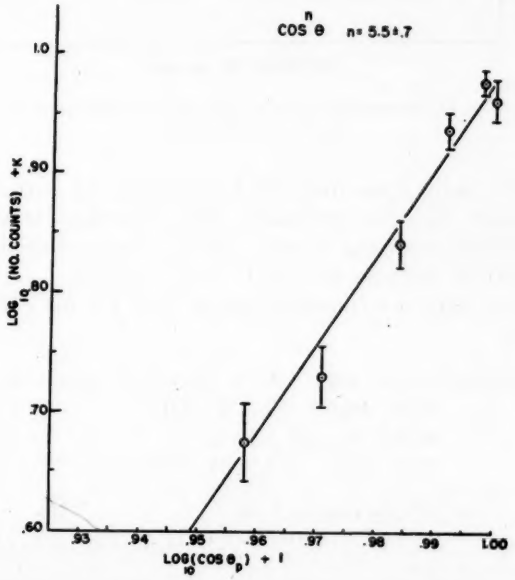

FIG. 8. Zenith angle dependence for primaries producing simple coincidences $A^1B^1C^2$ ($I=0$, $II=0$, $III=8$-in. Pb at *E.L.*).

absorber thickness would be to produce the same fractional decrease in counting rate, regardless of the initial thickness. Therefore the use of a thick generator does not change the shape of an exponential absorption curve, but merely changes the position of the zero point. Also, as mentioned in Neutral *vs.* Charged Primaries, back projected secondaries can produce coincidences of this type. Cocconi and Tongiorgi¶¶ have found that such particles have a very short mean range ($\frac{1}{2}$ in.–$\frac{1}{4}$-in. Pb), so that this effect should be constant after the addition of the first $\frac{1}{2}$-inch of absorber in position III. In the first $\frac{1}{2}$ inch of absorber III some shower production will make the apparent absorption a little too small.

The curves, both uncorrected and corrected for background showers produced by mesons, are given in Fig. 11.|| || The corrected curve has several interesting features. The first of these is the presence of many short range particles. The second feature is that the curve seems to have two distinct types of secondaries, one type having short range and another having long range.

The identity of the short-range secondaries is a point of interest. There are several possibilities:

a. Slow mesons
b. Electrons
c. Nuclear fragments (protons, α's, etc.)

We now consider the first possibility. From the range curve given in Fig. 11 it is seen that most of the short range component is absorbed out in 2–3 inches of lead. If III=8-in. Pb, only showers producing coincidences $A^1B^1C^{>2}$ (i.e., showers starting in III), can have short range secondaries capable of reaching row D. On the other hand, showers with long range secondaries could produce coincidences $A^1B^1C^{>2}$ or $A^{>0}B^{>1}C^{>2}$. The probability of stopping in the aluminum about D, having reached row C, is greater for a short range secondary than for a long range one. If the short range component and the long range component are each composed of about the same fraction of mesons, we would expect the coincidences $A^1B^1C^{>2}$ to be accompanied very much more often by delayed counts than coincidences $A^{>0}B^{>1}C^{>2}$. In Table VI is a comparison of rates with and without delayed counts.

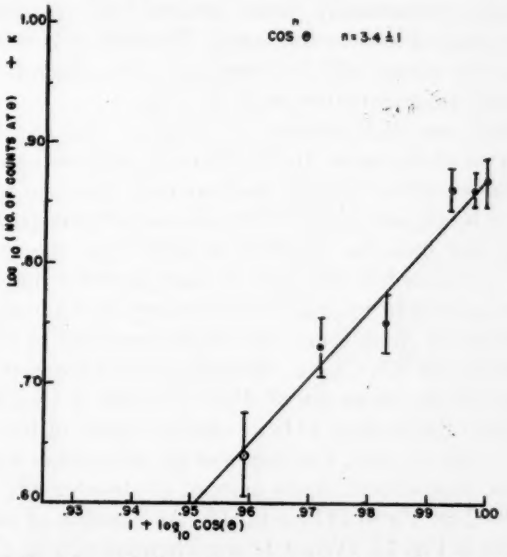

FIG. 9. Zenith angle dependence of primaries producing coincidences $A^1B^1C^{>2}$ ($I=II=0$, $III=8$-in. Pb at Ithaca).

¶¶ The author wishes to thank Drs. G. and V. T. Cocconi for communicating their results to him.

|| || As noted on the curve, the point $III=0$ was obtained from another coincidence, $A^1B^1C^{>2}$, with a different disposition of lead ($I=II=0$, $III=8$ in.). Consequently, this point gives only the order of magnitude.

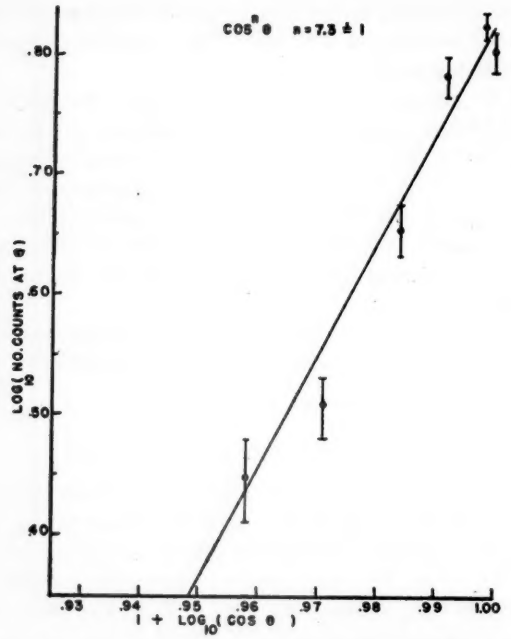

FIG. 10. Corrected zenith angle dependence for primaries producing coincidences $A^1B^1C^3$ ($I=II=0$, $III=8$-in. Pb at Echo Lake).

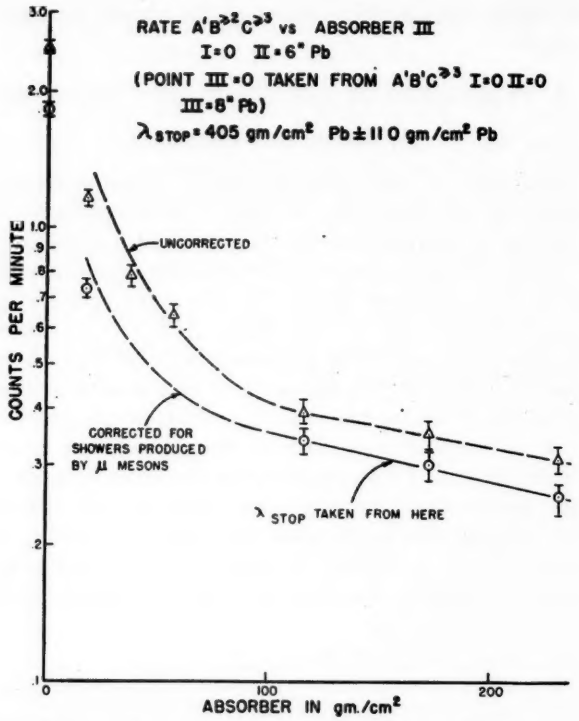
RATE A'B≥2C≥3 vs ABSORBER III
I=0 II=6" Pb
(POINT III=0 TAKEN FROM A'B'C≥3 I=0 II=0
III=8" Pb)
λSTOP=405 gm/cm² Pb ± 11 0 gm/cm² Pb
UNCORRECTED
CORRECTED FOR SHOWERS PRODUCED BY μ MESONS
λ STOP TAKEN FROM HERE
COUNTS PER MINUTE
ABSORBER IN gm./cm²

FIG. 11. Absorption of secondary particles produced in penetrating showers.

We see that mesons comprise a much larger fraction of the penetrating secondaries than of the non-penetrating, and that the fraction of the non-penetrating particles which are the mesons is extremely small.

According to Bridge and Hazen,[12] electrons in penetrating showers occur mostly in those of high energy which are much less numerous than showers of lower energy. According to the same authors, the lower energy showers occasionally have mesons but are usually composed of nuclear fragments. Therefore it is thought that the strong initial absorption is the absorption of nuclear fragments from such showers.

Next we shall attempt to interpret the less steep portion of the curve. In the following analysis we make the assumption that for each counter struck in row C there is only one particle.* In a shower of three particles only one must be absorbed in order that the shower not be recorded. Showers of four particles may lose one and still be recorded, etc. To carry such an analysis further we must know the relative number of coincidences $A^1B^{>1}C^3$, C^4, etc., for each value of absorber III. Plotting the frequency of $A^1B^{>1}C^N$ *versus* N ($N\geqslant 3$) for a given thickness of III, we obtain a curve of the form $N^{-\gamma}$ with $\gamma=2.67$. The slopes of all such curves seemed to be independent of the amount of absorber III from $III=2$-in. Pb to $III=8$-in. Pb. An example of such a curve is Fig. 12. (When II was changed to 6-in. C, the value of γ was unchanged.)

[12] H. Bridge and W. Hazen, Phys. Rev. **74**, 579 (1948).

* The validity of this obviously depends on the geometry of the showers. By limiting our analysis to the smallest showers we hope that this condition will be more nearly fulfilled.

If λ_s is the mean free path for stopping of a secondary particle, then the probability that 3 particles traverse x without stopping is $\exp[-3x/\lambda_s]$. The probability of a particle stopping in x is $(1-\exp[-x/\lambda_s])$.

Let $N(K, x)$ = counting rate of $A^1B^{>1}C^K$ for $III=x$. Then

$$\begin{aligned}N(3,x)&=N(3,0)\exp[-3x/\lambda_s]+N(4,0)\exp[-3x/\lambda_s]\\&\quad\times[1-\exp[-x/\lambda_s]]4!/3!1!\\&\quad+N(5,0)\exp[-3x/\lambda_s]\\&\quad\times[1-\exp[-x/\lambda_s]]^2 5!/3!2!+\cdots\\&=N(3,0)\exp[-3x/\lambda_s]\\&\quad\times[1+[N(4,0)/N(3,0)]4[1-\exp[x/\lambda_s]]\\&\quad+\cdots\\&\approx N(3,0)\exp[-3x/\lambda_s][1+4(3/4)^2 x/\lambda_s+\cdots]\\&\approx N(3,0)\exp[-3x/\lambda_s][1+2x/\lambda_s+\cdots]\\&\approx N(3,0)\exp[-x/\lambda_s].\end{aligned}$$

Consequently λ_s for a secondary particle is obtained directly from the slope of the graph in Fig. 12 and is approximately 405 g/cm². This sets an upper limit on the true value of λ_s because one counter discharge may correspond to more than one particle striking the counter.

Of the coincidences $A^1B^{>1}C^{>2}$, about one in 150 showed a delayed count (see Table VI). From the absorption curve one expects about one particle in seven to stop in the aluminum surrounding the counters of tray D. Calculating the efficiency of the detecting

TABLE VI. Comparison of total coincidence rate with that accompanied by delayed counts.

	$I=0$, $II=2$-in. Pb, $III=8$-in. Pb	
Coincidence	$(A^{>0}B^{>1}C^{>2})$ corr.	$(A^{1}B^{1}C^{>2})$ corr. (for μ-mesons)
Total rate	0.52 ± 0.02 min.$^{-1}$	1.31 ± 0.03 min.$^{-1}$
$+D$ delay	0.0035 ± 0.0008 min.$^{-1}$	0.0049 ± 0.001 min.$^{-1}$
Mesons per coincidence	1/150	1/270

system for decay electrons (taking into account capture, geometrical loss, time loss) we get 1/43. However, some of the counters of tray D will be struck by the shower particles, making them insensitive to delayed electrons. This decrease in efficiency for recording delayed counts has been estimated to be a factor of 2.†

Consequently,

$$1/150=\bar{N}_\pi/(2\times43\times7)$$
$$\bar{N}_\pi=4.$$

$\bar{N}_\pi$=average number of mesons incident on tray D in a shower producing a coincidence of the form $A^1B^{>1}C^{>2}$.

Piccioni[13] has shown that all, or nearly all, of the mesons produced in penetrating showers are π-mesons. In the calculation of the efficiency of the detecting system it was assumed that there are equal numbers of $\pm\pi$-mesons. The average energy of the decay electron was assumed to be about 40 Mev. As a result of possible errors in these assumptions and in other approximations made in this calculation the results could be wrong by a factor of at most 2.

In coincidences of the type selected above, on the average, four counters were struck in row C. As these coincidences are thought to be caused by showers of four particles penetrating 8 inches or so of lead, the above analysis would indicate that a large fraction of the particles stopping are π-mesons.

Since most of the long range secondaries are π-mesons, the flat portion of the range curve is approximately the integral range spectrum of π-mesons at production. Sands[14] has fitted the altitude variation of slow mesons by assuming the integral range spectrum at the point of production to be of the form $(R+\beta)^{-\alpha}$. The flat portion of the absorption curve in Fig. 11 may be fitted by this expression with the following values of β and α.

$$\alpha=1.6,\quad \beta=310\ \text{g/cm}^2\ \text{Pb}$$
$$\alpha=1.7,\quad \beta=460\ \text{g/cm}^2\ \text{Pb}.$$

† Because decay electrons have a short range (a 40-Mev electron has an average range of about 2 in. in Al), the electron from a meson is most apt to be detected near the point of stopping. In an average shower one or two counters will be struck in row D. If a meson of the shower stops, it will probably stop close (within 3 or 4 inches) to the counter struck. The decay electron can at most reach 4 counters in this region, and if two of the counters are dead then the probability of a delayed count being recorded is reduced by one-half.

[13] O. Piccioni, Bull. Am. Phys. Soc. 75, 1281 (1949).

[14] M. Sands, M.I.T. thesis (1948).

Sands' values were as follows:

$$\alpha=1.9,\quad \beta=350\ \text{g/cm}^2\ \text{Pb}\ (200\ \text{g/cm}^2\ \text{air}).$$

The agreement with the production spectrum of the mesons in the atmosphere indicates that the penetrating showers (and the subsequent π-μ-decays) are probably the mechanism of origin of the μ-mesons. Moreover, the small absorption indicates that π-mesons of moderate or low energy are not stopped by nuclear interactions, in agreement with the conclusion of Piccioni (reported at New York meeting of Physical Society in 1948 and at Echo Lake Conference in June, 1949). π-mesons may, however, have nuclear interactions in which they are not stopped.

C. Angular Spread

In studying the angular distribution of the secondary particles, the direction of reference is naturally the direction of the primary particle. To define an angle precisely we must also know the starting point of the shower. Therefore, it is difficult to obtain precise information because this apparatus has only three full rows of counters.

In this investigation we have chosen to use the coincidences $A^1B^{>2}C^{3,4,5}$ with absorbers $I=0$, $II=4$ in.

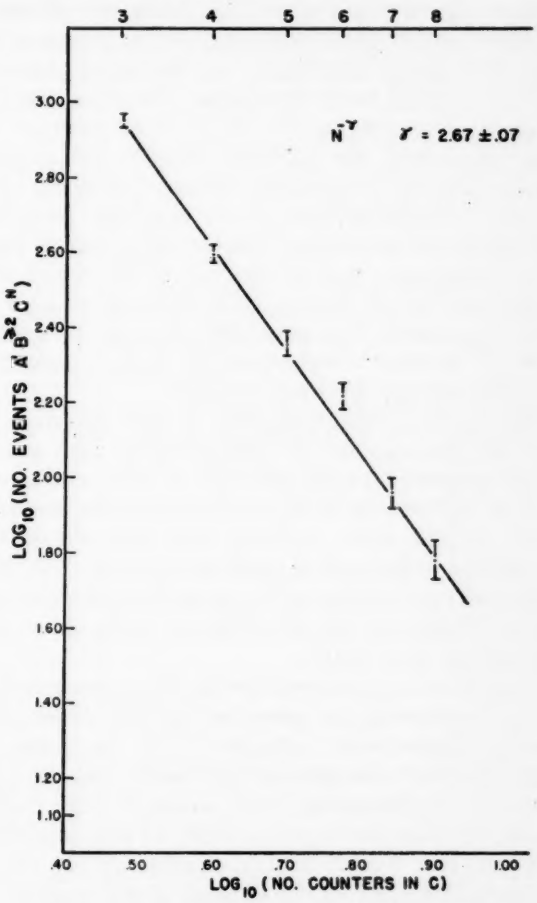

FIG. 12. Relative frequency of $A^1B^{>1}C^N$ vs. N.

TABLE VII. Range of secondaries.

Type of coincidence	Absorber (Pb) *I*	*II*	*III*	Rate Echo Lake (min.$^{-1}$)	Rate (min.$^{-1}$) Ithaca	Rate Echo Lake / Rate Ithaca	Fraction due to μ-mesons	Corrected rate (Echo Lake) (min.$^{-1}$)
$A^1B^1C^{>\frac{1}{2}}$	0	0	8 in.	2.52±0.03	0.61 ±0.02	4.13	0.272	1.83±0.03
$A^1B^{>1}C^{>\frac{1}{2}}$	0	6 in.	1.5 cm	1.17±0.04	0.35 ±0.02	3.35	0.378	0.73±0.04
$A^1B^{>1}C^{>\frac{1}{2}}$	0	6 in.	8 in.	0.31±0.02	0.058±0.007	5.35	0.176	0.26±0.02
$A^1B^{>1}C^{>\frac{1}{2}}$	0	6 in.	6 in.	0.35±0.02	0.058±0.007	6.04	0.142	0.30±0.02
$A^1B^{>1}C^{>\frac{1}{2}}$	0	6 in.	4 in.	0.39±0.015	0.058±0.007	6.7	0.115	0.34±0.02
$A^1B^{>1}C^{>\frac{1}{2}}$	0	6 in.	2 in.	0.64±0.03	No exp.			
$A^1B^{>1}C^{>\frac{1}{2}}$	0	6 in.	1¼ in.	0.78±0.05	No exp.			

and *III*=8-in. Pb. The origins of the showers were thereby located in absorber *II*, 13 in.±2 in. above row *C*. The angular separations of the penetrating secondaries were indicated by the counters struck in row *C*, while the reference direction or shower axis was determined by the line joining the counter struck in row *A* with the center of the group of counters struck in *B*.

Several features of this measurement should be noted. First, the angular distribution is obtained only for those secondaries capable of penetrating at least the 8-in. Pb in absorber *III*. Second, the results are limited to small showers (3 to 5 counters struck in row *C*), so that there should not be too much likelihood of several particles crossing a single counter, although some such effect undoubtedly occurs and tends to make the observed average angular spread too large. Third, it is possible that the angular distribution in the larger showers, which in general must have higher primary energy, is different from the angular distribution observed in these showers of few particles. Fourth, the angular interval defined by a counter in row *C* is pretty well known (0.08±0.013 radian), so that the projected angular spread between two secondaries does not have great uncertainty; but the direction of the shower axis is not very certain because more than one counter in row *B* is struck. This error, like that due to several particles crossing a single counter, tends to make the observed average deviation too large.

The results of this tabulation of data are given in Fig. 13. The number of times counters were struck when separated by n counters (i.e., $n-\frac{1}{2}$ to $n+\frac{1}{2}$) from the axis of the shower is plotted against the displacement, n. The curve indicates that the penetrating secondaries (those which traverse at least 8-in. Pb) show a strong tendency to be in the forward direction, although some do go off at large angles from the direction of the primary.

These data, as explained above, set an upper bound on the average angular spread on the secondaries. The average displacement, measured from the curve, is approximately 2 counters or 0.17 radian. Because only projected displacements were measured, this value should be multiplied by $\sqrt{2}$, so that we may say from this data that $\bar{\theta}<0.25$ radian. Considering the errors discussed above, $\bar{\theta}$ could be as small as 0.15 radian.

Assuming that the penetrating secondaries are mesons, in order to traverse eight inches of lead they must have momentum, p, greater than $3\mu c$ (where μ is the meson mass), and $\mu c/p$ must be less than 0.33. If the average angular divergence were of the order of $\mu c/p$,‡ then $\bar{\theta}<0.33$ radians. If, on the other hand, the angles of the secondaries were distributed uniformly in the center of mass system, velocities being greater than that of the center of mass, then $\bar{\theta}\approx(2M/E_0)^{\frac{1}{2}}$.¶ ($M$ and E_0 are the mass and energy of the primary.) Assuming the primaries to be protons, and setting 10^{10} ev as an upper limit on their average energy, we obtain $\theta\geqslant(2\times1/10)^{\frac{1}{2}}=0.45$ radians. We see that the second assumption is not consistent with these data, but that the data are consistent with smaller angular spreads, of the order of $\mu c/p$.

B. Mesons Produced Locally

The purpose of this part of the experiment was to estimate the number of low energy mesons locally

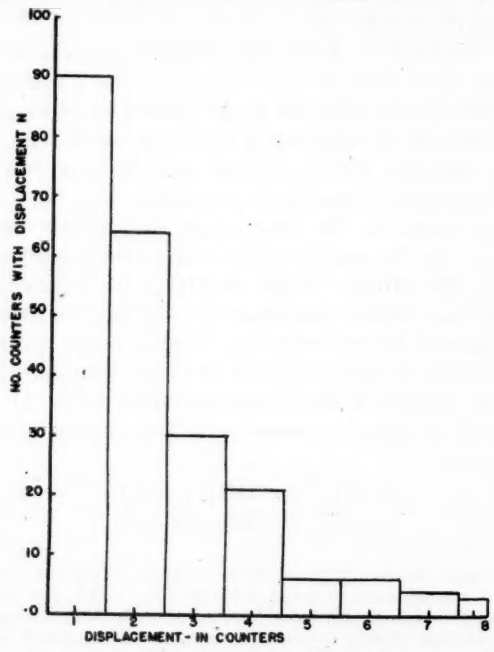

FIG. 13. Histogram. No. counters struck with displacement N *vs.* N, displacement from center of shower.

‡ According to the scalar theory of mesons. See Lewis, Oppenheimer, and Wouthuysen, Phys. Rev. 73, 127 (1948).

¶ According to the symmetric pseudoscalar theory (Lewis, Oppenheimer, and Wouthuysen, Phys. Rev. 73, 127 (1948)).

produced, relative to the number of μ-mesons arriving from the air and stopping. The apparatus was triggered on the coincidence $A^{>0}B^{>0}C^{>0}+D_{\text{delayed}}$ (between 1 and 4 μ-seconds). Using a delay discriminator, the lifetime of the meson was continuously checked (see Fig. 14).

Any simple coincidence, $A^1B^1C^1+D$ delayed, with the counters A, B, and C approximately in line, was attributed to a μ-meson arriving from the air. (Only in $\frac{1}{2}$ percent of the cases was there scattering which could not be accounted for by multiple scattering.) The next simplest coincidence, with two adjacent counters struck in any one row, could be the result of either local shower production, or a μ-meson plus a knock-on, or an inclined μ-meson. Mesons which stop in the apparatus have a very small probability of producing an energetic knock-on.[4] (See IIIB.) A calculation of the probability that any two adjacent counters will be struck by a single meson gives about 0.03 per row. This is seen, from Table VIII to be about the frequency of such a coincidence for rows B and C.

Any coincidence more complex than those mentioned above, i.e., two counters separated by one counter or three counters struck, etc., were thought to be caused by local shower production. A meson that stops in the aluminum could hardly be the primary of such an energetic shower; hence the meson must be a secondary particle produced in the shower.

The data from this experiment are given in Table VIII.

A coincidence in which several counters were struck in the top row could have been caused by a meson associated with an air shower. With regard to this possibility, it should be pointed out that, although the above data were taken with many different configurations of lead on the apparatus, there was always at least 230 g/cm² distributed between I, II, and III, and for about 85 percent of the experiment this included 57 g/cm² in I. In all, there were some 50 coincidences in which at least two non-adjacent counters were struck in row A. Certainly a large fraction can be accounted for by penetrating showers produced in $I=57$ g/cm² or in the roof above the apparatus, and by back projected particles from II. Therefore, we shall assume that most of these coincidences were caused by local shower production.

In order to find the fraction of the mesons that are produced locally, it is necessary to estimate the relative efficiency for detecting them. The efficiency for detecting mesons in showers is smaller than that for detecting single mesons for several different reasons. We estimate the various components of the efficiency as follows, the relative efficiency being the product of all of them.

TABLE VIII. Mesons produced locally *versus* mesons arriving from outside.

	Single mesons $A^1B^1C^1+D$ del.	Penetrating showers	$A^1B^1C^2$ tog. $+D$ del.	A^1B^2 tog. C_1 $+D$ del.
No. of cases	3490	212	134	88
Percent of total cases	86.3	6.2	3.9	2.6

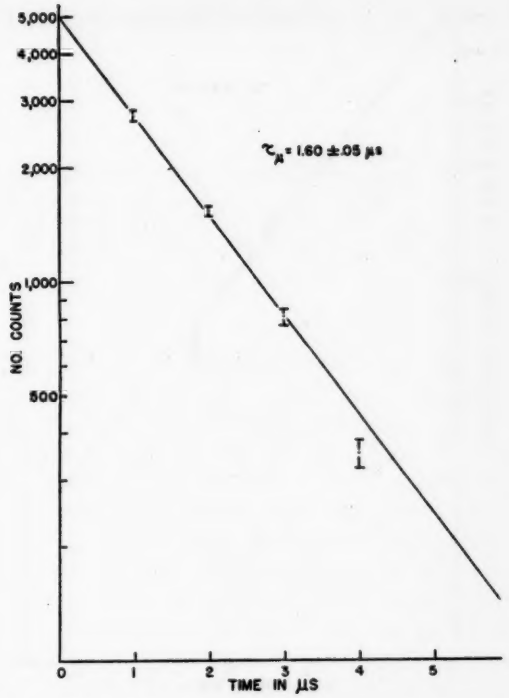

FIG. 14. Integral lifetime curve of mesons in aluminum.

(1) With 57 g/cm² Pb in I the efficiency for detection of the mesons that are produced by neutrons is about $\frac{1}{3}$ that for those produced by charged particles. The ratio of local showers produced by neutral particles to those produced by charged particles is approximately 0.9 from the section above. Therefore the efficiency factor is $1.3/1.9=0.7$.

(2) Since the locally produced mesons are π's, only the positive ones will be detected by π-μ-e-decay, whereas, of the μ-mesons arriving from the air, about $\frac{1}{3}$ of the negative mesons, as well as the positive ones will undergo decay. The factor, taking into account the shorter lifetime of the negative μ-mesons is 0.8.

(3) Because in a penetrating shower, on the average, $1\frac{1}{2}$ counters will be struck in row D, the efficiency for detecting the delay electron is smaller than that for a single meson, which will strike a counter in D with a probability of $\frac{1}{2}$. Since the decay electron can reach only about 4 counters in the region the efficiency factor is about 0.7.

As a result of these three factors, the efficiency for detecting mesons locally produced is $0.7\times0.8\times0.7=0.4$ of the efficiency for detecting mesons arriving singly from the air.

Since the fraction of mesons locally produced, detected by the apparatus, was 0.07, we have

$$\frac{0.07/0.4}{0.93+0.07/0.4}=0.16=\text{the fraction of mesons stopping that are produced locally.}$$

The lifetime curve for mesons arriving from the air is shown in Fig. 14. The lifetime of the mesons produced locally was measured by measuring the delay times

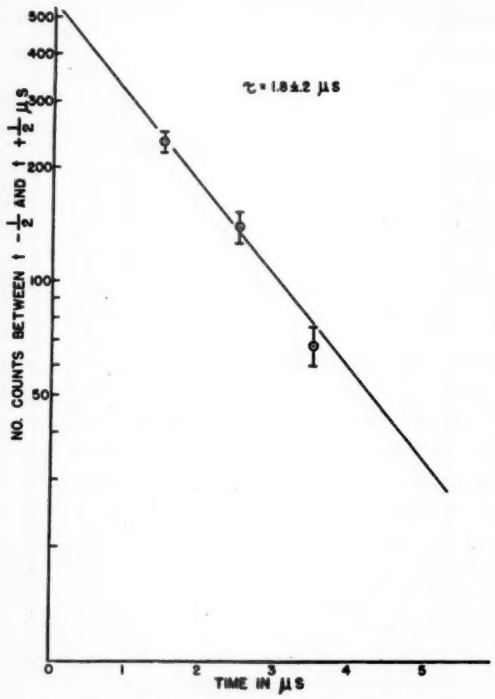

FIG. 15. Differential lifetime curve of mesons in penetrating showers.

associated with $A^{>0}B^{>0}C^{>2}+D$ delay. The differential lifetime curve obtained is given in Fig. 15. We expect a lifetime of about 2.15 μsec. (only π-mesons). The lifetime obtained from this curve is nearer 1.8 (±0.2 μsec. standard error). Repeated checks were made on the circuits, but nothing wrong could be found. The widths of the delay channels were measured and found to be equal to each other to within 5 percent. The reason for this discrepancy is not known at the present time, but the probability of a fluctuation of this magnitude is not very small. Also note that both curves, Fig. 14 and Fig. 15, err in the same direction by roughly the same amount, and that background effects such as that due to chance coincidences would make errors in the opposite direction.

CONCLUSIONS

From the data presented, the following conclusions have been drawn:

1. The mean free path for absorption or shower production of the charged primary particles decreases with increasing primary energy.
2. There are approximately equal numbers of charged and neutral particles producing penetrating showers, and the primary neutrons seldom change to protons without the production of a penetrating shower.
3. The charged primary particles have a very strong zenith angle dependence, indicating a mean free path in air of 100±17 g/cm².
4. There are large numbers of short range secondaries produced in penetrating showers; most of these particles are not mesons and are probably electrons or nuclear fragments (protons, α-particles, etc.).
5. The penetrating secondaries of a penetrating shower are projected mostly in the direction of the primary particle. The angles of divergence could be of the order of $\mu c/p$ if the secondary particles are mesons, μ and p being the mass and momentum of the secondary. A large fraction of these particles, probably almost all, are π-mesons.
6. At Echo Lake an appreciable fraction of the mesons which stop in our lowest absorber are locally produced in the absorbers above it. Considering the production by neutral as well as charged particles and the difference in efficiency of the apparatus for π- and μ-mesons and for single mesons as compared with those occurring in showers, we estimate the fraction of the slow mesons that are locally produced to be about 0.16.

ACKNOWLEDGMENT

The author wishes to thank Professor K. I. Greisen, at whose suggestion this work was undertaken, for his very generous aid, both in planning the experiment and in the analysis and presentation of the data. He also wishes to thank his wife for her help throughout the experiment.

The author is much indebted to Drs. Cohn and Iona of Denver University for their help and for making available the facilities of the Inter-University High Altitude Laboratory. He is grateful to the Research Corporation for a grant which made possible the stay at Echo Lake.

The expense of constructing the equipment was covered by an ONR contract.

A Remark on the Coupling of Gravitation and Electron*

HERMANN WEYL
Institute for Advanced Study, Princeton, New Jersey
(Received November 9, 1949)

In Einstein's theory of gravitation one may consider either the metric potentials g_{ik}, or both the metric potentials and the components of the affine connection, as independent quantities (metric *vs.* mixed theory) in the coupling of gravitational and electronic fields. This makes a difference for the ensuing equations, but one that can be easily straightened out by a slight change of the Lagrangian; see the Theorem at the end of the paper.

ON the level of classical field theory the welding together of Maxwell's electromagnetic, Dirac's electronic and Einstein's gravitational fields (**F**, **E** and **G**) affords no serious difficulty—whatever interpretation quantum physics may impose upon the resulting field equations, and however unsatisfactory a Lagrangian may be that is made up by addition of four separate parts, one for **F**, two for **E**, and one for **G**. The formulation of Dirac's theory of the electron in the frame of general relativity has to its credit one feature which should be appreciated even by the atomic physicist who feels safe in ignoring the role of gravitation in the building-up of the elementary particles: its explanation of the quantum mechanical principle of "gauge invariance" that connects Dirac's ψ with the electromagnetic potentials.

In contrast to Einstein's original "metric" conception in terms of the g_{pq} there was later developed, by Eddington, by Einstein himself, and recently by Schrödinger, an affine field theory operating with the components Γ_{pq}^{r} of an affine connection. But in 1925 Einstein also advocated a "mixed" formulation by means of a Lagrangian in which both the g_{pq} and the Γ_{pq}^{r} are taken as basic field quantities and submitted to independent arbitrary infinitesimal variations.[1] In certain respects this seems to be the most natural procedure. But even when the electromagnetic field is taken into account by adding the Lagrangian characteristic for Maxwell's theory, the resulting equations turn out to be the same as in Einstein's purely metric theory. This ceases to be true for the interaction between gravitation and electron; yet, as I shall show here, coincidence can be reestablished by adding to the Lagrangian one simple term, of a structure not dissimilar to that of the Dirac mass term.

A Cartesian frame E in a four-dimensional orthogonal vector space consists of four linearly independent vectors $\mathbf{e}(\alpha)$ ($\alpha=0, 1, 2, 3$), the transition between any two such ("equally admissible") frames being effected by an orthogonal transformation (rotation). Any vector $\mathbf{v}$ is uniquely representable relative to E in the form $\sum_\alpha v(\alpha)\mathbf{e}(\alpha)$ by its "*ortho-components*" $\mathrm{v}(\alpha)$. The square of the length of the vector $\mathbf{v}$ is the invariant $\sum_\alpha v^2(\alpha)$. We assume the reality conditions characteristic for the Lorentz-Minkowski vector geometry: $\mathbf{e}(1)$, $\mathbf{e}(2)$, $\mathbf{e}(3)$ are real space-like vectors while $\mathbf{e}(0)/i$ is a time-like vector pointing toward the future. An infinitesimal Lorentz rotation $d\mathbf{e}(\alpha)=\sum_\beta do(\alpha\beta)\cdot\mathbf{e}(\beta)$ is defined by a skew-symmetric matrix $\|do(\alpha\beta)\|$ of which the components $\alpha, \beta=1, 2, 3$ are real and the components $\alpha=0$, $\beta=1, 2, 3$ pure imaginary. With respect to the Lorentz frame E the wave function of the electron has four complex components $\psi_1, \psi_2; \psi_3, \psi_4$ which we arrange in a *column* ψ. Let $\bar{\psi}$ denote the *row* of the conjugate-complex numbers $\bar{\psi}_1, \bar{\psi}_2; \bar{\psi}_3, \bar{\psi}_4$ and form the following Hermitian expressions $s(\alpha)=\bar{\psi}S(\alpha)\psi$, $sp(\alpha)=\bar{\psi}Sp(\alpha)\psi$:

$s(\alpha),$ $\quad sp(\alpha)$	α
$i(\bar{\psi}_1\psi_1+\bar{\psi}_2\psi_2)\pm i(\bar{\psi}_3\psi_3+\bar{\psi}_4\psi_4)$	0
$(\bar{\psi}_1\psi_1-\bar{\psi}_2\psi_2)\mp(\bar{\psi}_3\psi_3-\bar{\psi}_4\psi_4)$	1
$(\bar{\psi}_1\psi_2+\bar{\psi}_2\psi_1)\mp(\bar{\psi}_3\psi_4+\bar{\psi}_4\psi_3)$	2
$i(\bar{\psi}_2\psi_1-\bar{\psi}_1\psi_2)\mp i(\bar{\psi}_4\psi_3-\bar{\psi}_3\psi_4)$	3

where the upper signs refer to $s(\alpha)$, the lower to $sp(\alpha)$. The ψ-components transform under the influence of a Lorentz rotation of the frame so as to make $s(\alpha)$ the ortho-components of an invariant vector (charge-current vector). $sp(\alpha)$ are then the components of a pseudo-vector (the spin, which changes sign if left and right in 3-space are interchanged). We make use also of the bilinear expressions $\bar{\psi}S(\alpha)\chi$ in which χ is a quantity transforming cogrediently with ψ. The components ψ are determined but for an arbitrary factor $e^{i\lambda}$, the phase λ of which is a real constant.

The metric field at a given point P in the real four-dimensional world is described by assigning to P a Lorentz-frame $E=E(P)$, but does not change if E is submitted to an arbitrary Lorentz rotation. Let the world around P be referred to (real) coordinates x^p ($p=0, 1, 2, 3$). The prototype of a "vector at P" is the line element joining the point P, coordinates x^p, with an infinitely near point P', coordinates x^p+dx^p. The coordinate increments dx^p are the *contravariant components* of this vector. The contravariant components $e^p(\alpha)$ of the four vectors $\mathbf{e}(\alpha)$ that constitute the frame $E(P)$ describe analytically the metric field at P in terms of the coordinates x^p. The laws of nature are

* This is an abbreviated version of a note that appeared under the same title in Actas de la Academía Nacional de Ciencias de Lima **11** (1948), but was made incomprehensible by numerous misprints.

[1] Sitzungsber., Preuss. Akad. der Wissensch. (1925), p. 414.

invariant (1) with respect to arbitrary transformations of the coordinates x^p and (2) with respect to arbitrary Lorentz rotations of the frames $E(P)$ at all points P (the rotation of the frame $E(P)$ at P depending in an arbitrary manner on the point P). Let $\|e_p(\alpha)\|$ denote the matrix reciprocal to $\|e^p(\alpha)\|$,

$$\sum_\alpha e^p(\alpha)\cdot e_q(\alpha)=\delta_q{}^p, \quad \sum_p e^p(\alpha)\cdot e_p(\beta)=\delta(\alpha\beta).$$

Here $\|\delta_q{}^p\|$ and $\|\delta(\alpha\beta)\|$ stand for the unit matrix. Let ϵ^{-1} be the absolute value of the determinant of the $e^p(\alpha)$. $\epsilon\cdot dx^0dx^1dx^2dx^3=\epsilon\cdot dx$ is the invariant volume element of the world. The contravariant, the ortho- and the covariant components v^p, $v(\alpha)$, v_p of a (real) vector $\mathfrak{v}$ are connected by the relations

$$\begin{aligned} v^p&=e^p(\alpha)\cdot v(\alpha) \quad \text{or} \quad v(\alpha)=e_p(\alpha)\cdot v^p, \\ v_p&=e_p(\alpha)\cdot v(\alpha) \quad \text{or} \quad v(\alpha)=e^p(\alpha)\cdot v_p \end{aligned} \tag{1}$$

(in the writing-down of which the well-known convention about the omission of summation signs has been adopted). Multiplication by ϵ changes a scalar into a scalar density, a vector into a vector density, etc. We indicate this process by transmuting an italic into the corresponding German letter.

Infinitesimal parallel displacement from P to P' carries the frame $\mathfrak{e}(\alpha)=\mathfrak{e}(\alpha;P)$ at P into a frame at P' that proceeds from the local frame $\mathfrak{e}(\alpha;P')$ at P' by a certain infinitesimal rotation

$$d\Omega=\|do(\alpha\beta)\|, \quad do(\alpha\beta)=o_p(\alpha\beta)\cdot dx^p.$$

We thus come to describe the metric field and the affine connection by the 16+24 quantities $e^p(\alpha)$ and $o_p(\alpha\beta)\{=-o_p(\beta\alpha)\}$.[2] The Riemann curvature tensor is given by

$$R_{pq}(\alpha\beta)=\left\{\frac{\partial o_q(\alpha\beta)}{\partial x^p}-\frac{\partial o_p(\alpha\beta)}{\partial x^q}\right\} +\{o_p(\alpha\gamma)o_q(\gamma\beta)-o_q(\alpha\gamma)o_p(\gamma\beta)\},$$

and hence the scalar curvature equals

$$R=e^p(\alpha)e^q(\beta)R_{pq}(\alpha\beta).$$

The integral $\int\mathfrak{R}\cdot dx$ of $\mathfrak{R}=\epsilon\cdot R$ is an invariant; following Einstein we adopt $\mathfrak{R}$ as the Lagrangian of the gravitational field.

Transcription of Dirac's theory of the electron into general relativity yields for the Lagrangian $\mathfrak{L}+m_0\mathfrak{l}$ of the electronic field the sum of two terms; the principal term $\mathfrak{L}$ is responsible for the most decisive general features of quantum mechanics, the accessory term $m_0\mathfrak{l}$ contains the mass m_0 of the electron as a constant factor:

$$L=\frac{1}{i}\left\{\tilde{\psi}e^p(\alpha)S(\alpha)\frac{\partial\psi}{\partial x^p}-\frac{\partial\tilde{\psi}}{\partial x^p}e^p(\alpha)S(\alpha)\psi\right\} -\frac{1}{i}\sum e^p(\alpha)o_p(\beta\gamma)sp(\delta), \tag{2}$$

with the sum $\sum$ extending over all even permutations $\alpha\beta\gamma\delta$ of 0123;

$$l=(\bar{\psi}_3\psi_1+\bar{\psi}_4\psi_2)+(\bar{\psi}_1\psi_3+\bar{\psi}_2\psi_4). \tag{3}$$

In general relativity the phase λ of the arbitrary factor $e^{i\lambda}$ of the ψ's is an arbitrary function of the position P. The infinitesimal transformation $d\psi=dZ\cdot\psi$ of the ψ's that is induced by an infinitesimal rotation $d\Omega=\|do(\alpha\beta)\|$ of the local frame, therefore, contains an indeterminate additive term $i\cdot df\cdot\psi$ with a pure imaginary scalar factor $i\cdot df$. Hence in a full description of the affine connection there will occur, in addition to the matrix $d\Omega$, also a scalar $df=f_pdx^p$ depending linearly on the dx^p. The derivative $\partial\psi/\partial x^p$ in L has to be replaced by $\partial\psi/\partial x^p+if_p\psi$, where f_p are the covariant components of a vector field, and all laws must be invariant with respect to the "gauge transformation" (or should one rather say "phase transformation"?)

$$\psi\longrightarrow e^{i\lambda}\cdot\psi, \quad f_p\longrightarrow f_p-\frac{\partial\lambda}{\partial x^p}.$$

Experience shows that f_p accounts for the effect of the electromagnetic field on the electron and is to be identified with the electromagnetic potential φ_p, measured in a suitable atomic unit, $f_p=(e/\hbar c)\cdot\varphi_p$. Form the field strength $f_{pq}=\partial f_q/\partial x^p-\partial f_p/\partial x^q$. The generation of the electromagnetic field by the electronic charge-current $s(\alpha)$ is accounted for by adding the electromagnetic term

$$\mathfrak{M}=f_{pq}\mathfrak{f}^{pq} \tag{4}$$

to the total Lagrangian.

In the Riemann-Einstein metric geometry the metric quantities $e^p(\alpha)$ determine the affine connection, i.e. the quantities $o_p(\alpha\beta)$, in the following manner. From the Poisson brackets

$$\frac{\partial e^p(\alpha)}{\partial x^q}\cdot e^q(\beta)-\frac{\partial e^p(\beta)}{\partial x^q}\cdot e^q(\alpha)=[e(\alpha),e(\beta)]^p,$$

and in accordance with the rules (1) for the juggling of indices

$$\begin{aligned} o(\gamma;\alpha\beta)&=e^p(\gamma)\cdot o_p(\alpha\beta), \\ [e(\alpha),e(\beta)](\gamma)&=e_p(\gamma)\cdot[e(\alpha),e(\beta)]^p. \end{aligned}$$

Then

$$o(\alpha;\beta\gamma)+o(\beta;\gamma\alpha)=[e(\alpha),e(\beta)](\gamma)$$

or more explicitly

$$2o(\gamma;\alpha\beta)=[e(\gamma),e(\alpha)](\beta) +[e(\beta),e(\gamma)](\alpha)-[e(\alpha),e(\beta)](\gamma). \tag{5}$$

In a quantity like L which involves the $o_p(\alpha\beta)$ one may replace the latter by their expressions $o_p(\alpha\beta)\{e\}$ in terms of the $e^p(\alpha)$ as derived from (5). Let the resulting expression be denoted by L^*, the asterisk indicating that $o_p(\alpha\beta)\{e\}$ has been substituted for $o_p(\alpha\beta)$. In particular R^* is Riemann's scalar curvature

[2] See for this whole analytic treatment: H. Weyl, Zeits. f. Physik **56**, 330 (1929).

written as an algebraic combination of the $e^p(\alpha)$, their first and second derivatives.

For the moment let us ignore the electromagnetic potentials f_p as well as the Dirac mass term, and let κ denote Einstein's gravitational constant multiplied by $\hbar/c$. Then Dirac's and Einstein's equations in the metric theory require the variation of

$$\int (\mathfrak{R}^*+\kappa\mathfrak{L}^*)dx$$

to vanish for such arbitrary infinitesimal variations $\delta\psi$ and $\delta e^p(\alpha)$ as vanish outside a bounded region, while in the mixed theory

$$\delta\int (\mathfrak{R}+\kappa\mathfrak{L})dx$$

is to vanish for similar variations of ψ, $e^p(\alpha)$ and $o_p(\alpha\beta)$. The latter variations result in a new set of field laws replacing the definitions (5). This set states that the differences

$$\Delta(\gamma;\,\alpha\beta)=[e(\alpha),\,e(\beta)](\gamma)-\{o(\alpha;\,\beta\gamma)+o(\beta;\,\gamma\alpha)\}$$

instead of being all zero, satisfy the relations

$$\Delta(\gamma;\,\alpha\beta)=\frac{\kappa}{2i}\cdot sp(\delta) \tag{6}$$

for any even permutation $\alpha\beta\gamma\delta$ of 0 1 2 3, and the relation

$$\Delta(\gamma;\,\alpha\beta)=0 \tag{6'}$$

whenever the three indices $\alpha\beta\gamma$ are not all distinct. *Thus by the influence of matter a slight discordance between affine connection and metric is created.*

Although the list of observables which describe the field in the mixed theory includes $o_p(\alpha\beta)$ beside ψ and $e^p(\alpha)$, it is possible to eliminate the $o_p(\alpha\beta)$ by means of the equations

$$o_p(\alpha\beta)=e_p(\gamma)\cdot o(\gamma;\,\alpha\beta),$$
$$2o(\gamma;\,\alpha\beta)=2o(\gamma;\,\alpha\beta)\{e\}-\Delta(\gamma;\,\alpha\beta)$$

and the laws (6), (6'). I have carried out the somewhat laborious calculations. Since the result applies to Lagrangians of a more general type than envisaged above I shall enounce it in this generality. In the expression (2) of L one has now to replace $\partial\psi/\partial x^p$, $\partial\bar\psi/\partial x^p$ by $\partial\psi/\partial x^p+if_p\psi$ and $\partial\bar\psi/\partial x^p-if_p\bar\psi$, respectively. Besides the terms R and L of the Einstein-Dirac theory which involve the $o_p(\alpha\beta)$ there exist four invariants which do not, to wit

$$l=(\bar\psi_3\psi_1+\bar\psi_4\psi_2)+(\bar\psi_1\psi_3+\bar\psi_2\psi_4),$$
$$l_2=(\bar\psi_3\psi_1+\bar\psi_4\psi_2)(\bar\psi_1\psi_3+\bar\psi_2\psi_4)\geq 0,$$
$$M=f_{pq}f^{pq} \quad\text{and}\quad Q=e^p(\alpha)e^q(\beta)F(\alpha\beta)f_{pq}.$$

The skew-symmetric tensor $F(\alpha\beta)$ which enters into Q is constructed out of the 16 products $\bar\psi\psi$ as follows:

$$F(01),\ F(23)=(\bar\psi_3\psi_1-\bar\psi_4\psi_2)\mp(\bar\psi_1\psi_3-\bar\psi_2\psi_4),$$
$$F(02),\ F(31)=(\bar\psi_3\psi_2+\bar\psi_4\psi_1)\mp(\bar\psi_2\psi_3+\bar\psi_1\psi_4),$$
$$F(03),\ F(12)=i(\bar\psi_3\psi_2-\bar\psi_4\psi_1)\pm i(\bar\psi_2\psi_3-\bar\psi_1\psi_4)$$

the upper signs to be used for $F(01)$, $F(02)$, $F(03)$, the lower for $F(23)$, $F(31)$, $F(12)$. Let H be of the general form

$$H=R+\kappa\{L+w(l,\,l_2,\,M,\,Q)\},$$

w being any function of four real variables.

THEOREM. *The mixed theory with the Lagrangian ϵH is identical with the metric theory based on the Lagrangian*

$$\epsilon H',\quad H'=R^*+\kappa\{L^*+w'(l,\,l_2,\,M,\,Q)\}$$

where

$$w'(l,\,l_2,\,M,\,Q)=w(l,\,l_2,\,M,\,Q)-\frac{3\kappa}{2}l_2.$$

To this extent then there is complete equivalence between the mixed metric-affine and the purely metric conceptions of gravitation.

Special relativity results if one lets the constant κ tend to zero. Then one obtains $e^p(\alpha)=\text{const.}$, $o_p(\alpha\beta)=0$, and one may choose

$$e^0(0)=i,\quad e^1(1)=e^2(2)=e^3(3)=1$$

and all other $e^p(\alpha)=0$. The Dirac equations and the energy-momentum tensor for the metric and the mixed theory coincide in the limit $\kappa\to 0$.

Relativistic Motion in a Magnetic Field

M. H. JOHNSON AND B. A. LIPPMANN
Nucleonics Division, Naval Research Laboratory, Washington, D. C.
(Received October 25, 1949)

A simple integral of the relativistic equations of motion for a charge in a magnetic field is used to reduce the Dirac equations to two simultaneous first-order differential equations. Eigenstates of this integral are the basis for a treatment of degeneracy and, in the case of a homogeneous field, for the construction of energy eigenfunctions from non-relativistic solutions. For a free particle the same integral leads directly to the only possible energy states with exactly defined spin projections.

I. INTRODUCTION

IN a recent paper[1] a treatment of the NR motion of a charge in a homogeneous magnetic field has been given which contains an exhaustive classification of the energy states in terms of integrals of the motion. While eigenfunctions were also given for the relativistic motion, there remained a twofold degeneracy in the energy, "accidental" in the sense that the degenerate states were not connected with an integral of motion. In the present paper this degeneracy is derived from and the degenerate states described by certain integrals which have not been previously considered.

In an inhomogeneous magnetic field (Section II) the relativistic equations of motion admit a simple integral, I, by which the problem of finding energy eigenfunctions can be reduced to the solution of two simultaneous first-order differential equations. For positive energy states with positive (negative) eigenvalues of I, the spin density is parallel (antiparallel) to the matter current. The energy is degenerate if a second integral exists which anticommutes with I or if the magnetic field satisfies certain symmetry conditions.

In a homogeneous magnetic field (Section III) explicit expressions are found for other integrals connected with the spin degeneracy. One of these involves only transverse motion and leads to a separation of the energy into transverse and longitudinal parts, each of which is a constant of motion. General solutions for the eigenfunctions of I are obtained in terms of NR wave functions. From these solutions spinor representations, as well as matter, spin and current densities, are derived for the energy eigenstates of the various integrals of motion.

For a free particle (Section IV) the energy eigenstates of I prove to be the only possible energy states in which a projection of the spin can be exactly defined. Solutions for the eigenfunctions of I are easily obtained for plane waves from which spinor representations are derived for the energy eigenstates of several integrals of motion. Free particle eigenfunctions can also be obtained from solutions in a homogeneous magnetic field by passing to the limit $\mathfrak{H}\to 0$.

[1] M. H. Johnson and B. A. Lippmann, Phys. Rev. **76**, 828 (1949). The notation of this paper will be followed here and equation references will be indicated by the suffix A.

II. INHOMOGENEOUS MAGNETIC FIELD

The Dirac Hamiltonian for a charge in any magnetic field is, in conventional notation,

$$H=c\rho_1\boldsymbol{\sigma}\cdot\boldsymbol{\pi}+\rho_3 mc^2, \tag{1}$$

where $\boldsymbol{\pi}$ is the kinetic momentum which satisfies the commutation relation of Eq. (3-A). Since $\boldsymbol{\sigma}$ commutes with ρ_1 and ρ_3,

$$I=c\boldsymbol{\pi}\cdot\boldsymbol{\sigma} \tag{2}$$

commutes with H and is therefore an integral of the motion. Simultaneous eigenfunctions for H and I necessarily exist and, as we shall see, represent states in which the spin is parallel or antiparallel to the current.

The Hamiltonian expressed in terms of I is

$$H=\rho_1 I+\rho_3 mc^2. \tag{3}$$

Thus the transformation from any representation in which I is diagonal to the principal axis of H involves only ρ_1 and ρ_3. In such a representation

$$H=\rho_1 F+\rho_3 mc^2, \tag{4}$$

where F is an eigenvalue of I. If the quantities ν_i are introduced

$$\nu_1=[\rho_1 mc^2-\rho_3 F][F^2+m^2c^4]^{-\frac{1}{2}}, \tag{5a}$$

$$\nu_2=\rho_2, \tag{5b}$$

$$\nu_3=[\rho_1 F+\rho_3 mc^2][F^2+m^2c^4]^{-\frac{1}{2}}, \tag{5c}$$

the Hamiltonian becomes

$$H=\nu_3[F^2+m^2c^4]^{\frac{1}{2}}. \tag{6}$$

Since $\nu_i^2=1$ and ν_i satisfy exactly the same commutation relations as ρ_i $(i=1, 2, 3)$, the eigenvalues of ν_3 are ± 1 and of H are

$$E=\pm[F^2+m^2c^4]^{\frac{1}{2}}. \tag{7}$$

Hence the energy eigenvalues occur in pairs $\pm E$ and, in magnitude are greater than or equal to mc^2.

The eigenfunctions of H are readily found from eigenfunctions of I by using the conventional matrix representation of $\boldsymbol{\sigma}$ and ρ_i with σ_z and ρ_3 diagonal. If

$$\psi_F=\begin{bmatrix} au_1 \\ au_2 \\ bu_1 \\ bu_2 \end{bmatrix}, \tag{8}$$

then ψ_F is an eigenfunction of I provided that

$$\pi_- u_2+(\pi_z-F/c)u_1=0, \tag{9a}$$

$$\pi_+ u_1+(-\pi_z-F/c)u_2=0. \tag{9b}$$

The constants a and b can be so chosen that ψ_F is an eigenfunction of H,

$$H\psi_{E,F}=(\rho_1 I+\rho_3 mc^2)\psi_{E,F}=E\psi_{E,F}. \tag{10}$$

We thus find

$$\psi_{E,F}=\begin{bmatrix}(E+mc^2)u_1\\(E+mc^2)u_2\\Fu_1\\Fu_2\end{bmatrix}[4E(E+mc^2)]^{-\frac{1}{2}}, \tag{11}$$

where E is given by Eq. (7). The problem of constructing energy eigenfunctions is thereby reduced to solving Eq. (9). In the next section general solutions are given for a homogeneous magnetic field.

The matter density and spin density, calculated from Eq. (11), are

$$\psi^*\psi=(1/2)(|u_1|^2+|u_2|^2), \tag{12}$$

$$\psi^*\sigma_z\psi=(1/2)(|u_1|^2-|u_2|^2), \tag{13}$$

$$\psi^*(\sigma_x+i\sigma_y)\psi=u_1^*u_2. \tag{14}$$

The matter current, calculated from Eq. (11), is given by the right-hand sides of Eqs. (13) and (14) multiplied by cF/E and therefore differs from the spin density by a constant factor. For positive energy states the matter current and spin density are parallel for positive eigenvalues of I and are antiparallel for negative eigenvalues of I.

It is evident that if the eigenvalues of I occur in pairs $\pm F$, the energy is degenerate in the sign of F. A sufficient condition is the existence of an operator, R, which anticommutes with I. For, in this case,

$$I(R\psi_F)=-RI\psi_F=-F(R\psi_F), \tag{15}$$

so that $R\psi_F$ is an eigenfunction of I for the eigenvalue $-F$. It should be noted that, if $RI=-IR$, an R can always be found which commutes with ρ_i (since I commutes with ρ_i) and that $\rho_3 R$ then commutes with H and is another integral of motion. The commutator, $[I, \rho_3 R]$, according to a general theorem, is then a third integral. Here the third integral is $iI\rho_3 R$ which anticommutes with both I and $\rho_3 R$.

The condition on the magnetic field that

$$\mathbf{A}(xyz)=-\mathbf{A}(-x-y-z) \tag{16}$$

is also sufficient for degeneracy in the sign of F. For under this condition the eigenvalue equation

$$-c\boldsymbol{\sigma}\cdot[ih\boldsymbol{\nabla}+(e/c)\mathbf{A}(xyz)]\psi_{E,F}(xyz)=F\psi_{E,F}(xyz) \tag{17}$$

is transformed into itself by changing the independent variables from xyz to $-x-y-z$, except that F is replaced by $-F$. Thus $\psi_{E,F}(-x-y-z)$ is an eigenfunction of I for the eigenvalue $-F$. According to Eq. (10) $i\rho_3\psi_{E,F}(-x-y-z)$ is then an eigenfunction of H for the eigenvalue E and is therefore a simultaneous eigenfunction of H and I. As $i\rho_3\psi_{E,F}(-x-y-z)$ is the spinor obtained from $\psi_{E,F}(xyz)$ by a reflection in the origin and as the matter, spin and current densities are scalar, pseudovector and vector quantities respectively, the matter and spin density for the state F at the point (xyz) and for the state $-F$ at $(-x-y-z)$ are the same while the current for the state F at (xyz) is equal in magnitude and opposite in direction to the current for the state $-F$ at $(-x-y-z)$. In general the matter densities for the two degenerate states are very different.

III. HOMOGENEOUS MAGNETIC FIELD

With $\mathbf{H}$ along the z axis, π_z is a constant of motion. In a representation with π_z diagonal all eigenfunctions contain z in a factor $\exp(ipz/h)$ where p is an eigenvalue of π_z. The field has the symmetry required by Eq. (16) and the energy is degenerate in the sign of F. The solution derived from $\psi_{E,F}$ by a reflection in the origin clearly has the eigenvalue $-p$ for π_z and represents motion in a reversed sense along the z axis. New solutions can also be derived from $\psi_{E,F}$ because of the high degree of symmetry in the field, by reflections in the xy plane or in the z axis. It is easily shown that the eigenvalue for π_z, x_0 or y_0 changes sign in the derived solutions which are therefore contained in a classification of states according to a complete set of constants chosen from π_z, x_0 and y_0.

The solutions in Eq. (54-A) show another degeneracy in which the matter density for the two degenerate states is very nearly the same in contrast to the pairs of states discussed. This spin degeneracy may be inferred by writing

$$I=c(\sigma_x\pi_x+\sigma_y\pi_y)+c\sigma_z p, \tag{18}$$

where the two terms on the right-hand side anticommute with each other and therefore their product anticommutes with I. Hence

$$T=i\rho_3(I-c\sigma_z p)\sigma_z=i\rho_3(I\sigma_z-cp) \tag{19}$$

anticommutes with I and commutes with H so that I, T and iIT are three anticommuting integrals of motion leading to degeneracy in the sign of F. As these integrals commute with π_z, x_0 and y_0, the degeneracy is in addition to any degeneracy in which the degenerate states have different eigenvalues of π_z, x_0 or y_0.

To determine the eigenvalues of I, T and iIT, it is sufficient to consider their squares as the commutation properties insure the eigenvalues occur in pairs of the form $\pm F$. For example

$$I^2=c^2\pi^2+2e\hbar c\sigma_z\mathcal{H}. \tag{20}$$

The eigenvalues of π^2 have been determined, Eqs. (16-A) and (17-A), while those of σ_z are ± 1. We conclude

$$F=\pm[c^2p^2+2e\hbar c\mathcal{H}n]^{\frac{1}{2}}. \tag{21}$$

In a similar way the eigenvalues of T are $\pm[2ehc\mathcal{H}n]^{\frac{1}{2}}$ and those of iIT are $\pm|F|[2ehc\mathcal{H}n]^{\frac{1}{2}}$. While, according to Eq. (21) F is related to both transverse and longitudinal motion, the eigenvalues of T depend only on the motion in the transverse plane.

Another integral of motion which involves only the longitudinal motion can be constructed from I and iIt. Let L be defined by

$$I^2L=-mc^2(iIT)+c\pi_z HI, \tag{22a}$$

$$L=mc^2\rho_3\sigma_z+c\rho_1\pi_z. \tag{22b}$$

From its construction, Eq. (22a), L anticommutes with T. Its eigenvalues are $\pm[c^2p^2+m^2c^4]^{\frac{1}{2}}$. The Hamiltonian can be simply expressed in terms of L and T,

$$H=\sigma_z(L+\rho_2 T), \tag{23a}$$

$$H^2=L^2+T^2. \tag{23b}$$

The eigenfunctions of I are easily derived from the ψ_n of Eqs. (36-A) and (37-A). In fact, setting $u_1=a'\psi_{n-1}$ and $u_2=b'\psi_n$, Eq. (9) is satisfied provided that

$$(cp-F)a'+(2ehc\mathcal{H}n)^{\frac{1}{2}}b'=0, \tag{24a}$$

$$(2ehc\mathcal{H}n)^{\frac{1}{2}}a'+(-cp-F)b'=0. \tag{24b}$$

Upon solving Eq. (24) and inserting the corresponding functions u_1 and u_2 into Eq. (11),

$$\psi_{E,F}=\begin{pmatrix}(E+mc^2)(2ehc\mathcal{H}n)^{\frac{1}{2}}\psi_{n-1}\\(E+mc^2)(F-cp)\psi_n\\F(2ehc\mathcal{H}n)^{\frac{1}{2}}\psi_{n-1}\\F(F-cp)\psi_n\end{pmatrix}\times[4E(E+mc^2)F(F-cp)]^{-\frac{1}{2}}, \tag{25}$$

where F is given by Eq. (21). According to Eq. (24) only the minus sign should be used in Eq. (21) for $n=0$, in which case Eq. (25) remains valid. The state $n=0$ is not degenerate in the spin variables.

The matter and spin densities, obtained by inserting the solution of Eq. (24) into Eqs. (12), (13) and (14), are

$$\psi^*\psi=p_1|\psi_{n-1}|^2+p_2|\psi_n|^2, \tag{26}$$

$$\psi^*\sigma_z\psi=q(p_1|\psi_{n-1}|^2-p_2|\psi_n|^2), \tag{27}$$

$$\psi^*(\sigma_x+i\sigma_y)\psi=2q'(p_1p_2)^{\frac{1}{2}}\psi^*_{n-1}\psi_n, \tag{28}$$

where

$$p_1=(2ehc\mathcal{H}n)\div 2F(F-cp), \tag{29a}$$

$$p_2=(F-cp)/(2F), \tag{29b}$$

$$q=q'=1. \tag{29c}$$

The matter current is obtained by multiplying the spin density by cp/F. The quantities p_1 and p_2 can be interpreted as the probabilities for finding the NR "orbital states" ψ_{n-1} and ψ_n, respectively, in an eigenstate of H and I. Equation (27) then shows that ψ_{n-1} and ψ_n are associated with spin projections $+1$ and -1, respectively, along the z axis. In the two eigenstates $\pm|F|$, both probabilities p_1 and p_2 are different, the transverse spin densities are equal but opposite in sign and the transverse currents are the same. The expectation values of all transverse currents are zero while those of the longitudinal components are p/F and c^2p/E for spin and current, respectively.

Simultaneous eigenfunctions of H and T can now be found from Eq. (25) by projection operators. If the eigenvalues of T are $T'=\epsilon(2ehc\mathcal{H}n)^{\frac{1}{2}}$, where $\epsilon=\pm1$, then $(T+T')\psi_{E,F}$ is an eigenfunction of T for the eigenvalue T'. We get

$$\psi_{E,T'}=\begin{pmatrix}(E+mc^2)\psi_{n-1}\\i\epsilon(E+mc^2)\psi_n\\i(T'-icp)\psi_{n-1}\\\epsilon(T'-icp)\psi_n\end{pmatrix}[4E(E+mc^2)]^{-\frac{1}{2}}. \tag{30}$$

The matter and spin density, calculated from Eq. (30), are given by Eqs. (26)–(28) with

$$p_1=p_2=\tfrac{1}{2}, \tag{31a}$$

$$q=1, \tag{31b}$$

$$q'=i\epsilon mc^2/E. \tag{31c}$$

The longitudinal current is given by the right-hand side of Eq. (27) with $q=c^2p/E$ and the sign before the second term changed to $+$ while the transverse current is given by the right-hand side of Eq. (28) with $q'=c|T'|/E$. In the two eigenstates $\pm|T'|$, the current and longitudinal spin densities are the same while the transverse spin densities are equal but opposite in sign. The expectation values of all transverse components is zero while those of the longitudinal components are 0 and c^2p/E for spin and current, respectively.

Simultaneous eigenfunctions for H and L are obtained in a similar way from the projection operator $L+L'$, where $L'=\pm[c^2p^2+m^2c^4]^{\frac{1}{2}}$.

$$\psi_{E,L'}=\begin{pmatrix}(E+L')(L'+mc^2)\psi_{n-1}\\cp(2ehc\mathcal{H}n)^{\frac{1}{2}}\psi_n\\(E+L')cp\psi_{n-1}\\(L'+mc^2)(2ehc\mathcal{H}n)^{\frac{1}{2}}\psi_n\end{pmatrix}\times[4E(E+L')L'(L'+mc^2)]^{-\frac{1}{2}}. \tag{32}$$

The matter and spin densities, calculated from Eq. (32), are given by Eqs. (26), (27) and (28) with

$$p_1=(E+L')/(2E), \tag{33a}$$

$$p_2=(2ehc\mathcal{H}n)\div 2E(E+L'), \tag{33b}$$

$$q=1, \tag{33c}$$

$$q'=cp/L'. \tag{33d}$$

The longitudinal current is given by the right-hand side of Eq. (27) with $q=c^2p/L'$ while the transverse current is given by the right-hand side of Eq. (28) with $q'=c$. In the two eigenstates $\pm|L'|$, the probabilities p_1 and p_2 are different, the transverse spin densities are equal but opposite in sign while the transverse currents are the same. The expectation values of all transverse components is zero while those of the longitudinal com-

ponents are L/E and c^2p/E for spin and current, respectively.

It is interesting to see how the addition of a Pauli term, $\mu\mathbf{H}\cdot\boldsymbol{\sigma}$, to the Hamiltonian removes the spin degeneracy. Since σ_z commutes with L, $\psi_{E,L'}$ are correct zeroth order eigenfunctions. The first-order correction to the energy[2] is given by the expectation value of σ_z.

$$\Delta E=\mu\mathcal{H}L'/E=\pm\mu\mathcal{H}[1-(2e\hbar c\mathcal{H}n)/E^2]^{\frac{1}{2}}. \quad (34)$$

Since, in most cases, $2e\hbar c\mathcal{H}n\ll E^2$, the additional energies are those of a dipole of strength μ, parallel or antiparallel to $\mathbf{H}$. The degenerate states are thus split by the energy $2\mu\mathcal{H}$.

III. FREE PARTICLE

In the absence of a field the kinetic momentum can be identified with the usual momentum, $\mathbf{p}$, whose eigenvalues we will designate by p_x', p_y' and p_z'. It is obvious that I is still an integral and it is easily verified that T is the z component of a vector all of whose components are integrals. The seven integrals, I, T and iIT may be expressed in terms of three independent integrals as can most easily be seen by taking the z axis along $\mathbf{p}'$ ($p_x'=p_y'=0$). In that case T_z and iIT_z are identically zero and the five remaining integrals reduce to σ_z, $\rho_3\sigma_y$ and $\rho_3\sigma_x$. It is evident that the component of $\boldsymbol{\sigma}$ along $\mathbf{p}$ is a constant of the motion and that no other component of $\boldsymbol{\sigma}$ has this property. The eigenstates of I are therefore the only possible states with exactly defined values of a spin projection.[3] The eigenstates of $\rho_3\sigma_y$ or $\rho_3\sigma_x$ are eigenstates of σ_y or σ_x only in the limit of small velocities ($\rho_3\rightarrow 1$).

From Eq. (21) the eigenvalues of I are $F=\pm cp'=\pm c[p_x'^2+p_y'^2+p_z'^2]^{\frac{1}{2}}$. Simultaneous eigenfunctions of H and I can again be found from Eqs. (9) and (11). Setting $u_1=a''\exp(i\mathbf{p}'\cdot\mathbf{r}/\hbar)$ and $u_2=b''\exp(i\mathbf{p}'\cdot\mathbf{r}/\hbar)$, Eq. (9) becomes algebraic and its solutions substituted into Eq. (11) yield

$$\psi_{E,F}=\exp[i\mathbf{p}'\cdot\mathbf{r}/\hbar]\begin{pmatrix}(E+mc^2)(F+cp_z')\\(E+mc^2)c(p_x'+ip_y')\\F(F+cp_z')\\Fc(p_x'+ip_y')\end{pmatrix}\times[4E(E+mc^2)F(F+cp_z')]^{-\frac{1}{2}}. \quad (35)$$

The matter and spin densities, obtained by substituting the solutions of Eq. (9) into Eqs. (12)–(14), are

$$\psi^*\psi=1, \quad (36)$$

$$\psi^*\sigma_z\psi=cp_z'/F, \quad (37)$$

$$\psi^*(\sigma_x+i\sigma_y)\psi=c(p_x'+ip_y')/F. \quad (38)$$

Thus the spin densities are just the projections of a unit vector, parallel to $\mathbf{p}'$ for F positive and antiparallel to $\mathbf{p}'$ for F negative, on the coordinate axes. The matter current, obtained by multiplying the spin density by cF/E, is identical with the classical velocity vector, c^2p'/E for both eigenstates $\pm|F'|$.

Simultaneous eigenfunctions of H and other integrals of motion associated with spin degeneracy can now be obtained by projection operators. For example the eigenfunctions of L are

$$\psi_{E,L'}=\exp(i\mathbf{p}'\cdot\mathbf{r}/\hbar)\begin{pmatrix}(E+L')(L'+mc^2)\\cp_z'c(p_x'+ip_y')\\(E+L')cp_z'\\(L'+mc^2)c(p_x'+ip_y')\end{pmatrix}\times[4E(E+L')L'(L'+mc^2)]^{-\frac{1}{2}}. \quad (39)$$

The matter and spin density, calculated from Eq. (39) are

$$\psi^*\psi=1, \quad (40)$$

$$\psi^*\sigma_z\psi=L'/E, \quad (41)$$

$$\psi^*(\sigma_x+i\sigma_y)\psi=cp_z'c(p_x'+ip_y')/(EL'). \quad (42)$$

The matter current is again identical with the classical velocity vector. In the two eigenstates $\pm|L'|$, the currents are the same and the spin densities are equal but opposite in sign.

Free particle solutions can also be obtained from solutions in a homogeneous field by passing to the limit $\mathcal{H}\rightarrow 0$. The ψ_n of Eq. (37-A) contain λ (Eq. (19-A)) as a scale factor for the transverse coordinates and λ is proportional to $\mathcal{H}^{-\frac{1}{2}}$. If n is held fixed, ψ_n approaches the value of ψ_n at $x=y=0$ for any finite value of x and y as $\mathcal{H}\rightarrow 0$. Thus the space parts of the wave functions approach plane waves along the z axis as should be expected for, in this limit, the energy of transverse motion is zero. The spinor parts of the eigenfunctions go over into the corresponding spinors for a free particle. Thus $\psi_{E,F}$ goes over into the solution of Eq. (35) and $\psi_{E,L'}$ into the solution of Eq. (39) with $p_x'=p_y'=0$ in both cases.

[2] The exact eigenvalues of the Hamiltonian $H=c\rho_1\boldsymbol{\pi}\cdot\boldsymbol{\sigma}+\rho_3mc^2+\mu\mathbf{H}\cdot\boldsymbol{\sigma}$ are $E'=\pm[E^2+\mu^2\mathcal{H}^2\pm 2\mu\mathcal{H}cE(1-2e\hbar c\mathcal{H}n/E^2)^{\frac{1}{2}}]^{\frac{1}{2}}$, where E is given by Eqs. (7) and (21).

[3] This has been discussed in detail from a different standpoint in A. Sommerfeld's, *Wellenmechanik* (Frederick Ungar Publishing Company), p. 330 ff.

Conductivity Pulses Induced in Insulating Liquids by Ionizing Radiations

NORMAN DAVIDSON AND A. E. LARSH, JR.
Gates and Crellin Laboratories of Chemistry, California Institute of Technology, Pasadena, California*
(Received November 8, 1949)

Conductivity pulses due to electron collection have been observed in liquid and solid argon exposed to α- or γ-radiation. The maximum pulse sizes, P_M, for α-particles depend only on the field strength, E, and not on the electrode spacing, proving that the pulse limiting effect is columnar recombination and not electron trapping by impurities. The maximum pulse sizes obey the equation $(P_M/P_0)=1-\exp(-AE^{\frac{1}{2}})$, where P_0 is the α-pulse size in an argon gas counter. The counting efficiency for α-particles is close to 100 percent, but there is some variation in pulse size due to variation of columnar recombination with angle of emission. No α- or γ-pulses were observed in liquid nitrogen or heptane, but weak α-induced pulses were observed in liquid methane.

The effects of nitrogen and oxygen in solution in liquid argon in decreasing the pulse sizes are interpreted as being due to electron capture by these molecules.

I. INTRODUCTION

THERE has recently been considerable interest in the study of crystal counters.[1,2] In this experiment bound electrons in a crystal are excited into a conducting state by the passage of an ionizing radiation, and the rapid motions of these electrons through the crystal toward a collecting electrode are observed. If the freed electrons are trapped at sites in the crystal before they move a sufficiently large fraction of the distance to the collecting electrode, no voltage pulse is detected. From an elementary theoretical point of view one would expect that free electrons introduced into a pure liquid composed of molecules with no electron affinity would move in an applied field without being trapped. The study of liquid counters might therefore provide information about the electron trapping properties of various molecules. A practical difficulty with crystal counters is the development of space change during operation due to the accumulation of nonmobile positive and negative charges at sites in the crystal. A successful liquid counter would avoid this difficulty, because of the slow mobilities ($\sim 10^{-3}$ cm^2/volt-sec.) of ions in liquids. For these reasons we have carried on the investigations on liquid counters described below. A brief account of our early results has already appeared,[3] and G. W. Hutchinson[4] has independently worked in the same field, A. N. Gerritsen[5] has measured the d.c. ionization currents due to α-particles for liquid nitrogen, hydrogen, helium, and argon.

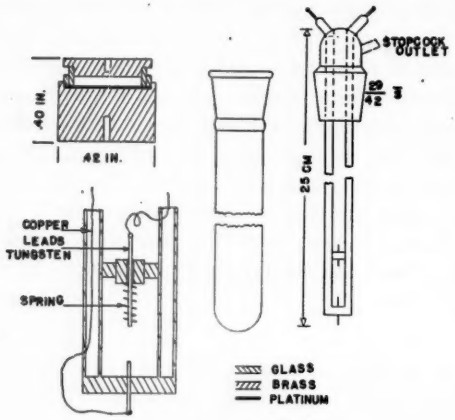

FIG. 1. Liquid ionization chamber.

II. EXPERIMENTAL

a. Materials

"Welding Argon" supplied by the Linde Air Products Company was used without further purification. It was stated by the supplier to be better than 99.8 percent pure, with nitrogen the principal impurity, and with the oxygen content "nil." Further purification of the argon by passage through the deoxidizer described did not noticeably affect its counting characteristics.

Linde "High Purity Dry" nitrogen which is stated to be 99.99 percent pure was passed over reduced copper supported on diatomaceous earth at *ca.* 300°C, and over phosphorus pentoxide.[6] Cylinder oxygen was passed over P_2O_5. Phillips Petroleum Company "Pure" methane, with a minimum purity of 99 percent, was used directly. The Phillips' "Pure" *n*-heptane of a stated minimum purity of 99 percent was washed with concentrated sulfuric acid and water, dried over potassium hydroxide, refluxed in vacuum over molten sodium, and then distilled into the liquid counter. The various gases were condensed into the counter tube using liquid air whose temperature was controlled when necessary by bubbling oxygen through it or by cooling it by evacuation.

b. Measurements

Figure 1 shows the ion chamber used for most of the measurements. A RaD-polonium source on a platinum

* Contribution No. 1349.

[1] P. J. Van Heerden, *The Crystal Counter* (N. V. Noord-Hollandsche Uitgevers Maatschappij, Amsterdam, 1945).

[2] For a general summary, see R. Hofstadter, Nucleonics 4, No. 4, 2 (1949); 4, No. 5, 29 (1949).

[3] N. Davidson and A. E. Larsh, Jr., Phys. Rev. 74, 220 (1948).

[4] G. W. Hutchinson, Nature 162, 610 (1948).

[5] A. N. Gerritsen, Physica 14, 381 (1948).

[6] Pollock, Pringsheim, and Terwood, J. Chem. Phys. 12, 295 (1944); F. B. Meyer and G. Ronge, Zeits. f. angew. Chemie 52, 63 (1939).

foil could be held in place on the surface of the lower electrode by the glass spacers. Several glass spacers were used to give collecting electrode spacings (at the temperature of liquid air) of 0.094, 0.360, and 1.08 mm. Voltage pulses due to electron collection were amplified with a fast linear amplifier constructed according to the directions of Bell and Jordan.[7] This instrument contains a pulse height selector for determining the size distribution of the output pulses. As used for most of our measurements, there was an instrumental rise time of about 4 μsec. and a decay time of about 20 μsec. The gain calibration was made using a well-shielded voltage divider and the trigger pulses from a P4-E M.I.T. Radiation Laboratory synchroscope. The capacitances of the counters and associated input circuit were measured with a General Radio Company Impedance Bridge, Type 650-A, at 1000 cycles/sec. These capacitances were: (1) Liquid counter, 0.094-mm spacing, containing liquid argon, plus input circuit, 30 $\mu\mu$f; (2) the same, 0.4- or 1.1-mm spacing, 27 $\mu\mu$f; (3) gas counter plus input circuit, 29 $\mu\mu$f; (4) input circuit alone, 16 $\mu\mu$f. That the capacitance measurements and the amplifier gain measurements were at least roughly consistent was shown by the observed maximum size of the polonium alpha-pulses of 1.015 mv in the argon gas counter. Using the value of 25.4 ev/ion pair for argon,[8] the calculated pulse size for a 5.30-Mev α-particle is 1.15 mv. The visually estimated rise time of the pulses in the gas counter was 7.5 μsec., the fall time, 20 μsec.; this introduces a "clipping" correction of 83 percent, so the theoretical pulse size is 0.95 mv.

The counter tubes and preamplifier were housed in a $1\frac{1}{2}$ ft.$\times$2 ft.$\times 2\frac{1}{2}$ ft. grounded box shielded with copper screening and 0.020-in. sheet steel. With the preamplifier in the middle of this space and grounded to the box by a wire, there was considerable pick-up by the counter leads of the miscellaneous electrical disturbances in the laboratory. This was true even though multiple ground connections were avoided. The most effective measure in removing these difficulties was simply to mount the preamplifier chassis flush against the conducting walls of the box. It was also helpful to use batteries for a high voltage supply instead of a transformer-rectifier voltage source. The batteries were external to the box to avoid pick-up of radiated battery noise, and the voltage led into the counter through *RC* filters.

III. RESULTS AND DISCUSSION

a. Liquid Argon

Conductivity pulses due to α-particles and γ-rays have been observed with liquid argon. Large α-particle pulses were observed only with the collecting electrode positive and hence are due to electron collection. Figure 2 displays a set of pulse height distribution curves for the 0.094-mm spacing. The maximum pulse sizes were determined by the indicated extrapolations, and by subtracting 95 μvolts for the contribution of noise. Figure 3 exhibits the dependence of the maximum pulse size, P_M (normalized to an input capacitance of 30 $\mu\mu$f), on the field strength, E, for the three different electrode spacings. The plot is actually one of $\ln(1-P_M/P_0)$ *vs.* $E^{\frac{1}{2}}$, where P_0 is the maximum calculated pulse size assuming that, just as in argon gas, an energy of 25.4 ev is required per electron and that every electron liberated moves all the way to the collecting electrode. The observed P_M's are all less than one-half of P_0. There is no evidence in Fig. 3 that the maximum pulse size has reached a saturation value at the voltages used, and hence no indication whether the energy per ion pair is different in liquid argon than in the gas. *The data of Fig. 3 show that the pulse size is dependent on the field strength alone and is independent of electrode spacing. Therefore the pulse limiting event for α-particles in liquid argon is recombination of the liberated electrons with the column of positive ions left in the track of the α-particle (columnar recombination) and not electron trapping.* The trapping hypothesis predicts that the pulse size would be inversely proportional to the electrode spacing for a fixed field strength. Indeed, the pulse sizes for the two larger spacings are slightly greater than those for the 0.094-mm spacing at the same field; we are unable to explain this small discrepancy. Hutchinson[4] has already suggested that columnar recombination might be the cause of our relatively small pulse sizes.

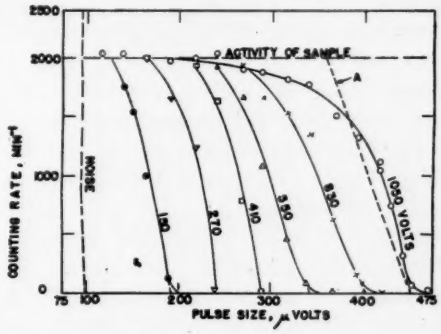

FIG. 2. Pulse size distribution curves for different collecting voltages (0.094-mm gap). (For all the curves except that at 1050 collecting volts, 10-sec. counts; one-minute counts for this case.)

We now consider the question of the causes of the distribution of pulse sizes for a given collecting voltage. We will discuss in detail the pulse size distribution curve for 1050 collecting volts and the 0.094-mm electrode gap displayed in Fig. 2. There is a plateau in the curve of counting rate *vs.* pulse size which corresponds closely to the counting rate of the sample observed in a gas counter (the horizontal line of Fig. 2). There is an observed spread in pulse size of about 250 μvolts. This

[7] W. Jordan and P. Bell, Rev. Sci. Inst. **18**, 703 (1947); Manhattan District Report, Mon. P-323, "Instructions for use of A-1 amplifier and preamplifier" (July 28, 1947).

[8] Rutherford, Chadwick, and Ellis, *Radiations from Radioactive Substances* (Cambridge University Press, London, 1930), p. 81.

could be due to (a) variation in the contributions of noise to different pulses, (b) variation in pulse size with the angle of emission of the α-particles. Item (a) contributes only about 30 μvolts to the pulse size spread. This was determined by observations on pulses of uniform size from a pulse generator. Item (b) includes two factors. There is the possibility that the efficiency of columnar recombination varies with the angle of emission. There is also a geometrical effect since electrons liberated from an α-track that is perpendicular to the electrodes move on the average a smaller fraction of the electrode spacing to reach the collecting electrode than do electrons liberated from an α-track that is parallel to the collecting electrode and necessarily the maximum distance away from the collecting electrode. The calculated range of polonium α-particles in liquid argon is 0.05 mm, therefore assuming no difference in columnar recombination, pulses due to electron collection from α-tracks perpendicular to the electrodes should be of the order of 75 percent of the size of those due to α-particles moving parallel to the plates for the 0.094-mm spacing. (We do not consider in this approximate treatment the effect of the variation of specific ionization along a track in view of the difficulty in treating the dependence of the columnar recombination on this variable.) If θ=the azimuthal angle of emission of the α-particles, then the fractional number of α-particles between zero and θ is $1-\cos\theta$. For the particular dimensions under consideration, the pulse size at angle θ is calculated to be $P_M(1-(\cos\theta)/4)$ and the pulse size distribution curve is predicted to be $N(P)=4(1-P/P_M)$, where $(3P_M/4)<P<P_M$ and $N(P)$ is the fractional number of pulses of size greater than P. This is the dotted curve A of Fig. 2. (It must be remembered that the true pulse sizes, P, are obtained from those in Fig. 2 by subtracting 95 μvolts for the noise level.)

The reality of this geometrical effect as an influence on pulse size is most convincingly demonstrated by

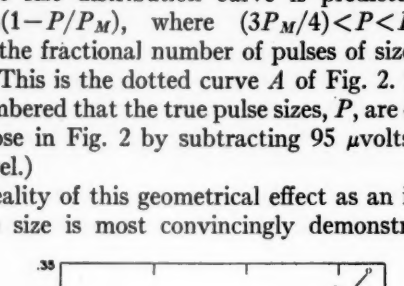

FIG. 3. Dependence of maximum pulse size, P_M, on field strength, E, for three different electrode spacings. (The pulse sizes have been normalized to an input capacitance of 30 $\mu\mu$f.) ○, □, △, 0.094, 0.36, 1.08-mm spacings; ●, Gerritsen's data (see reference 5) for the variation of the d.c. ionization current, I, induced in liquid argon by polonium α-particles, plotted in the form $\ln(1-I/I_0)$ *vs.* $E^{\frac{1}{2}}$.

TABLE I. Pulses in liquid argon with α-active electrode positive.*

Counting rate (percent of total)	Maximum azimuthal angle	Minimum pulse size (μvolts) (obs.)	(calc.)
3	14°	70	84
17	34°	58	72
30	46°	46	61
75	76°	33	22

* 0.094-mm spacing, 1040 collecting volts.

observing the small pulses due to the collection of electrons at the lower (active) electrode when it is positive. Table I records some observations on this effect. (Calculation shows that for the narrow spacing used, the effects of Table I cannot be due to Ra-E β-rays.)

In the table, the azimuthal angles were calculated from the fractional counting rate for a given pulse size and the calculated minimum pulse sizes as $(P_M\cos\theta)/4$ (P_M being the maximum pulse size for the active electrode negative).

In view of the small pulse sizes involved, the agreement between calculations and observations in Table I is satisfactory. This in turn gives one confidence in the reliability of curve A of Fig. 2 to represent the variation of pulse size with angle of emission due to the geometrical factor. The discrepancy between the experimental curve and A may then be due to an increasing efficiency of columnar recombination for α-tracks with small θ. For example, at 1800 c/m (corresponding to an angle of emission of 26°) the pulse size is *ca.* 18 percent smaller than that (275 μvolts) predicted by curve A. There are so few α-rays that are closely parallel to the field (10°) that one has no information on the columnar recombination in this case.

To consider the variation of maximum pulse size with voltage one might look for a saturation curve of the type $P_M/P_0=1-\exp(-AE^n)$. The plot of Fig. 3 shows that $n=\frac{1}{2}$ fits the data reasonably well; in view of the experimental uncertainties and the uncertainty as to real value of P_0 for liquid argon, we have not attempted to find a function that fits the data better. We can offer no theoretical explanation for the value $n=\frac{1}{2}$.

Gerritsen[5] has observed the d.c. ionization current, I, induced in liquid argon by polonium-α's that is plotted in Fig. 3 as $\ln(1-I/I_0)$ where I_0 is the saturation current in argon gas. He finds much larger ionization currents in liquid argon and helium than in nitrogen or hydrogen. Furthermore, the dependence of current on field strength in nitrogen and hydrogen is in accordance with that expected on the basis of the theory of columnar recombination of heavy ions, and this is not the case for argon and helium. This is in accordance with our observations presented below that electrons can move freely through liquid argon but are trapped by nitrogen molecules. In Fig. 3 it is seen that Gerritsen's data also give a linear plot of $\ln(1-I/I_0)$ *vs.* $E^{\frac{1}{2}}$. The slope of this curve is about 0.4 of the slope of the

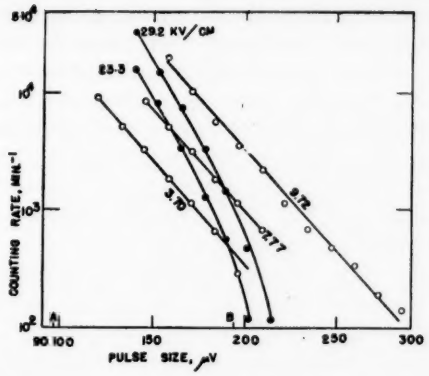

FIG. 4. Gamma-ray counting with liquid argon (the pulse sizes have been corrected for noise level). (A and B, maximum α-pulse sizes for 9.6 and 28.9 kv/cm, respectively.) ●, 0.36-mm gap; ○, 1.08-mm gap.

curve for our data on P_M/P_0. Gerritsen's data for the average current should really be compared not with our values of P_M but with suitably averaged values of P obtained from the distribution curves of Fig. 2. This averaging process would recognize that there is no reduction in d.c. current in Gerritsen's measurements corresponding to the reduction in pulse size in our electron collection experiments due to the geometrical effect for which curve A of Fig. 2 was calculated. Without making detailed calculations, it is evident that the averaged value of P is not less than 0.9 P_M and that there is a real discrepancy between our results and those of Gerritsen. Small concentrations of electron trapping impurities in Gerritsen's argon that did not influence the columnar recombination but subsequently captured the electrons would not affect a d.c. ionization current. In view of our indications reported in a subsequent section that small concentrations of nitrogen in the argon reduce the pulse size by increasing the columnar recombination as well as by trapping electrons, it is conceivable that Gerritsen's low results are due to nitrogen impurity in the argon he used.

In concluding the section on α-particles in liquid argon we note that with the crude apparatus used for the data of our preliminary report,[3] we underestimated the field at which conductivity pulses of a given size are obtained. We have not extended the qualitative observations recorded there that when the argon was solidified in the counter, presumably in a polycrystalline condition, conductivity pulses were still observed. Hutchinson[4] has confirmed and extended these observations. One is led to believe that the height of the conduction band in crystalline argon is such that electrons can readily enter or leave the crystal from or to the vapor phase.

Figure 4 displays some pulse size *vs.* activity curves for Compton electrons from γ-rays in liquid argon. The data were obtained with a 1.7-mc radium needle mounted in the plane of the counting electrodes and at a fixed distance of about 2 cm away. These data agree in a general way with Hutchinson's description[4] of his experiences counting γ-rays in liquid argon. Although radium-γ's are less energetic than polonium-α's, there is less columnar recombination and the maximum pulse sizes observed are larger for the γ-rays than for the α's at the same field. Because of geometrical effects, more large pulses are observed with the wider electrode spacings; and, of course, the pulse sizes are independent of the direction of the applied field. We do not know the causes of the variations of pulse size with field strength at a fixed electrode spacing.

b. Solutions of Oxygen and Nitrogen in Liquid Argon

In order to learn something about the electron trapping properties of oxygen and nitrogen molecules, we have investigated conductivity pulses due to α-particles with dilute solutions of these components in liquid argon. We set: $u(c, E)$ = drift velocity of an electron toward a collecting electrode in a field E and in a solution of concentration c (mole fraction) of the dilute component, $k(c, E)$ = probability of capture in unit time, $n(c, E)$ = number of electrons escaping columnar recombination from an α-track in such a solution, $P_s(c, E)$ = maximum pulse size for the solution, $n_0(E)$ = number of electrons escaping columnar recombination in pure argon, $P_M(E)$ = maximum pulse size in pure argon, l = electrode spacing, $m = u/k$. The quantity m is readily shown to be the mean drift distance of electrons before capture. By a well-known derivation[9] one obtains

$$(P_s/P_M) = (n/n_0)(m/l)[1-\exp(-l/m)]. \qquad (1)$$

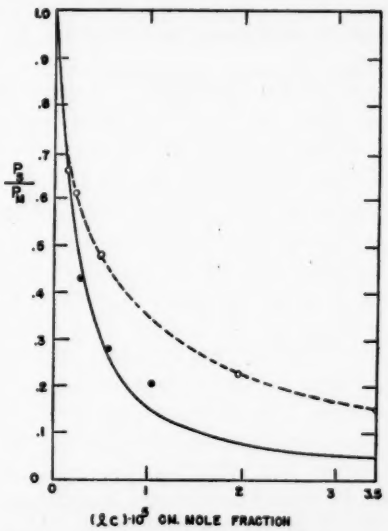

FIG. 5. P_s/P_M for solutions of oxygen in liquid argon as a function of lc. ○, 0.094-mm gap, 113 kv/cm; ●, 0.36-mm gap, 29 kv/cm. The dotted line goes through the experimental points for the narrow gap. The solid line is the theoretical curve of Eq. (1), assuming $(n/n_0) = 1$ and $m = (1.55\times10^{-6}/c)$ cm.

[9] N. F. Mott and R. W. Gurney, *Electronic Processes in Ionic Crystals* (Oxford University Press, London, 1940), p. 122.

The observed values of P_s/P_M for dilute solutions of oxygen in argon are plotted in Fig. 5 as a function of lc. The results plotted are for the maximum available field strengths for the two electrode spacings used because greater accuracy in the measurements was obtained in this way. However, with the 0.094-mm spacing, there was no marked dependence of P_s/P_M on E. Thus with $c=2.6\times10^{-4}$, we observed for P_s/P_M 0.61 (113 kv/cm), 0.59 (87 kv/cm), 0.55 (58 kv/cm), 0.54 (29 kv/cm). The fact of electron trapping is unambiguously proved by the decrease in P_s/P_M with increasing electrode

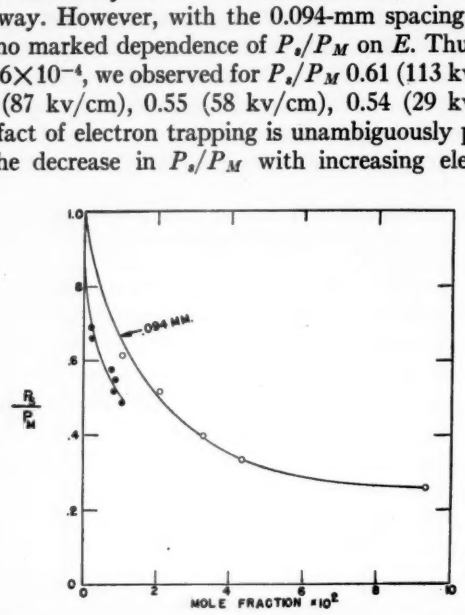

FIG. 6. Pulse sizes in solutions of nitrogen in argon, ○, 0.094-mm gap, ●, 0.36-mm gap.

spacing (remembering that P_s/P_M is approximately independent of field strength). The plot of Fig. 5 shows that the variation of P_s/P_M with l fits Eq. (1) with the assumption that $n=n_0$ and indeed one cannot explain the variation of P_s/P_M with l unless n is approximately equal to n_0 at O_2 concentrations of about $1-2\times10^{-4}$ mole fraction.

For sufficiently dilute solutions one would expect that the mean drift path, m, would be inversely proportional to the concentration, c. However, with the short spacing and larger concentrations of O_2 the observed values of P_s/P_M are higher than those calculated from Eq. (1) at a fixed field strength assuming that $n=n_0$ and that $m=a/c$, using the more dilute solutions to determine a value of a, the constant. This deviation is also noticeable for the highest concentration ($c=2.6\times10^{-4}$) used with the 0.37-mm gap. It seems improbable that $n/n_0>1$ for high concentrations of oxygen and we therefore propose that the equation $m=a/c$ does not hold at high concentrations ($>3\times10^{-4}$). This is not unreasonable for the following reasons. The capture cross section by oxygen molecules is dependent on the agitation velocity of the electrons in the liquid and the mean agitation velocity probably decreases in the presence of small quantities of oxygen.[10] Now, k, the probability of capture in unit time, equals the mean agitation velocity times the capture cross section times the concentration of oxygen molecules in units of molecules per cc. We do not know how the capture cross section depends on the electron velocity. However the contribution of the first term is to make k decrease as the agitation velocity decreases. Since $m=u/k$, and u increases as the agitation velocity decreases,[10] there are two known factors which would make m increase with decreasing agitation velocity.

Since the drift velocity is expected to be proportional to the field strength and k should not be strongly dependent on the field, it is surprising that P_s/P_M is approximately independent of the field strength. This probably means that the drift velocity is not proportional to the field strength, but a constant. The same situation occurs at high field strengths in argon gas.[10,11] The value of E/p for argon gas at which the drift velocity becomes a constant is about 1 volt per cm per mm Hg. Using p simply as a measure of density, the values of "E/p" for liquid argon in our work are in the range of 0.015–0.15.

Assuming the order of magnitude figures for the drift velocity and the mean agitation velocity in liquid argon in a field of 10^4–10^5 volts/cm of 10^6 cm/sec. and 2×10^8 cm/sec. (this latter figure corresponding to a mean agitational energy of 10 ev[10]) one calculates from the values of m of *ca.* 0.016 cm for a concentration of O_2, c of 10^{-4} (obtained from Fig. 5) a value of the cross section for electron capture by O_2 molecules of 10^{-19} cm²/molecule, using the relation stated above.

As shown in Fig. 6, the concentrations of N_2 required to diminish the pulse size a given amount are about 20 times greater than the equivalent O_2 concentrations. The approximation that the nitrogen is present as a very dilute solution and functions only as an electron trapping impurity without affecting n/n_0 or the velocity distribution of the electrons (and hence the capture cross section) does not work at all. Just as in the oxygen case, the values of P_s/P_M are independent of field strength. Thus with 1.04 percent N_2, we observe $P_s/P_M=0.61$ (111 kv/cm), 0.57 (86 kv/cm), 0.61 (56 kv/cm), 0.65 (43 kv/cm) and 0.67 (28 kv/cm). Similar results were obtained with 2.08 percent N_2. The fact displayed in Fig. 6 that for a fixed N_2 concentration, the value of P_s/P_M decreases as the electrode spacing increases proves that electron trapping by N_2 molecules does take place. One can fit the data at $c=ca.\ 2.5\times10^{-3}$ by assuming that $m=0.028$–0.12 cm and that $n/n_0=0.94\pm0.1$. To fit the data at $c=ca.$ 1 percent one must assume that $m=0.028$–0.12 cm and that $n/n_0=0.7\pm0.1$. Furthermore the values of P_s/P_M do not fall off as rapidly with N_2 concentration (for the short spacing) as would be expected if n/n_0 were constant and $m=a/c$. There are indications therefore that n/n_0 decreases with increasing concentration of nitrogen and

[10] J. Allen and B. Rossi, "Time of collection of electrons in ionization chambers," MDDC 448, United States AEC, Oak Ridge, Tennessee (1944).

[11] D. E. Hudson, "Method of measuring the drift velocity of electrons in gases," MDDC 524, United States AEC, Oak Ridge, Tennessee (1946).

that m is not inversely proportional to the concentration. In view of the experimental inaccuracy, more precise conclusions are not possible.

c. Other Materials

With purified nitrogen no α-induced pulses were observed with the 0.094-mm spacing and no γ-induced pulses with the 1.0-mm spacing (the large spacing being more favorable for the detection of γ-pulses). The failure to obtain α-pulses might be attributed to a high efficiency for columnar recombination in liquid nitrogen but presumably with the relatively low specific ionization of the Compton electron ejected by a γ-ray the failure to observe γ-induced pulses is due to electron capture by nitrogen and confirms the conclusion of the preceding section that N_2 molecules do have an electron affinity.

We have observed no α-induced pulses with purified heptane, either at 0°C or −80°C, and Hutchinson[4] observed no γ-induced pulses in purified hexane. However with methane just above its triple point we have observed weak α-induced pulses with 10^5 volts/cm and the 0.094-mm electrode spacing. The pulses were about 65 μvolts above noise. Because of the very weak pulses and the relatively low purity of the methane we have not tried to investigate this substance further to distinguish between the effects of columnar recombination and of electron trapping.

IV. ACKNOWLEDGMENT

Without the financial support of the ONR this work could not have been performed. We are indebted to Mr. Alvin Tollestrup for many helpful conversations about the operation of our amplifier and associated problems.

PHYSICAL REVIEW VOLUME 77, NUMBER 5 MARCH 1, 1950

Do the Equations of Motion Determine the Quantum Mechanical Commutation Relations?

EUGENE P. WIGNER
Palmer Physical Laboratory, Princeton University, Princeton, New Jersey
(Received November 9, 1949)

The commutator of the Hamiltonian with the operator corresponding to any physical quantity gives the operator which corresponds to the time derivative of that quantity. One can ask, hence, whether the postulate, that the quantum mechanical operators obey the classical equations of motion, uniquely determines the commutation relations. The answer is found to depend on the form of the Hamiltonian and is in the negative for a free particle and for the harmonic oscillator.

1. SCHRÖDINGER[1] obtained his wave mechanical equation by postulating that the waves' motion correspond to the classical motion of a particle if the field of force in which it is moving does not change too rapidly with position. Later on, Ehrenfest[2] has shown that Schrödinger's work can be summarized most neatly by observing that the operators in the Heisenberg picture satisfy the classical differential equations:

$$\dot{q}=p/m; \quad \dot{p}=-\partial V/\partial x \tag{1}$$

if one assumes that the Hamiltonian has the simple form

$$H=p^2/2m+V(x). \tag{2}$$

As is well known, the time derivative of any operator in the Heisenberg picture is its commutator with the Hamiltonian so that (1) is equivalent with (2) and

$$(i/\hbar)[H, q]=p/m; \quad (i/\hbar)[H, p]=-\partial V/\partial x, \tag{1a}$$

or

$$(i/\hbar)[\tfrac{1}{2}p^2, q]=p; \quad (i/\hbar)[V, p]=-\partial V/\partial x. \tag{3}$$

These equations are usually derived from the Heisenberg-Born-Jordan relation

$$[p, q]=-ih. \tag{4}$$

Since, however, (1) and (1a) have a more immediate physical significance than (4) (see in particular Ehrenfest's discussion), it is natural to ask whether, conversely, (4) can be derived from (1a). The present writer has considered this question some time ago but its significance in consequence of Heisenberg's recent paper[3] and of their own work has been pointed out to him only recently by Pais and Uhlenbeck.

Some doubt on the fundamental nature of relations of the type (1a) must arise, of course, even apart from the results of the present analysis, by the observation that Dirac's equation of the electron does not lead to the classical equation of motion for the operators. Furthermore, because of the non-commuting character of the p and q, there are many forms in which the Hamiltonian can be written. In particular, in the example to be discussed below, $H=\frac{1}{2}(x+iv)(x-iv)$ could

[1] E. Schrödinger, *Abhandlungen zur Wellenmechanik* (J. A. Barth, Leipzig, 1927).
[2] P. Ehrenfest, Zeits. f. Physik 4, 455 (1927).
[3] W. Heisenberg, Zeits. f. Physik 123, 93 (1944), p. 108 ff.

have been written for the H of (5) and this would have altered the final result. In spite of these objections and ambiguities, it was felt that the above mentioned articles justify the publication of evidence that (4) is *not* a consequence of (1a).

2. The example which we shall consider is that of the harmonic oscillator. It was chosen because it seemed the simplest example except for the case of a free particle. This latter is, however, clearly anomalous because the second equation of (1a) is identically fulfilled. It so happens that the example of the harmonic oscillator is also the relevant one from the point of view of the considerations of Pais and Uhlenbeck.

Since the purpose of the above-mentioned considerations[4] is to avoid using Hamiltonian theory, we shall write the energy

$$H=\tfrac{1}{2}(x^2+v^2) \tag{5}$$

of an oscillator of mass one and classical frequency $1/2\pi$, in terms of coordinates and velocity rather than coordinates and momenta. If we choose units in which $\hbar=1$, the fundamental Eqs. (1a) become

$$v=\dot{x}=i[H, x] \tag{6a}$$

$$\dot{v}=-x=i[H, v]. \tag{6b}$$

3. The simplest method to solve Eqs. (5) and (6) seems to be essentially that of Born and Jordan.[5] One assumes that H is diagonal, its diagonal elements, which are because of (5) all positive, shall be denoted by $E_0, E_1, E_2, \cdots$. Then (6a) and (6b) read for the matrix elements x_{nm} and v_{nm} of x and v

$$v_{nm}=i(E_n-E_m)x_{nm} \tag{7a}$$

$$-x_{nm}=i(E_n-E_m)v_{nm}. \tag{7b}$$

Combining the two equations, we have

$$x_{nm}=(E_n-E_m)^2x_{nm}. \tag{8}$$

It follows that x_{nm} can be finite only if $E_n-E_m=\pm 1$ and it follows from (7a) that v_{nm} vanishes if x_{nm} does. As a result, the E_n which are connected by a finite matrix element of either x or v form an arithmetical series

$$E_n=E_0+n \tag{9}$$

if we restrict our attention to irreducible systems of operators satisfying (6).

Off hand, every E_n of (9) could occur in the diagonal form of H several times. It appears, however,[6] that one can decompose any system of matrices in which E_n occurs more than once by means of a unitary transformation which leaves H unchanged. Hence we can assume that all characteristic values (9) are simple.

Among the matrix elements x_{nm} only those of the form x_{nn+1} and x_{n+1n} can be different from zero; the former can be made real and positive by a transformation with a unitary diagonal matrix. Because of the Hermitean nature of x, the $x_{n+1n}=x_{nn+1}$ will then be real also. The matrix elements of v will be purely imaginary:

$$\begin{aligned} v_{nn+1}&=-ix_{nn+1}=-ix_{n+1n} \\ v_{n+1n}&=ix_{n+1n}=-v_{nn+1} \end{aligned} \tag{10}$$

as follows from (7a) and (9).

So far, the $x_{01}, x_{12}, x_{23}, \cdots$ are entirely free but only (6) is satisfied. In order to fulfill (5), we have to calculate $\frac{1}{2}(x^2+v^2)$. One notes that this is, as a result of (10), automatically a diagonal matrix, the diagonal element corresponding to E_n being

$$E_n=E_0+n=x_{n-1n}{}^2+x_{nn+1}{}^2, \tag{11}$$

except that $x_{01}{}^2=E_0$. Hence the x_{nn+1} can be determined one after another

$$\begin{aligned} x_{nn+1}&=(E_0+\tfrac{1}{2}n)^{\frac{1}{2}} \quad \text{for even } n \\ x_{nn+1}&=(\tfrac{1}{2}n+\tfrac{1}{2})^{\frac{1}{2}} \quad \text{for odd } n. \end{aligned} \tag{12}$$

The commutator of v and x is also automatically diagonal as a result of (10), its diagonal elements are $-2ix_{01}{}^2, -2i(x_{12}{}^2-x_{01}{}^2), -2i(x_{23}{}^2-x_{12}{}^2), \cdots$. Because of (12), these are $-2iE_0, -2i(1-E_0), -2iE_0, -2i(1-E_0), \cdots$. The usual solution is, of course, $E_0=\frac{1}{2}$ and, hence, $[v, x]=-i$. Our somewhat more general solution can be written as

$$([v, x]+i)^2=-(2E_0-1)^2, \tag{13}$$

E_0 being a constant characterizing the solution.

It is worth noting that for large n, all solutions converge to the usual one. It may also be worth mentioning that the situation here described obtains for a large class of quantum mechanical problems. However, there are other cases in which the equations of motion entail the relation $[v, x]=-ih/m$. A trivial case of this nature is that of a potential which is a linear function of the coordinate, $V(x)=ax^3$ is a less obvious case therefore.

[4] W. Heisenberg see reference 3; A. Pais and S. Uhlenbeck (to be published).

[5] M. Born and P. Jordan, Zeits. f. Physik **34**, 858 (1927).

[6] This question will not be further pursued since not even those solutions of (5) and (6), in which every diagonal element of H occurs only once, are all equivalent to the usual solution.

Letters to the Editor

PUBLICATION of brief reports of important discoveries in physics may be secured by addressing them to this department. The closing date for this department is five weeks prior to the date of issue. No proof will be sent to the authors. The Board of Editors does not hold itself responsible for the opinions expressed by the correspondents. Communications should not exceed 600 words in length.

Nuclear Cross Sections of High Energy Pi-Mesons

KENNETH GREISEN
Cornell University, Ithaca, New York
January 17, 1950

THE experiment of Piccioni[1] on the secondary particles of local penetrating showers is the first experiment to give direct information about the interaction with nuclei of pi-mesons of high velocity. The result, that the nuclear absorption is small, is presented as being in contrast to the absorption of high energy nucleons; and the inference (although Piccioni was careful not to state this) is that the cross section for nuclear interaction of high energy pi-mesons is at least an order of magnitude smaller than the geometric cross section of the nuclei. This inference has been accepted by other authors such as Lovati, Mura, Salvini, and Tagliaferri,[2] who have used it as an established fact in the interpretation of their cloud-chamber experiments. Because of the importance of such a conclusion and because it is contrary to other indirect evidence about pi-mesons, as is explained later, we think it is justified to examine the Piccioni experiment in an especially critical manner.

The conclusions rest on three observations: (1) The comparative absorbing powers of iron and lead are about equal, instead of in the ratio of geometric cross sections; (2) the number of pi-mesons that stop and decay near the lowest counters (tray C) is practically unchanged by increasing the iron from 1 inch to 5 inches between the tray C and the 12-inch lead filter; and (3) the number of pi-mesons that stop in the 4 inches of iron, in such a way that the positive ones decay, is about equal to the net absorption of ionizing secondaries in that layer of iron.

We wish first to discuss Piccioni's experiment III, an auxiliary experiment which showed that some of the pi-mesons stopping near tray C were produced in its immediate vicinity by neutral particles emerging from the thick lead filter. A tray D, above C, failed to be discharged in $11/60=18\pm5$ percent of the cases when hard shower delayed coincidences $(HS)_{del}$ were recorded in C. Therefore in at least (not at most) this many cases, the stopped pi-meson was produced in the 3 inches of iron about tray C. Since the HS on the average contained 4 penetrating ionizing particles, most of the times when a neutral particle entered the iron and produced a pi-meson there, another ionizing particle would discharge tray D. Moreover, if secondary neutral particles (presumably neutrons since (γ, μ) reactions are known to be unimportant in these showers) can produce slow mesons in the iron about tray C, some of the charged particles crossing tray D probably do so also. Hence, Piccioni's experiment III gives evidence that a *large* fraction of the stopped pi-mesons are produced in the lower layers of absorber, which act, therefore, not only as absorbing layers but also as producing layers. The flatness of the differential absorption curve in experiment II is likely due to a cascade process, and does not mean that the only process of energy loss is ionization.*

Secondly, we wish to question the nature of the nuclear interactions by which pi-mesons are expected to be prevented from making a delayed coincidence. Piccioni's counter geometry was such that nuclear scattering could not be effective even if the cross section were large. It is true that negative pi-mesons of practically zero velocity can be captured in a process that gives rise to no new mesons; but is such a process to be expected for pi-mesons of high energy? We know of no evidence to this effect. Indeed, a nuclear interaction of a high energy pi-meson is likely to result in one or more mesons of reduced energy, so that the occurrence of such a reaction in the iron just above tray C might be expected to *increase* the probability of recording a delayed coincidence not to decrease this probability. Actually, however, we can only conjecture on this point, since cloud-chamber observations of penetrating showers never have allowed identification of both the primary and the secondary particles.

At any rate, in experiment IV the coincidences $(HS)_{del}$, are proportional to the sum of (1), the number of pi-mesons entering the absorber and brought to rest there by any combination of energy loss processes (not necessarily by ionization alone) and, (2) the number of mesons produced and stopped in the layer. This sum was 19.8 ± 1.8 hr.$^{-1}$. The term (1), according to Piccioni's experiment III, was certainly less than 16 ± 2 hr.$^{-1}$, and possibly much less. The net absorbing effect of the same layer on all ionizing particles (absorption minus production in the layer) was $(HS)_F=15.7\pm1$ hr.$^{-1}$. This is quite reasonable, and does not exclude either the presence of some protons, or nuclear interactions of pi-mesons as a process of energy loss.

Consider next the absorption experiment (I), in which rather thin (83–90 g-cm^{-2}) lead or iron absorbers were placed underneath the thick lead filter, just above the lowest counter tray, C. We suggest that nuclear reactions are likely an important process of energy degradation for pi-mesons as well as nucleons, as long as the energy is high; but that when the kinetic energy becomes about equal to μc^2 for mesons, or 2 μc^2 for protons, the nuclear cross section is low and ionization loss predominates. At this energy the residual range is still about 80 g-cm^{-2}. Thus, nuclear collisions degrade the energy, but ionization stops the particles. The last hundred g-cm^{-2} of absorber causes mainly the ionization loss that stops the particles, not the catastrophic reactions that degrade the energy, for those particles that stop. Hence lead and iron are expected to be equivalent stopping agents in thin layers at the bottom, even if the chief process of energy degradation is nuclear collisions that occur with geometric cross section. If the latter is true, iron should appear a more effective absorber than lead if placed near the top of the pile, rather than at the bottom.

Fourthly, in condensed materials the cross section for absorption of the hard shower producers arriving from the air (nucleons) is much less than the geometric nuclear cross section. Actually no indisputable measurements have been made of the absorption mean free path λ_a in condensed materials, because of experimental difficulties. Bridge[3] has published the values $\lambda_a(\text{Pb})=430\pm90$ and $\lambda_a(\text{Fe})=320\pm70$ g-cm^{-2}, and Hudson[4] has obtained the value $\lambda_a(\text{Pb})=600\pm250$ g-cm^{-2}, by study of bursts containing penetrating particles. Tinlot and Gregory[5] have found $\lambda_a>310$ g-cm^{-2} Pb by study of hard showers. For star producers, λ_a has been measured with greater certainty[6] and is about 310 g-cm^{-2} in Pb, 160 in carbon and 200 in ice. Stars are on the average phenomena of lower energy than hard showers, so that star producers may not multiply as much as HS producers. However, in all the measurements, λ_a appears much longer than the collision mean free path λ_i, which has been well measured[7] in Pb and is 160 g-cm^{-2}, while in carbon it is about 83 g-cm^{-2}.[8] Presumably the difference between λ_a and λ_i is due to production of secondaries that are capable of further nuclear interactions, like those observed in cloud chambers. Hence even if pi-mesons have an absorption mean free path several times longer than the value corresponding to the geometric cross section, this does not imply that they are less strongly absorbed than high energy nucleons, nor that their collision cross section is less than the geometric value.

In air, λ_a and λ_i are more nearly equal (taking λ_i from measurements on condensed materials of similar atomic number).[8] This is most easily explained by assuming that the nuclear cascade process in condensed materials involves nuclear interactions of pi-mesons. In air the pi-mesons cannot play this role because of their short lifetime.

Therefore we think there still exists no conclusive direct evidence about the nuclear interaction properties of fast pi-mesons, and that indirect evidence favors a large cross section.

[1] O Piccioni, Phys. Rev. **77**, 6 (1950).
[2] Lovati, Mura, Salvini, and Tagliaferri, Phys. Rev. **77**, 284 (1950).
* Dr. Piccioni has kindly pointed out that the tray D has an apparent inefficiency of six percent, as judged by the difference between the rates A_2BC and A_2BCD; and that the HS defined only by A_2B contain on the average only one ionizing particle striking tray C in experiment III, when it contains only four counters. These facts modify the above statements only slightly. Still it appears that 2×12 or 24 percent of the stopped mesons are locally produced by neutrons, and likely an equal number are produced in secondary reactions by charged particles. The large statistical errors in experiment III make the precise magnitude of this effect very uncertain, but many cloud-chamber photographs (as well as recent, unpublished counter experiments) support the contention that the cascade multiplication of penetrating particles in hard showers is a process of major importance.
[3] H. S. Bridge and B. Rossi, Phys. Rev. **75**, 810 (1949).
[4] D. E. Hudson, Echo Lake Conference (June 1949).
[5] J. Tinlot and B. Gregory, Phys. Rev. **75**, 519 (1949). Their experimental arrangement was such as to measure a length intermediate between λ_s and λ_i.
[6] Bernardini, Cortini, and Manfredini, Phys. Rev. **74**, 845 and 1878 (1948); E. P. George and A. C. Jason, Proc. Phys. Soc. London **A62**, 243 (1949) and *Research* (Special Supplementary Volume, Colston Papers) (1949); Harding, Lattimore, Li, and Perkins, Nature **163**, 319 (1949).
[7] G. Cocconi, Phys. Rev. **75**, 1074 (1949) and **76**, 984 (1949); E. P. George and A. C. Jason (unpublished communication).
[8] λ_s(air) = 118, J. Tinlot, Phys. Rev. **74**, 1197 (1948); λ_i(carbon) = 90–100, G. Cocconi (reference 7); λ_i(carbon) = 85, W. D. Walker and K. Greisen (unpublished); λ_i(carbon) = 70, E. P. George and A. C. Jason, reference 7.

Cross Sections for the Photo-Disintegration of Nitrogen and Oxygen Nuclei by 100-Mev Betatron X-Rays*

E. R. Gaertner and M. L. Yeater
Research Laboratory, General Electric Company, Schenectady, New York
January 16, 1950

NUCLEAR disintegrations caused by x-rays from the 100-Mev betatron have been investigated with a cloud chamber.[1] The disintegrations studied are those occuring in the filling gas of the cloud chamber; they are observed as single, double (flag), and multiple (star) tracks. The singles are nuclear recoils mostly from (γ,n) processes; according to our preliminary analysis most of the flags in nitrogen result from (γ,pn) reactions; the stars represent various modes of disintegration involving the emission of several charged particles and probably neutrons. Approximate values of the integrated cross sections have been obtained for the flags in air, and for singles, flags, and stars in nitrogen and oxygen, for a peak betatron energy of 100 Mev. The latter measurements give the total integrated photo-disintegration cross sections for nitrogen and oxygen.

The experimental procedure is as follows. X-rays from the General Electric 100-Mev betatron pass through an aperture in a lead shield, which defines a beam $\frac{1}{8}$ in.×$\frac{3}{4}$ in. in cross section, and enter the cloud chamber through a thin window. The data for air are taken with the x-ray intensity adjusted so that an average of one positron-electron pair in ten expansions is formed in the gas. The data for nitrogen[1] and oxygen are taken at a higher intensity, yielding an average of one nuclear disintegration in five expansions; the growth time of the tracks is shortened in this case to reduce the background caused by electron tracks.

The measurements with the air-filled chamber involve a simultaneous observation of flags and positron-electron pairs. This gives a ratio of the flag cross section to the pair cross section, when account is taken of the x-ray energy interval in which flags are produced. The mean x-ray energy for producing flags in nitrogen is about 30 Mev, according to our previous measurements.[2] The ratio of the flag cross section to the pair cross section is given by a total count of 27 flags and a count of 344 pairs with energy in the range 30±10 Mev.[3] Using the pair cross section suitably averaged over this energy interval, we find the integrated flag cross section to be 0.3 Mev-barn. The estimated error is ±20 percent, determined mostly by the number of events counted.

The flag cross sections for nitrogen and oxygen can be derived from the value for air if their relative cross sections are known.[4] A comparison of these cross sections has been made by counting the flags produced in oxygen and in nitrogen by strong x-ray beams monitored with a Victoreen r-meter. The oxygen cross section is 90 percent of the nitrogen cross section, according to a count of 185 flags in nitrogen and 166 in oxygen for equal r-meter readings. The integrated flag cross section for each is, therefore, approximately equal to the measured value for air.

The flag cross section for nitrogen has been measured in an independent way by comparing the number of flags observed in nitrogen with the number of x-ray quanta in the appropriate energy interval at 30 Mev. The latter number is obtained from the reading of a Victoreen r-meter by the use of a previous absolute calibration[5] of the number of quanta per Mev at 30 Mev per unit r-reading. In this way we obtain an integrated flag cross section of 0.36 Mev-barn, in satisfactory agreement with the value measured by our first method. This result is based on a count of 212 flags. The estimated error is ±40 percent, determined primarily by the probable error of the intensity calibration.

The (γ,n) cross sections for nitrogen and oxygen have been derived from the ratio of singles to flags, on the assumption that these reactions are produced by x-rays in the same energy interval. For nitrogen the (γ,n) cross section is 25 percent[1] of the flag cross section, or 0.08 Mev-barn. For oxygen the (γ,n) cross section is 52 percent of the flag cross section, or 0.15 Mev-barn, based on a count of 315 flags and 164 singles.

The total photo-disintegration cross sections can be derived from the single and flag cross sections and our data relating to multiple disintegrations. The ratio of flags to stars is 3.0 for nitrogen;[1] for oxygen it is 4.4, as given by a count of 636 flags and 144 stars. Assuming the x-ray spectrum to be of the form dE/E and taking the energy range for star production to be about 30–60 Mev, we find the star cross section to be 0.16 Mev-barn for nitrogen and 0.11 Mev-barn for oxygen. The total integrated photo-disintegration cross section, up to 100 Mev, is therefore about 0.6 Mev-barn for both nitrogen and oxygen.

Our results for the (γ,n) cross sections are in good agreement with other measurements made in this Laboratory. Perlman and Friedlander[6] give values of 2.2 and 2.3, respectively, for the (γ,n) cross sections in oxygen and in carbon relative to nitrogen. Using the value of 0.15 Mev-barn for carbon measured by Lawson and Perlman,[7] one obtains a (γ,n) cross section of 0.14 Mev-barn for oxygen and 0.07 Mev-barn for nitrogen.

The cooperation of the betatron staff is gratefully acknowledged.

* The cloud-chamber equipment used in this investigation was developed under Contract N7onr 332 with the ONR.
[1] For additional information about the photo-disintegration of nitrogen see E. R. Gaerttner and M. L. Yeater, Phys. Rev. **77**, 570 (1950). The apparatus is described in Rev. Sci. Inst. **20**, 588 (1949).
[2] The energy dependence of flags and stars in nitrogen is discussed in reference 1. The same energy dependence is assumed for oxygen.
[3] The numerical value of the flag cross section is not sensitive to the choice of interval up to about ±20 Mev.
[4] About 1 percent argon is present in the air. A preliminary study of the flags produced in an argon-filled cloud chamber indicates that the effect of this contaminant is negligible.
[5] E. R. Gaerttner and M. L. Yeater, Phys. Rev. **76**, 363 (1949).
[6] M. L. Perlman and G. Friedlander, Phys. Rev. **74**, 442 (1948).
[7] J. L. Lawson and M. L. Perlman, Phys. Rev. **74**, 1190 (1948).

The Half-Life of Carbon Fourteen and a Comparison of Gas Phase Counter Methods*

Warren W. Miller, Robert Ballentine, William Bernstein, Lewis Friedman, A. O. Nier, and R. D. Evans
Brookhaven National Laboratory, Upton, New York, University of Minnesota, Minneapolis, Minnesota, and Massachusetts Institute of Technology, Cambridge, Massachusetts
January 16, 1950

OF the published determinations of the half-life of C^{14}, three have been done by methods that would allow accuracy of 5 percent or better. All are by mass spectrometry of a rich sample of active material and absolute gas counting of a diluted aliquot of the same material. The first[1,2] was done by diluting as carbonate ion in solution, and counting in a differential CO_2-CS_2 G-M counter which eliminates end effects. The value found for the half-life was 6360±200 years. Two more recent papers[3,4] have

reported determinations by very similar methods and the values obtained are in close agreement, 5720±47 and 5589±75 years, respectively. Both of the latter procedures involve expansion and dilution of active CO_2 gas to obtain samples which were counted as small partial pressures of CO_2 in argon-alcohol G-M counters.

Over the last two years we have carried out a series of experiments that sum up to two completely separate and independent determinations of this half-life with different source materials, isotope abundance determinations on different mass spectrometers, different counting methods, and many of the steps of the experimental procedures by different operators. The work does not clear up the discrepancy between the two values previously reported but does indicate a basis on which to make a choice of values, and a possible source of discrepancy.

Determination I.—This determination was carried out on a lot of Oak Ridge C^{14} as $BaCO_3$ identified as MIT-1. The isotopic abundance of C^{14} in the total CO_2 obtained from a portion of this material by vacuum fusion with $PbCl_2$ was determined on a mass spectrometer previously described by one of us.[5] Applying the usual corrections and accounting for the presence of natural C^{13} and O^{18} gave the abundance of C^{14} as 3.80 mole percent.

The CO_2 content of MIT-1 was determined gas volumetrically by a method known to be better than 1 percent from determinations on $BaCO_3$ of known purity. It assayed 98.3 percent of theoretical.

Direct stepwise dilution and homogenization of solid $BaCO_3$, by evolution of the CO_2 from the active and diluent $BaCO_3$ and reabsorption in $Ba(OH)_2$ solution, was employed as a reliable method of dilution to a specific activity suitable for counting. By two different procedures, samples F and K were obtained from MIT-1 diluted by the factors 5.247×10^5 and 3.343×10^5 respectively. The procedures were checked in blank runs and the factors are good to better than 1 percent.

The activity of the CO_2 obtained from portions of materials F and K above was measured in CO_2 filled G-M counters. The counters, associated circuits, and the operating characteristics of the system have been previously described,[6,7] as has also the factor V_T/V_C, the ratio of the total volume to the cathode volume, that has been shown to normalize large variations of counter geometries to the same response. It is this point, together with the independence of the system to other parameters that has been taken to justify the assumption that the adjusted counter response very nearly represents an absolute count. From four determinations on the two dilutions in two different counter tubes the average value of the disintegration rate of MIT-1 is 2.36×10^7 d.p.m./mg with a spread of less than 1 percent.

Combining the specific activity, the chemical assay, and the isotopic abundance, the half-life is calculated to be 6360 years. The limiting error is in the isotopic abundance and is not more than 3 percent.

Determination II.—A different lot of Oak Ridge C^{14} as $BaCO_3$ identified as AUI-30 was assayed gas volumetrically for CO_2 and found to yield 92.4 percent of theoretical.

One of the samples of active gas obtained in the chemical assay was run on a Consolidated-Nier isotope-ratio mass spectrometer using standard techniques for this commercial instrument. The value found, after accounting for the natural C^{13} and O^{18} abundances, was 4.18 mole percent C^{14} in the active CO_2.

The CO_2 obtained from a weighed sample of AUI-30 and diluent $BaCO_3$ was absorbed in NaOH and aliquots of this solution or dilutions made from it with inert carbonate solution were taken for counting.

The gas sample filled proportional counter method used for the measurement of the activity of these diluted solutions has been recently described.[8] In substance it is a cylindrical counter tube of conventional design filled with methane and CO_2, high voltage supply, amplifier, discriminator, and scaler circuit. It is sensitive to 1-kev electrons, does not produce multiple pulses, and its response in the region of the characteristic curve in which the measurement is made is flat within 1 percent. The V_T/V_C factor used with the G-M counters has been shown to apply in the same manner and its use has been justified for the same reason.

Two separate determinations of the specific activity of AUI-30 made on the above solution, each consisting of a series of values obtained on different counter tubes and circuit components combined with their appropriate dilution factors, give an average value of 2.81×10^7 d.p.m./mg with an error of less than 2 percent.

In the same manner as before, the half-life is calculated to be 5513 years, with an over-all error limited by the isotopic abundance determination to about 3 percent.

Activity K, used in determination I, was assayed by the proportional counter method and the ratio of specific activities shown by the two methods, 1.15, is the same as the ratio of the half-lives by the two methods, and indicates that the sole source of the discrepancy between the two determinations must lie with the counter methods. Including the work presented here, the five determinations fall into two groups, two values at 6400 years, and three at 5600 years. The unique difference between the two groups is the type of counter system used. The latter three values have been done with two radically different counter methods, while both of the former values were determined with the CO_2-CS_2 G-M counter system. It seems unlikely that the two different methods used for the second value would be erroneous by the same amount and we are inclined to the tentative view that the CO_2-CS_2 G-M counters may have an efficiency of only about 85 percent, in spite of the recent careful work of Hawkings.[9] Further work on the absolute efficiency of the CO_2-CS_2 G-M counter is being undertaken.

* This work was carried out in part at M.I.T., with the support of the Joint Program of the AEC and ONR and in part at Brookhaven National Laboratory with the support of the AEC.

[1] Hawkings, Hunter, Mann, and Stevens, Phys. Rev. 74, 696 (1948).
[2] Hawkings, Hunter, Mann, and Stevens, Can. J. Research 27, 545 (1949).
[3] Engelkemeir, Hamill, Inghram, and Libby, Phys. Rev. 75, 1825 (1949).
[4] W. M. Jones, Phys. Rev. 76, 885 (1949).
[5] A. O. Nier, Rev. Sci. Inst. 18, 398 (1947).
[6] W. W. Miller, Science 105, 123 (1947).
[7] S. C. Brown and W. W. Miller, Rev. Sci. Inst. 18, 496 (1947).
[8] W. Bernstein and R. Ballentine, Rev. Sci. Inst. (in press).
[9] Hawkings, Hunter, and Mann, Can. J. Research 27, 555 (1949).

The Lateral Distribution of Photons in Extensive Air Showers

G. MOLIÈRE
University of Tübingen and Kaiser-Wilhelm-Institut für Physik, Heckingen, Germany
January 16, 1950

THE lateral structure of single cosmic-ray extensive air showers has recently been investigated, using "core selectors" (CS), by Cocconi, Coccori-Tongiorgi, and Greisen[1] and independently by Amaldi and co-workers.[2] As far as the electron density, measured by unshielded G-M counters with varied distances from the CS, is concerned, both groups of experimenters found fairly good agreement with the theoretical results obtained by the author on the basis of cascade theory and Coulomb scattering.[3] Amaldi in his experiments apart from unshielded counters also used lead shielded ones. His results in the latter case, where multiplication due to photons plays an important role, seemed strongly to contradict the author's theory. This conclusion had been drawn under the implicit assumption that the photon density (which had actually not yet been calculated by us) will be roughly proportional to that of the electrons.

To check this assumption we recently extended our theory to the photons in a single extensive shower. As a result, the number of photons of energy E within dE striking an element of area dS at a distance r (radiation units) from the core may be described with good approximation by the formula:

$$g(E,r)dEdS=\frac{2dEdS}{\pi K^2}\left\{\frac{1.03}{0.1}\frac{\exp[-2Er/(0.1)^{\frac{1}{2}}K]}{2Er/(0.1)^{\frac{1}{2}}K}+\frac{0.26}{3.25}\exp[-2Er/(3.25)^{\frac{1}{2}}K]\right\}. \quad (1)$$

For easy comparison our corresponding result for electrons may be reproduced here:

$$f(E,r)dEdS=\frac{2dEdS}{\pi K^2}\left\{\frac{2.8}{1.36}L_{-1/6}\left(\frac{2Er}{(1.36)^{\frac{1}{2}}K}\right)-\frac{1.8}{0.71}L_{5/6}\left(\frac{2Er}{(0.71)^{\frac{1}{2}}K}\right)\right\},\quad(2)$$

with the abbreviation

$$L_p(x)=(\pi/2)(x/2)^p i^{p+1}H_p^{(1)}(ix)/p!.$$

[$K\approx 2\times 10^7$ ev in (1) and (2).] Both formulas are valid for particle energies above the critical one and for big air showers at their maximum development, the normalization being chosen so that the energy spectrum is given by $E^{-2}dE$ for electrons and by $1.29E^{-2}dE$ for photons [as approximately valid for big showers at maximum, apart from a common constant factor in (1) and (2)].

The photon density (1) differs greatly from that of electrons by its more rapid singularity at $r=0$; varying as r^{-1} for photons as compared with $r^{-\frac{1}{2}}$ for electrons. This means a much stronger concentration of photons within the core and a more rapid variation of photon density in its vicinity than expected from the corresponding behavior of electrons. (The somewhat larger r.m.s.-spread of photons is almost entirely due to the tail of (1) and does not, therefore, contradict the above result.) This seems, at least qualitatively, to agree with the above-mentioned results of Amaldi and also with those recently obtained by Clay[4] with six- and eightfold coincidences of shielded counters. Our result further suggests that the stars which, according to observations of Blackett,[5] occur with an abnormally high frequency in the cores of cascade showers and which are evidently produced by some neutral radiation, are eventually due to energetic photons. Processes of this kind could be the source of fast nucleons and of the weak meson component accompanying the extensive air showers according to results of Cocconi and Greisen,[1] Brown and McKay,[6] and others.

The details of our theory will be published elsewhere.

Note added in proof: The first direct experimental determination of the lateral structure of single extensive air showers has been carried through by R. W. Williams.[7] His results are consistent with those of the other experimenters quoted (references 1 and 2, below) and with the authors calculations.

[1] Cocconi, Cocconi-Tongiorgi, and Greisen, Phys. Rev. 76, 1020 (1949).
[2] E. Amaldi, Como Congress (September, 1949).
[3] G. Molière, Naturwiss. 30, 87 (1942); W. Heisenberg, *Cosmic Radiation* (Dover Publications, New York, 1946). See also Zeits. f. Physik 125, 250 (1948-49).
[4] J. Clay, Proc. Konink. Nederland. Akad. Wetenschap. 52, No. 4, 2 (1949).
[5] P. M. S. Blackett, Como Congress (September, 1949).
[6] W. W. Brown and A. S. McKay, Phys. Rev. 76, 1034 (1949).
[7] R. W. Williams, Phys. Rev. 74, 1689 (1948).

On the Magnetic Moments of Mn^{55}, Co^{59}, Cl^{37}, N^{15}, and N^{14} *

W. G. Proctor and F. C. Yu
Department of Physics, Stanford University, Stanford, California
January 18, 1950

USING the nuclear induction radiofrequency spectrometer described earlier,[1] the nuclear magnetic resonances of Mn^{55}, Co^{59}, Cl^{37}, N^{15}, and N^{14} have been observed. The magnetic moments listed in column 2 of Table I have been computed directly from our measured frequency ratios and the value of the magnetic moment of the nucleus used as a standard. Diamagnetic corrections were not applied; they are listed separately in column 3, and have been determined by linear interpolation from the values for specific atoms given by Lamb, using Hartree fields.[2] These corrections are to be applied so as to increase the magnitudes of the magnetic moments.

TABLE I. Magnetic moments and diamagnetic corrections.

Nucleus	Nuclear moment in nuclear magnetons	Diamagnetic correction in percent
Mn^{55}	$+3.4624\pm0.0004$	0.191
Co^{59}	$+4.6399\pm0.0006$	0.214
Cl^{37}	$+0.6835\pm0.0001$	0.113
N^{15}	-0.28302 ± 0.00003	0.034
N^{14}	$+0.40369\pm0.00004$	0.034

The resonance of Mn^{55} was located near 8.3 Mc, using a field of 7900 gauss and a 2.0-molar solution of $LiMnO_4$ in water as the sample. Comparing the resonance frequency three times with that of Na^{23}, from a sample containing 0.25-molar NaCl in 1.0-molar $MnSO_4$, we found

$$\nu(Mn^{55})/\nu(Na^{23})=0.9372\pm0.0001.$$

The sign of the magnetic moment, and spin, agreed with the h.f.s. data,[3] which indicated a spin of 5/2 and a magnetic moment of $3.0\mu_N$.

The frequency of the Co^{59} resonance was measured, by use of a 1.0-molar aqueous solution of the diamagnetic compound $K_3Co(CN)_6$ at a field of 6600 gauss and a radiofrequency near 6.6 Mc. Comparing this frequency to that of Na^{23} five times, we found

$$\nu(Co^{59})/\nu(Na^{23})=0.89709\pm0.00009.$$

Verifying that the spin is 7/2 and that the magnetic moment is positive,[4] we find this frequency ratio leads directly to a magnetic moment of $(4.6399\pm0.0006)\mu_N$, which is much larger than the value 2.0 to 3.0 nuclear magnetons obtained by More.[4] The new value indicates that the odd-proton is in an $f_{7/2}$ orbit, as proposed by Mayer;[5] this nucleus has hitherto been regarded as an exception to her single-particle model of the nucleus.

The frequencies of resonance of the chlorine isotopes were compared four times, using concentrated HCl and a field of 9400 gauss, with the result that

$$\nu(Cl^{35})/\nu(Cl^{37})=1.2014\pm0.0001.$$

Omitting the negligible correction from the reduced electron mass ratios, this differs by about 0.1 percent from the ratio $a_{35}/a_{37}=1.20272\pm0.00008$ of the magnetic dipole interaction constants as determined by Davis, Feld, Zabel, and Zacharias[6] by the atomic beam method. In computing $\mu(Cl^{37})$ we have made use of the frequency ratio $\nu(Cl^{35})/\nu(H^1)=0.09799\pm0.00007$ as determined by Chambers and Williams.[7]

The resonance frequency of N^{15} at a field of 11,000 gauss was compared with that of deuterium, the sample being 5 ml of liquid ammonia together with 1.18 grams of NH_4NO_3 and 1.25 grams of $Cr(NO_3)_3\cdot 9H_2O$ in a sealed tube. The N^{15} in the ammonia was enriched to about 7.5 percent; the deuterium was from a 1.8-molar aqueous solution of $MnSO_4$ containing 25 percent D_2O. We found

$$\nu(N^{15})/\nu(D^2)=0.66004\pm0.00006.$$

The sign of the magnetic moment, which was previously unknown, has been determined to be negative; its value is in good agreement with the molecular beam value.[8]

The frequencies of the resonance of N^{14} and D^2, from samples of concentrated HNO_3 and 0.6-molar $MnSO_4$ in 85 percent D_2O, respectively, were compared at 11,000 gauss with a General Radio Model 271 frequency meter, with the result that

$$\nu(N^{14})/\nu(D^2)=0.47070\pm0.00005.$$

The magnetic moment is in good agreement with the molecular beam value.[9] Since we have observed that the frequency of resonance of N^{14} in liquid samples depends strongly upon the compound in which it is contained (see the following letter), we have felt that it is important to state carefully what compounds have been used as our samples.

The magnetic moment of Na^{23} has been computed by taking $\mu(H^1)=2.79348\pm0.00014$ nuclear magnetons,[10] and $\nu(Na^{23})/\nu(H^1)=0.26450\pm0.00003$;[11] the magnetic moment of D^2 was similarly computed using $\mu(D^2)/\mu(H^1)=0.307013$.[12]

We would like to express our appreciation to Professor Felix Bloch for his continued interest in our work. Thanks are also due Mr. William S. Gorton Jr. of the Department of Chemistry for preparing the liquid ammonia sample.

* Assisted by the Joint Program of the AEC and the ONR.
[1] W. G. Proctor, Phys. Rev. **75**, 522 (1949).
[2] W. E. Lamb, Jr., Phys. Rev. **60**, 817 (1941).
[3] R. A. Fisher and E. R. Peck, Phys. Rev. **55**, 270 (1939).
[4] K. R. More, Phys. Rev. **46**, 570 (1934); Phys. Rev. **47**, 256 (1935).
[5] M. G. Mayer, Phys. Rev. **75**, 1969 (1949).
[6] Davis, Feld, Zabel, and Zacharias, Phys. Rev. **76**, 1076 (1949).
[7] William H. Chambers and Dudley Williams, Phys. Rev. **76**, 638 (1949).
[8] J. R. Zacharias and J. M. B. Kellogg, Phys. Rev. **57**, 570 (1940).
[9] S. Millman and P. Kusch, Phys. Rev. **60**, 91 (1941).
[10] H. Taub and P. Kusch, Phys. Rev. **75**, 1481 (1949).
[11] F. Bitter, Phys. Rev. **75**, 1326 (1949).
[12] This figure is that given by Bloch, Levinthal, and Packard, Phys. Rev. **72**, 1125 (1947), rounded to six places.

The Dependence of a Nuclear Magnetic Resonance Frequency upon Chemical Compound*

W. G. Proctor and F. C. Yu
Department of Physics, Stanford University, Stanford, California
January 18, 1950

In the course of measurements on N^{14}, mentioned in the previous letter, we made the surprising observation that its frequency of resonance, in liquid samples, depended strongly upon the chemical compound in which it was contained.[1,2] This effect is strikingly demonstrated by the appearance of two resonances, separated by 1.6 kc in the neighborhood of 3300 kc, corresponding to a field of 10,500 gauss, using a solution of NH_4NO_3 in 2.0-molar $MnSO_4$ as a sample. These resonances presumably arise from the NH_4^+ and NO_3^- complexes, since samples of $NH_4C_2H_3O_2$ and HNO_3 separately give rise to two different resonances whose frequencies approximate those from the above sample. The separation is four times greater than the line widths measured between points of maximum slope.

We have observed, within a resolution of 0.1 kc, that the N^{14} resonances from the ion NH_4^+ from the compounds NH_4NO_3, $NH_4C_2H_3O_2$, and MH_4Cl coincide at one frequency, while those from the ion NO_3^- from the compounds NH_4NO_3, HNO_3, and $Cu(NO_3)_2$ coincide at another frequency. Measuring the N^{14} resonances from other molecules relative to that arising from the ion NO_3^- from HNO_3 or NH_4NO_3, we have obtained the results given in Table I. All such frequency shifts have been in the direction of lower frequency.

The separations of resonances from four pairs of compounds were also measured at 6700 gauss, corresponding to a frequency of 2100 kc, to determine whether or not the frequency separations were independent of the field intensity. They are apparently proportional to it, for the ratios of the separations are in agreement with the ratio 6700/10,500=0.64, within our experimental resolution. (See Table II.)

We further made the observation that the separation of the two resonances arising from NH_4NO_3 was dependent on the concentration of the paramagnetic salt $MnCl_2$ added to it. A 7.5-molar solution of this salt without $MnCl_2$ shows two resonances separated by 1.0 kc, as given in Table I, but with 1.0- and 2.0-molar concentrations of $MnCl_2$ the separations become 1.4 kc and 1.6 kc, respectively.

We shall continue to investigate this phenomenon because of its direct significance for the interpretation of nuclear magnetic resonance frequencies in terms of nuclear moments, as well as to obtain an insight into its origin. With the largest observed line shift amounting to about 5 parts in 10^4, this effect is almost twice as large as the total diamagnetic correction calculated for the atom. These calculations, however, do not hold for the polyatomic molecules which we have studied and appreciable modification of the diamagnetism, as well as terms due to induced paramagnetism (high frequency matrix elements) can be expected, particularly in cases where three out of seven electrons may be strongly influenced by the chemical bond. The fact that the shifts are of the same order of magnitude as the diamagnetic correction and exhibit likewise proportionality to the applied field suggests a similar origin, although we have not been able to explain satisfactorily the observed magnitude of the effect. Until it is clearly understood, the accuracy of magnetic moments determined under certain chemical conditions remains somewhat in doubt.

We should like to express our appreciation to Professor Felix Bloch for stimulating discussions about this work.

Table I. Frequency shifts relative to the resonance from the ion NO_3^- at 10,500 gauss.

Compound observed	Frequency shift (kc)
NH_4^+ from NH_4NO_3, $NH_4C_2H_3O_2$, NH_4Cl	−1.0
Liquid NH_3, containing 0.6-molar $Cr(NO_3)_3$; NH_4OH	−1.2
$(NH_2)_2CO$	−1.0
KCN	−0.2

Table II. Resonance frequency separations with different compounds and field intensities.

Compounds compared	Separation (kc) at 10,500 gauss	Separation (kc) at 6700 gauss	Ratio
NH_4^+ and NO_3^- from 7.5-molar NH_4NO_3 in 2.0-molar $MnSO_4$	1.6	0.9	0.58
HNO_3 and $NH_4C_2H_3O_2$	1.0	0.7	0.70
HNO_3 and $(NH_2)_2CO$	1.0	0.6	0.60
NH_3, containing 0.6-molar $Cr(NO_3)_3$ and NO_3^-, from NH_4NO_3	1.2	0.7	0.58

* Assisted by the Joint Program of the AEC and the ONR.
[1] W. C. Dickinson, at M. I. T., has also observed similar shifts for F^{19} in different compounds. We are grateful to Professor F. Bitter for communicating this information to us.
[2] W. D. Knight, Phys. Rev. **76**, 1259 (1949), has observed a large frequency difference between the nuclear magnetic resonance frequency of a metal and its salt. The satisfactory explanation which he has given for this difference does not apply, however, to our case.

Spallation Products of Arsenic with 190-Mev Deuterons*

H. H. Hopkins, Jr.
Department of Chemistry and Radiation Laboratory, University of California, Berkeley, California
January 5, 1950

Recent investigations[1] of the nuclei formed when arsenic is bombarded with 190-Mev deuterons in the 184-in. cyclotron have been extended.

The target material consisted of twice sublimed arsenic. Spectrographic analysis[2] showed no impurity in sufficient quantity to account for the formation of any of the isotopes reported here with the observed yield.

The use of improved chemical separations and counting techniques has enabled the identification of 38 nuclear species among the elements from chromium through selenium. Table I lists the isotopes identified, the observed and the "nominal" half-lives as reported in the literature,[3] and the yields relative to that of As^{72} taken as 1.00.

In calculating yields, the extent of electron capture has been taken from the data collected in reference 3. For Se^{73}, Ge^{69}, and Ga^{66}, crude absorption measurements indicated that approximately two-thirds of the decays are by electron capture. The yield of As^{72} is based on the count of beta-particles, as no x-rays were observed (<50 percent of the disintegrations). The yields reported here should all be accurate to within a factor of two and many accurate to within 20 percent, depending on the certainty with which electron-capturing ratios and counting efficiencies of x-rays are known.

Table I contains two changes in isotope assignment differing from those previously reported.[1] The 44-min. selenium and 52-min.

arsenic daughter are placed at mass 70 since careful separations revealed no active germanium daughter. The 40-hr. germanium cannot be found when germanium is chemically separated from the 60-hr. As^{71}, so the former is assigned to mass 69, in agreement with the work of McCown, Woodward, and Pool.[4]

It is reasonable to assume that stable nuclei are formed in the spallation process with yields of the same order of magnitude as those of the adjacent isotopes. On this basis we assign a yield to each isotope which we cannot observe, following the trends apparent among the observed isotopes. The resultant yield pattern can be described as follows: (1) For each element below arsenic, the yields of the isotopes increase towards the line of nuclear stability. (3) For each mass number the yields of isobars increase towards the line of stability. (3) The lower the atomic number, the lower becomes the total yield of a given element.

TABLE I. Isotopes produced by $_{33}As^{75}+D^+$ (190 Mev).

Isotope	Radiation type[a]	Nem. half-life[a]	Obs. half-life	Yield rel. As^{72}[b]
$_{34}Se^{75}$	K	127 days	120 days	0.14
Se^{73}	β^+, K	6.7 hr.	6.7 hr.	0.3
Se^{72}	K	9.5 days	9.7 days	0.08[c]
Se^{70}	β^+	44 min.	~44 min.	0.004[c]
$_{33}As^{74}$	β^+, β^-	17.5 days	19 days	1.25
As^{73}	K	90 days	(long)	2
As^{72}	β^+	26 hr.	26.7 hr.	1.00[b]
As^{71}	K	60 hr.	60 hr.	0.7[c]
As^{70}	β^+	52 min.	52 min.	0.1
$_{32}Ge^{71}$	K	11 days	11 days	2.0
Ge^{69}	β^+, K	39.7 hr.	40 hr.	0.9
Ge^{68}	K	250 days	250 days	0.3[c]
Ge^{67}	β^+	23 min.	21 min.	0.1[c]
Ge^{66}	β^+(?)	140 min.	~150 min.	0.008[c]
$_{31}Ga^{70}$	β^-	20.3 min.	20 min.	0.018
Ga^{68}	β^+	68 min.	70 min.	0.56
Ga^{67}	K	78.3 hr.	80 hr.	1.0
Ga^{66}	β^+, K	9.4 hr.	9 hr.	0.6
$_{30}Zn^{72}$	β^-	49 hr.	~50 hr.	0.0002
Zn^{69m}	I.T.	13.8 hr.	13.5 hr.	0.015
Zn^{65}	β^+, K	250 days	(long)	0.2
Zn^{63}	β^+, K	38 min.	39 min.	0.02
Zn^{62}	K	9.5 hr.	10 hr.	0.002[c]
$_{29}Cu^{67}$	β^-	56 hr.	61 hr.	0.013
Cu^{64}	β^+, β^-, K	12.8 hr.	12.8 hr.	0.20
Cu^{62}	β^+	10.5 min.	10 min.	0.10
Cu^{61}	β^+, K	3.4 hr.	3.3 hr.	0.03
$_{28}Ni^{65}$	β^-	56 hr.	56 hr.	0.0006[c]
Ni^{65}	β^-	2.6 hr.	2.6 hr.	0.003
Nu^{57}	β^+	36 hr.	34 hr.	0.00003
$_{27}Co^{61}$	β^-	1.75 hr.	1.83 hr.	0.014
Co^{58}	β^+, K	72 days	~100 days	0.006
Co^{55}	β^+	18.2 hr.	~18 hr.	0.0002
$_{26}Fe^{59}$	β^-	46.3 days	46 days	0.005
$_{25}Mn^{56}$	β^-	2.59 hr.	2.6 hr.	0.0026
Mn^{52}	β^+, K	5.8 days	6.2 days	0.0003
$_{24}Cr^{51}$	K	26.5 days	25 days	0.002
Cr^{49}	β^+	41.9 min.	40 min.	0.00006

[a] See reference 3.
[b] Absolute yield of As^{72}: 0.02 barn.
[c] Determined from measurement of daughter activity.

From a consideration of the Q-values of the reactions and the energy necessary for Coulombic barrier penetrations, we conclude: (1) Reactions leading to arsenic, germanium, and gallium isotopes are mostly non-capture excitation reactions, in which only a fraction of the deuteron's energy is imparted to the nucleus. These comprise more than 90 percent of all the reactions. (2) Less likely processes involving preliminary capture of the deuteron lead to isotopes of lower lying elements. (3) The formation of nuclear species lower than Fe^{59} involves the emission of one or more alpha-particles. Such reactions occur approximately one percent of the time.

The author wishes to thank Mr. James Vale and the members of the 184-in. cyclotron group for performing the many bombardments. He acknowledges the helpful advice of Professors B. B. Cunningham and G. T. Seaborg.

* This work was performed under the auspices of the AEC.
[1] H. H. Hopkins, Jr. and B. B. Cunningham, Phys. Rev. **73**, 1406 (1948).
[2] Analysis performed by Mr. John Conway.
[3] Table of Isotopes from G. T. Seaborg and I. Perlman, Rev. Mod. Phys. **20**, 585 (1948).
[4] McCown, Woodward, and Pool, Phys. Rev. **74**, 1311 (1948).

Electron Recombination in Helium

D. R. BATES
Department of Mathematics, University College, London, England
January 18, 1950

RECENTLY, Biondi and Brown[1] have applied microwave techniques to the study of the rate of decay of ionization in helium. Their main object was the investigation of ambipolar diffusion, but they also took the opportunity of measuring the effective electron recombination coefficient, α, under the following conditions: mean electron energy, 0.039 ev; electron concentration from 8×10^9 to 3×10^{10}/cm³; gas pressure from 20 to 30 mm Hg. They found it to be 1.7×10^{-8} cm³/sec.

With ions of an *atomic* nature only three types of mechanism seem possible, either (a) that the excess energy of the recombining electrons appears as radiation, (b) that it is given up to some third body, or (c) that the electrons disappear through attachment to impurities. We will consider these separately.

(a) Goldberg[2] and Huang[3] have computed the relevant matrix elements associated with direct radiative recombination to the 1^1S, 2^1S, 2^3S, 2^1P and 2^3P levels; those for the remaining levels can be taken as hydrogenic.[4] An elementary calculation shows that the total contribution to α is only about 4×10^{-12} cm³/sec.

In the case of helium there are no suitably located doubly excited states so that dielectronic recombination[5] can be ignored.

(b) A slow electron can lose only about 10^{-3} to 10^{-4} of its kinetic energy in a single collision with a helium atom.[6] Very many collisions are therefore required to bring about any considerable reduction. When allowance is made for this in the well-known Thomson theory[7] of three-body recombination, it appears that the process, $He^+ + e + He \rightarrow 2He$, is negligible. Other electrons may be more important as third bodies. The necessary formulation of the problem has not yet been developed in detail. However, the cross section for the energy-loss collisions is likely to be less than πr^2, where r is the distance such that e^2/r is equal to the mean energy of the electrons; and this yields an α which is too small by more than an order of magnitude.

(c) If η is the coefficient associated with the postulated attachment process, $n(x)$ is the concentration of foreign molecules, and $n(e)$ is the concentration of electrons, then $\eta n(x)/n(e)$ is the maximum possible contribution to α. It appears that $n(x)$ is perhaps 10^{13}/cm³ at a pressure of 25 mm Hg. Thus, η would have to be some 2×10^{-11} cm³/sec. to account for an α of 1.7×10^{-8} cm³/sec. when $n(e)$ is, say, 10^{10}/cm³. This is improbably high.[8] Furthermore, α would only be independent of $n(e)$ if detachment was also rapid so that a quasi-equilibrium could be established between it and attachment;[5] and in this case a still greater η is needed.

It would seem, therefore, that the recombination measurements of Biondi and Brown are difficult to reconcile with the assumption that the ions involved were He^+. If, instead, they were He_2^+, the position would be quite different for dissociative recombination, $He_2^+ + e \rightarrow 2He$, could occur and quantal considerations indicate that this may well be of the required rapidity. It is perhaps relevant to mention that Bates and Massey[9] have suggested that reactions of this type may be mainly responsible for recombination in the ionosphere. Their hypothesis demands that the associated coefficient be of the order 10^{-8} cm³/sec. The ions concerned are of course different, and α may vary greatly from gas to gas.

He_2^+ is known to be stable and has been observed in the laboratory.[10] It may be formed from He^+ through the three-body

process, $He^+ + 2He \rightarrow He_2^+ + He$. Substitution of the interaction constants of Massey and Mohr[11] in the Thomson formula gives that the mean lifetime of a He^+ ion in helium at 25 mm Hg is only about 10^{-5} sec.[12] Since the age of the ions studied by Biondi and Brown ranged from 5×10^{-3} to $1\cdot1\times10^{-2}$ sec., it would seem probable that they were indeed He_2^+. In view of the importance of being certain of the nature of the recombination mechanism, it would be useful if this could be verified by means of a mass spectrograph.

The ambipolar diffusion measurements were conducted at lower pressures but the conditions were still such that He_2^+ might well predominate over He^+. Unfortunately the discrepancy between the results of Biondi and Brown and those of Tyndall and Powell[13] cannot be attributed to this, for Meyeratt[14] claims these latter probably also worked with molecular ions. It is difficult to predict the mobility of He_2^+ as certain collision reactions may introduce complications.

Finally I would like to thank Professor H. S. W. Massey for several helpful discussions.

[1] M. A. Biondi and S. C. Brown, Phys. Rev. **75**, 1700 (1949).
[2] L. Goldberg, Astrophys. J. **90**, 414 (1939).
[3] Su-Shu Huang, Astrophys. J. **108**, 354 (1948).
[4] Bates, Buckingham, Unwin, and Massey, Proc. Roy. Soc. **A170**, 322 (1939).
[5] D. R. Bates and H. S. W. Massey, Proc. Roy. Soc. **A187**, 261 (1947).
[6] R. H. Healey and J. W. Reed, *The Behaviour of Electrons in Gases* (Amalgamated Wireless, Ltd., Australasia, 1941).
[7] J. J. Thomson, Phil. Mag. **47**, 337 (1924).
[8] H. S. W. Massey, *Negative Ions* (Cambridge University Press, London, 1938).
[9] D. R. Bates and H. S. W. Massey, Proc. Roy. Soc. **A192**, 1 (1947).
[10] F. L. Arnot and M. B. M'Ewen, Proc. Roy. Soc. **A171**, 106 (1939).
[11] H. S. W. Masey and C. B. O. Mohr, Proc. Roy. Soc. **A144**, 188 (1934).
[12] *Note.*—The corresponding mean lifetime of Li^+ in the inert gases has been observed to be even shorter [see R. J. Munson and K. Hoselitz, Proc. Roy. Soc. **A172**, 28 (1939)].
[13] A. M. Tyndall and C. F. Powell, Proc. Roy. Soc. **A134**, 125 (1931).
[14] R. Meyeratt, Phys. Rev. **66**, 242 (1944).

Microwave Spectra and Molecular Constants of Trifluorosilane Derivatives. SiF_3H, SiF_3CH_3, SiF_3Cl, and SiF_3Br *

JOHN SHERIDAN† AND WALTER GORDY
Department of Physics, Duke University, Durham, North Carolina
January 12, 1950

$Si^{28}F_3H$ and $Si^{29}F_3H$. The rotational transitions $J=1\rightarrow2$ and $J=2\rightarrow3$ have been observed for $Si^{28}F_3H$. Precise measurements on the $J=1\rightarrow2$ transition yield: $\nu=28{,}831.90\pm0.10$ mc, $B_0=7207.98$ mc, and $I_B=116.39_4\times10^{-40}$ g cm² (with Planck's constant $=6.624_2\times10^{-27}$ erg sec.). With the assumptions, $d_{SiH}=1.55\pm0.05$A and $\angle FSiF=110°\pm1°$, the silicon-fluorine distance, $d_{SiF}=1.555\pm0.005$A, is obtained.

The $J=2\rightarrow3$ transition has been observed for $Si^{29}F_3H$. Failure to detect a hyperfine structure is evidence, but not proof,[1] that the nuclear spin of Si^{29} is ½. Precision measurements are being made on the rotational frequency of this and other transitions. Also, it is expected that measurements can be made on $Si^{30}F_3H$, with Si^{30} in naturally occurring concentrations.

$Si^{28}F_3C^{12}H_3$. Observations of the $J=3\rightarrow4$ and $J=5\rightarrow6$ transitions[2] have been made for $Si^{28}F_3C^{12}H_3$. Precise measurements yield: $\nu=29{,}724.91\pm0.18$ mc for the $J=3\rightarrow4$ transition, $B_0=3715.62$ mc, and $I_B=225.79_4\times10^{-40}$ g cm² (with $h=6.624_2\times10^{-27}$ erg sec.). Assuming all angles to be tetrahedral and assuming $d_{SiF}=1.555$A and $d_{CH}=1.10$A, the SiC distance obtained is 1.88A.

$Si^{28}F_3Cl^{35}$ and $Si^{28}F_3Cl^{37}$. The pure rotational transitions, $J=6\rightarrow7$, $7\rightarrow8$, and $8\rightarrow9$, have been observed for $Si^{28}F_3Cl^{35}$ and the $J=7\rightarrow8$ for $Si^{28}F_3Cl^{37}$. A hyperfine structure, which has not yet been completely analyzed, was observed for each transition. The moments of inertia (I_B) are 338.6×10^{-40} g cm² and 347.5×10^{-40} g cm² for $Si^{28}F_3Cl^{35}$ and $Si^{28}F_3Cl^{37}$, respectively. If $\angle FSiCl$ is taken as 110°30′, as indicated by electron diffraction,[3] the preliminary values, $d_{SiF}=1.55_9$A and $d_{SiCl}=1.99_8$A, are obtained. The SiCl distance thus appears to be shorter than that[4] in SiH_3Cl by about 0.05A.

$Si^{28}F_3Br^{79}$ and $Si^{28}F_3Br^{81}$. The pure rotational transitions $J=15\rightarrow16$ and $16\rightarrow17$ have been observed for $Si^{28}F_3Br^{81}$ and the $J=16\rightarrow17$ for $Si^{28}F_3Br^{79}$. The hyperfine structure has not been completely analyzed. The moments of inertia are 541.4×10^{-40} g cm² and 547.3×10^{-40} g cm² for $Si^{28}F_3Br^{79}$ and $Si^{28}F_3Br^{81}$, respectively. If $\angle FSiBr$ is taken as 110°30′, as is $\angle FSiCl$ in SiF_3Cl, preliminary figures for the bond distances are obtained as follows: $d_{SiF}=1.55_6$A, $d_{SiBr}=2.15_9$A. The SiBr distance is thus probably some 0.05A shorter than that[5] (2.20₉A) in SiH_3Br.

Further work on these molecules is planned to complete the structure determinations and to determine the nuclear couplings and molecular dipole moments.

* The research reported in this document has been made possible through support and sponsorship extended by the Geophysical Research Directorate of the Air Force Cambridge Research Laboratories under Contract No. W(19-122)ac-35. It is published for technical information only and does not represent recommendations or conclusions of the sponsoring agency.
† On leave from Department of Chemistry, University of Birmingham, England.
[1] From the relation between nuclear quadrupole moment and nuclear shell structure found by Gordy [Phys. Rev. **76**, 139 (1949)] one would not expect a large quadrupole moment for Si^{29}. Because of the symmetry of the tetrahedral bonds to Si, the quantity $(\partial^2V)/(\partial z^2)$ would be very small. Hence, if a hyperfine structure exists for $Si^{29}F_3H$, it might be unresolvable.
[2] Concurrently with our work, Minden, Mays, and Dailey (private communication) have made approximate measurements on the $J=2\rightarrow3$ and $3\rightarrow4$ transitions of SiF_3CH_3. They report several lines caused by molecules in excited vibrational states.
[3] Livingston and Brockway, J. Am. Chem. Soc. **66**, 94 (1944).
[4] A. Harry Sharbaugh, Phys. Rev. **74**, 1870 (1948); Dailey, Mays, and Townes, Phys. Rev. **76**, 136 (1949).
[5] Sharbaugh, Bragg, Madison, and Thomas, Phys. Rev. **76**, 1419 (1949).

Multiple Meson Processes and Nucleon Recoil

ALEX E. S. GREEN
University of Cincinnati, Cincinnati, Ohio
January 11, 1950

AN investigation of the effects of multiple meson processes and nucleon recoil has been carried out with an adaptation of the functional formalism of Fock.[1] An iterative method was employed to deduce from the set of integro-differential equations the explicit interaction $U={}^2U+{}^4U+{}^6U+\cdots$, where

$$ {}^2U=-\int\{G_0^*(\mathbf{k})G_0(\mathbf{k})/\hbar\omega\}d\mathbf{k}, \tag{1} $$

$$ {}^4U=+\int\{G_0^*(\mathbf{k})[H_p, G_0(\mathbf{k})]/(\hbar\omega)^2\}d\mathbf{k}, \tag{2} $$

$$ {}^6U=-\int\{G_0^*(\mathbf{k})[H_p, [H_p, G_0(\mathbf{k})]]/(\hbar\omega)^3\}d\mathbf{k}, \tag{3} $$

$$ G_0(\mathbf{k})=\Sigma_u\, g(2\pi)^{-\frac{1}{2}}\beta_u c(\hbar/2\omega)^{\frac{1}{2}}\exp(-i\mathbf{k}\cdot\mathbf{x}_u). \tag{4} $$

H_p is the Hamiltonian for free nucleons and $\omega=c(\mathbf{k}\cdot\mathbf{k}+\kappa^2)^{\frac{1}{2}}$.

Equation (4) is for a neutral one-mass scalar field with scalar coupling. It may be modified for other types of fields and couplings. ${}^2U$ is the usual second-order interaction. Using this very same formalism but neglecting nucleon recoil, Tomonaga[2] obtained only ${}^2U$. In contrast with previous results by others ${}^4U$, ${}^6U$, ${}^8U$, etc. here are quadratic in the coupling constant. In deriving ${}^6U$ and ${}^8U$ certain questions as to the order of the operators involved in self-energy terms arose which we resolved in view of the symmetry requirements for bosons by assuming that expressions like $[G_{0u}(\mathbf{k}_2), [H_{pu}, G_{0u}(\mathbf{k}_1)]]\psi_0$ may be ignored. Apart from this unsettled point the work was straightforward. We believe it reasonable to anticipate that an indefinite extension of our method or a valid alternative perturbation method will lead to the following conclusions.

(a) The exact interaction is quadratic in the coupling constant.

(b) The results of any development employing power series in the coupling constant must be regarded with very great suspicion. The fact that in electrodynamics such a perturbation method

when augmented by cut-off devices may be used to predict unambiguously a wide range of physical phenomena, is due to a combination of circumstances which is not duplicated in meson theory.

(c) Our generalization principle[3] is effective in removing divergences even from these higher order effects. The relations $\Sigma_\sigma \xi_\sigma^i/\gamma_\sigma$ for $i=0$ and $i=2$ which follow from our generalized field theory for arbitrary meson mass assignments are just the regularization conditions $\Sigma_i C_i=0$ and $\Sigma_i C_i M_i^2=0$. Thus the Pauli-Villars[4] treatment will also be effective here although to a lesser extent since in allowing the masses of the auxiliary particles (including the negative energy bosons) to become infinite some of the milder divergences reappear.

This work was based upon the original quantum field methods of Heisenberg, Pauli, Dirac, Fock and others. It probably can be translated into the Tomonaga-Schwinger invariant methodology which, in meson theory, suffers from significant ambiguities and the use of the unreliable power series method.

[1] V. Fock, Physik. Zeits. Sowjetunion 6, 425 (1934).
[2] S. Tomonaga, Prog. Theor. Phys. 2, 10 (1947).
[3] A. Green, Phys. Rev. 75, 1926 (1949); 73, 519 (1948).
[4] W. Pauli and F. Villars, Rev. Mod. Phys. 21, 434 (1949).

The Near Infra-Red Spectrum of the Polar Aurora

W. Petrie
Physics Department, University of Saskatchewan, Saskatoon, Saskatchewan, Canada
January 9, 1950

During the past year, infra-red spectra of the aurora have been secured by Meinel[1] at the Lick Observatory and Petrie[2] at the University of Saskatchewan. Low level permitted multiplets of OI and NI are features of the spectra, but it appears that atoms of these elements are not excited to levels with energies greater than around 11.5 ev. The low level forbidden and permitted lines of OII and NII are absent from the spectra, hence it is unlikely that the many faint auroral features which have been attributed to ionized oxygen and nitrogen really arise from these ions. The relative intensities of the OI multiplets indicate that the excitation temperature during an auroral display is of the order of 7000°K. The relative intensities of the NI and OI lines suggest that the ratio of the numbers of nitrogen and oxygen atoms in low energy levels is of the order of 1.5. This result is of interest and must be considered in any theory of atmospheric ionization.

A number of N_2 bands of the first positive system are present in the infra-red auroral spectrum. These bands show structure, but higher resolution is needed to measure the several maxima which can be seen.

[1] A. B. Meinel, Pub. Astr. Soc. Pac. 60, 373–377 (1948).
[2] W. Petrie, J. Research (to be published).

A Possible Isomeric State of RaE*

H. M. Neumann, J. J. Howland, Jr.,† and I. Perlman
Radiation Laboratory and Department of Chemistry, University of California, Berkeley, California
January 18, 1950

The neutron irradiation of bismuth at high neutron flux has produced a new bismuth alpha-emitter of very low activity which can best be assigned to Bi^{210m}, an isomeric state of RaE. In a previous report[1] this activity was indicated on an alpha-energy *vs.* mass number plot as Bi^{208} (with the mass number in question) on the assumption that it was formed by a $(n,2n)$ reaction from the relatively small number of fast neutrons. The alpha-particle energy of this new activity is 5.03±0.05 Mev as determined in an ionization chamber coupled to a pulse-height analyzer. This value for the energy is one of the arguments against the assignment to Bi^{208} since, according to the systematics of alpha-radioactivity,[1,2] we would expect the alpha-energy of Bi^{208} to be even less than that of Bi^{209} which itself must be about 4 Mev or less. In addition, the bismuth alpha-emitter was not noted following the irradiation of lead with 20-Mev deuterons although an extremely long half-life could explain this.

The alpha-activity was observed by allowing the irradiated bismuth to stand for six months until all of the 5-day RaE had decayed after which it was rigorously purified, first from the great alpha-activity of Po^{210} present and then from all other possible alpha-activities. To reduce any extraneous beta- and gamma-activity that might be present, special purification from such elements as silver was performed in addition to purification from heavy elements. The bismuth finally reached a constant specific activity of 1.9±0.1 alpha-disintegrations per minute per milligram and 2.0±0.2 electrons or beta-particles.

The principal experimental evidence that this alpha-emitter is an isomer of Bi^{210} is the identification of a thallium[3] daughter with the properties of Tl^{206}. The half-life obtained was 4.2±0.5 min. in agreement with the reported value for Tl^{206}, 4.23 min.[4,5] There was available insufficient activity to determine the beta-particle energy precisely but through a factor of ten in absorption, the absorption curve looks like that reported by Krishnan and Nahum[6] for Tl^{206}. Within the experimental uncertainty of about 10 percent then, all of the radioactivity of the Bi^{210m} may be explained by the alpha-particles for Bi^{210m} in equilibrium with its 4-min. beta-emitting daughter Tl^{206}.

It is recognized that the assignment of this activity to Bi^{210m} will imply extraordinary half-life energy relationships for modes of decay other than alpha-emission. If it is a metastable state of Bi^{210}, it should decay to the ground state and directly to Po^{210} by β^--emission. Indeed, if we accept the data to be discussed, this nucleus should also be unstable with respect to RaD. It is possible to calculate these decay energies from the alpha-energies of the two states of Bi^{210} and known beta-energies and to set some lower limits on the half-lives for the different processes.

Let us first consider the isomeric transition energy, that is the difference between Bi^{210m} and RaE, the ground state. This can be obtained by comparing the alpha-energies of the two states making the assumption that both alpha-transitions go to the ground state of Tl^{206}. The alpha-decay energy for Bi^{210m} as determined in the present study is 5.12±0.05 Mev. That for RaE can be calculated by closing a cycle involving the beta-decay energies for RaE and Tl^{206} and the alpha-decay energy of Po^{210}. Broda and Feather[7] who discovered the alpha-branching of RaE made this calculation arriving at the decay energy 4.86 Mev for the alpha-decay of RaE; but in re-evaluating the data of Krishnan and Nahum[6] and of Fajans and Voigt[4] for the beta-energy of Tl^{206}, we have selected 1.63±0.10 Mev which revises the alpha-energy of RaE to 4.94±0.10 Mev. The energy difference between the isomeric states of Bi^{210} would then be 0.18±0.11 Mev. The unobserved beta-decay energy of Bi^{210m} is accordingly 1.35 Mev and the electron-capture energy to RaD 0.1 Mev.

The alpha-half-life for Bi^{210m} is not known other than that it must be greater than 25 years based on observation of the alpha-activity over a period of 15 months. From the failure to find Po^{210} growing into the sample which would result from both the isomeric transition and beta-decay, it is possible to say that these decay modes are at least 2000 times slower than the alpha-decay and therefore have minimum half-lives of 5×10^4 years.

It is obvious that the most stringent requirement in explaining the long half-lives will be demanded by the isomeric transition. Using the expression and conventions given by Segrè and Helmholz[8] relating decay constant to the *order of the transition* and the transition energy, it would appear impossible to explain the $>5\times10^4$-yr. half-life if the transition energy is as great as 0.18 Mev even if one assumes a fifth-order transition. However, if the

transition energy is 0.07 Mev, the calculated half-life can become sufficiently long.

With the uncertainties still existing in this study, it is not considered profitable to attempt to assign spin numbers to the different nuclear states in these transitions nor to interpret such states in terms of the newer considerations of shell structure. It is perhaps worth pointing out that other cases of nuclear isomerism in odd-odd nuclei have been found in the heavy element region, for example, $Am^{242}-Am^{242m}$ and $UZ^{234}-UX_2^{234}$.

* This work was performed under the auspices of the U. S. AEC.
† Now at Brookhaven National Laboratory, Upton, Long Island, New York.
[1] Perlman, Ghiorso, and Seaborg, Phys. Rev. **74**, 1730 (1948).
[2] Perlman, Ghiorso, and Seaborg, Phys. Rev. **77**, 26 (1950).
[3] We are indebted to Dr. C. P. Keim and the Isotopes Division of the AEC for furnishing the separated thallium isotopes, and to Dr. B. H. Ketelle of the Oak Ridge National Laboratory for his cooperation in assigning the 4-min. thallium activity.
[4] K. Fajans and A. F. Voigt, Phys. Rev. **60**, 619 (1941).
[5] At the time this work was done the principal evidence that the 4-min. period was Tl^{206} rather than Tl^{204} was that of Broda and Feather (reference 7) who identified this activity from the rare alpha-branching of RaE. Dr. D. H. Templeton and one of the authors (I.P.) irradiated some enriched thallium isotopes (reference 3) with moderated cyclotron neutrons and obtained evidence that the 4-min. period was indeed Tl^{206}. More conclusive confirmation of this assignment was obtained by Dr. B. H. Ketelle (reference 3) who irradiated some separated thallium isotopes with pile neutrons.
[6] R. S. Krishnan and E. A. Nahum, Proc. Camb. Phil. Soc. **36**, 490 (1940).
[7] E. Broda and N. Feather, Proc. Roy. Soc. **A190**, 20 (1947).
[8] E. Segrè and A. C. Helmholz, Rev. Mod. Phys. **21**, 271 (1949).

A Confirmation of the Workman-Reynolds Effect

VINCENT J. SCHAEFER
General Electric Research Laboratory, Schenectady, New York
January 19, 1950

THE recent discovery by Workman and Reynolds[1] of the formation of a large electrical potential as water containing small quantities of certain salts is in the process of freezing has impressed the writer as being a phenomenon of great importance in the field of meteorology and physical chemistry.

Having attended the meeting in Washington in 1949 when the effect was first described to meteorologists and noting the skepticism voiced at the conclusion of the paper by certain of the audience, it was decided by the writer to check the experiments by an independent investigation.

A simple electrometer and freezing unit was constructed following, in general, the description of the apparatus described[2] in a report issued by Workman and Reynolds.

The electrical effects as described in this report were immediately observed using a good grade of laboratory distilled water containing a 1×10^{-5} molar concentration of NH_4I. Lack of time has thus far prevented a complete survey of the many salts on which data have accumulated, but it is felt that a sufficient variety of salts has been studied to confirm their claims without question, both as to voltage magnitude and sign of the current flow generated in the freezing process. The peculiar structural detail of the curves produced by a specific salt has also been checked.

It is interesting to note that the molar concentrations of the dilute electrolytes which give the maximum effects are in the same range as those we use to obtain good monomolecular reactions in surface chemistry.[3]

In addition to the salts studied which included NaOH, CsF, NH_4I $Ba(CO_3)_2$, NaCl, and NH_4CO_3, two samples of sea water from the Atlantic near Bermuda and northwest of Puerto Rico were used. These were essentially similar. The results from the latter are shown in Table I.

The extreme simplicity of the experiment and the very important implications of the Workman-Reynolds effect as it pertains to the development of lightning in thunderstorms and as a possible new method for microchemical analysis suggests that a careful study of its physical and chemical nature should be actively pursued.

TABLE I. Electrical potentials developed in the freezing of salt solutions.

Approx. molar concentration (with respect to salts in the sea water)	Max. potential
5×10^{-2} molar	0.0 volt
5×10^{-3}	+0.2
2.5×10^{-3}	+12.
1×10^{-3}	+11.
5×10^{-4}	+16.5
5×10^{-5}	+15.0
2.5×10^{-5}	+4.5
5×10^{-6}	0.0

[1] E. J. Workman and S. Reynolds, Phys. Rev. **74**, 709 (1948).
[2] Final Report, Signal Corps Research Contract No. W-36-039-SC-32286, New Mexico School of Mines, Research and Development Division.
[3] I. Langmuir and V. J. Schaefer, J. Am. Chem. Soc. **59**, 2400 (1937).

Statistics of the Three-Dimensional Ferromagnet

D. TER HAAR AND B. MARTIN
Department of Physics, Purdue University, Lafayette, Indiana
January 19, 1950

SINCE Kramers' variational method[1] appeared to be so much superior to other methods in approximating the partition function of the two-dimensional ferromagnet, it was felt to be worth while to use the same method for the three-dimensional case.[2] We have used a simple cubic Ising model[3] with only nearest neighbor interaction. It turns out that now the partition function has to be approximated in two steps, both involving the variational principle. We shall denote by J the interaction energy, i.e., the difference in energy between a situation where two neighboring spins are parallel or antiparallel. If we restrict ourselves to the case where no magnetic field is present, the total energy of the system is given by

$$E=-\tfrac{1}{2}J\sum\mu\mu', \tag{1}$$

where the summation extends over all nearest neighbor pairs in the crystal. The quantities μ and μ' can take on the values $+1$ and -1, corresponding to the two possible directions of the spins. The partition function f is now given by

$$f=\sum_{\mu=\pm1}\exp(K\sum\mu\mu'), \tag{2}$$

where the summation is extended over all spins in the crystal and where

$$K=J/2kT. \tag{3}$$

By the same method as used by Kramers and Wannier,[1] one can show that the partition function will be given by the largest eigenvalue of the matrix

$$H(\mu_{ij},\mu_{ij}')=\exp[K\sum_{i,j}\mu_{ij}\mu_{ij}'+\tfrac{1}{2}K\sum_{ij}(\mu_{ij}\mu_{ij+1}+\mu_{ij}\mu_{i+1j}+\mu_{ij}'\mu_{ij+1}'+\mu_{ij}'\mu_{i+1j}')], \tag{4}$$

where the μ_{ij} denote the spins in one plane and μ_{ij}' the spins in the next plane: the problem is reduced from a three-dimensional problem to a bi-planar problem. The largest eigenvalue of $H(\mu_{ij},\mu_{ij}')$ can be approximated by the Ritz method, and it turns out that one then has to use the Ritz method once more in order to find a solvable equation. Detailed calculations will be published elsewhere but we may mention here that one finally has to evaluate the partition functions of crystals consisting of 4, 2, and 1 neighboring linear chains which leads to 16th, 4th, and 2nd degree equations.

For high temperatures, the equations can be simplified and one can solve the equations either by numerical methods, the

results of which we hope to publish in the near future, or by series expansions. If one solves by series expansion, one finds for the partition function:

$$f=2\left[1+\frac{3}{2}K^2+\frac{31}{8}K^4+\frac{5461}{240}K^6+\frac{2180851}{13440}K^8+\cdots\right], \quad (5)$$

which up to the K^6 term agrees with the exact expression as determined by one of us.[4]

From the partition function one can easily calculate the configurational energy and specific heat which are given by

$$E=-kT\cdot K\cdot\partial \log f/\partial K, \quad c_v=kK^2\partial^2 \log f/\partial K^2. \quad (6)$$

The series expansions for these two quantities are found to be:

$$E=-kT[3K^2+11K^4+(542/5)K^6+(107587/105)K^8+\cdots] \quad (7)$$

and

$$c_v=k[3K^2+33K^4+542K^6+(107587/15)K^8+\cdots]. \quad (8)$$

[1] H. A. Kramers and G. H. Wannier, Phys. Rev. **60**, 252, 263 (1941).
[2] A preliminary account of the method was given at the New York meeting of the American Physical Society; see Phys. Rev. **75**, 1298 (1949).
[3] E. Ising, Zeits. f. Physik **31**, 253 (1925).
[4] D. ter Haar, Phys. Rev. **76**, 176 (1949). The same result was also obtained by Dr. E. Trefftz and Dr. E. Somers. We are endebted to Dr. E. Trefftz and Dr E. W. Montroll for communicating to us these results prior to publication.

Nuclear Spin and Isotope Shift of Xenon Investigated with Separated Isotopes

JØRGEN KOCH
Institute for Theoretical Physics, University of Copenhagen, Copenhagen, Denmark
AND
EBBE RASMUSSEN
Department of Physics, Royal Veterinary and Agricultural College, Copenhagen, Denmark
January 19, 1950

PURE samples of the xenon isotopes 129, 130, 131, 132, 134, and 136 have been prepared by using a mass-spectrographic technique previously described.[1] According to recent experiences with isotopes of neon and krypton,[2] Geissler tubes with aluminum electrodes were prepared containing some micromoles of xenon with helium as a carrier gas at a pressure of about 10 mm.

In order to reduce Doppler broadening the tubes were operated at liquid air temperature, which turned out to be possible without much loss of intensity. The interferometric investigations carried out by means of a Fabry-Perot etalon using 15–25-mm spacers, were especially devoted to the study of infra-red lines resulting from $1s-2p$ transitions.

Because of the high purity of the isotopic samples the interferograms of the magnetic structures of Xe^{129} as well as of Xe^{131}, did not show any lines due to impurities of even isotopes, which were checked to be present with less than one percent. Also the tubes containing the different even isotopes were prepared with great care in order to avoid any displacements of the observed lines.

From the exposures with Xe^{129} the spin value could at first sight be determined to be $\frac{1}{2}$, since all levels appeared split up into two levels, also for j-values 2 and 3. This result is in accordance with earlier determinations,[3] and also our measurements of term separation showed good agreement with earlier experiments, using normal xenon.[4,5]

Also in the case of Xe^{131} we could fully confirm[3] the spin value ($i=\frac{3}{2}$), but in this case by making use of the exact validity of the interval rule for a level ($2p_4$) having spherical symmetry. The two intervals for this level were measured directly by means of the line 8206A ($1s_3-2p_4$) for which only the upper term can split. The experimental values were found to be 0.1085 and 0.0655 cm^{-1}, closely agreeing with the calculated values 0.1087 and 0.0653 cm^{-1}.

Because of the high purity of the Xe^{131} tube with respect to other isotopes it was possible to measure the intervals directly for most of the $1s$ and $2p$ terms. Among these should be mentioned only the intervals of the term $1s_2$, which by means of the line 7887A ($1s_2-2p_1$) were measured to be 0.145 and 0.081 cm^{-1}, while the calculated values are 0.141 and 0.085 cm^{-1}. These deviations confirm the supposed existence of a quadrupole moment[6] of the same size as in Kr^{83}, but with opposite sign.

By using the method of alternating exposures previously described[2] the existence of an isotope shift between the even isotopes 130, 132, 134, and 136 was investigated. An isotope shift of the same order of magnitude as found in krypton[2] was measured under favorable experimental conditions (constancy of atmospheric pressure and temperature). However, the order was found to be reversed with respect to that of krypton, the heavier isotopes having the greatest wave-lengths. Further, in the present case no exact equidistance seems to be present, as shown in Table I.

TABLE I. Isotope shift of some even xenon isotopes expressed in 10^{-3} cm^{-1}.

Wave-length	Combination	132–134	134–136
8819A	$1s_5-2p_8$	2.5	3.6
8280	$1s_4-2p_8$	1.1	2.9
8231	$1s_5-2p_6$	2.4	3.5

Preliminary measurements indicate moreover that the center of gravity of the hyperfine structures for the odd isotopes Xe^{129} and Xe^{131} are situated close to the lines due to the even isotopes of one unit higher mass, i.e., Xe^{130} and Xe^{132}, respectively. All these results indicate that the isotope shift in Xenon is due to a nuclear volume effect rather than to a mass effect.

The investigation will be continued and further details will be published in the Communications of the Royal Danish Academy.

We wish to thank Professor Niels Bohr for his continued interest in this investigation. We should further like to thank Mr. S. Møller-Holst and Mr. K. O. Nielsen for having carried out several separation experiments.

[1] J. Koch, Nature **161**, 566 (1948).
[2] J. Koch and E. Rasmussen, Phys. Rev. **76**, 1417 (1949).
[3] H. Kopfermann and E. Rindal, Zeits. f. Physik **87**, 460 (1934).
[4] E. Gwynne Jones, Proc. Roy. Soc. **144**, 587 (1934).
[5] E. Gwynne Jones, Proc. Phys. Soc. London **46**, 634 (1934).
[6] H. Korsching, Zeits. f. Physik **109**, 349 (1938).

Possible Experimental Determination of Whether the Neutral Meson is Scalar or Pseudoscalar

C. N. YANG
Institute for Advanced Study, Princeton, New Jersey
January 16, 1950

NEUTRAL mesons with a mass of ~300 Mev which decay into two photons have been reported.[1] It can be proved[2,3] on general grounds of rotation-inversion invariance that a particle which dematerializes into two photons cannot have spin 1. Furthermore,[3] if the neutral meson is a scalar meson, the two photons would always have parallel planes of polarization, while if the neutral meson is a pseudoscalar meson, the two photons would always have perpendicular planes of polarization. One is tempted to investigate whether this may possibly lead to an experimental determination of the symmetry nature of the neutral mesons. Some calculation along this direction has been carried out. The results are summarized herein.

The experimental set-up considered is schematically illustrated in Fig. 1. The two photons produce pairs at L and L'. The counters A and A' are supposed to be identical and symmetrically situated with respect to M. So are B and B'. The sizes of the counters have not been assumed to be small. Fourfold coincidence rate is recorded, and then the whole apparatus to the left of M is rotated

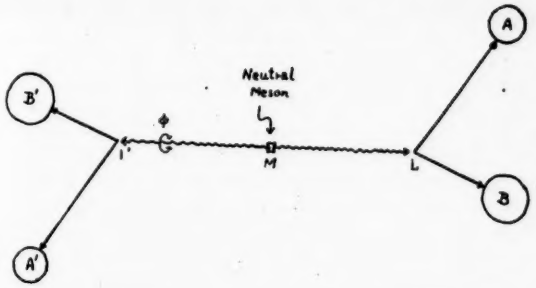

FIG. 1. Schematic diagram of experiment (angles ALB, $A'L'B'$ much exaggerated).

around the axis LML' through an azimuthal angle ϕ and the fourfold coincidence rate N plotted against ϕ.

The calculation of the theoretically expected dependence of N on φ is rather straightforward, but somewhat complicated. The result is

$$N=\alpha(1\pm\beta^2\cos 2\phi) \quad \begin{matrix} + \text{ for scalar meson} \\ - \text{ for pseudoscalar meson,} \end{matrix}$$

where β^2 is a positive constant dependent on the geometry of the counters A and B with respect to the points M and L. One sees that

$$^N\phi=0°>{}^N\phi=90° \quad \text{for scalar meson,}$$
$$^N\phi=0°<{}^N\phi=90° \quad \text{for pseudoscalar meson.}$$

To get an idea of the order of magnitude of β^2, the hypothetical case that the counters A and B are infinitesimal in size is considered in detail. If the angles MLA and MLB are equal, the value of β^2 is approximately $\frac{1}{16}$ for all values of the angle MLA for which pair production is abundant. In such a case

$$\frac{^N\phi=0°}{^N\phi=90°}=\frac{17}{15}=1.13 \quad \text{for a scalar meson,}$$

$$\frac{^N\phi=0°}{^N\phi=90°}=\frac{15}{17}=0.88 \quad \text{for a pseudoscalar meson.}$$

[1] Bjorklund, Crandall, Moyer, and York, Phys. Rev. **77**, 213 (1950).
[2] L. D. Landau, Dokl. Akad. Nauk USSR **60**, 207–9 (1948). A summary in English of this article appeared in Phys. Abstracts **A52**, 125 (1949).
[3] C. N. Yang, Phys. Rev. **77**, 242 (1950).

Neutron Capture Gamma-Rays from Be^9, C^{12}, and N^{14}

B. B. KINSEY, G. A. BARTHOLOMEW, AND W. H. WALKER
Division of Atomic Energy, National Research Council of Canada, Chalk River, Ontario, Canada
January 20, 1950

MATERIALS containing carbon and nitrogen were exposed to a high flux of thermal neutrons in the Chalk River pile. The radiations emitted were examined with the aid of a coincidence pair spectrometer similar to that described by Walker and McDaniel.[1]

In our method the coincidence counting rate between two counters recording positrons and negatrons is obtained for a series of values of the magnetic field. The field is measured by means of a proton resonance magnetometer. In a plot of coincidence rate against field strength a homogeneous gamma-ray appears as a sharp peak which falls rapidly to zero toward high field strengths. The upper limit of the peak corresponds to pairs which are produced at the center of the radiator, the components having equal energy. The energy of the gamma-ray can be calculated, to a first approximation, from the distance between the inner edges of the slits covering the counters and the value of the magnetic field obtained by extrapolating the high field slope of the peak to zero. The true energy of the gamma-ray is obtained by adding a correction of about 25 kev computed from the pair production cross section and from the geometry.

With a graphite sample in the pile a conspicuous radiation was identified as resulting from neutron capture in C^{12} which must be the direct transition to the ground state of C^{13}. The energy of this radiation is 4.947 ± 0.008 Mev. Another value for this energy may be obtained by the addition of the following equations:

$$C^{12}+H^2=N^{13}+n-0.281\pm0.003 \text{ Mev}^2, \quad (1)$$
$$N^{13}=C^{13}+2m_0c^2+1.198\pm0.006 \text{ Mev}^3, \quad (2)$$
$$n+H^1=H^2+2.230\pm0.007 \text{ Mev}^4, \quad (3)$$
$$n-H^1=0.782\pm0.002 \text{ Mev}.^5 \quad (4)$$

The result is:

$$C^{12}+n=C^{13}+4.951\pm0.010 \text{ Mev}. \quad (5)$$

A recent measurement of the energy balance in the $C^{13}(d,p)C^{13}$ reaction gives $Q_0=2.729\pm0.009$ Mev.[6] From this result, together with (3), we find:

$$C^{12}+n=C^{13}+4.959\pm0.012 \text{ Mev} \quad (6)$$

in agreement with our own figures and with (5). Taking into account the probable errors of these three results the mean energy is:

$$4.951\pm0.006 \text{ Mev}. \quad (7)$$

Nitrogen was investigated with the aid of samples of beryllium nitride, urea, and beryllium oxide. From the spectra of these

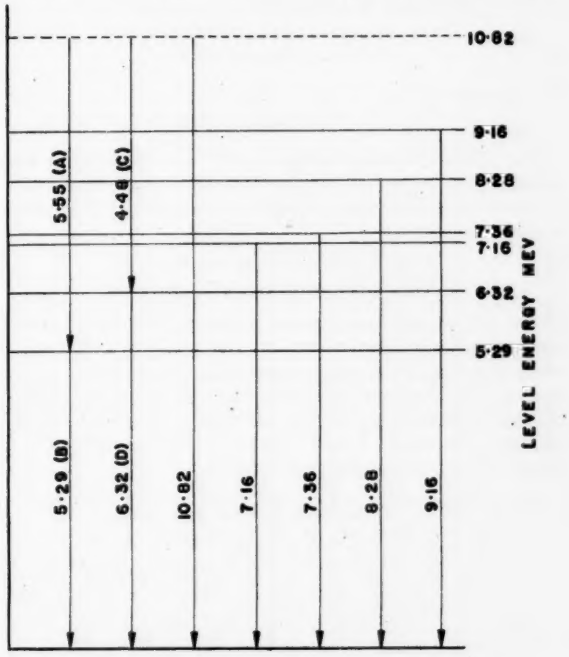

FIG. 1. Capture gamma-radiation from nitrogen.

compounds nine radiations due specifically to nitrogen were identified. These radiations are given in Table I and can be fitted to the level scheme of Fig. 1 which, with the exception of the levels at 7.16 and 9.16 Mev, has already been published.[7,8]

Rough values for the relative intensities appearing in Table I were obtained from the heights of the coincidence peaks after corrections had been made for the variation with energy of the pair production cross section and of the angular distribution of the electron pairs.

By comparing the intensities of the nitrogen and beryllium radiations from beryllium nitride we estimate that the radiative capture cross section of nitrogen is about 100 millibarns. This

TABLE I. Gamma-rays from nitrogen under neutron bombardment.

Energy Mev	Relative intensity
10.816±0.015	1.0
9.156±0.030	0.1
8.278±0.016	0.4
7.356±0.012	0.8
7.164±0.010	0.1
6.318±0.010	2
5.554±0.010	4
5.287±0.010	5
4.485±0.010	3

follows from the capture cross section of beryllium, 9 millibarns, and our observation that only one radiation is emitted, its energy being 6.80±0.01 Mev. Now the total absorption cross section of nitrogen is about 1.7 barns[9] and the penetrability of the Coulomb barrier for a proton of 600 kev is about 0.03. If, then, the radiation width is of the order of a few volts,[10] the proton width without barrier must be of the order of a kilovolt, a very low result.

Another surprising feature is the relative weakness of the direct transition to the ground state. If, as seems likely, the parities of the ground states of N^{14} and N^{15} are even and odd, respectively, the transition is of the electric dipole type. It is, however, no more intense than the radiation of 5.55 Mev which competes with it and has about half the energy.

Correcting for recoil, the energy of the direct transition to the ground state of N^{15} is found to be 10.820±0.015 Mev. The sums of the corrected energies of the two pairs of cascading transitions (AB) and (CD) in Fig. 1 are:

$$A+B=10.843\pm0.014 \text{ Mev},$$
$$C+D=10.805\pm0.014 \text{ Mev}.$$

The average of the three determinations is:

$$N^{14}+n=N^{15}+10.823\pm0.012 \text{ Mev}. \quad (8)$$

The neutron binding energies of C^{13} and N^{15} may be used to calculate the values of certain mass differences which may be compared with mass spectrographic measurements. From (4), (7), and (8), we obtain:

$$C^{12}H^1-C^{13}=44.78\pm0.06\times10^{-4} \text{ mu},$$
$$N^{14}H^1-N^{15}=107.85\pm0.11\times10^{-4} \text{ mu}.$$

The first of these two results is significantly higher than that obtained directly by Ewald,[11] *viz.*, $44.10\pm0.08\times10^{-4}$ mu. Our measurement of the binding energy of the neutron in C^{13} therefore confirms a discrepancy between the transmutation and mass spectrographic data indicated by the results (5) and (6). For the nitrogen difference, Ewald obtained $107.76\pm0.20\times10^{-4}$ mu, which is in agreement with our results.

[1] R. L. Walker and B. D. McDaniel, Phys. Rev. **74**, 315 (1948).
[2] Bonner, Evans, and Hill, Phys. Rev. **75**, 1398 (1949).
[3] E. M. Lyman, Phys. Rev. **55**, 234 (1939).
[4] Private communication from R. E. Bell.
[5] Taschek, Argo, Hemmendinger, and Jarvis, Phys. Rev. **76**, 325 (1949).
[6] Buechner, Strait, Sperduto, and Malm, Phys. Rev. **76**, 1543 (1949).
[7] W. F. Hornyak and T. Lauritsen, Rev. Mod. Phys. **20**, 191 (1948).
[8] L. D. Wyly, Phys. Rev. **76**, 316 (1946).
[9] J. H. Coon and R. A Nobles, Phys. Rev. **75**, 1358 (1949).
[10] Brostrom, Huus, and Tangen, Phys. Rev. **71**, 661 (1947).
[11] H. Ewald, Zeits. f. Naturforschung **1**, 131 (1946).

On the Low States of Li^7 and Be^7

D. R. INGLIS
Argonne National Laboratory, Chicago, Illinois
January 27, 1950

TO the problem of interpreting the ground level and 480 kev level of Li^7, recent experiments[1] have added as a new feature the necessity of understanding the apparent lack of further levels up to at least 3.6 Mev, with a similar but not quite so clear-cut situation in the mirror nucleus Be^7.

This scarcity of levels might be considered to favor a return to the original interpretation,[2] in terms of a rather extreme $L-S$ coupling scheme with a ^2P splitting of 480 kev and the ^2F elevated now about 4 Mev or more above this. The most striking experimental evidence[3] against this interpretation,[4] the intensity ratio of the $B^{10}(n,\alpha)Li^7$ transitions, could then be attributed to a minor misbehavior of incalculable matrix elements. It would be a further concession to accept such extreme $L-S$ coupling in these light nuclei, unless an adequate theory of the large spin-orbit coupling could be found much less sensitive to nuclear radius than is the inadequate theory that has been discussed.[2] (It varies about as l^3R^{-4}, to be compared with lR^{-3} for the competing integral[5] of the inter-nucleon attraction.) We wish therefore to examine an alternative.

In a description of the low states of Li^7 in the $j-j$ coupling scheme, the two p-neutrons, each having individual $j=3/2$, form a total neutron moment $J_\nu=0$ or 2, of which $J_\nu=0$ is presumably associated with the ground state. In zeroth order the low excited states are then described[6] by coupling this moment $J_\nu=2$ with the proton moment $j=3/2$, to make the nuclear moment $I=7/2$, 5/2, 3/2, and 1/2. In first order the state with $I=3/2$ is mixed with the ground state. The relative energies of these various states are most easily studied phenomenologically in terms of the familiar non-exchange (Wigner), space-spin-exchange (Heisenberg), space-exchange (Majarana) and spin-exchange (Bartlett) interactions. It is a rather remarkable and intriguing fact that the states with $I=7/2$, 5/1, and 1/2 remain degenerate in first order with an arbitrary combination of non-exchange and space-spin-exchange terms of arbitrary range. The excited $I=3/2$ state lies somewhat higher. In second order, as one departs from extreme $j-j$ coupling, admixture of states with higher spin-orbit energy begins to lift the degeneracy, but it seems possible that the departure from $j-j$ coupling might be small enough to leave the second-order splitting unobserved with present resolution, if one identifies the degenerate level as the 480 kev level. Its complexity satisfies the simple demands of relevant intensity-ratio, lifetime, and angular-distribution data.[6]

In addition to a narrow triple level at 480 kev, we would then have a single level (with "statistical weight" 1/4 as great) probably one or several hundred kev higher. The fact that it has not been observed[1,7] in the two sufficiently exoergic reactions $Be^9(d,\alpha)Li^7$ and $Li^6(d,p)Li^7$ would have to be attributed to unexpected behavior of the transition intensities, which seems no more implausible than the other alternative.

In the excited spectrum of Be^7, observations of the reactions $Li^6(d,n\gamma)Be^7$ at about 1.5 Mev bombarding energy[8] and $Li^7(p,n)Be^7$ at several bombarding energies[9] up to almost 4 Mev have revealed the level at 430 kev, but no other level up to the limit of the observations, perhaps 1 Mev. The latter reaction with cyclotron bombardment[10] at 5 Mev seems to show a level near 700 kev, in addition to the one near 430 kev (and still another less consistently resolved near 200 kev). This observation of an additional level (or two), if verified by more extensive investigation at high bombarding energies, would indeed demonstrate unexpected behavior of the transition probabilities and encourage attempts to find a mirror level and to resolve the multiple level.

The separation of the 480 kev level from the ground level arises mainly from the separation of $J_\nu=2$ from $J_\nu=0$ by the like-nucleon attraction, and the corresponding separation is less in Be^7 (430 kev) because the like-nucleon attraction is there weakened by the Coulomb repulsion of the two protons.

This interpretation would require mainly non-exchange interaction with, perhaps, an additional weak space-spin exchange term (even weaker between like nucleons, in order to leave $J_\nu=0$ below $J_\nu=2$, than suggested for unlike nucleons by the deuteron states). Saturation would then be attained not by exchange but perhaps by interactions between three nearly coincident nucleons which might be relatively unimportant for the three loosely bound nucleons here discussed. Such an origin of saturation is characteristic of pair theories of nuclear forces, and there is a rather attractive μ-meson pair theory (with π-mesons as pairs in the same field), according to recent discussions of Gregor Wentzel.

It has become apparent in discussions with Maria Goeppert Mayer and Dieter Kurath that just such a combination of non-exchange and space-spin-exchange terms seems also to be needed to understand the nuclear spins of Li^6 and B^{10} in the $j-j$ model, and less satisfactorily that, as a result of the first-order mixing of the $I=3/2$ states, the magnetic moment of Li^7 is about seven percent low with non-exchange forces symmetrical between all pairs of nucleons.

[1] W. W. Buechner and E. N. Strait, Phys. Rev. **76**, 1547 (1949); D. R. Inglis (to be published in Phys. Rev.).
[2] D. R. Inglis, Phys. Rev. **50**, 783 (1936); G. Breit and J. R. Stehn, Phys. Rev. **53**, 459 (1938).
[3] J. K. Bøggild, Kgl. Danske Vid. Sels. Math.-fys. Medd. **23**, 4, 26 (1945).
[4] D. R. Inglis, Phys. Rev. **74**, 1876 (1948).
[5] M. G. Mayer, Phys. Rev. **75**, 1969 (1949); **77**, (to be published). Haxel, Jansen, and Suess, Phys. Rev. **75**, 1766 (1949); Naturwiss. **36**, 155 (1949).
[6] S. S. Hanna and D. R. Inglis, Phys. Rev. **75**, 1767 (1949).
[7] Unpublished observations of $Li^6(d,p)Li^7$ by Buechner *et al.*, and by Heydenburg and Inglis.
[8] T. Lauritsen and R. G. Thomas (to be published in Phys. Rev.).
[9] Johnson, Laubenstein, and Richards (to be published in Phys. Rev.) and recent unpublished work of J. H. Roberts and of B. Hamermesh and V. Hummel.
[10] J. C. Grosskreutz and K. B. Mather, Phys. Rev. **77**, 580 (1950).

Crucial Experiment Demonstrating Single Domain Property of Fine Ferromagnetic Powders

C. KITTEL, J. K. GALT AND W. E. CAMPBELL
Bell Telephone Laboratories, Murray Hill, New Jersey
January 18, 1950

IT is now well known that fine ferromagnetic powders have high coercivities and this has been explained on the supposition that a sufficiently fine particle will consist of a single magnetic domain, as suggested by domain theory. The objection is sometimes raised that it might be possible to explain the high coercivity without the single-domain assumption, by supposing that internal strains are very large in fine powders, and that the strains hinder and retard magnetization changes by domain boundary displacement, thereby giving high coercivity. It may seem difficult to prove that the internal strain hypothesis will not account for the observed corecivities of 200 and 600 oersteds in fine nickel and iron powder, although it appears most improbable that strains are responsible for the unusually high coercivities observed in fine powders of MnBi ($H_c=12{,}000$ oersteds) and FePt ($H_c=20{,}000$ oersteds).

We have, however, devised and carried out a simple experiment applicable to iron and nickel by which single-domain effects have been clearly distinguished from the ordinary processes of bulk magnetization. We consider the field required to saturate a specimen consisting of a dilute solid suspension of magnetic particles embedded in a non-magnetic matrix. If the degree of dilution is sufficient the magnetic interactions between particles may be neglected, and each particle will behave as if it were alone. In this limit the field required to saturate a spherical particle of nickel or iron will be very considerably larger in a multi-domain particle than in a single-domain particle. We shall show this by considering the magnetization of: (A) a particle so small that it never forms a domain wall or closed-flux arrangement and thus is always a single domain; and (B) a larger particle which normally consists of a large number of domains.

(A) The energy of orientation of the magnetization arises from crystalline and shape anisotropy; therefore if the particle is spherical it will saturate for $H_s(A)\approx 2K/I_s$, while agglomeration may tend to increase this value. We observed $H_s=550\pm 50$ oersteds for a sample of fine nickel particles in 0.1 percent concentration in a 0.01-cc matrix of paraffin wax. The particles were prepared by decomposition of nickel formate in dimethyl phthlate at 250°C and were determined with an electron microscope to be nearly spherical in shape and of diameter 200 ± 50A.

(B) In order to saturate the particle it will be necessary to overcome the maximum demagnetizing field of the particle on itself, which is $4\pi I_s/3$ for a sphere. If the material is magnetically hard H_s may be still larger, so that we have $H_s(B)\geq 4\pi I_s/3=2100$ for Ni. We observed $H_s=2100\pm 100$ oersteds for a 0.1 percent solid suspension of commercial carbonyl process nickel particles in the form of spheres about 8×10^{-4} cm in diameter.

If the particles agglomerate into chains of spheres, oriented at random, $H_s(B)\geq \pi I_s$. There appears to be no way in which the energy density required to saturate a random distribution of multi-domain crystals can be made less than about πI_s^2, so that the samples discussed in (A) must consist of single-domain particles (or at least of particles so very close to single-domain particles that the exchange energy is comparable with the demagnetizing energy).

The expected dividing line in nickel below which the single-domain state is lowest in energy[1] occurs at a diameter of about 600A, which is between (A) and (B).

We may summarize the idea of the experiment by saying that a saturated sphere in isolation must always have a demagnetizing energy density of $\frac{1}{2}NI_s^2=2\pi I_s^2/3$; with multi-domain particles this energy must be supplied by the external magnetic field, whereas with single-domain particles this amount of energy is always present.

We acknowledge with thanks assistance given by W. O. Baker, W. C. Ellis, H. Hopper, W. Shockley, and F. H. Winslow.

[1] C. Kittel, Rev. Mod. Phys. **21**, 541 (1949), Eq. (6.1.8).

Effect of Exchange Interaction on Ferromagnetic Microwave Resonance Absorption

C. KITTEL AND CONYERS HERRING
Bell Telephone Laboratories, Murray Hill, New Jersey
January 18, 1950

IT is well known that exchange forces have no effect on the ferromagnetic resonance frequency in a uniformly magnetized specimen, as a consequence of the fact that the magnetization operator $\Sigma_i S_i^z$ commutes with the exchange operator $\Sigma_{i,j}' \mathbf{S}_i\cdot\mathbf{S}_j$; in classical language,[1] the Weiss molecular field $\mathbf{H}_w=q\mathbf{M}$ is always parallel to the magnetization $\mathbf{M}$, and hence the torque $\mathbf{M}\times q\mathbf{M}$ must vanish. In the most common experimental arrangement for studying ferromagnetic resonance the specimen is in the form of a thin plate, and the microwave field penetrates only partially into the plate, perhaps to a depth of the order of 10^{-5} to 10^{-4} cm. The microwave component of the magnetization in these conditions is non-uniform and the exchange energy will play a role in determining the resonance frequency and the line width. It turns out that at microwave frequencies the exchange effects are not likely to be of importance in pure metals at room temperature, or in alloys at any temperature; at low temperatures, however, the exchange effects must be considered in pure metals, the skin depths being smaller.

The exchange energy density in a body-centered cubic lattice may be written semi-classically[2] as

$$f_{ex}=(A/M_s^2)(\nabla\mathbf{M}\cdot\nabla\mathbf{M}), \tag{1}$$

where $A=2JS^2/a\cong 2.0\times 10^{-6}$ erg/cm for iron. We shall treat the exchange energy as a small perturbation on the motion of the system. Taking the plane of the plate as the x–z plane, the unperturbed state of the system is described by H_x, M_x, $M_y\sim e^{-ky}$, where $k^2=j\mu(4\pi\omega/\rho c^2)$. At resonance $\mu_1=0$ and $\mu=-j\mu_2$, so that

$$k_0=(4\pi\omega\mu_2/\rho c^2)^{\frac{1}{2}}=1/\delta \tag{2}$$

is real, where δ is the classical skin depth for permeability $2\mu_2$. As the phenomenon is essentially a modified Zeeman effect, we

may calculate the first-order shift in resonance frequency from the relation

$$\Delta\omega/\omega=\Delta W/W, \tag{3}$$

where W is the unperturbed energy.

The time-average unperturbed energy per unit area of plate, referred to the static condition, is

$$W=\left\langle \tfrac{1}{2}\int[4\pi M_y^2+(M_x^2+M_y^2)(H_x/M_s)]dy\right\rangle_{Av}; \tag{4}$$

at resonance $(M_x^0)^2=(B_x/H_x)(M_y^0)^2$, so that

$$W=\tfrac{1}{2}(B_x/M_s)\int(M_y^0)^2e^{-2ky}dy=(B_x/M_s)[(M_y^0)^2/4k]. \tag{5}$$

The perturbation energy is

$$\Delta W\cong\left\langle(A/M_s^2)\int[(\partial M_x/\partial y)^2+(\partial M_y/\partial y)^2]dy\right\rangle_{Av}$$
$$=(A/M_s^2)[B_x+H_x)/H_x]k(M_y^0)^2/4. \tag{6}$$

We have the result

$$\Delta\omega/\omega=(Ak^2/M_s)(B_x^{-1}+H_x^{-1}), \tag{7}$$

which corresponds to

$$\Delta H_x=2Ak^2/M_s=2A/\delta^2M_s. \tag{8}$$

It may be noted that this is just equal, but opposite in sign, to what one obtains by treating the exchange incorrectly as an effective field $\mathbf{H}_{eff}=(2A/M_s^2)\nabla^2\mathbf{M}$ in the equations of motion; the effective field treatment will give erroneous results unless we add to the effective field at the boundary the term $-(2A/M_s^2)\delta(y)(\partial\mathbf{M}/\partial y)$, where $\delta(y)$ is a delta-function.

For iron at 24,000 mc/sec. we may take $2\mu_2\approx20$ at resonance, so that at room temperature $\delta\approx2.14\times10^{-5}$ cm and

$$\Delta H\approx4\times10^{-6}/(1.7\times10^3)(4.6\times10^{-10})\approx5 \text{ oersteds},$$

so that the neglect of exchange effects will give a g value too high by about 0.1 percent. At liquid hydrogen temperature the resistivity of iron is about 10^{-2} of the room temperature value, so that for the same μ_2 we would have $\Delta H\approx500$ oersteds.

There will be a contribution to the line width from exchange effects of the same order of magnitude as the extra contribution to the field. We may accordingly expect that the line width of pure iron, nickel, and cobalt single crystals will increase appreciably at low temperatures as a result of exchange effects. Microwave resonance at low temperatures may thus provide a new tool for the study of exchange interactions in ferromagnetic substances.

[1] C. Kittel, Phys. Rev. 71, 270 (1947); 73, 155 (1948).
[2] C. Kittel, Rev. Mod. Phys. 21, 541 (1949); see Section 2.1.

The β-Spectrum of Be^{10}

D. J. HUGHES* AND C. EGGLER
Argonne National Laboratory, Chicago, Illinois
AND
D. E. ALBURGER
Brookhaven National Laboratory, Upton, Long Island, New York
January 20, 1950

MARSHAK[1] has pointed out that the shape of the Be^{10} spectrum is a crucial test of the theory of beta-decay. He has shown that only three interactions, tensor, axial vector, and vector can explain the observed half-life of 2.7×10^6 years, and furthermore that each of these interactions should produce the same spectrum shape, a shape greatly different from the allowed shape. Several measurements of the spectrum have already been made using the extremely weak sources of Be^{10} which were available. Hughes, Eggler, and Huddleston[2] inferred from the shape of the absorption curve of extremely weak sources that the spectrum was near the allowed shape. Bell and Cassidy[3] then measured the spectrum with somewhat stronger sources in a scintillation counter, finding some deviations from the allowed shape which were less than the shape predicted by Marshak (usually called the D_2 shape). Wu and Feldman[4] used quite thick samples (~10 mg/cm²) in a conventional spectrometer and also found deviations less than D_2 but concluded that the true shape might well be D_2 because of the source thickness used. Fulbright and Milton,[5] however, recently measured the spectrum in a proportional counter and found agreement with the forbidden D_2 shape. The work of the last three groups was all done with cyclotron-produced Be^{10} of about the same specific activity (Be^9 containing 0.01 percent Be^{10}). Because the available material was not intense enough for use in a conventional spectrometer, it was of great importance to obtain material of sufficient activity for a spectrometer measurement using a thin source.

Fortunately, the preparation of an intense Be^{10} spectrometer source had been started two years ago. This Be^{10} became available recently and we have used it for a thin source spectrum measurement in a magnetic lens spectrometer. Be metal, which had been irradiated for some time in the Hanford pile, was purified chemically at Argonne using the basic acetate process. The radioactivity of the impurities was about 10^6 times greater than the Be^{10} activity, so extensive purification was necessary. The purified material, which contained about 3 ppm Be^{10} in Be^9, was converted to anhydrous chloride and sent to the Isotope Research and Production Division at the AEC's electromagnetic plant at Oak Ridge for enrichment. The very careful runs which were made on the chloride concentrated the Be^{10} by a factor of 1200 with the result that the collected material (about 4 mg Be) contained 0.3 percent Be^{10}. In accordance with the planned irradiation and electromagnetic separation, this material was just intense enough to give a good spectrum determination.

The beta-spectrum was measured with the Brookhaven magnetic lens spectrometer after a preliminary run using a sample several mg thick, kindly performed by H. Agnew at the University of Chicago, had shown that such a source produced too much distortion. At Brookhaven the effects of source thickness and resolution were first investigated very carefully using Na^{22} as a standard. Na^{22} was first shown to have an allowed shape by a measurement with a thin source (mounted on 0.08 mg/cm² Nylon kindly supplied by J. Richards) and high resolution.[6] The Na^{22} was then run with a thin source and 17 percent resolution (full width at half-maximum) which was the resolution to be used for the Be^{10}. The lower curve in Fig. 1 shows the Na^{22} Kurie plot for

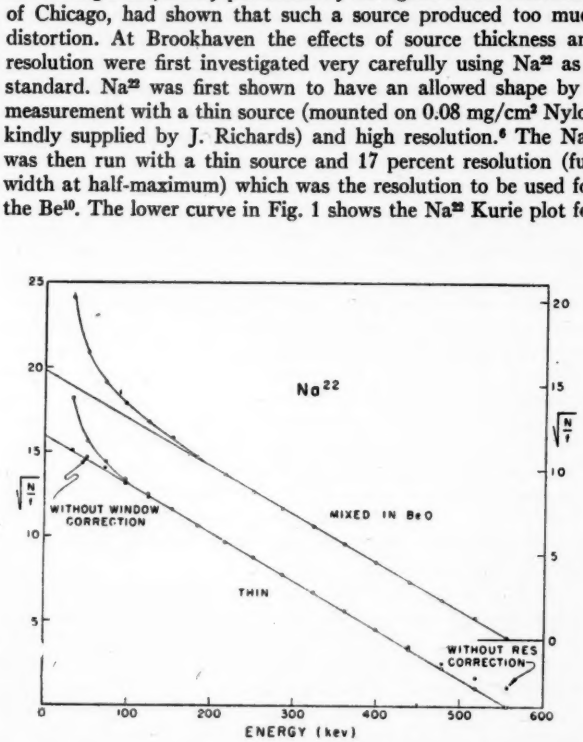

FIG. 1. Kurie plots of Na^{22} showing effect of 0.4 mg/cm² BeO source thickness, 17 percent resolution and 0.5 mg/cm² window thickness.

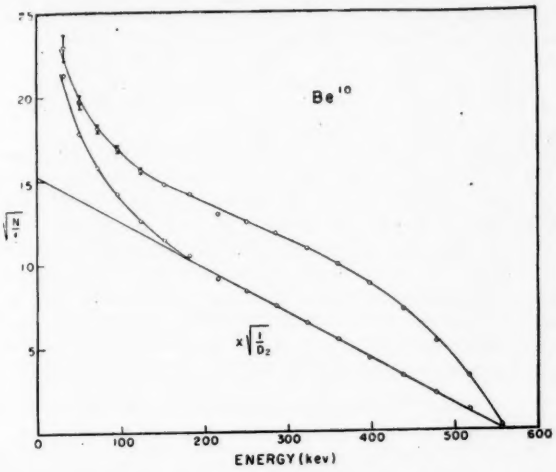

FIG. 2. Kurie plot of Be^{10} spectrum with and without the theoretical "D_2" correction factor.

this run with a resolution correction made by graphical integration (the resolution function of the spectrometer having been determined with a conversion electron line) as well as a correction below 100 kev for the 0.5 mg/cm² Nylon counter window. The straight Kurie plot shows that the resolution correction is quite accurate. The Na^{22} was then mixed with a 0.4 mg/cm² inert BeO source (the thickness to be used for the Be^{10} run), and the upper curve in Fig. 1 (which includes resolution and window corrections) obtained. The effect of the source thickness is seen to be a deviation from the straight line present only below about 180 kev.

The Be^{10} spectrum was obtained with a source of active BeO also 0.4 mg/cm² thick, and the Kurie plot of the data is shown in Fig. 2 both with and without the D_2 correction. The spectrum including the D_2 shape is a straight line from the end point of $560\neq5$ kev down to the point where the source thickness deviation, already determined from Na^{22}, becomes appreciable. The fact that the deviation below this energy is so nearly the same as that observed with Na^{22} implies that the Be^{10} spectrum follows the D_2 shape to an energy lower than 180 kev, that is, at least to 100 kev. The fact that D_2 fits the observed shape so well implies that the disintegration is determined mainly by a single interaction. Marshak[7] has pointed out that the D_2 spectrum is a unique prediction even for an arbitrary linear combination of the fundamental interactions. The one linear combination $(T+A)$ which is consistent with the lifetime of Be^{10} adds a factor $(1+1/W)$ to the D_2 spectrum; but the same factor would then multiply the allowed spectrum and this contradicts experiment. Be^{10} is thus the first example of a highly forbidden transition to be explained as directly as the previously found first forbidden and allowed transitions.

We wish to express our gratitude to many persons whose cooperation has made this experiment possible. Mr. J. Schumar supplied the machined Be metal for the irradiation, which in turn was handled by Mr. E. Montgomery at Hanford. Mr. M. Rodin and Dr. T. S. Chapman expedited the transfer of the material to Hanford and Oak Ridge. The electromagnetic separation at Oak Ridge was under the direction of Dr. C. P. Keim and we wish to extend special thanks to him, and to Mr. H. W. Savage and Mr. L. O. Love who performed the separation with such skill.

* Now at Brookhaven National Laboratory, Upton, L. I., New York.

[1] R. Marshak, Phys. Rev. 75, 513 (1949).
[2] Hughes, Eggler, and Huddleston, Phys. Rev. 74, 1239 (1948).
[3] P. R. Bell and J. M. Cassidy, Phys. Rev. 76, 183 (1949).
[4] C. S. Wu and L. Feldman, Phys. Rev. 76, 698 (1949).
[5] H. W. Fulbright and J. C. D. Milton, Phys. Rev. 76, 1271 (1949).
[6] This finding is in agreement with recent work under the direction of Professor Deutsch (private communication).
[7] R. Marshak (private communication).

Infra-Red Absorption in Silicon

H. B. BRIGGS
Bell Telephone Laboratories, Murray Hill, New Jersey

THE high transparency of pure and nearly pure bulk silicon for infra-red energy makes possible the direct measurement of the extinction coefficient, k, for bulk silicon of small impurity content.[1] Samples of silicon of known impurity content were on hand from a previous investigation.[2] These were prepared for transmission tests by grinding to convenient size and thickness, and polishing. The thicknesses used were all in the range of micrometer caliper measurement. Transmission measurements were made with the aid of a PbS photo-conduction cell placed in a monochromatic beam of infra-red energy. The ratio, p, of transmitted energy to incident energy was determined for two or more thicknesses of each silicon sample. Reflection and scattering losses were minimized by careful polishing of the surfaces. Extinction coefficients were obtained from[3]

$$k=\frac{\lambda}{4\pi}\cdot\frac{\log p_1-\log p_2}{d_1-d_2},$$

where p_1 is the ratio for the thickness d_1, etc.

Figure 1 shows the results of measurements on seven silicon samples, prepared by alloying high purity silicon from the E. I.

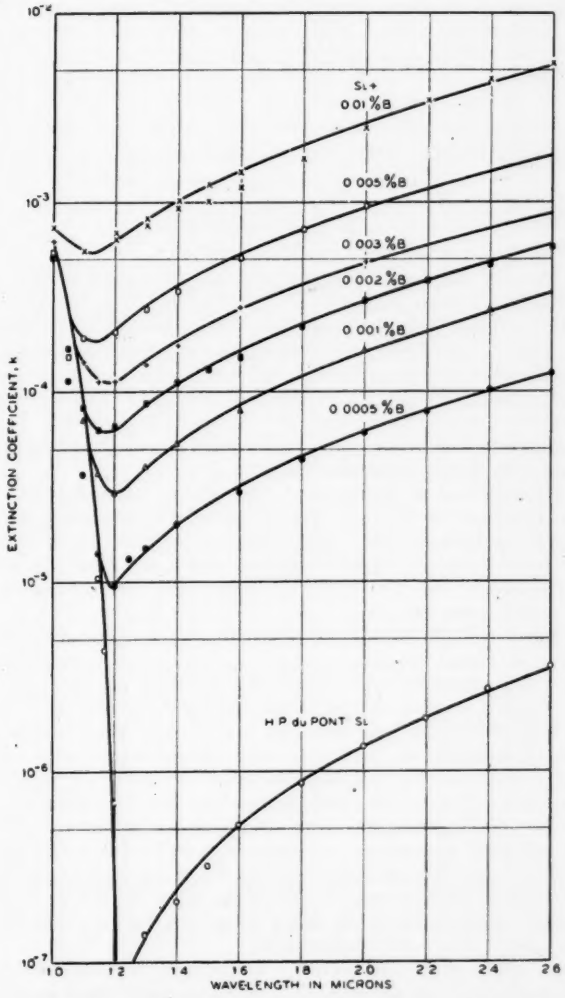

FIG. 1. Extinction coefficient *versus* wave-length for several samples of silicon to which have been added known amounts of boron. The weight percentages of added boron are indicated on each curve.

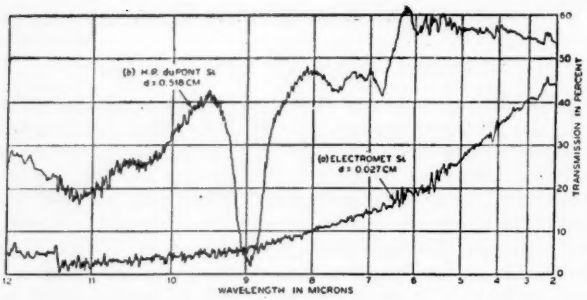

FIG. 2. Transmission of infra-red energy as a function of wave-length. (a) Electromet silicon with a resistivity of about 0.2 ohm cm. (b) Du Pont silicon with a resistivity of about 30 ohm cm.

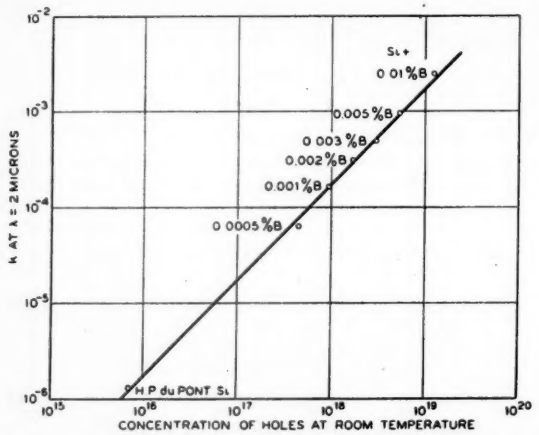

FIG. 3. Extinction coefficient at 2μ *versus* concentration of holes. The 45° line corresponds to direct proportionality.

du Pont de Nemours Company, with small amounts of boron. These samples were prepared by J. H. Scaff and H. C. Theuerer.

In the range of photoelectric activity the extinction coefficients are high for all samples; they drop sharply to minimum values at the photoelectric long wave limit. Beyond the long wave limit, the absorption increases with increasing wave-length for all the samples tested.

Figure 2 shows transmission as a function of wave-length in the range from 2 microns to 12 microns.

The record for the high purity du Pont silicon sample shows very low absorption in the range from 2 microns to 6½ microns, after which absorption increases with the wave-length. At 9 microns there is a strong and sharp absorption band, and a weaker one at 6–8 microns. These are similar to bands found in the absorption spectra of some diamonds.

The record for the sample prepared from Electromet silicon shows only a wide region of absorption, beginning at the long wave limit, and extending out to 11 microns. The 9 micron band is not in evidence, possibly because of the thinness of the sample.

Absorption in the band extending to about 1.2μ is due to excitation of electrons from the filled band to the conduction band, and this absorption gives photo-conductivity. Beyond 1.2μ light is absorbed mainly by the mobile holes which give the conductivity of the p type material. As shown in Fig. 3, the values of k at 2μ are directly proportional to the concentration of holes, N_h, derived from Hall and resistivity data.[2] The degree of ionization of the boron impurity varies with concentration so that N_h is not directly proportional to the added boron. Neutral acceptors may also contribute to the absorption.

According to the classical theory of absorption by free electrons at frequencies high compared with the reciprocal of the relaxation time, τ, the value of nk is

$$nk = e^2\lambda^3 N_h/4\pi^2 mc^3\tau.$$

The observed values of nk are approximately proportional to λ^3, and, at $\lambda=2\mu$, nk is about $6.0\times10^{-22}\ N_h$, giving $\tau=0.32\times10^{-14}$. The value of τ corresponding to the lattice scattering mobility at low frequencies, 100 cm² volt sec., is about 5.7×10^{-14}, which is more than 10 times larger than the optical value. A similar discrepancy is observed by Becker and Fan.[1]

Absorption in the Electromet silicon sample beyond 2μ, shown in Fig. 2, is roughly proportional to λ^3 and is probably due to mobile holes. Absorption by holes is small in the du Pont silicon sample, and the sharp peak at 9μ is probably associated with a vibrational transition of the lattice. The remaining absorption may be associated with transitions from the filled band to acceptor levels. It is believed that study of infra-red absorption will be a useful method for investigating impurities present in concentrations below the limit of ordinary chemical methods but which are of importance in connection with the electrical properties.

[1] M. Becker and H. Y. Fan, Phys. Rev. **76**, 1531 (1949); H. B. Briggs, Phys. Rev. **77**, 287 (1950).
[2] G. L. Pearson and J. Bardeen, Phys. Rev. **75**, 865 (1949).
[3] This relation assumes that $\log p$ is a linear function of d; it neglects the effect of internally reflected energy.

The Neutron Density in the Free Atmosphere up to 100,000 Feet*

LUKE C. L. YUAN**
Princeton University, Princeton, New Jersey
December 19, 1949

IN carrying further the studies[1,2] of the intensity distribution of slow neutrons in the free atmosphere, balloon flights similar to those described in a previous paper[2] were made at the latitude of Princeton, New Jersey (geomagnetic latitude 51° 46′ N).

A pair of identical proportional counters filled with enriched boron trifluoride (96 percent B^{10}) at a pressure of 50 cm Hg were used. One counter was shielded with 0.030 inch of cadmium and the other was shielded with tin of the same thickness for the compensation of possible effects caused by stars produced in the cadmium shield. Both counter systems including the high voltage supply were pressurized to eliminate possible effects caused by corona discharge of the high voltage system. The counters were operated at a voltage plateau centered at 2000 volts.

The results obtained in these flights confirmed our previous measurements[2] made with counters of lower pressure. In one flight, the balloon-borne equipment ascended to an altitude of

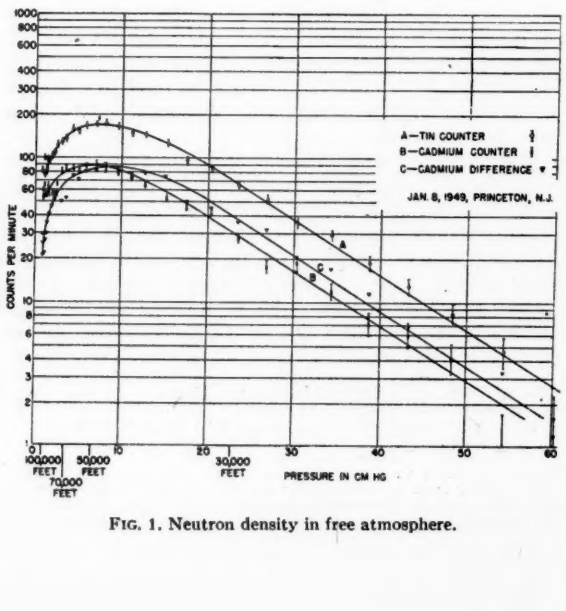

FIG. 1. Neutron density in free atmosphere.

102,000 ft. (0.75 cm Hg pressure). The altitude dependence of the neutron intensity obtained in this flight is shown in Fig. 1, where the counting rate is plotted against pressure in centimeters of Hg. The maximum in the slow neutron distribution as a function of altitude appears at about 8.5 cm Hg and drops down sharply to about one-fourth of its maximum value at 1 cm Hg.

A detailed account of the experiment and the analysis of the results are being prepared for publication and will appear shortly.

* Assisted by the Joint Program of the AEC and the ONR.
** Now at Brookaven National Laboratory, Upton, L. I., New York.
[1] Luke C. L. Yuan, Phys. Rev. **76**, 1267, 1268 (1949). Luke C. L. Yuan and R. Ladenburg, Bull. Am. Phys. Soc. **23**, No. 2, 21 (1948).
[2] Luke C. L. Yuan, Phys. Rev. **74**, 504 (1948).

The Zenith Angle Dependence of the Cosmic Radiation above the Atmosphere at $\lambda = 41°N$* †

S. F. Singer
Applied Physics Laboratory, Johns Hopkins University, Silver Spring, Maryland
January 9, 1950

In a previous note[1] we gave preliminary results on the average flux and primary specific ionization above the atmosphere as measured with a G-M counter telescope (Fig. 1) in a V-2 rocket. We wish to present here a more refined breakdown of these results based on analysis of the motion and orientation of the rocket during flight.

In the present experiment, the telescope pointed along an axis parallel to the longitudinal axis of the V-2 rocket. The zenith angle of the missile, therefore, gave the zenith angle of the axis of the telescope independent of the roll orientation of the missile. Very good information on the zenith angle and azimuth during flight was obtained through analysis of photographs of the earth taken by a camera which was mounted in the rocket (Fig. 2). The coincidences of telescope ABC and $AB'C$, not accompanied by guard counts, were assigned to the proper zenith angle interval leading to the results of Table I and Fig. 3.

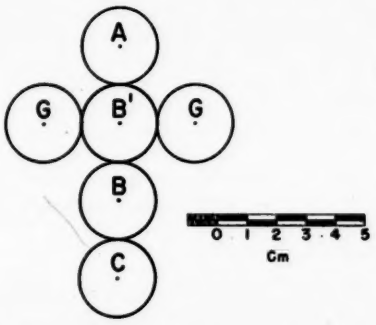

FIG. 1. Low efficiency telescope. All counters have an effective diameter of 2.38 cm and an effective length of 14.5 cm. The low efficiency counter B' is filled with hydrogen to a pressure of 5 cm Hg. Telemetered coincidences: (ABC), $(AB'C)$, and (ACG).

TABLE I. Zenith angle dependence of coincidence counting rate.

Time interval (sec.)	Zenith angle interval	No. of coinc. (ABC)	No. of coinc. $(ABC)\cdot(AB'C)$	Av. directional intensity (telescope ABC) (particles-sec.$^{-1}$-cm^{-2}-sterad.$^{-1}$)	Efficiency: $\frac{(ABC)\cdot(AB'C)}{(ABC)}$
70–130	0°–15°	58	37	0.078 ± 0.010	0.646 ± 0.045
130–180	15°–30°	55	36	0.087 ± 0.012	
180–270	30°–60°	128	87	0.112 ± 0.010	0.680 ± 0.041
270–318	>60°	69	51	0.114 ± 0.014	0.730 ± 0.054

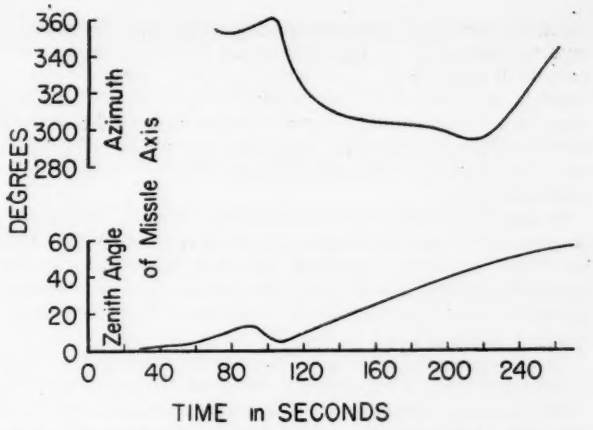

FIG. 2. Zenith angle and azimuth of V-2 rocket fired on February 17, 1949 at the White Sands Proving Ground, New Mexico.

All errors quoted in Table I are standard errors assigned only on the basis of the number of counts.

The values of the directional intensity were obtained by dividing the counting rates (after minor corrections for telescope inefficiency, deadtime, and accidental coincidences) by the telescope's geometric factor (12.6 cm²-sterad.) corresponding to flux incident isotropically from the upper hemisphere, assuming the flux incident from the lower hemisphere to be zero. Because of the "smearing out" caused by the rather wide aperture of the telescope used in this exploratory experiment, the data of Table I and Fig. 3 refer to a directional intensity *averaged* over the geometry of the telescope. The actual variation with zenith angle is probably more rapid than that shown.

From geomagnetic theory and an estimate of the penumbra[2] an "effective" cut-off energy for primary protons has been assigned to sets of zenith and azimuth angles taken from Fig. 2. These cut-off energies range from 4.0 to 3.4 Bev. Assuming a differential energy spectrum of primary protons of the form $E^{-\gamma}dE$, expected intensities have been computed for two extreme values of the

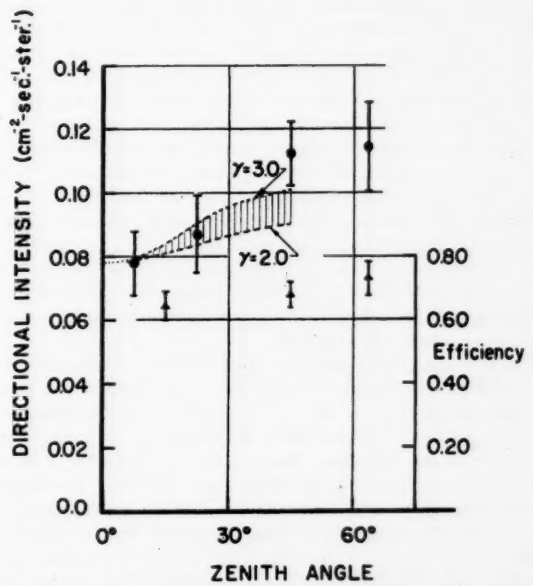

FIG. 3. The average directional intensity (circles) and efficiency of the telescope $AB'C$ (triangles) as a function of zenith angle in a northwesterly direction at $\lambda = 41°N$. The shaded area represents the spread of expected intensities assuming values of the spectrum exponent γ between 2.0 and 3.0.

exponent: $\gamma=2$ and $\gamma=3$. We have superimposed the spread of expected intensities on the experimental points of Fig. 3 for the purpose of comparison. There appears to be a rather definite increase in experimental intensity above the expected value, starting near a zenith angle of 45°.[3] There is also the barest indication of a rise in efficiency with zenith angle, but the number of counts is not large enough to place the increase definitely outside of the statistical error.

Taking these results at their face value, we reach the tentative conclusions: (i) that the near vertical intensity ($j=0.078\pm0.010$ sec.$^{-1}$-cm^{-2}-sterad.$^{-1}$) represents the best upper limit to the primary intensity, and (ii) that low energy secondary radiation produced within the atmosphere contributes to the directional intensity at large zenith angles.

These conclusions are in good accord with those of Van Allen, which are based on a telescope experiment[4] in an Aerobee sounding rocket (Round A-5) at $\lambda=41°$N and also with theoretical considerations by Vallarta[5] on the zenith dependence of the albedo.

I wish to thank Dr. J. A. Van Allen and Professor M. S. Vallarta for valuable discussion, and Messrs. L. W. Fraser, R. S. Ostrander, and F. W. Loomis for their aid in carrying out the experiment and analyzing the camera record.

* This work was supported by the Navy Bureau of Ordnance under Contract NOrd 7386.
† A preliminary account of this work was given at the Echo Lake Conference (June, 1949).
[1] S. F. Singer, Phys. Rev. **76**, 701 (1949).
[2] M. S. Vallarta, Phys. Rev. **74**, 1837 (1948); R. A. Alpher, APL/JHU Internal Report CF-1308 (July 18, 1949).
[3] Based on vertical intensity measurements at $\lambda=0°$ and $\lambda=41°$N, Van Allen and Gangnes have deduced a value for γ of 1.9 [Phys. Rev. (to be published)].
[4] J. A. Van Allen, Echo Lake Conference (June, 1949), and private communication.
[5] M. S. Vallarta (private communication).

On the Nature of the Cosmic Radiation near the Pfotzer Maximum at $\lambda=41°$N* †

S. F. Singer
Applied Physics Laboratory, Johns Hopkins University, Silver Spring, Maryland
January 9, 1950

A DIRECT measurement of the primary specific ionization of the cosmic radiation above the atmosphere by means of a "low efficiency telescope"[1] in a V-2 rocket launched at White Sands, New Mexico ($\lambda=41°$N) has been previously reported.[2] The measurement was carried out essentially by comparing the efficiency of a low pressure hydrogen-filled G-M counter near sea level and above the atmosphere. A small but definite increase was found in the efficiency above the atmosphere leading to the conclusion that the radiation above the atmosphere is predominantly singly charged, but has an average primary specific ionization appreciably higher than minimum. This result is consistent with the interpretation that the charged radiation consists predominantly of high energy (primary) protons of minimum specific ionization with an admixture of (primary) alpha-particles and/or low energy (secondary) protons.

The purpose of this note is to report on data obtained by the telescope in its passage through the atmosphere. In spite of a rather small number of counts, it is apparent that the efficiency of the low pressure counter, and, therefore, the primary specific ionization of the radiation, show a maximum near the position of the Pfotzer maximum of the total cosmic-ray flux. The efficiency measured for the altitude interval 9 to 29 km (approximately 330 to 14 g-cm^{-2}) was 0.764 ± 0.058, compared to a sea-level efficiency[2] of 0.585 ± 0.019 and efficiency above the atmosphere[2] of 0.670 ± 0.027. After applying the corrections discussed previously,[2] this result leads to an average primary specific ionization near the Pfotzer maximum of 1.65 ± 0.35 times the sea-level value. This ratio may have a much higher peak value since it is "smeared out" by the large altitude interval over which the data were taken.

The immediate gross conclusion, which is valid in spite of the large statistical error of the result, is that the bulk of the cosmic-ray flux at high altitudes, which is known to be easily absorbable,[3] does not consist of low energy electrons (5–50 Mev). The argument runs as follows: The particles registered by the telescope after traversing the low pressure counter must possess an additional range of about 2 g-cm^{-2} of copper. For electrons this corresponds to an energy of at least 6 Mev. However, electrons in this energy range exhibit a primary specific ionization near the minimum value. Our experimental result can be interpreted plausibly in terms of slow protons and mesons. A 100-Mev proton, for example, has a residual range of about 10 g-cm^{-2} and a primary specific ionization slightly higher than that of an alpha-particle.

Further experiments within the atmosphere are planned to determine the composition of the cosmic-ray flux at various altitudes; however, the present result, though somewhat crude, is sufficiently discriminating to provide evidence against the electronic nature of the bulk of the soft component at very high altitudes. A similar conclusion, based on entirely different considerations, has been reached by others.[3]

I am greatly indebted to Dr. J. A. Van Allen for valuable discussion.

* This work was supported by the Navy Bureau of Ordnance under Contract NOrd 7386.
† A preliminary account of this work was given at the Echo Lake Conference (June, 1949).
[1] See Fig. 1, preceding letter.
[2] S. F. Singer, Phys. Rev. **76**, 701 (1949).
[3] M. A. Pomerantz, Phys. Rev. **75**, 69 (1949).

Resonance Neutron Scattering in Na^{23} at 3000 Ev

C. T. Hibdon, C. O. Muehlhause, W. Selove, and W. Woolf
Argonne National Laboratory, Chicago, Illinois
January 16, 1950

NEUTRON resonance overlapping between sodium and manganese has been observed by using a neutron scattering counter[1] and an epi-cadmium neutron beam from the Argonne heavy water reactor. With either material serving as scattering detector and the other as absorber about 20 percent overlapping was observed. That is, about 20 percent of the scattered neutrons from one material had a transmission cross section of approximately 120 b for the other material. Similarly, when sodium was used as both scattering detector and absorber about 50 percent of the scattered neutrons had a high transmission cross section.

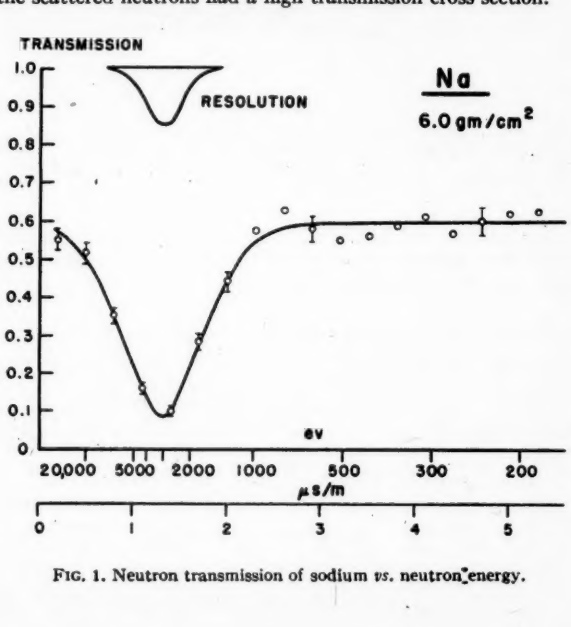

FIG. 1. Neutron transmission of sodium *vs.* neutron energy.

A comparison of the average epi-cadmium scattering of sodium with that of carbon ($\sigma_c=4.60$ b) yielded a resonance scattering integral, $\int\sigma_r dE/E$, for sodium of 51 b.[2] From the self-absorption measurements on sodium a peak value of the resonance cross section, σ_0, of 550 b was obtained. Resonance activation of sodium also indicated that the resonance capture integral, $\int\sigma_\gamma dE/E$, for sodium was less than one percent of the sodium resonance scattering integral. From these data one concludes that (a) $\Gamma_n/\Gamma>0.99$ and (b) $E_0=1770$ ev ($J=1$), or $E_0=2950$ ev ($J=2$).

The neutron transmission of sodium as a function of energy was measured with the new resonance-region time-of-flight spectrometer[3] at the Argonne. The results for the highest resolution used are shown in Fig. 1. The resonance energy, E_0, was determined to be 3000 ± 600 ev (the quoted uncertainty is estimated, and is principally due to various small time uncertainties, each of the order of a fraction of a microsecond). From this, one concludes that (a) $J=2$ and (b) $\Gamma\approx170$ ev. An approximate calculation on the basis of the area under the resonance dip in the transmission *vs.* energy curve gives $\sigma_0\Gamma^2\approx13\times10^6$, which is in agreement with the values given.

Spectrometer measurement of manganese in the energy region covered in Fig. 1 showed that the Na-Mn resonance overlap originally observed was due to a manganese resonance a few hundred ev below the sodium resonance.

Several interesting points can be noted in connection with the sodium resonance observed here. First, sodium is the lightest element ever observed to have a resonance at this low an energy. The average spacing of resonance levels for neutrons incident on sodium is of the order of 100 kev.[4] Second, the energy of the present resonance is at the upper end of the region now reached by time-of-flight spectrometers, and at the lower end of the region accessible to particle-accelerator neutron sources; sodium thus constitutes a convenient test substance for measuring the performance of either type of apparatus.

Third, since this sodium resonance is almost purely scattering, one might expect to observe interference between resonant and potential scattering, leading to a dip in the cross section on the low energy side of resonance. Measurements were made down to thermal energies and show no such dip. The explanation lines in the spin dependence of neutron scattering by sodium. In fact, one can obtain a separate determination of the spin state associated with the resonance, $J=2$, from the fact that the cross section does not change by as much as 0.1 b from 800 ev to 1 ev ($\sigma=3.3$ b in this range), and from the measurement of the coherent scattering from Na, by Wollan and Shull.[5] From the smallness of the variation in σ over the large energy range, one can calculate that for the spin state associated with the resonance the contribution to the potential scattering must be between about 0.3 and 1.0 b, and that the contribution of this spin state to the scattering cross section at low energies must be less than about 0.05 b. From the coherent scattering data one then finds that[6] $J=I+\frac{1}{2}$, $=2$.

Thus it is seen that for the spin state associated with the resonance, the potential scattering is so small that the "dip" in the cross section is extremely shallow and broad. The cross section probably *does* have a minimum at some energy above zero, but the scattering cross section at zero neutron energy is only about 0.01 b greater than at the minimum. Zero neutron energy is simply not far enough from the resonance energy to allow the cross section to rise appreciably from the dip.

Finally, it is of interest to compare the widths of the 3-kev level and the 60-kev level[4] ($\Gamma\approx3$ kev after correcting roughly for instrument spread) in Na^{23}. We have $(E_0/\Gamma)_{3\text{ kev}}=3000/170\simeq18$ and $(E_0/\Gamma)_{60\text{ kev}}\approx60{,}000/3000=20$. It appears, then, from this example that Γ_n varies approximately as E_0.

[1] C. T. Hibdon and C. O. Muehlhause, Phys. Rev. **76**, 100 (1949).
[2] C. O. Muehlhause, Phys. Rev. **77**, 739(A) (1950).
[3] W. Selove, Phys. Rev. **76**, 187 (1949). A detailed description of this apparatus and of other measurements made with it is in preparation.
[4] Adair, Barschall, Bockelman, and Sala, Phys. Rev. **75**, 1124 (1949).
[5] E. O. Wollan and C. G. Shull, Phys. Rev. **73**, 830 (1948).
[6] Reference 5, Table IV. There is an error in this table—the columns should be interchanged.

Showers of Minimum Ionizing Particles from Cosmic-Ray Induced Nuclear Disintegrations in Nuclear Emulsions*

B. T. Feld, I. L. Lebow, and L. S. Osborne
Physics Department and Laboratory for Nuclear Science and Engineering, Massachusetts Institute of Technology, Cambridge, Massachusetts
January 4, 1950

Recent improvements in nuclear emulsions[1,2] make possible the observation of singly charged particles of relativistic energies, allowing the detection of all charged particles associated with nuclear disintegrations in the emulsion. In these emulsions, exposed to cosmic radiation, stars are frequently observed to involve the emission of a multiplicity of relativistic particles, usually confined to a relatively narrow cone.[3–7]

We have analyzed fifteen disintegrations, each involving at least five relativistic particles, in plates exposed at over 90,000 feet.[3] The results are summarized in Table I. The tracks are divided into three categories:

1. "Minimum" tracks: Grain densities corresponding to a singly charged particle of kinetic energy greater than mc^2. These tracks show no observable Coulomb scattering,[8] indicating few electrons of less than ~100-Mev energy.
2. "Near-minimum" tracks: Grain densities from minimum to 5 ×minimum. On eight long tracks, simultaneous scattering and grain count measurements identified seven protons and one meson. We conclude that *most near-minimum tracks are due to high energy protons.*
3. "Heavy" tracks: Grain densities greater than 5 ×minimum, distributed spherically symmetrically and assumed to be evaporation products—low energy protons, alpha-particles, and nuclear fragments.

By grain counting, we estimate the charge carried by evaporation products from each star (column 5). With respect to charge evaporated, the stars divide into two groups; five ascribable to disintegrations of light nuclei (C, N, O), and ten to heavy (Br, Ag). This division is maintained when the near-minimum tracks are included (column 6). However, if the total charge observed (column 7) were assumed to be nucleonic, no events could be ascribed to light nuclei; and two would involve a charge greater than that of Ag(47).

Now, the constitution of the emulsion[9] predicts a ratio of events in heavy to light nuclei of ~3, if the nuclei are opaque to the disintegration-producing radiation, or ~5 if they are transparent. Therefore, *the minimum tracks must be predominantly of non-nucleonic origin.* We assume, in agreement with previous evidence,[10] that they are due to π-mesons.

Furthermore, on the basis of column 6, *we can distinguish experimentally between disintegrations of light and heavy nuclei.*

For each disintegration, we have measured the direction of each track with respect to the geometric axis of the minimum tracks. The distributions of all minimum and near-minimum tracks are plotted in Fig. 1. A significant difference is observed between light and heavy nuclei.

Table I. The salient features of observed nuclear disintegrations containing more than 5 relativistic particles.

Star	No. of min. tracks	No. of near-min. tracks	Angle of primary with the shower axis	Charge in the heavy	Charge in the heavy and near-min.	Total charge observed
L-1	6	2	10°	4	6	12
L-2	7	3	10°	4	7	14
L-3	9	5		4	9	18
L-4	10	4		3	7	17
L-5	13	5		4	9	22
H-1	5	9		27	36	41
H-2	9	6	20°	28	34	43
H-3	10	8		24	32	42
H-4	11	1	20°	15	16	27
H-5	12	6	18°	18	24	36
H-6	12	6	9°*	17	23	35
H-7	13	8		19	27	40
H-8	14	5		43	48	62
H-9	15	4	19°	22	26	41
H-10	27 (20)	12 (19)	25°	19	31 (38)	58

* The particle, assumed incident, has a grain density approximately four times minimum, which corresponds to a relativistic alpha-particle.

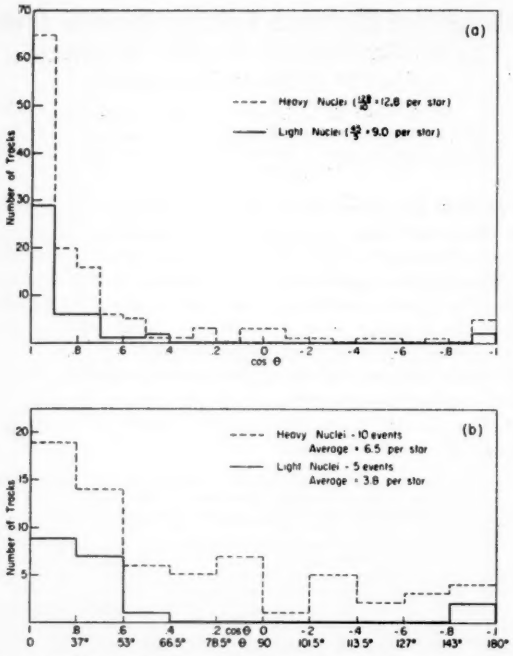

FIG. 1. Angular distribution, with respect to their shower axes, of (a) all minimum tracks (kinetic energy $>mc^2$) and (b) all near-minimum tracks (kinetic energy between 0.08 and 0.6 mc^2) from light and heavy nuclei.

The average angle with respect to the shower axis of the minimum tracks in each star *vs.* their multiplicity is plotted in Fig. 2. *For the same multiplicity of meson production, the angular spread is much smaller for light than for heavy nuclei.*

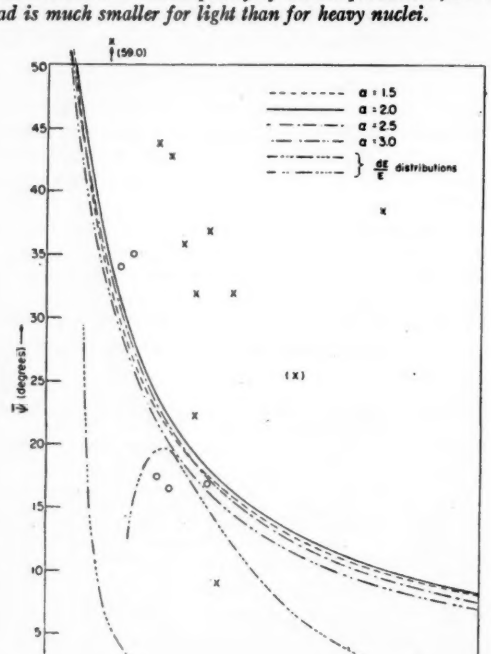

FIG. 2. Average angular spread of the minimum tracks *vs.* their multiplicity. The circles represent light nuclei; the crosses, heavy nuclei. The curves are predictions based on a completely inelastic single nucleon-nucleon collision, with a spherically symmetric angular distribution of charged mesons in the center of mass system. The upper group of four curves assume that all the mesons are produced with a single energy, α (total energy in meson rest energy units) in the center of mass system. The lower two curves assume a bremsstrahlung energy distribution, with high energy cut-offs at 0.155 and 1.0 times the energy available in the center of mass system.

The curves in Fig. 2 represent predictions of a simple theory in which all the charged mesons are produced in a single, completely inelastic nucleon-nucleon collision, with a spherically symmetrical angular distribution and various energy distributions in the center of mass system. The meson distributions from light nuclei are not in disagreement with these predictions; the heavy nuclei are in disagreement.

On the other hand, the fast proton component in the showers and the increased angular spread of showers from heavy, as compared to light, nuclei suggest that meson production in all nuclei is by a cascade process, with a small multiplicity in each nucleon-nucleon collision. Accordingly, nuclei must be considered opaque to high energy nucleons, and the observed[10] exponential absorption, with longer-than-geometric mean free path, of the star-producing radiation, must be explained in terms of the cascade multiplication process.

We are indebted to Mrs. T. Kallmes for much detailed observation.

* Assisted by the Joint Program of the ONR and the AEC. We are especially grateful to J. Hornbostel and E. O. Salant, Brookhaven National Laboratory, for their cooperation in making available emulsions exposed at high altitudes.

[1] R. W. Berriman, Nature **161**, 432 (1948); **162**, 992 (1948); R. H. Herz, Phys. Rev. **75**, 478 (1949).
[2] Brown, Camerini, Fowler, Muirhead, Powell, and Ritson, Nature **163**, 74, 82 (1949).
[3] J. Hornbostel and E. O. Salant, Phys. Rev. **76**, 468(A), 859 (1949); L. S. Osborne and B. T. Feld, Phys. Rev. **76**, 468(A) (1949).
[4] Leprince-Ringuet, Bousser, Hoang-Tchang-Fong, Jauneau, and Morellet, Phys. Rev. **76**, 1273 (1949).
[5] Brown, Camerini, Fowler, Heitler, King, and Powell, Phil. Mag. **40**, 862 (1949); Camerini, Coor, Davies, Fowler, Lock, Muirhead, and Tobin, Phil. Mag. **40**, 1073 (1949).
[6] Kaplon, Peters, and Bradt, Phys. Rev. **76**, 1735 (1949).
[7] Cosyns, Dilworth, Goldschmidt-Clermont, Occhialini, Schonberg, and Vermaesen, Report at the Como Conference. We are grateful to the above for making available to us the results of their investigations prior to publication.
[8] Goldschmidt-Clermont, King, Muirhead, and Ritson, Proc. Roy. Soc. **61**, 183 (1948).
[9] J. H. Webb, Phys. Rev. **74**, 511 (1948).
[10] B. Rossi, Rev. Mod. Phys. **20**, 537 (1948).

The Neutrons from the Disintegration of Beryllium by Deuterons*

W. D. WHITEHEAD AND C. E. MANDEVILLE
Bartol Research Foundation of the Franklin Institute, Swarthmore, Pennsylvania
January 16, 1950

THE neutrons from the reaction $Be^9+D\rightarrow B^{10}+n+Q$ have been previously investigated by Bonner and Brubaker,[1] Powell and Fertel,[2] and Staub and Stephens.[3] In all three instances, a bombarding energy of less than 1 Mev was employed and neutron groups were observed corresponding to energy levels in the residual nucleus, B^{10}, at 0.65, 2.0, and 3.4 Mev.[4] More recently, Evans, Malich, and Risser[5] have noted the presence of an additional neutron group, endothermic in character, and corresponding to an excitation level in B^{10} at 5.13 Mev. Their estimated Q-value for this group is (-0.74) Mev. Indication of the endothermic group was obtained solely from an analysis of the counter data of the excitation curve for neutrons from $Be^9(D,n)B^{10}$, whereas in the earlier measurements,[1-3] recoil proton spectra of the neutrons were actually observed in cloud chambers and photographic plates.

In the measurements to be described, Ilford C_2 emulsions, located 10 cm from the target and making an angle of zero degrees with the incident deuterons, were irradiated by neutrons from the reaction $Be^9(D,n)B^{10}$. In order to activate the level in B^{10} corresponding to the endothermic Q-value, a mean bombarding energy of 1.62 Mev was employed to irradiate a beryllium target of thickness 100 kev. The energy spectrum observed in a microscope is shown in Fig. 1 where five groups of neutrons are seen to

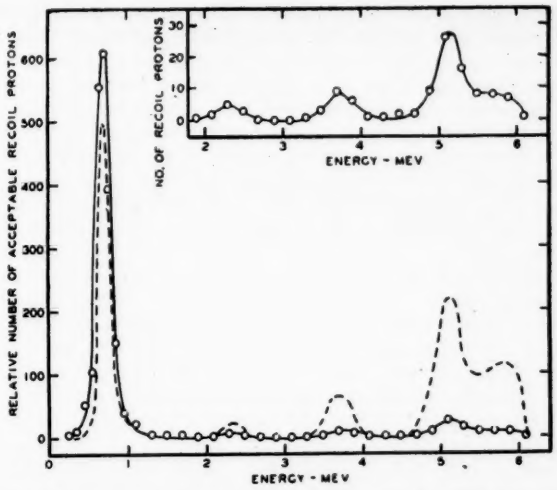

FIG. 1. Distribution in energy of the recoil protons of the neutrons from $Be^9(D,n)B^{10}$. The energy of the incident deuterons was 1.62 Mev.

be present having energies of 0.70, 2.32, 3.72, 5.17, and 5.86 Mev. In order to ascertain positively that the group of lowest energy was not distorted by the presence of neutrons from $C^{12}(D,n)N^{13}$, a carbon target also of thickness 100 kev was irradiated by deuterons at 1.62 Mev, and the recoil protons of the emitted neutrons were observed in C_2 plates. The observed peak of the monochromatic neutrons occurred at 1.14 Mev, showing clearly that the neutrons of carbon could have made no contribution to the group of lowest energy in Fig. 1. The Q-values given by the curve of Fig. 1 are -0.74, 0.73, 2.19, 3.70, and 4.39 Mev. In obtaining the Q-values, the observed neutron energies were increased to allow for the use of a finite angle of acceptance in the emulsions.

In a separate experiment, the same beryllium target was bombarded by deuterons of mean energy 1.15 Mev. The energy distribution of the recoil protons is shown in Fig. 2, where the endothermic group of the beryllium reaction has disappeared and has been replaced by the neutrons from $C^{12}(D,n)N^{13}$, since carbon had begun to form in appreciable quantity upon the surface of the target. Disappearance of the endothermic group at a bombarding energy of 1.15 Mev is attributed to the fact that the recoils of the neutrons of low energy did not make tracks of sufficient length to be distinguishable against the general background of the plates.

The energy levels in B^{10} calculated from Figs. 1 and 2 are 0.69 ± 0.10, 2.20 ± 0.10, 3.66 ± 0.10, and 5.13 ± 0.08 Mev. In Figs. 1 and 2, the energy distributions were corrected for variation with energy of the $n-p$ scattering cross section and acceptance probability as indicated by the broken line. It is to be noted that the relative intensities of the neutron groups fluctuate considerably with bombarding energy. From the areas under the curves and, assuming spherical symmetry in the c.g. system of coordinate axes, it is estimated that at $E_D=1.62$ Mev, the relative intensities are, in the order of ascending Q-value, 14.5, 1.9, 9.4, 35.6, and 38.6. At $E_D=1.15$ Mev, for the four beryllium groups, the relative intensities are 7, 15, 39 and 39.

Recently, spectrometric studies have been made of the gamma-rays related to the reaction $Be^9(D,n)B^{10}$. A gamma-ray of energy 5.20 Mev was observed, with an intensity amounting to about two percent of the total gamma-ray yield. The low intensity of the gamma-ray is in agreement with the fact that the total gamma-ray yield does not increase appreciably with the appearance of the endothermic group of neutrons.[5] It has been suggested,[6] therefore, that the following reactions occur:

$$Be^9+D\rightarrow{}^*B^{10}+n-0.74 \text{ Mev},$$
$$^*B^{10}\rightarrow Li^6+He^4+0.84 \text{ Mev}.$$

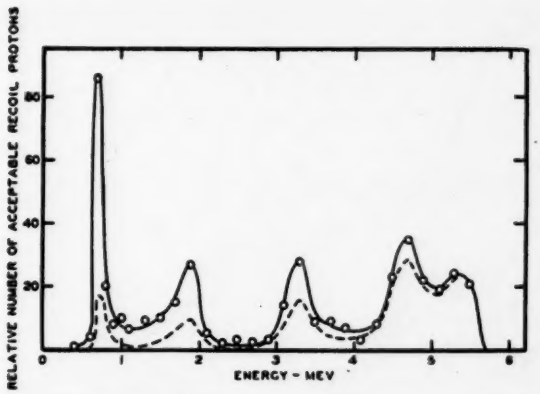

FIG. 2. Distribution in energy of the recoil protons of the neutrons from $Be^9(D,n)B^{10}$. The energy of the incident deuterons was 1.15 Mev. The group of lowest energy is from the reaction $C^{12}(D,n)N^{13}$.

The high probability of particle emission explains, of course, the low intensity of the nuclear gamma-ray at 5.20 Mev.

* Assisted by the Joint Program on the ONR and the AEC.
[1] T. W. Bonner and W. M. Brubaker, Phys. Rev. **50**, 308 (1936).
[2] C. F. Powell and G. E. G. Fertel, Nature **144**, 115 (1939).
[3] H. H. Staub and W. E. Stephens, Phys. Rev. **55**, 131 (1939).
[4] W. F. Hornyak and T. Lauritsen, Rev. Mod. Phys. **20**, 191 (1948).
[5] Evans, Malich, and Risser, Phys. Rev. **75**, 1161 (1949).
[6] Rasmussen, Lauritsen, and Lauritsen, Phys. Rev. **75**, 199 (1949); Rasmussen, Hornyak, and Lauritsen, Phys. Rev. **76**, 581 (1949); Chao, Lauritsen, and Rasmussen, Phys. Rev. **76**, 582 (1949).

Evidence for a Charged Heavy Meson*

H. H. FORSTER
University of Southern California, Los Angeles, California
December 12, 1949

IN the course of recent experiments with nuclear emulsion plates exposed for several hours at 30,000 feet an interesting cosmic-ray event was found which is discussed below. A photomicrograph of the event is shown in Fig. 1: A charged particle

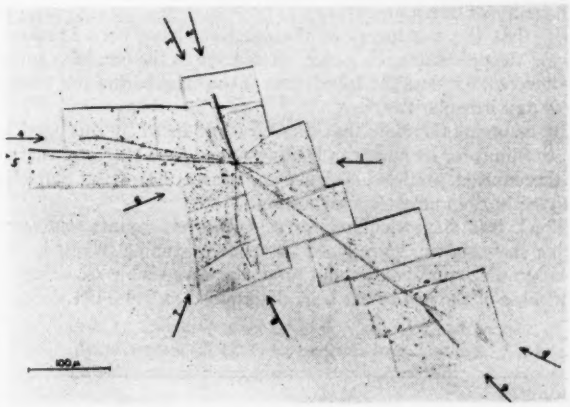

FIG. 1. Disintegration of a heavy nucleus originated by a charged particle coming to rest in the emulsion.

(track 1) enters the emulsion from the air and after progressing 50μ comes to rest in the emulsion. The end of its range is coincident with a nuclear disintegration in which 10 charged particles are ejected. One particle (track 8) is strongly scattered, stops in the emulsion and shows an increase in ionization typical for mesons. An enlargement of track 1 is shown in Fig. 2; with regard

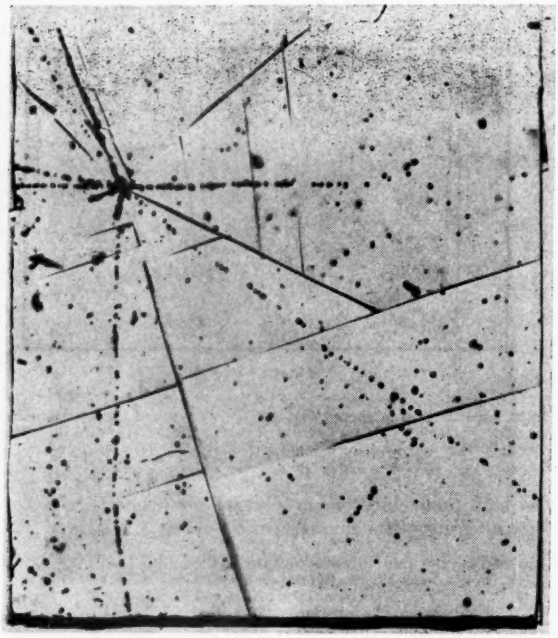

FIG. 2. Enlargement of center section of Fig. 1.

to this track it is pointed out that the coincidence between the star and the track is perfect when examined under the highest magnification. Careful examination leaves no doubt that the grain density increases from right to left indicating that the particle progresses toward the star and does not originate in it. Other possible causes for a change in grain density were considered: Since the track dips 17μ before reaching the end of its range near the center of the 50μ thick emulsion an interpretation other than that of an incident particle would imply

(a) that the deeper layers of the emulsion were more developed than the top layers; but, as is well known, exactly the opposite effect takes place in non-uniform development of nuclear emulsion plates. Furthermore, none of the other tracks indicate any non-uniformity of development; or,

(b) that the top layers of the emulsion have been impaired during the processing. However, no damage to the emulsion could be detected, nor does the appearance of the neighboring star tracks show any irregularities.

By assuming therefore that the star is produced by this particle a lower limit for its mass can be determined from the total energy of the emitted particles. Table I contains a list of the particles emitted in the nuclear disintegration.

Track 8 is of particular interest since grain counts and scattering show that it is produced by a meson coming to rest in the photographic emulsion without producing any visible secondaries. The mass of the meson has been determined as 214±124 electron masses; while no reliance can be placed in the quantitative mass determination of an individual meson this method can be used to distinguish with certainty between a proton and a meson track of the same age. Track 9 is produced by an energetic particle which appears to collide elastically with another particle in the emulsion (9′). From conservation of momentum and energy the ratio of the mass of the incident particle to that of the knock-on is determined as 2.1:1 corresponding to a deuteron proton collision. From the residual range of the scattered deuteron its energy immediately after the collision can be determined as 4.1 Mev. Its energy just before the collision is then calculated from the conservation laws as 18 Mev. From known range energy relations the kinetic energy of the deuteron when leaving the nucleus is found to be 21.1 Mev.** Particles 10 and 11 listed in Table I could not be shown in the photo-micrograph because of the shortness and large angle of dip of their tracks. They are energetic particles which pass out of the emulsion and which have tentatively been identified as protons. (Identification with alpha-particles would yield a higher total energy.)

TABLE I. Particles emitted in the disintegration.

Track number	Track ending	Particle	Kinetic energy (Mev)	Total energy (Mev)
2	glass	alpha	11.3	13.8
3	emulsion	proton	2.2	10.2
4	emulsion	proton	5.6	13.6
5	emulsion	proton	6.3	14.3
6	emulsion	alpha	5.1	7.6
7	emulsion	alpha	2.5	5.0
8	emulsion	meson	2.0	2.0
9	emulsion	deuteron	21.1	23.6
10	air	proton	0.8	8.8
11	air	proton	0.7	8.7

Column 5 in Table I contains the energies of the star particles computed from known range energy relations for the photographic emulsion. In this table the binding energy of protons has been taken as 8 Mev, that of alpha-particles as 2.5 Mev. In the case of particles which do not end in the emulsion the minimum energy is listed, that is, the energy corresponding to the length of track lying entirely in the emulsion. The total energy of the 10 particles is at least 107 Mev.

If the mass of the emitted meson is taken as 285 electron masses the rest mass of the incident particle must be larger than 500 electron masses. The assumption of 210 electron masses corresponding to identification of track 8 with a μ-meson yields, as a lower limit, a mass of 425 electron masses for the incident particle. The actual mass of the particle can only be inferred by speculation; an assumption that the total energy of the star particles not detectable in the photographic plate (particles with minimum ionization and neutral particles) is of the same order of magnitude as that obtained from Table I places the mass of the incident particle in the neighborhood of 700 to 800 electron masses.*** It may be worth mentioning that these mass values yield a lower limit for the lifetime of the particle of the order of 10^{-12} sec.

It is a pleasure to thank Dr. W. Arnquist of the ONR and Mr. C. L. D'Ooge of the Naval Ordnance Test Station at Inyokern, California, for the assistance rendered in exposing the plates.

* The exposure of the plates was made possible through the cooperation of the Pasadena office of the ONR and the Air Force at the Naval Ordnance Test Station at Inyokern, California.

** The alternative that track 9′ is the track of the primary particle and track 9 that of the knock-on can be ruled out. A calculation similar to the one given above yields a mass ratio of 3:1 for the two colliding particles. However, the energy calculated for the triton after the collision would not be sufficient to account for the observed range and ionization of track 9′.

*** A similar event has been reported by Leprince-Ringuet in Rev. Mod. Phys. 21, 42 (1949).

Thermoelectric Power and Mobility of Carriers in Selenium*

HERBERT W. HENKELS
University of Pennsylvania, Philadelphia, Pennsylvania
December 23, 1949

THE theromoelectric power of single crystal and microcrystalline selenium has been investigated as a function of temperature with parameters of crystallization temperature and oxygen content. Simultaneous measurements of resistivity were made in the cases of the microcrystalline samples. The thermoelectric power of a semiconducting crystal may be related to the density of current carriers, when carriers of one sign and of electronic mass are assumed by:

$$Q=\frac{k}{e}\left(\ln\frac{3\pi T^{\frac{1}{2}}}{8en}-5.32\right). \quad (1)$$

Our previous work on the dark resistivity of "pure" hexagonal microcrystalline selenium has shown that the resistivity and activation energy depend on the temperatures of quench and crystallization. Quenched samples, crystallized rapidly (i.e., at higher temperatures), exhibited very marked non-equilibrium conditions in the temperature dependence of resistance. Both positive and negative temperature coefficients were obtained in different temperature ranges as has been previously reported by other investigators. However, samples prepared without quenches always have negative temperature coefficients. The resistivities of the single crystals have been reported previously.[1]

The thermoelectric power was checked with different temperature gradients but most of the measurements were made with a gradient of approximately 25°C. Figure 1 gives data on the thermoelectric power and resistivity of differently crystallized samples including a single crystal grown from a melt. Figure 2 presents data on the simultaneous measurement of thermoelectric power and resistivity as a function of oxygen content.

Although the relation (1) is not obviously applicable to any microcrystalline aggregate, it should hold for single crystals. However, it is noticed that the behavior of the thermoelectric power is similar for the single crystal and microcrystalline samples. It should be noted that all selenium samples, including single crystals, exhibit to some extent the existence of non-equilibrium conditions. In what follows it must be assumed that in the individual temperature intervals used to measure the thermoelectric power the "acceptor" densities are constant and there are activation energies constant in the small intervals. In a few cases the temperature was raised to within a few degrees of the melting point but the thermoelectric power showed no tendency to reverse or decrease sharply.

An estimate of the density of carriers in different temperature ranges was obtained by use of the formula. The densities calculated are given in Table I, while Table II gives the corresponding mobilities.

To our knowledge there is in the literature no data on the mobility of carriers in single crystal selenium for comparison.

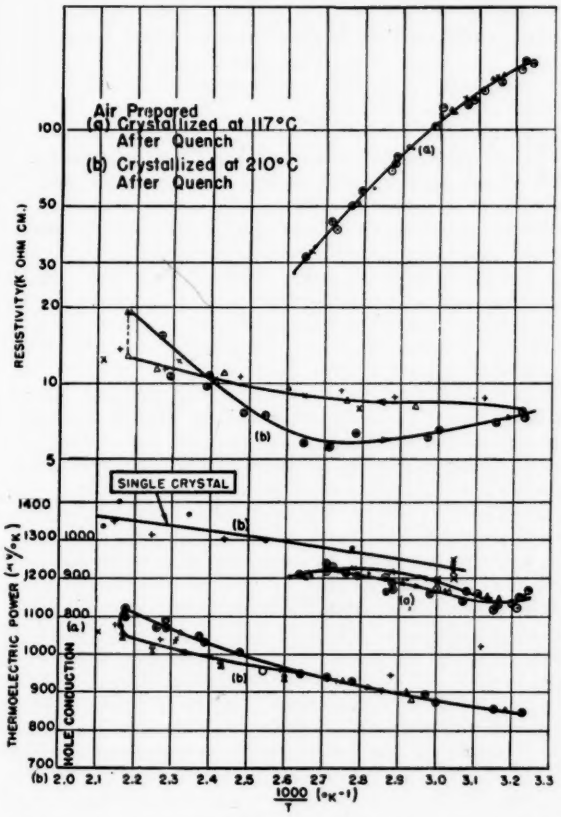

FIG. 1. Resistivity and thermoelectric power of various samples of microcrystalline selenium.

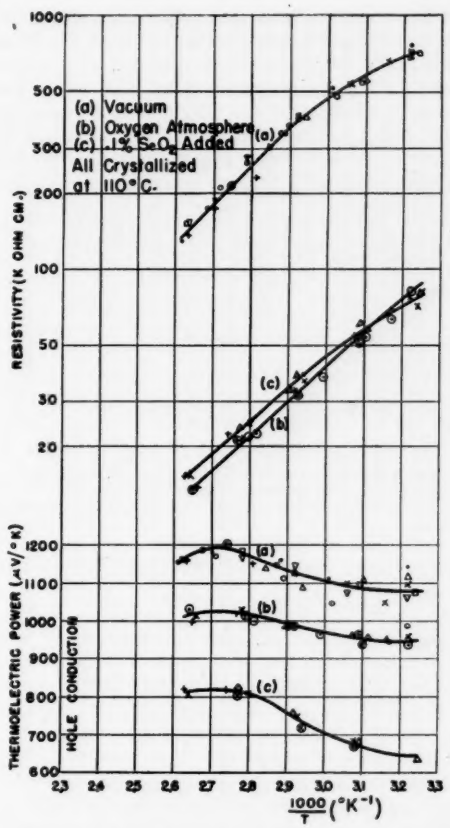

FIG. 2. Thermoelectric power and resistivity of microcrystalline selenium as functions of oxygen content.

TABLE I. Density of carriers in selenium (cm^{-3}).

	50°C	100°C	190°C
Single crystal sample	1.5×10^{14}	1.0×10^{14}	0.6×10^{14}
Microcrystal samples, Lot A			
(a) Air prepared, quenched, crystallized at 110°C	1.1×10^{16}	6.1×10^{15}	—
(b) Air prepared, quenched, crystallized at 210°C	9.9×10^{15}	4.8×10^{15}	1.0×10^{15}
Microcrystal samples, Lot B			
(a) vacuum prepared	7.2×10^{14}	2.7×10^{14}	—
(b) Oxygen atmosphere prepared	3.6×10^{15}	2.0×10^{15}	—
(c) 0.1 percent SeO_2 added, all quenched, crystallized at 110°C	9.2×10^{16}	1.9×10^{16}	—

TABLE II. Mobility of carriers in selenium (cm^2/volt sec.).

		50°C	100°C	190°C
Single crystal sample	$\parallel C$ axis	0.4	1	5
	$\perp C$ axis	0.1	0.3	1
Microcrystal samples, Lot A				
(a) Air prepared, quenched, crystallized at 110°C		0.004	0.03	—
(b) Air prepared, quenched, crystallized at 210°C		Av. 0.09	Av. 0.2	Av. 0.4
Microcrystal samples, Lot B				
(a) Vacuum prepared		0.02	0.1	—
(b) Oxygen atmosphere prepared		0.03	0.2	—
(c) 0.1 percent SeO_2 added, all quenched, crystallized at 110°C		0.001	0.02	—

Estimates have been made of the mobility of carriers in microcrystalline selenium with carrier densities based on the capacity of rectifiers. In view of the failure of rectifier theory to explain the observed results in selenium rectifiers and the demonstration of the presence of selenides at the intersurfaces of such rectifiers,[2] the results are considered unreliable. The existence of grain boundary resistance in the case of microcrystalline selenium can readily explain the large difference in mobilities of such samples and single crystals.

* This work was done under Naval Contract NObsr 42487.
[1] H. W. Henkels, Phys. Rev. 76, 1737 (1949).
[2] H. W. Henkels, Proc. Nat. Electronics Conf. 5 (1949).

Production of C^{15}

EMMETT L. HUDSPETH* AND CHARLES P. SWANN
Bartol Research Foundation of the Franklin Institute,† Swarthmore, Pennsylvania
AND
N. P. HEYDENBURG
Carnegie Institution of Washington, Department of Terrestrial Magnetism, Washington, D. C.
January 19, 1950

THE bombardment of C^{14} with deuterons has been shown to yield d,n and d,α reactions, both of which were recently reported.[1] We have utilized the larger generator of the Carnegie Institution of Washington to make bombardments with deuterons of energy up to 2.8 Mev in order to look for the $C^{14}(d,p)C^{15}$ reaction. The mass estimated for C^{15} is[2] 15.0165, which would indicate that this reaction would have a Q-value of about -2 Mev.

A target of $BaCO_3$ (containing about 40 percent C^{14}), of weight about 400 $\mu g/cm^2$, was used in our bombardments.[3] A preliminary check showed that, when bombarding with deuterons of 2.4-Mev energy, a beta-emitter of half-life much greater than that of B^{12} was also formed. We were able to measure the half-life by simply following the activity of the target with a stop-watch; counts were recorded after the bombarding beam had been shut off for varying lengths of time. The results of these observations are shown in Fig. 1, where the data for three separate runs have been combined and averaged. All of the sets of data indicated a half-life of 2.4 seconds, with an estimated error of about 0.3 second. Some scatter in the points is probably caused by non-uniformity of the target and slight variations in bombarding current.

When it was established that the half-life is so much greater than that of B^{12} (formed in the competing (d,α) reaction) it was possible to make absorption measurements on the beta-rays from C^{15} decay—again by taking observations directly after bombardment was stopped. It was found that the extrapolated end point of the beta-ray spectrum corresponds to 4.6 g/cm² of aluminum absorber; this would indicate a beta-ray energy of 8.8 Mev, with a tentatively estimated error of about 0.5 Mev. This value of the energy, together with the half-life measurement, indicates that the postulated $C^{15}-N^{15}$ decay is a first-forbidden transition.

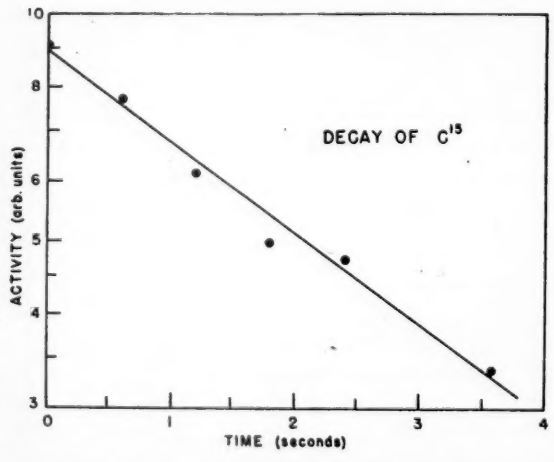

FIG. 1. Activity of C^{15} as measured by counting of beta-rays emitted at various times following deuteron bombardment of C^{14}.

We have also obtained a rough excitation curve; it rises smoothly with increasing energy of deuterons in the region from 1.4 to 2.8 Mev, except for some indication of a resonance at about 1.9 Mev. This, however, must be confirmed.

The calculated mass of C^{15}, based on the beta-ray data, is 15.01434, which makes the Q-value for $C^{14}(d,p)C^{15}$ only slightly negative. However, decay of C^{15} may not be to the ground state of N^{15}, which would alter this mass value as calculated. Indeed, we have some evidence for delayed gamma-emission.

Bombardment of normal $BaCO_3$ was also made, and no beta-emitter of appreciable intensity and of half-life comparable to 2.4 seconds was observed.

More complete details of this investigation will be published in the near future.

* Present address: Department of Physics, University of Texas, Austin, Texas.
† Assisted by the Joint Program of the ONR and AEC.
[1] E. L. Hudspeth and C. P. Swann, Bull. Am. Phys. Soc. 25, No. 1, 32 (1950), New York Meeting.
[2] H. A. Bethe, *Elementary Nuclear Theory* (John Wiley and Sons, Inc., New York, 1947).
[3] Target material was obtained from Oak Ridge; the estimated value of enrichment was supplied by L. D. Norris (private communication).

Dependence of the F^{19} Nuclear Resonance Position on Chemical Compound*

W. C. DICKINSON
Research Laboratory of Electronics, Massachusetts Institute of Technology, Cambridge, Massachusetts
January 9, 1950

MOST unexpectedly, it has been found that for F^{19} the value of the applied magnetic field H_0 for nuclear magnetic resonance at a fixed radiofrequency depends on the chemical compound containing the fluorine nucleus. The assumption has generally been made that the time average of all internal magnetic fields is zero, excluding of course the small diamagnetic field at the nucleus due to the Larmor precession of its atomic electrons in H_0. Nuclear resonance shifts in metals,[1] interpreted as being due to the conduction electrons, are larger by about an order of magnitude than those reported here.[2]

To investigate the effect in fluorine, two identical magnetic resonance absorption bridges,[3] both fed by the same oscillator, were employed. The two sample holders were placed side by side in the magnet so that the F^{19} resonance traces occurred simultaneously on separate recording milliammeters. This "null" method allows a precision of about 0.0005 percent of the applied field in measuring relative shifts of resonance position and has been used by the author in measuring such shifts due to the addition of paramagnetic ions.

The maximum separation of F^{19} resonances observed so far is 1.05 gauss (see Fig. 1) for $C_2F_3Cl_3$ (freon 113) and BeF_2 in a magnetic field $H_0 \approx 7000$ gauss, the freon resonance coming at the lower *applied* field. Although the resonances in SbF_3 and BeF_2 are separated by 0.99 gauss when observed in separate samples, the separation reduces to 0.82 gauss for a mixture of the two compounds (see Fig. 2). On the other hand, the resonances in SbF_3 and HF are separated by 0.83 gauss in separate samples, but a half and half mixture of the two results in a single resonance located halfway between the positions where the separate resonances would be expected. Increasing the relative amount of SbF_3 shifts

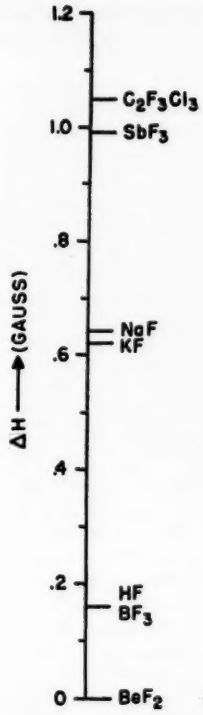

FIG. 1. Dependence of F^{19} nuclear resonance position on chemical compound. $H_0 \approx 7000$ gauss. ΔH represents an aiding field at the nucleus and has arbitrarily been set equal to zero for BeF_2. All compounds except $C_2F_3Cl_3$ and BF_3 (ether complex) were in aqueous solution.

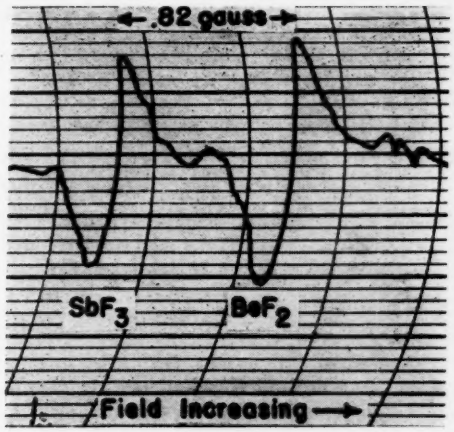

FIG. 2. The nuclear resonances of F^{19} in a single sample containing a half and half mixture of SbF_3 and BeF_2 (saturated aqueous solutions). The applied resonance magnetic field is about 7000 gauss at a radiofrequency of 28.0 megacycles.

the single resonance toward the position of the resonance in pure SbF_3. The observed line widths were about 0.15 gauss in all cases. The F^{19} resonance separations in the chemical compounds listed in Fig. 1 were remeasured at a resonance field of 2500 gauss (10.0 megacycles). Within the experimental error, proportionality of the separations with the applied field was found.

It might be added here that a discrepancy exists between the $F^{19}-H^1$ resonance frequency ratio measurements by Siegbahn and Lindstrom[4] (using $C_2F_3Cl_3$) and by Poss[5] (using HF). The magnitude and direction of the relative shift for these two compounds as observed here accounts for this discrepancy but of course the *true* value of this frequency ratio is now uncertain by at least 0.015 percent.

The internal diamagnetic corrections[6] H'/H_0 for the neutral fluorine atom and the singly charged negative ion have been calculated by the author using Hartree-Fock wave functions[7] giving 0.0464 and 0.0472 percent, respectively. Thus for $H_0=7000$ gauss the difference between the two diamagnetic fields would be approximately 0.06 gauss. This seems to be the wrong order of magnitude to explain the observed shifts.[8] Further investigation as to the nature and cause of these shifts is now in progress.

Proton resonances were compared with each other in acetone, mineral oil (Nujol), distilled water, glacial acetic acid, glycerin, and anhydrous ether. No shifts could be detected within the accuracy of the experiment of about 5 parts in 10^6.

The author wishes to express his thanks to Professor F. Bitter for his advice and guidance during the course of this work.

* This work has been supported in part by the Signal Corps, the Air Materiel Command, and the ONR.

[1] W. D. Knight, Phys. Rev. **76**, 1259 (1949).

[2] In a private communication, Professor F. Bloch reports that W. G. Proctor and F. C. Yu at Stanford University, while recently working with N^{14}, found a similar but even more pronounced dependence of the resonance position on the chemical compound.

[3] Bloembergen, Purcell, and Pound, Phys. Rev. **73**, 679 (1948).

[4] K. Siegbahn and G. Lindström, Arkiv. Mat. Astr. o. Fys. **1**, 6, 193.

[5] H. Poss, Phys. Rev. **75**, 600 (1949).

[6] W. E. Lamb, Jr., Phys. Rev. **60**, 817 (1941).

[7] F. W. Brown, Phys. Rev. **44**, 214 (1933).

[8] Molecular perturbations of the electrons in the outer electronic shells would be expected to have only a small effect on the value of H'/H_0 since for F^- the entire contribution of the $(2s)^2(2p)^6$ shell to H'/H_0 is only about 30 percent.

PHYSICAL REVIEW VOLUME 77, NUMBER 5 MARCH 1, 1950

Proceedings of the American Physical Society

MINUTES OF THE MEETING AT CHICAGO, NOVEMBER 25 AND 26, 1949

THE 295th meeting of the American Physical Society, being the 1949 Thanksgiving meeting, was held at Chicago in the buildings of the University of Chicago on Friday and Saturday, November 25 and 26, 1949. The Secretary thinks that in number of papers (143 contributed!) this was by far the largest meeting yet held west of Washington, D. C. Since by reason of the Thanksgiving holiday it was cramped into two days, the number of papers per day fell short of that of our greatest meetings by about a third, whence the unwelcome necessity of scheduling four and even five simultaneous sessions. In number of people in attendance it fell much shorter of our New York and Washington meetings: the number of registrants, somewhat under 500, is supposed to be not far below the number who actually came. Arrangements were very capably handled by the Local

Committee, consisting apparently in the main of S. K. Allison and his secretarial staff.

There were nineteen invited papers: seven of these belonged to two Symposia—their subjects, "Electron Emission" and "Gaseous Electronics," respectively—arranged by our Division of Electron Physics, and five others pertained to solid-state physics, some of these being provided by our Division of Solid-State Physics. The titles of these papers and the names of the speakers are given hereinafter.

The banquet of the Society was held on the Friday evening at the Shoreland Hotel; the after-dinner speakers were S. K. Allison and E. C. Bullard, who did not have nearly so large an audience as they deserved.

The Council met on the Friday morning and again on the Saturday afternoon. It elected to Fellowship eleven candidates and to Membership the very large number of 406 candidates, the names of whom are printed hereinafter. Various other actions of the Council will be of general interest to our members. "Double publication" of the abstracts of the ten-minute papers given at our meetings—i.e., publication in both Bulletin and *The Physical Review*—will be continued throughout 1950: no promise is made as to subsequent years. The preparation of an Author and Subject Index to *The Physical Review*, covering the years since 1920 (to which year the previous index extended) was authorized and has already been begun. The page-charge for *The Physical Review* will be raised to eight dollats at a date to be fixed by the Managing Editor. The American Institute of Physics offered to supply *Physics Today* to the entire membership of the Society at two dollars per head for the year 1950. The stringency of our financial situation obliged the Council to decline this offer, but the membership of the Society will have an opportunity during 1950 to say whether or not they want a similar arrangement made in 1951 *at the price of a corresponding raise in annual dues.* F. W. Loomis and J. T. Tate were nominated to the Governing Board of the Institute for three-year terms commencing in February, 1950, and F. W. Loomis and W. Shockley were appointed to the Board of Editors of the Society for three-year terms also commencing in February, 1950.

According to reports reaching the office of the Society, we have lost through death D. R. Blosser, R. M. Buffington, A. Christy, C. L. Coggins, C. B. Crawley, J. H. Ellis, H. H. Goldsmith, H. M. Goodwin, J. W. Hake, W. J. Humphreys, F. B. Jewett, P. S. Millar, E. S. Moore, R. P. Penrose, R. S. Rasmussen, G. H. Rockwood, Jr., E. B. Stephenson, and A. G. Worthing.

Elected to Fellowship: E. S. Akeley, F. J. Belinfante, Ernst Bleuler, S. S. Dharmatti, H. Y. Fan, Wolfgang Finkelnburg, R. O. Haxby, A. G. Meister, E. R. Piore, C. F. Squire, and H. J. Yearian.

Elected to Membership: Leonard C. Aamodt, Eugene Ackerman, Norman Adams, Gerald A. Allard, Gene M. Amdahl, Carl E. Anderson, Stephen Antkiw, Edmond A. Arnous, Julius Aronofsky, Robert A. Artman, Giulio Ascoli, Andrew L. Atkins, Jr., Harry A. Atwater, Walter B. Baker, Clarence F. Barnett, Robert J. Beeber, Stuart A. Been, Samuel Belchis, George I. Bell, Albert I. Bellin, Joel Bengston, Louis E. Benitez, Pierrette Benoist-Gueutal, Margot E. Bergmann, Bernard Berman, Clifford E. Berry, *J. R. Bird, Robert D. Birkhoff, Robert J. Blackwell, Norman W. Blake, Donald J. Blattner, Myer Bloom, Stanley Bloom, Irving Boekelheide, Jorgen K. Bøggild, Conrad R. Bohn, Forrest I. Boley, Duis D. Bolinger, Donald R. Born, William A. Bowen, Jr., Charles B. Bradley, William E. Bradley, Rev. Brother T. Brendan, F.S.C., George R. Brewer, James S. Brierley, George R. Briggs, Sam Broder, Russel K. Brown, Frank A. Bury, Georg Busch, Clifford C. Butler, Carlos F. M. Cacho, George W. Callendine, Jr., Bille Chandler Carlson, Robert L. Carroll, Arthur N. Carson, Walter L. Carss, Jr., Robert L. Carter, William H. Chambers, Kenneth G. Chapman, Georges Charpak, Robert A. Charpie, Joel W. Chastain, Talbot Chubb, George W. Clark, John W. Cleland, Morrel H. Cohen, Robert J. Collins, David Conrad, Philip W. Constance, Stuart P. Cooke, Charles D. Cornwell, Hans W. J. Courant, Donald A. Cowan, George F. Crable, William H. Cuffey, Jr., Norman E. Cusack, Maynard A. Cutler, Arthur C. Damask, Julian L. Davis, Donald E. Dawson, Maynard H. Dawson, Albert L. de Graffenried, Jean F. Delord, Wendell C. De Marcus, James M. DePue, Vernon E. Derr, Roger S. Dildine, John A. Dillon, Jr., Thomas H. Dimmock, C. Eugene Dixon, John R. Donaldson, Jr., Clifford L. Dotson, Harry G. Drickamer, George H. Duffey, Everett P. Dulit, Marion M. Duncan, Jr., Maurice F. Duret, Harold C. Early, Harry T. Easterday, Douglas E. Eastwood, Jewell J. Ebers, Howard D. Edwards, James T. Elder, William R. Elliott, Osmand H. El-Mofty, Norman H. Enenstein, Robert D. Enzmann, Bela K. Erdoss, Paul M. Erlandson, Frank B. Estabrook, Evan C. Evans III, LeRoy Eyring, Stephen H. Fairweather, Richard A. Fayram, Milton H. Feldman, John D. Ferry, Gabriel A. Fialho, Gerard Field, Gail T. Flesher, Donald J. Fluke, Robert S. Foote, Jay W. Forrester, Daniel R. Frankl, Benjamin C. Frazer, Alexander J. Frolich, Wallace F. Fuller, Fausto Gherardo Fumi, Andrew L. Gardner, Joseph F. Genna, Robin Giles, M. Alten Gilleo, Charles-Aime Giroux, Colman Goldberg, Murrey D. Goldberg, Bernard Goldstein, John S. Gooden, Harold R. Grady, Michael B. Grandy, Glen A. Graves, Evon C. Greanias, Cyril O. Green, Raymond G. Green, Melvin L. Griem, Thomas W. Griswold, Edward E. Gross, Gordon L. Guernsey, John E. Haggenmacher, Harold H. Hall, William M. Hall, Frederick Halverson, Harold T. Hammel, Melvin Hanberg, T. Lyle Harlor, John M. Harriman, Lawrence A. Harris, Wilma Harris, Otto Heinz, Louis R. Henrich, Roland F. Herbst, Mathias Hettinger, Walter A. Heywood, *E. R. Hill, *Kenneth C. Hines, Robert E. Hoffman, Leonhard W. Holmboe, William M. Honig, John R. Hood, Jr., John I. Hopkins, Maurice Horowitz, William Robert Hosler, William S. Hough, Kerson Huang, Hugh M. Hulburt, Erdal I. Inonu, Carlyle W. Jacob, Derek Jakeman, Robert L. Jepsen, Arthur F. Johnson, Harold G. Johnstone, Donald W. Jones, Emily W. Jones, George Jura. Louis L. Kaplan, Maurice Karnaugh, Jack Katzenstein, Peter E. Kaus, Doris J. Kay, Benjamin Kazan, Richard W. Kebler, Alfred A. H. Keil, Charles N. Kelber, James B. Kelley, Paul S. Kelly, Ralph O. Kerman, Sidney Klein, Walter H. Kleiner, Carl Kligman, John W. Knowles, Sol N. Koblick, Werner

*One sponsor only.

Kopp, Heinz Koppe, Ezra S. Krendel, George C. Kruger, Jerome Kurshan, Walter I. Lang, Philip D. LaRiviere, Richard R. LaTorre, Vincent R. Learned, Jean V. Lebacqz, Albert Lederman, John M. Leffler, Bowen R. Leonard, Jr., Simon Levin, Solomon Levine, Carl A. Levinson, Maurice M. Levy, Arthur M. Lewis, David V. Lieberman, Wilbur Liebson, Robert A. Liedtke, J. Gordon Likely, Jr., Ralph H. Lilienkamp, Charles V. Litton, Merle K. Loken, J. S. Lomont, Hugh C. Longuet-Higgins, Jerome D. Luntz, Joan S. Lyttle, Edward F. Mac Nichol, Jr., Alan C. Macpherson, John F. Marion, Gene R. Marner, Luis Marquez, David H. Martin, Geraldo Martynes, Sebastian V. R. Mastrangelo, Carmine Masucci, Warren E. Mathews, Jean Maurice, Howard C. McAllister, Elmer D. McArthur, John M. McCrea, Harry G. McGuire, Colin D. McKenzie, Edward B. McNeil, Michel A. Melkanoff, Albert M. L. Messiah, Robert A. Meyer, Irving Michael, Henry S. Mika, Richard H. Milburn, Fred P. Miller, Knox Millsaps, James M. Mitchell, Eugene I. Mohr, Edmund G. Muirhead, Marcel W. Muller, John J. Murphy, Jack F. Music, Marcel W. Nathans, John E. Naugle, Robert A. Naumann, Loyd B. Nesbitt, Maurice Neuman, Roger G. Newton, Nathan L. Nichols, B. R. A. Nijboer, George D. O'Neill, Girard L. Ordway, William C. Orr, William C. G. Ortel, Paul W. Ott, Serge Pakswer, Thomas R. Palfrey, Jr., James P. Palmer, John Pappademos, Harvey M. Parkhurst, Philippe M. Passau, Robert M. Pearce, Robert W. Peelle, Morris L. Perlman, Janice R. Pisem, Roy F. Potter, John C. Potts, David R. Powers, Patrick D. Pratt, Jacques Prentki, Ernest R. Rae, Norman T. Rasmussen, Ned S. Rasor, Paul A. Redhead, Willard A. Reenstra, Kenneth E. Relf, Marlin E. Remley, Jacob L. Rhodes, Jr., Joaquim C. Ribeiro, Gerald C. Rich, Charles M. Richards, Roland W. Roberts, Herman P. Robinson, Hilliard Roderick, Dean C. Rogers, E. de L. Rogers, William A. Rogers, Jerome D. Rosenberg, William M. Sadock, Hans W. G. Salinger, Ernest W. Salmi, Robert A. Satten, George A. Sawyer, Victor E. Scherrer, Theodore Schiffman, Robert J. Schmelzer, Otto Schnepp, Irvin H. Schroader, Richard G. Seed, Paul Sekelj, Israel R. Senitzky, Andrew M. Sessler, William J. Sette, Otis H. Shuart, Adel Silveira, S. Fred Singer, William E. Siri, Willard Skolnik, William P. Slichter, George F. Smith, Raymond V. Smith, Thomas J. Smith, Thomas S. Smith, Roderick W. Spence, Lee Spetner, Gale C. Sprague, Tor B. Stavar, Brenton F. Stearns, Paul H. Stelson, Frank Stern, Noel Stone, Clarence N. Stover, Jr., Philip A. Stowell, Thomas F. Stratton, James W. Sturgess, Asa W. Swain, Paul J. Sykes, Jr., Peter E. Tannenwald, Andrew Tasch, Eugene S. Taylor, Harry W. Taylor, Julius H. Taylor, J. Teillac, Sidney J. Tetenbaum, Robert G. Thomas, Donald O. Thompson, Virgil S. Thurlow, Marvin Tidwell, Jr., Arthur N. Tifford, M. Elaine Toms, James F. Tracy, Lynne E. H. Trainor, Ralph F. Trambarulo, R. Q. Twiss, Robert Ullman, Vachaspati, Alan Van Bronkhorst, Allan Van Duren, L. C. Van Hove, Edward S. Wajda, David H. Walker, Edward J. Walker, James R. Walker, John Walker, Frederick T. Wall, Chao Chen Wang, Sylvan D. Wanlass, John C. Ward, Andrea Wataghin, Neil J. Waterman, Walter L. Weeks, Harold F. Weiler, Marvin A. Weinstein, William Weltner, Jr., Glenn Werth, John R. Weske, William J. West, Jan Weyssenhoff, Nathan R. Whetten, John R. Whinnery, Robert C. Whitney, Daniel Willard, Frederick K. Willenbrock, H. Bartel Williams, Paul D. Williams, Robert S. Wilson, James R. Wilts, August F. Wittenborn, Richard M. Wolfe, Robert L. Woodhouse, David F. Woods, *I. F. Wright, Louis Wynberg, Lloyd D. Yates, James A. Young, George B. Yntema, Theodore A. Zegers, and Otto H. Zinke.

KARL K. DARROW, *Secretary*,
American Physical Society
Columbia University
New York 27, New York

Invited Papers in the General Programme

Properties of liquid helium 3 and of mixtures of helium 3 and helium 4. BERNARD ABRAHAM, *Argonne National Laboratory.*

The use of fast neutrons for the study of nuclear energy levels. H. H. BARSCHALL, *University of Wisconsin.*

The origin of terrestrial magnetism. E. C. BULLARD, *University of Toronto.*

Recent developments in cryogenics. J. G. DAUNT, *Ohio State University.*

Resonance neutron scattering. C. O. MUEHLHOUSE, *Argonne National Laboratory.*

High speed digital computers: an elementary survey of present developments and future trends. L. N. RIDENOUR, *University of Illinois.*

Recent work on microwave spectroscopy at the State University of Iowa. ARTHUR ROBERTS, *State University of Iowa.*

Invited Papers in Solid-State Physics

Optical behavior of semiconductors. H. Y. FAN, *Purdue University.*

"Drift mobility" and lifetimes of injected electrons and holes in germanium. J. R. HAYNES, *Bell Telephone Laboratories.*

Fundamental mechanisms of diffusion in metals. J. H. HOLLOMON, *General Electric Company.*

Stability of color centers in alkali-halide crystals. P. PRINGSHEIM, *Argonne National Laboratory.*

Neutron diffraction and magnetic crystallography. C. G. SHULL, *Oak Ridge National Laboratory.*

Symposia of the Division of Electron Physics
Electron Emission

Photoelectric emission in strong fields: a progress report. A. H. WEBER, *St. Louis University.*

Activity studies on pulsed oxide cathodes. E. A. COOMES, *University of Notre Dame.*

The leady-condenser oxide-cathode interface. A. S. EISENSTEIN, *University of Missouri.*

Gaseous Electronics

The glow-to-arc transition. J. T. WINANS, *University of Wisconsin.*

A double-probe method for measurements in steady and time-varying discharges. E. O. JOHNSON AND L. MALTER, *RCA Laboratories.*

Electromagnetic propagation in ion streams. L. R. WALKER, *Bell Telephone Laboratories.*

Supersonic wind at low pressures produced by magnetically driven arc. H. C. EARLY AND W. G. DOW, *University of Michigan.*

Band and Microwave Spectroscopy

A1. Raman Spectrum and Force Constants for Fluorotrichloromethane. JAMES P. ZIETLOW, FORREST F. CLEVELAND, AND ARNOLD G. MEISTER, *Illinois Institute of Technology.*—Raman displacements, semi-quantitative relative intensities, and precise depolarization factors were obtained for liquid CCl_3F. Assignments were made for the fundamental frequencies, and fourteen force constants in a modified valence-force potential function were obtained. The constants of the CCl_3 group were transferred from CCl_3H and CCl_3D, and the other constants were evaluated from the observed frequencies, as was done previously for CCl_3Br.[1] Further proof of the trans-

ferability of these constants was obtained by calculating the frequencies of carbon tetrachloride, with a maximum difference between observed and calculated values of 1.7 percent. Below are the Raman displacements $\Delta\nu$ in cm^{-1}, the relative intensities I, the depolarization factors ρ, and the calculated displacements $\Delta\nu_c$. The calculated displacements are identical with the mean of all $\Delta\nu$ values thus far obtained (present results included).

	$\nu_4(E)$	$\nu_2(A_1)$	$\nu_3(E)$	$\nu_3(A_1)$	$\nu_4(E)$	$\nu_1(A_1)$
$\Delta\nu$	247	352	399	538	837	1066
I	25	30	15	100	5	1
ρ	0.83	0.42	0.81	0.11	—*	—*
$\Delta\nu_c$	244.6	350.5	397.8	535.8	835.4	1068.1

* The bands obtained up to now are too weak for precise measurement of ρ.

[1] Zietlow, Cleveland, and Meister, Phys. Rev. **75**, 333 (1949).

A2. Vibrational Spectra and Calculated Thermodynamic Properties of Deuterotrichloromethane. JOHN R. MADIGAN, FORREST F. CLEVELAND, WILLIAM M. BOYER, AND RICHARD B. BERNSTEIN, *Illinois Institute of Technology.*—Raman displacements $\Delta\nu$ in cm^{-1}, semi-quantitative relative intensities I, and quantitative depolarization factors ρ for the liquid, and infra-red frequencies ν for the liquid and CS_2 solution at different concentrations, in the region 400–5000 cm^{-1}, have been obtained for $CDCl_3$. The present $\Delta\nu(I)\rho$ values for the liquid were: 262(100)0.87; 365(92)0.10; 649(72)0.03; 735(14)0.84; 908(3)0.87; 2255(15)0.26, and the ν values for the solution were: 648; 727; 756; 904; 2247 cm^{-1}. No previous infra-red data or quantitative depolarization factors were found for this molecule. The infra-red band at 2247 was obtained with NaCl optics and the others with KBr optics. A band observed at 1202 is caused by *ca* 10 percent $CHCl_3$. The broad infra-red band at 735 cm^{-1} was resolved into the doublet 727, 756 for dilute solutions. Heat capacity, heat content, free energy, and entropy were calculated at temperatures of 298.16°, 300°, 400°, 500°, 600°, 700°, 800°, 900°, and 1000°K. The values for 298.16°K were: $C_p=16.40$ cal. deg.$^{-1}$ mole^{-1}, $(H-H_0)/T=11.56$ cal. deg.$^{-1}$ mole^{-1}, $-(F-F_0)/T=59.43$ cal. deg.$^{-1}$ mole^{-1}, and $S^0=71.00$ cal. deg.$^{-1}$ mole^{-1}. Thermodynamic calculations and infra-red investigations are also being carried out on $CHCl_3$, $CBrCl_3$, and CCl_4.

A3. Vibrational Spectra and Calculated Thermodynamic Properties of Deuterotribromomethane. SALVADOR M. FERIGLE, FORREST F. CLEVELAND, WILLIAM M. BOYER, AND RICHARD B. BERNSTEIN, *Illinois Institute of Technology.*—Raman frequencies and intensities have been given for CBr_3D by Redlich and Stricks.[1] No depolarization factors or infra-red data have been found in the literature. As a part of the work on substituted methanes and ethanes that is being carried out in this laboratory, Raman displacements, semi-quantitative relative intensities, depolarization factors, and infra-red frequencies have been obtained for CBr_3D. The Raman frequencies are in good agreement with the values previously reported. Depolarization factors have been measured with a Leeds and Northrup Recording Microphotometer. Infra-red spectra have been run with both NaCl and KBr optics. Depolarization factors for CBr_3H and CBr_3Cl have also been obtained and thermodynamic properties for all the tribromomethanes have been calculated to a rigid rotator, harmonic oscillator approximation.

[1] O. Redlich and W. Stricks, Sitz. Akad. Wiss. Wien, IIb, **145**, 192 (1936).

A4. Raman and Infra-Red Spectra of 1,1,1-Trichloroethane. M. ZAKI EL-SABBAN AND FORREST F. CLEVELAND, *Illinois Institute of Technology.*—Raman displacements $\Delta\nu$, semi-quantitative relative intensities I, and quantitative depolarization factors ρ for the liquid, and infra-red frequencies ν for both liquid and gaseous states in the region 400–5000 cm^{-1} have been obtained for $H_3C\text{-}CCl_3$. The present $\Delta\nu(I)\rho$ values for the liquid are: 242(45)0.86; 344(74)0.58; 523(100)0.12; 544(vw); 698(vw); 710 and 721(19)0.84; 1073(3) and 1083(3)-0.82; 1383(1); 1422(2) and 1449(4)0.81; 1789(w); 2740(1); 2880(2); 2938(80)0.15; and 3005(21)0.81 (w = weak, vw = very weak). The only depolarization factors previously reported are those by Wagner, whose $\Delta\nu(I)\rho$ values were: 240(90)0.81; 308(0?); 342(99)0.48; 522(100)0.03; 690(0); 713(49)0.78; 760(0); 1068 and 1082(12)0.64; 1179(w?); 1378(w); 1420 and 1444(9)0.81; 2740(w); 2938(29)0.32; 3002(25)0.97. The 713 cm^{-1} line was resolved into the doublet 710,721 cm^{-1} in the present work. The infra-red data, ν (percent absorption), were, for the liquid: 523(70); 688(11); 708(75); 786(61); 858(19); 950(16); 1000(38); 1075(91); 1224(45); 1366(60); 1423(59); 1960(12); 2938(28); 4300(6); and for the gas: 525(70); 534(64); 709(92); 734(84); 796(23); 863(18); 964(13); 1007(36); 1082(99); 1242(23); 1372(58); 1435(43); 2062(3); 2954(13). These seem to be the first infra-red data for this molecule, except for the band at 343 cm^{-1} reported by Hyde. Calculation of force constants and thermodynamic properties is now in progress.

A5. Raman and Infra-Red Spectra for Hexachloroethane and Hexabromoethane, and Force Constants for Hexachloroethane. ROSE A. CARNEY,* ARNOLD G. MEISTER, AND FORREST F. CLEVELAND, *Illinois Institute of Technology.*—Infra-red data in the region 400–5000 cm^{-1}, and Raman frequencies, relative intensities, and depolarization factors, are reported for solutions of hexachloroethane and hexabromoethane. Critical evaluation was made of all the Raman data obtained for these molecules, including previous data, in order to set up tables of "most probable values." However, since no previous infra-red data were found in the literature, only the results of the present investigation were available when the calculations were started. These, then, were the values used in determining, by a normal-coordinate treatment, the force constants for hexachloroethane that would give the best fit with the observed vibrational frequencies, assuming a D_{3d} symmetry. Recently Mizushima[1] and his co-workers have obtained the near infra-red spectrum of hexachloroethane and their results are in good agreement with those obtained in the present investigation. Calculation of the force constants for hexabromoethane is in progress.

* Now at St. Procopius College, Lisle, Illinois.

[1] Mizushima, Morino, Simanouti, and Kuratani, J. Chem. Phys. **17**, 838 1949).

A6. Raman and Infra-Red Spectra of 2,3-Dibromo-2,3-Dimethylbutane. J. E. LAMPORT AND FORREST F. CLEVELAND, *Illinois Institute of Technology.*—Using methods described earlier,[1] Raman displacements, relative intensities and depolarization factors for solutions of 2,3-dibromo-2,3-dimethylbutane were obtained. Kahovec and Wagner[2] had previously obtained the Raman spectrum of the compound in the powdered crystalline state. Eleven Raman displacements were found by Kahovec and Wagner, while eighteen have been found in the present investigation. A comparison of the results of this investigation with those of Kahovec and Wagner will be made. Ten frequencies have been observed in the infra-red absorption spectrum using a Beckman Model IR-2 infra-red spectrophotometer equipped with KBr optics, covering the range from 400 to 5000 cm^{-1}. The fact that none of the intense infra-red absorption bands correspond to strong Raman lines is taken to indicate a center of symmetry for the molecule. This is further borne out by the appearance of only 18 Raman lines for a molecule of 20 atoms which should have 54 fundamental

vibrations. There are also fewer infra-red absorption bands than is normal for a molecule of this size.

[1] Forrest F. Cleveland, J. Chem. Phys. 11, 1 (1943); 13, 101 (1945).
[2] L. Kahovec and J. Wagner, Zeits. f. physik. Chem. B47, 48 (1940).

A7. Band Spectrum of GaCl. F. K. LEVIN* AND J. G. WINANS, *University of Wisconsin.*—The absorption spectrum of GaCl showed vibrational but no rotational structure in the 2490A to 2700A system, $^1\Pi_1 \leftarrow {}^1\Sigma_0^+$. The predissociation limit indicated a dissociation energy for the ground state 4.99 ± 0.01 volts. A short continuum at 2430A indicated $^1\Pi$ causing predissociation. Vibrational analyses of $^3\Pi_1 \leftrightarrow {}^1\Sigma_0^+$ and $^3\Pi_0 \leftrightarrow {}^1\Sigma_0^+$, systems 3200A to 3500A gave constants:

$\omega_e'' = 365.3$ cm^{-1}, $\omega_e'' x_e'' = 1.2$ cm^{-1} for $^1\Sigma_0^+$.
$\omega_e' = 395.3$ cm^{-1}, $\omega_e' x_e' = 2.3$ cm^{-1}, $\omega_e' y_e' = 0.015$ cm^{-1}, $\nu_e = 29{,}524.3$ cm^{-1} for $^3\Pi_0$.
$\omega_e' = 395.3$ cm^{-1}, $\omega_e' x_e' = 2.5$ cm^{-1}, $\nu_e = 29{,}856.3$ cm^{-1} for $^3\Pi^1$.

Rotational constants obtained are:

$B_0'' = 0.1490$ cm^{-1}, $D_0'' = 2.4 \times 10^{-8}$ cm^{-1},
$B_1'' = 0.1487$ cm^{-1} for $^1\Sigma_0^+$.
$B_0' = 0.1568$ cm^{-1} for $^3\Pi_1$.
$B_0' = 0.1568$ cm^{-1}, $D_0' = 2.4 \times 10^{-8}$ cm^{-1} for $^3\Pi_0$.

* Now with Carter Oil Co., Tulsa, Oklahoma.

A8. Absolute Absorption Coefficients in N_2 in the Vacuum Ultraviolet.* G. L. WEISSLER AND E. I. MOHR, *University of Southern California.*—Absolute absorption coefficients k_λ in N_2 for light of 600A to 1300A were measured in a grazing incidence two-meter vacuum spectrograph of average dispersion of 3A/mm using Eastman 103-0 plates sensitized for the u.v. with a fluorescent lacquer. A Lyman source provided the wave-length continuum. On a single plate two exposures were taken at known, different pressures of N_2 in the spectrograph, five overlapping exposures were taken in a high vacuum. In addition this plate contained two series of calibration exposures using Schneider's** method. The exposure ratios were monitored by electronically counting the number of Lyman flashes. In spite of reaming of the capillary by the discharges this proved to be reliable. The overlapping exposures provided for a check at various wave-lengths of the characteristic curve of the plate obtained by the Schneider method. Nine plates were taken providing 27 independent determinations of k_λ as a function of wave-lengths. A modified Zeiss microphotometer is used in the evaluation of the plates. Preliminary results will be presented. Work on other gases is in progress.

* Supported by ONR.
** F. G. Schneider, J. Opt. Soc. Am. 30, 129 (1940).

A9. The Absorption of Radiation in the Very Near Infra-Red by Water Vapor.* ROBERT M. CHAPMAN, *The Ohio State University (Introduced by Dudley Williams).*—A quantitative experimental study was made on the infra-red absorption of the water vapor bands at 1.35μ and 1.85μ using a low dispersion prism spectrometer. The effect on the absorption of changing the water vapor concentration, changing the absorption path length by means of a multiple reflection absorption cell, and increasing the total pressure by the addition of dry air were investigated. It was found that the average fractional absorption in each band, A fits the theoretically derived expression,[1,2] $A = erf(t) = \frac{2}{\sqrt{\pi}} \int_0^t e^{-t^2} dt$, in which $t = [1/2\beta(\pi w)^{\frac{1}{2}} f(p)]$, β is a generalized absorption coefficient for each band, w is the water vapor concentration in precipitable centimeters of water, and $f(p)$ is a function of pressure alone. An analysis of the data permitted evaluation of the form of the pressure function $f(p)$ as $f(p) = [(P_t + P_p)/760]^{\frac{1}{2}}$, where P_t is the total pressure in the absorption cell, in mm of Hg; and P_p is the partial pressure of the water vapor, in mm of Hg.

* The work described in this paper was carried out, in part, under contract between the Engineer Research and Development Laboratories of the Engineer Center, Ft. Belvoir, Virginia, and The Ohio State University Research Foundation.
[1] W. M. Elsasser, Harvard Meteorological Studies No. 6 (1942).
[2] T. G. Cowling, Rep. on Prog. in Physics 9, 29 (1942).

A10. Microwave Spectrum of Methyl Alcohol.* D. K. COLES, W. E. GOOD, AND R. H. HUGHES, *Westinghouse Research Laboratories.*—The microwave spectrum of CH_3OH is complicated by hindered rotation of the O—H group around the CH_3 axis. We have measured and identified 59 lines of $C^{12}H_3OH$ and $C^{13}H_3OH$ in the frequency interval between 16,900 Mc and 34,000 Mc. A short *series* of lines in the neighborhood of 25,000 Mc was first noticed by W. D. Hershberger. B. P. Dailey made more extended observations. D. M. Dennison suggested that the series was due to simultaneous internal and over-all rotational transitions in which the quantum number J does not change. We have employed the Stark effect to identify early lines in the series and have been able to follow the series from $J=2$ at a frequency of 24,934.38 Mc up to $J=20$ at 31,358.31 Mc and then down to $J=30$ at 16,941.6 Mc. $C^{13}H_3OH$ and $CH_3O^{18}H_3$ have been prepared. The corresponding series for the C^{13} molecule has been followed from 27,052.97 Mc for $J=2$ up to 33,220.05 Mc for $J=20$, and down to 17,870.5 Mc for $J=31$. It is hoped that the additional information provided by the O^{18} substitution will make possible a complete determination of the molecular structure.

* This work was supported in its entirety by the Westinghouse Electric Corporation.

A11. Microwave Spectrum of Nitrosyl Chloride.* W. J. PIETENPOL, J. D. ROGERS, AND DUDLEY WILLIAMS, *The Ohio State University.*—The microwave absorption spectrum of nitrosyl chloride has been observed by means of a recording Stark spectrograph. The transitions $1_0 \rightarrow 2_{-1}$, $1_{-1} \rightarrow 2_{-2}$, and $1_{+1} \rightarrow 2_0$ have been observed for each of the two chlorine isotopes Cl^{35} and Cl^{37}. Rotational constants determined from these transitions are $A(Cl^{35}) = 5.3136$ cm^{-1}, $B(Cl^{35}) = 0.19001$ cm^{-1}, $C(Cl^{35}) = 0.18345$ cm^{-1}, and $A(Cl^{37}) = 5.6765$ cm^{-1}, $B(Cl^{37}) = 0.18900$ cm^{-1}, $C(Cl^{37}) = 0.18291$ cm^{-1}, and agree quite favorably with electron diffraction[1] data. This shows NOCl to be nearly an accidentally symmetric top with asymmetry constant being $b(Cl^{35}) = -0.00064$ and $b(Cl^{37}) = -0.00055$. Hyperfine structure observed for these lines gives a quadrupole coupling coefficient of $-eQq(Cl^{35}) = 62 \pm 6$ Mc/sec. and $-eQq(Cl^{37}) = 48 \pm 8$ Mc/sec. The Stark effect for Cl^{35} has been observed and follows the law $\Delta\nu = \alpha E^2 M$, where $\alpha = 5.45 \pm 0.05$ cm^2/sec. volts.[2]

* The work reported was done under a contract between O. S. U. Research Foundation and Watson Laboratories of the Air Materiel Command, Red Bank, New Jersey.
[1] Ketelaar and Palmer, J. Am. Chem. Soc. 59, 2629 (1937).
[2] H. H. Nielsen, Phys. Rev. 38, 1432 (1931).

A12. Pressure Broadening and Line Shift in Microwave Spectra. L. C. JONES, *St. Louis University (Introduced by A. V. Buskovitch).*—Approximate formulas for pressure broadening and line shift have been derived for an absorber surrounded by N_j foreign perturbers located at r_j with respect to the absorber, and N_i non-foreign perturbers at r_i, assuming the resonant interaction potential is of the form $a_i r_i^{-3}$, and the non-resonant potential is of the form $b_j r_j^{-6}$. Orders of magnitude are computed for the average interaction coefficients, the line shift and the ratio of half-width to shift for carbonyl sulfide (OCS) perturbed by cyanogen chloride (ClCN) and ammonia (NH_3) perturbed by methyl chloride (CH_3Cl).

A13. Nuclear and Molecular Information from the Microwave Spectrum of FCl. D. A. GILBERT AND A. ROBERTS, *State University of Iowa.*—The triplets due to the $J=0\rightarrow1$ rotational transitions in FCl^{35} and FCl^{37} have been observed near 30,000 mc both for the ground vibrational state and the first excited vibrational state. Stark effect measurements give for the molecular dipole moment 0.88 Debye. Observed deviations from the predicted hyperfine structure spacings may be explained by assuming an interaction[1] of the form $cI\cdot J$, where $c\cong0.03$ mc for FCl^{35}. The ratio $B_e^{37}/B_e^{35}=30{,}378.468/30{,}967.404$ yields for the Cl^{35}/Cl^{37} mass ratio 0.9459771 ±0.0000036, agreeing better with the previous determination in ICl,[2] 0.9459801$\pm$0.000005 than with the best mass-spectroscopic values,[3] 0.9459445$\pm$0.000007. We conclude that the latter is probably in error. The vibration-rotation constants are $\alpha^{35}=130.696\pm0.02$ mc and $\alpha^{37}=126.972\pm0.02$ mc. The quadrupole coupling constants are $eqQ^{35}=-146.00\pm0.12$ and $eqQ^{37}=-144.89\pm0.13$. Their ratio agrees only moderately well with that found by Davis and Zabel.[4]

[1] W. Nierenberg and N. F. Ramsey, Phys. Rev. **72**, 1075 (1947).
[2] Townes, Merritt, and Wright, Phys. Rev. **73**, 1334 (1948).
[3] Recalculated from Okuda *et al.*, Phys. Rev. **58**, 578 (1940) with H and C masses from K. T. Bainbridge, *Isotopic Weights of the Fundamental Isotopes* (National Research Council, Washington, D. C., 1948).
[4] L. Davis and C. W. Zabel, Phys. Rev. **74**, 1211A (1948).

A14. Nuclear Spin and Quadrupole Coupling of S^{35}.* VICTOR W. COHEN, WALTER S. KOSKI, T. WENTINK, JR., *Brookhaven National Laboratory.*—The rotational transition $J=1\rightarrow2$ of COS^{35} has been observed at a frequency of 23461 ± 5 mc using a Stark modulation microwave spectroscope operating at 100 kc. The observed pattern is consistent with a nuclear spin of S^{35} of $\frac{3}{2}$. The quadrupole coupling constant is observed to be $+20\pm4$ mc/sec. Comparison of this with S^{33} which also has a spin of $\frac{3}{2}$[1] shows the signs of the two quadrupole coupling constants is opposite. This reversal of the sign of the nuclear quadrupole moment in going from S^{33} to S^{35} is in accord with the theory of shell structure and electric quadrupole moments as described by Townes, Foley, Low,[2] and Hill.[3]

* Work performed at Brookhaven National Laboratory under contract with the AEC.
** Permanent address: Chemistry Department, Johns Hopkins University.
[1] Townes and Geschwind, Phys. Rev. **74**, 622 (1948).
[2] Townes, Foley, and Low, Phys. Rev. (to be published).
[3] Hill, Phys. Rev. **76**, 998 (1949).

Artificial Radioactive Substances

B1. Ra DEF Standard Sources for Beta-Disintegration Rate Determinations. T. B. NOVEY, *Argonne National Laboratory.*—Ra DEF equilibrium sources for absolute beta-counting have been prepared and calibrated. The sources are essentially weightless and are mounted on a thin backing to avoid self absorption and backscattering correction problems. The sources were calibrated by determination of the alpha-disintegration rate of the Ra F in a parallel plate alpha-ionization chamber. No secondary standards are required and the sources can be recalibrated at any time. As an example of the application of such standards, details of the calibration of a P^{32} solution distributed by the Bureau of Standards for intercalibration in February, 1949 will be given. The final result is 88.8 mrd/ml at 8 A.M., C.D.T., March 1, 1949. The precision of the measurement is 0.3 percent. The accuracy is estimated to be 1–2 percent.

B2. The Production of Li^8 from Various Gases. S. COURTENAY WRIGHT, *University of California, Berkeley.*—Li^8 has been produced by 340-Mev proton and 190-Mev deuteron bombardments of C, N, Ne, A, Kr, and Xe. The target element formed the gas of a proportional counter. The 0.88-second beta-decay of Li^8 produces Be^{8*} which disintegrates into two alpha-particles with a half-life of 10^{-21} second. Li^8 was detected by observation of these alpha-particles and identified by its half-life. Deuteron excitation functions for the production of Li^8 are given for C, N, Ne, and A. In the case of 190-Mev deuterons the cross section varies from about 10^{-27} cm^2 for C to 2×10^{-29} cm^2 for Xe. For 340-Mev protons the variation is from about 7×10^{-27} cm^2 for C to 3×10^{-29} cm^2 for Xe. A discussion of the process involved is given.

B3. γ-Rays from N^{16}. C. H. MILLAR, A. G. W. CAMERON, AND M. GLICKSMAN, *Chalk River Laboratories.*—The energies and relative intensities of the γ-rays from N^{16} have been measured with deuterium loaded emulsions. The source was the effluent cooling water of the Chalk River pile. The reaction is presumed to be $O^{16}(n,p)N^{16}$. An Ilford C2 emulsion (100 μ-thick) containing 0.40 mg/cm^2 deuterium in the form of hexadeutero diacetin was used to register photo-proton tracks. The plate was exposed to 2 r of γ-rays at the end of a lead collimator and then developed normally. Background tracks were measured in an unirradiated plate from the same batch. Measurements of α-particle tracks from contamination in the emulsions showed that the stopping power was 7 percent less than in standard C2 emulsions. The range-energy relationship given by Lattes *et al.*[1] was accordingly modified and used. A histogram of the photo-proton tracks indicates γ-rays at 6.2 and 7.0 Mev, in agreement with the well-known excitation energies 6.16 and 7.06 Mev[2] of O^{16}. The relative intensities of the γ-rays are 6:1 respectively.

[1] Lattes, Fowler, and Cuer, Proc. Phys. Soc. **59**, 885 (1947).
[2] See, for example, Rasmussen, Hornyak, and Lauritsen, Phys. Rev. **75**, 1462 (1949).

B4. Beta-Spectra of Cl^{38}. LAWRENCE M. LANGER,* *Los Alamos Scientific Laboratory.*—The beta-spectra of the 38-minute Cl^{38} activity have been studied in a magnetic lens spectrometer. The source was 10 mg/cm^2 of NH_4Cl which was irradiated in the thermal neutron column of a nuclear reactor. Three distinct groups of beta-rays were observed. The highest energy group was found to have a shape characteristic of a once forbidden transition. The shape is completely satisfied by the forbidden factor $W^2-1+(W_0-W)^2$. This suggests that the transition involves an angular momentum change of 2 units and a parity change. Because of the low atomic number and the high maximum energy, W_0, this conclusion is not as uniquely determined as in the case of a heavier element.[1] However, from the theory of nuclear shell structure,[2] one would expect a parity change and a change of *at least* 2 units of angular momentum. The end-point energies and the branching ratios of the three groups are: 4.81 Mev, 53.4 percent; 2.77 Mev, 15.8 percent; 1.11 Mev, 30.8 percent.

* Indiana University.
[1] L. M. Langer and H. C. Price, Jr., Phys. Rev. **75**, 1109 (1949).
[2] M. G. Mayer, Phys. Rev. **75**, 1969 (1949).

B5. Nuclear Gamma-Radiation from Positron Emitters.* H. E. KUBITSCHEK,[1] A. LONGACRE, AND M. GOLDHABER, *University of Illinois.*—Absorption measurements of low intensity gamma-radiation from positron emitters are complicated by the annihilation radiation present. Spectroscopic methods are preferred, but these become tedious in the search for unknown radiation, since the lifetimes of positron emitters are usually short. A simple absorption technique has been devised which permits a more rapid survey. The source, thin to self-absorption for positrons, is placed in a vacuum chamber. Positrons escape to the chamber walls to produce annihilation radiation from which the detector can now be shielded. In this manner the nuclear gamma-radiation of Cu^{64} was substantiated. With 0.1 ml foils the detection of annihilation radiation was reduced to 4 percent of the maximum observable with a thick source. Measurements on Ti^{45} showed the exist-

ence of two gamma-rays, of 0.51±0.02 and 0.82±0.03 Mev. The ratio of the number of positrons to 0.5-Mev gamma-rays to 0.8-Mev gamma-rays was (19±2):(4.1±0.8):(1). Verification for these gamma-rays was obtained from the photo electron spectrum obtained with a 180° spectrometer. The energies were 0.48±0.02 and 0.80±0.01 Mev. A Kurie plot of the positron spectrum gave an end point of 1.00±0.02 Mev.

* This work was supported by the ONR. Service irradiations of copper were done by Oak Ridge National Laboratory.
[1] Atomic Energy Commission Fellow.

B6. The Shape of the Positron Spectrum of Cu^{61}. GEORGE E. OWEN AND C. SHARP COOK,* *Washington University.*—The remaining low energy excess of particles in the allowed beta-spectra have been assumed to be caused by the finite thickness of the source. In order to test this, a source of Cu^{61} has been prepared by evaporation from a tungsten filament onto an aluminum foil backing. The thickness calculated from the activity of the source was of the order of magnitude of $(10)^{-4}$ micrograms per square centimeter. This thickness corresponds to less than one complete atomic layer. The resulting spectrum gives a Fermi-Kurie plot identical with those previously obtained using chemically deposited sources and still shows an excess of positrons in the region below 500 kev. Although the aluminum backing was much thicker than the source, evidence will be shown indicating that the backings used most probably do not produce the deviations observed. Attempts are being made to obtain a comparable source of Cu^{64} and the results from this isotope will be reported if available at the time.

* Assisted by the Joint Program of the ONR and AEC.

B7. On the Disintegration of Sr^{85}.* MICHEL TER-POGOSSIAN, *Washington University.*—The disintegration of the 65-day Sr^{85} was studied in a 180° β-ray spectrometer. This isotope has been previously reported to decay by K-capture with emission of a gamma-radiation of 0.8 Mev.[1] The source was prepared by bombarding a sample of rubidium chloride with deuterons in the Washington University cyclotron, and by separating chemically the strontium after addition of carrier. The source was found to emit a single gamma-radiation of 0.510±0.005 Mev partially internally converted. This energy was obtained by measuring the energy of secondary photo electrons emitted by a uranium radiator placed in front of the source and by measuring the energy of the internal conversion electrons emitted by the source. Two groups of low energy electrons were found to be emitted by the source, corresponding to Auger electrons emitted from the L and M shell of the daughter atom. Any attempt to detect the presence of positrons failed. The fact that no coincidences were observed between the photons emitted by the source at 180° ruled out the possibility for the observed radiation to be due to the annihilation of positrons.

* Assisted by the Joint Program of the ONR and AEC.
[1] DuBridge and Marshall, Phys. Rev. Phys. Rev. 58, 7 (1940).

B8. Assignment and Disintegration Scheme of the 6.75-hour Molybdenum Activity. D. N. KUNDU, JOHN L. HULT, AND M. L. POOL, *Ohio State University.*—A redetermination of the assignment of the 6.75-hour Mo activity was undertaken because (1) contrary to the observations of others that this activity was produced by Mo+d, no measurable amount of this activity could be produced by our 10-Mev deuterons even from enriched Mo^{92}; (2) $Mo^{92}+n$ and $Mo^{94}+\gamma$ have been found not to produce this activity.[2] The 6.75-hour Mo activity is still attributed to Mo^{93} by virtue of the reactions $Cb^{93}(p, n)$, $Cb^{93}(d, 2n)$, $Zr^{90}(\alpha, n)$, $Zr^{91}(\alpha, 2n)$, and $Mo^{93}(n, 2n)$ using enriched isotopes in the last three cases. A disintegration scheme has been worked out using absorption, beta-ray spectrograph and coincidence counter measurements. The decay does not take place by positron emission or K-capture. After the emission of three gamma-rays of energies 0.30, 0.70, and 1.7 Mev in cascade of which the first is about 90 percent internally converted, the 6.75-hour Mo^{93} passes into a long-lived isomeric state. MoK_α x-rays resulting from the conversion have been found. The absence of the (d, p) and (n, γ) reactions may be related to the fact the Mo^{92} is a nucleus with the magic number 50 neutrons.

[1] M. L. Wiedenbeck, Phys. Rev. 70, 435 (1946).
[2] R. B. Duffield and J. D. Knight, Phys. Rev. 76, 573 (1949).

B9. Radiations from Long-Lived Tin Isotopes. J. W. MIHELICH AND R. D. HILL, *University of Illinois.**—The radiations produced in four samples of enriched Sn isotopes, which were activated by neutrons in the Oak Ridge pile, have been investigated using absorption and spectrographic techniques. Three hitherto unreported γ-ray transitions have been observed and their nature is at present being investigated. The energy values of the transitions and their assignments to particular Sn isotopes are given in Table I. No converted

TABLE I.

Isotope	Half-Life	γ-Transition
Sn^{117m}	14 days	159 and 162 kev
Sn^{119m}	$\geqslant$ 100 days	69 kev
Sn^{123}	130 days	394 kev

γ-ray was detected in the 28-hr Sn^{121}. The 159-kev transition had been tentatively assigned to Sn^{119m}.[1] The conversion lines of the 69-kev transition are of very low intensity and an estimate for the activation cross section for the production of Sn^{119m} is ~0.004 barn. The 394-kev γ-transition associated with Sn^{123} probably follows the beta-ray activity and is converted in Sb.

* Assisted by the Joint Program of the ONR and AEC.
[1] M. Lindner and I. Perlman, unpublished. Reported by G. T. Seaborg and I. Perlman, Rev. Mod. Phys. 20, 585 (1948).

B10. Disintegration of Sn^{125}.* ROBERT B. DUFFIELD, *University of Illinois*, AND LAWRENCE M. LANGER, *Indiana University.*—We have examined the beta- and gamma-rays emitted by the 9.5-minute Sn^{125} with a magnetic lens spectrometer. The radioactive sources used were prepared by neutron irradiation of tin metal foils enriched to 83 percent in Sn^{124}.[1] The source used for the determination of the beta-spectrum had a thickness of 6 milligrams per square centimeter. The beta-spectrum was found to be complex: There are two groups with end points at 2.04 and 1.17 Mev and a probable third group with an end point at 0.51 Mev. Conversion electrons from a gamma-ray of 0.326 Mev were found. The gamma-radiation was examined using uranium and lead radiators. Photo electrons from the 0.326-Mev gamma-ray were observed and also Compton electrons from one or more gamma-rays of energy greater than 1 Mev. The high energy gamma-radiation was of low intensity and the energy could not be accurately determined.

* Research done at the Los Alamos Scientific Laboratory of the University of California.
[1] Supplied by the Y-12 Plant, Carbide and Carbon Chemicals Corporation, on allocation by the Isotopes Division of the U. S. AEC.

B11. 14-Day Tin 117. E. C. MALLARY AND M. L. POOL, *The Ohio State University.*—The tin isotope which decays with a 14-day half-life by an isomeric transition is definitely assigned to mass number 117. By comparison of results of different bombardments of samples of electromagnetically enriched cadmium and tin, and by chemical separations, it was verified that the reactions $Cd^{114}(\alpha, n)$, $Sn^{116}(d, p)$, $Sn^{118}(n', 2n)$, $Sn^{117}(n', n)$, and $Cd^{116}(d, n)$, followed by decay to tin, pro-

duced this tin activity. By comparison of specific activities induced by the same neutron flux, the cross section of the reaction $Sn^{117}(n', n)$ was found to be about 1.8 times larger than the cross section of the reaction $Sn^{118}(n', 2n)$. Characteristic radiations are K and L conversion electrons of 0.146 ±0.006-Mev and 0.171±0.006-Mev energy respectively, tin x-rays, and 0.175±0.006-Mev gamma-rays. These values were determined with a beta-ray spectrograph. By means of copper absorptions the x- and gamma-ray intensities from tin 117 were compared with those from indium 111. Indium 111, which decays with a 2.84-day half-life, is known to emit 1.72 gamma-rays to each x-ray. As a result of this comparison of x- and gamma-rays of comparable energies, it was found that the gamma-rays from tin 117 were about 50 percent internally converted.

B12. Disintegration of I^{124} and I^{126}. ALLAN C. G. MITCHELL, J. Y. MEI, FRED C. MAIENSCHEIN, AND CHARLES L. PEACOCK, *Indiana University.*—The nuclear radiations from I^{124} (4 days) and I^{126} (13 days) have been measured. I^{124} decays to Te^{124} with the emission of three positron groups with end points at 2.20±0.01, 1.50±0.01, and 0.67±0.05 Mev, possibly accompanied by some K electron capture. Gamma-rays of energy 0.603±0.002, 0.73±0.01, 1.72±0.02, and 1.95±0.05 are given off in the disintegration. I^{126} decays to Xe^{126} with the emission of two beta-ray groups of energies 1.268±0.010 and 0.085 ±0.01 Mev, together with a gamma-ray of energy 0.395 ±0.005 Mev. A state of I, of 13.0±0.5 hours half-life, which decays under the emission of an internally converted gamma-ray of energy 0.159 Mev has been found. This state is assigned to I^{125}. The high energy group of positrons from I^{124} for a forbidden shape of the type associated with $\Delta j = \pm 2$, first forbidden.

B13. Low Energy Beta-Ray Spectra: Pm^{147}, S^{35}.* H. C. PRICE, JR., J. MOTZ AND L. M. LANGER, *Indiana University.*—The beta-spectra of S^{35} and $_{61}Pm^{147}$ have been measured in an attempt to study further the nature of the low energy deviation from the Fermi theory previously reported.[1,2] Measurements were made with thinner sources and improved techniques in both the 40-cm radius of curvature spectrometer and also in a small 180 degree focusing Helmholtz coil spectrometer designed specifically for low energy spectra. The excess of particles at low energies was found to be a function of source thickness. The thinnest sources used were less than 10 micrograms/cm². Both S^{35} which is allowed and Pm^{147} which is probably once forbidden were found to have spectra of the allowed shape. Using counter windows of 3 micrograms/cm² and also a windowless counter technique, Fermi plots were obtained which, for Pm^{147}, were straight down to 8 kev. The end point of Pm^{147} was found to be 223.2±0.5 kev. On the basis of an improved calibration of the instrument, the present results for S^{35} yield an end point of 167.0±0.5 kev.

* Assisted by a grant from the Frederick Gardner Cottrell Fund of the Research Corp. and by the Joint Program of the ONR and AEC.
[1] Cook, Langer, and Price, Phys. Rev. 74, 548 (1948).
[2] R. D. Albert and C. S. Wu, Phys. Rev. 74, 847 (1948).

Contributed Papers on Electron-Emission

D1. X-Ray Absorption Factors for Coated Cylinders.* EUGENE B. HENSLEY, *University of Missouri.*—Absorption corrections for the calculation of Debye-Sherrer powder pattern diffraction intensities from a thin crystalline film of thickness l on a cylindrical absorbing base material have been computed using numerical methods. These are plotted as functions of μl at 10° intervals of the Bragg angle θ. Also computed over the same range are the corresponding absorption factors for x-rays diffracted from the underlying base material.

Possession of these correction curves affords a useful method for the measurement of the thickness of thin crystalline films on cylindrical wires.** This method is based on a comparison of the intensities of the diffracted lines from the surface material with the intensities of the lines from the underlying base material. The accuracy of the method has been checked using coatings of copper electroplated on nickel wires. An application of the method has been made in studying the growth in thickness of oxide cathode interfaces as a function of cathode life.

* This work was supported in part by the ONR.
** A. Eisenstein, J. App. Phys. 17, 874 (1946).

D2. Luminescence of Barium Oxide.* VIRGIL L. STOUT, *University of Missouri.*—Studies of the luminescence spectra of BaO were made on active and inactive samples in the temperature range 340° to 575°K. Excitation was by means of electron bombardment of 3-Kev energy. The active sample was prepared by drawing a thermionic emission current from the heated oxide in the manner used for activation of oxide coated cathodes. The relative intensity distribution of the luminescence was recorded over the wave-length range 250 to 860 mμ. Several relatively strong luminescence bands were found from both active and inactive samples. The active material gave a luminescence band at 410 mμ which was not present from the inactive oxide. Similarly the inactive sample had a strong band at 460 mμ which appeared only weakly from the active sample. All luminescence bands did not exhibit the same temperature dependence.

* This work was supported in part by the ONR.

D3. Mass Spectrometric Production of Oxide Cathodes.* L. T. ALDRICH AND C. E. SMITH, *University of Missouri.*—A high intensity Nier-type mass spectrometer has been used as a source of pure BaO to coat a cathode of approximately 0.01 cm² area to thicknesses up to one monolayer. The thickness of the layer is monitored by continuously measuring the ion current to the cathode surface and assuming that all ions incident on the cathode are retained. Retarding potential measurements are used to measure the zero field, saturation emission current from the cathode. A pure nickel base cathode was produced in this manner. At a temperature of 1125°K, the thermionic emission is about 3×10^{-6} A/cm^2 for BaO layer of approximately one-half monolayer thickness. Cathodes produced using tungsten, molybdenum, and tantalum sleeves will be studied.

* This work was supported in part by the ONR.

D4. Extraction of Ions from Solids by Electrons in High Fields.* JEROME ROTHSTEIN, *Signal Corps Engineering Laboratories.*—Certain observations of Germer and Haworth[1] on anode pitting seem explainable only if electrons bombarding a metal surface in a high field can cause emission of positive ions with high yield. The voltages employed exceed positive ion thermionic work functions by at least several volts. Elastic transfer of energy from electron to surface atom can be neglected, leaving only inelastic transfer for consideration. In the absence of a high gradient at the surface a quantum would be emitted, or, alternatively, the excitation energy of the surface atom would appear as energy of thermal agitation, perhaps after wandering in the lattice as an exciton. Surface atom excitation is presumably accompanied by considerable increase in the effective atomic radius, and, in a high field, the strained binding between excited atom and lattice is broken with emission of a positive ion, the field overcoming image forces. The process is analogous to molecular dissociation under electronbombardment, with the metal a macromolecule, or to dissociation of excited atoms in high fields. From another viewpoint an excited atom is one of low effective

ionization potential making the process analogous to formation of Cs^+ from Cs impacting on W. The sharp threshold voltage for the pitting process to be expected on this picture has been observed.

[1] L. H. Germer and F. E. Haworth, Phys. Rev. **73**, 1121 (1948).

Optical Physics; Line-Spectroscopy; Nuclear Magnetic Resonance; Mass Spectrometry

G1. The Establishment of Mean Points of Transition Between Spectral Bands.* ZABOJ V. HARVALIK AND JOHN H. BOWEN,[1] *University of Arkansas.*—A method for obtaining the mean spectral band transition points is outlined and the mean values are presented. Comparison is made between transition values of this study and the values given in contemporary literature. The spectral transition points for binocular vision of light adapted eyes are: red, 739–613; orange, 613–597: yellow, 597–585; green, 585–517; blue, 517–479; violet, 479–422, at the brightness of the eyepiece slit of 0.002 foot candles/cm². The data were obtained from 125 individuals of the ages from 17 to 36 years of both sexes (42 women and 83 men). The selection of these subjects was made without selection with respect to eye deficiencies. Data on color ranges of monocular vision and binocular vision for the dark and light adapted eye are given.

* Based on work performed under contract with the Office of Chief of Ordnance, Department of Army.
[1] Ordark Research Fellow in Psychology, Department of Psychology.

G2. The Use of "Exploding Wires" as a Light Source of Very High Intensity and Short Duration. WILLIAM M. CONN, *Rockhurst College.*—The flash of light obtained in discharging a large condenser through a very thin wire has been used as a light source for obtaining high speed photographs and for making visual observations of rapidly moving objects. Copper wire was found most suitable for photographic exposures, while wires made of silver and chromel gave good results in visual work. Examples of some typical settings are presented using wires of silver, gold, aluminum, copper, steel, constantan, and chromel. Arrangements for increasing the intensity of single flashes of light and for multiple flashes are briefly discussed, as well as means for electrically exploding materials not available in the shape of thin wires.

G3. Forbidden $s-ns$ Lines in Alkali Metal Atomic Absorption Spectra. J. E. MACK, *University of Wisconsin.*—A reexamination of Kratz' long-path absorption spectrograms[1] shows that at least on the Rb plates there are, in addition to the series from the normal state to high d-, f-, g- . . . levels, transitions to s-levels in the neighborhood of 50s. These levels were overlooked before because they are only barely or partly resolved from those in the f series, where the asymptotic quantum defect is less by almost 3 units. The significance of their presence lies in their evidence that the unusual transitions must arise from disturbances attributable to other atoms, since the $0-0$ transition in l is strictly forbidden.

[1] H. R. Kratz and J. E. Mack, Phys. Rev. **76**, 193A (1949).

G4. Isotope Shift in the $2p\ ^1S_0-3s\ ^1P_1$ Line of Carbon.* JOHN R. HOLMES, *University of Southern California.*—A study has been made of appropriate methods of excitation of small samples of carbon in order to make a measurement of isotope shift in the atomic spectrum of carbon. It has been found that milligram amounts of carbon can be excited to give the 2479 A ($2p\ ^1S_0-3s\ ^1P_1$) line with good intensity and sharpness in a liquid nitrogen cooled electrodeless discharge tube of rectangular cross section, but that no other carbon lines appeared. The carrier gas was about 4 mm of helium but it is essential that it contain about 0.5 mm of oxygen to make the carbon line appear. Using a mixture of $C^{13}-C^{12}$ enriched to 52 percent C^{13}, a measurement of the isotope shift in this line was made with a Fabry-Perot interferometer crossed with a medium Hilger spectrograph. The normal mass effect, based simply on the change in the Rydberg constant, would predict an isotope shift in this line of plus 0.142 cm^{-1}. The observed shift, however, is minus 0.156 ± 0.002 cm^{-1}, indicating a "specific mass effect"[1] of minus 0.298 cm^{-1}.

* Supported by the ONR.
[1] D. S. Hughes and Carl Eckart, Phys. Rev. **36**, 694 (1930).

G5. Departure of the Lamb Shift from the n^{-3} Law in He^+. J. G. HIRSCHBERG, JR. AND J. E. MACK, *University of Wisconsin.**—Light of the Paschen line, λ4686, from a liquid-air-cooled hollow-cathode discharge was diffracted from a 21-foot grating, and the extreme violet portion ($3_i-4_{i'}$, in the notation n_j), isolated by a knife-edge, was subjected to a Fabry-Perot interferometric examination with several spacers ranging from 16 to 21 mm. The separation of the two[1] components, which (neglecting any p- and d-shifts) is just the 3s-shift, is $0.1314\left\{\begin{matrix}+\text{ about }0.003\\-\text{ about }0.006\end{matrix}\right\}$ cm^{-1}, and thus definitely smaller than the 0.139 ± 0.003 which an n^{-3} extrapolation from the 2s-shift[2] would yield. Other values to be compared, all based on the 3_i-4_i component and incorporating the assumption (4s-shift)/(3s-shift) = 27/64, are our previous tentative grating value[3] of 0.113 ± 0.014 cm^{-1} and Kopfermann's[4] 0.137 ± 0.015 and[5] 0.118 ± 0.003 cm^{-1}.

* Supported by contract with the ONR.
[1] J. E. Mack and N. Austern, Phys. Rev. **74**, 1262A (1948).
[2] M. Skinner and W. E. Lamb, Jr., Phys. Rev. **75**, 1325A (1949).
[3] J. E. Mack and N. Austern, Phys. Rev. **72**, 972 (1947).
[4] H. Kopfermann and W. Paul, Nature **162**, 33 (1948).
[5] H. Kopfermann, Zeits f. Physik manuscript sent to us in advance of publication.

G6. Hyperfine Structure and Isotope Shift in Barium. O. H. ARROE, *University of Wisconsin.**—Spectroscopic h.f.s. studies have been made with concentrated samples of the isotopes Ba^{137} and Ba^{135}.** The resonance lines of Ba II show that both isotopes have the spin 3/2 and that the splittings from Ba^{137} are 12 percent larger than those from Ba^{135}. A small isotope shift, in which the even isotopes are displaced with respect to the odd, is found in these lines. Earlier studies with natural barium have indicated the values 5/2 or 3/2 for both odd isotopes; the current acceptance of 3/2 has come from a consistency test by Hay,[1] who found by a molecular beam resonance method that the nuclear magnetic moments have the ratio $\mu_{137}/\mu_{135}=1.1174\pm0.0010$, although the structure of Ba^{135} had never been resolved from that of Ba^{137}. The disagreement among earlier investigations probably arose from the blending caused by the difference in the h.f.s. splittings of Ba^{137} and Ba^{135} (natural abundances respectively 11.32 and 6.59 percent).

* Supported by contract with the ONR.
** Produced by the Y-12 plant, Carbide and Carbon Chemicals Corporation, and obtained by allocation from the United States AEC.
[1] R. H. Hay, Phys. Rev. **60**, 75 (1941).

G7. Nuclear Moments of Mg^{25}. F. M. KELLY, A. L. SCHAWLOW, W. M. GRAY, AND M. F. CRAWFORD, *University of Toronto.*—The h.f.s. of the Mg I line 5167A ($3s3p\ ^3P_0-3s4s\ ^3S_1$) and the Mg II line 2796A ($3s\ ^2S_{1/2}-3p\ ^2P_{3/2}$), excited in an atomic beam source, have been resolved with a Fabry-Perot etalon. 5167A shows two faint components due to Mg^{25} at $+0.0303$ and -0.0341 cm^{-1}, and a Mg^{26} component at -0.0138 cm^{-1}, from the strong Mg^{24} component. If the Mg^{25} centroid is assumed midway between the Mg^{24} and Mg^{26} components, the interval rule gives $I=5/2$ and the inverted structure of $^3S_1$ shows that the magnetic moment is negative. The $^3S_1$ splitting gives $\mu(Mg^{25})=-0.97\pm0.05$ n.m. 2796A shows

a strong Mg^{24} component and weaker Mg^{25} and Mg^{26} components $+0.0786$ and $+0.1021$ cm^{-1}, respectively, to higher frequencies. The intensity ratio between the Mg^{25} and Mg^{26} components confirms the negative moment and is consistent with $I=5/2$. Assuming that the Mg^{25} centroid is midway between the Mg^{24} and Mg^{26} components $\mu(Mg^{25})=-0.93\pm0.09$ n.m. The spin and the negative magnetic moment, but not its magnitude, agree with predictions for shell structure based on the individual particle model.

G8. The Effect of Electronic Paramagnetism on Nuclear Magnetic Resonance Frequencies in Metals.* W. D. KNIGHT,** *Brookhaven National Laboratory.*—Experiments have been performed[1] which show conclusively that nuclear magnetic resonance absorption in many metals occurs at frequencies which are appreciably higher than might be expected from the known nuclear g-values and the applied magnetic fields. This deviation in resonance frequency varies from 0.036 percent of the expected value in Li^7 to 1.20 percent in Pb^{207}. Measurements on Be^9, accurate to about ±0.002 percent, fail to disclose the existence of such a frequency shift. Assuming $g(I)$ to be invariant for a given isotope, one can describe the effect in terms of a paramagnetic contribution to the total magnetic field at the nucleus. To be sure, the volume susceptibility of most metals is too small (in many cases negative) to account for the effect. However, the average magnetic field at the nucleus will be greater than the average field in the volume of the metal if the conduction electrons, in addition to being paramagnetic, exist in states which allow them to spend appreciable time near the nucleus. The shift should be proportional to the hyperfine structure splittings of the corresponding atomic states and to the electronic paramagnetism. Quantitative agreement with experiment is obtained for Na^{23}.

* Work performed at Brookhaven National Laboratory under the auspices of the AEC.
** Permanent address: Trinity College, Hartford, Connecticut.
[1] W. D. Knight, Phys. Rev. **76**, 1259 (1949).

G9. Spin Echoes.* E. L. HAHN, *University of Illinois.*—A technique for obtaining nuclear resonance after the applied r-f field is turned off has been discovered. While the d.c. magnetic field is held at the resonance value the sample is subjected to two r-f pulses of high intensity, separated by time interval τ at pulse width $\ll\tau$. At time τ after the leading edge of the second r-f pulse a single spontaneous nuclear induction signal appears. This single echo is predicted by integrating the solution of Bloch's equation** of motion for a monochromatic spin group over all Larmor frequencies. The distribution of spins at thermal equilibrium over a range of Larmor frequencies imposed by magnetic field inhomogeneities provides a distribution in precessing spins grouped at frequency intervals of approximately π/τ following the application of the twin r-f pulses. Measurements of the spin phase memory time T_2 for various substances agree with values obtained by conventional resonance methods. Advantages of the spin echo technique are (1) direct and accurate measurements of T_2, (2) elimination of balancing procedures in conventional resonance methods, (3) high signal to noise ratio, (4) higher stability and speed for hunting unknown resonances.

* Done under auspices of the ONR.
** F. Bloch, Phys. Rev. **70**, 460 (1946).

G10. Nuclear Quadrupole Effects in Solids. C. KIKUCHI, *Michigan State College.*—The discovery of the h.f.s. in solids by Penrose *et al.*[1,2] prompted us to consider the effects of the electric quadrupole moments of nuclei in crystalline solids. The quantum mechanical operators convenient for the calculation of this effect can be shown to be

$$(W_Q)_{\text{cryst}}=\tfrac{1}{4}(\partial^2V_{\text{cryst}}/\partial z^2)_0[eQ/I(2I-1)](3I_z^2-I^2), \quad (1)$$

$$(W_Q)_{\text{electron}}=-\tfrac{1}{2}(e^2Q/I(2I-1))1/r^3[(3I\cdot rI\cdot r/r^2)-I^2]. \quad (2)$$

In the above, Eqs. (1) and (2) are due to the crystalline and the electron electric fields respectively. Polder's model of copper sulfate crystal was used in carrying through our provisional calculations. The effects of strong and weak magnetic fields were investigated.

[1] Penrose, Abragam, and Pryce, Nature **163**, 922 (1949).
[2] Bleaney, Ingram, and Pryce, Nature **164**, 116 (1949).

G11. Retardation of High Velocity Ions in Gases. A. J. DEMPSTER AND A. E. SHAW, *Argonne National Laboratory.*—In connection with the measurement of the masses of isotopes with a double focusing mass spectrograph using 8000-volt ions, it was observed that differences in the spacing of narrow doublets occur when small amounts of gas are present. The differences are no doubt due to different retardations of the ions in the residual gas, and from the doublet changes it is possible to deduce the energy losses, even when they are only 2 parts in 100,000 or 0.16 volt in the 8000 used. At pressures of 10^{-5} mm the singly charged NO^+ ion was retarded 1.05 volts more than the doubly charged nickel ions. At higher pressures when benzene was introduced to give comparison lines, energy losses in Sm^{+2} and Sm^{+3} ions were as much as 16 volts more than in the corresponding hydrocarbon ions. With quadruply charged samarium ions an unexpected phenomenon was observed—two ionic types of the Sm^{+4} isotopes are formed. One suffers very large energy losses compared with the other, up to 58 volts, and is strongly scattered, while the second type of Sm^{+4} isotopes remain as sharp as at low pressure.

G12. A Simplified Emission Regulator for Mass Spectrometer Ion Sources. E. B. WINN AND ALFRED O. NIER, *University of Minnesota.*—A simplified electron emission regulator has been developed which operates by controlling the space current instead of the filament heater current. Regulation is accomplished by the insertion of a control plate between the filament and the shield. The control plate is connected to the filament through a biasing battery and control resistor, through which the emission current is allowed to pass. In spite of the fact that no vacuum tubes are required in this circuit, the regulation characteristics are essentially the same as those of the electronic devices previously used.[1]

[1] Alfred O. Nier, Rev. Sci. Inst. **18**, 398 (1947).

G13. Atomic Mass Determinations with a Mass Spectrometer.* T. R. ROBERTS AND ALFRED O. NIER, *University of Minnesota.*—The double focusing mass spectrometer previously described[1] has been employed to measure the mass doublets H_2-D, $C^{12}H_2-N^{14}$, $C^{12}H_4-O^{16}$, $H_2O^{16}-A^{36}/2$, $C_3^{12}H_4-A^{40}$. The mass differences in 10^{-4} a.m.u. were found to be 15.49, 126.1, 364.5, 267.7, and 688.5, respectively. Although the internal consistency was such as to indicate a p.e. of a few parts in 10^6 of the ion mass number measured, the results on the first three are all about 5 parts per 10^6 higher than those compiled by Bainbridge.[2] The measurement on H_2-D supports the results from recent disintegration experiments;[3,4] however, the existence of an undiscovered systematic error of the magnitude suggested above would put the doublet in direct agreement with that of Mattauch and Bonisch.[5]

* Supported by Joint Program of the AEC and the ONR.
[1] Nier, Roberts, and Franklin, Phys. Rev. **75**, 346 (1949).
[2] K. T. Bainbridge, National Research Council Preliminary Report No. 1, Nuclear Science Series, 1948.
[3] R. F. Taschek *et al.*, Phys. Rev. **75**, 1268 (1949).
[4] A. V. Tollestrup *et al.*, Phys. Rev. **75**, 1947 (1949).
[5] J. Mattauch, Phys. Rev. **57**, 1155 (1940).

Artificial Radioactive Substances; Radioactivity of Neutron; Capture and Scattering of Neutrons

H1. 9.0-Minute La^{136}. B. E. ROBERTSON, W. L. CARSS, AND M. L. POOL, *The Ohio State University.*—The 9.0±0.5-minute activity[1] in lanthanum is assigned to mass number 136. This activity was produced in the lanthanum fraction when Hilger CsCl was bombarded with 20-Mev alpha-particles and is ascribed to the reaction $Cs^{133}(\alpha, n)$. Barium samples, electromagnetically enriched in Ba^{134}, Ba^{135}, and Ba^{136}, respectively, when bombarded with 10-Mev deuterons, produced the 9-minute lanthanum activity with relative yields in agreement with the above mass assignment, the reactions being $Ba^{135}(d, n)$ and $Ba^{136}(d, 2n)$. Characteristic radiations are positrons, x-rays, and gamma-rays. The maximum energy of the positrons is 1.8±0.1 Mev as obtained by aluminum-absorption measurements.

[1] W. Maurer, Zeits. f. Naturforschung **2a**, 586 (1947).

H2. Beta-Spectrum of Pr^{143}.* J. BRUNER,** L. M. LANGER, AND D. MOFFAT, *Indiana University.*—The beta-spectrum of Pr^{143} (13.8*d*) has been studied in the 40-cm radius of curvature-shaped magnetic field spectrometer and also in a smaller version employing a 15-cm radius of curvature. Although the comparative half-life ($ft \sim 4.5\times10^7$) indicates that the transition is once forbidden, the spectrum was found to have the allowed shape. This suggests that the spin change must be less than 2. In order to satisfy these conditions it is necessary that, in this case, the $2d_{5/2}$ and $1g_{7/2}$ states be inverted in the nuclear shell model of M. G. Mayer.[1] The end point was found to be 0.922±0.003 Mev.

* Assisted by a grant from the Frederick Gardner Cottrell Fund of the Research Corporation and by the Joint Program of the ONR and AEC.
** AEC Fellow.
[1] M. G. Mayer, Phys. Rev. **75**, 1969 (1949).

H3. $\beta-\gamma$ Angular Correlation in Au^{198} and Rb^{86}. SHERMAN FRANKEL, *University of Illinois.**—$\beta-\gamma$ angular correlations have been investigated using scintillation counter detectors. The angular correlation in Au^{198} was found to be isotropic from $\frac{2}{3}\pi$ to π ($R/Q=1.00\pm0.01$). This is in agreement with an allowed shape for the beta-spectrum. The isotropy was unaltered by biasing the beta-detector to accept only the upper 10 percent of the beta-spectrum. Using Rb^{86}, from which Cs^{134} impurities were removed with an ion-exchange column, the correlation coefficient for the $\beta-\gamma$-branch was determined as -0.094 ± 0.015. This coefficient is consistent with either of two theoretical coefficients, both requiring the interaction to be Gamow-Teller, first forbidden, (L=2). The coefficient leading to a spin of 2 for Rb^{86} is consistent with the shape of the spectrum of the direct beta-transition to Sr^{86}, the empirical lifetime, and the parity of Rb^{86} as obtained from the nuclear shell model. It requires a spin of 2 for the excited state in Sr^{86} and specifies the γ-radiation as electric quadrupole.

* Assisted by the Joint Program of the ONR and the AEC.

H4. Investigation of Momentum Relations in the Decay of Be^7. PHILIP B. SMITH AND JAMES S. ALLEN, *University of Illinois.*—In the 90 percent branch of the decay of Be^7 through orbital electron capture to the ground state of Li^7, the excess energy is carried away by the neutrino, according to the usual neutrino hypothesis. Accordingly the Li^7 recoil nucleus must have a well-defined momentum. A highly concentrated source of Be^7 has been deposited as a thin film by successive evaporation. Using an electron multiplier tube and a retarding potential method, the energy distribution of the Li^7 recoils has been studied. Due to energy losses in the source a spectrum of energies appeared. The maximum energy of the recoils has been found to be 56.6±1.0 ev. This is to be compared with the expected value of 57.3 ev predicted from the known Be^7-Li^7 mass difference. In addition we have made time-of-flight measurements on the 10 percent branch of the decay in which a γ-ray is emitted. The γ-ray is used to trigger a sweep and the time-of-flight spectrum of the recoils is displayed on a CRT. Preliminary results indicate the presence of recoils of the expected energy. Auger electrons of approximately the expected energy of 35 ev have also been observed with the electron multiplier.

H5. Excited States of Be^7. J. C. GROSSKREUTZ AND K. B. MATHER,* *Washington University.*—Evidence for the existence of excited states of Be^7 below 1 Mev has been found from a study of the neutrons produced in the reaction $Li^7(p, n)Be^7$. Using a beam of homogeneous protons of 5-Mev energy from the Washington University cyclotron, the neutrons were detected by a standard photographic plate method. In addition to the ground state group of neutrons, three additional lower energy groups were observed indicating a level structure for Be^7. Three separate runs on three separate targets of varying thickness gave the same results. Observations were made at 20° and 90° to the proton beam for each target. In every case the shift in energy of the peaks as one goes from 90° to 20° is consistent with the assignment of definite levels to Be^7. Values obtained for the excitation energies are: 0.205±0.070 Mev, 0.470±0.070 Mev, and 0.745±0.070 Mev above the ground state. The level at 470 kev is analogous to the well-known level at 478 kev in the mirror nucleus Li^7. The other two levels have no correspondence as yet observed in Li^7. Q for the ground state reaction was found to be −1.65±0.04 Mev in good agreement with previously obtained values.

* Assisted by the Joint Program of the ONR and the AEC.

H6. Radioactive Decay of the Neutron. J. M. ROBSON, *Chalk River Laboratory.*—The positive particle from the radioactive decay of the neutron has been identified as a proton from a measurement of charge to mass. A collimated beam of neutrons emerging from the Chalk River pile passes between two electrodes in an evacuated tank. One electrode is held at a positive potential, up to 20 kev, while the other electrode is grounded and forms the entrance aperture to a thin lens magnetic spectrometer, the axis of which is perpendicular to the beam of neutrons. The positive decay particles can be focused on the first electrode of an electron multiplier. The background counting rate is 60 c.p.m. A peak of 80 c.p.m. is observed above background when the magnetic field is adjusted for protons of energy expected from the electrostatic field. When a thin boron shutter is placed in the neutron beam, the proton peak disappears. Preliminary estimates of the collecting and focusing efficiency and the neutron flux indicate a minimum half-life of 9 minutes and a maximum of 18 minutes for the neutron.

H7. Thermal-Neutron Capture Cross Sections of Sixty Eight Elements. H. POMERANCE, *Oak Ridge National Laboratory.*—The Oak Ridge pile oscillator, previously described,* has been used for a uniform survey of the thermal neutron capture cross sections of the elements. Sixty eight elements from atomic number 3 to 82, nine of them not previously measured, have been measured by comparison with gold. The capture cross section of gold is known from other work. From the internal consistency of the measurements, the care in selecting samples, and the accuracy of the value for gold, a precision of 5 percent is estimated. A comparison will be given with the results of other methods such as time-of-flight and activation.

* J. I. Hoover *et al.*, Phys. Rev. **74**, 864 (1948).

H8. Total Fast Neutron Cross Section of Potassium. R. E. PETERSON, *University of Wisconsin.*—The total neutron cross

section of potassium has been measured for neutron energies ranging from 15 to 600 kev. The cross section was obtained by transmission measurements, using a neutron energy spread of 15 kev. Maxima in the cross section were found for neutron energies of 70, 110, 160, 305, 360, 430, 490, and 560 kev. The largest cross section observed was about 3.7 barns, at 70 and 305-kev neutron energy, while in the region between maxima, the cross section was less than 2 barns. It is interesting to note that for both potassium and calcium,[1] whose most abundant isotopes contain "closed shells"[2] of twenty neutrons, the total neutron cross section between maxima is considerably smaller than that of other nuclei in this region of the periodic table.

* This work was supported in part by the AEC and in part by the Wisconsin Alumni Research Foundation.
[1] Adair, Barschall, Bockelman, and Sala, Phys. Rev. **75**, 1124 (1949).
[2] M. G. Mayer, Phys. Rev. **74**, 235 (1948).

H9. Dependence of Neutron Cross Sections on Mass Number.* R. K. ADAIR,** *University of Wisconsin.*—The total neutron cross sections of Ti, Zn, Cu, Sn, and W have been measured for energies from 50 to 1400 kev, using a neutron energy spread of about 100 kev. The cross sections were determined by means of simple transmission measurements as previously described.[1] The neutron energy spread is assumed to be large enough compared to the average spacing between energy levels, so that the values represent an average over many resonances and can be compared to the predictions of statistical theories.[2] The results show the anomalous variation of cross sections with mass number which was noticeable in previous work.[1,3] The cross sections of Ti, Zn, Cu, and W reach their highest values at the lowest neutron energies and decrease with increasing neutron energy. The cross section of Sn, in common with other elements of mass number near 100, is almost independent of neutron energy.

* This work was supported in part by the AEC and in part by the Wisconsin Alumni Research Foundation.
** AEC Predoctoral Fellow.
[1] Bockelman, Peterson, Adair, and Barschall, Phys. Rev. **76**, 277 (1949).
[2] Feshbach, Peaslee, and Weisskopf, Phys. Rev. **71**, 145 (1947).
[3] Barschall, Bockelman, and Seagondollar, Phys. Rev. **73**, 659 (1948).

H10. Total Cross Sections of C, O, Mg, Si, and S for Neutrons in the Energy Range 0.6 Mev to 1.8 Mev.* G. D. FREIER, E. E. LAMPI, AND J. H. WILLIAMS, *University of Minnesota.*—The fast neutron total cross sections of light nuclei which may be considered to consist of an integral number of alpha-particles were determined by measuring the transmission of disks of C, Mg, Si, S, and SiO_2. The thickness of each scatterer was adjusted so that the average transmission was about 50 percent. By using the $Li^7(p, n)Be^7$ reaction as a source of neutrons with a 30-kev thick Li target source the neutrons were sufficiently monoergic to resolve apparently most of the excited levels of the compound nucleus when bombarded with neutrons in the energy range 0.6 Mev to 1.8 Mev. A pulse ionization chamber with a paraffin radiator was used as a detector and was placed at 0 degrees with respect to the incident proton beam where the neutron energy varied only a fraction of a percent in the solid angle subtended by the detector. All elements except C showed a rather complex set of resonance levels in the above energy range and the complexity increased with atomic number. Enough counts were taken to make the probable errors in the measurements ±5 percent. The data will be presented in the form of curves showing total cross section as a function of incident neutron energy.

* This research was supported in part by the ONR.

H11. Total Neutron Scattering Cross Section of Helium.* S. BASHKIN, B. PETREE, F. P. MOORING, AND R. E. PETERSON, *University of Wisconsin.*—The total cross section of helium for fast neutrons has been determined by comparing the transmission of a thin-walled cylinder filled with 8000 p.s.i. of helium with that of an identical, empty cylinder. Neutrons were obtained from the $Li(p, n)$ and $d-d$ reactions and were detected by a hydrogen recoil counter. Measurements were carried out under conditions of good geometry for neutrons of energies between 40 kev and 6.4 Mev. The helium cross section increases smoothly from 0.8 barn at 40 kev to 6.7 barns at 1.1 Mev, and then decreases to 2.3 barns at 6.4 Mev, the statistical uncertainty being 0.1 barn. From 0.95 Mev to 1.32 Mev, measurements were taken in 30-kev steps with a neutron energy spread of 30 kev. No evidence was found for the two maxima reported by Staub and Tatel.[1] As a check on the present helium measurements, the hydrogen cross section was determined at 1 Mev by the same method. The value of 4.2 ± 0.1 barns agrees with the results of Lampi *et al.*[2]

* This work was supported in part by the AEC and in part by the Wisconsin Alumni Research Foundation.
[1] H. Staub and H. Tatel, Phys. Rev. **58**, 820 (1940).
[2] Lampi, Freier, and Williams, Phys. Rev. **76**, 188 (1949).

H12. Neutron Scattering in the Resonance Region. J. TITTMAN, C. SHEER, J. RAINWATER, AND W. W. HAVENS, *Columbia University.*—The Columbia neutron velocity spectrometer,[1] hitherto used only for transmission experiments, has been applied to the direct measurement of neutron scattering in the 1–100-ev region. The neutron beam is collimated by a 3-inch square tube lined with small bricks made of B_4C. It then enters a large chamber similarly lined. The scattering target, located near the center of the chamber, is placed with its front face at 45° to the beam. The neutrons scattered in the general direction perpendicular to the beam leave the scattering chamber through a 1-foot square port and are detected by twenty BF_3 counters in parallel. The counter pulses are fed into the velocity selector. The total path of the scattered neutrons, consisting of the distance from the paraffin source slab to the scattering target plus the distance from the scattering target to the BF_3 counters is known. Since the velocity selector sorts the neutron pulses fed to it according to the time of flight over the known path, the energy distribution of the scattered neutrons is determined. Results on resonance and potential scattering will be presented.

[1] J. Rainwater and W. W. Havens, Jr., Phys. Rev. **70**, 136, 154 (1946).

H13. Interaction of 12–13-Mev Neutrons with Deuterons. G. L. GRIFFITH, M. E. REMLEY, AND P. G. KRUGER, *University of Illinois.*—12–13-Mev neutrons produced by bombarding a thin deuterium gas target with 10-Mev deuterons have been scattered from deuterons in a high pressure cloud chamber filled with CD_4. 4229 tracks with the appropriate lengths to be deuteron recoils were observed between 0° and 70° in the laboratory system. A small percentage of these tracks were due to a 3 percent contamination of ordinary hydrogen, and the remainder were recoil deuterons or protons from the $d(n, 2n)p$ reaction. That this reaction exists was evident by the presence of tracks between 60° and 90° in the laboratory system which were too long to be accounted for by either deuteron or proton recoils. Because of lack of sufficient information at this time no correction on the $n-d$ scattering angular distribution has been made for this reaction. The angular distribution of observed tracks shows a minimum at 60° for the center of mass recoil angle with a forward peak 6.5 times as large as the minimum and rises to 4.5 times minimum at 130° and 20°.

Solid-State Physics

J1. Thermoluminescence of Calcium Sulfate: Mn Phosphor. K. WATANABE, *Naval Research Laboratory.*—As part of the program on upper atmosphere research, observations* of extreme ultraviolet and x-rays from the sun were recently

made with thermoluminescent calcium sulfate: Mn phosphors mounted on V-2 rockets. To permit their use as detectors of radiation it was necessary to establish several properties. The sensitivity was found to commence at 1300A, as reported by Lyman, and extended to x-rays and gamma-rays. The phosphor was excited conveniently by radiation between 1100 and 1300A produced by a hydrogen discharge tube with LiF window. The thermoluminescence extended from 4480 to 5790A with the maximum at 5020A. The sensitivity was constant for exposure temperatures from 80°C to at least −40°C. Near 25°C the emission was proportional to $1/t$ and to the total initially stored energy. The stored energy was reduced by near ultraviolet but was not affected by infra-red or visible. The stored energy was a function of tI and was directly proportional until saturation set in. The total thermoluminescence was independent of the heating cycle.

* Purcell, Tousey, and Watanabe, Phys. Rev. 76, 165 (1949).

J2. Diffraction Effects Observed in Partially Ordered CoPT Crystals. JOHN B. NEWKIRK AND R. SMOLUCHOWSKI, *Carnegie Institute of Technology.*—A detailed x-ray study of single crystals of CoPt at early stages of the ordering process shows the presence of lattice aperiodicities in some of the [110] directions. This is demonstrated by the presence of [110] rods in the reciprocal lattice which run through matrix points. It is found that different rods of the ⟨110⟩ family are missing at different matrix points. This is interpreted to indicate that the aperiodicities have their origin in the strains which accompany the transformation from disordered cubic to the ordered tetragonal phase, rather than in the presence of platelets of different concentration. It is proposed to correlate these internal strains with the high coercive force which this alloy exhibits when at an intermediate state of order, as predicted by Becker's theory.

J3. Electronic Band Structure in Disordered Alloys.* HUBERT M. JAMES AND ARTHUR S. GINZBARG,** *Purdue University.*—Disordered alloys and crystals with randomly distributed substitutional impurities resemble pure crystals in the regular arrangement of crystal cells, but differ in the random distribution of atoms into cells. To investigate the applicability of the idea of electronic band structure to these non-periodic systems, an equivalent one-dimensional wave equation has been studied, in which the potential energy in successive cells of length a is randomly assigned one of two forms, A and B, with probabilities p_a and p_b. The number of states $N(E)$ below energy E is proportional to the average number of nodes per cell of any solution, and the energy density of states is obtained as dN/dE. One can reduce the problem of determining the average number of nodes per cell to that of solving a functional equation for the distribution of initial phases in the cells, or can count the nodes in a long sequence of randomly chosen cells. Illustrative calculations show the gradual washing out of the original band structure of the pure type A crystal, and the spreading out of "impurity states" to form a diffuse impurity band, as the "impurity" density (p_b) is increased.

* Work partially supported by Signal Corps contract.
** Present address: Shell Oil Company, Houston, Texas.

J4. The Energy Absorbed in Twinning Single Crystals of Zinc.* EDWARD I. SALKOVITZ AND JAMES S. KOEHLER, *Carnegie Institute of Technology.*—The energy absorbed in producing twins in single crystals of zinc by means of ballistic impacts has been measured in the manner first described by B. Chalmers. Chalmers found an absorption of 0.8×10^6 erg/cc of twin for single crystals of tin. Data on 14 specimens indicate that zinc behaves differently from tin. It was found necessary to deform the zinc crystals plastically before twinning could be produced. Seven one-inch specimens, cut from three different crystals with (001) pole at 83° with the specimen axis, required, on absorption, of from 0.71×10^6 to 1.33×10^6 erg/cc of sample before twinning. Subsequent twinning occurred with an absorption of 0.45 to 4.6×10^6 erg/cc of twin. Five one-inch specimens, cut from the same crystal whose orientation was 80°, absorbed between 0.21×10^6 and 0.59×10^6 erg/cc of sample before twinning. An additional absorption of between 0.21×10^6 and 1.48×10^6 erg/cc of twin was required for the production of twins. Two specimens cut from the same 75° crystal required 0.50×10^6 and 0.56×10^6 erg/cc of sample before twinning. Subsequent twinning occurred with an absorption of 0.92×10^6 and 2.07×10^6 erg/cc of twin. In the latter specimen severe bending occurred. In general the "fore" energy and the "twinning" energy depend on the kinetic energy of the striker at the moment of impact.

* This work was supported by ONR contract.

J5. Revised Procedure for Measuring Internal Friction.* J. S. KOEHLER AND J. W. MARX, *Carnegie Institute of Technology.*—The use of an auxiliary piezoelectric gauge in conjunction with an a.c. bridge as a means of measuring both strain amplitudes and decrement over wide ranges is described. Consistent and reproducible decrement values varying from 10^{-6} to 10^{-2}, measured over strain amplitudes of from 10^{-8} to 10^{-4}, have been obtained for single crystals of copper, lead, and quartz, using the improved technique. A previously established method of decrement measurement with the a.c. bridge alone, involving the determination of the width of the resonance peak, which has been extensively employed by T. A. Read and others, including the authors, is shown to be invalid for those cases in which the a.c. resistance varies appreciably with the strain amplitude. Comparison of data obtained on the same specimens by the two procedures shows excellent agreement for quartz samples, for which the decrement is virtually independent of the strain amplitude, but a very marked disagreement exists for copper and lead specimens, particularly at high strain amplitudes. In the latter case, decrement calculated by the resonance peak width method is frequently more than ten times as great as that calculated by the revised procedure. A supplementary calculation, involving piezoelectric relationships, has been devised which permits the salvage of data previously calculated by the resonance peak width method over regions in which the latter is not applicable.

* This research was sponsored by the ONR.

J6. Effects of Etching, Annealing, and Threshold Deformation on the Internal Friction of Copper.* J. W. MARX AND D. A. PATTERSON, *Carnegie Institute of Technology.*—(1) Unannealed and annealed copper single crystals were first weighed, then cemented to quartz driver-gauge combinations and piezoelectrically driven at their fundamental frequency of 37 kc at a constant strain amplitude of 5×10^{-7}. The cylindrical surfaces of the rod shaped specimens were etched away by periodic immersion in nitric acid, with the loss in mass of about two percent per etch determined by chemical analysis of the etchant. After each etch the decrement in vacuum was measured and plotted against the decreasing mass. Unannealed crystals showed *decreases* of as much as 50 percent in decrement with a loss of less than five percent in mass, but annealed specimens without exception exhibited marked *increases* in decrement following the first few etches. (2) The decrement of copper single crystals was first measured at a reference strain amplitude of about 5×10^{-7}, after which the vibrational amplitude of the composite resonator at resonance was raised from this value to a maximum working strain of about 5×10^{-5} in a series of small steps. After each increment in working strain the reference level strain was restored and the decrement

remeasured. The first change in the reference level decrement was a slight increase occurring after applications of working strain amplitudes of about 1×10^{-5}, while very pronounced increases were observed following larger working strains.

* This research was sponsored by the ONR.

J7. Internal Friction of Metals at Very High Temperatures. T'ING-SUI KÊ, *University of Chicago.*—In connection with the study of the internal friction peak (*versus* temperature) associated with the viscous behavior of grain boundaries in metals, some other effects were observed at higher temperatures causing an additional internal friction in superposition with the high temperature branch of this internal friction peak. This additional internal friction was found to have its origins in some effects of cold-working introduced in the interior of the grains which remain even after the complete recrystallization of the specimen. It increases with the amount of cold-work the specimen was subjected to before and after recrystallization; it decreases with annealing at successively higher temperatures until a stable value is reached; and it increases with the precipitated impurity content in the specimen. This high temperature internal friction is very high in an aged specimen of 99.991 aluminum alloyed with four percent copper. These observations are consistent with the viewpoint that this internal friction is caused by the presence of dislocations in the interior of the specimen although the mechanism of giving rise to the internal friction is unknown. It is pointed out that a study of high temperature creep under very low stress may be conveniently carried out through the internal friction measurements described.

J8. The Creep of Pure Copper and Lead Single Crystals.* PETER W. NEURATH AND J. S. KOEHLER, *Carnegie Institute of Technology.*—Single crystals of 99.999 percent purity were grown by the Bridgman method in the form of standard tensile specimens of one-inch gauge length. The strains range from 10^{-5} to 10^{-3}. Measurements were made at 90°K and 295°K. Loads are applied by sliding a weight along a lever using a motor drive. The applied stress is increased by small increments (10 g/mm² for Pb). Below the yield stress such an increment results in a transient increment of strain which is less than 10^{-4}; however the first increment which exceeds the critical stress results in a transient strain of about 10^{-3} which occurs in less than five minutes. The yield stress did not depend on the temperature for copper and lead. For lead the yield stress is 100 g/mm²±10 g/mm²; for copper it is 300 g/mm². Steady-state creep was observed in lead for periods up to 1000 minutes, the steady-state rate decreases with decreasing temperature. For example at a stress of 150 g/mm² the transient creep is still less than 10^{-2}; the steady-state rate is 10^{-4} per minute at 295°K whereas it is only 1×10^{-6} per minute at 90°K. The rates mentioned in the example are the extreme rates measurable. Changing the orientation, annealing the copper, and adding 0.0015 percent Bi to the lead did not influence the behavior.

* This research supported in part by NACA contract and by ONR contract.

J9. Measurement of the Activation Energy for Motion of Dislocations in Single Crystals of Copper. A. S. NOWICK, *Columbia University.*—Measurements of internal friction were made on single crystal rods of copper in forced longitudinal vibration. The method was that of Read[1] extended by positioning the composite oscillator in a cryostat which permitted temperature variation between +30°C and −60°C, and by the use of a liquid adhesive which prevented strain of the specimen due to differential thermal expansion at the quartz-specimen interface. The variation of decrement with strain amplitude at constant temperature was observed to decrease with decreasing temperature proportionately to $\exp(-\epsilon/kT)$. It has been shown[1] that in single crystals of copper, amplitude-dependent internal friction results from the motion of dislocations already present in the crystal lattice. Therefore, it was concluded that the observed values of ϵ correspond to the activation energy for such motion. Values of ϵ were obtained for two crystals initially annealed in vacuum and subsequently subjected to static compressional stress which introduced a definite amount of cold work. The results were 1300 and 1600 cal./mole, the second representing the more highly worked crystal.

[1] T. A. Read, Phys. Rev. **58**, 371 (1940); Trans. A.I.M.E. **143**, 30 (1941).

J10. Growth of Alkali Halide Crystals from the Vapor Phase onto Substrates of Mica. L. G. SCHULZ, *University of Chicago.*—Thin films of alkali halides were formed by evaporation in a vacuum on mica substrates and studied by means of electron diffraction. It was found that the crystals of all substances had a [111] direction normal to the substrate. In addition there was an angular orientation about this direction which depended on the lattice constant, a_0, in the following way: (1) when a_0 was larger than 5.36A (a_0 for KF) the angular orientation of the hexagonal net of atoms in the deposit at the interface matched exactly the orientation of the network of potassium atoms in the cleavage face of mica. (2) For LiCl (a_0 equal to 5.14A) the angular orientation was random but the [111] fiber structure was well defined. (3) NaF (a_0 equal to 4.62A) had a definite [111] fiber structure but was mixed with a large component of crystals having random orientation. (4) For LiF (a_0 equal to 4.02A) the hexagonal network at the interface was turned 30° in respect to the potassium atom network of the substrate. By considering the crystal structure of mica an attempt is made to explain the observed orientation of each substance.

J11. Magnetic Properties of Zinc Alloys at Low Temperatures. JULES A. MARCUS,* *Northwestern University.*—The de Haas-van Alphen effect and the temperature dependence of susceptibility have been investigated for pure zinc and zinc alloyed with small amounts of copper and aluminum. Measurements were made on single crystals by the Faraday method in fields ranging from 2.5 to 11 kilogauss and temperatures down to 14°K. The addition of copper (up to 0.32 atomic percent) to New Jersey super-pure zinc shifted the d.H.-v.A. oscillations to higher fields, increased their frequency, increased the amplitude of the high field oscillations, and decreased the amplitude at low fields. The addition of aluminum (up to 0.26 atomic percent) decreased the frequency of the oscillations by an amount comparable with the experimental error while the amplitude decreased markedly for all field strengths. The temperature dependence of susceptibility was investigated at temperatures above that at which the d.H.-v.A. effect becomes negligible. The anomalous maxima and minima characteristic of the susceptibility parallel to the hexagonal axis of pure zinc were found in all the alloys. For the copper alloys, the extremes were less pronounced and shifted to slightly higher temperatures. For the aluminum alloys, the mean value of susceptibility decreased but the temperature dependence curves were otherwise identical with those for pure zinc.

* This work was carried out while I was a Union Carbide and Carbon Postdoctoral Fellow at The Institute for the Study of Metals, University of Chicago.

J12. Paramagnetic Anisotropy of Manganous Fluoride. J. W. STOUT AND MAURICE GRIFFEL, *University of Chicago.*—The magnetic anisotropy of single crystals of MnF_2 has been measured over the temperature range 12 to 300°K. The measurements were made with a torsion balance. Temperature con-

trol was obtained with baths of hydrogen, nitrogen, oxygen, and ethane boiling under regulated pressure. At temperatures above 100°K the anisotropy is of the order of 0.1 percent of the susceptibility, and the greater susceptibility is in the direction of the c-axis of the tetragonal crystal. Below 70°K the anisotropy becomes extraordinarily large and the susceptibility in the direction of the c-axis is smaller than that perpendicular to the c-axis. Previous investigators have found a maximum in the powder susceptibility and in the heat capacity in the neighborhood of 70°K. Combining the present measurements with those of the powder susceptibility, the directional susceptibilities parallel and perpendicular to the c-axis can be calculated. The parallel susceptibility approaches zero at zero temperature and the perpendicular susceptibility increases by about 12 percent as the temperature drops from 70°K to 14°K. These results will be discussed in connection with the theory of antiferromagnetism proposed by Van Vleck.

[1] J. H. Van Vleck, J. Chem. Phys. **9**, 85 (1941).

Cosmic Rays and Artificial Mesons

M1. Neutron Production in Elements at High Altitudes.* J. A. SIMPSON, H. W. BALDWIN,† AND S. MOLNER, *University of Chicago.*—Measurements of the local production of fast neutrons from C, Al, Cu, Sn, and Pb have been made at altitudes of 30,000 and 35,000 feet pressure altitude using large paraffin neutron moderator geometries in aircraft during the past year and a half. Between 40° and 55°N magnetic latitude the local production from lead showed a factor of increase of 1.4 to 1.5 at 30,000 feet corresponding to the increase for the measured production of nuclear disintegrations and neutrons in the atmosphere.[1] An estimate of the absorption in lead for the incident neutron producing radiation of 200–400 g/cm² was obtained by stacking successive layers of lead in the paraffin geometry. A transition maximum for neutrons in lead occurs at about 18 g/cm². The relative rates of local production of neutrons give a factor of increase of ~2.8 from carbon to lead. Assuming that nucleons are the incident particles leading to neutron production, the relative multiplicity of neutrons from a nucleus of C, Al, Cu, Sn, or Pb may be determined. The ratio of neutron multiplicity of lead to carbon is ~7.5 which is not in disagreement with the recent measurements of Tongiorgi[2] at lower altitudes.

* Assisted by the Joint Program of the ONR and AEC.
† Deceased.
[1] J. A. Simpson, Jr. and R. B. Uretz, Phys. Rev. **76**, 569 (1949).
[2] V. Tongiorgi, Phys. Rev. **76**, 517 (1949).

M2. Primary Helium Flux in Cosmic Radiation.* L. GOLDFARB, H. L. BRADT, AND B. PETERS, *University of Rochester.*—Electron sensitive Kodak NTB3 plates were exposed under 16 and 10 g/cm² of air at geomagnetic latitudes of $\lambda = 30°$N and 51°N, respectively. The specific energy loss distribution of particles as measured by their track grain densities is found to show a distinct peak at four times the ionization of a relativistic singly charged particle. This corresponds to the grain density for a relativistic alpha-particle. Many of the particles with this grain density have been uniquely identified as fast He nuclei by the constancy of specific energy loss over long ranges of track (up to 60 g/cm²). Arguments will be presented which show that these He nuclei are not of secondary origin. The following results based on the indicated values for the mean free path for alpha-particles, λ_α, are obtained for the primary flux of He nuclei at the top of the atmosphere:

Flight	Geomagnetic latitude	(Number of alphas/cm² sec. ster.) $\times 10^2$ $\lambda_\alpha = 30$ g/cm²	$\lambda_\alpha = 40$ g/cm²	$\lambda_\alpha = 50$ g/cm²
1	$\lambda = 30°$N	1.1±0.3	0.9±0.3	0.8±0.3
2	$\lambda = 51°$N	4.5±1.5	3.8±1.3	3.4±1.2

According to these values the alpha particles constitute 20–30 percent of the primaries, in agreement with the results of M. A. Pomerantz and F. L. Hereford.[1]

* This work was assisted by the Joint Program of the ONR and the AEC.
[1] Phys. Rev. **76**, 997 (1949).

M3. Magnetic Deflection of Cosmic-Ray Mesons Using Nuclear Plates.* IAN BARBOUR, *University of Chicago.*—A method has been described[1] for investigating the mass and charge sign of mesons by exposing two nuclear plates with an air gap separating their parallel emulsion surfaces in a perpendicular magnetic field. From the orientation of the tracks of a given particle in the two emulsions is computed the radius of magnetic curvature of the trajectory in the intervening air gap, and hence the momentum which, with the range, allows the mass of the particle to be computed. Preliminary results reported[2] have been extended with plates exposed for 6 hours at 90,000 ft. in the 12,800 gauss field of our 65 lb. permanent magnet. Some 150 meson tracks have been analyzed, the signs of the charges determined, and values for the mass computed. In about 30 of these cases the trajectories are long enough to allow good mass determinations with probable errors of the order of 10 to 20 percent. These mass measurements and probable errors will be discussed.

* Assisted by the Joint Program of the ONR and the AEC.
[1] C. F. Powell, Nature **161**, 473 (1948); I. Barbour, Phys. Rev. **74**, 507 (1948).
[2] I. Barbour, Phys. Rev. **76**, 320, (1949).

M4. Concerning the Knock-On Secondaries of Mesons.* FRANK L. HEREFORD,† *Bartol Research Foundation.*—The average number of secondary electrons accompanying a meson traversing and emerging from thin foils of various materials ($t \ll$ radiation length) has been computed using the spin zero collision probability given by Bhabha.[1] The data are of interest in connection with low pressure G-M counter cosmic-ray experiments. The probability, ν, is computed that at least one secondary is produced with sufficient energy to emerge from a foil upon passage of a meson. Families of ν *vs.* t curves for various meson momenta, $P/\mu c$, are thus obtained. For $P/\mu c = 10$ the curve for lighter elements ($Z < 50$) attains equilibrium for $t \sim 1.5$ g/cm² at $\nu = 0.075$. This corresponds to $\nu_{Pb} = 0.065$ in good agreement with recent experimental results.[2] Computational details and curves will appear elsewhere.[3]

* Assisted by Joint Program of the ONR and the AEC.
† Now at University of Virginia.
[1] H. J. Bhabha, Proc. Roy. Soc. **164**, 257 (1938).
[2] Brown, McKay, and Palmatier, Phys. Rev. **76**, 506 (1949).
[3] J. of Frank. Inst.

M5. East–West Asymmetry of Positive and Negative Mesons.* GERHART GROETZINGER AND GORDON W. MCCLURE, *University of Chicago.*—With a magnetic lens telescope, focusing either positive or negative mesons with an energy of approximately 800 Mev, but excluding protons, the counting rates W_+, W_-, and E_+, E_- of positive and negative mesons coming from the west and east, respectively, were measured for various values of the zenith angle of incidence. The east–west asymmetries $\alpha_\pm = \dfrac{2(W_\pm - E_\pm)}{W_\pm + E_\pm}$ and the positive excess $\beta = \dfrac{2(W_+ + E_+ - W_- - E_-)}{W_+ + E_+ + W_- + E_-}$ were found to be:

Zenith angle	Mt. Evans (Altitude 14,000 feet) 24°	58°	Chicago 17°
	$\alpha_+ = +$ 7.1±2.1%	$\alpha_+ = +37.0 \pm 6.1\%$	$\alpha_+ - \alpha_- = 12.7 \pm 3.2\%$
	$\alpha_- = -$ 5.6±2.1%	$\alpha_- = -37.4 \pm 6.0\%$	
	$\beta =$ 17.6±1.2%	$\beta =$ 7.4±2.8%	$\beta = 12.0 \pm 1.4\%$

Our data thus indicate: (a) The east-west asymmetry is the same for positive and for negative mesons. (b) The positive excess increases with altitude, which is in agreement with results previously obtained by others.

* Assisted by the Joint Program of the ONR and the AEC.

M6. Multiple Production of Mesons. E. P. NEY AND PHYLLIS FREIER, *University of Minnesota.*—Definite examples of multiple production of mesons have been observed in cloud chambers and supporting evidence obtained in photographic emulsions. The multiplicity and angular distribution in carbon and lead will be discussed.

M7. Properties of the Heavy Primaries. PHYLLIS FREIER, E. P. NEY, F. OPPENHEIMER, *University of Minnesota.*—Recent results concerning the energy distribution and the mean free path of the heavy primaries will be discussed.

M8. Electrical Detection of Artificially Produced Mesons. L. W. ALVAREZ, A. LONGACRE, V. G. OGREN, AND R. E. THOMAS, *University of California, Berkeley.*—Scintillation counters have been used to detect the electrons from the decay of μ-mesons. The decay of the μ-meson has been followed over an intensity range of almost 10^4, and the measured mean life is 2.09 ± 0.03 μ-sec. The fact that this may be less than the free space lifetime may be explained by the presence of a small component of negative μ's. Almost all of the μ's are positive, as they come from the decay of π's. Although the latter have both signs, negative π's produce stars in matter and so do not give negative μ's unless the process occurs "in flight." Now that the technique has been shown to be reliable, it becomes possible to determine the energy spectrum, the angular distribution, and the total cross sections for the production of positive π-mesons as functions of Z and the proton-bombarding energy. For such determinations, the μ-decay is used as a "tracer," to tell where a π-meson has ended its range. Since the combined ranges of the μ and electron are small compared to the π-range, no appreciable errors are introduced by the tracer technique.

Reactions of Transmutation

N1. *P-N* Thresholds for Calibration Points on the Nuclear High Voltage Scale.* H. T. RICHARDS AND R. V. SMITH, *University of Wisconsin.*—The nuclear absolute voltage scale established by Herb, Snowdon, and Sala[1] has been extended to higher energies by accurate determinations of the $p-n$ thresholds of Be^9, B^{11}, C^{13}, and O^{18}. The same electrostatic proton analyzer with slits adjusted for 0.1 percent resolution was used for bombarding heated thin targets of Li, Be, B, TaO_3, and a thick carbon target. The proton energies in Mev at the observed neutron thresholds are as follows:

Li^7	Be^9	B^{11}	C^{13}	O^{18}
1.882 (Standard)	2.059	3.015	3.236	2.592

The largest uncertainty in these values is believed to be the 0.1 percent uncertainty in the Li standard.

* This work was supported in part by the AEC and in part by the Wisconsin Alumni Research Foundation.
[1] Herb, Snowdon, and Sala, Phys. Rev. **75**, 246 (1949).

N2. A Comparison of Several Nuclear Absolute Voltage Determinations. WILLIAM J. STURM AND VIRGIL JOHNSON, *University of Wisconsin.*—An experiment has been performed which was designed to evaluate the consistency between the absolute voltage determination of the threshold energy of the $Li^7(p, n)Be^7$ reaction as measured by Herb, Snowdon, and Sala[1] and earlier independent absolute voltage measurements. The comparison was effected by employing the natural alpha-particles from polonium and radium C′, the energy of which has been measured absolutely by several authors using magnetic deflection methods.[2] In this comparison the alpha-particles from these substances have been deflected electrostatically in the 90° cylindrical electrostatic analyzer at the University of Wisconsin. Alpha-particle line measurements were analyzed by numerical integration of resolution and source functions and in themselves contributed negligibly to the uncertainties of the comparison. The resulting alpha-particle energies, evaluated by comparison with the energy of the $Li^7(p, n)Be^7$ threshold, agree with the earlier measurements, and indicate that within the limits of accuracy of Herb's determination, all determinations give identical results.

[1] Herb, Snowdon, and Sala, Phys. Rev. **75**, 246 (1949); cf. also Schoupp, Jennings, and Jones, Phys. Rev. **76**, 502 (1949).
[2] S. Rosenblum and G. Dupouy, J. Phys. Rad. **4**, 262 (1933); W. W. Lewis and B. V. Bowden, Proc. Roy. Soc. **145**, 235 (1934); G. H. Briggs, Proc. Roy. Soc. **157**, 183 (1936).

N3. Fast Neutron Yield From the Cyclotron.* A. J. ALLEN AND J. F. NECHAJ, *University of Pittsburgh,* AND K. H. SUN AND B. JENNINGS, *Westinghouse Research Laboratories.*—Previous measurements of the fast neutron yield from various thick targets bombarded with 15-Mev deuterons and 30-Mev alphas have been extended.[1] The reaction, $S^{32}(n, p)P^{32}$, was used for neutron detection and defines the term "fast" neutron. The total neutron yield, N, obtained from angular distribution data, was found to be (410, 320, 290, 280, 168, 150, 137, 33, and 21)$\times10^7$/sec./μa deuterons for Ti, Cr, Co, Cu, Cb, Mo, Ag, Ta, and Pb targets respectively, and (650, 189, 106, 105, 42, 6.5, and 4.6)$\times10^7$/sec./μa alphas for Be, Al, Co, Cu, Ag, Au, and Bi targets respectively. For data obtained thus far, N may be calculated from the nuclear charge, Z, of the target by the empirical relationships: $\log N=10.18-0.024Z$ (for deuterons) and $\log N=9.72-0.024Z$ (for alphas). There is evidence that the strong forward neutron peak reported previously may be resolved into double or triple peaks.

* Assisted by the Joint Program of the AEC and the ONR.
[1] Allen, Nechaj, Sun, and Jennings, Phys. Rev. **76**, 188, 463 (1949).

N4. Deuterium (p, n) Threshold and the Deuteron Binding Energy.* R. V. SMITH AND D. H. MARTIN, *University of Wisconsin.*—The threshold has been carefully investigated for the previously reported $D(p, n)2H$ reaction.[1] Protons from the Wisconsin electrostatic generator, limited to 0.1 percent energy spread by the cylindrical electrostatic analyzer and calibrated in energy against the $Li(p, n)Be$ threshold, were used to bombard a target of frozen ND_3. The reaction neutrons, which at threshold are collimated forward and monoenergetic at 370 kv, were detected with a small hydrogen recoil counter biased to count only neutrons above 100-kv energy.

A preliminary evaluation of the data has been made, using for extrapolation near threshold a theoretical cross section curve which is based upon a $E^{\frac{1}{2}}$ variation for the outgoing neutrons and Coulomb barrier penetration for the outgoing protons. This extrapolation gives 3.340 ± 0.015 Mev for the threshold proton energy, and -2.227 ± 0.010 Mev for the reaction Q. This Q-value is then directly the deuteron binding energy.

* This work was supported in part by the AEC and in part by the Wisconsin Alumni Research Foundation.
[1] R. V. Smith and H. T. Richards, Phys. Rev. **74**, 1871 (1948).

N5. Photo-disintegration of Deuterium by 4.5 to 20.3-Mev X-Rays.* EVERETT G. FULLER, *University of Illinois.*—Nuclear emulsions have been used to detect the photo-protons produced by the passage of the collimated x-rays from a thin target (0.005-in. Pt.) betatron doughnut through a deuterium gas filled scattering chamber. The preliminary analysis of these plates has been reported.[1] Using the quanta distribution with energy for a thin target betatron determined by Koch and

Carter,[2] the observed distribution of the photo-protons, after correction for the neutron background, was used to obtain a curve for the relative cross section of the photo-disintegration process as a function of photon energy. This curve falls off slower than the Bethe-Peierls expression. At high energies it goes as $1/(h\nu)^{\frac{1}{2}}$. Angular distributions indicate a differential cross section in the center of mass system, obeying a $\sin^2\theta$ law at low energies. For energies above 10 Mev the data are fitted by a $\sin^2\theta(1+\alpha\cos\theta)$ law. There is no evidence for an isotropic component except in the high energy group (mean photon energy of 17 Mev), where the data are fitted by the expression: $\sin^2\theta(1+0.4\cos\theta)+0.15$.

* This work was assisted by the Joint Program of the ONR and AEC.

[1] E. G. Fuller, Phys. Rev. **76**, 576 (1949).
[2] H. W. Koch and R. E. Carter, Phys. Rev. **75**, 1950 (1949).

N6. Angular Distribution of Photo-Protons from Deuterium.* GERSON GOLDHABER, *University of Wisconsin.*—The angular distribution of photo-protons from the $D^2(\gamma, n)H^1$ reaction was measured in photographic emulsions loaded with deuterium and exposed to $F^{19}+H^1$ gamma-rays. The emulsions (Eastman, NTA, 100μ) were loaded by soaking in D_2O and were exposed while wet together with control emulsions loaded with H_2O (D_2O content 50 percent of emulsion weight). The gamma-rays were obtained by bombarding a thick CaF_2 target with 2.6-Mev protons from the Wisconsin electrostatic generator. A 35 μamp. hr. exposure was used. The emulsions were exposed at an average distance of 12.5 cm from the target, with the plane of the emulsion containing the proton beam direction. All the information is thus obtained on a single emulsion. The scanning of the emulsions is still in progress. To date ~600 acceptable tracks were found on an area of 40 mm^2 of the D_2O emulsion. The number of tracks on the H_2O emulsion of the same range is negligible. The two gamma-ray lines from $F^{19}+H^1$ at 6.13 and 7.00 Mev are clearly resolved, when the angular dependence of photo-proton energy is taken into consideration. The present preliminary value of a/b for the two gamma-rays combined is ~0.1 (where the angular distribution is of the form $a+b\sin^2\theta(1+\alpha\cos\theta)$ and α has the value $0.4\geq\alpha>0.1$).

* This work was supported in part by the AEC and in part by the Wisconsin Alumni Research Foundation.

N7. Differential Cross Section of the Reaction $He^3(d, p)He^4$ at 10.2-Mev Bombarding Energy and Search for Excited State in He^4. J. C. ALLRED, *Los Alamos Scientific Laboratory and University of Texas.*—Measurements of the differential cross section of the reaction $He^3(d, p)He^4$ at 10.2-Mev bombarding energy have been made using the focused cyclotron beam by means of a nuclear multiple photographic plate camera recently constructed at the Los Alamos Laboratory. The camera-target arrangement used permitted simultaneous observation of the reaction protons at laboratory angles from 20° to 155°. In the center of mass system the differential cross section shows two minima at 44° and 112°, the peak between them occurring at 65°. For the angular region investigated the cross section varied between two and five millibarns/unit solid angle. A comparison was made of the low energy particle spectrum from He^3 with that of H^3 and He^4 bombarded under similar conditions. The results indicate that, at a proton angle of 90° lab, residual excited He^4 nuclei are not produced with a cross section as great as 0.2 millibarn/unit solid angle for an excited level as high as 20.9±0.4 Mev. Values of the differential cross section at 5° intervals will be given and limits of the excited level energy as determined at 45° lab will be discussed.

N8. The Energies of Neutrons from the $Be^9(\alpha, n)$ Reaction. C. E. BRADFORD AND W. E. BENNETT, *Illinois Institute of Technology.*—A thick beryllium target was bombarded with 1.4 Mev α-particles produced in a Van de Graaff machine. The neutron spectrum was inferred by measuring the tracks of recoil protons in an Ilford C2 plate placed at 90° to the target. Two groups of neutrons were found. The group of higher energy corresponded to the formation of C^{12} in the ground state, and the Q-value derived from the masses (5.72 Mev) was used to find the stopping power of the plates. The second group of neutrons was found to have a Q-value of 1.27 Mev, yielding 4.45 Mev as the energy of the excited state of C^{12}. Lower excited states were definitely missing. Any excited state higher than 6 Mev would not have been observed at this low bombarding energy. The yield of neutrons in the low energy group was 1.30 times the yield of high energy neutrons. A plate exposed in the forward direction gave 0.40 for this ratio, as indication that the angular distribution of the two groups is different.

N9. Interpretation of the Angular Distribution of Long and Short Range Protons from the $O^{16}(d, p)O^{17}$ Reaction. LEO DIESENDRUCK, *Rhode Island State College.*—The theoretical expansion of the resonance formula for nuclear reactions for the differential cross section of an unpolarized reaction leads to a power series in the cosine, the coefficients of which are the sums of many terms each of which contains three types of factors: energy dependent (functions of the resonance denominators and "penetration" factors), "kinematic" (depending only on the quantum numbers), and unknown complex (arising from the matrix elements). The experimental results[1] show a fourth power of the cosine and odd powers necessary for both groups and for the long-range case (spin of $\frac{5}{2}\hbar$ and even parity for the ground state of O^{17}) are consistent with resonant levels located at 1.4 Mev, 2.00 Mev, and 2.60 Mev and widths 0.5 Mev. The complexity of the distribution sets a lower value and estimates of the penetrability set an upper value to the permitted angular momentum quantum numbers. Evaluation of the "kinematic" factors permits further limitations and the best choice of states for the three levels giving the long-range protons is $J=2^+$, 1^-, and 3^+. The complete theoretical expansion for these assumptions can be checked by attempting a fit of the experimental results, evaluating the unknown complex factors under the assumption that their magnitudes are not too different. A similar procedure for the short-range protons does not result in a unique choice of states.

[1] N. P. Heydenburg and D. R. Inglis, Phys. Rev. **73**, 230 (1948).

N10. Angular Distribution of Photo-Protons from Magnesium.* M. E. TOMS, J. HALPERN, AND W. E. STEPHENS, *University of Pennsylvania.*—The protons ejected from a four-mil magnesium foil by the bremsstrahlung from 22.5-Mev electrons were observed in Ilford C-2 emulsions. The magnesium foil was irradiated by 13,500 roentgen units in the $\frac{1}{4}$-in. diameter beam defined by a collimator in front of a betatron. Several Ilford plates (1 in.×$\frac{1}{2}$ in., 100 microns thick) were placed at various angles and one inch from the target so as to intercept the protons with glancing incidence. Equal areas (24 mm^2) of five plates were scanned and 423 protons found which entered the top surface of the emulsion and pointed from the target. The background of recoil protons was small enough to require no correction to the photo-protons. The angular distribution of photo-protons was observed to be: 30°, 79; 60°, 80; 90°, 93; 120°, 65; 150°, 106. The energy distribution of the protons as inferred from the measured range corrected for the target thickness is: 2–3 Mev, 34; 3–4 Mev, 73; 4–5 Mev, 80; 5–6 Mev, 66; 6–7 Mev, 87; 7–8 Mev, 62; 8–9 Mev, 18; 9–10 Mev, 3. From induced radioactivities, it was estimated that less than 5 percent of the protons were produced by the $Mg^{24}(n, p)$ reaction, that $\frac{3}{4}$ of the protons were probably from $Mg^{25}(\gamma, p)$ and $\frac{1}{4}$ from $Mg^{26}(\gamma, p)$.

* Supported by the Joint Program of the ONR and the AEC.

N11. $P-N$ Reactions in Light Elements.* C. P. BROWNE, R. V. SMITH, AND H. T. RICHARDS, *University of Wisconsin.*—The yield of neutrons from $Be^9(p, n)B^9$, $O^{18}(p, n)F^{18}$, and $K^{41}(p, n)Ca^{41}$ has been investigated from threshold to about 3.5-Mev proton energy. For the Be reaction a thin evaporated target was used. No resonance structure was observed except that at 2.56 Mev previously reported by Hushley.[1] For the O^{18} reaction, thin TaO_2 and Al_2O_3 targets were prepared by electrolyzing water enriched to 1.5 percent O^{18}. Resonances in the forward direction neutron yield were observed at the following proton energies: 2.67, 3.05, 3.29, 3.40, and 3.50 Mev. For the potassium reaction, thin K_2O targets were used. Resonances in neutron yield were observed at the following proton energies: 1.60, 1.90, 2.24, 2.46, 2.60, 2.80, 2.96, and 3.12 Mev. The K^{41} threshold was observed at 1.242 ± 0.015 Mev in agreement with the previous value 1.25 ± 0.05 Mev.[2] Work is in progress on $p-n$ reactions in chlorine and iron.

* This work was supported in part by the AEC and in part by the Wisconsin Alumni Research Foundation.
[1] W. J. Hushley, Phys. Rev. **67**, 34 (1945).
[2] H. T. Richards and R. V. Smith, Phys. Rev. **74**, 1257 (1948).

N12. The $(n-2n)$ and $(n-p)$ Cross Sections. BERNARD L. COHEN, *Carnegie Institute of Technology.*—The cross sections of about $15(n-2n)$ and $30(n-p)$ reactions produced by neutrons from the University of Pittsburgh 47-inch cyclotron were measured by counting the induced activity of the product isotopes. Corrections were made for the self-absorption of the beta-rays and for all other recognizable factors. Due to the slow variation of these cross sections with energy, the results could be readily integrated over the energy spestrum of the neutrons and compared with the predictions of Weisskopf's Nuclear Statistics.* The neutron energy spectrum was determined by proton recoils in a photographic plate, and in a triple coincidence—anticoincidence counter telescope with aluminum absorbers. Although fair agreement was found in several cases, there were deviations that are not consistent with any reasonable choice of nuclear temperatures. The results will be discussed in connection with the degree of validity of statistical theories of nuclei, and applications will be suggested to the identification of doubtful isotopes and the use of threshold detectors for determining neutron energies. This work was done with the assistance of the ONR.

* See, for example, "Lecture series in nuclear physics" MDDC 1175.

N13. The Values of Certain (p, γ) Resonances Below 400 Kv. S. K. ALLISON, J. H. MONTAGUE, AND A. H. MORRISH. *University of Chicago.*—A cylindrical electrostatic deflector has been constructed with average radius 15 cm, spacing 0.5 cm, and 90° deflection, in which the deflecting potential can be in the neighborhood of 50 kv, focusing protons up to 750 kv. Movable slits have been incorporated in the design and the geometry of the entrance and exit apertures of the deflecting channel is such that the stray field may be calculated analytically. The predictions have been compared with experiments on the focusing of electron beams by the instrument under controlled conditions and agreement to within 0.3 percent has been demonstrated. The instrument has been used to measure the lower voltage thresholds of the $F^{19}(p, \alpha, \gamma)$ and the $B^{11}(p, \alpha)$ and $B^{11}(p, \gamma)$ resonances, obtaining 0.3404 ± 0.0004 Mev for fluorine and 0.1628 ± 0.0002 for boron respectively. The agreement is good with recent measurements of Tangen[1] and Heydenburg.[2]

[1] R. Tangen, Kgl. Norske. Vid. Sels. Skrifter (1946) NRI.
[2] N. P. Heydenburg (private communication).

N14. The Low Energy Cross Section and Angular Distribution of the $D(d, p)$ Reaction. J. H. SANDERS,* J. MOFFATT, AND D. ROAF, *Oxford University.*—A thin deuterium target has been used to study the $D(d, p)$ reaction at low energies.[1,2] Using beams of from 35 μA to 250 μA of analyzed deuterons and a nuclear emulsion camera which favored the detection of low yields, sufficient proton tracks could be counted to measure the cross section and the angular distribution down to 15-kev bombarding energy. The deuteron beam was admitted to the camera through two successive canals, with differential pumping between them to reduce the gas flow into the accelerator. A velocity-selector type analyzer was used, and the beam intensity was measured calorimetrically owing to the large amount of ionization and charge-exchange in the target gas. The distribution can be represented as $Y_\theta = Y_{90°}(1+A\cos^2\theta)$. Values of A and the integrated cross-section σ are tabulated below:

Ekv	14.53	19.45	24.33	29.13	33.88	38.82	50.00
A	0.207	0.223	—	0.274	—	0.308	0.374
$\sigma\times10^{29}$	7.06	24.8	59.6	112.0	176.0	255.0	—

* Now at National Research Council of Canada, Chalk River, Ontario.
[1] A. P. French, Phys. Rev. **73**, 1474 (1948).
[2] Bretscher, French, and Seidl, Phys. Rev. **73**, 815 (1948).

Miscellany of Nuclear Experiments; Theoretical Nuclear Physics

P1. Resonance Scattering of X-Rays by Atomic Nuclei.* RALPH DRESSEL, M. GOLDHABER, AND A. O. HANSON, *University of Illinois.*—An attempt has been made to detect possible resonance radiation expected on the basis of the nuclear model suggested by Goldhaber and Teller.[1] Using x-rays from the 22-Mev betatron the radiation scattered from lead at 90° and 145° was measured by the 3.3-minute activity from the $Pr^{141}(\gamma, n)Pr^{140}$ reaction. Absorption measurements indicated that about half the activity could be attributed to fast neutrons from the scatterer. Comparison of the angular distribution of the remaining activity with that from 17-Mev electrons on thick lead indicated that about 50 percent of this activity at 90° and 5 percent of that at 145° might be associated with bremsstrahlung generated in the scatterer by multiple processes. The residual activities indicate differential cross sections for nuclear scattering in lead of (1.1 ± 0.6) and $(2.0\pm1.0)\times10^{-27}$ cm² per steradian, at 90° and 145° respectively. These values are approximately those expected from the above model using a resonance width of 4 Mev. Scattering from lighter elements was considerably less in agreement with the observations of Gaerttner and Yeater.[2]

* This work was supported by the Joint Program of the ONR and AEC.
[1] M. Goldhaber and E. Teller, Phys. Rev. **74**, 1046 (1948).
[2] E. R. Gaerttner and M. L. Yeater, Phys. Rev. **76**, 363 (1949).

P2. The Penetration of Protons in Several Metals. T. A. HALL AND S. D. WARSHAW,* *University of Chicago.*—The energy loss and average charge of fairly low energy protons (from 50 to 400 kev) passing through thin metallic foils have been studied for five elements: Be, Al, Cu, Ag, and Au. The data should be more accurate than previous results[1] because of improvements in the preparation and measurement of the thin foils[2] and the greater precautions taken against oil vapor effects in the vacuum system. At the energy extremes, the stopping data are consistent with the low energy theory of Fermi and Teller[3] and the high energy theory of Bethe,[4] but neither theory applies well in the energy range studied.[5] The data on average ionic charge will be compared with Bohr's estimates.[6]

* This work was in part supported by the Joint Program of the ONR and the AEC.
[1] H. Wilcox, Phys. Rev. **74**, 1747 (1948); Hall and Warshaw, Phys. Rev. **75**, 891 (1949).
[2] S. D. Warshaw, Rev. Sci. Inst. **20**, 623 (1949).
[3] E. Fermi and E. Teller, Phys. Rev. **72**, 399 (1947).
[4] M. S. Livingston and H. A. Bethe, Rev. Mod. Phys. **9**, 264 (1937).
[5] S. D. Warshaw, Phys. Rev. (to be published).
[6] N. Bohr, *The Penetration of Atomic Particles through Matter* (Copenhagen, 1948).

P3. Fission Yields of 65-day Zr^{95} and 17-hr. Zr^{97}; Search for Other Zr and Nb Fission Chains.* C. D. CORYELL, A. Y. SAKAKURA, AND A. M. ROSS, *Massachusetts Institute of Technology.*—No precise values have been reported[1] for fission yields of chain 95 (65*d* Zr−35*d* Nb) and chain 97 (17*h* Zr −75*m* Nb) in U^{235} fission. Values of 6.0±0.3 percent and 6.2±0.3 percent respectively are found by chemical separation of zirconium. Search for other zirconium fission activities (of mass numbers 93, 98, 99, 100) of half-life between 2*m* and 65*d* gave negative results; other work[1-3] also eliminates activities in appreciable yield of periods between 2*m* and 100*y*. Calculations indicate minimum half-lives for Zr^{93} and Zr^{98} of 1.7*d* and 1.5*m* respectively. It is thus shown that Zr^{93} is very long-lived; Zr^{98} might have been missed. Samples of niobium (columbium) separated rapidly after fission fail to show any short-lived constituent of half-life between 10*m* and 10*h* except 75*m* Nb^{97}, although 30*m* Nb^{98} has been reported to exist.[4] If Zr^{98} has a short life, Nb^{98} should have been found here unless its half-life is less than 10*m*.

* Assisted by the Joint Program of the ONR and the AEC.
[1] The Plutonium Project, J. Am. Chem. Soc. 68, 2411 (1946); Rev. Mod. Phys. 18, 513 (1946).
[2] S. Katcoff and L. J. Brown, J. Chem. Phys. 17, 505 (1949).
[3] L. Jacobson and R. Overstreet, paper 91, Vol. 9, Div. IV, Nat. Nucl. En. Series (in press).
[4] G. E. Boyd, private communication to G. T. Seaborg and I. Perlman, Rev. Mod. Phys. 20, 607 (1948).

P4. Further Interpretations of Closed-Shell Perturbations in Fission Yields.* L. E. GLENDENIN** AND C. D. CORYELL, *Massachusetts Institute of Technology.*—In previous papers[1,2] the authors have treated the distribution of nuclear charge in fission and showed that there is a pronounced perturbation in fission yields caused by enhanced stability of fission fragments with 50 or 82 neutrons. At present two competitive hypotheses exist which are in fair agreement with the mass spectrometric observations of Thode on xenon fission yields and of Nagle on the ratio of the yields of Cs^{135} to Cs^{137} (1.1±0.1). The first hypothesis is that primary fission fragments with 83 neutrons eject promptly an extra neutron, and the yield of primary fission fragments is that set by the postulate[1] of equal charge displacement of light and heavy fragments; the second is an elaboration[1] of the theory of the division of charge in fission of Present. For some interesting chains, the ratio of observed fission yields to smooth-curve[3] yields are: *132* 1.00; *133* 1.26; *134* 1.35; *135* 1.0_2; *136* 1.0_2; *137* 0.8_8. It is seen that the effects are large; it will be shown that they are understood semi-quantitatively.

* Assisted by the Joint Program of the ONR and the AEC.
** Presently at the Argonne National Laboratory, Chicago, Illinois.
[1] Glendenin, Coryell, and Edwards, paper 52, Vol. 9, Div. IV, Nat. Nucl. En. Series (in press); Phys. Rev. 75, 337 (1949).
[2] L. E. Glendenin, Ph.D. thesis in Chem. M.I.T. (August, 1949); Phys. Rev. 75, 337 (1949).
[3] The Plutonium Project, J. Am. Chem. Soc. 68, 2411 (1946); and also Rev. Mod. Phys. 18, 513 (1946).

P5. Properties of Deuteron and Triton from h.f.s. Measurements. EDWARD N. ADAMS II,* *University of Wisconsin.*—Using Aage Bohr's model[1] of deuterium it is found that there is a contribution to the anomaly in the deuterium h.f.s. due to the small orbital moment of the deuteron. This contribution is of the order $2D/a$ relative to the total h.f.s. contribution of the orbital moment, in which D denotes the radius of the adiabatic region[1] and a the Bohr radius. Estimates of D indicate that this effect may be large enough to provide a new relation between the ^3D probability in the deuteron and the range of the neutron-proton interaction if experimental uncertainties can be reduced somewhat.[2] The adiabatic approximation should be equally valid in the case of tritium, which has no h.f.s. anomaly. For reasonable estimates of D conclusions can be drawn about several possible explanations of the anomaly in the triton magnetic moment.

* AEC predoctoral fellow.
[1] Aage Bohr, Phys. Rev. 73, 1109 (1948).
[2] However, calculations of this effect by Francis Low (private communication) indicate that the adiabatic model may be too crude for accurate calculations.

P6. Relativistic Meson Theory of the Deuteron. S. M. DANCOFF, *University of Illinois.*—The properties of the deuteron have been studied on the basis of scalar and pseudoscalar meson theories in a treatment which considers the nucleons to obey the Dirac equation. Weak coupling was assumed. For separations larger than the nucleon Compton wave-length, the conventional potential expressions are derived in the low velocity limit. Relativistic corrections introduce (1) the "Thomas precession" spin-orbit coupling, first postulated for nuclei by Inglis; and (2) higher order spin-orbit couplings. Spin-orbit coupling energies are invariably characterized by very singular dependences on separation. However, for separations less than the nucleon Compton wave-length, the notion of a point potential energy does not apply; the singular potentials have no significance for this region. Instead one can solve directly for the binding energy of the lowest state; this binding energy is always finite. It remains to be determined to what extent one can account quantitatively for the phenomenological properties of the deuteron with the introduction of a single (coupling) constant. It is interesting that with the relativistic treatment, even the scalar theory permits a qualitative account of all the deuteron properties and is to be discarded, if at all, only on the basis of numerical disagreement.

P7. On Generalized Meson Theories.* ALEX E. S. GREEN, *University of Cincinnati.*—Choosing an approximate deuteron wave function we calculate energy expectation values to show that a generalized, multiple meson, weak coupling theory predicated only upon relativistic pole interactions or non-relativistic dipole interactions is numerically feasible. The closely related fact that our potential function corresponds to a deep spherical well at nuclear ranges suggests the interpretation that the interaction of nucleons is due to the virtual emission and absorption of connected meson complexes (super-particles) or interfering meson waves (a super-superposition). We call attention to a marked confluence of some consequences of recent work by Born and Green,[1] Pauli and Villars,[2] DeBroglie[3] and others with those of our own work despite divergent premises and interpretations.

* A. Green, Phys. Rev. 73, 26, 519 (1948); 75, 1926 (1949); 76, 460, 871 (1949).
[1] M. Born and H. S. Green, Nature 163, 207, 208 (1949).
[2] W. Pauli and F. Villars, Rev. Mod. Phys. 21, 434 (1949).
[3] L. DeBroglie, Phys. Rev. 76, 862 (1949).

P8. Theory of the D+D Reactions: Analysis of the Energy Dependence.* F. M. BEIDUK,** J. R. PRUETT, AND E. J. KONOPINSKI, *Indiana University.*—The variations with energy of the newly extended observations on the D+D reaction products are analyzed. It is found adequate to assume that all these variations, including details of the angular distributions, are due to differences in centrifugal barriers met by different components of the incident deuteron waves. This is found possible only if considerable spin-orbit interaction is allowed for. The possibility is investigated that numerical measures of the interactions can be obtained from the experimental data. Such conclusions as are permitted by the nature of the data are presented.

* Supported in part by Joint Program of the AEC and the ONR.
** AEC Fellow.

P9. Theory of the D+D Reactions: Relation to the Internucleonic Forces.* J. R. PRUETT, F. M. BEIDUK,** AND E. J. KONOPINSKI, *Indiana University.*—The adequacy of current

ideas about the internucleonic forces in accounting for the observations as analyzed in the foregoing abstract is investigated. In particular, the adequacy of the spin-orbit coupling provided by the tensor forces is examined. To this end, a "minimal" formulation of the four-body problem is attempted. The interaction responsible for the reaction is derived. Some order-of-magnitude comparisons with the experimental data are presented.

* Supported in part by Joint Program of the AEC and the ONR.
** AEC Fellow.

P10. Dipole Transitions in the Nuclear Photo-Effect. J. S. LEVINGER AND H. A. BETHE, *Cornell University.*—The G. E. experiments[1] on the cross section and energy dependence of the nuclear photo-effect indicate strong dipole transitions. Using sum rules for dipole transitions, we find agreement with the general features of their experiments. We do not need to assume dipole vibration of the entire nucleus.[2] Exchange forces modify the sum rules.[3] The summed oscillator strength for dipole transitions for heavy nuclei becomes $\Sigma f_{on}=(NZ/A)\times(1+0.8x)$. (Here N is the number of neutrons; and x is the fraction of attractive exchange force.) For $N=Z$, $\int\sigma dW=0.015A\ (1+0.8x)$ Mev-barns. The mean energy for photon absorption is about 20 Mev for pure ordinary forces, and is greatly increased by attractive exchange forces. From another sum rule we show that quadrupole transitions can account for only about 6 percent of the experimentally determined integrated cross section.

[1] Lawson and Perlman, Phys. Rev. **74**, 1190 (1948); Baldwin and Klaiber, Phys. Rev. **73**, 1156 (1948).
[2] M. Goldhaber and E. Teller, Phys. Rev. **74**, 1046 (1948).
[3] Siegert, Phys. Rev. **52**, 787 (1937).

Nuclear and General Theory

S1. Magic Numbers and the Principle of Continuity and Regularity of Nuclear Series. WILLIAM D. HARKINS AND M. POPELKA, *University of Chicago.*—In a series of 24 papers (1915 to 1923) Harkins showed that *the most important of all "magic" nuclear numbers is two for protons and two for neutrons, giving four for nucleons.* This is illustrated by the latest data (Greenstein) which show that *the cosmic abundance of helium is 70 times that of all other elements* (hydrogen excluded). In the building of nuclei from neutrons (protons also for light atoms) the same general stability relations rule as for the naturally radioactive series (except a *general* decrease in stability with increase in mass). If the uranium 238 disintegration series is continued to heavy hydrogen, there are 83 species: only one of these, $_{38}Sr^{90}$, is unstable. In the Helium-Thorium series 85 species are stable: five unstable. No even-even nucleus is stable which does not belong to the He−Th or the H^2-U^{238} series. Of the 173 species in both series each of the unstable six is adjacent to but not at the end of a nuclear shell. The seemingly abnormal existence of $_{20}Ca^{48}$ is due to the magic 20.

S2. The Principle of Continuity as Related to the Existence of Stable Even *N*-Odd *P* and Odd *N*-Even *P* Nuclei. MARTIN POPELKA AND WILLIAM D. HARKINS.—The continuity principle indicates two isotopes each for elements 43 and 61. However, these should not exist in nature, since they are adjacent isobars to stable species: thus elements 43 and 61 do not exist in nature. If all stable nuclear species of odd mass (nucleons) are considered as a single series, an extremely interesting pattern, *very unlike* that for the even-even series, is revealed. When plotted as number of extra neutrons (I) against the number of protons (P) all species arrange themselves in 23 single horizontal steps, which are neither below nor above other steps, except at the end. *Thus there is only one isotope per element except at the end of a step* where the pattern exhibits an increase of I to the next higher odd value, except between $P-44$ Ru and $P=56$ Ba. In the region $P=56$ to 62 the pattern is greatly disturbed by the end of the 82 neutron shell. Here four species adjacent to the 82 neutron shell are missing: 80NLa, 81NCe, 83NCe, 84NPr (N=neutrons).

S3. The Low States of Li^7.* C. H. BLANCHARD AND R. AVERY, *University of Wisconsin.*—Recent measurement[1] shows that the Li^7 quadrupole moment is positive. This result was unexpected since previous theory[2] predicted a negative value. Assuming an s^4p^3 configuration, we find that only one spin and angular dependence for the wave function is consistent with the positive quadrupole moment as well as other known data (spin; magnetic moment; $Be^7\xrightarrow{K}Li^{7*}$, Li^7 lifetime and branching ratio). This wave function, 80 percent D and 20 percent P state, is necessarily very different from the wave function predicted by the previous theory. The validity of the analysis depends on the accuracy of the assumption that the quadrupole moment is due only to the charge distribution of the nucleons, with no contribution arising from their interaction. Similar analysis shows that assigning the s^4p^3 configuration and a spin 5/2 to the 480 Kev excited state is consistent with experimental data ($Li^{7*}\rightarrow Li^7+\gamma$ lifetime; Be^7 K-capture data). The inability of any s^4p^3, spin $\frac{1}{2}$ function to agree with these data is considered further evidence favoring the higher value of the excited state spin.

* Work supported by the AEC.
[1] Kusch, Phys. Rev. **76**, 138 (1949).
[2] Feenberg and Wigner, Phys. Rev. **51**, 95 (1937).

S4. Evaluation of $f_{\pm}(Z, W_0)$ in the Fermi Theory of Beta-Decay.* GEORGE L. TRIGG, *Washington University.*—The values of $f_{\pm}(Z, W_0)$,[1] the integral of the allowed distribution function in Fermi theory of beta-decay, are necessary for the evaluation of the ft product. Since the charts given by Konopinski are inconvenient in form for the interpretation of a large quantity of data, and since their accuracy is not uniform over the entire range of the variables, it was found desirable to calculate the values of f_- itself and plot them as a function of W_0 for values of Z in steps of 10 from 0 to 100 for negatron emitters. For positron emitters the function f_k which plays the analogous part in K- capture theory was also evaluated; the sum and the ratio of f_+ and f_k are plotted as functions of W_0 for Z in steps of 10, from 0 to 80. The mathematical methods used in arriving at the values are discussed, including the Nordheim and Yost[2] approximation and its limitations.

* Assisted by the Joint Program of the ONR and the AEC.
[1] E. J. Konopinski, Rev. Mod. Phys. **15**, 209 (1943).
[2] L. W. Nordheim and F. L. Yost, Phys. Rev. **51**, 942 (1937).

S5. The Interpretation of *ft* Values in the Fermi Theory of Beta-Decay.* EUGENE FEENBERG, *Washington University.*—The ft product in the Fermi theory of beta-decay provides a useful criterion for the classification of radioactive transitions as allowed or forbidden to various degrees.[1] Using f values computed by G. L. Trigg (see preceding abstract) tables have been prepared including all transitions for which the determination of energy, half life and branching ratios is sufficiently complete to permit the calculation of the ft product. Separate histograms have been prepared, for odd and even mass numbers, showing the distribution of $lgft$ values for transitions between ground states. These histograms provide useful information for the study of: (a) the correct covariant formulation of the beta-decay theory and (b), the type of coupling between orbital and spin angular momenta in nuclei.

* Assisted by the Joint Program of the ONR and the AEC.
[1] E. J. Konopinski, Rev. Mod. Phys. **15**, 209 (1943).

S6. Multiple Scattering. MELVIN LAX, *Syracuse University.*—Foldy's[1] treatment of the multiple scattering of waves by isotropic scatterers has been generalized to the case of non-isotropic scattering. The wave function in a medium of

scatterers, averaged over the position of the scatterers, is found, as before, to obey a modified wave equation. The index of refraction and attenuation of the wave in the medium are shown to be determined by the scattering amplitude in the forward direction of a single scatterer. An integral equation is found for $\langle\psi^*(r)\psi(r')\rangle$, a quadratic in the field variables. This integral equation describes incoherent scattering effects. The notation has been generalized sufficiently to describe the scattering of quantized waves.

[1] L. L. Foldy, Phys. Rev. **67**, 107 (1945).

S7. Charge Conjugation in Two Component Wave Equations. HERBERT JEHLE, *University of Nebraska.*—The set of two component equations

$$\gamma^\kappa(\partial/\partial x^\kappa - i\varphi_\kappa)\psi = \mu\psi^*,$$
$$\tfrac{1}{2}(\gamma^\kappa\gamma^\lambda + \gamma^{\lambda*}\gamma^{\kappa*}) = -g^{\kappa\lambda}1,$$

admit the Lorentz group; but not reflections except in the trivial case $\varphi_\kappa = 0$. We abandon the demand of invariance with respect to reflections. The solutions of these equations fall into two classes describing the motion of charges of opposite signs in a given field φ_κ. J. Serpe[1] and C. W. Kilmister[2] have recently commented on the covariance properties of this system, the matrices γ^λ have been extensively studied by O. Veblen several years ago.[3] Serpe showed the relation to Majoranas theory.[4]

[1] Phys. Rev. **76** 1538 (1949).
[2] Phys. Rev. **76**, 568 (1949).
[3] Unpublished manuscript, geometry of two-component spinors.
[4] J. Serpe, Nuovo Cimento **14**, 171 (1937); H. A. Kramers, Proc. Amst. Akad. Sci. **40**, 814 (1937); F. J. Belinfante, Physica **6**, 859 (1939); W. H. Furry, Phys. Rev. **54**, 56 (1938); H. Jekle, Zeits. f. Physik **100**, 702 (1936).

S8. Interaction Representation of General Fields. F. J. BELINFANTE AND J. S. LOMONT, *Purdue University.*—The possibility of a transformation to interaction representation was investigated for the most general first-order Lagrangian field theory in which the identities give the derived variables as uniquely determined sums of products of canonical variables and their derivatives but may contain interaction terms. In order to make the transformed variables ${}^\sigma q(x)$ point functions, it was necessary to let the space-like surface of transformation be tangent at x to the xyz-plane of the Lorentz frame in which $q(x)$ was measured. Also $W(x)$ appearing in the generalized Schrödinger equation $i\hbar c\delta\Psi[\sigma]/\delta\sigma(x) = {}^\sigma W(x)\Psi[\sigma]$ consists of the interaction terms in the Hamiltonian energy-density evaluated in a Lorentz frame "tangent" to σ at x. Under these conditions the integrability of this Schrödinger equation was proved. In interaction representation, in general not the ${}^\sigma q(x)$ form tensor-undors as the $q(x)$ did in Heisenberg representation. Instead, one has to replace the derived variables by new functions obtained by omitting all interaction terms from the identities, while the canonical variables are left unchanged. The new functions thus defined are tensor-undors in interaction representation satisfying field equations without interaction and satisfying the commutation relations for non-interacting fields.

S9. Elimination of the Self-Electromagnetic Field. STUART P. LLOYD,* *University of Illinois.*—A non-quantized Dirac spinor field is in interaction with a classical electromagnetic field. Elimination of the electromagnetic field gives a non-linear equation for the stationary states of the electron wave function. A variational integral is constructed and a four parameter $J = \frac{1}{2}$ spinor is used as a trial function. There is a stationary point and the value $e^2/\hbar c = 0.842^{-1}$ is obtained. The total energy, matter plus coulomb, is negative and works out to be $-0.875\ mc^2$, where m is the coefficient of the matrix beta in the wave equation.

* AEC Predoctoral Fellow.

S10. Relation between *S*-Matrix and Hamiltonian. H. EKSTEIN, *Armour Research Foundation of Illinois Institute of Technology.*—The question has been raised recently whether the scattering potential $V(\mathbf{r})$ is uniquely determined by the S-matrix, and has been answered in the affirmative[1] for the case of a central force. An extended result, without restriction to central forces, can be obtained as follows: For sufficiently large particle momentum $\mathbf{k}_0$, the R-matrix element is, by Born's approximation, proportional to $(\mathbf{k}'|V|\mathbf{k}^0)$ which is a function of $(\mathbf{k}'-\mathbf{k}^0)$ only. By joining two points of the surface $k'^2 = k^{02}$, one can obtain any value of $(\mathbf{k}'-\mathbf{k}^0)$ and therefore, V is fully determined by the knowledge of the *asymptotic* form $(|\mathbf{k}^0|\to\infty)$ of the S-matrix. This argument holds also for many-particle scattering and for relativistic equations. The observation that the asymptotic values of the S-matrix fully determine the potential has the implication that an arbitrarily chosen S-matrix will in general be incompatible with the existence of a potential. When the Hamiltonian is of a more general form, it cannot be shown that the asymptotic values of the S-matrix determine *all* values of the interaction Hamiltonian, but there will still be severe restrictions on the S-matrix if it is to be compatible with a Hamiltonian.

[1] V. Bargmann, Phys. Rev. **75**, 301 (1949); Rev. Mod. Phys. **21**, 488 (1949).

S11. Free Vibrations of An Isotropic Cube. T. SCHIFFMAN AND H. EKSTEIN, *Armour Research Foundation of Illinois Institute of Technology.*—Approximate solutions for free vibrations of an isotropic cube are derived by the perturbation method.[1] The modes are classified by group theory. Three rigorous degenerate modes are known.[2] Three longitudinal plane waves in the X, Y, and Z direction, respectively, are also solutions for the case of zero Poisson's ratio. These six functions are used as "zero order" modes. The operations of the cubic group are applied to these six zero-order eigenfunctions and the linear combinations which are the basis for the irreducible representations are determined. The modes are found to belong to the A_1, A_2, and $2E$ irreducible representations,[3] exhibiting the symmetric "breathing" mode, one rigorous mode belonging to A_2, two rigorous and two coupled modes belonging to the two-dimensional irreducible representation. Thus, the triple degeneracy is accidental. The corresponding frequencies are functions of Lamé's constants, λ and μ:

$$\rho\omega_1^2 = 2\mu k^2\left(1+\frac{\pi^2+16}{\pi^2}\frac{\lambda}{2\mu}\right), \quad \rho\omega_{2,3,4}^2 = 2\mu k^2,$$

$$\rho\omega_{5,6}^2 = 2\mu k^2\left(1+\frac{\pi^2+4}{\pi^2}\frac{\lambda}{2\mu}\right),$$

where $k \equiv \pi/\text{length of edge}$.

[1] H. Ekstein, Phys. Rev. **66**, 108 (1944); **70**, 76 (1946).
[2] H. Mähly, Helv. Phys. Acta **19**, 412 (1946).
[3] Notation as in Eyring, Walter, and Kimball, *Quantum Chemistry* (1944).

Apparatus of Nuclear Physics; Crystal Counters

T1. The Illinois Cyclotron Oscillator. G. F. TAPE AND P. G. KRUGER, *University of Illinois.*—The 11-mc oscillator now in operation on the University of Illinois cyclotron was chosen for simplicity of components and operation and for flexibility in changing frequency when changes of energy from the cyclotron are desirable. Two type 880 power triodes are self-excited in push-pull operation. Following general designs of the Pittsburgh and M.I.T. oscillators, each tube is mounted directly over a concentric dee line. The inductive coupling loop feeding the dee line is connected directly to the plate of the tube. The two grids are coupled together by a single inductance coil. Thus the tank circuit of the oscillator is effectively the resonant circuit of the cyclotron and power is transferred without

transmission lines. Water-cooling of tubes and loops is simplified by operating the plates at d.c. ground and leading the water in and out on the r-f ground side of the loops. The r-f measurements have shown the cold resonant frequency of the grid circuit to be about 1.3 mc above the operating frequency. Operation has shown that for reliable starting and for riding through load changes (gas bursts in the chamber) a large grid drive is necessary.

T2. The Pole Tips on the Carnegie Institute of Technology Cyclotron Magnet. MARTIN FOSS, *Carnegie Institute of Technology.*—The pole tips on the Carnegie Institute of Technology cyclotron magnet have complex contours, the surfaces of which near the outside radius have a series of ridges and valleys which rise above and below the average position. This structure enables the magnet to produce a higher energy proton beam than would otherwise be possible in a magnet with the same yoke, pole base, and coil. The scheme was suggested by the solution of a series of two-dimensional problems and the actual contour was determined by a cut-and-try procedure in which the field was measured to one-one-hundredth percent. Recently, a three-dimensional method for determining the potential associated with a given field has been developed. This may be applied to the design of poles for β-ray spectrographs or other apparatus. This work was supported by the ONR.

T3. Voltage Stabilizer for Electrostatic Generator. W. C. MILLER, B. WALDMAN, J. C. NOYES,* AND J. E. VAN HOOMISSEN, *University of Notre Dame.*—The use of a tank liner (i.e., insulated shield enclosing entire column and terminal assembly) to stabilize the potential of an electrostatic generator has been suggested by several workers in this field. A partial liner has been installed in the Notre Dame generator. This liner is an aluminum cylinder eight feet long of four-foot radius, coaxial with the high voltage terminal, and is mounted between the terminal and tank. It is supported at a distance of two inches from the tank wall by Mykroy insulators. Because of the capacitive coupling between linear and terminal, a change of potential of the liner induces a proportional change in the potential of the terminal. The potential of the liner can be varied rapidly from 0 to 30 kv by an r-f-type power supply. This induces a change in the potential of the terminal of approximately 15 kv. An error signal from a generating voltmeter controls this power supply. Preliminary results indicate that a stability of better than ± 5 kv can be obtained with this method. This work has been partially supported by the Joint Program of the ONR and AEC.

* AEC predoctoral fellow.

T4. The Use of Selenium Rectifiers in a 500-Kev Generator. W. R. ARNOLD, *State University of Iowa.*—A 500-kilovolt linear accelerator recently placed in operation is described. This voltage is obtained by the use of a voltage multiplier circuit using selenium rectifiers and one-microfarad condensers in 22 stages. The input is nine kilovolts at 750 cycles, and the peak inverse voltage across each rectifier and condenser is 25 kilovolts. Because of the large condensers and relatively high frequency, the ripple should be less than 0.2 percent and the regulation appears to be quite good in spite of the large multiplication (44 times). The generator is capable of handling a one-to-two-milliampere total beam. The large number of stages allows use of lower voltage condensers and a series of constant voltage points to tie into an accelerating tube which eliminates the usual corona gaps.

T5. Fast Neutron Detector. W. G. MOULTON AND C. W. SHERWIN, *University of Illinois.*—A simple fast neutron detector suitable for health physics applications has been constructed using two 931A photo-multiplier tubes in coincidence to reduce background. A "sandwich" made of Lucite and activated zinc sulfide is used to produce scintillations. The efficiency for fast neutrons from a Ra-Be source is 1.5 ± 50 percent $\times 10^{-4}$. It detects a fast neutron flux of 20 neutrons/cm^2 sec. with a counting rate that is over ten times background. The counter has the advantage that by proper choice of discriminator bias it may be rendered essentially insensitive to gamma-radiation without an appreciable decrease of the neutron efficiency.

T6. Measurement of Fast Neutron Energies by Observation of $Li^6(n, \alpha)H^3$ in Photographic Emulsions. GEORGE R. KEEPIN, JR. AND JAMES H. ROBERTS, *Department of Physics, Northwestern University.*—A new technique of neutron energy measurement not requiring neutron collimation is described. The method employs the nuclear reaction $Li^6(n, \alpha)H^3$ (Q 4.64 Mev) observed within photographic emulsions impregnated with enriched Li^6. Results on monoenergetic neutrons indicate a resolution of at least ± 0.1 Mev in the region studied (from thermal energies up to 1.3 Mev). For this resolution, good discrimination between the alpha-particle and triton tracks is required. To extend the method for use as a precision neutron spectrometer suitable for continuous neutron spectra, both the excitation function and the angular distribution of the Li^6 disintegration process should be known. For immediate practical application both these measurements might be circumvented by calibrating the method with a well-known spectrum. The Li^6 method is particularly well suited to energy measurements on neutrons within a material medium where perturbations introduced by the detector must be minimized and where collimation is clearly impossible.

T7. Space-Charge Effects in Diamond Conduction Counters.* R. K. WILLARDSON, A. C. DAMASK, AND G. C. DANIELSON, *Iowa State College.*—The accumulation and removal of space charge in diamond counters has been investigated by McKay and by Newton for electron bombardment and by Ahearn for alpha-particle bombardment. Space-charge effects for bombardment of diamonds with gamma-rays have been suggested by Hofstadter. We have investigated in some detail the variation in counting rate of several diamonds which count not only alpha-particles but also cobalt^{60} gamma-rays. Prior to the usual decrease in counting rate attributed to negative space charge from trapped electrons, we observe a conspicuous increase in counting rate which we interpret in terms of an accumulation of positive space charge. This effect is observed when counting gamma-rays, but has not been observed when counting alpha-particles. With increasing bombardment time the deeper traps become occupied. This is indicated by a decreasing counting rate recovery when the source is periodically removed. The space charge is removed by irradiation with red light when using a gamma-source. This has been observed by Chynoweth using alpha-particles. New effects are observed with violet light.

* This work was performed in the Ames Laboratory of the AEC.

T8. Efficiencies of Calcium Tungstate and Calcium Fluoride as Scintillators for Low Energy Electrons.* WALDO RALL** AND R. G. WILKINSON, *Indiana University.*—Natural polished calcium tungstate crystals from Kern County, California, and synthetic calcium fluoride crystals from Harshaw Chemical Company were tested for their low energy response to beta-rays. A commercial 5BP1 tube was mounted in a vacuum system as an electron gun which could accelerate electrons up to 5600 volts. The electron beam which was operated between 10^{-10} and 10^{-12} ampere was monitored by passing it through an electrometer grid of about ten percent transmission placed just in front of the crystal. The 1P28 photo-multiplier tube was operated at -600 volt, which was also the potential

placed on a secondary electron guard ring for the electrometer grid. Curves will be shown giving pulse-height distributions and efficiencies from 500 to 5600 volts. The absolute efficiencies are probably accurate within 50 percent, the relative efficiencies within 20 percent. The integral bias curves are logarithmic over three orders of counting magnitudes. The efficiencies for 5000-volt electrons are 10^{-4} and 5×10^{-4} for calcium fluoride and calcium tungstate, respectively, for pulses >120 microvolts.

* Supported by the ONR.
** Now at Yale University.

T9. Response of an Anthracene Counter to Monoenergetic Electrons of Energies 1.4, 2.2, and 2.6 Mev.* JAMES F. NORTON, *University of Rochester* (*Introduced by S. W. Barnes*).—By means of magnetic analysis a beam of monoenergetic electrons was obtained from a Sr+Y source. Curves of counting rate *versus* pulse height were measured for electron energies of 1.4, 2.2, and 2.6 Mev with a clear anthracene crystal of dimensions $\frac{3}{4}$ in. diam.$\times\frac{1}{4}$ in. The scintillations were detected with a 1P21 photo-multiplier. The curves showed plateaus in all cases. The existence of a plateau and the value of the pulse height cut-off indicate uniformity and proportionality of the response. Such curves will be shown.

* Supported in part by the ONR.

T10. Proportional Counter Spectrometer.* C. J. BORKOWSKI AND E. FAIRSTEIN, *Oak Ridge National Laboratory*.—The use of a proportional counter with high gas amplification for the determination of beta- and x-ray energies[1-3] has been used to examine the beta-ray spectra of C^{14}, S^{35}, Tm^{171} all of which have been previously examined with magnetic lens beta-ray spectrometers. The proportional counter used in this study was designed to give 50 percent geometry for solid samples. A sweep-type differential discriminator automatically plots the differential curve on a Brown recorder chart. The width at half-maximum of photo-electron peaks produced by 6.9-Kev x-rays is 17 percent. This resolution allows one to "resolve" adjacent elements in this part of the periodic table from their K x-rays.

* This document is based on work performed under contract for the AEC at Oak Ridge National Laboratory.
[1] C. J. Borkowski and E. Fairstein, "The use of a proportional counter for low energy beta-measurements," MonN-311, Oak Ridge National Laboratory Progress Report, March 1947.
[2] Curran, Angus, and Cockroft, Nature 162, 302 (1948).
[3] Kirkwood, Pontecorvo, and Hanna, Phys. Rev. 74, 497 (1948).

T11. Scintillation Studies on Potassium Iodide. M. FREEDMAN, B. SMALLER, AND J. MAY, *Argonne National Laboratory*.—Scintillation studies have been conducted on the effect of thallium impurity on the fluorescence properties of potassium iodide. Coincidence techniques have demonstrated the presence of single photon emission as expected from electron trapping at impurity sites. It has been possible to distinguish between the characteristic radiation due to the impurity and the fundamental or lattice radiation from the pure potassium iodide crystal. The fluorescence efficiencies of both types of emission have been determined as a function of temperature. Measurements of the K^{40} radioactivity in the crystal result in the values $\lambda(\beta)=3.92\times10^{-10}$ per year and $\lambda(\gamma)/\gamma(\beta)\cong0.04$. Comparison of pulse-height distribution with that from Cs^{137} activity gave a provisional $E_{max}(\beta)\cong1.3$ Mev.

Semiconductors; Miscellany in Electron Physics

U1. Mobility of Electrons and Holes in Germanium. W. C. DUNLAP, JR., *General Electric Company*.—In a previous paper[1] the author presented results of a study of the conduction properties of high purity germanium. These measurements have been extended to cover samples from about three hundred ingots of germanium. Mobility values (R/ρ) as high as 4000 cm³/volt sec. have been found for N type single crystals. Values as high as 3000 have been found for P type single crystals. These values are higher than those of Lark-Horowitz *et al.*, and of Pearson. It was found that higher Hall coefficients were obtained when point pressure contacts were used than when broad soldered or plated contacts were used. It was noted that high purity germanium annealed at 500–550°C has usually a low mobility figure (R/ρ), and thus is inhomogeneous, probably possessing a fine intermixture of N and P regions. It is also pointed out that the conduction properties of germanium also vary with time, and that the apparent mobility often decreases somewhat with time, even at room temperatures. It is concluded that only a lower limit on the mobility can be given from present Hall effect data.

[1] W. C. Dunlap, Jr., Phys. Rev. 71, 471 (1947).

U2. Resistivity of Germanium Samples in External Magnetic Fields at Various Temperatures and Orientations.* A. FONER AND I. ESTERMANN, *Carnegie Institute of Technology*.—The effect of magnetic fields on the resistivity of isotropic conductors was first investigated by Gans[1] on the basis of a Maxwell-Boltzmann energy distribution for the conducting particles. In contrast to metals, the density of conducting particles in reasonably pure semiconductors is so low that they may be treated in accordance with classical statistics. Experiments were carried out with N and P type germanium samples at various temperatures between 20 and 300°K and with different angular orientations between electric and magnetic fields. In the case of a P type sample, the change in resistance as function of field strength and orientation was in fair agreement with theoretical results. The hole mobility was calculated to 1900 cm²/volt-sec. which is higher than calculated from Hall constant and conductivity, but in good agreement with Pearsons[2] value for single crystals. In N type samples, the observed effect is always several times larger than calculated, and does not disappear for longitudinal orientation. According to unpublished calculations by Seitz, the inclusion of anisotropic terms could produce the additional increase in resistance in all orientations.

* This work is supported by the ONR.
[1] R. Gans, Ann. d. Physik 20, 293 (1906).
[2] G. L. Pearson, Phys. Rev. 76, 179 (1949).

U3. The Reflectivity of Germanium Semiconductors. K. LARK-HOROVITZ AND K. W. MEISSNER, *Purdue University*.—The reflectivity of germanium alloys of the N type (electron conductor) and P type (hole conductor) has been investigated. Samples with a small number of carriers ($\sim10^{16}$/cm³) and with high impurity content ($\sim5.10^{18}$/cm³) were used.

In the range from 0.6μ to 12μ a rocksalt spectrometer and a Nernst filament as a radiation source were used. The semiconductor sample was mounted in exactly the same plane as a comparison aluminum mirror and the reflectivity determined for various settings of the spectrograph expressed in terms of the reflectivity of the aluminum mirror. Between 0.6μ and 0.8μ the reflectivity of all the samples is between 47 percent and 51 percent. The reflectivity then decreases and remains almost constant about 35 percent up to about 40μ. In the range from 8.7μ to 152μ the method of residual rays was used. Radiations selected from the incident continuous radiation with wave-length $\lambda=8.70\mu$, 20μ, 30μ, 41μ, 52μ, 117μ, and 152μ were employed. The highly conducting samples show a high reflectivity at 117μ which decreases again at 152μ, but is still considerably higher than the reflectivity of the high resistance samples which remains essentially constant through the whole wave-length range.

U4. Dependence of the Germanium High Back Voltage Rectifier Resistance on Frequency.* R. BRAY AND H. J. YEARIAN, *Purdue University.*—Germanium high back voltage rectifier units show anomalously poor rectification at high frequency. Detailed investigation,[1] involving measurement of the rectified d.c. current for voltages of frequencies from 60 cycles to 60 mc showed the forward resistance to increase with frequency f, for $f \lesssim 100$ kc. The effect is small at low voltage, increases with voltage and becomes almost constant above 0.6 volts r.m.s. where predominantly spreading resistance determines the current. The effective back resistance at 1000 cycles and 30 mc were compared. It was found to be lower at 30 mc only when there was a forward swing to the applied voltage, otherwise it was higher. An interpretation is suggested in terms of the motion in the high frequency field of the holes injected into the germanium from the point contact. Thus for $f \lesssim 2/\tau$, (τ is lifetime of the holes), a decrease in the depth of penetration of the holes results which increases the spreading resistance. The back resistance can be decreased by the return to the contact, and the collection there, of the holes injected during the forward swing of the voltage.

* Work partially assisted by Signal Corps Contract.
[1] H. J. Yearian, "Dependence of forward conductance and back resistance of high back voltage germanium on voltage and frequency," NDRC Report (October 1945).

U5. Infra-Red Transmission of Germanium and Silicon.* M. BECKER AND H. Y. FAN, *Purdue University.*—In the investigation of photoelectric effects in germanium, it was found that these effects can still be observed when a piece of silicon or germanium several millimeters thick is interposed in the incident beam. This shows that infra-red transmission or absorption can be measured on bulk material instead of being measured on thin films or deduced from reflection measurements. Transmission measurements were made on germanium and silicon using slabs of thicknesses up to 15 mm. Germanium shows very little absorption from 12μ to 2μ, the transmission being determined primarily by reflection. The absorption coefficient is between 0.1 and 1 cm^{-1} for samples of resistivity $\rho \sim 5$ ohm cm and between 1 and 10 cm^{-1} for samples $\rho \sim 0.015$ ohm cm. It rises sharply at 2μ toward short wave-length. The absorption coefficient of silicon ($\rho = 0.03$ ohm cm) shows a minimum $\mu \sim 15$ cm^{-1} around 1.2μ at room temperature. It rises sharply toward short wave-length and more gradually toward longer wave-length. Measurements of silicon have been extended from liquid nitrogen temperature to 400°C. The absorption increases with increasing temperature with the minimum shifting toward longer wave-length. The reflecting power for polished surfaces is 0.35 for germanium and 0.27 for silicon.

* Assisted by a Signal Corps Contract.

U6. Resistivity at Boundaries Between Crystallites in Semiconducting Materials. V. A. JOHNSON, *Purdue University.*—It is found that the observed electrical resistivities of pure tellurium[1] samples and some silicon[2] samples at low temperatures are not accounted for theoretically[3] by the combination of only resistivity due to lattice scattering and resistivity due to impurity scattering. It is apparent, for these samples, that there exists an additional source of scattering characterized by a mean free path almost independent of temperature. An earlier study by Goodman[4] has described scattering of electron waves at crystallite boundaries as a source of electrical resistivity; this process is characterized by a mean free path dependent upon crystallite size and independent of temperature. The combination of such a resistivity due to scattering at crystallite boundaries with resistivities due to lattice and impurity scattering removes the discrepancy between theory and experiment mentioned above.

[1] Virgil E. Bottom, Phys. Rev. **75**, 1310 (1949).
[2] K. Lark-Horovitz, Contractor's Final Report, NDRC 14-585 (November, 1945), pp. 57-61.
[3] K. Lark-Horovitz and V. A. Johnson, Phys. Rev. **69**, 258 (1946).
[4] B. Goodman, NDRC Div. 14 Report, University of Pennsylvania (April 25, 1945).

U7. Dielectric Breakdown in Simple Non-Polar Crystals.* W. R. HELLER, *Washington University.*—A treatment of the interaction of conduction band electrons with atomic lattice vibrations shows that breakdown in non-polar crystals may be grouped into three classes, A, B, C. Ideal crystals (with a relatively small number of shallow trapping centers) compose classes A and B, according as $\hbar^2/8m\lambda_{min}^2 \lesssim I_{cr}$ where λ_{min} is the minimum wave-length of the sound quanta, and I_{cr} is the energy separation between the top of the filled band and the lowest conduction level. Class A is analogous, as regards breakdown criterion, to the ideal polar crystal treated by Frohlich, and permits the definition of only a lower limit to the actual breakdown field, F_A. Class B allows derivation of an actual breakdown field, F_B, but occurs only infrequently. Class C includes crystals in which impurities and lattice defects act as important ionizable centers (energy $I_i < I_{cr}$) and also yields (if only one type of trap is present) a unique breakdown criterion, F_C. As an example, a clear diamond (without absorption bands in the visible $-I_{cr} = 4.1$ volts) and with centers of mean depth 0.75 volt should reach F_A at 136,000 volts/cm and F_C at 88,000 volts/cm, independent of temperature for $T \ll T_{Debye}$, the physical reason for the inequality $F_A > F_C$ being apparent from the theory.

* This work was done under the tenure of an AEC pre-doctoral fellowship and assisted by the Joint Program of the AEC and the ONR.

U8. Multiple Scattering of Electrons in Argon.* FRED L. RIBE, MARTIN J. BERGER AND GERHART GROETZINGER, *University of Chicago.*—The multiple scattering of electrons with energies from 50 to 1700 kev in one atmosphere of argon was measured by means of a magnetic cloud chamber. 132 tracks with a total path length of 1800 cm were examined. For each individual track the angles between successive chords connecting points two centimeters apart along the track were measured and from the mean and the mean square of these angles the most probable momentum and mean square angle of multiple scattering were determined. The experimental multiple scattering (as a function of the momentum) obtained from the measurement of the 132 tracks was compared with that predicted by the theories of (a) Bothe, (b) Williams, (c) Saunderson and Goudsmit, (d) Molière, and (e) Snyder and Scott. Theories (d) and (e), as well as (b) if an available parameter is suitably adjusted, give a root mean square angle of multiple scattering which agrees fairly well with that found by us. The maximum deviations (at the endpoints of the momentum range investigated) do not exceed 2.5 times the probable experimental error (~10 percent) while over most of the momentum range the agreement is within the limits of the experimental error.

* Assisted by the Joint Program of the ONR and the AEC.

U9. Radiation Transients in Brief Gas Discharges. R. G. FOWLER, JACK S. GOLDSTEIN, R. J. LEE, AND B. E. CLOTFELTER, *University of Oklahoma.*—Abrupt discharge of a condenser through a gas has been investigated for effects of the type described by Rayleigh.[1] The discharge tube used was in the form of a T, with electrodes at the ends of the top. Subsequent to the discharge ($\sim 10^{-7}$ sec.) fronts of excitation and ionization have been detected passing down the stem of

the T at velocities up to 2×10^6 cm/sec., and advancing up to 10 cm. Behavior of these fronts indicates strongly that they have the nature of powerful shock waves. Examination of the radiation emitted when hydrogen gas is used shows the Balmer line series and Balmer continuum in about equal intensities. Experiments show that the Balmer continuum is emitted within 10^{-7} sec. of the emission of the Balmer line series, and co-spatially. It is concluded that rapid recombination acts may precede the emission of the line spectrum.

[1] R. J. Strutt (Lord Rayleigh), Proc. Roy. Soc. **183**, 26 (1944–45).

U10. On the Use of Coaxial Lines to Produce and Measure Short Time Delays.* DONALD C. MOORE AND WILLARD A. REENSTRA,** *Rensselaer Polytechnic Institute.*—Coaxial lines have been used as delay elements and pulse delays of 2.5×10^{-9} second have been produced and measured. Negative pulses of approximately 2.5×10^{-8} second in length and with an amplitude of 100 volts were generated with the discharge of a thyratron into a delay line with its end open circuited. These pulses were narrowed still further by clipping all but their extreme negative point with a biased germanium diode (1N48). These signals were then sent through two coaxial lines (RG 63-U) to a Rossi coincidence circuit and a coincidence was detected with a discriminator circuit. By measuring the difference in delay line necessary to produce or lose coincidence, it is possible to find the inherent resolving time of the circuits for pulses of such a shape. Some of the possibilities and limitations of the circuit as an instrument for the measurement of actual time delays will be discussed.

* Supported by the Rensselaer Polytechnic Institute Research Fund.
** Now at the Bell Laboratories, New York City.

U11. Electron Dynamics in a Standing Wave Accelerator. GERALD HOFFMAN AND EDWARD AKELEY, *Purdue University.*—The axial motion of an electron in a standing wave accelerator will be given by

$$du/dx = A\{\cos(t-x/V)+\cos(t+x/V)\},$$

and an equation for dt/dx. x represents the position of electron on axis, t time, u relativistic kinetic energy and V a mean wave speed. Certain natural units are used and A is a dimensionless constant proportional to longitudinal component of electric field strength. A synchronous particle is defined and the deviations of u and t as functions of x for an actual particle from those of the corresponding synchronons one are expressed as power series in the initial values of these deviations. The first- and second-order coefficients, expressed as power series in A have been computed through their second-order terms. This expansion makes possible a discussion of the energy and time distribution of those particles whose orbits do not differ too much from the synchronons. Graphs of u and t as functions of x have been obtained for the Purdue accelerator.

Papers Not Classed Elsewhere

V2. Time Delays for Plastic Flowing. JOHN KAUFFMAN AND WALLER GEORGE, *Naval Research Laboratory.*—Under suitable conditions, appreciable time intervals are observed between the application of a load and the response of a solid to this load by plastic flowing. These time intervals are termed delay times, and appear to have been first systematically studied by Clark and Wood in mild steel.[1] The phenomenon will be demonstrated in polymeric films. The delay time in Nylon films is found to vary slowly with applied stress, from 1 to 10^3 sec. for stresses between 4400 and 3000 p.s.i., with an apparent activation energy of about 120,000 cal./mole. Similar effects are found in polyethylene films. Under dead-weight loading, the flowing appears after the time delay, as one or more severe localizations or "necks" which, in turn, propagate slowly along the specimen with the evolution of heat. The macroscopic phenomenological similarities between delay times in mild steel and high polymers will be discussed.

Note added in proof.—P. W. Bridgman has pointed out to one of us (JK) his earlier report of similar time delay effects in highly alloyed steels under combined compressive loads; see J. App. Phys. **17**, 225 (1946).

[1] D. S. Clark and D. S. Wood, Proc. A.S.T.M. Preprint No. 25 (June, 1949).

V3. Multiple Diffuse Small Angle Scattering of X-Rays.* D. L. DEXTER AND W. W. BEEMAN, *University of Wisconsin.*—The problem of multiple x-ray scattering from spherical particles of radius much larger than the wave-length ($a/\lambda\sim10^2$ or 10^3) is treated using the Guinier approximate scattering function.[1] The total coherently scattered intensity is found to be a sum of Gaussians in the polar angle with coefficients dependent on the sample thickness. A method is discussed for determining particle sizes from the variation of the width of the scattering curve with sample thickness in the region of high multiplicities ($\lesssim10$). Experimental radii of Godfrey L. Cabot P-33, Sterling L, and Spheron Grade 6 carbon blacks are 770, 480, and 180A, respectively. The results for P-33 and Grade 6 are in better agreement with weighted average radii obtained from nitrogen adsorption and electron-micrograph data[2] than with sizes obtained from the usual log of intensity *versus* angle squared curves. This method may be useful for particles too large to be treated by standard single scattering techniques.

* Assisted by the ONR and the Wisconsin Alumni Research Foundation.
[1] A. Guinier, Ann. de physique **12**, 161 (1939).
[2] Anderson and Emmet, J. App. Phys. **19**, 367 (1948).

V4. Direction-of-Fall of Sedimenting Particles. E. E. MILLER AND C. B. TANNER, *University of Wisconsin.*—Kunkel has recently reported[1] that unsymmetrical particles drift to one side in falling through viscous media. Such behavior would invalidate most sedimentation methods of determining particle-size distributions. Since Kunkel used only a few special shapes and was concerned with charge-analysis of dusts, a simple experiment was devised for testing naturally occurring particle shapes. A continuous but dilute stream of particles was injected from a point at the top of a motionless, thermally stabilized body of water. After some hours of operation, the accumulation of particles on the bottom of the container was examined. Qualitatively, it was noticed that most natural particles actually do plane to one side when falling, but at the same time they rotate. The result is a small regular spiral about a vertical axis. Quantitatively, the experiment showed that sideward drifts can be neglected for normal sedimentation equipment. Soil samples showed less dispersion than powdered mica, which suggests a possible method for shape-factor analysis.

[1] W. B. Kunkel, J. App. Phys. **19**, 1056 (1948).

V5. Some New Techniques in the Calorimetry of Solids,* MALCOLM DOLE, JOHN A. WETHINGTON, JR., NORMAN LARSON AND W. P. HETTINGER, JR., *Northwestern University.*—In setting up an apparatus for the measurement of specific and latent heats and heats of transition of solid high polymers we have been led to develop an automatic device for adiabatic temperature control which may be of interest to workers in the field of calorimetry. We also make use of a special watt-hour meter for the estimation of the electrical energy input which

simplifies the operation of the equipment. The introduction of continuously recording potentiometers enables us to correct the observed rises in temperature for any inequality in temperature between the calorimeter and its adiabatic jacket. Furthermore, our automatic equipment not only makes possible a quantitative study of the effect of gas pressure and other factors on the temperature drifts of the calorimeter with time, but also is especially adaptable to the measurement of slowly occurring heat effects. We hope to present a short moving picture sequence of the calorimeter apparatus in actual operation.

* This work was aided by grants from the Visking Corporation, the Rayon Technical Division of the E. I. Du Pont de Nemours and Company, The Richardson Company, and the Research Corporation (Frederick Gardner Cottrell Grant). R. C. Wilhoit and A. E. Worthington assisted in some of the measurements.

V6. Distribution of Phases in Two-Phase Solids. LEONARD D. JAFFE, *Watertown Arsenal.*—The quasi-equilibrium distribution of a disperse phase, B, within a polycrystalline second phase, A, is investigated by methods of statistical thermodynamics. Phase B is assumed to consist of spherical particles of uniform size within the A crystals, and of lenticular particles of uniform size at the boundaries between two A crystals. The concentration (Mf) of B at the grain boundaries of A is found to be related to the sizes (r_1 and r_2) of the B particles at and away from grain boundaries, in terms of the interfacial energies (γ_{aa} and γ_{ba}), the temperature (T), the over-all concentration (M), and the size of the A crystals (R), by

$$\left(\frac{Mf}{1-Mf}\right)\left(\frac{Mw}{1-Mw}\right)^{-r_1^3/r_2^3} = \exp\left\{-\frac{\gamma_{aa}r_1^2}{kT}\left[\frac{9\pi Z-\left(\frac{9\pi}{2}\right)^{\frac{1}{2}}(3Z^3+2\pi)\frac{r_1}{r_2}}{3Z^3-4\pi}\right]\right\},$$

where

$$w=1-\frac{2.66fr_1}{R\left(Z-\frac{\pi}{3}Z^{-2}\right)} \quad \text{and} \quad Z=\left[\frac{2\pi\left(4\frac{\gamma_{ba}}{\gamma_{aa}}+1\right)}{3\left(2\frac{\gamma_{ba}}{\gamma_{aa}}-1\right)}\right]^{\frac{1}{3}}.$$

Temperature will significantly affect the distribution only if $\gamma_{aa}r_1^2$ is of the order of kT, or if $\gamma_{ba}/\gamma_{aa}\sim\frac{1}{2}$.

V7. Thermodynamic Functions of Crystals from the Moments of the Frequency Distribution.* WILLIAM J. TAYLOR, *The Ohio State University.*—Montroll[1] has proposed the expansion in Legendre polynomials of the distribution function $g(\nu)$ for the frequencies (ν) of normal modes of vibration of a crystal, and has related the coefficients of the expansion to the even moments of $g(\nu)$. This expansion has the disadvantage that in practice, when only a few terms of the series are retained, a non-vanishing value will in general be obtained for $g(0)$, whereas for all crystals $g(\nu)$ must approach the Debye form, $g(\nu)\propto\nu^2$, for small ν. This difficulty may be overcome in a simple way by expanding the quantity $\nu^{-2}g(\nu)$ in even Legendre polynomials; the coefficients then involve also the second *inverse* moment of $g(\nu)$. Substitution of this expansion in the definite integral defining a thermodynamic function (integrand a product of $g(\nu)$ by an Einstein function), yields a convergent series of functions (of temperature) with coefficients depending on the moments of $g(\nu)$. The first of these functions is the familiar Debye function—a point in favor of the modified expansion proposed here. Tabulation of succeeding functions will make possible the calculation of higher order corrections to the Debye value directly from the moments of $g(\nu)$.

* This work was supported in part by the ONR under contract with the Ohio State University Research Foundation.
[1] E. W. Montroll, J. Chem. Phys. 10, 218 (1942); 11, 481 (1943); 12, 98 (1944).

V8. A New Piezoelectric Effect? A. E. BENFIELD, *Harvard University.*—It seems likely that a stress gradient in a metal will produce a small separation of the electric charge in its interior, and a consequent small potential gradient, in a manner somewhat similar to that caused by a temperature gradient in the Thomson effect of thermo-electricity. Attention is drawn to this, and to the possibility of measuring it, since the effect does not seem to have been directly observed. Its existence has recently been predicted theoretically[1] by considering the maximum energy of the electrons in the Fermi-Dirac gas of a metal under appreciable hydrostatic compression. P. W. Bridgman, in measuring the Peltier heat between a number of compressed and uncompressed metals,[2] has apparently studied a closely related effect. The observed values of the Peltier heat are, however, many times smaller than would be expected from the above-mentioned theory; it is not entirely clear to what extent the observations correspond with the ideas presented here.

[1] A. E. Benfield, Phys. Rev. 75, 211 (1949).
[2] P. W. Bridgman, Proc. Am. Acad. 53, 269 (1918).

V9. Characteristics of Piezoids with Surfaces of Cylindrical Shape.* CHARLES R. MINGINS, CARL A. STEVENS, AND ROBERT W. PERRY, *Research Laboratory of Physical Electronics, Tufts College.*—In a previous paper[1] was described a method of studying the vibrational characteristics of a piezoid by a method of probing, employing the response spectrometer developed in this laboratory several years ago.[2] The work previously reported involved quartz plates with surfaces of spheroidal shape, with the vibrational effects of which this laboratory has been concerned for some time. The investigations presently discussed concern plates having major surfaces which are cylindrical in shape, wherewith something of the anatomy of surface shape influences can be studied. It is found that the 1,1,3 and 1,3,1 modes of the thickness-shear family can be placed in radically different spectral positions relative to each other and to the main response, and by varying the orientation of the cylinders further unusual effects can be obtained, such as the inhibiting of certain flexures and the selective use of portions of the plate.

* This work is sponsored by the Frequency Control Branch of the Signal Corps.
[1] Mingins, Stevens, and MacLeod, Phys. Rev. 76, 467 (1949).
[2] C. R. Mingins *et al.*, Reports to U. S. Army Signal Corps (1944 ff.).

V10. Measurement of Small Curvatures by Optical Interference.* HAROLD R. LETNER, *Mellon Institute.*—The curvatures of nearly flat, specularly reflecting surfaces can be measured with good precision by means of optical interferometry. A simple instrument for producing and photographing the interference patterns is described and a method of obtaining highly magnified profiles of the surface directly from the resulting photographic negatives is illustrated. The method is applicable to the study of residual stresses of the type encountered in: (1) machining, grinding, lapping, honing, or shot-peening; (2) heat treatment; (3) differential thermal expansion; (4) electrodeposition; (5) shrinkage of protective coatings; (6) polymerization of plastic films.

* A contribution from the L. Leslie Byers Memorial Fellowship sustained at Mellon Institute by the Grinding Wheel Institute.

SUPPLEMENTARY PROGRAMME

SP1. Electrostatic Potential Energy of Crystals and Molecules from X-Ray and Electron Diffraction Data.* WILLIAM J. TAYLOR, *The Ohio State University.***—Methods for calculating the electrostatic potential energy of ionic crystals have been developed by Madelung, Ewald, Born, and others.[1] The method of Ewald, involving the Fourier expansion of the charge and potential functions, may be extended to the general crystal, thus obtaining an exact expression for the electrostatic energy in terms of the structure factors for positive and negative charge.[2,3] The latter may be calculated from assumed atomic functions or obtained from x-ray diffraction data. This method has also been extended to molecules, in which case the energy may be expressed in terms of the Fourier transforms of the radial charge density functions, which determine the molecular diffraction of x-rays and electrons.[3] The electrostatic energy is equivalent to the quantum-mechanical coulomb energy of the method of one-electron wave functions, if the latter is written in the symmetrical (unprimed) form, and represents the limiting value of this coulomb energy for an exact wave-mechanical calculation.

* This work was supported in part by the ONR under contract with the Ohio State University Research Foundation.

** To be given at the end of Session V if the Chairman rules that time permits.

[1] *Handbuch der Physik*, second edition, Vol. 24, Part 2, p. 705.

[2] C. N. Wall, Phys. Rev. 36, 1243 (1930), has given a rather obscure derivation of this relation, which has apparently been overlooked in the subsequent literature.

[3] Tech. Report No. 2, ONR Project NR 019 113 (June 15, 1949).

Author Index to Papers Presented at the Chicago Meeting

Abraham, Bernard—No. C3
Adair, R. K.—No. H9
Adams, Edward N. II—No. P5
Aldrich, L. T. and C. E. Smith—No. D3
Allen, A. J., J. F. Nechaj, K. H. Sun, and B. Jennings—No. N3
Allison, S. K., J. H. Montague, and A. H. Morrish—No. N13
Allred, J. C.—No. N7
Arnold, W. R.—No. T4
Alvarez, L. W., A. Longacre, V. G. Ogren, and R. E. Thomas—No. M8
Arroe, O. H.—No. G6

Barbour, Ian—No. M3
Barschall, H. H.—No. C1
Bashkin, S., B. Petree, F. P. Morring, and R. E. Peterson—No. H11
Becker, M. and H. Y. Fan—No. U5
Beiduk, F. M., J. R. Pruett, and E. J. Konopinski—No. P8
Belinfante, F. J. and J. S. Lomont—No. S8
Benfield, A. E.—No. V8
Blanchard, C. H. and R. Avery—No. S3
Borkowski, C. J. and E. Fairstein—No. T10
Bradford, C. E. and W. E. Bennett—No. N8
Bray, R. and H. J. Yearian—No. U4
Browne, C. P., R. V. Smith, and H. T. Richards—No. N11
Bruner, J., L. M. Langer, and D. Moffat—No. H2
Bullard, E. C.—No. F1

Carney, Rose A., Arnold G. Meister, and Forrest F. Cleveland—No. A5
Chapman, Robert M.—No. A9
Cohen, Bernard L.—No. N12
Cohen, Victor W., Walter S. Koski, and T. Wentink, Jr.—No. A14
Coles, D. K., W. E. Good, and R. H. Hughes—No. A10
Coomes, E. A.—No. D6
Conn, William M.—No. G2
Coryell, C. D., A. Y. Sakakura, and A. M. Ross—No. P3

Dancoff, S. M.—No. P6
Daunt, J. G.—No. F3
Dempster, A. J. and A. E. Shaw—No. G11
Dexter, D. L. and W. W. Beeman—No. V3
Diesendruck, Leo—No. N9
Dole, Malcolm, John A. Wethington, Jr., Norman Larson, and W. P. Hettinger, Jr.—No. V5
Dressel, Ralph, M. Goldhaber, and A. O. Hanson—No. P1
Duffield, Robert B. and Lawrence M. Langer—No. B10
Dunlap, W. C., Jr.—No. U1

Early, H. C. and W. G. Dow—No. E4
Eisenstein, A. S.—No. D7
Ekstein, H.—No. S10
El-Sabban, M. Zaki and Forrest F. Cleveland—No. A4

Fan, H. Y.—No. L1
Feenberg, Eugene—No. S5
Ferigle, Salvador M., Forrest F. Cleveland, William M. Boyer, and Richard B. Bernstein—No. A3
Foner, A. and I. Estermann—No. U2
Foss, Martin—No. T2
Fowler, R. G., Jack S. Goldstein, R. J. Lee, and B. E. Clotfelter—No. U9
Freedman, M., B. Smaller, and J. May—No. T11

Frankel, Sherman—No. H3
Freier, Geo. D., E. E. Lampi, and J. H. Williams—No. H10
Freier, Phyllis, E. P. Ney, and F. Oppenheimer—No. M7
Fuller, Everett G.—No. N5

Gilbert, D. A. and A. Roberts—No. A13
Glendenin, L. E. and C. D. Coryell—No. P4
Goldfarb, L., H. L. Bradt, and B. Peters—No. M2
Goldhaber, Gerson—No. N6
Green, Alex E. S.—No. P7
Griffith, G. L., M. E. Remley, and P. G. Kruger—No. H13
Groetzinger, Gerhart and Gordon W. McClure—No. M5
Grosskreutz, J. C. and K. B. Mather—No. H5

Hahn, E. L.—No. G9
Hall, T. A. and S. D. Warshaw—No. P2
Harkins, William D. and M. Popelka—No. S1
Harvalik, Zaboj V. and John H. Bowen—No. G1
Haynes, J. R.—No. L2
Heller, W. R.—No. U7
Hensley, Eugene B.—No. D1
Hereford, Frank L.—No. M4
Hirschberg, J. G. and J. E. Mack—No. G5
Hoffman, Gerald and Edward Akeley—No. U11
Holmes, John R.—No. G4
Hollomon, J. H.—No. L4

Jaffe, Leonard D.—No. V6
James, Hubert M. and Arthur S. Ginzbarg—No. J3
Jehle, Herbert—No. S7
Johnson, V. A.—No. U6
Johnson, E. O. and L. Malter—No. E2
Jones, L. C.—No. A12

Kauffman, John and Waller George—No. V2
Kê, T'ing-Sui—No. J7
Keepin, George R., Jr. and James H. Roberts—No. T6
Kelly, F. M., A. L. Schawlow, W. M. Gray, and M. F. Crawford—No. G7
Kikuchi, C.—No. G10
Knight, W. D.—No. G8
Koehler, J. S. and J. W. Marx—No. J5
Kubitschek, H. E., A. Longacre, and M. Goldhaber—No. B5
Kundu, D. N., John L. Hult, and M. L. Pool—No. B8

Lamport, J. E. and Forrest F. Cleveland—No. A6
Langer, Lawrence M.—No. B4
Lark-Horovitz, K. and K. W. Meissner—No. U3
Lax, Melvin—No. S6
Levin, F. K. and J. G. Winans—No. A7
Levinger, J. S. and H. A. Bethe—No. P10
Letner, Harold R.—No. V10
Lloyd, Stuart P.—No. S9

Mack, J. E.—No. G3
Madigan, John R., Forrest F. Cleveland, William M. Boyer, and Richard B. Bernstein—No. A2
Mallary, E. C. and M. L. Pool—No. B11
Marcus, Jules A.—No. J11
Marx, J. W. and D. A. Patterson—No. J6
Mihelich, J. W. and R. D. Hill—No. B9
Millar, C. H., A. G. W. Cameron, and M. Glicksman—No. B3
Miller, E. E. and C. B. Tanner—No. V4
Miller, W. C., B. Waldman, J. C. Noyes, and J. E. Van Hoomissen—No. T3
Mingins, Charles R., Carl A. Stevens, and Robert W. Perry—No. V9
Mitchell, Allan C. G., J. Y. Mei, Fred C. Maienschein, and Charles L. Peacock—No. B12
Moore, Donald C. and Willard A. Reenstra—No. U10
Moulton, W. G. and C. W. Sherwin—No. T5
Muehlhouse, C. O.—No. C2

Ney, E. P. and Phyllis Freier—No. M6
Neurath, Peter W. and J. S. Koehler—No. J8
Newkirk, John B. and R. Smoluchowski—No. J2
Norton, James F.—No. T9
Nowick, A. S.—No. J9
Novey, T. B.—No. B1

Owen, George E. and C. Sharp Cook—No. B6

Peterson, R. E.—No. H8
Pietenpol, W. J., J. D. Rogers, and Dudley Williams—No. A11
Pomerance, H.—No. H7
Popelka, Martin and William D. Harkins—No. S2
Price, H. C., Jr., J. Motz, and L. M. Langer—No. B13
Pringsheim, P.—No. V1
Pruett, J. R., F. M. Beiduk, and E. J. Konopinski—No. P9

Rall, Waldo and R. G. Wilkinson—No. T8
Ribe, Fred L., Martin J. Berger, and Gerhart Groetzinger—No. U8
Richards, H. T. and R. V. Smith—No. N1
Ridenour, L. A.—No. F2
Roberts, Arthur—No. M9
Roberts, T. R. and Alfred O. Nier—No. G13
Robertson, B. E., W. L. Carss, and M. L. Pool—No. H1
Robson, J. M.—No. H6
Rothstein, Jerome—No. D4

Salkovitz, Edward I. and James S. Koehler—No. J4
Sanders, J. H., J. Moffatt, and D. Roaf—No. N14
Schiffman, T. and H. Ekstein—No. S11
Schulz, L. G.—No. J10
Shull, C. G.—No. L3
Simpson, J. A., H. W. Baldwin, and S. Molner—No. M1
Smith, Philip B. and James S. Allen—No. H4
Smith, R. V. and D. H. Martin—No. N4
Stout, J. W. and Maurice Griffel—No. J12
Stout, Virgil L.—No. D2
Sturm, William J. and Virgil Johnson—No. N2

Tape, G. F. and P. G. Kruger—No. T1
Taylor, William J.—Nos. V7 and SP1
Ter-Pogossian, Michel—No. B7
Tittman, J., C. Sheer, J. Rainwater, and W. W. Havens—No. H12
Toms, M. E., J. Halpern, and W. E. Stephens—No. N10
Trigg, George L.—No. S4

Walker, L. R.—No. E3
Watanabe, K.—No. J1
Weber, A. H.—No. D5
Weissler, G. L. and E. I. Mohr—No. A8
Willardson, R. K., A. C. Damask, and G. C. Danielson—No. T7
Winans, J. G.—No. E1
Winn, E. B. and Alfred O. Nier—No. G12
Wright, S. Courtenay—No. B2

Zietlow, J. P., Forrest F. Cleveland, and Arnold G. Meister—No. A1